AMIRA
International

Final Report

P544 – Proterozoic Sediment-hosted Copper Deposits

October 2003

CODES – University of Tasmania
Colorado School of Mines

Contents

Introduction 1.1

Stratigraphy, regional alteration and mineralisation of the Zambian Copperbelt 2.1
David Broughton

Chambishi basin studies; Chambishi SE Prospect 3.1
Stuart Bull and David Selley

Development of the Lower Roan basin system: controls on Cu-Co mineralisation 4.1
David Selley, Stuart Bull, Robert Scott, Mawson Croaker, David Broughton and Nicky Pollington

The evolution of Willouran Trough 5.1
Wallace Mackay

Architecture and evolution of the Yeneena Basin, Paterson Orogen, W.A. 6.1
Robert Scott

Alteration history of the Roan 7.1
David Selley, Robert Scott, Mawson Croaker, David Broughton, Stuart Bull and Nicky Pollington

Lufilian metamorphism in the Zambian Copperbelt: implications for the interpretation of mineral assemblages and alteration paragenesis 8.1
Robert Scott, Ron Berry, David Selley and Stuart Bull

Introduction to Zambian Copperbelt geochemical and stable isotope studies 9.1
Peter McGoldrick

Lithogeochemistry and alteration halos to stratiform copper mineralisation in the Chambishi Basin, Zambian Copperbelt 10.1
Ross Large, Peter McGoldrick, Stuart Bull, Rob Scott and Dave Selley

Carbon and oxygen isotopic composition of ore-related and sedimentary carbonates in the Roan, ZCB 11.1
Ross Large, Stuart Bull, Mawson Croaker, Peter McGoldrick, Nicky Pollington, Rob Scott and Dave Selley

Minor element geochemistry of Zambian Copperbelt deposits 12.1
*Peter McGoldrick, Robert Scott, David Selley and *David Broughton*

Controls on mineral zones at Konkola mine 13.1
David Broughton

Sulfide mineral zonation and chemistry at Konkola North 14.1
Nicky Pollington and Rob Scott

Mwambashi B: Keys to arenite-hosted Cu–Co mineralisation 15.1
David Selley & Robert Scott

Stratigraphy, alteration history and copper mineralisation at Ndola West, Zambian Copperbelt 16.1
Robert Scott

Structural development and controls on Cu-Co mineralisation at Nkana-Mindola 17.1
Mawson Croaker and David Selley

Geochemical and isotopic character of Cu mineralisation in the Tapley Hill Formation, South Australia 18.1
Peter McGoldrick and Stuart Bull

Alteration, geochemical, and isotopic signatures of stratabound copper mineralisation in the Yeneena Basin, Paterson Orogen, W.A. 19.1
Robert Scott

Phosphate geochronology and geochemistry of hydrothermal events the Zambian Copperbelt 20.1
Galvin Dawson

Zambian Copperbelt geochemistry, geochemical modelling and stable isotopes: implications for mineralising processes 21A.1
Peter McGoldrick and David Cooke

Geochemical modelling: implications for mineralising processes in the Zambian Copperbelt 21B.1
David R Cooke

Comparison of Cu mineralised basins: the Zambian Copperbelt, the Polish Kupferschiefer, the Adelaide Fold Belt and the Yeneena Basin 22.1
Stuart Bull et al.

Numerical fluid flow, salinity and heat transfer modelling in an attempt to understand basin-scale mineralisation processes in the Zambian Copperbelt 23.1
Lyudmyla Koziy, Ross Large, Stuart Bull, Jianwen Yang and Dave Selley

Synthesis of P544 data for a genetic and exploration model for the Zambian portion of the African Copperbelt 24.1

Murray Hitzman

Introduction

Project P544 "Proterozoic sediment-hosted copper deposits" was a collaboration between researchers from CODES SRC at the University of Tasmania and from the Colorado School of Mines. It was jointly funded by AMIRA from July 2000 to June 2003 and by the Australian Federal Government through the ARC Linkage scheme from January 2001 to December 2003. This is the Final Report to AMIRA for this project.

Project objectives and key insights

When it began P544 had two simple objectives:

- To provide new data on Zambian Copperbelt to better understand its geology and genesis and develop new exploration tools for this style of deposit.
- To compare and contrast the Zambian Katangan with the similar sequences from the Adelaidean of South Australia

Later, these were extended to include a review of Cu metallogeny and geological evolution of the Paterson Province in Western Australia.

After three years work we now believe we have important insights in a number of areas that address these objectives. In Zambia, for instance, we now recognise the importance of structural controls for sedimentation in the Lower Roan and we have a more robust stratigraphy up to the lower Kundelungu and we recognise broad-scale basin architecture of the Zambian Copperbelt area. Evaporites, and evaporite-related breccias are, or were, an important component of Upper Roan rocks. We can recognise regional alteration (potassic and sodic) and its relationship to mineralisation, and have developed at least one vectoring tool (C isotopes) to mineralisation. Lastly, the availability of reductants (which may take several forms) is recognised as a critical control on the localisation of Cu mineralisation.

In South Australia, we recognise that Cu deposits related to the Tapley Hill Formation share the same oxidised fluid/reducing trap site process with the Zambian Copperbelt deposits, but, they occur at a different tectono-stratigraphic position, lack the intense alkali alteration and don't have the isotopically very light carbonate C seen in the Zambian deposits. More focused work in the Willouran Trough has revealed that the stratigraphic equivalent of the Lower Roan rocks may present, but they are not intact. Also we see the effects of catastrophic salt withdrawal during, or soon after, the Sturtian glaciation in regional-scale collapse of Callana and Burra Group rocks.

Our review of the Paterson Orogen in Western Australia suggests a fundamentally different style, and relative timing, for its Cu mineralisation compared to the Zambian Copperbelt.

This report

This report comprises three CDs. The first contains new detailed reports, in screen readable PDF format, written to accompany the Powerpoint presentations made at the P544 Final meetings held in Hobart and Kitwe last July. It also has a series of spreadsheets with sample information and geochemical data for samples analysed over the course of the project. The second CD contains the same material, in printable PDF format. The third CD contains copies of previous annual progress reports (2001, 2002), quarterly reports to AMIRA, other major reports and a field guide prepared for the May 2002 South Australian meeting.

Acknowledgements

The project was sponsored through AMIRA by the following companies and organizations:

Anglo American
Anglovaal Mining
BHP Billiton
First Quantum – Mopani
Inco
MIM Exploration
Phelps Dodge Exploration
Outokumpu
Department of Primary Industry & Resources SA
Rio Tinto Exploration
Straits Resources
Teck Cominco
WMC Resources

Alan Goode was the AMIRA Research Co-ordinator for this project, and his efforts in many areas are greatly appreciated.

We would like to particularly thank the three Zambian-based sponsors (Anglo American – Zamanglo, Anglovaal Mining and First Quantum-Mopani) for their logistical support, without which very little would have been achieved in Zambia. Special mention goes to Hugh Carruthers and Mike Stewart (FQ), Peter Mann and Jon Woodhead (Anglo) and Claus Schlegal and the 'two James' Mwali and McMaster from Avmin. Dave Armstrong, Wellington Mukumba and Giddy Mwali from MCM were a great help at the Nkana end of the Chambishi Basin. It was Nick Franey from Anglo who suggested over a couple of Mosi's that 'perhaps CODES should come and do some work in Zambia'. Dugi Wilson from MIM also thought this would be a good idea! At Zamanglo, Anne Musunga was a great help in getting people and rocks in and out of Zambia, Spider and Mfutu kept the 'Love Bus' running most of the time and Mike Kondani kept Peter McGoldrick and David Selley out of jail (most of the time)!

In South Australia, discussions and guidance from Wolfgang Preiss and Stuart Robertson was invaluable, and Brian Logan and crew at the PIRSA core store worked hard to keep the cores rolling out.

Closer to home, sample preparation and much of the analytical support was provided by Christine Cook, Keith Harris and Dave 'the animal' Steele from the University of Tasmania's Central Science Laboratory, and by Phil Robinson, Katie McGoldrick, Marc Norman, Seb Meffre, Sarah Gilbert and Fernando Della Pasqua from CODES SRC.

June Pongratz has done a great job with the layouts for all the P544 reports (including this one), and ultimately won the battle against the nasty black backgrounds!

Mike Blake toiled hard to produce the slick navigable pdf versions of the reports you are now reading.

Finally, we want to personally thank all the P544 Researchers for their efforts and sacrifices that have given us new insight into how Cu mineralizing systems develop in sedimentary basins, and, hopefully, how to find them. The research team comprised David Selley, Robert Scott, Stuart Bull, Peter McGoldrick, Ross Large, David Cooke, Lyudmyla Koziy, Wallace Mackay, Nicky Pollington and Mawson Croaker from CODES; Murray Hitzman and David Broughton from CSM; and Galvin Dawson (UWA). A very special mention goes to D1 and D2 (Dave Selley and Dave Broughton) who contributed hugely to P544 over the entire three years.

Peter McGoldrick
Stuart Bull
Murrray Hitzman

October 2003

Stratigraphy, regional alteration and mineralisation of the Zambian Copperbelt

David Broughton
Colorado School of Mines

This report summarises the stratigraphy, sedimentology, and basinal architecture of the Neoproterozoic Katangan Supergroup host to the Zambian Copperbelt (ZCB), and in addition provides an overview of the regional alteration, and the distribution of mineralisation, within the Katangan. A tentative correlation between the ZCB and the southern part of the Congolese Copperbelt (CCB) is proposed. The report is based upon four field seasons of core logging, mine visits and limited field mapping in all major areas of the ZCB, including Lonshi, Bwana Mkubwa, Ndola/Itawa, Mufulira, Luansobe, Lubembe (DRC), Kinsenda (DRC) Mokambo, Kawiri South, Konkola, Konkola North, Kakosa, Nchanga, Chambishi, Nkana, Mindola, Nkana West Limb, Chibuluma, Chibuluma South, Kabula, Luanshya, Baluba, and Samba. Observations from the main Shaba province of the CCB are also included. Reference is made to numbered Powerpoint slides presented at the final meetings.

The Katangan Supergroup in the ZCB comprises some 1–2 km of metamorphosed continental and marine sedimentary rocks deposited on a major unconformity. The lower part of the ZCB Katangan section is divided into Lower Roan Group (dominantly clastic rocks), Upper Roan Group (carbonates, clastics and interpreted evaporitic breccias), Mwashia Group (carbonates and generally fine-grained clastics) and Nguba (Lower Kundelungu) Group (diamictite and overlying carbonates and carbonate-bearing clastics) (Slide 5). Stratigraphic nomenclature adopted here is modified from Clemmey (1976), Binda (1994), Cailteux (1994) and Cailteux and Kampunzu (2002) (see table 1). In accordance with the North American Stratigraphic Code (1983), lithological references have been removed from the Zambian formation and member names (e.g., Rokana Evaporites Member replaced by Rokana Member).

Throughout most of the ZCB, the basal Katangan rocks overlie basement granitic, intermediate metavolcanic, and metasedimentary rocks dated at ~1800-2000 Ma. However, the maximum age of Katangan sedimentation is constrained by U-Pb dates on zircons from the Nchanga granite, at 877 ± 11 Ma (Armstrong et al., 1999; Slide 5). Field relations between the granite and the basal Roan arkoses can be puzzling, and have previously been ascribed to sedimentation between exfoliated slabs of granite (Slide 6). Other contacts are more difficult to explain (Slide 7), but may result from intense K-feldspar metasomatism of selected arkosic beds. Coarse-grained K-feldspar alteration of basement clasts occurs elsewhere in the ZCB (Slide 8).

The only other age constraint on the Katangan sedimentation is provided by U-Pb dates of zircons from mafic volcanics and sills within the Mwashia and Nguba Groups, at ~735 to 760 Ma (Key et al., 2001; Barron, 2003; this study). Given the relative thinness of the Katangan section in the ZCB, and the apparent lack of a major unconformity within the section, it is possible that the basal Katangan sediments are much closer in age to the upper than to the lower age constraint.

Copper-(cobalt) orebodies occur at all stratigraphic levels of the lower Katangan Supergroup in the ZCB and CCB, up to and including the Kakontwe Fm in the Nguba Group (Lonshi deposit, Slide 5). The stratigraphic position of the Congolese mineralisa-

Table 1. Stratigraphy and Nomenclature of the Zambian Copperbelt.

Group	Formation	Member	Clemmey, 1976	Nkana	Chambishi	Nchanga (Binda and Mulgrew, 1974)	Konkola	Musoshi (Lefebvre, 1989)	Lubembe (Lefebvre, 1989)
Kundelungu (Upper Kundelungu)	Plateaux (Ku 3) (Mokambo Fm?)								
	Kiubo (Ku 2)								
	Kalule	Ku 1.3							
		Ku 1.2							
		Petite Conglomerate (Ku 1.1)							
Nguba (Lower Kundelungu)	Monwezi	Ng 1.2							
	Likasi	Ng 1.3							
		Kakontwe (Ng 1.2)							
		Grand Conglomerate (Ng 1.1)							
Mwashia	Upper					Mwashia	Mwashia	Upper Mwashia	
	Middle					Upper Roan			
	Lower			Ultra Far Water Formation				Lower Mwashia	Mines Group RAT
Upper Roan			Bancroft Fm		Dolomite Formation		Upper Roan	Kanwangungu Fm.	
Lower Roan	Kitwe	Antelope	Antelope Clastics Mbr.	Far Water Sediments	Sandy Talc Schist	Shale with Grit	Shale with Grit	Kibalongo Fm.	Musoshi Fm
		Chambishi	Chambishi Dolomites Mbr.	Far Water Dolomite Dolomite - Argillite Seq	Cherty Dolomite Interbedded Arg & Dol	Chingola Dolomite Dolomitic Schist Upper Banded Shale	Hangingwall Aquifer	Chingola Fm.	Kitotwe Mbr Kabemba Mbr.
		Nchanga	Nchanga Quartzite Mbr.	Upper Quartzite	Upper Quartzite	Feldspathic Quartzite	Hangingwall Quartzite	Pelito-Arkosic Fm.	
		Rokana	Rokana Evaporites Mbr.	Near Water Sediments	Intbdd Arg & Dol Intbdd Qtzite & Shale Intbdd Arg Qtzite & Dol HW Quartzite	Banded Sandstone Upper Pink Quartzite Shale Marker Banded Sandstone Lower Chert Marker			
		Copperbelt	Copperbelt Orebody Mbr.	Hangingwall Argillite Ore Shale	Ore Shale	Lower Banded Shale	Ore Shale	Ore Shale	F.Q.
	Mindola	Kafue	Kafue Arenites Mbr.	Footwall Conglomerate Arkosic Sandstone Lower Conglomerate	Footwall Conglomerate Arkose and Argillite Cobble Conglomerate	Transition Arkose Arkose Conglomerate	Footwall Conglomerate Footwall Sandstone Porous Conglomerate	Mutonda Fm.	Simbi Mbr. Lubembe Mbr.
		Konkola	Basal Quartzites Mbr.	Footwall Transition Footwall Quartzite Basal Conglomerate	Footwall Quartzite Basal Conglomerate		Footwall Quartzite Pebble Conglomerate Basal Conglomerate	Kafufya Fm. Chimfunsi Fm.	

Recommended nomenclature in columns 1-3. Lower Katangan follows Clemmey (1976), upper Katangan follows Cailteux and Kampunzu (2002). Approximate correlations based on local mine terms, not to scale, see text for details.

tion remains uncertain, and will be further discussed. There is no evidence to support widely different ages of mineralisation at different stratigraphic levels, and indeed the styles of mineralisation are broadly similar throughout the ZCB and CCB. This suggests that mineralisation developed later than ~740–750 Ma, the interpreted age of the Nguba. All available robust geochronological data on mineralisation and associated alteration reflect the Lufilian orogenic event at ~590–500 Ma (586 Ma biotite from Luanshya, 592 Ma monazite from Chambishi, Rainaud *et al.*, 2002a; numerous dates on monazite, rutile, molybdenite, uraninite, at ~530–500 Ma). Re-Os dating of copper sulfides is in progress and may provide a better constraint on the timing of the onset of mineralisation.

The lowermost portion of the Katangan (Lower Roan Group, Mindola Formation, below the Copperbelt Member or Ore Shale) is characterised by locally variable thicknesses of immature continental clastic rocks typical of an early-stage rift basin fill. Volcanic rocks and intrabasinal volcanic clasts are absent, and in most places the early-stage rift fill is only hundreds of meters thick, to a maximum of approximately one kilometer in the Konkola North area. At least in the ZCB, the Katangan basin did not evolve to a typical rift, with kilometers of sediment fill and attendant volcanics. In comparison, the Nosib Group records the rift-fill stage of the correlative Neoproterozoic Damara Supergroup in Namibia, and in many places is more than 6 km thick, with thick accumulations of alkalic volcanic rocks (Miller, 1983)

The majority of the Lower Roan coarse detritus was derived from the basement granites and quartz sandstones. Clasts of basement metavolcanic rock (Lufubu schist) are rare or absent except in the basal conglomerates. Contrary to interpretations of copper 'porphyries' and 'fertile granitoids' (Samba deposit, Wakeford, 1978; Rainaud *et al*., 2002b) providing a copper-rich source rock for the Katangan deposits, all basement mineralisation including Samba examined during P544 is similar in style to that seen in the Katangan, and is most commonly restricted to the uppermost portion of the basement, in close proximity or contact with overlying mineralised Katangan rocks. In summary, the evidence suggests that the footwall rocks for the ZCB deposits were if anything relatively poor in copper, in comparison to other world class sediment-hosted copper districts.

Local and regional thickness variations and facies changes in the rift-phase Lower Roan are related to syn-sedimentary NW, NNW and NE faults, which may coincide with basement contacts (e.g., between granite and Lufubu schist at Mufulira, Slide 34). Reactivation during Lufilian deformation produced basement 'ridges' and 'paleohills'. Many of the ZCB deposits occur along or in proximity to such faults, including Konkola, Mufulira, Luansobe and Lubembe (Slides 34, 37, 39, 44). In some deposits, the higher-grade mineralisation is restricted to localised stratigraphic units developed within grabens (e.g., Lubembe, Slides 39, 40).

The Ore Shale (Copperbelt Member) and its equivalent in the Mufulira area, the 'Mudseam', represent regionally transgressive deposits that show relatively minor facies and thickness changes associated with the early faults. They resulted from a relative sea level rise, or maximum flooding surface, probably related to widespread fault death (Selley, this volume). Above this marker the Lower Roan sequence becomes progressively siltier and more carbonate-rich, with local evaporitic textures, and is much more laterally continuous, reflecting a stable, near- to shallow-marine basin environment and gradual subsidence. The base of the Ore Shale–Mudseam therefore marks a major change in basin architecture, from a tectonically active, compartmentalised, coarse clastic continental rift-fill stage in its footwall (Mindola Formation), to a relatively quiescent, laterally continuous, mixed clastic-carbonate, marine-influenced stage (Kitwe Formation).

In the Chambishi Basin and Nchanga areas, above the ore shale, the Kitwe Fm contains two sequences of fining upwards, metre-scale, clastic-to-carbonate cycles, the Rokana Member and Chambishi Member (Slide 12). Laminated, probably algal dolomites, and local centimetre- to decimetre-sized dolomite nodules after sulfate are present at the tops of some cycles. These two members are separated by the Nchanga Member (TFQ), of thick, fluvial sandstones. The Chambishi cycles become more carbonate-dominant up-section, and are capped by a massive dolomite bed, the Chingola Dolomite.

In the Konkola area, the Kitwe Formation contains a higher proportion of coarse clastic material than is present in the Chambishi Basin and at Nchanga. This is attributed to the proximity of a basement high related to at least two major WNW faults (Kawiri and Fitwaola, Slide 44) that were active post-Ore Shale time. The carbonate-capped cycles are poorly developed, and a second, thinner, transgressive siltstone, the weakly mineralised Upper Ore Shale, is developed below the Chingola Dolomite equivalent carbonate bed that marks the top of the Chambishi Member (Hangingwall Aquifer Formation at Konkola).

The Chambishi Member is abruptly overlain by a sequence of thinly to rhythmically bedded fine and coarse-grained clastics, which lack significant carbonate beds and gradually fine upwards. This, the Antelope Member (former 'shale with grit'), is characterised by very poor sorting, outsized sand and granule 'grit' within siltstone layers, and distinctive sand/grit dykes that indicate widespread basin dewatering (Slide 13). Although the grit and dyke textures are developed to varying extents throughout the Lower and Upper Roan Groups, they are by far most abundant in this member.

The top of the Antelope Member is defined at base of the first significant (~metre-thick) dolomite bed. The overlying sequence of gritty sandstones, siltstones and dolomites, commonly with dolomite nodules after sulfate evaporates, forms the Upper Roan Group (Bancroft Dolomite Formation in Clemmey, 1976). The Upper Roan is characterised by laterally extensive fining upwards cycles of sandstone, siltstone, dolomite and local anhydrite, which become finer grained and more dolomitic-anhydritic up-section. The dolomites, and to a lesser extent the sandstones and siltstones, commonly contain nodules and 'chicken wire' structures of dolomite, talc, quartz, and/or anhydrite diagnostic of evaporitic, sabkha conditions. In some areas the amount of anhydrite increases substantially up-section, again suggesting increasingly evaporitic, restricted basin conditions. In general, the Upper Roan section records gradual regional subsidence and filling of accommodation space. The section is punctuated by two coarse-grained, cross-bedded fluvial sandstone beds, traced throughout the Konkola area, with possible correlative beds at Nchanga and Chambishi (Slide 32).

Correlation of the Roan stratigraphy above the Ore Shale–Mudseam is difficult between the western (Konkola) and eastern (Mufulira) limbs of the Kafue Anticline. Available drill holes at Kawiri and Lubembe (Slides 37, 39-42) indicate that the Roan is represented by a condensed, transitional section in this area, interpreted as a basement high at the northern closure of the Kafue Anticline. The Antelope Member (shale with grit), present at western Kawiri, is not recognised at eastern Kawiri, Lubembe, Luansobe and Mufulira, although poorly bedded to massive gritty siltstones and fine-grained sandstones are present throughout the Roan section above the Ore Shale–Mudseam. In these eastern areas, the Upper Roan fining-upward sabkha cycles directly overlie the Glassy Quartzite (Slides 33, 35-38), which was previously correlated with the Nchanga Member (Binda, 1994).

The Glassy Quartzite is a sequence of partially to intensely K-feldspar/albite/quartz–altered ('glassy') sandstone and siltstone, well developed at Mufulira and Luansobe. The glassy character of the unit is not unique, as all of the fluvial sandstone beds above the Ore Shale–Mudseam at least locally host this alteration. This lithological control on alteration is demonstrated northwest of Luansobe, at Lubembe and Kinsenda in the DRC, where siltstone dominates the Glassy Quartzite unit, and the alteration is less pervasive. The Nchanga and Glassy Quartzites are not considered stratigraphic equivalents, and correlation of the base of the Upper Roan is made on the basis of the stratigraphic equivalence of the sabkha cycles that overlie the Glassy Quartzite and Antelope Member, in the eastern and western parts of the Copperbelt. The Nchanga Quartzite is instead correlated with the Marker Grit at Mufulira, as suggested by Binda and Mulgrew (1974).

The Upper Roan Group in Zambia is characterised by the presence of unusual polylithic or conglomeratic breccias, lithologically equivalent to similar breccias in the DRC. They are comprised of rounded to subangular intrabasinal (Katangan) fragments supported within a matrix that contains some or all of dolomite, albite, quartz, anhydrite and chlorite. Fragment size ranges from sand-sized to beyond the limit of resolution in core, as it is difficult to evaluate whether sections of stratigraphy between breccia zones are

beds or large fragments. The fragments tend to be locally derived, and commonly the most abundant fragment lithology can be recognised in the adjacent stratigraphy. In some instances fragments are derived from both above and below the stratigraphic position of the breccia. Typically, the breccias are internally structureless: unsorted, ungraded, and lacking evidence of internal bedding. Contacts in drill core range from apparently concordant to highly discordant, the latter suggesting the breccias form dyke- or pipe-like injections. For example, in drill hole KS17 from Mokambo, the breccias occur several hundreds of metres above the base of the Mwashia Group, with discordant contacts (Slide 18).

The breccias occur as single centimetre- to tens-of-metres-thick bodies, usually at the contact between the Roan and Mwashia, as breccia complexes hundreds of metres thick within the Roan, and, at Mokambo east of Mufulira, as isolated bodies within the Mwashia. Within the complexes, large blocks of intact stratigraphy can be recognised. The breccias are broadly stratiform at the local (mine) scale, but regionally discordant. Similar breccias are recognised throughout the Lufilian Arc in northern Zambia and the southern DRC, at Luamata, Kalengwa, West Lunga, and Kipushi, as well as in the ZCB and CCB. In the DRC where field relations can be observed, the breccias form piercement structures into the Mwashia, Nguba and Kundelungu stratigraphy, and isolate 'megafragments' of Mines Group stratigraphy that contain the Congolese Cu–Co orebodies (Slide 19).

West of the Kafue Anticline, some of the breccias occur in association with irregular, podiform, metagabbroic bodies, and were termed 'hybrid rock'. However, gabbros at Kabula and Chibuluma South have non-brecciated footwall contacts with Roan rocks, and breccias east of the Kafue Anticline (Mufulira, Luansobe) and in the CCB lack any associated gabbros. Pebble- to cobble-sized fragments of gabbro and tuff have been found within breccias at Kalengwa, Shituru, and Kipushi. These observations indicate that many of the breccias are unrelated to the igneous activity, in some cases post-date the gabbros.

The polylithic breccias typically have a highly veined (crackle brecciated) and dolomite-talc-albite altered footwall, suggesting they localised overpressuring and/or faulting (Slide 17; these are termed 'friction breccias' in the CCB). In a given drill hole, the hangingwall to the uppermost polylithic breccia body completely lacks any such veining and alteration, and is instead often characterised by strongly foliated and deformed rocks (Mwashia Group). Although the polylithic breccias are common within deformation zones, or zones marking abrupt changes in strain, they themselves appear comparatively to completely undeformed. This contrasts markedly with the well-developed foliation and deformed clasts seen in the other matrix-supported conglomeratic rocks in the Katangan section, the Grand Conglomerate diamictites and the Lower Roan conglomerates.

The breccias are interpreted as resulting from dissolution and mobilisation of anhydrite and salt in the Upper Roan sequence. In many cases, it is not possible to demonstrate significant tectonic movement associated with individual breccia bodies, and they are interpreted to reflect the position of former evaporitic beds. The dyke and pipe-like breccias appear to have formed and emplaced at various stages in the basin history, from Mwashia and Nguba time (~740–760 Ma) through to Lufilian deformation.

In the CCB, major thicknesses of former evaporite have been interpreted from the presence of breccias at several stratigraphic levels broadly correlative with the Roan-Mwashia in the ZCB (DeMagnee and Francois, 1988; Jackson et al., 2003). Jackson et al. (2003) suggested that formation of diapiric breccias began in Roan time, based on breccias cross-cutting Roan (pre-Mwashia) strata within the Kolwezi klippe.

The rocks overlying the breccias, dolomites, and clastics of the Upper Roan Group belong to the Mwashia Group, and comprise generally finer-grained siltstones and mudstones, intermixed with dolomites and minor sandstones. The determination of the Upper Roan–Mwashia contact is made difficult by the breccias, a greater degree of deformation in the Mwashia rocks, and in some instances, apparent loss of stratigraphic section at the contact. The clastic sedimentary rocks in the Mwashia are distinguished from

those of the Upper and Lower Roan by their lack of sandy, outsized quartz – feldspar grit. Geochemically, the Mwashia Group siltstones and mudstones have higher Ti/Zr ratios than the Roan clastics, indicative of a more mafic provenance (Slide 25). However, individual siltstones and mudstones within the Roan sequence commonly have comparable Ti/Zr ratios to those in the Mwashia. The Mwashia sequence may therefore record a greater relative input of mafic to felsic detritus as compared to the Roan, rather than a change in source area.

Traditionally and as shown on most of the geological maps, the Mwashia Group is defined in Zambia as a siltstone-mudstone (shale) facies immediately underlying the Grand Conglomerate diamictite. In the Konkola and Mufulira areas, it is possible to recognise a three-part sequence of lower dolomitic, intermediate mixed dolomitic-clastic, and upper clastic (traditional Mwashia) rocks. This sequence defines a gradual upward-deepening trend and is here used to define a lower, middle and upper Mwashia. In the Chambishi and Ndola areas, the contact between the Upper Roan and Mwashia Groups is transitional, and again defines an upward-deepening trend.

The lowermost, dolomitic sequence contains only minor clastic input, and is characterised by millimetre- to centimetre-sized silicified grey nodules, and local stromatolitic laminations. These may be correlative with the 'black oolite' dolomites of the Mwashia in the DRC (Cailteux, 1994). The middle unit contains both massive dolomite and interbedded centimetre-thick beds of dolomite or dolomitic siltstone, and siltstone. In the Mufulira–Luansobe area its lower boundary is placed at the base of a persistent, slightly carbonaceous shale. Unlike the lower unit dolomites, the middle unit dolomites are commonly ferroan. The upper unit consists predominantly of thinly interbedded siltstone and variably carbonaceous mudstone, with only minor dolomitic beds. Disseminated and locally framboidal pyrite mineralisation is the norm, but transitions upwards to pyrrhotite close to the contact with the overlying diamictite. Locally, fine- to medium-grained sandstone is present within the upper Mwashia, as metre-thick beds with cross-bedding, and/or as thin beds rhythmically interbedded with siltstone/mudstone. Thin, fining-upward, and possibly turbiditic beds of conglomerate–sandstone may also be present. These sandstones are morphologically similar to some of the Roan sandstones, and clasts of the two would be difficult to distinguish in provenance studies of conglomerates and breccias.

The top of the Mwashia is defined by the base of the Grand Conglomerate diamictite, which comprises predominantly subangular intrabasinal clasts and rare rounded basement clasts within a ferroan dolomitic mudstone (locally carbonaceous) matrix similar to that of the underlying Mwashia mudstones. The majority of the intrabasinal clasts are derived from the Mwashia and Upper Roan, and it does not appear as though significant erosion of the Lower Roan or basement occurred in the ZCB. Also lacking are clasts of the Upper Roan breccias, although it is debatable whether this may be due to preservation potential. In the Ndola and Mufulira areas, the Grand Conglomerate contains thin interbeds of laminated siltstone and coarse lithic sandstone, which mark the contacts between distinct diamictite (debris flow) beds. The thickness of the Grand Conglomerate in the ZCB varies from approximately 10–100 m, and major thickness variations occur on a local scale. It is considerably thicker (+600 m) in the CCB.

The Grand Conglomerate marks a major sea level fall, and destabilisation of the Katangan platform and shallow marine environment, correlated worldwide with similar Sturtian age diamictites at approximately 750 Ma. Global 'Snowball Earth' glaciation has been proposed as a mechanism to explain the worldwide distribution of Sturtian age diamictites (Hoffman et al., 1998). The Grand Conglomerate also has a broad temporal association with extension and mafic igneous activity (gabbroic sills and mafic volcanic flows and tuffs), which mark a significant heat influx into the basin. All of the above points to a tectonically and hydrologically active Katangan basin during late Mwashia – Nguba (~750 Ma) time. It is considered likely that saline fluids were produced both by seawater concentration during glaciation, and by dissolution of Upper Roan evaporites through circulation of fluids along tectonically active faults.

The Grand Conglomerate marks the lowest unit, Ng 1.1, of the Nguba (Lower Kundelungu) Group (Cailteux and Kampunzu, 2002). There is no evidence

of a non-depositional hiatus at the base of the diamictite. The overlying Nguba sequence is lithologically and stratigraphically similar to the Mwashia, and in the Konkola–Mufulira area is characterised by a deepening upward succession of dolomite / limestone (Kakontwe Formation) to mixed dolomite-siltstone to siltstone-mudstone. The Mwashia is therefore more closely related to the Nguba (and to a similar cycle in the overlying Upper Kundelungu) than to the Roan sequence. In the southeastern ZCB (Ndola, Lonshi areas) the Grand Conglomerate is immediately overlain by thinly interbedded mudstones, siltstones and carbonates similar to those in its footwall, before passing upwards into massive shallower-water carbonates and siltstones. This indicates a more distal setting within the Katangan basin, and is comparable to the Nguba sequence seen in the CCB. There, the interbedded lower sequence is defined as Ng 1.2.1, and the massive limestone (Kakontwe) as Ng 1.2.2. This sequence also hosts the Kansanshi deposit west of the ZCB.

The Kundelungu Group (formerly the Upper Kundelungu Group) was intersected in one drill hole in the Mufulira Syncline near Luansobe, and comprises a similar sequence of diamictite (Petit Conglomerate), carbonate (Calcaire Rose), and mixed carbonate-siltstone as in the Nguba. In this hole the thickness of the Nguba Group is constrained at approximately 400–500 m. If the Petit Conglomerate is correlated globally with the Marinoan diamictites at circa 600–620 Ma, the Zambian portion of the Nguba basin was tectonically quiescent and received only modest input over a protracted (+130 Ma) interval.

In the Mokambo area on the eastern side of the Mufulira Syncline, the Kakontwe dolomite is abruptly truncated by a more than 300 m-thick sequence of immature, hematitic, continental molasse deposits, which contain poorly sorted intrabasinal clasts of Kundelungu, gabbro, Mwashia and possibly Upper Roan derivation. Gabbroic clasts are unaltered and present only at the base of the sequence, indicating gradual unroofing of the underlying Katangan sediments. These deposits apparently post-date the deposition of the Petit Conglomerate at circa 600 Ma, and may record the development of a Lufilian foreland basin between 600 and 500 Ma. The name Mokambo Formation is suggested for this sequence. Further work is required to determine whether they are the stratigraphic equivalent to the Plateaux Sub-Group, Ku 3, of the Kundelungu, interpreted as the foreland basin deposits in the northern CCB (Cailteux, 1994; Cailteux and Kampunzu, 2002).

Cailteux and Kampunzu (2002) and Wendorff (2000) presented opposing views of stratigraphic correlation between the ZCB and CCB. With respect to the lowermost Katangan stratigraphy in each area, Cailteux and Kampunzu (2002, and references therein) presented the commonly held view that Zambian Copperbelt Mbr (Ore Shale) is equivalent to the Congolese Mines Group. This view is based partly on the interpretation of the red hematitic RAT (Roches-Argilo-Talqueuses, thin-bedded to massive siltstones and fine sandstones underlying the Mines Group) as a distal fine-grained equivalent of the immature first-cycle, hematitic Mindola Formation. Significantly, the RAT is not known to show the same local facies changes, and associated syn-sedimentary fault-controlled thickness changes, that are so characteristic of the Mindola Formation. Additionally, exposures in the Luiswishi open pit in the southeastern part of the CCB suggest that the overlying lower Mines Group does not represent a fundamental tectonic reorganisation of the basin, as it consists of variably dolomitic rocks interbedded with siltstones that are indistinguishable from the RAT. The presence of hematite (and mineralisation) cannot be considered a basis for correlation.

The second view, proposed by Wendorff (2000) based upon an early paper by Grujenschi (1978), also holds that the CCB and ZCB orebodies are stratigraphically equivalent, but in the CCB are allochthonous, as olistoliths within syn-orogenic Lufilian foreland olistostromes, the polylithic breccias described above. This view is difficult to reconcile with the diapiric and piercement geometries typical of the breccia bodies in the CCB, and with the other breccia features detailed above.

An alternative correlation is suggested here, based on drill cores from Luansobe in Zambia, and Lubembe in the southern DRC (Slides 37-41). Lubembe is located just north of the Zambian border, south of the Luina Dome, and geologically within the ZCB. In the DRC holes, Congolese geologists recognised

RAT and Mines Group lithologies overlying an intact section of Lower and Upper Roan stratigraphy (Slide 40; Lefebvre, 1989; Lefebvre and Tshiauka, 1986). Relogging demonstrated that the Roan stratigraphy correlates with that at Luansobe and Mufulira, the RAT with Upper Roan massive siltstones and fine-grained sandstones, and the Mines Group with lower and middle Mwashia (Slide 40). The contact between the RAT and the Mines Group is marked by a polylithic breccia, as is the Upper Roan–Mwashia contact at Luansobe. This correlation suggests that Lower Roan equivalent stratigraphy, favourable for copper mineralisation, exists and is untested below the RAT in the CCB.

Further work would be required to determine whether the unmineralised RAT and Mines Group identified at Lubembe are in fact correlative with the mineralised RAT and Mines Group north of the Luina Dome, in the CBB *senso stricto*. The Lubembe Mines Group does not correlate with the Upper Roan mineralisation in drill hole DH218 at Mufulira, which was interpreted as Mines Group by Cailteux et al. (1994), but is here seen to occur within the Zambian Upper Roan.

As noted earlier, alteration and mineralisation are widespread throughout the Katangan section. Anhydrite is found in varying amounts at all stratigraphic levels, including the basement, but focused in the Upper Roan. Regionally, the basement and Lower Roan are typified by potassic alteration and hematite, with zones of sulfide mineralisation in the ore shale and sandstone orebodies. The Upper Roan is characterised by carbonate-anhydrite and albite alteration, the latter associated with the polylithic breccias, and dominant but weak pyritic mineralisation. The Mwashia is also characterised by carbonate and albite alteration, local potassic alteration (K-feldspar, biotite), and predominantly pyritic mineralisation. The upper Mwashia and Grand Conglomerate are commonly mineralised with pyrrhotite, rather than pyrite, indicating more reduced conditions. Lithogeochemical samples reveal the same broad trends of strongly potassic-altered Lower Roan and variably sodic- or potassic-altered Upper Roan and Mwashia (Slide 8).

The recognition of regional alteration throughout the lower part of the Katangan Supergroup, and at least the uppermost tens to hundreds of metres of basement, suggests that the entire lower part of the basin was involved in the mineralizing system. Virtually nothing is known about the presence or absence of alteration above the level of the Kakontwe Formation, however, it is perhaps noteworthy that in the ZCB and CCB there are no known base metal deposits higher in the section. The lack of deposits may reflect a lack of alteration and hence of ore fluid circulation. The small but high-grade Dikulushi Cu deposit in the eastern DRC is thought to occur in Upper Kundelungu equivalent sandstones and siltstones, but its regional stratigraphy needs better constraint before the relevance of Dikulushi to the Copperbelt can be addressed.

References

Armstrong, R.A., Robb, L.J., Master, S., Kruger, F.J. and Mumba, P.A.C.C. (1999). New U-Pb age constraints on the Katangan sequence, Central African Copperbelt. In: Frimmel, H.E., (ed), Special Abstracts Issue, 11th International Conference of the Geological Society of Africa: Earth Resources for Africa. J. African Earth Sciences, v. 28, pp 6-7.

Barron, J.W., 2003. The Stratigraphy, Metamorphism and Tectonic History of the Solwezi area, North West Province, Zambia: Integrating Geological Field Observations and Airborne Geophysics in the Interpretation of Regional Geology. Unpublished PhD dissertation, Colorado School of Mines, Golden, USA, 233 p.

Binda, P.L., (1994), Stratigraphy of Copperbelt Orebodies. J. Afr. Earth Sci, v19, no.4, pp. 251-264.

Binda, P.L., and Mulgrew, J.R., 1974. Stratigraphy of Copper Occurences in the Zambian Copperbelt. In Bartholome, P. (ed), Gisements Stratiformes et Provinces Cupriferes. Societe Geologique de Belgique, Liege, pp 215-233.

Cailteux, J. (1994); Lithostratigraphy of the Neoproterozoic Shaba-type (Zaire) Roan Supergroup and metallogenesis of associated stratiform mineralization; Journal of African Earth Sciences. 19; 4; pp 279-302.

Cailteux, J., Binda, P.L., Katekesha, W.M., Kampunzu, A.B., Intiomale, M.M., Kapenda, D., Kaunda, C., Ngongo, K., Tshiauka, T., and Wendorff, M., 1994. Lithostratigraphical correlation of the Neoproterozoic Roan Supergroup from Shaba (Zaire) and Zambia, in the Central African copper-cobalt metallogenic province. J. African Earth Sci., v.19, p. 265-278.

Cailteux, J.L.H., and Kampuzu, A.B.H, 2002. Lithostratigraphic Position and Petrological Characteristics of R.A.T. (Roches Argilo Talqueues) Subgroup Sedimentary Rocks, Neoproterozoic Katangan Belt (Congo). In: Robb, L. and Montjoie,

(eds), 11th Quadrennial IAGOD Symposium and Geocongress 2002, Extended Abstract Volume (CD ROM).

Clemmey, H. (1976), Aspects of Stratigraphy, sedimentology, and ore genesis on the Zambian Copperbelt. Ph.D. Dissertation, University of Leeds, U.K., pp. 356.

De Magnee, I. and Francois,A. (1988); The origin of the Kipushi (Cu,Zn,Pb) Deposit in direct relation with a Proterozoic salt diapir; Copperbelt of Central Africa, Shaba, Republic of Zaire; In: Friedrich,G.H. and Herzig, P.M. (editors); Base metal sulfide deposits in sedimentary and volcanic environments. Special Publication of the Society for Geology Applied to Mineral Deposits. No. 5; pp 74-93.

Grujenschi, C. (1978), Quelques observasations sur la position stratigraphique de la "serie des mines" du shaba; Annals Society Geological Belgique, 101; pp. 1-11.

Hoffman, P.F., Kaufman, A.J., Halverson, G.P.and Schrag, D.P. (1998) A Neoproterozoic Snowball Earth, Science, Vol. 281, 1342-1346.

Key, R.M., Liyungu, A.K., Njamu, F.M., Somwe, V., Banda, J. Mosley, P.N., and Armstrong, R.A., 2001. The western arm of the Lufilian Arc in NW Zambia and its potential for copper mineralization. J. African Earth Sci, v. 33, pp 503-528.

Jackson, M.P.A., Warin, O.N., Woad, G.M., and Hudec, M.R., 2003. Neoproterozoic salt tectonics during the Lufilian orogeny in the Katangan copperbelt, central Africa. Geol. Soc. Amer. Bull., v. 115, no. 3, pp 314-330.

Lefebvre, J.J., 1989. Depositional Environment of Cu-Co Mineralization in the Katangan Sediments of Southeast Shaba (Zaire). In: Boyle, R.W., Brown, A.C., Jefferson, C.W., Jowett, E.C., and Kirkham, R.V. (eds.), Sediment-hosted Stratiform Copper Deposits, Geol. Assoc. Canada Sp. Paper 36, p. 401-426.

Lefebvre, J.J. and Tshiauka, T., 1986. Le Groupe de Mines a Lubembe, Shaba, Zaire. Annales de la Societe geologique de Belgique, T. 109, pp. 557-571.

Miller, R.McG., 2002. Guide to the Excursion through the Damara Orogen. 11th Quadrennial IAGOD Symposium and Geocongress 2002; Geological Society of Nambia, Windhoek, Namibia. 106 pp.

North American Stratigraphic Code, 1983. AAPG Bull, v. 67, p 841-875.

Rainaud, C., Master, S., Armstrong, R.A., Phillips, D., and Robb, L.J., 2002a. Contributions to the Geology and Mineralization of the Central African Copperbelt: IV. Monazite U-Pb dating and Ar-Ar Thermochronology of Metamorphic Events during the Lufilian Orogeny. In: Robb, L. and Montjoie, (eds), 11th Quadrennial IAGOD Symposium and Geocongress 2002, Extended Abstract Volume (CD ROM).

Rainaud, C., Armstrong, R.A., Master, S., Robb, L.J., and Mumba, P.A.C.C., 2002b. Contributions to the Geology and Mineralization of the Central African Copperbelt: I. Nature and Geochronolgy of the Pre-Katangan Basement. In: Robb, L. and Montjoie, (eds), 11th Quadrennial IAGOD Symposium and Geocongress 2002, Extended Abstract Volume (CD ROM).

Wakefield, J. (1978); Samba; a deformed porphyry-type copper deposit in the basement of the Zambian copperbelt; Institution of Mining and Metallurgy, Transactions, Section B: Applied Earth Science. 87, May; pp 43-52. PB: Institution of Mining and Metallurgy.

Wendorff, Marek, 2000. Revision of the stratigraphical position of the "Roches Argilo-Talqueuse' (R.A.T.) in the Neoproterozoic Katangan Belt, south Congo. J. Afr. Earth Sci, v30, no.3, pp717-726.

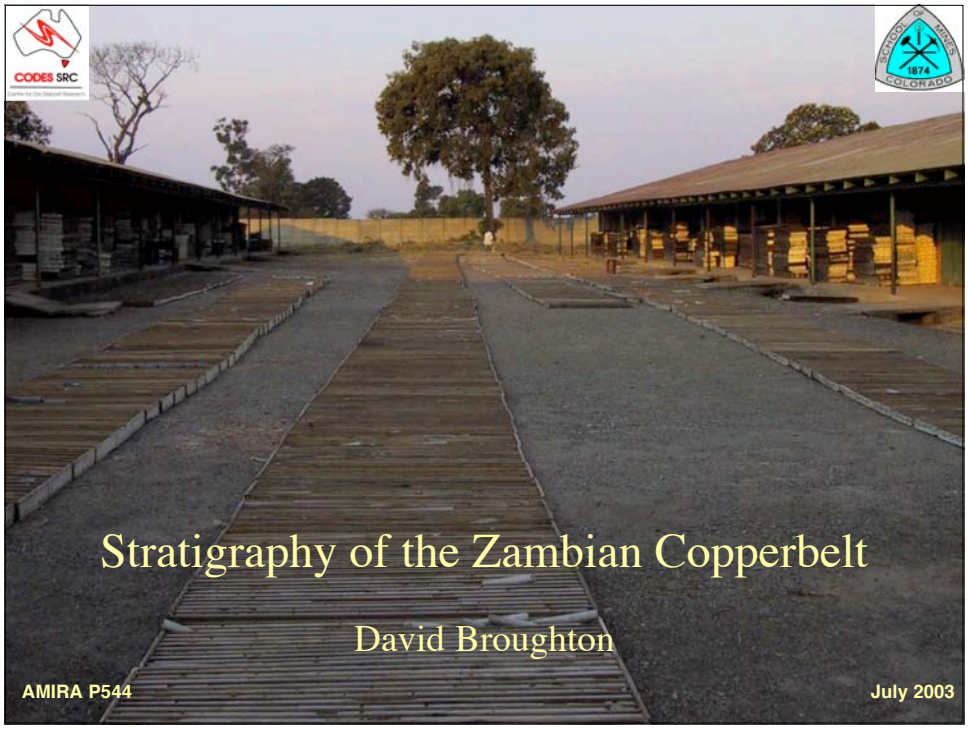

Acknowledgements

- P544 team
- Zambian geologists and companies
- Zambian Chamber of Mines
- SEG, GSA funding

Results

- Characterization of Lower Katangan basin in Zambian Copperbelt
- Correlation between Eastern and Western parts of the Copperbelt
- Initial correlation with southern DRC
- Salt-related breccias – source of brine
- Regional Alteration of entire Lower Katangan
- Consistent structural control of orebodies

Zambian Copperbelt

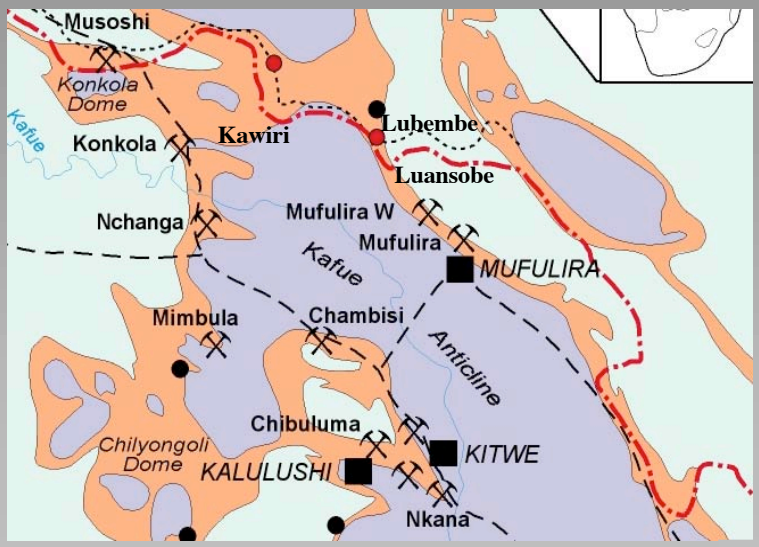

Lower Katangan Lithostratigraphy

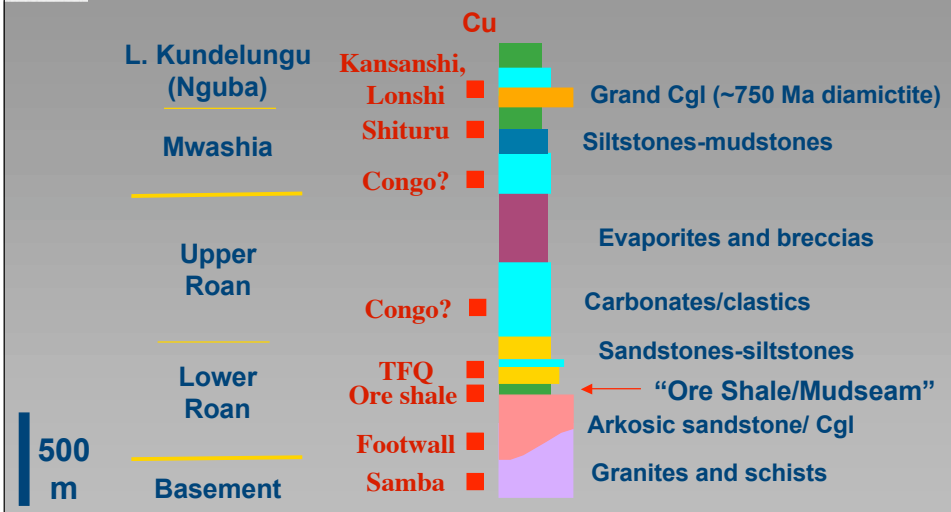

Beginning of Katangan sedimentation < 880 Ma

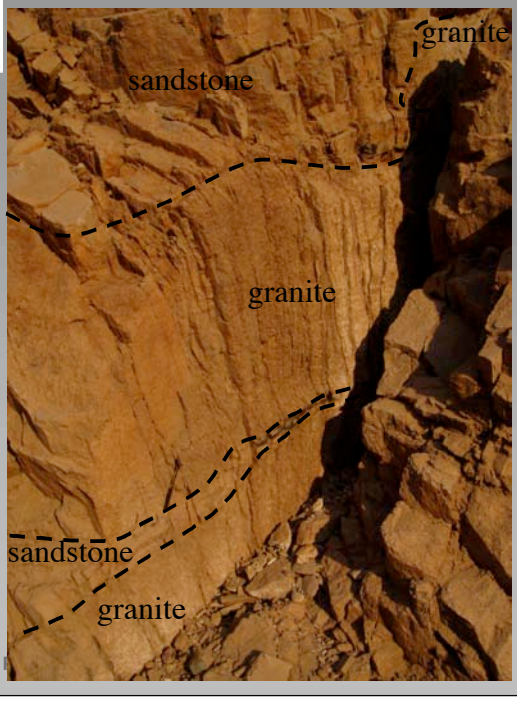

The Basement Problem: "exfoliation slabs" of Nchanga granite

Intrusive Contacts?

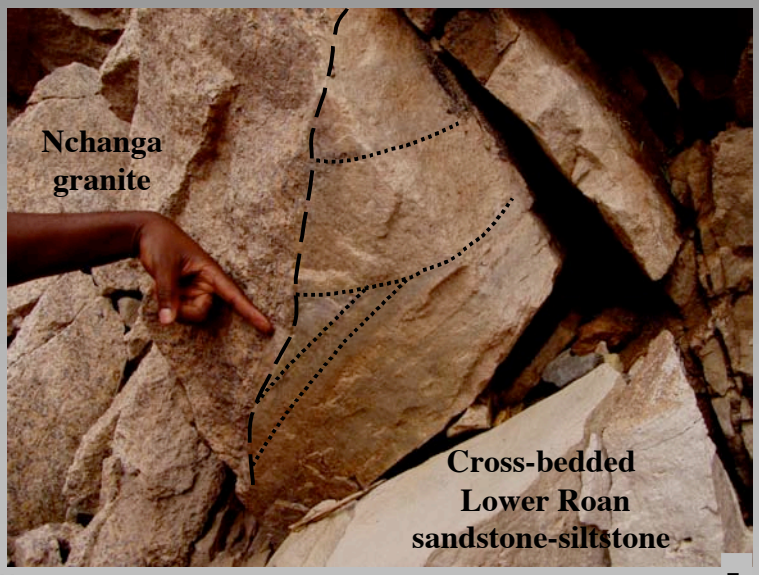

Kspar –(qtz) alteration in Roan and basement

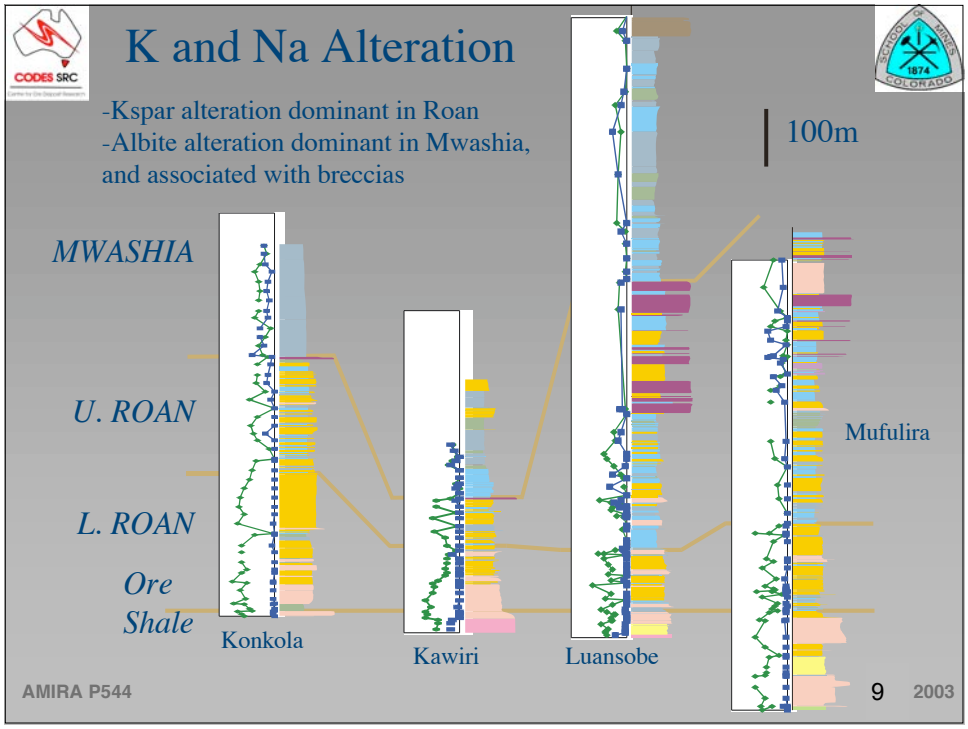
K and Na Alteration
-Kspar alteration dominant in Roan
-Albite alteration dominant in Mwashia, and associated with breccias
100m
MWASHIA
U. ROAN
L. ROAN
Ore Shale
Konkola
Kawiri
Luansobe
Mufulira
AMIRA P544
9
2003

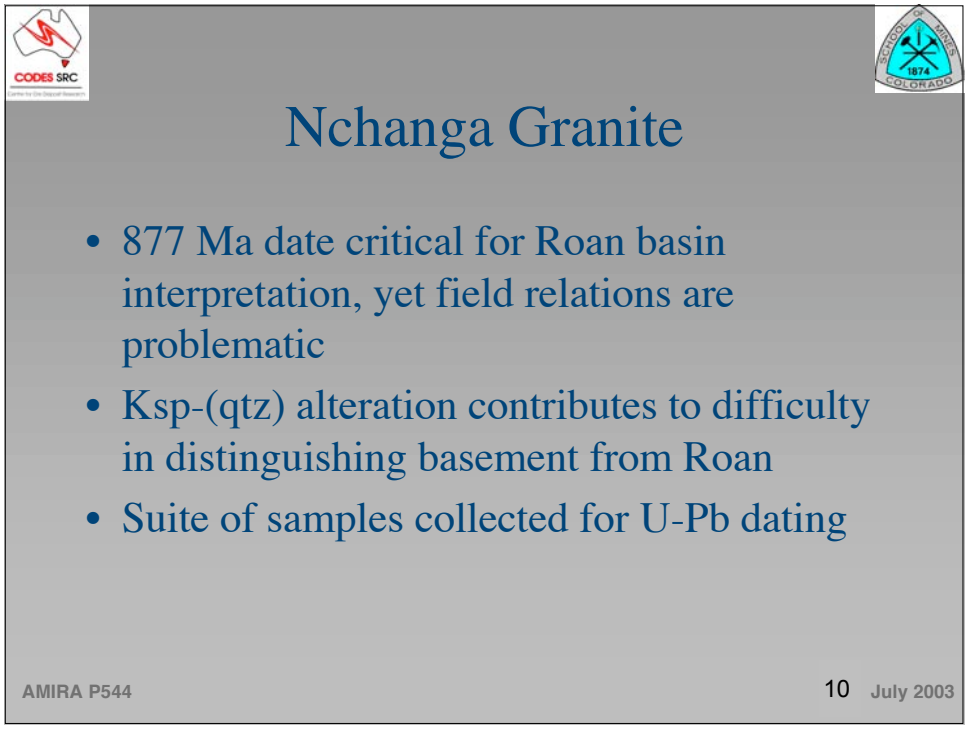
Nchanga Granite
• 877 Ma date critical for Roan basin interpretation, yet field relations are problematic
• Ksp-(qtz) alteration contributes to difficulty in distinguishing basement from Roan
• Suite of samples collected for U-Pb dating
AMIRA P544
10
July 2003

Ore Shale – Mudseam regional transgressive marker

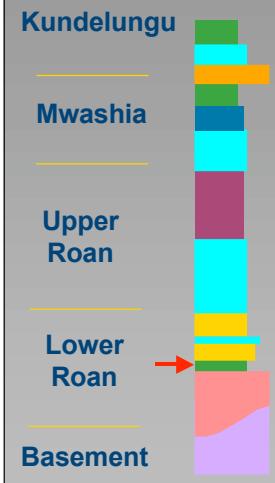

AMIRA P544 11 July 2003

Ore Shale Hangingwall: shallow marine fining upwards clastic-carbonate cycles

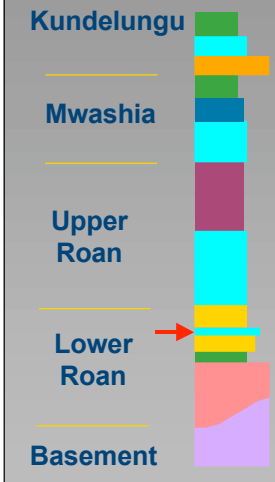

AMIRA P544 12 July 2003

Lower Roan "Shale-with-Grit": Extensive Dewatering Event

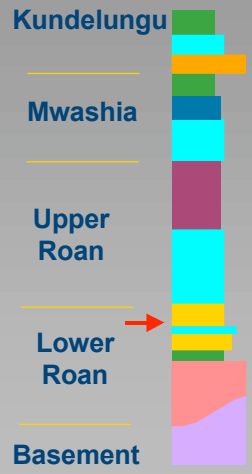

Upper Roan: algal dolomites

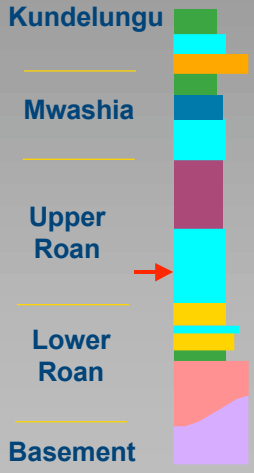

Upper Roan: evaporitic textures

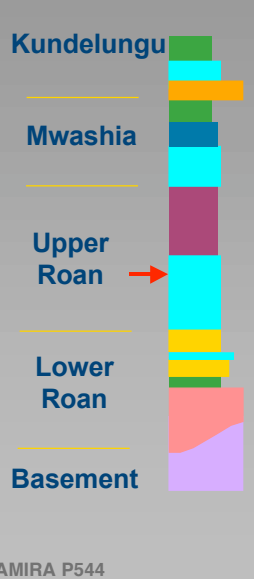

Enterolithic "chicken wire" texture, anhydrite-dolomite-pyrite

Upper Roan: polylithic breccias = evidence of former salt

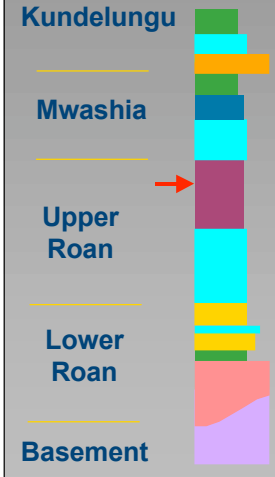

Breccias: crackle-brecciated and dolomite-talc-albite altered footwall

Breccias: form injections, dykes

Fungurume: breccias envelop and inject into blocks of Mines Group

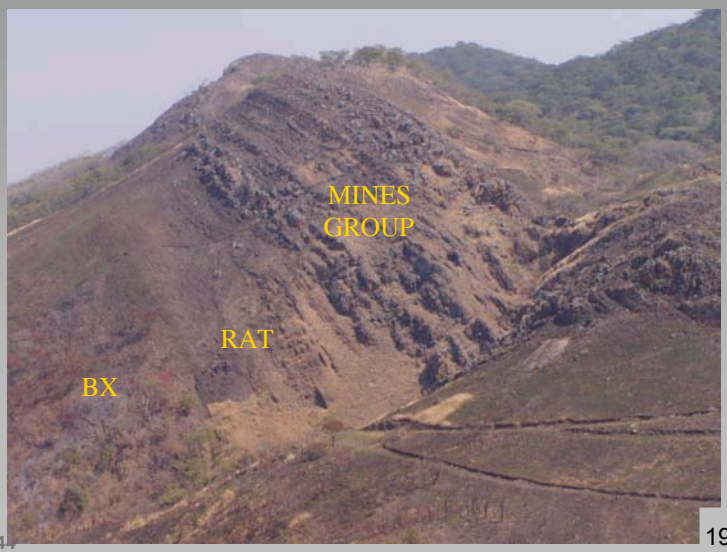

Polylithic Breccias: summary

- Form broadly stratigraphic unit within Upper Roan, but are both locally and regionally discordant (injections), occurring up into the Kundelungu in the DRC
- Contain intrabasinal clasts, commonly derived from adjacent stratigraphy, including gabbros and Mwashia volcanics (~750 Ma)
- Occupy thrust zones but show relatively little strain
- Contain mineralized blocks of Mines Group and are locally mineralized by late calcite-Cu-Co veins (Kamoya pit)

Lower Mwashia: massive and algal dolomites, with silicified nodules

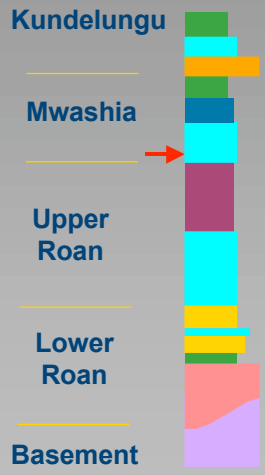

AMIRA P544 21 July 2003

Middle Mwashia: Interbedded Dolomites and Siltstones

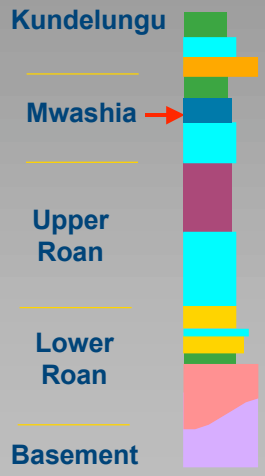

AMIRA P544 22 July 2003

Upper Mwashia: deeper water mudstones

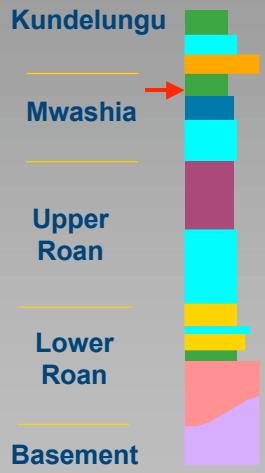

AMIRA P544 23 July 2003

Mafic igneous event, local Fe formations at ~740-760Ma

Mafic tuff in Lower Mwashia at Shituru

Gabbro intruding Upper Roan at Chambishi

AMIRA P544 24 July 2003

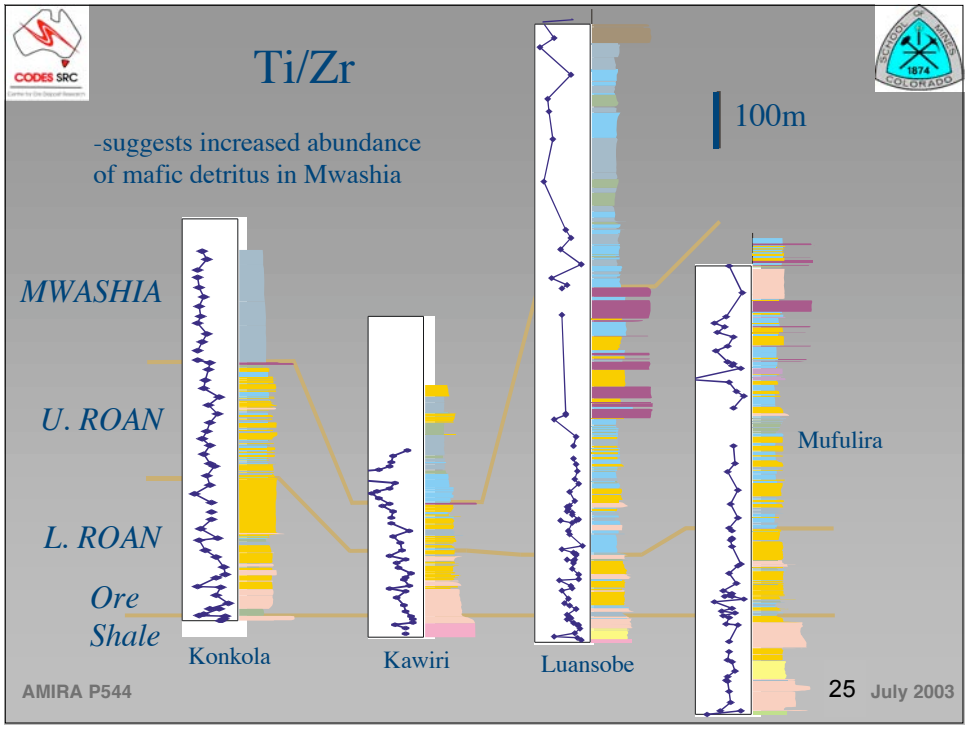
Ti/Zr
-suggests increased abundance
of mafic detritus in Mwashia
100m
MWASHIA
U. ROAN
L. ROAN
Ore
Shale
Konkola
Kawiri
Luansobe
Mufulira
AMIRA P544
25 July 2003

Lower Kundelungu (Nguba 1.1):
Grand Conglomerate
Kundelungu
Mwashia
Upper
Roan
Lower
Roan
Basement
AMIRA P544
26 July 2003

Nguba 1.2

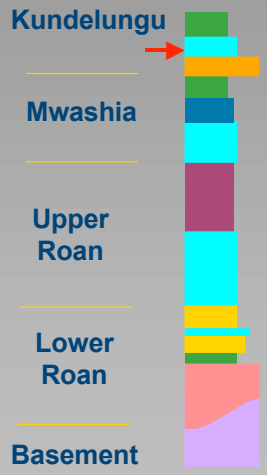

AMIRA P544 27 July 2003

Kakontwe Dolomite (Nguba 1.3)

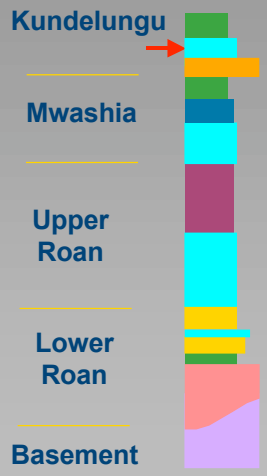

AMIRA P544 28 July 2003

Upper Kundelungu?: Foreland Molasse

Summary

Lower Roan: thin, compartmentalized rift fill, regional transgressive ore shale/mudseam, overlying mixed clastics – carbonates

Upper Roan: shallow marine clastics, carbonates, increasingly evaporitic, salt withdrawal breccias

Mwashia: carbonate to deeper water mudstones, similar cycle to Kundelungu (difficult to distinguish lithologies!)

Nguba-Kundelungu: 2 cycles of diamictite-carbonate –mudstone – glacial water recharge into basin?

Gabbros: intrude Lower Katangan, related to breccias in western Copperbelt – source of heat and brine convection

Upper Kundelungu: continental molasse, Lufilian foreland basin?

Zambian Copperbelt

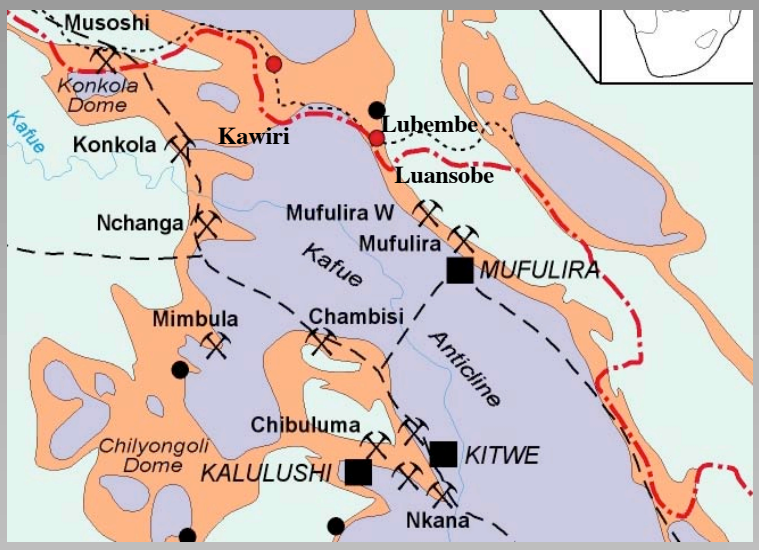

AMIRA P544 31 July 2003

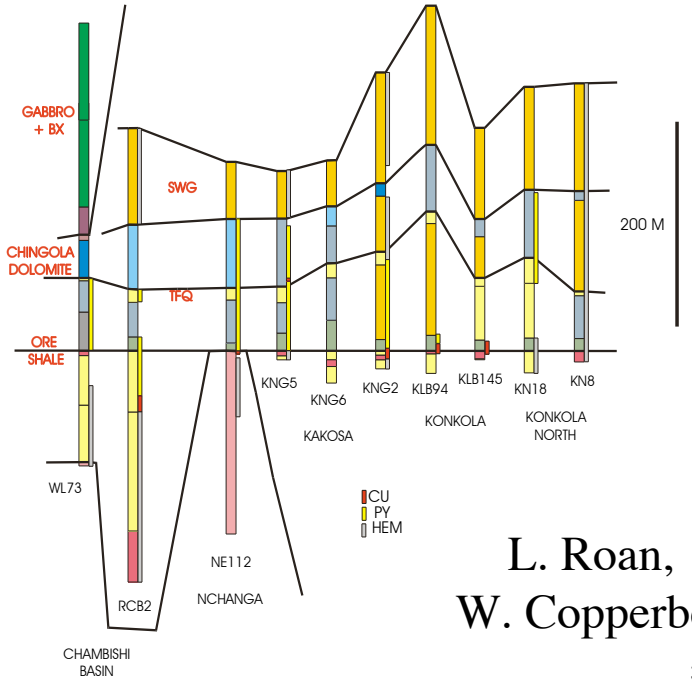

L. Roan, W. Copperbelt

32

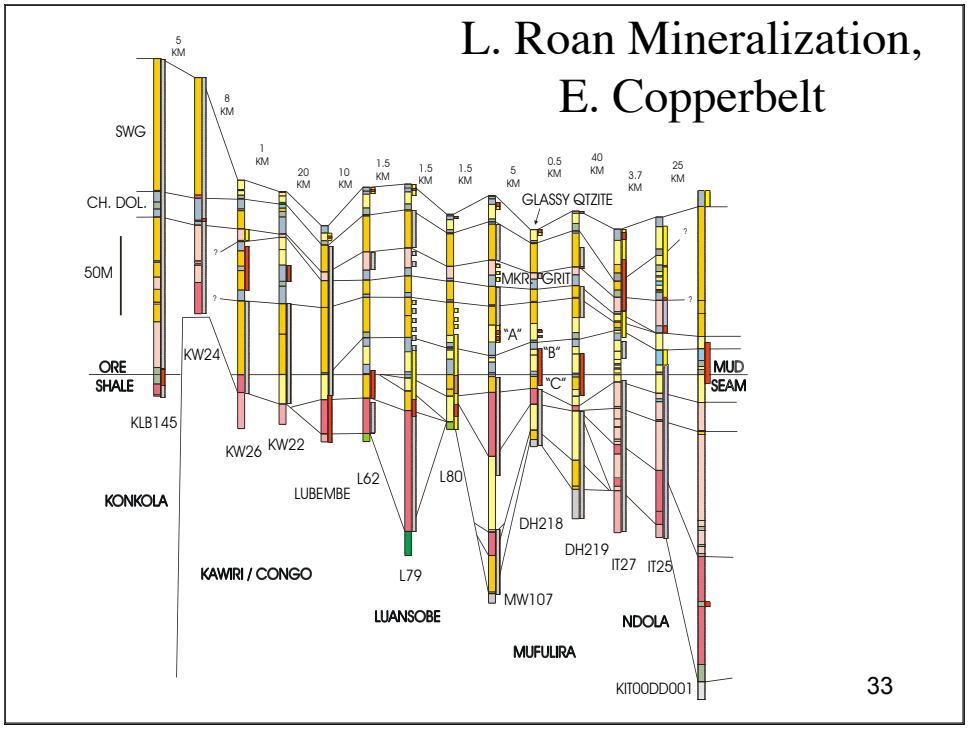
L. Roan Mineralization,
E. Copperbelt
SWG
CH. DOL.
50M
ORE SHALE
KLB145
KW24
KW26
KW22
LUBEMBE
L62
L80
L79
MW107
DH218
DH219
IT27
IT25
GLASSY QTZITE
MKR
GRIT
"A"
"B"
"C"
MUD SEAM
KONKOLA
KAWIRI / CONGO
LUANSOBE
MUFULIRA
NDOLA
KIT00DD001
33

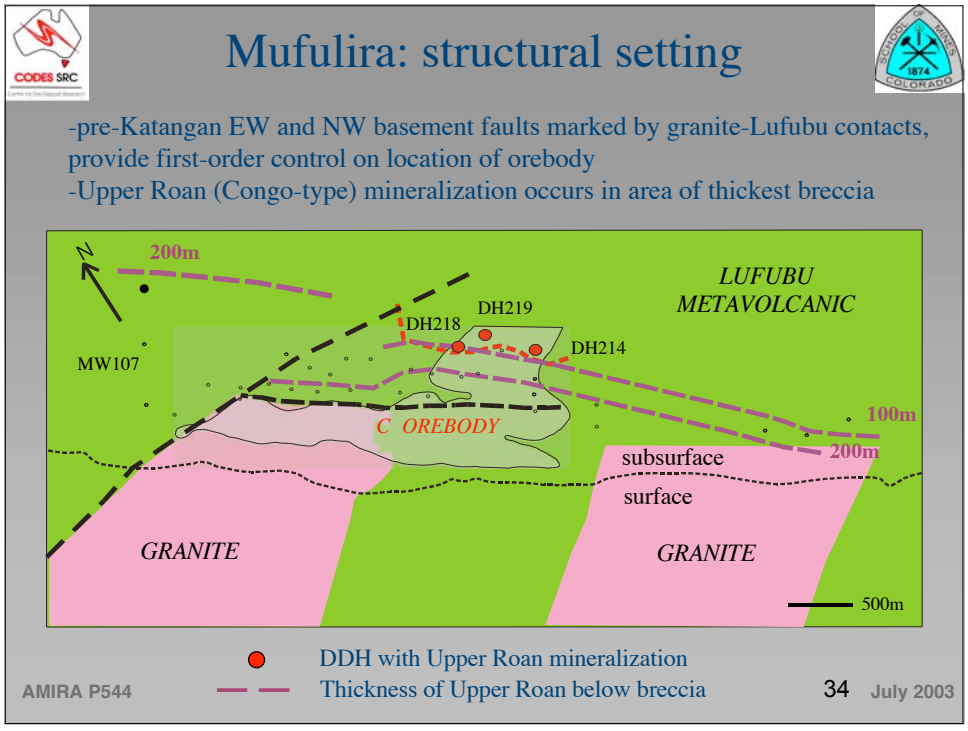
Mufulira: structural setting
-pre-Katangan EW and NW basement faults marked by granite-Lufubu contacts, provide first-order control on location of orebody
-Upper Roan (Congo-type) mineralization occurs in area of thickest breccia
200m
LUFUBU METAVOLCANIC
DH219
DH218
DH214
MW107
C OREBODY
100m
200m
subsurface
surface
GRANITE
GRANITE
500m
DDH with Upper Roan mineralization
Thickness of Upper Roan below breccia
AMIRA P544
34
July 2003

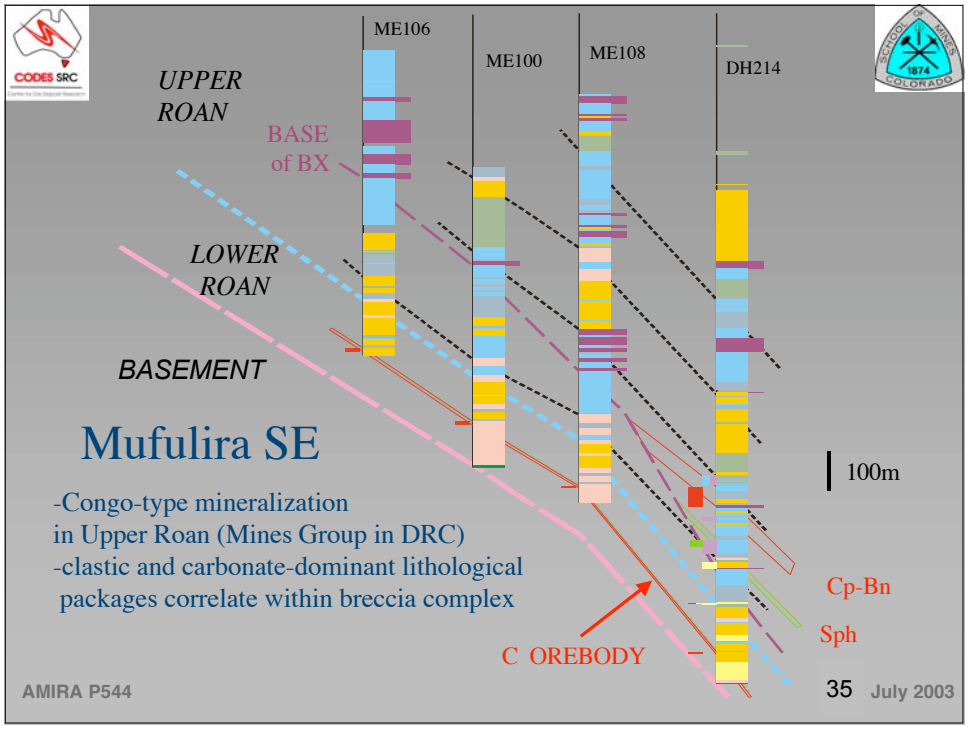
ME106
ME100
ME108
DH214
UPPER ROAN
BASE of BX
LOWER ROAN
BASEMENT
Mufulira SE
-Congo-type mineralization in Upper Roan (Mines Group in DRC)
-clastic and carbonate-dominant lithological packages correlate within breccia complex
100m
Cp-Bn
Sph
C OREBODY
AMIRA P544
35
July 2003

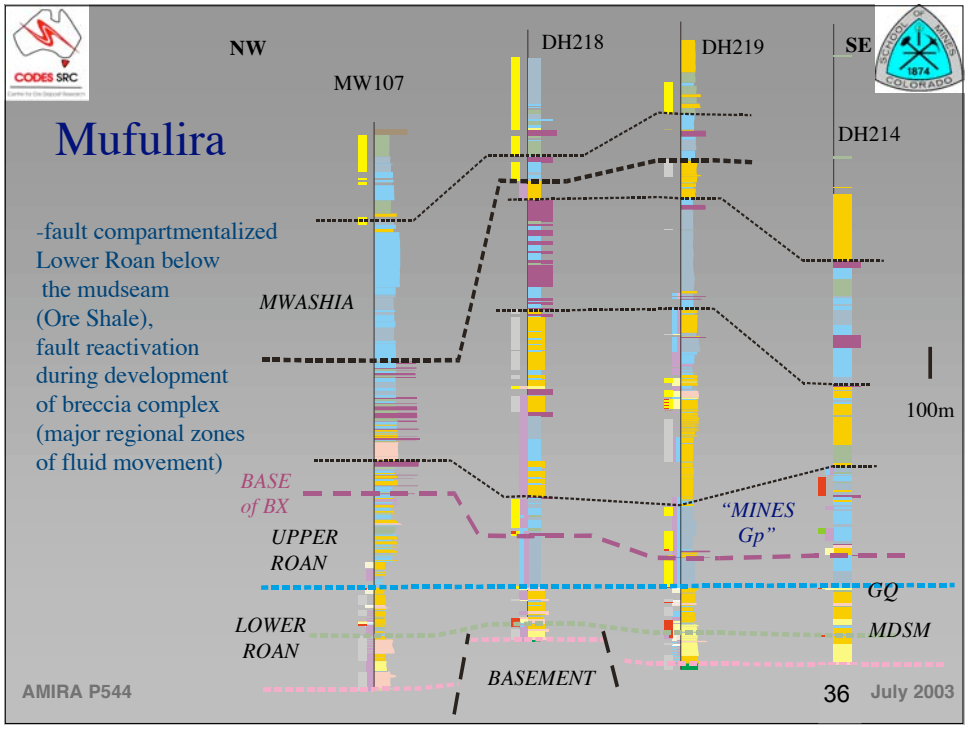
NW
MW107
DH218
DH219
SE
DH214
Mufulira
-fault compartmentalized Lower Roan below the mudseam (Ore Shale), fault reactivation during development of breccia complex (major regional zones of fluid movement)
MWASHIA
100m
BASE of BX
UPPER ROAN
"MINES Gp"
GQ
MDSM
LOWER ROAN
BASEMENT
AMIRA P544
36
July 2003

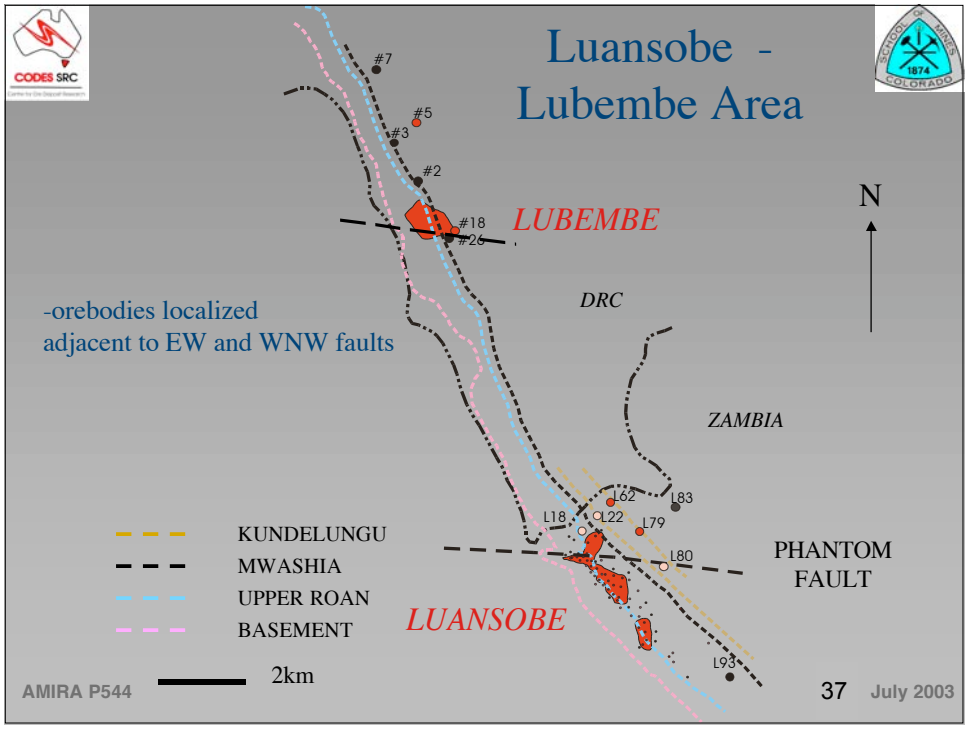
Luansobe - Lubembe Area
#7
#5
#3
#2
#18
#26
LUBEMBE
N
DRC
-orebodies localized
adjacent to EW and WNW faults
ZAMBIA
L62
L83
L18
L22
L79
L80
PHANTOM FAULT
KUNDELUNGU
MWASHIA
UPPER ROAN
BASEMENT
LUANSOBE
L93
2km
AMIRA P544
37
July 2003

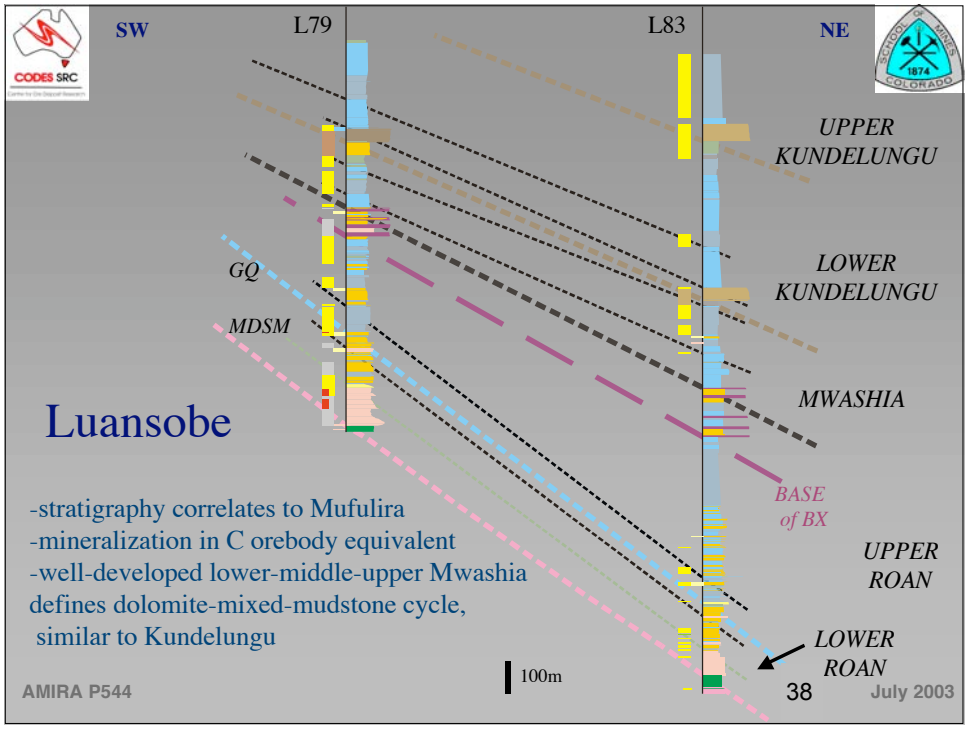
SW
L79
L83
NE
UPPER KUNDELUNGU
LOWER KUNDELUNGU
GQ
MDSM
MWASHIA
BASE of BX
UPPER ROAN
LOWER ROAN
Luansobe
-stratigraphy correlates to Mufulira
-mineralization in C orebody equivalent
-well-developed lower-middle-upper Mwashia defines dolomite-mixed-mudstone cycle, similar to Kundelungu
100m
AMIRA P544
38
July 2003

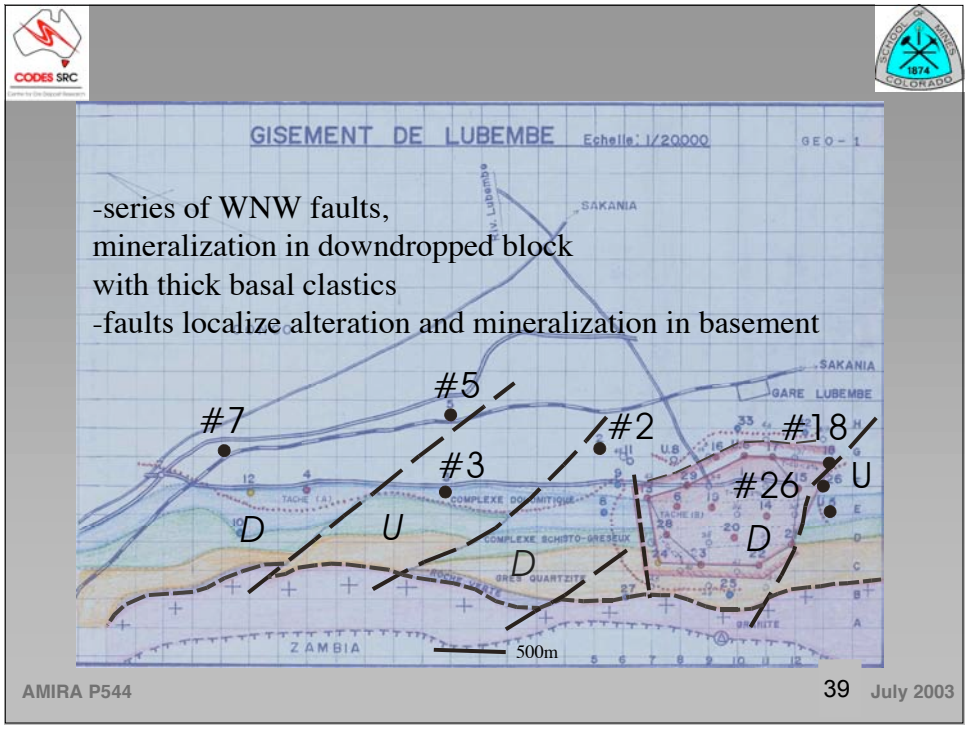
GISEMENT DE LUBEMBE
Echelle: 1/20000
-series of WNW faults,
mineralization in downdropped block
with thick basal clastics
-faults localize alteration and mineralization in basement
#7
#5
#3
#2
#18
#26
U
D
U
D
D
SAKANIA
GARE LUBEMBE
ZAMBIA
500m
AMIRA P544
39
July 2003

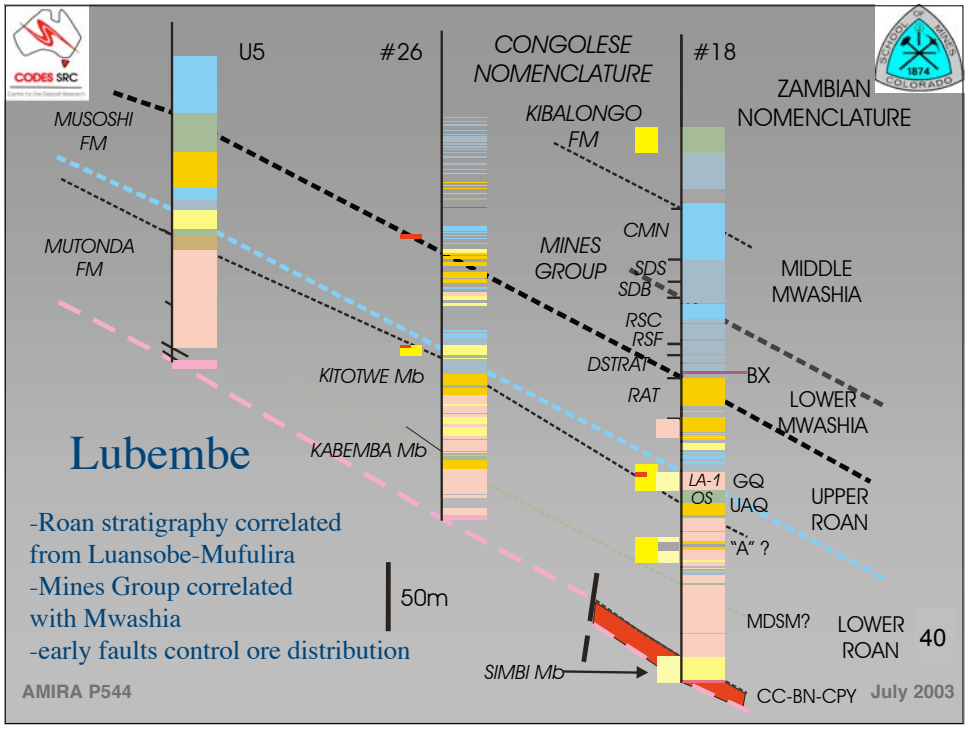
U5
#26
CONGOLESE NOMENCLATURE
#18
ZAMBIAN NOMENCLATURE
MUSOSHI FM
MUTONDA FM
KIBALONGO FM
MINES GROUP
CMN
SDS
SDB
RSC
RSF
DSTRAT
RAT
BX
MIDDLE MWASHIA
LOWER MWASHIA
UPPER ROAN
LOWER ROAN
KITOTWE Mb
KABEMBA Mb
LA-1
OS
GQ
UAQ
"A" ?
MDSM?
SIMBI Mb
CC-BN-CPY
Lubembe
-Roan stratigraphy correlated from Luansobe-Mufulira
-Mines Group correlated with Mwashia
-early faults control ore distribution
50m
AMIRA P544
40
July 2003

Lubembe

Shales Dolomitiques

RSC

RAT

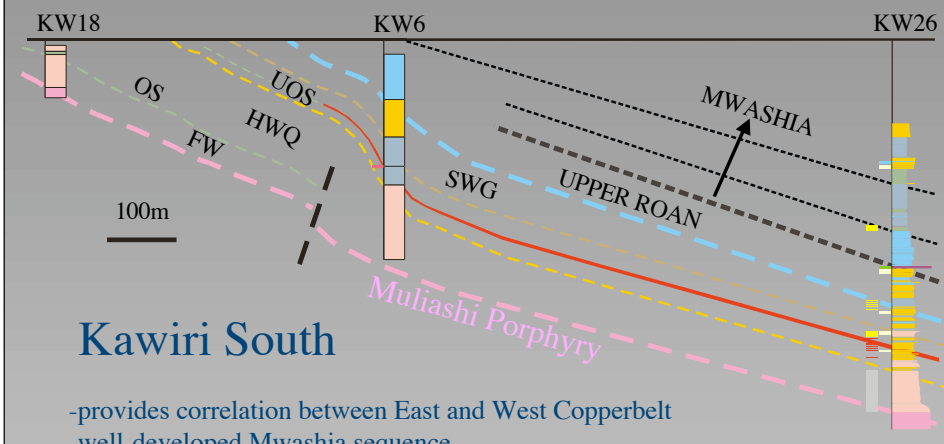

Kawiri South

-provides correlation between East and West Copperbelt
-well-developed Mwashia sequence
-sandy facies Ore Shale recognizable in shallow holes and trenches, cannot distinguish in deeper holes across Kawiri-Lubengele Fault
-persistent subore mineralization in Upper Ore Shale

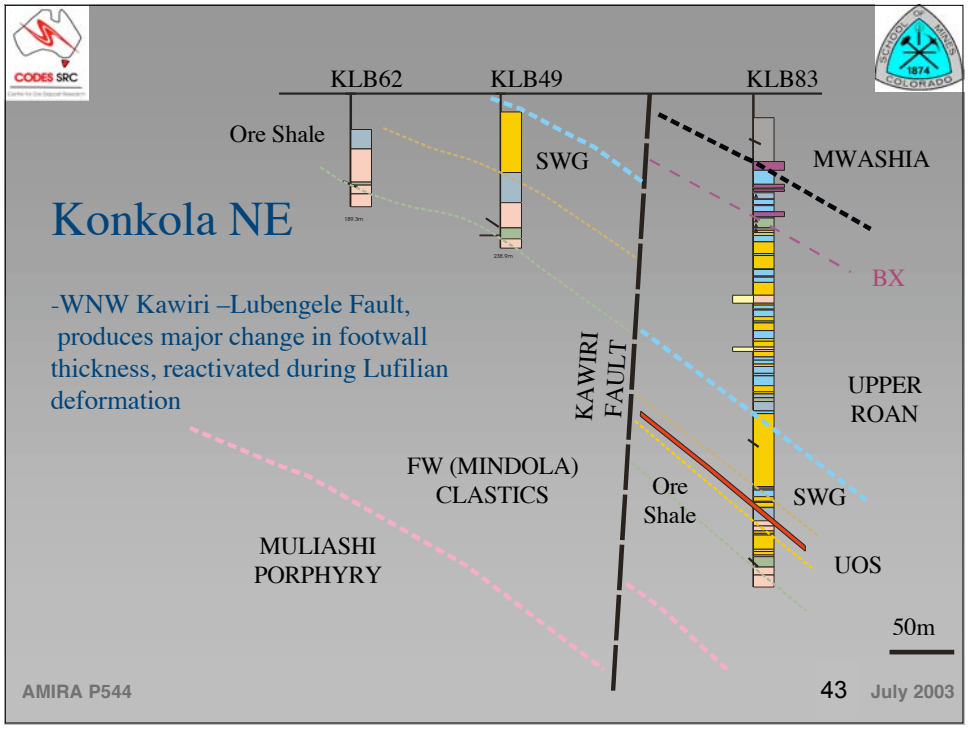
KLB62
KLB49
KLB83
Ore Shale
SWG
MWASHIA
Konkola NE
-WNW Kawiri –Lubengele Fault, produces major change in footwall thickness, reactivated during Lufilian deformation
BX
KAWIRI FAULT
UPPER ROAN
FW (MINDOLA) CLASTICS
Ore Shale
SWG
MULIASHI PORPHYRY
UOS
50m
AMIRA P544
43
July 2003

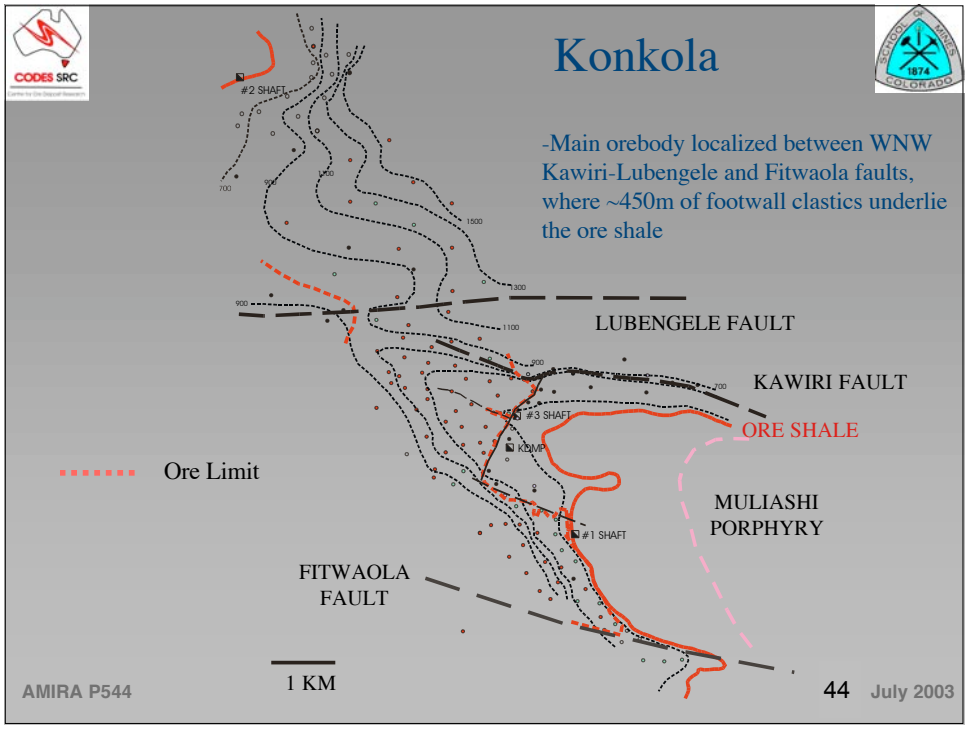
Konkola
-Main orebody localized between WNW Kawiri-Lubengele and Fitwaola faults, where ~450m of footwall clastics underlie the ore shale
#2 SHAFT
LUBENGELE FAULT
KAWIRI FAULT
#3 SHAFT
ORE SHALE
Ore Limit
MULIASHI PORPHYRY
#1 SHAFT
FITWAOLA FAULT
1 KM
AMIRA P544
44
July 2003

Conclusions

-Maximum thickness of "rift-phase" Lower Roan is about 1 kilometre – Copperbelt is probably on the basin margin

-Ore Shale – Mudseam represents regional relative sea level rise, fundamental change in basin architecture

-Regionally developed and locally discordant breccias record former presence of salt in Roan

-Congolese Mines Group appears to correlate with Upper Roan/Lower-Middle Mwashia

-Mwashia sedimentation and igneous activity marks new phase of basin development, but locally shows basement source

-Entire Lower Katangan section is altered, and orebodies occur throughout the section

-L.Roan orebodies are localized along faults active during Roan sedimentation, and reactivated during Lufilian deformation

Chambishi basin studies; Chambishi SE Prospect

Stuart Bull & David Selley
Centre for Ore Deposit Research, University of Tasmania

Summary

The Chambishi SE prospect (CSE) consists of two ore zones separated by a well-defined "barren gap" where non-mineralised carbonate has been interpreted by previous researches as an ore shale-equivalent microbial bioherm. Footwall architecture at CSE is the same as that recorded from the previous deposits. Rapid thickness and facies changes reflect half graben style sedimentation controlled by NNW-trending growth faults. Conglomerates are sourced locally from growth fault scarps, however most of the footwall succession comprises well-sorted, laminated and cross-bedded subarkose. Contemporary rift models indicate these deposits accumulated in axial braided fluvial systems.

The CSE provides the first opportunity to study facies patterns at the level of the ore shale and into the hanging wall. The hangingwall architecture is effectively layercake, with the Ore Shale overlain successively by; the Rokana evaporates a marginal marine sabkha succession recording a period of tectonic quiescence; the Nchanga quartzite and upper ore shale that represents a subsequent period of activity on the controlling growth structures; an upper evaporitic succession similar in character to the Rokana Evaporites; the Chambishsi dolomite, a clean anhydritic marble that has a coherent internal stratigraphy across the entire deposit area, and is interpreted to represent a microbial bioherm that records another period of tectonic quiescence; and ultimately the Shale With Grit characteristic of the upper lower Roan. In the absence of primary evaporitic (e.g., playa lake) facies associations in the footwall sandstones, the evaporitic cements (now recrystallised anhydrite and carbonate) common at this level are interpreted to have originated at the level of the Rokana Evaporites, which is the first major brine/evaporite 'factory' in the CB.

The layercake facies architecture of the hangingwall allows confident interpretation of facies patterns at the level of the ore shale. Results indicate that the NW edge of the NW ore shoot reflects an along strike pinchout of the ore shale and associated mineralisation. The distinctive Copperbelt Orebody Member is still recognisable, however the reduced siltstone facies (ore shale) is replaced by biotitic sandstone that occurs within a coarse-grained apron of evaporitic sandstone and conglomerate. This succession is interpreted as a hangingwall fan emanating from a lateral sediment entry-point into the half graben (e.g., a transfer zone). Such areas were subject to greater clastic sediment supply and were topographically higher and than areas of the graben floor where ore shale accumulated in relatively starved conditions.

Across strike pinchouts of the ore shale also occur in this area, but are best manifested in the central barren gap. As recorded by previous workers, sub-wave base siltstones (Ore Shale) are abruptly replaced by correlative clean anhydritic marbles. These resemble the microbial Chambishi dolomite, and this origin is confirmed by C and O isotopic data which clearly show these units preserve a marine C signature.

Introduction

This is the final in a series of detailed reports focussing on three Chambishi Basin (CB) deposits (Slide 2). The results from the Chibuluma West and Mwambashi B studies concentrated on the relationship between mineralisation and the facies architecture of the footwall (Mindola Clastics Formation), and the results have been reported at earlier meetings. When combined with Mawson Croaker's PhD study of Nkana system, these provide the basis for a detailed model for the development and mineralisation of the lower Roan (Selley et al., this volume, report 4).

The Chambishi SE prospect (CSE; Slide 3) consists of two main ore zones located on the NW and SE edges of a well-defined "barren gap" of non-mineralised carbonate. This was interpreted by previous researches as an ore shale-equivalent bioherm (Annels, 1974, 1989) on the basis of the presence of oncolite stromatolites, however, the location of these structures was not cited and they were not described in any detail. Mineralisation is Ore Shale hosted and occurs at depths of > 500 m below surface across most of the prospect. As a result most of the drill holes were collared in upper Roan and most were also continued to basement, giving excellent coverage of the footwall and hangingwall stratigraphy.

The current study of CSE involved logging three fences of holes, north, central and south (Slide 3) with three main aims:

- The current study has demonstrated the significance of the origin and geochemistry of the lower Roan carbonates for the genesis of the Cu mineralisation (Large et al., this volume, report 11). The southern fence was therefore designed to re-evaluate the origin of the "barren gap" carbonates.
- CSE also provides the opportunity to examine the nature of the margin to one of these CB mineralised system, at the NW end of the NW ore zone, and the northern fence was designed to investigate this area.
- The central fence was designed to study facies patterns from the footwall through the ore shale and into the hanging wall through the main ore zone at the NW margin of the barren gap. This facies base work was carried out in parallel to geochemical studies looking at trends from the main ore to zone to distal holes in fringe positions (McGoldrick, this volume, report 9).

Footwall Architecture

The facies architecture of the lower Roan footwall at CSE is the same as that recorded in the previous deposit studies. Rapid thickness and facies changes (e.g., Slide 7; NN45 to NN48) reflect half graben style sedimentation controlled by NNW-trending growth faults. Sedimentation comprises two broad facies associations (Slide 9); Conglomerates record cross-strike sedimentation sourced locally from growth fault scarps (Slide 8); however most of the footwall succession comprises well-sorted, laminated and cross-bedded subarkose. Contemporary rift models indicate these deposits record braided fluvial systems flowing axially within the half graben (Slide 8).

No primary evaporitic (e.g., playa lake) facies associations were intersected in the footwall sandstones in any of the CB deposits studied, indicating a marginal position with respect to the rift axis (Slide 11; alluvial fan/sandflat/dry mudflat zone). However, evaporitic components are widespread at CSE in the form of anhydrite and carbonate, which although they are now recrystallised (Slide 10; bottom two photomicrographs), we interpret to have originated as evaporitic cement components. Biotite is also abundant in the matrix of the sandstones, some of which represents a protolith with a muddy matrix, but much of which is clearly patchy alteration (Slide 10; top photo) of previously well-sorted deposits.

Hangingwall Architecture

The hangingwall architecture at CSE is effectively layercake (Slide 12), and the stratigraphic scheme erected by Clemmy (1976) in his work at Mindola a few km to the south works here with only minor modification. In summary, the ore shale is overlain successively by;

- The Rokana evaporates (Slide 13) comprising a cyclically interbedded succession of muddy

(biotitic) sandstone with abundant carbonate and anhydrite cements/vughs/nodules, thin microbially laminated carbonates and minor clean sandstone (quartzite) and reduced siltstone beds. Some of the anhydrite nodules are clearly of primary evaporitic origin, and given the amount of sulfate present and the associated facies, we interpret this succession to represent a marginal marine sabkha recording a period of relative tectonic quiescence. Significantly, it represents the first major brine/evaporite 'factory' in the CB. In the absence of primary evaporitic (e.g., playa lake) facies associations in the footwall sandstones, the locally abundant evaporitic cements in these units are interpreted to have originated at the level of the Rokana Evaporites. This most likely occurred during early diagenesis, when dense evaporitic brines could sink through the unconsolidated sediments and displace the less dense pore fluids (i.e., brine reflux; Slide 15). In this model, the presence of evaporitic components in the footwall sandstones was not related to primary evaporites, but was controlled by factors such as the distribution of evaporitic facies in the hangingwall and access points where descending dense brines could breach the Ore Shale. It therefore explains why some CB basin lack sulfate (e.g. Mwambashi B) while others with basically identical stratigraphy have it in abundance (e.g., CSE);

- The Rokana Evaporites are abruptly overlain by the Nchanga or Glassy quartzite (Slide 16, 17), comprising several to >10 m of thick, clean, massive to stratified and cross-bedded, coarse to very coarse-grained arkose. It is similar to some of the footwall facies and represents the resumption of basement erosion and fluvial braidplain sedimentation. It is always overlain by intervals of non-evaporitic siltstones similar to the Ore Shale indicating increased rate of generation of accommodation space at this time. This combination of basement uplift and increased accommodation space indicates that this cycle is of tectono-sedimentary origin and represents a resumption of activity on the controlling growth faults.
- The intervals of upper ore shale are interbedded with/overlain by progressively more evaporitic sediments as the accommodation space is used up (Slide 18), and the facies association is ultimately similar in character to the Rokana Evaporites. It is likewise interpreted as a marine sabkha succession indicating the end of the tectonically active period.
- The Chambishsi or Cherty Dolomite (Slide 19) comprises a <10 to >15 m thick clean anhydritic marble that abruptly overlies the upper evaporitic succession. It preserves good microbial textures (Slide 20) and has a coherent internal stratigraphy across the entire prospect that includes a > 1 m thick mudstone marker within a few metres of the upper contact (Slide 19; left end of pale CD, younging towards viewer). It is therefore interpreted as a biohermal reef system that records complete tectonic quiescence in this part of the Chambishi Basin.
- The Chambishi Dolomite is abruptly overlain by the 'Shale With Grit' unit characteristic of the upper lower Roan (Slide 19; left end of core overlying pale CD).

Ore Shale

The layercake facies architecture of the hangingwall allows confident interpretation of facies patterns at the level of the Ore Shale. 'Normal' Ore Shale intersections in CSE, i.e., those that occur within half graben depocentres, comprise 10–20 m of carbonaceous and dolomitic siltstone (Slide 21). This caps a tens-of-metres-thick tectono-stratigraphic cycle termed the Copperbelt Orebody Member by Clemmy (1976). It comprises a basal conglomerate (Slide 19) that may be immediately overlain by Ore Shale, but is more commonly separated from it by an interval of poorly-sorted biotitic, or less commonly clean well-sorted sandstone. The Ore Shale itself also has a crude internal stratigraphy. It comprises carbonate-rich sand/siltstone at the base, fining up to more carbonaceous siltstone that is the focus of the ore grade mineralisation. This is overlain by barren or pyrite mineralised siltstone with distinctive sulfate nodules often altered to carbonate and rimmed by pyrite (Annels, 1974).

CSE provides the opportunity to examine pinch outs of this typical ore shale intersection both along and

across strike. The NW edge of the NW ore shoot preserves an along strike pinch out of the ore shale and associated mineralisation between NN60 and NN69 (Slide 22). The distinctive Copperbelt Orebody Member with its basal conglomerate is still recognisable in NN69, however the reduced Ore Shale siltstone facies is replaced by biotitic sandstone that occurs within a coarse-grained apron of evaporitic sandstone and conglomerate. This succession is interpreted as a hangingwall transfer zone fan (Slide 23) emanating from a lateral sediment entry-point into the half graben (e.g., a transfer zone). Such areas were subject to greater clastic sediment supply and were topographically higher and than areas of the graben floor where ore shale accumulated in relatively starved conditions.

Across strike pinch outs of the ore shale also occur in the northern fence, but are best manifested in the southern fence from the central barren gap area (Slide 24). As reported by previous workers, 'normal' sub-wave-base Ore Shale siltstones present in NX4 and NN15 are abruptly replaced to the NE by clean anhydritic marbles. Correlation of the hangingwall stratigraphy confirms these are direct lateral correlatives of the Ore Shale. They resemble the microbial Chambishi Dolomite (Slide 25) although unequivocal microbial fabrics are not preserved this case. However, a microbial origin is confirmed by C and O isotopic data (Slides 27, 28) which clearly show these units preserve a marine C signature, while the laterally equivalent mineralised ore shale shows the excursion to typically light C values identified in the P544 research program (Large et al., this volume, report 11). In the context of the overall rift architecture that controlled deposition of the lower Roan (Slide 29), these zones represent remnant intra-basinal highs that were less affected by the subsidence event that controlled the abrupt transgression recorded by the Ore Shale. In the case of CSE at least, this area is coincident with a zone where extension was transferred between two active rift segments (Selley et al., this volume, report 4).

Conclusions

The central 'barren gap' that separates the two ore zones at Chambishi SE formed as a microbial bioherm. It is situated on an area of elevated basement that represents a transfer zone between normal fault arrays that controlled the footwall clastics.

The along strike ore shale pinch out of the NW ore zone is caused by a hangingwall fan that corresponds to an area sediment input point across the controlling normal faults, usually also a transfer zone. It elevated the floor of the graben above wave base.

The generation of accommodation space in the Chambishi Basin slows markedly post ore shale, although one distinct tectono-stratigraphic pulse is recorded by the Nchanga Quartzite – upper Ore Shale. The latter hosts minor mineralisation around the Kafue Anticline.

Evaporitic facies in the hangingwall (Rokana Evaporites) generated brines that sank though the basin fill (brine reflux) and precipitated evaporitic cements in the footwall aquifers.

References

Annels, A. E. 1974. Some aspects of the stratiform ore deposits of the Zambian Copperbelt and their genetic significance. Centenaire de la Société de Belgique Gisements Stratiformes et Provinces Cupriferes, Liege. p. 235-254.

Annels, A. E. 1989. Ore genesis in the Zambian Copperbelt, with particular reference to the northern sector of the Chambishi Basin. In Boyle et al., eds, Sediment-hosted stratiform copper deposits: Geol. Assoc. Canada Spec. Pap. 36, p. 427-452.

Clemmy, H. 1976. aspects of stratigraphy, sedimentology and ore genesis on the Zambian Copperbelt. Unupublished PhD thesis, University of Leeds, 357 pp.

1

Chambishi Basin Studies; Chambishi Southeast Prospect

Stuart Bull and David Selley

Introduction

2

Final of a series of deposit case studies to constrain relationship between basin architecture and mineralisation in the CB

Why Chambishi Basin?

- Widespread high density drilling ~ 3d control
- Diversity of deposits and ore hosts
- Pronounced thickness and facies variation in the LR

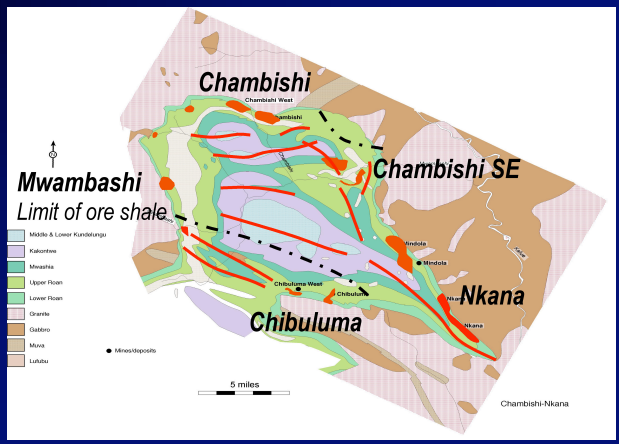

Introduction

3

Why Chambishi SE?

- Primarily ore shale-hosted system
- Large deposit with well-defined edge associated with ore shale pinch out to N
- Well-defined central barren gap coincident with a change from "normal" to dolomitic ("biohermal") ore shale

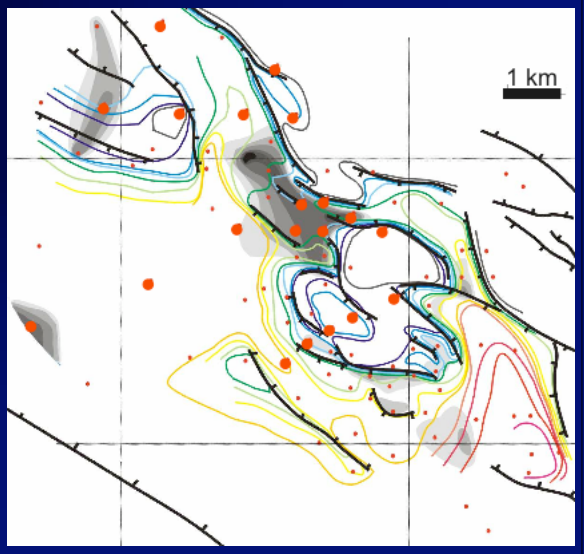

AMIRA /ARC ProjectP544 *Final Sponsors Meeting* *July 2003*

Introduction

4

Footwall architecture has been reported previously from Chibuluma & Mwambashi

Main BA points I am going to cover today are

- Facies variations at the level of the ore shale "barren gaps"
- Facies characteristics and architecture of the hangingwall succession

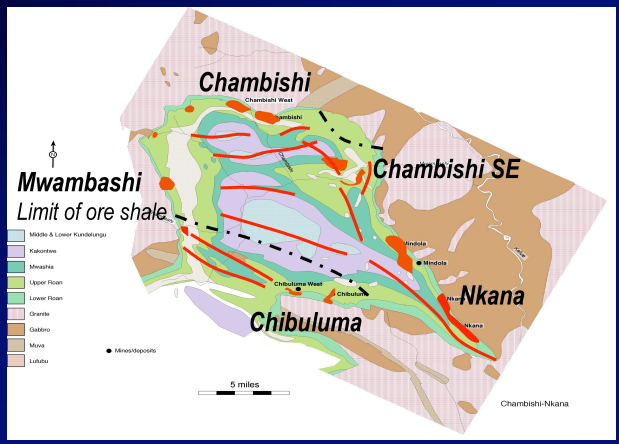

AMIRA /ARC ProjectP544 *Final Sponsors Meeting* *July 2003*

Chambishi SE

5

Preliminary interpretation indicates:

- Basin evolution during "footwall deposition" was controlled by WNW to NNW trending growth faults
- Broadly SW dipping ramp with interference of NNW trending troughs (significant fold modification)
- Broad barren gap coincident with intra-basinal high
- Control on high grade zones similar to those on footwall orebodies - coincident with fault step-overs and footwall pinchouts

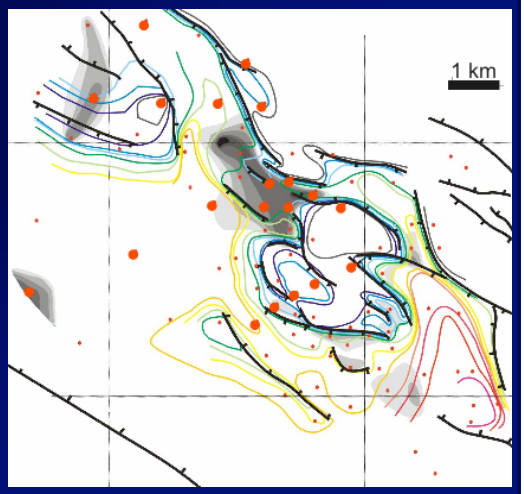

AMIRA /ARC ProjectP544 *Final Sponsors Meeting* *July 2003*

Chambishi SE

6

Latest study involved logging three drill fences to test our basin architecture model

More specifically:

- N fence examines the fringe of the system in the form of along and cross-strike pinch outs of the ore and ore shale
- Central fence examines the guts of one of the two main ore zones
- S fence examines the central barren gap

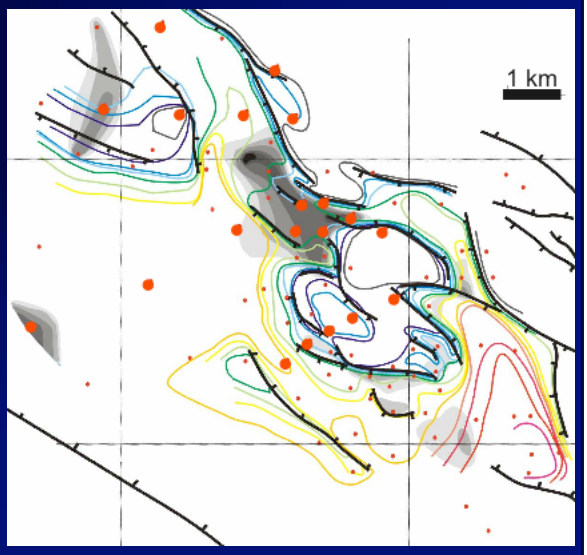

AMIRA /ARC ProjectP544 *Final Sponsors Meeting* *July 2003*

Chambishi SE; basement

7

Study made possible because most holes went to basement

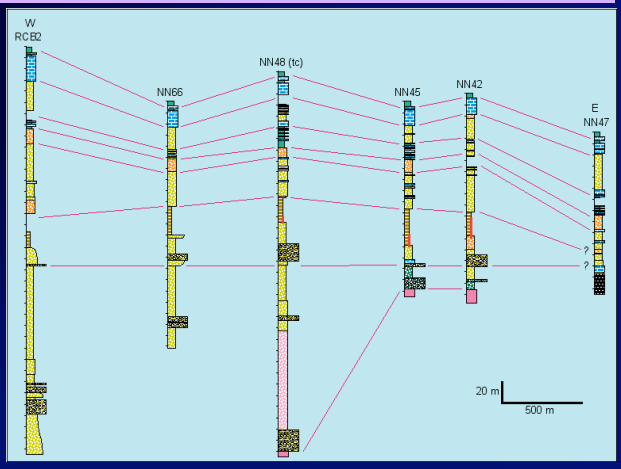

AMIRA /ARC ProjectP544 *Final Sponsors Meeting* *July 2003*

Chambishi SE; footwall

8

Abrupt thickness and facies variations controlled by NW-trending SW-dipping growth faults

Two broad sedimentary facies associations

Conglomerates represent across strike debris flow and associated high-energy tractional sedimentation sourced from proximal controlling growth faults

Thick footwall intersections dominated by stratified and cross-bedded hematitic sub-arkose - represent axial braided fluvial systems draining the half grabens

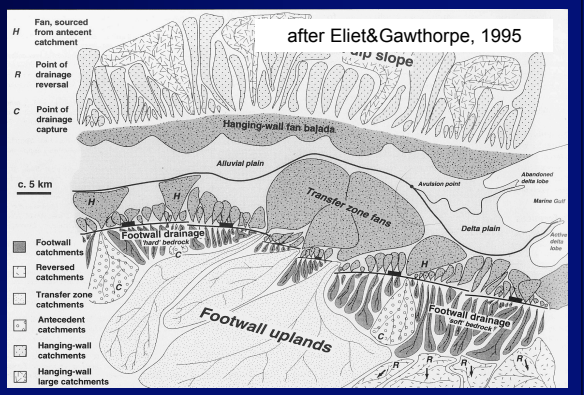

AMIRA /ARC ProjectP544 *Final Sponsors Meeting* *July 2003*

Chambishi SE; footwall

9

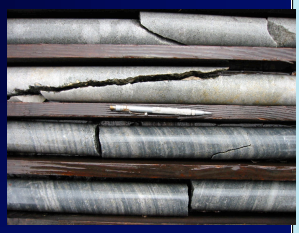

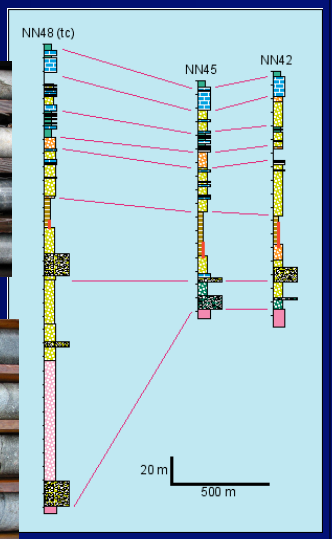

AMIRA /ARC ProjectP544 *Final Sponsors Meeting* *July 2003*

10

Patchy biotite distribution partly muddy protolith & partly alteration

Locally abundant evaporitic components in the sandstones (now recrystallised) we interpret as original cements

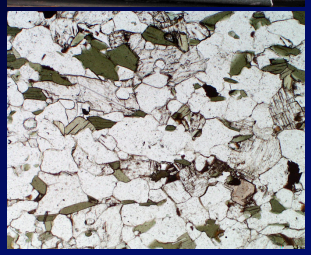

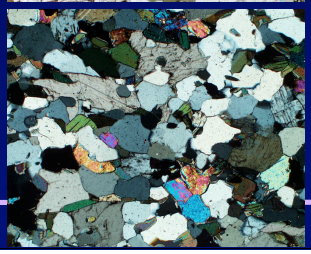

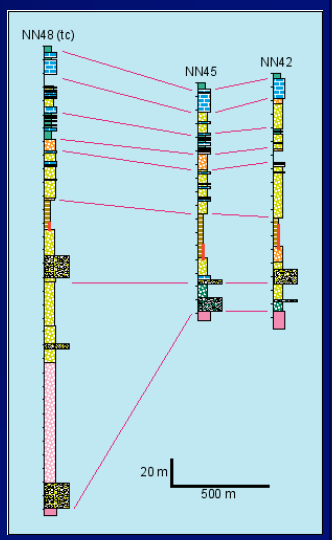

AMIRA /ARC ProjectP544 *July 2003*

Chambishi SE; footwall

11

No primary evaporitic-carbonate (playa lake) facies preserved in the CB

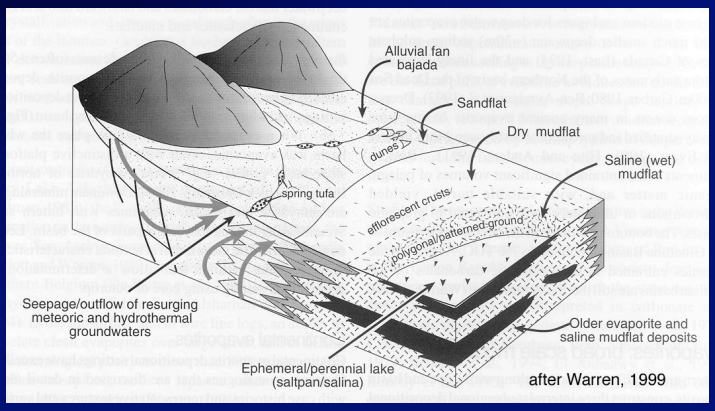

AMIRA /ARC ProjectP544 *Final Sponsors Meeting* *July 2003*

Chambishi SE; hangingwall

12

Effectively layercake stratigraphy that thickens gradually SW into basin centre

- Shale with grit
- Chambishi dolomite
- Upper evaporites
- Upper ore shale
- Nchanga quartzite
- Rokana evaporites

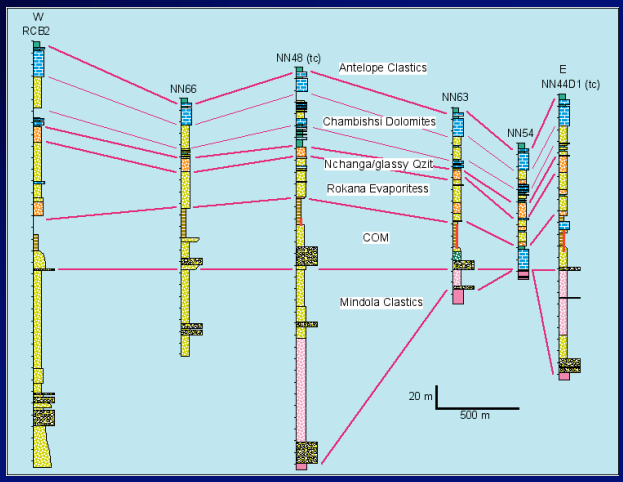

AMIRA /ARC ProjectP544 *Final Sponsors Meeting* *July 2003*

Chambishi SE; hangingwall

13

Rokana Evaporites are a cyclically interbedded succession;

- Muddy (biotitic) sandstone with abundant carbonate and anhydrite cements/vughs/nodules
- Thin microbially laminated carbonates
- Minor clean sandstone (quartzite) and reduced siltstone beds

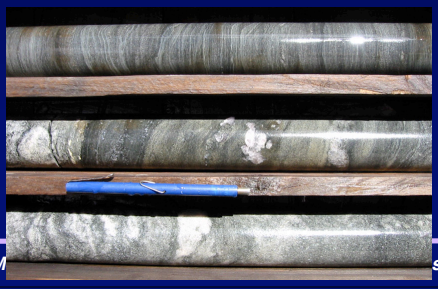

Chambishi SE; hangingwall

14

Marginal marine sabkha succession - first major Roan evaporite & brine factory

Reflected in the preserved nodular textures & abundant anhydrite & carbonate (now recrystallised) in the fine-grained units compared to those in the footwall

Suggests, given the absence of primary evaporite facies in the footwall, the Rokana Evaporites were the source of the anhydrite & carbonate cements in the clean (permeable) sandstones

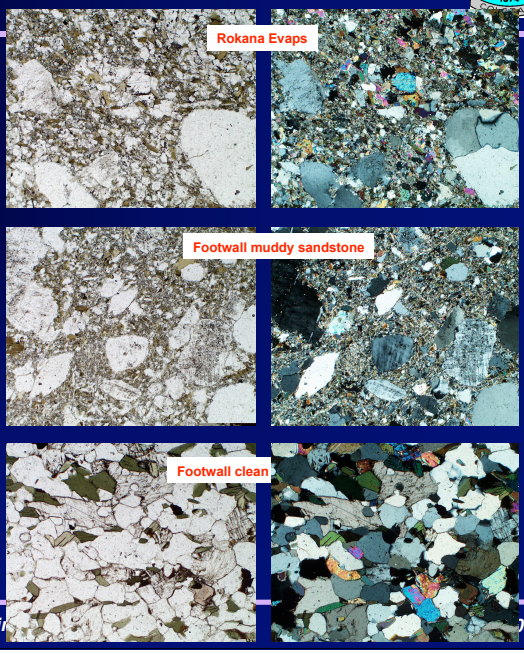

Chambishi SE; hangingwall 15

Descent of sulfate rich fluids could have originated during earliest diagenesis (few 100s of m burial) by brine reflux

Or slightly later in burial history by release of sulfate enriched fluids from dehydration of gypsum

The distribution of sulfate in the footwall controlled by;

- the distribution of evaporitic facies in the hanging wall
- the access points where descending fluids could breach the ore shale
- the permeability distribution in the footwall

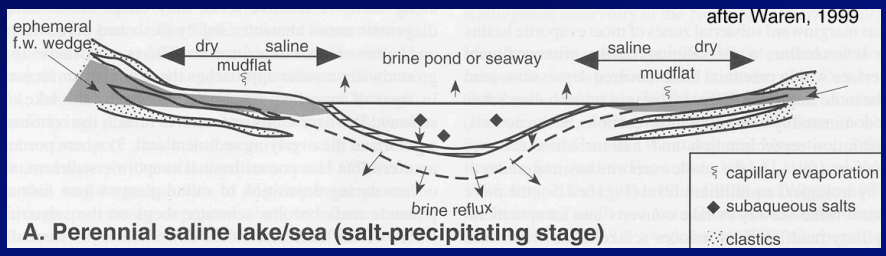

A. Perennial saline lake/sea (salt-precipitating stage)

AMIRA /ARC ProjectP544 *Final Sponsors Meeting* *July 2003*

Chambishi SE; hangingwall 16

Nchanga or glassy quartzite - upper ore shale

Several to >10 m thick, clean, massive to stratified and cross-bedded, coarse to v coarse grained arkose marker

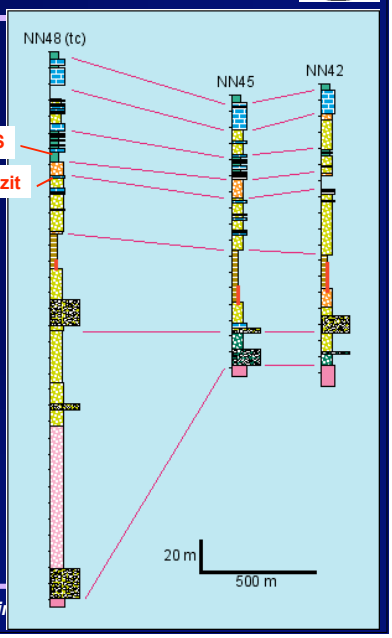

Chambishi SE; hangingwall 17

Represents resumption of basement erosion & fluvial braidplain sedimentation

Always overlain by intervals of non-evaporitic siltstones (~ore shale)

Combination of basement uplift and generation of accommodation space = this cycle is of tectono-sedimentary origin & records a resumption of activity on the controlling growth faults

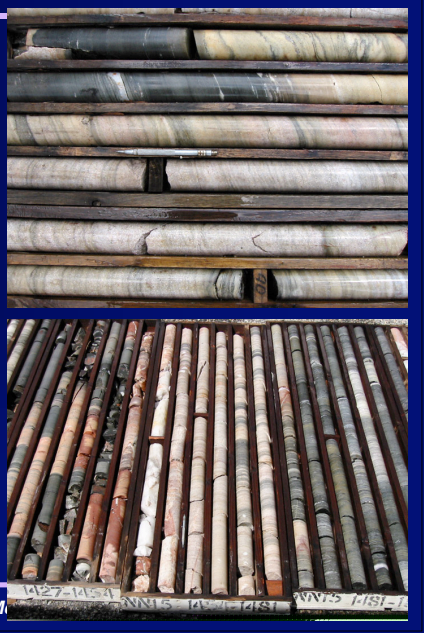

AMIRA /ARC ProjectP544 *Final Sponsors M*

Chambishi SE; hangingwall 18

Upper evaporitic sequence

Return to Rokana Evaporites marginal sabkha facies association

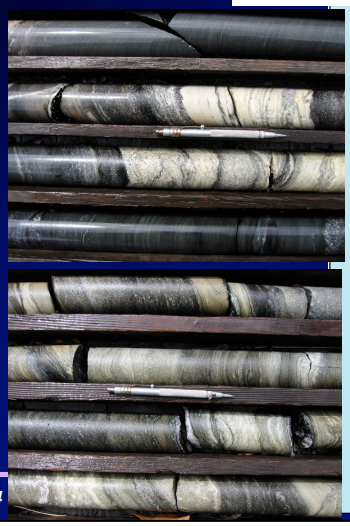

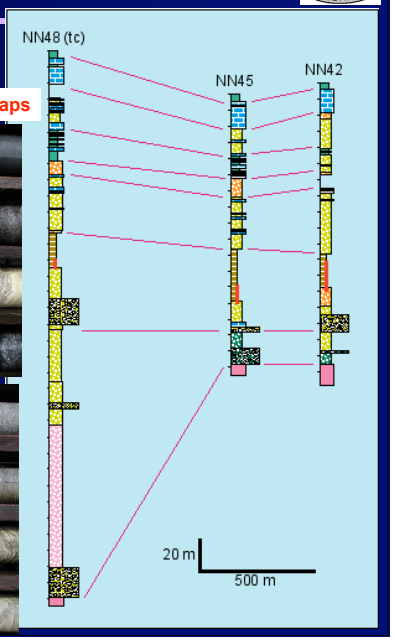

AMIRA /ARC ProjectP544

Chambishi SE; hangingwall

19

Chambishsi or cherty dolomite

<10 - >15 m dolomite that preserves a coherent internal stratigraphy across the entire prospect

Microbial carbonate reef system that records complete tectonic quiescence

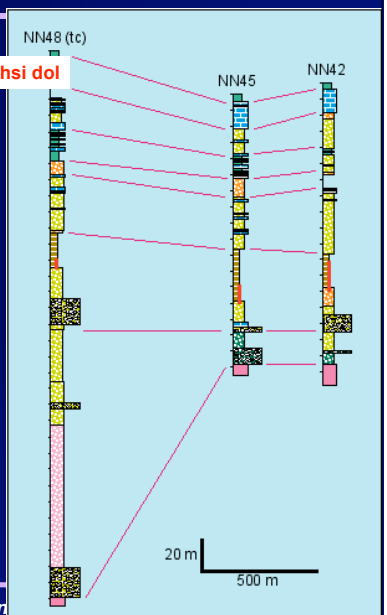

Meetin

nsors Meeting July 2003

Chambishi SE; ore shale & equivalents 21

Typical ore shale intersection

AMIRA /ARC ProjectP544 *Final Sponsors Meeting* *July 2003*

Chambishi SE; ore shale & equivalents 22

Along strike OS pinchouts

Ore shale replaced by biotitic sandstone within a coarse-grained apron of well-sorted evaporitic sandstone and conglomerate

Approach sediment entrypoints (eg transfer fan) into axial graben

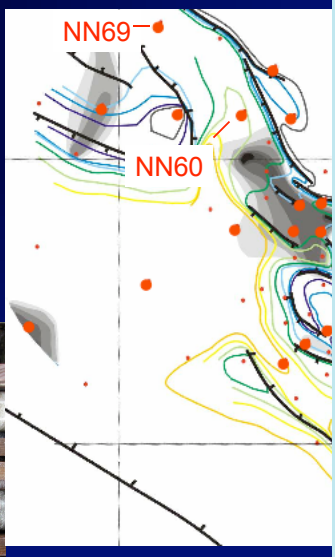

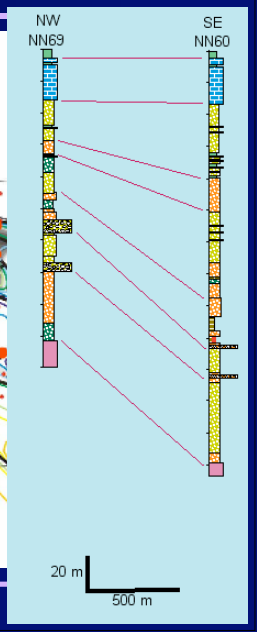

Final Sponsors Meeting

Chambishi SE; ore shale & equivalents 23

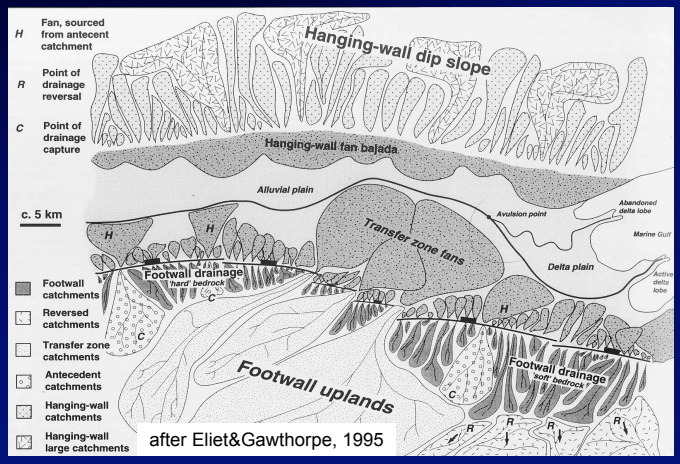

after Eliet&Gawthorpe, 1995

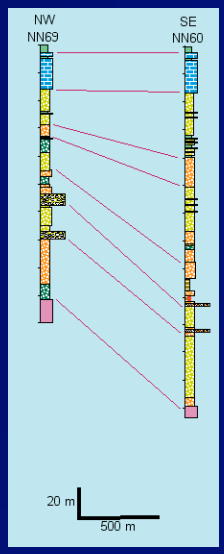

Chambishi SE; ore shale & equivalents 24

Across strike OS pinchouts - Northern section & barren Gap

Ore shale replaced by "biohermal" carbonate

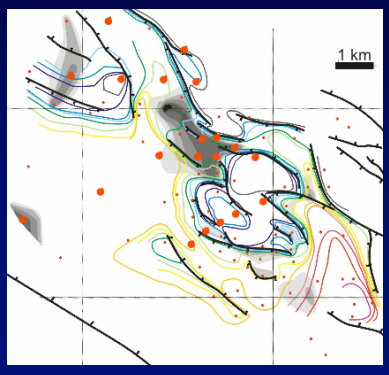

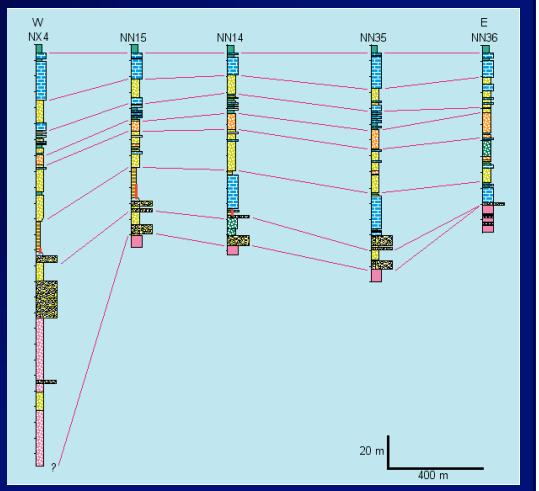

Chambishi SE; ore shale & equivalents 25

Barren Gap section

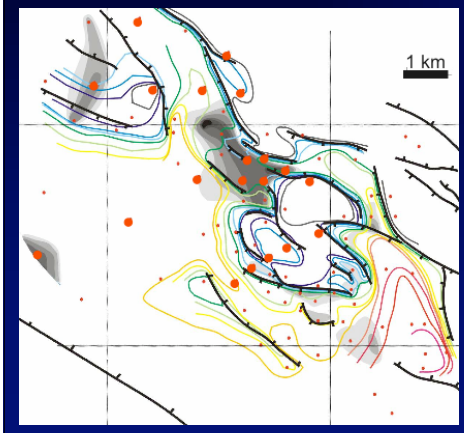

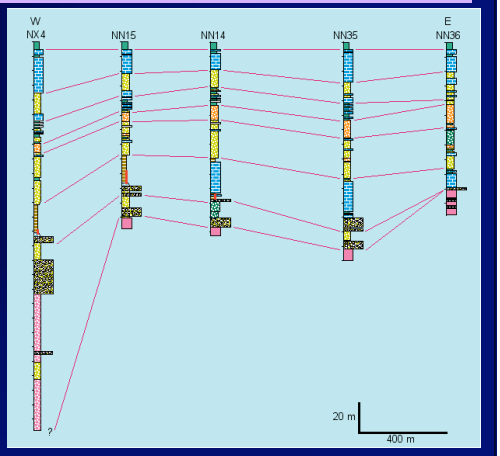

AMIRA /ARC ProjectP544 *Final Sponsors Meeting* *July 2003*

hale and equivalents 26

Chambishi SE; ore shale & equivalents 27

Resort to isotopes!

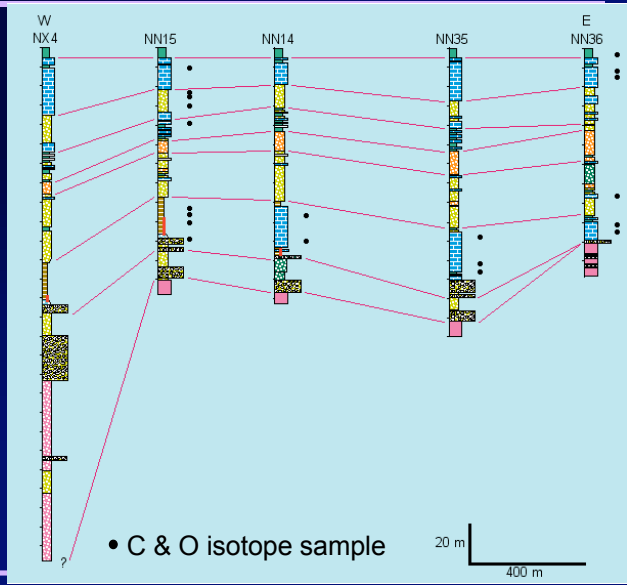

AMIRA /ARC ProjectP544 Final Sponsors Meeting July 2003

Chambishi SE; ore shale and equivalents

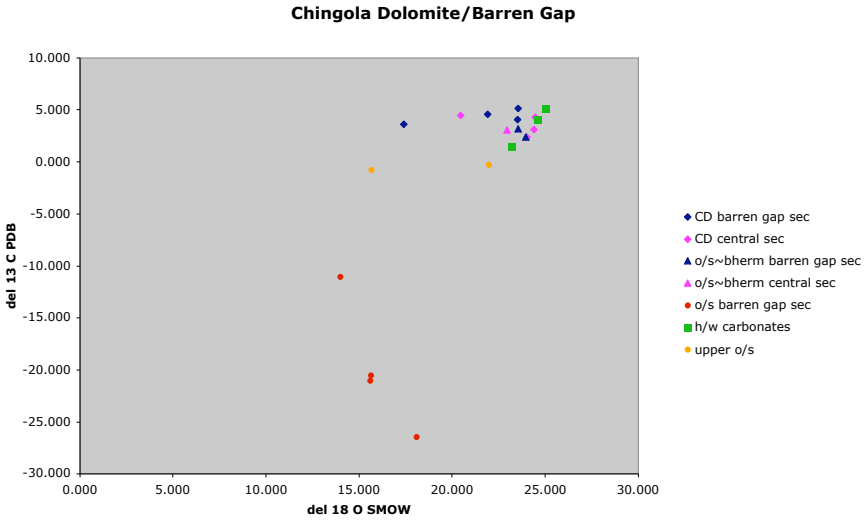

Chambishi SE; ore shale & equivalents 29

Barren Gap section

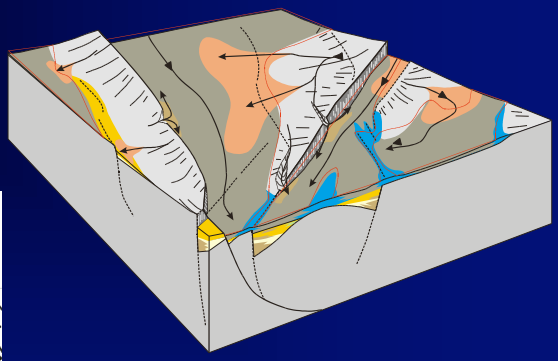

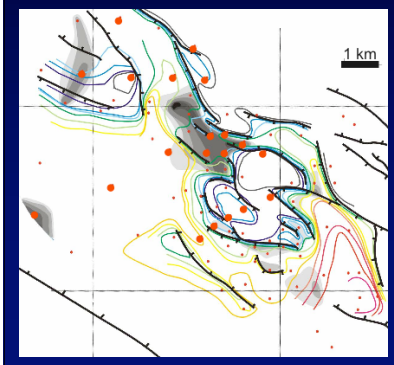

AMIRA /ARC ProjectP544 *Final Sponsors Meeting* *July 2003*

Conclusions 30

Chambishsi SE central main "barren gap" is a microbial bioherm

Situated on a area of elevated basement that represents a transfer zone between zones of extension that controlled the footwall clastics

Along strike ore shale pichout is a hangingwall fan

Generation of accommodation space slows post ore shale - one major distinct tectono-stratigraphic pulse that hosts minor mineralisation around the KA

Evaporitic facies in the hangingwall (Rokana Evaporites) generated brines that sank though the basin fill (brine reflux) and precipitated evaporitic cements in the footwall aquifers

AMIRA /ARC ProjectP544 *Final Sponsors Meeting* *July 2003*

31
AMIRA /ARC ProjectP544
Final Sponsors Meeting
July 2003

Development of the Lower Roan basin system: controls on Cu-Co mineralisation

David Selley, Stuart Bull, Robert Scott, Mawson Croaker, David Broughton & Nicky Pollington
Cemtre for Ore Deposit Research, University of Tasmania

Abstract

The Lower Roan records rift-dominated basin development at the onset of Katangan sedimentation. Accommodation development, sediment dispersal patterns and resultant stratigraphic architecture, were controlled by an evolving network of WNW- and NNW-trending structures. During initial rifting, the fault array was highly segmented, resulting in small, compartmentalised depocentres and predominantly coarse-grained fluviatile accumulation. With continuing extension, linkage of fault segments led to the evolution of a master fault system. The ability of master faults to accommodate greater rates and degrees of displacement resulted in an abrupt increase in subsidence and opening of the rift system. The Copperbelt Orebody Member records the onset of this phase of basin development, which was characterised by initial sediment starvation and the formation of a broad, subaqueously deposited argillaceous seal to underlying basin compartments. The final tectono-stratigraphic phase involved episodic re-emergence of basement source areas, possibly due to extensional rebound, and the deposition layer-cake cycles of fluviatile and evaporitic strata.

The distribution of Cu-Co mineralisation appears strongly partitioned into linkage zones between WNW- and NNW-trending fault zones. In the cases of arenite-hosted ore, this relationship results from accumulation of mobile hydrocarbons within distinctive physical traps formed at fault intersections. The reasons for localisation of Ore Shale-hosted ore at or above similar structural configurations is less clear, but is likely to involve one or a combination of the following features: (1) concentration of available sulphur and/or reductant, (2) enhanced fracture-induced permeability, (3) geometry of footwall aquifers.

Introduction

In this paper, we present a synthesis of results from detailed tectono-stratigraphic studies of the Lower Roan from a number of deposits located on the eastern flank of the Kafue Anticline (i.e., Nkana-Mindola, Chibuluma West, Mwambashi B, Chambishi, Chambishi SE, Konkola and Konkola North) and Mufulira. Much of the data have been sourced from the 'Chambishi Basin' where drilling commonly persists to basement, allowing constraints to be placed on the stratigraphic architecture at the onset of basin growth. Deposits where 'footwall' data are limited, such as Konkola and Konkola North, are incorporated however, as they provide critical information on basin development during accumulation of upper levels of the Lower Roan.

Our results have demonstrated that the fundamental stratigraphic subdivision of the Lower Roan erected by previous workers (e.g., Clemmey, 1976) is essentially valid. The basic elements of this stratigraphy comprise: (1) Mindola Clastics Formation (MCF), a basal alluvial-fluvial dominated succession, characterised by small compartmentalised basins separated by areas of pronounced basin topography, and (2) Kitwe Formation (KF), a broadly layer-cake, mixed fan-delta, evaporite, carbonate succession, that was largely subaqueously deposited (Slides 2, 14). Our principal contribution in terms of resolving basin development during deposition of these sequences, has been to relate facies architecture to evolution of a

systematic network of extensional faults. In doing so, we have identified four major tectono-stratigraphic events, each of which records a discrete phase in displacement and/or linkage history of the fault network. Despite the restricted thickness of the Lower Roan, its tectono-stratigraphic development is typical of modern rift systems.

Regional fault architecture

Fundamental to our model, is the recognition of a systematic association of two distinct basin-controlling structural orientations, WNW and NNW, throughout the deposits studied (Slides 6–13). These structural grains are most demonstrable within the MCF, where basin-bounding elements are more densely distributed, but also influence facies architecture at a broader scale within the KF. WNW- to E–W trending half grabens appear to represent the principal extensional fault array, and are interpreted to have formed under regional NNE-SSW directed extension at the onset of Katangan sedimentation. The NW- to NNW-grain is generally less continuous and interpreted to reflect sub-ordinate linkage structures or accommodation zones, located at the tip-points of WNW-trending extensional faults. An important exception to this relationship occurs on the eastern flank of the Chambishi Basin, where a significant NNW-trending graben system was developed (Slide 3). This graben system effectively hosts the major deposits of Nkana-Mindola & Chambishi SE, and potentially steps westward near the northern margin of the Chambishi Basin to include the Chambishi deposit. That this anomalous NNW-trending graben system flanks the Kafue Anticline, may indicate 'inheritance' from deep seated, pre-existing basement structures.

Relationship of Lufilian fold geometry and extensional fault architecture

The geometry of structures generated during Lufilian commonly exhibits 'inheritance' from early rift architecture. This relationship is most clearly seen in terms of Lufilian fold patterns, which effectively mimic the shape and distribution of basin compartments generated at the onset of rifting. Classic examples of partitioning of strain and nucleation of folds parallel to inverted rift shoulders occur at Chambishi open pit and Chibuluma West (Slide 4). In the latter case, Selley & Bull (2001) demonstrated that an array of high amplitude, low-wavelength basement-cored anticlines represent inverted tilt-blocks developed within the footwall of WNW-trending half-grabens. Similarly Croaker & Selley (2003) show that folds generated above inverted growth faults at Nkana-Mindola have resulted in marked deflections in the orientation of the Lower Roan-Basement contact.

Regional fold patterns from the Chambishi Basin indicate that the expression of early basin architecture is recorded at least to the level of the Mwashia. As shown in Slide 3, a relatively simple array of E-W trending fold axial traces developed at the level of the Kundelungu, passes eastward into a complex interference pattern of WNW- and NNW-trending folds within Mwashia and Upper Roan strata, the latter coinciding closely with the distribution and orientation of early rift faults. This relationship highlights the potential of using changes in regional fold geometry, gleaned from either surface outcrop of remote sensing datasets, as a guide to basin architecture.

Structural control on ore distribution

Through restoration of original basin architecture at a number of Copperbelt deposits, we have demonstrated a consistent 'structural control' on the distribution of classical Lower Roan ore (Selley & Bull, 2001; Selley et al., 2002; Scott et al., 2003; Croaker and Selley, 2003; Broughton, 2003). In doing so, we have refined the long recognised spatial association of mineralisation with basement highs, to a systematic and hence predictable association involving the interference of WNW- and NNW-trending growth structures. Localisation of ore near the intersection of these structural grains results in part from the anomalous stratigraphic architecture developed at these sites, but also from the focussing of hydrothermal fluids into damage zones generated during stages of basin growth, and possibly inversion.

The relationship between transfer, or fault accommodation zones, with ore is best demonstrated within arenite-hosted deposits: e.g., Chibuluma West, Mwambashi B, Chambishi and Mufulira (Slides

6–11). In each of these cases, interaction of NNW-trending transfer zones with WNW-trending graben systems resulted in the development of narrow, confined depocentres, characterised by condensed and relatively coarse-grained sediment infill. This distinctive stratigraphic architecture was responsible for the trapping of mobile hydrocarbons or sour gas, which in turn reacted with oxidised metal-bearing hydrothermal fluids to precipitate sulphides (e.g., Scott et al., 2003).

The distribution of Ore Shale-hosted Cu mineralisation at Chambishi SE is also partly accounted for by variations in facies architecture of the host sequence developed at the intersection of extensional fault arrays (Bull & Selley, 2003). However the stratigraphic architecture of the footwall succession, and potentially the faults themselves, are likely to have played an additional role. Shown in Slide 12 is the basin architecture developed during accumulation of the MCF (ie. footwall to the Ore Shale). Principal elements include major WNW- and NNW-trending graben systems, at the intersection of which is a zone of subdued accommodation development, resulting in a broadly south-westerly thickening clastic wedge, as well as discrete emergent basement blocks. Mineralisation within the overlying Ore Shale closely corresponds to confined fault-controlled footwall compartments (Slide 13), distributed about the periphery of the central basement block.

Tectono-Stratigraphic Evolution of the Lower Roan

Evolution of the extensional fault network is recorded by four laterally mappable tectono-stratigraphic units, which from oldest to youngest include: (1) Basal Quartzite Member (BQM), (2) Kafue Arenites Member (KAM), (3) Copperbelt Orebody Member (COM), (4) Rokana Evaporites Member (REM) and Antelope Clastics Member (ACM) (Slide 14). We have attempted to retain as much as possible the stratigraphic terminology introduced by Clemmey (1976).

Basal Quartzite Member

Initial rift strata comprise a facies association of well stratified subarkose and subordinate talus and debris flow conglomerate, deposited under subaerial conditions (Slide 15). Rapid lateral facies and thickness variation are characteristic of this stratigraphic level and attest to the compartmentalised nature of the basin framework during this period of sedimentation (Slides 16, 17).

The palaeographic model shown in Slide 18 highlights the interrelated aspects of fault architecture, accommodation development and sediment dispersal active during this stage. Incipient WNW-trending trough systems had limited lateral extent, dying out onto oblique basement ridges or fault arrays. This discontinuous nature of the basin system reflects the segmented form of extensional faults that typifies the onset of rifting (Gawthorpe and Leeder, 2000). Under these conditions, displacement is partitioned into the central part of each fault segment, dissipating rapidly towards tip points at either end. Strain at tip points is 'accommodated' or 'transferred' to neighbouring fault segments by oblique transfer systems. These transfer systems are interpreted to be recorded by the NNW- to NW-structural grain.

Detritus in each sub-basin was derived from immediately adjacent basement sources. The main points of supply were via topographically low domains at the lateral tips of sub-basins, where condensed, chaotic assemblages of conglomerate and sandstone accumulated. From these drainage points, braided fluvial systems formed, depositing well-structured sheets of well sorted subarkose. Talus breccias were confined to the immediate hangingwalls of half grabens (Slide 16) and were fed by small footwall canyon systems.

Kafue Arenites Member

Resurgence of tectonic activity at the onset of KAM sedimentation is heralded by a widely recognised, basal alluvial fan/fan-delta association, and an upward transition to partly subaqueously deposited argillaceous sandstones and minor dolomitic siltstones (Slides 20–22). The onset of subaqueous sedimentation records increased rates of subsidence relative to sediment input, accompanying greater

displacement on basin-bounding structures. This relationship suggests an increased connectivity between adjacent fault segments, but not so efficient as to change fundamental drainage systems and basin geometry (compare Slides 18, 25). That is, the aerial distribution of the KAM was roughly compatible with that of the BQM and provenance remained unchanged (i.e., locally derived detritus).

Transfer systems remained active throughout accumulation of the entire MCF as shown by vertical amalgamation of condensed, chaotically structured, subaerial deposits at sediment input points (Slides 23, 24). These relatively 'clean' pinch-out zones were important reservoir sites for migrating hydrocarbons during late diagenesis.

Copperbelt Orebody Member

The COM is characterised by an abrupt shut-off of sediment supply, leading to deposition of predominately subaqueously deposited fine-grained siliciclastics with variable carbonate and evaporitic components, and microbial carbonate reefs (Bull & Selley, 2003). This sediment-starved system is interpreted to reflect a new stage in tectonic activity, involving regional and rapid basin-floor subsidence, rather than a simple eustatic sea-level rise. Evidence for an event that involved a fundamental reorganisation of the fault network is three-fold. Firstly was the ubiquitous influx of coarse-grained sediment immediately below the COM, i.e., 'Footwall Conglomerate'. In some cases, this facies defines a distinct upward coarsening and thickening fanglomerate cycle, indicating increased activity on basin controlling structures during the latest MCF (Slide 27). The uppermost contact of this cycle records immediate sediment starvation, suggesting a catastrophic change in sediment dispersal systems, rather than gradual flooding of source areas in response to thermal relaxation.

Secondly, many of the faults that controlled accommodation development during deposition of the MCF, suddenly became inactive at the onset of the COM. This stage of basin evolution is recorded by a fundamental change in stratigraphic architecture from lower compartmentalised clastic accumulations, to more layer-cake facies patterns at higher levels (Slide 28). At a regional scale, the COM formed a fine-grained blanket that transgressed and effectively sealed the underlying sub-basin compartments. 'Ghosts' of the older basin architecture are locally preserved, however, with the formation of the 'reef facies' of the COM atop MCF controlling transfer zones and possibly footwall tilt blocks (Slide 30). Significantly, this broadly layer-cake architecture persists throughout the overlying Rokana Evaporites phase, despite clear evidence for tectonically-related coarse clastic input (Bull & Selley, 2003; Broughton, 2003). Thus faults that became inactive at the end of the KAM phase, were never reactivated during subsequent tectonism, implying an important change in fault displacement and propagation mechanisms.

The final line of evidence for tectonically controlled reorganisation of depocentres during the COM is perhaps the weakest. It relates to broad areas of either non-deposition or preservation of the COM documented from the northeastern and southern margins of the Chambishi Basin (Annels, 1989), and the Konkola region (Broughton, 2003). Comparison of stratigraphic profiles from Nkana and Chibuluma West on the southern margin of the Chambishi Basin demonstrate the highly condensed character of both the COM and overlying Rokana Evaporites Member in 'pinch-out' zones, despite ubiquitous thick accumulations of the underlying MCF. Although we cannot discount tectonic thinning at the level of the COM in response to extensional collapse, the apparently condensed section may indicate that areas of significant accommodation development (ie. thick MCF), suddenly became areas of emergence. If this were the case, the change in basin configuration at the onset of the COM would be best interpreted to reflect displacement along a new or evolved array of basin-controlling faults.

Rokana Evaporites – Antelope Phase

Sedimentation throughout the final phase of Lower Roan basin development involved cyclical packages of argillaceous sandstone, dolomitic siltstone, microbial carbonate and evaporite (Slide 33). Although broadly similar to the KAM (though richer in evaporitic and carbonate components), the

REM is distinguishable by its remarkable layer-cake facies architecture (Bull & Selley, 2003; Broughton, 2003). Subtle thickening of the package does occur adjacent to major growth structures however, areas where greater subsidence and accommodation development was accompanied by persistent deeper water sedimentation, are conspicuously lacking in an evaporitic component (Slides 34, 35). By contrast, evaporitic anhydrite-dolomite cements were intensely developed within more 'emergent' parts of the basin system, such as above older basement topographic highs at Chambishi SE (Slide 35; also Bull & Selley, op cit.)

The cyclical character of the package records periods of tectonic activity during which basement source areas became emergent. The first of these tectonic pulses is recorded by an upward coarsening and thickening profile from the underlying COM, and possibly relates to post extensional rebound following the COM event. Older MCF basin-controlling structures had little influence on facies architecture at this time, implying that displacement was re-partitioned into the younger fault system that controlled deposition of the COM. An extensive sheet of subarkose at the top of the REM (Nkana Quartzite) heralds the final tectono-stratigraphic element of the Lower Roan. This major braided fluvial system marks a regional increase in sediment input prior to prolonged subaqueous sedimentation and flooding of source regions during accumulation of the Chambishi Dolomite/Shale-With-Grit facies association (ACM).

Summary and conclusions

Lower Roan strata record early rift-dominated phases of the Katangan system. The upward transition in stratigraphic architecture involving progressively deeper water sedimentation and more layer-cake profiles is interpreted to reflect a history of growth fault propagation and linkage that typifies more modern rift systems (e.g., McLeod et al., 2000; Gawthorpe & Leeder, 2000). Initial accommodation development was controlled by a discontinuous array of WNW-trending growth faults, which terminated or interacted with a predominantly subordinate set of NNW-trending transfer faults and basement ridges (Slides 18, 25). Transfer zones were the loci for sediment input, and are characterised by the accumulation condensed, amalgamated fanglomerate systems within confined, weakly subsident troughs.

A fundamental change in fault configuration is recorded by the abrupt cessation of coarse clastic supply and transition to marginal marine conditions at the KAM-COM boundary. These features, coupled with widespread 'death' of the fault system that controlled the MCF, is consistent with a sudden linkage of a small number of through-going master faults (Slide 30). Evolution of the master fault system that was to control subsequent accommodation development resulted in opening of the rift system and widespread subsidence. However, concomitant uplift along the margins of major basin compartments directed drainages away from the depocentres to feed small arenaceous hangingwall fan systems (Slide 30; Bull and Selley, 2003). As the transition to finer-grained, transgressive units of the COM was so widespread, the linkage event was unlikely to have been related to the mechanics of a specific part of the basin system. The most plausible explanation involves fault reorganisation in response to a regional extensional pulse and/or change in stress orientation.

Cyclical fluvial and marginal marine conditions characteristic of the Rokana-Antelope event record the final stage of rifting prior to the Upper Roan phase of protracted platformal sedimentation (Broughton, 2003). Accommodation development remained controlled by master faults, the positions of which are revealed by abrupt changes in thickness at the level of the REM: eg. Kawiri & northeastern Chambishi Basin (Broughton, 2002; Bull & Selley, 2003).

The basin evolution of the Lower Roan system played important roles in mineralisation process, mainly through the localisation of reductants. The change in basin configuration at the KAM-COB boundary and resultant transgression of older basin compartments provided numerous physical trap sites for mobile hydrocarbons, principally within restricted transfer related troughs. Organic rich facies of the COM were the likely source of kerogen, but also served as an *in situ* reductant.

Localisation of several Ore-Shale hosted deposits above transfer zones (e.g., Chambishi, Chambishi SE) could be taken to indicate that the geometry of MCF compartments was also responsible for direction of hydrothermal Cu-bearing fluids towards more reducing facies of the COM. However, alteration studies have demonstrated that hydrothermal fluid flow was not obviously restricted to, or even intensified within an MCF 'aquifer' system (Selley et al., 2003; Large et al., 2003; Scott et al., 2003). Reasons for the spatial association of Ore Shale-hosted mineralisation with 'footwall pinchouts' are therefore potentially complex, and may involve one or a combination of the following. (1) Cu mineralisation occurred during the early stages of hydrothermal evolution, during which fluids were partitioned into a permeable MCF aquifer. With progressive cementation of the basal aquifer, fluids were directed through initially less permeable strata at higher stratigraphic levels. (2) The high density of faults and hence fracture-enhanced permeability that typifies transfer zones (Morley et al., 1990) provided a focussing mechanism for hydrothermal fluid flow. (3) The marked rheological contrast between the COM and underlying rigid crystalline basement and coarse siliciclastic units promoted tectonically induced decoupling at this level, again enhancing fracture-induced permeability along the base of the COM. At a number of deposits, highest strains recorded at the base of the COM occur where either the MCF is very thin or absent (ie. the COM lies close to, or directly on basement). (4) Transfer zones represented sites of reductant concentration within coarser-grained facies of the COM, via leakage of hydrocarbons from underlying MCF reservoirs. (5) Evaporitic conditions during deposition of the REM were enhanced above older basement highs, resulting in local concentration of available sulphur in the form of diagenetic anhydrite cements.

References

Annels, A.E., 1989. Ore genesis in the Zambian Copperbelt, with particular reference to the northern sector of the Chambishi Basin, in Boyle, R.W., et al., *Sediment-hosted stratiform copper deposits*: Geological association of Canada Special Paper 36, p. 427-452.

Broughton, D., 2002. Stratigraphy, regional alteration and mineralization patterns in the Zambian Copperbelt. AMIRA P544 Progress Report, Dec 2002. pp. 11.1-11.9.

Broughton, D., 2003. Stratigraphy, regional alteration and mineralisation of the Zambian Copperbelt. This volume.

Bull, S. & Selley, D., 2003. Chambishi basin studies; Chambishi SE Prospect. This volume.

Clemmey, H., 1976. Aspects of stratigraphy, sedimentology and ore genesis on the Zambian Copperbelt. PhD thesis, Univ. Leeds, 357pp.

Croaker, M. & Selley, D., 2003. Structural development and controls on Cu-Co mineralisation at Nkana-Mindola. This volume.

Gawthorpe, R. L., & Leeder, M. R. 2000. Tectono-sedimentary evolution of active extensional basins. Basin Research, 12, 195-218.

Large, R., McGoldrick, P., Bull, S., Scott, R., Selley, D. 2003. Lithogeochemistry and Alteration Halos to Stratiform Copper Mineralisation in the Chambishi Basin, Zambian Copper Belt. This volume.

McLeod, A., Dawers, N., Underhill, J., 2002. The propagation and linkage of normal faults: insights from the Starthspey-Brent-Statfjord fault array, northern North Sea. Basin Research, 12, 263-284.

Morely, C. K., Nelson, R. A., Patton, T. L., Munn, S. G. 1990. Transfer zones in the East African Rift System and their relevance to hydrocarbon exploration in rifts. AAPG Bulletin, 74, 1234-1253.

Scott, R., Selley, D., & Cooke, D., 2003. Arenite-hosted copper mineralisation east of the Kafue Anticline: A comparison of tectono-stratigraphic, mineralogical, geochemical and C- and O-isotopic characteristics of small and large deposits. This volume.

Selley, D. & Bull, S., 2001. Stratigraphy and basin geometry at the Chibuluma West copper-cobalt deposit, Zambia. AMIRA P544 Progress Report, Dec 2001. pp. 101-132.

Selley, D., Bull, S., Scott, R., Cooke, D., 2002. Chambishi Basin progress report 2: Basin geometry and its controls on mineralisation at Mwambashi B. AMIRA P544 Progress Report, Dec 2002. pp. 5.1-5.40.

Selley, D., Scott, R., Croaker, M., Broughton, D., Bull, S. & Pollington, N., 2003. Alteration history of the Roan. This volume.

Development of the Lower Roan Basin System, W Kafue Anticline

AMIRA P544 Team

Slide 1

Slide 2

Previous Work

- Previous sedimentological studies (eg. Clemmey, 1976) were basically correct
  - Intracontinental rift succession
  - Basal coarse siliciclastic package
    - Significant basement topography
  - Upper mixed succession of dominantly fine siliciclastics, carbonates and evaporites
    - Transgresses pre-existing basement topography

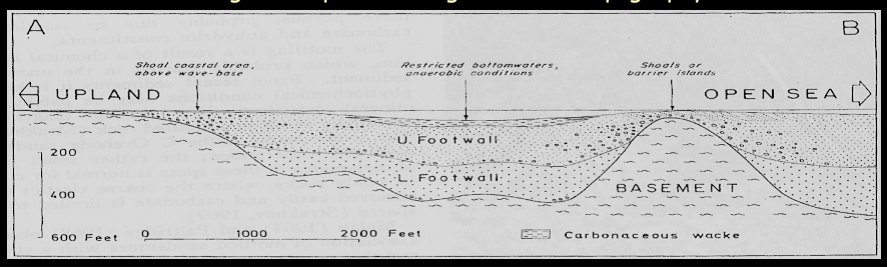

Slide 3

Key Outcomes

- Structural control on basin development
  - Facies variation, drainage patterns are intimately linked to a *systematically* evolving network of extensional faults
  - WNW-trending ½ graben & NNW-trending transfers
  - *Fault evolution was typical of modern rift systems*
- Basin configuration influenced inversion-related structures
  - Fold patterns reflect shape & distribution of early basin compartments
  - *Strain patterns can be used to determine initial basin geometry*

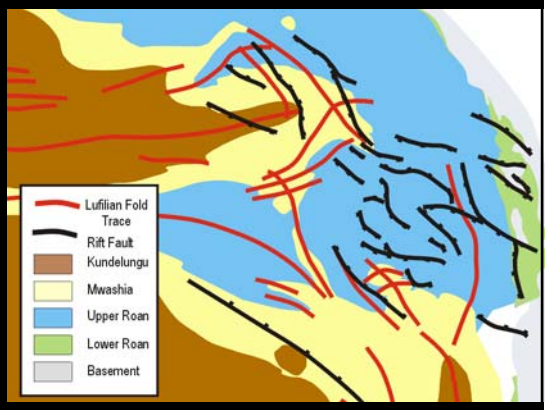

Chambishi

- E-W trending folds nucleated above a similarly oriented rift shoulder

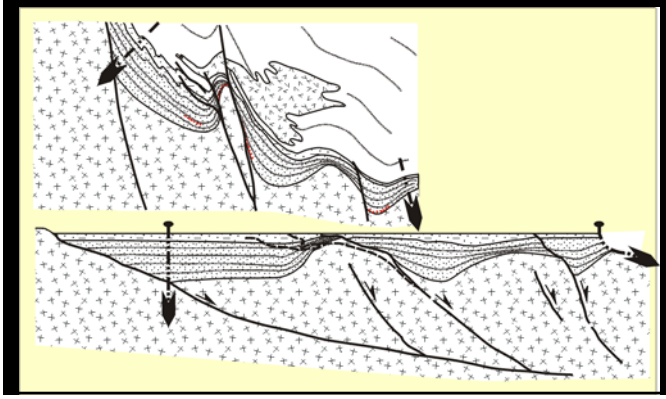

Chibuluma West

- Fold geometries reflect inversion of initial basin compartments

Slide 4

Key Outcomes

- Systematic link between basin architecture and Cu-Co distribution
  - Basin architecture controlled hydrological system
    - Geometry and spatial association of aquifers & aquicludes
    - Geometry of fault conduit system
  - Basin architecture dictated the distribution of reductants and sulphur sources

Slide 5

Chibuluma West

- FW deposited in series of discrete sub-basins:
  - N thickening ramp to NE
  - pinch outs onto WNW-trending basement highs in central zone
  - pinch out onto NNW-trending basement ridge to W

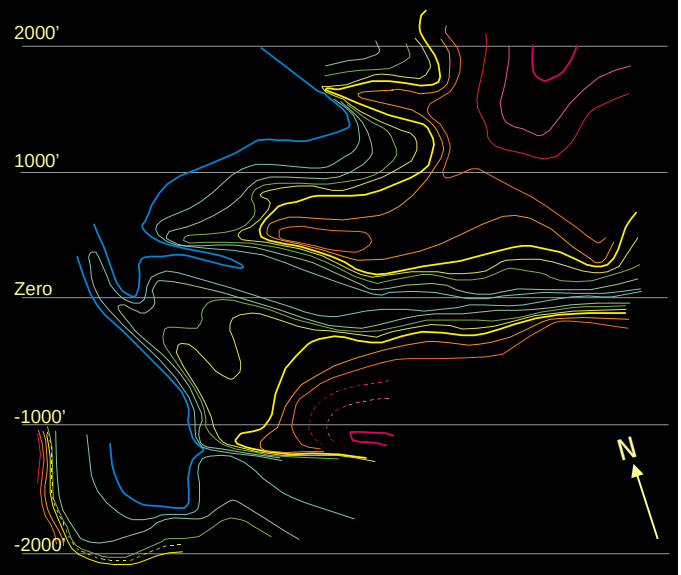

Slide 6

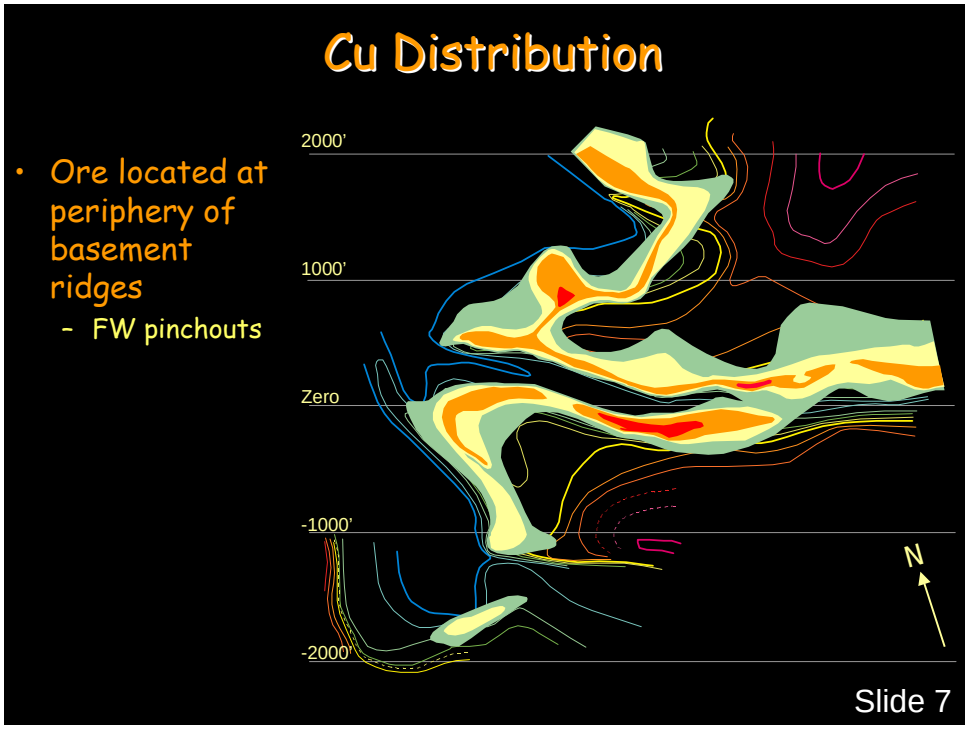
Cu Distribution
• Ore located at periphery of basement ridges
– FW pinchouts
2000'
1000'
Zero
-1000'
-2000'
N
Slide 7

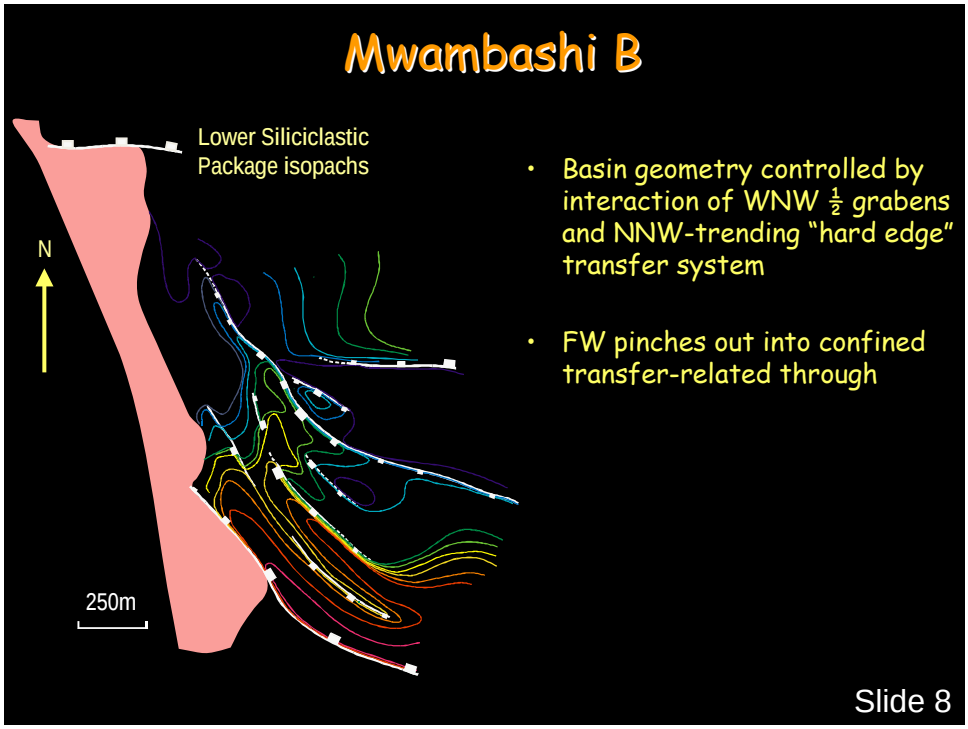
Mwambashi B
Lower Siliciclastic Package isopachs
N
250m
• Basin geometry controlled by interaction of WNW ½ grabens and NNW-trending "hard edge" transfer system
• FW pinches out into confined transfer-related through
Slide 8

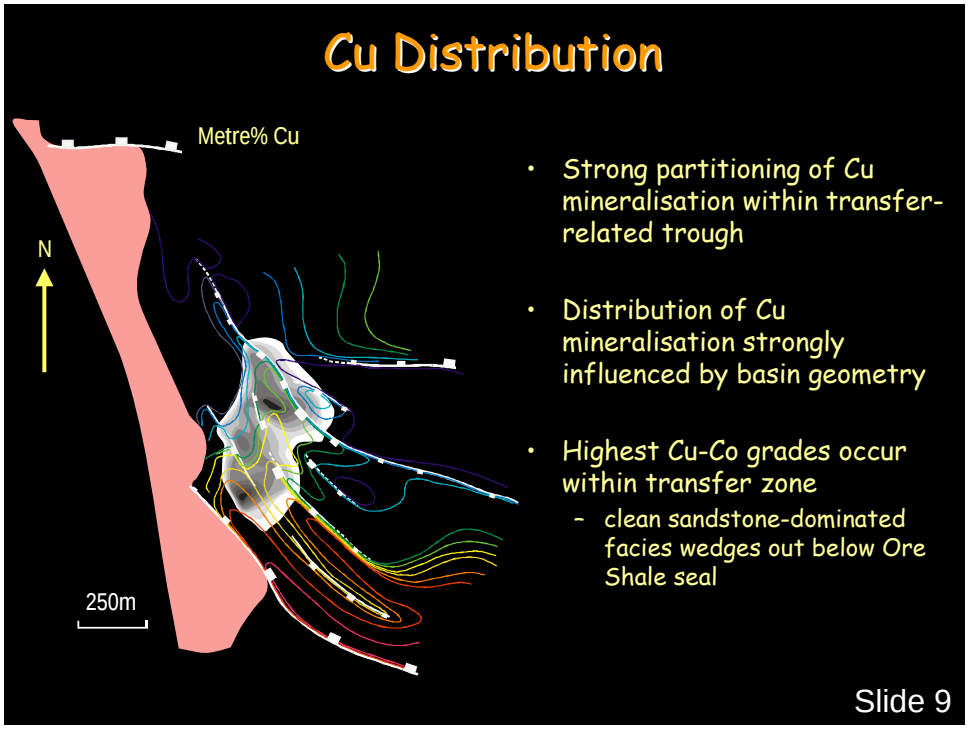
Cu Distribution
Metre% Cu
N
250m
• Strong partitioning of Cu mineralisation within transfer-related trough
• Distribution of Cu mineralisation strongly influenced by basin geometry
• Highest Cu-Co grades occur within transfer zone
– clean sandstone-dominated facies wedges out below Ore Shale seal
Slide 9

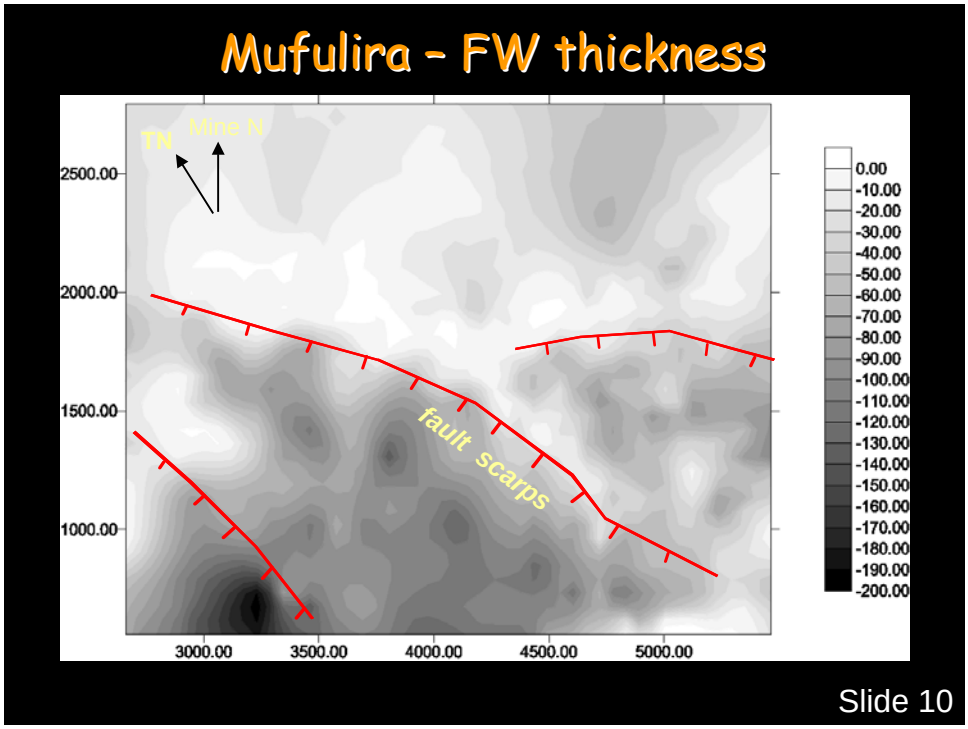
Mufulira – FW thickness
TN
Mine N
2500.00
2000.00
1500.00
1000.00
fault scarps
3000.00
3500.00
4000.00
4500.00
5000.00
0.00
-10.00
-20.00
-30.00
-40.00
-50.00
-60.00
-70.00
-80.00
-90.00
-100.00
-110.00
-120.00
-130.00
-140.00
-150.00
-160.00
-170.00
-180.00
-190.00
-200.00
Slide 10

Mufulira – COB thickness

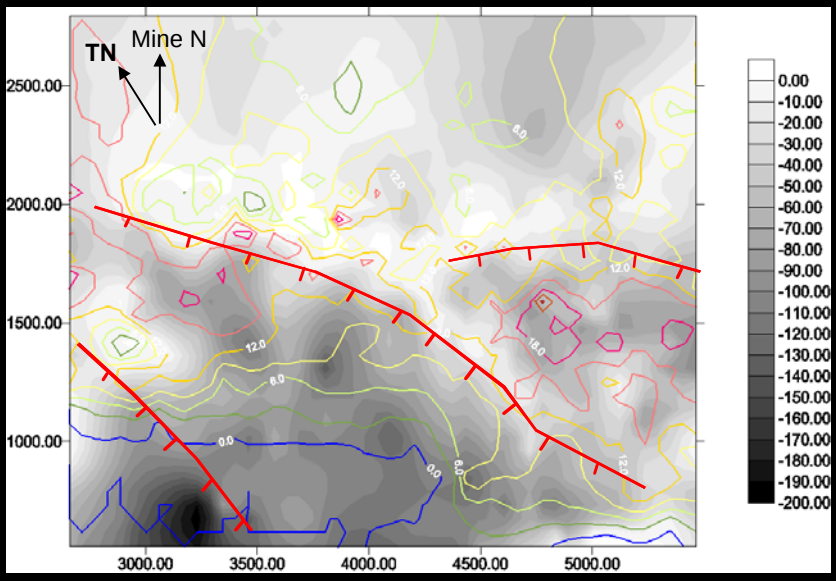

Slide 11

Chambishi SE

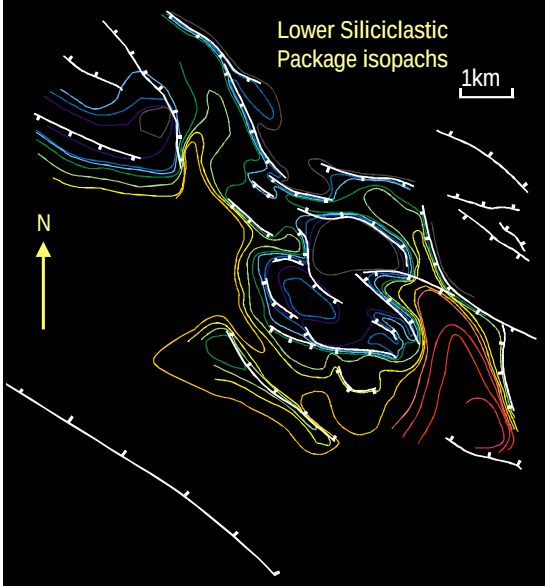

- Ore Shale hosted
- Complex fault system with WNW & NNW trending segments
- Numerous confined transfer fan systems around basement high

Slide 12

Cu Distribution

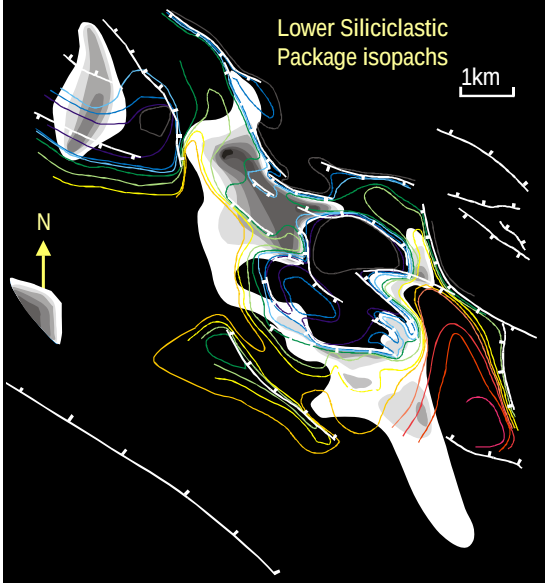

- Significant Cu occurrences fringe basement high, particularly above FW troughs
- Corresponds in part to facies variation in Ore Shale
- However, deposits clearly also controlled by FW basin architecture

Slide 13

Basin Development

- What are the main basin controlling elements?
- What are the critical stages in basin evolution?
- Four main tectono-stratigraphic events
  - Basal Quartzite Member
  - Kafue Arenites Member
  - Copperbelt Ore Body Member
  - Rokana Evaporites - Antelope Clastics

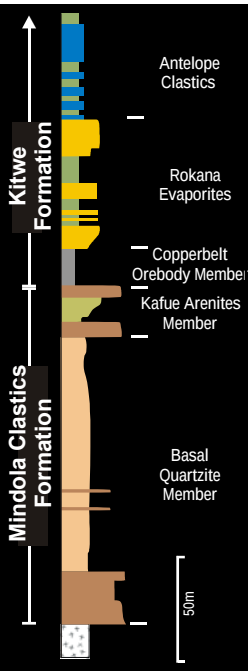

Slide 14

Basal Quartzite Member

Facies Association

- Talus breccia, debris flow conglomerate, fluvial sandstone
- Detritus derived from immediate Basement

Slide 15

Basal Quartzite Member

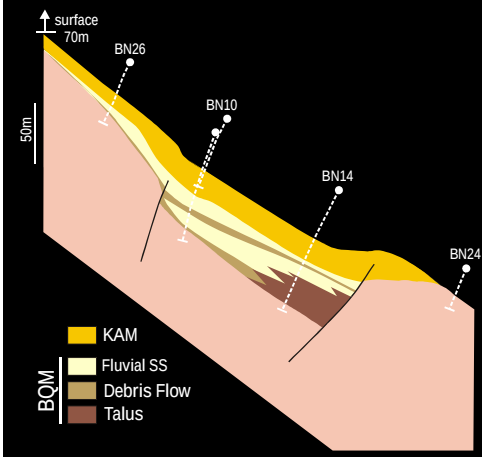

Facies Architecture

- Significant thickness variation
- Asymmetric facies patterns
- Rapid pinch-out of basin fill along axis

Slide 16

Basal Quartzite Member

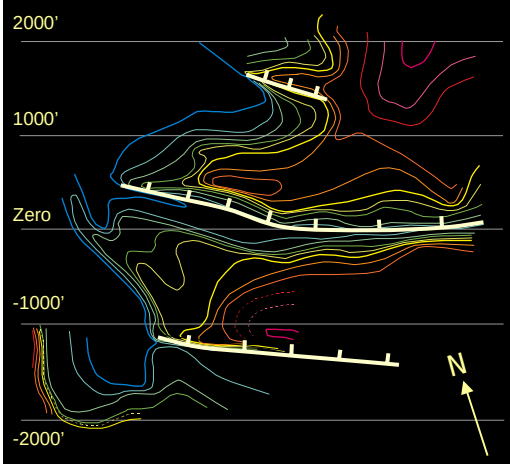

Facies Architecture

- Significant thickness variation
- Asymmetric facies patterns
- Rapid pinch-out of basin fill along axis

Slide 17

Basal Quartzite Member

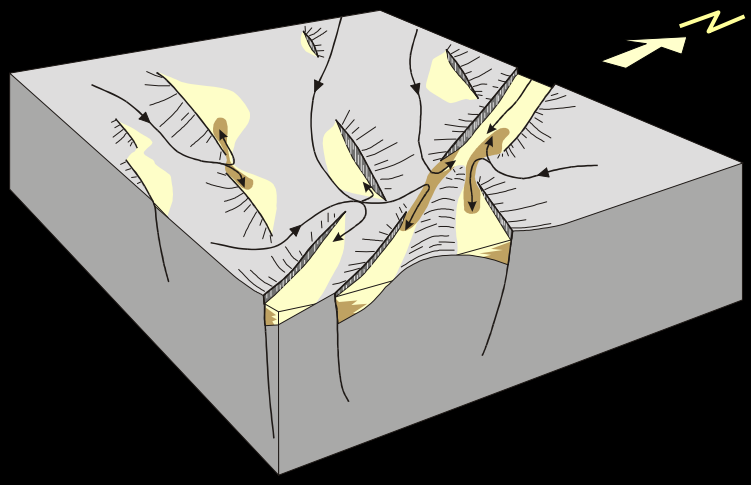

Slide 18

Basal Quartzite Member

Basin Architecture

- Facies architecture is typical of that generated at the onset of rifting
- Highly compartmentalised ½-graben basins formed within the hangingwalls of discontinuous fault arrays
- Minor sediment input across the footwall block
- Drainage systems directed mainly through topographically low transfer systems
  → axial fluvial systems

Slide 19

Kafue Arenites Member

Facies Association

- Conglomerate – poorly structured argillaceous sandstone – well stratified sub-arkose - dolomitic siltstone
- Coarse detritus remains sourced from immediately adjacent basement

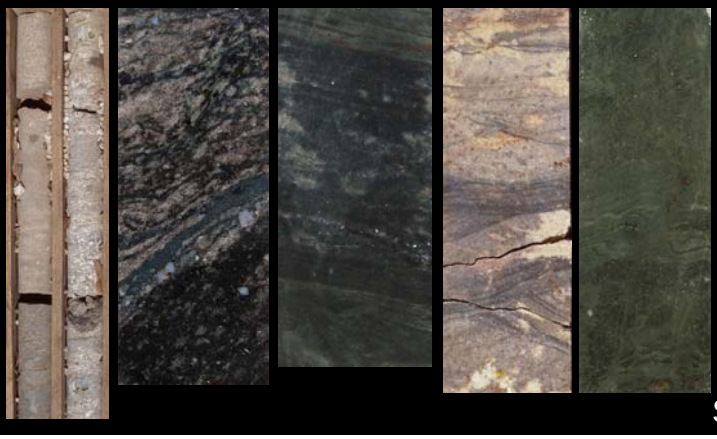

Slide 20

Kafue Arenites Member

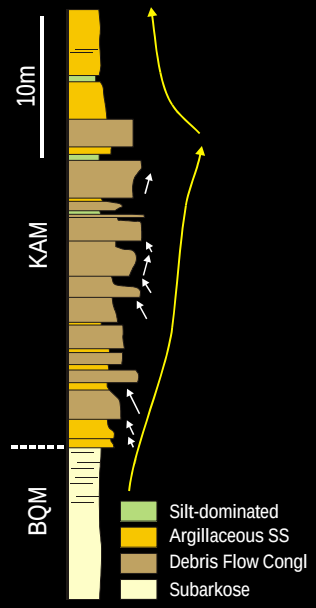

Facies Architecture

- Basal units are generally coarser grained than immediately underlying BQM, recording renewed fault activity
- Progradational cycles recorded close to active faults

Basinal Position

- Interfingering of conglomerate, argillaceous sandstone, locally significant thickness of dolomitic siltstone, rare subarkose sheets
- Transition to probable subaqueous conditions
- Fan-delta environment
- Rare axially-directed fluvial incursions

Slide 21

Kafue Arenites Member

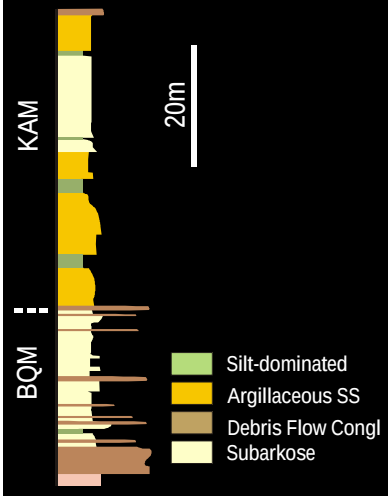

Facies Architecture

- Basal units are generally coarser grained than immediately underlying BQM, recording renewed fault activity
- Progradational cycles recorded close to active faults

Basinal Sections

- Interfingering of conglomerate, argillaceous sandstone, locally significant thickness of dolomitic siltstone, rare subarkose sheets
- Transition to probable subaqueous conditions
- Fan-delta environment
- Rare axially-directed fluvial incursions

Slide 22

Kafue Arenites Member

Facies Architecture

- Basal units are generally coarser grained than immediately underlying BQM, recording renewed fault activity
- Prograding cycles recorded close to active faults

Marginal Position

- Condensed, chaotic intercalation of argillite-poor sub-arkose & debris flow conglomerate
- Restricted to transfer zones
- Persisting subaerial depositional environment

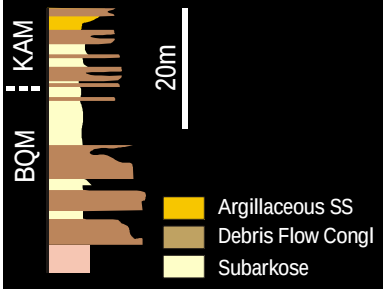

Slide 23

Kafue Arenites Member

- Transfer zones = points of sediment input
- Amalgamated coarse, "clean" transfer fans
- Excellent reservoir potential – critical for hydrocarbon accumulation

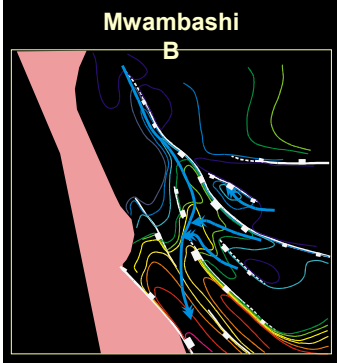

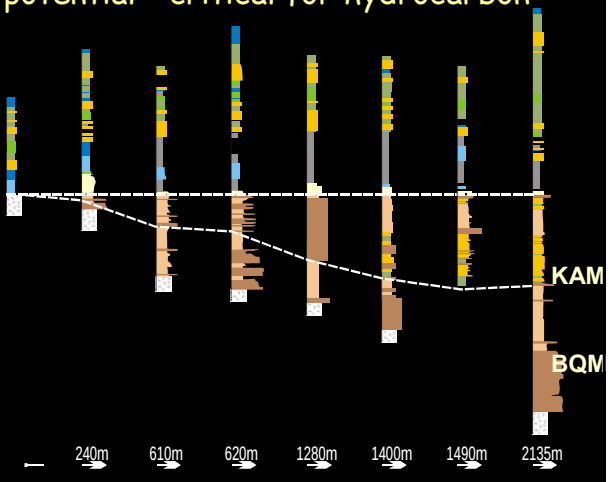

Slide 24

Kafue Arenites Member

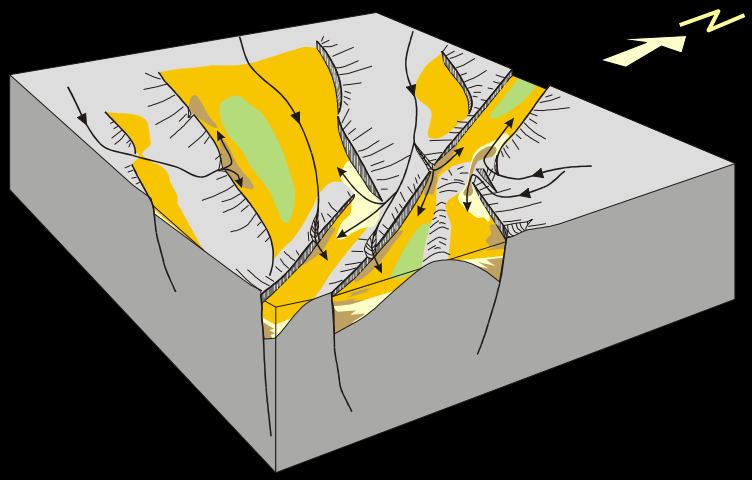

Slide 25

Kafue Arenites Member

Basin Architecture

- Transition to subaqueous sedimentation indicates basin subsidence (relative sea level rise)
- Increased fault linkage, but not sufficient to fundamentally change basin compartments and regional drainage patterns

Slide 26

Copperbelt Orebody Member

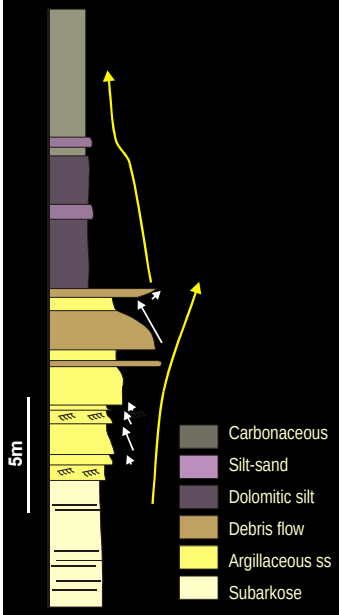

Facies Association

- Dolomitic siltstone – microbial carbonate – evaporite – argillaceous sandstone association *(marginal marine)*
- Abrupt cessation of coarse detrital input
  - *sediment starvation*
  - *drowning of older source areas*

Facies Architecture

- 3 lines of evidence indicate that COM basin phase *starts with a BANG!*
  - Tectonic event heralded by progradational fanglomerate systems within uppermost MCF
  - Upward coarsening + thickening cycle followed by immediate sediment starvation

Slide 27

Copperbelt Orebody Member

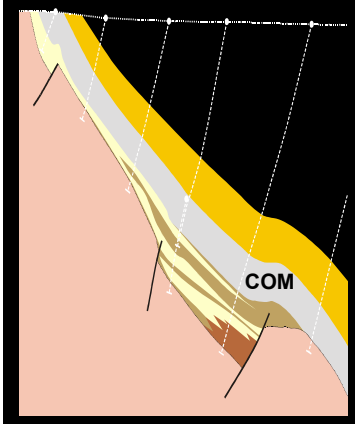

- Numerous faults which controlled development of older basin phases became inactive
  - *Never reactivated*
- *Fundamental change in fault architecture*

Slide 28

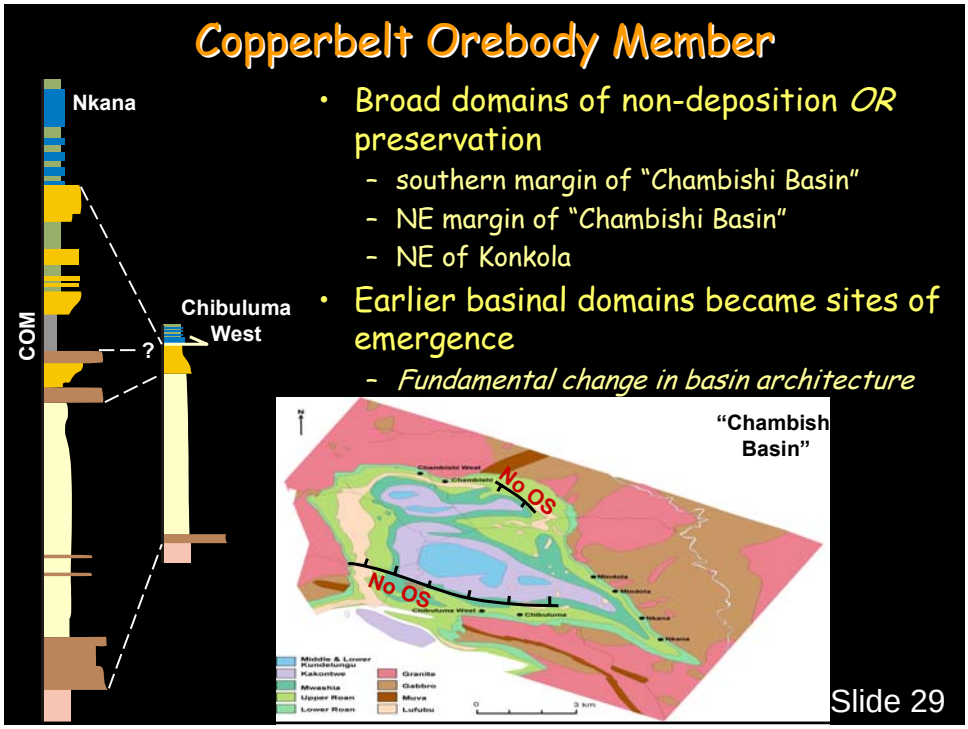
Copperbelt Orebody Member
Nkana
COM
Chibuluma West
?
Broad domains of non-deposition OR preservation
southern margin of "Chambishi Basin"
NE margin of "Chambishi Basin"
NE of Konkola
Earlier basinal domains became sites of emergence
Fundamental change in basin architecture
"Chambish Basin"
No OS
No OS
Slide 29

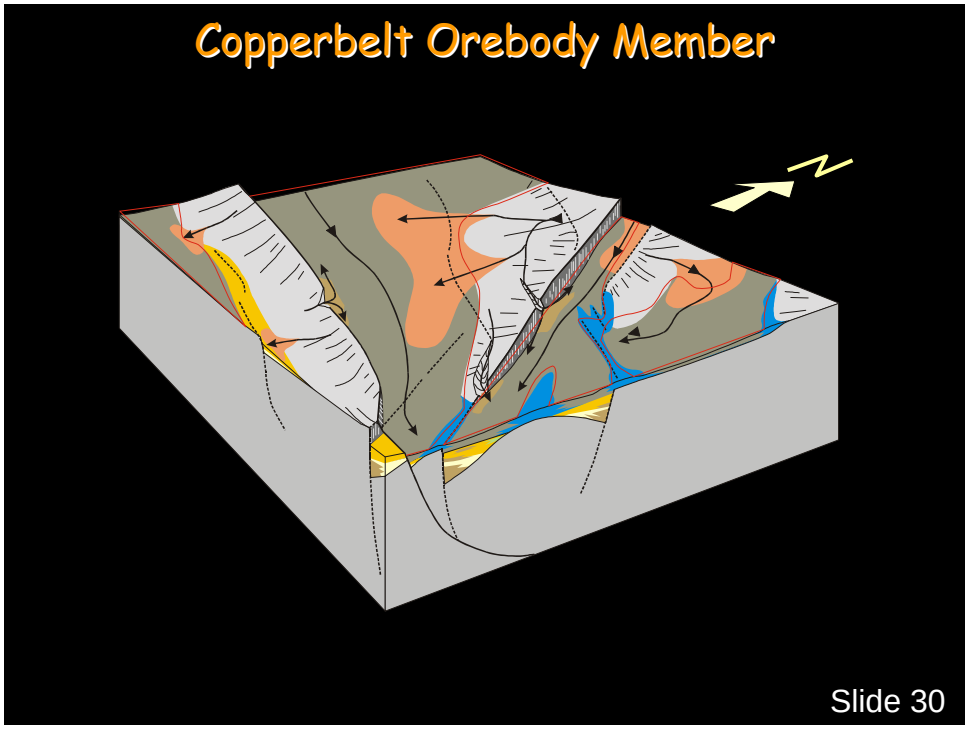
Copperbelt Orebody Member
N
Slide 30

Copperbelt Orebody Member

Tectonic Significance

- Increased accommodation development *BUT* widespread "fault death"
- Ultimate linkage stage – fundamental reorganisation of basin-controlling fault system
  - Increased displacement on smaller number of through-going faults
  - Drowning of source regions and/or redirection of drainage systems
- Event so widespread in the stratigraphic record implies fundamental change in stress conditions
  - Increased rate of extension and/or change in orientation

Slide 31

Copperbelt Orebody Member

Hydrological Significance

- Development of transgressive "seal" to lower "aquifer" system + *older fault system*
- Creates loci of elevated strain at tectono-stratigraphic boundary ⟶ *fracture-induced permeability*
  - mechanical and/or rheological contrast
  - decoupling of the stratigraphy during subsequent tectonism (extension and/or inversion)

Slide 32

Rokana - Antelope Phase

Chambishi

Facies Association

- Sheet arenite - dolomitic siltstone - microbial carbonate - evaporite association
- Fluctuating subaerial - marginal marine environments

Facies Architecture

- Layer-cake stratigraphy
- Episodic re-emergence of basement source areas, *but no reactivation of old fault system*
- Final tectonic pulse heralded by Nchanga Quartzite ➔ persistent subaqueous "quiescent" sedimentation

Slide 33

Rokana - Antelope Phase

Konkola Nth

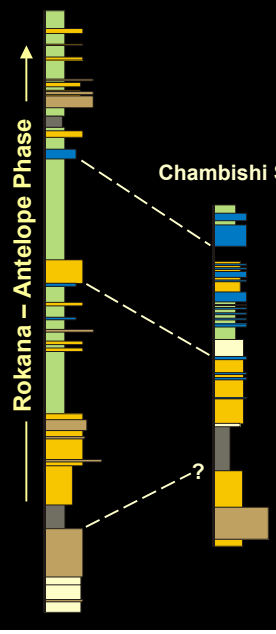

- Sections proximal to "master fault systems" record thicker, deeper water sedimentation
  - greater accommodation development
- Lack of significant evaporitic association
  - ie. Konkola

Slide 34

Rokana – Antelope Phase

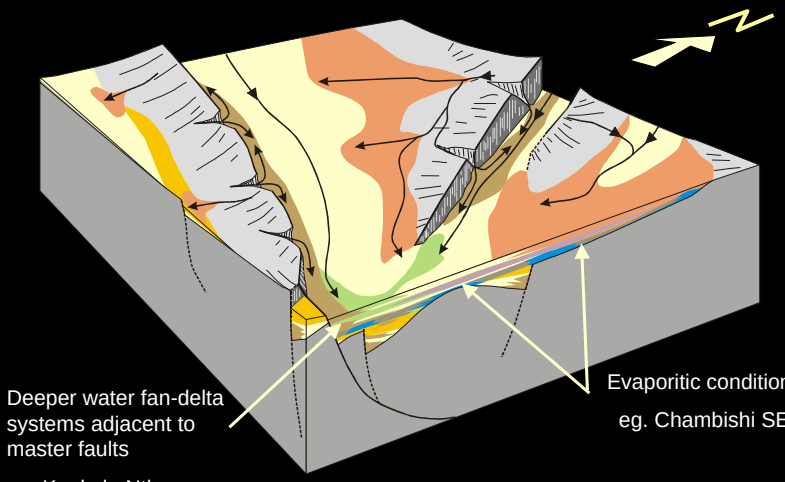

Slide 35

Key Points

- Lower Roan basin evolution is typical of modern rift systems
- Basin architecture records lateral propagation and ultimate linkage of initially discontinuous fault segments
- Principal phase of fault linkage is recorded by the Copperbelt Orebody Member
  - widespread "fault death"
  - transgression of older basin compartments and fault systems
- Basin architecture from onset of rifting to Copperbelt Orebody Member was critical in terms of hydrology & localisation of reductants
  - hydrocarbon accumulations in FW pinch-outs

Slide 36

The evolution of the Willouran Trough

Wallace Mackay
Centre for Ore Deposit Research, University of Tasmania

Introduction

The Willouran Trough is a major depositional compartment within the northern Adelaide Fold Belt. It records the initial rifting of the Adelaide Fold Belt, beginning at about 850 Ma and continuing to about 550 Ma. Within the context of P544, the importance of the Adelaide Fold Belt is that it provides a comparison with the Zambian Copper Belt. Both areas share a similar tectonic setting, they are of a similar age and in both, there is copper, albeit on a much larger scale in the Zambian Copperbelt. The excellent outcrop in the Adelaide Fold Belt and the weight of previous research provide an opportunity to examine basin-scale processes within the Adelaide Fold Belt.

Outcrop within the Willouran Range records the development of the Willouran Trough, with the important exception of the basal package, although its presence is inferred from megaclasts within breccias. It contains the most complete section of the Curdimurka Subgroup, the upper package of the basal Callanna Group, the thickest deposits of the Burra Group within the Adelaide Fold Belt and the important basal sections of the Umberatana Group. The structure within the Willouran Range records the final extension that led to the break-up of Rodinia and the Delamerian Orogeny, which marked the end of rifting within the Adelaide Fold Belt, after about 300 million years of sedimentation. Diapiric breccias cropping out within the Willouran Range provide evidence for the timing and extent of salt tectonic processes within the Willouran Trough, as well as recording the underlying stratigraphy which otherwise does not crop out. And, within the Willouran Range are a number of copper occurrences, which provide data on the mineralisation processes within the Adelaide Fold Belt. Slide 5 shows the locality of the Willouran Trough.

Studies of the Willouran Trough have helped in gaining an understanding of the development of the Adelaide Fold Belt, and the lessons learnt have been used to assist in the understanding of the development of the Zambian Copperbelt. At the same time, the lessons learnt from studying the mineralisation of the Zambian Copperbelt have been used to help understand the mineralisation within the Adelaide Fold Belt and assist in the development of new models that could be applied to the Adelaide Fold Belt.

The Willouran Trough

The Willouran Trough was first named by Preiss (1987), who identified the Willouran Trough as being a northwest trending trough, extending from the Willouran Range to the Peak and Denison Range. It was thought to have been offset by transcurrent faults southwest of Lake Eyre, and narrowing to the north. From Preiss (1987), the Willouran Trough is inferred to refer only to a depocentre into which Callanna Group sediments were deposited. The eastern margin of the trough was not named but it could be inferred to be the Muloorina Gravity Ridge. Likewise, a southern margin is not identified but it could be inferred to be the southern end of the Willouran Range. (Preiss, 1987).

The Willouran Trough continued to be a depocentre during the deposition of the Burra Group but

sedimentation was beginning to step beyond the margins of the trough to the west, onto the Torrens Hinge Zone. To the east, the Muloorina Gravity Ridge likely remained a positive feature in the early to mid Sturtian, but by the Late Sturtian, it too began to be covered by sedimentation (Preiss, 1993). It was in the Sturtian that the Willouran Trough ceased to be a major depocentre, with the depocentre of the northern Adelaide Fold Belt moving to the east, adjacent to the Paralana Fault Zone (Paul et al., 1999).

To better define the Willouran Trough, a South Australia gravity data set was combined with digital geological data, both provided by PIRSA, (Slide 6). From this combination of data sets, it can be seen that the Willouran Trough is best defined as the deep regional gravity low, trending northwest–southeast. The Norwest Fault marks the western edge of the Willouran Trough, with the Torrens Hinge Zone west of the Norwest Fault. It is difficult to define an eastern boundary but there are likely a series of normal faults that define the boundary. At this time, the more general statement of the boundary being the Muloorina Gravity high is retained. To the north, the Willouran Trough thins and is probably cut-off by a transfer fault system. The southern boundary is more complex, with a series of interpreted and mapped faults rotating from parallel to the Norwest Fault in the west to being sub-parallel with the Paralana Fault Zone to the east.

Within the area of the Willouran Trough there are two gravity lows, one along the Norwest Fault and a second broader low to the east, separated by a local gravity high which broadens to the south, rotating from northwest– southeast to east–west. The boundary between the gravity lows and the intermediate high follows interpreted and mapped faults that likely represent individual fault blocks.

Outcrop of the Curdimurka Subgroup and the Burra Group are restricted to the areas of low gravity. Diapiric breccias occur along the margins of the trough and along mapped and interpreted faults within the trough.

The area surrounding the Mt Painter Inlier and the inlier are considered to form part of the Paralana Fault Zone, a transfer fault zone that offsets the southern end of the Willouran Trough. The Mt Babbage Inlier on the other hand is likely a part of the Muloorina Gravity Ridge (Preiss, 1987).

Gravity model of the Willouran Trough

To better define the eastern margins of the Willouran Trough, a gravity profile was modelled, beginning at 174000 mE, 6642000 mN, with an azimuth of 38.5°, and extending for about 100 km. The data that the profile was created from was taken from a set specific to the area of the Willouran Trough, selected from the South Australian gravity data base. The data varies widely in its density, from high data density in the area of the Leigh Creek Coal Field to very low-density regional data set, with a spacing of about nine kilometres. In areas of widely spaced data, there may also be concentrations of more closely spaced data following roads and tracks (Slide 7).

To account for the wide variation in data density, the point data was gridded using Surfer®, with a final grid spacing of one kilometre square. The gridding algorithm used was a standard Surfer® kriging algorithm. Grid data was then exported to the Potent® potential-field modelling program.

The geological constraints for modelling the gravity are from the 1:250,000 Curdimurka and Andamooka map sheets, and the 1:100,000 digital geological data set for the Marree 1:250,000 map sheet. Additional data from fieldwork done as part of this study was used to better define the structure. In areas of no outcrop along the line of the section, geological contacts and structures were extrapolated from areas of outcrop, with the assistance of the gravity data image and the South Australia state magnetic data image.

Density data collected by Utah Development Corporation as part of a gravity survey they undertook in the early 1980s (Rowlands et al., 1981) was used as a guide when assigning bulk densities to stratigraphic blocks used in the model. Additional information for assigning basement bulk densities was taken from Kearey and Brooks (1991). Bulk densities for evaporitic sediments were estimated using data from Barrows and Fett (1985). Densities used for the blocks modelled are listed in Table 1.

Table 1. Densities applied to blocks in preparing the gravity models.

Unit	Density
Basement (granodiorite)	2.72
Basement – low density, model 2	2.58
Paralana Quartzite	2.67 (background)
Evaporites (salt-rich)	2.30
Basalt	3.00
Curdimurka Subgroup (siltstone)	2.58
Emeroo Subgroup (sandstone)	2.65
Skillogalee Dolomite (siltstone-carbonate west of Norwest Fault)	2.68
Skillogalee Dolomite (dolomite-rich, elsewhere)	2.72
Myrtle Springs Formation (i/b carbonate – siltstone)	2.65
Umberatana (undifferentiated)	2.65
Tapley Hill Formation (siltstone)	2.62
Lower Wilpena	2.62, 2.65, 2.70
Upper Wilpena	2.70

The densities taken from the above references were used mainly as a guide, and where necessary were altered to slightly to improve the fit between the observed and modelled gravity. The densities used for the lower Wilpena Group were varied to model individual short-wavelength features. No attempt was made to model the Jurassic to recent sediments that obscure the Adelaidean sediments east and west of the Willouran Range. A background density of 2.67 t/m^3 and a regional value of –20.348 mgal were used.

Slide 8 shows the modelled cross-section with two possible solutions. The long wavelength features reflect the broad geology, a deep trough filled with mostly low-density sediments bounded by steadily rising higher density basement. There is good agreement in the upper part of the density model (above about 8000 m) with the interpreted geology. The position of the Norwest Fault matches the deep, narrow gravity low, and the shape and position of the Burra Group bodies matches the mapped and interpreted geology. The small peaks or inflections in the regional field on the Torrens Hinge Zone and east of the Willouran Trough coincide with the position of known or interpreted fold closures.

The problematic features in the gravity model are the long wavelength anomalies, particularly the deep lows with adjacent highs, which are interpreted to reflect the geology at depth (below 8000 m). Deep level strata comprise the Arkaroola Subgroup. Although highly fragmented in the Willouran Trough, its stratigraphic components and architecture can be inferred from clast-types in diapiric breccias and exposures in the Mt Painter and Peak and Denison Inliers. From mapped geology, the presence of basalt (the Noranda Volcanics) is inferred to be widespread at depth, the thickness of which is estimated to be about 1000 m, from the outcrop of Wooltana Volcanics around the Mt Painter Inlier (Preiss, 1987). The presence of quartzite, the Paralana Quartzite equivalent is also assumed and although its thickness varies, it may be up to 1000 m thick.

In the first model (Slide 8a), a basement bulk density of 2.72 t/m^3 is used, this figure being from the upper end of average values for granodiorite (Kearey and Brooks, 1991). The gravity model suggests that to balance the high-density basement and basalt, about 1500 m of lower density material is required. As field evidence suggests that the source of diapirs in the Willouran Trough is the Arkaroola Subgroup (see below) the first model has an evaporite sheet at depth. The second problem is the narrow deep gravity low along the Norwest Fault. Modelling of this feature suggests the presence of a narrow body of low-density material approaching the surface. A diapir is modelled to account for the gravity low. Although there are no diapirs mapped on the section, diapirs have been mapped along the Norwest Fault to the northwest and southeast.

A second model (Slide 8b) excludes salt at depth. That is, the salt that caused the diapirism has been removed by salt evacuation and dissolution. Salt may still be present in diapirs however. To account for the long wavelength gravity lows, a block of low-density

basement beneath the Willouran Trough was introduced. The density for this material was taken from the published density of the Hiltaba Granite Suite (Gow et al., 1993), which is present in the Gawler Craton, west of the Willouran Trough. It is unlikely that a block of low-density basement, either Hiltaba Suite Granite or a Mt Painter Block equivalent, would be restricted to beneath the Willouran Trough only. Salt diapirs are still required along the Norwest Fault however to produce the pronounced gravity low at this position.

Evidence, albeit circumstantial, in favour of there being low-density basement beneath the Willouran Trough comes from three sources. Gow et al. (1993) interpret a regional gravity low on the Stuart Shelf to be due to a body of Hiltaba Suite Granite, intruded into metagranite beneath an eroded caldera complex filled with Gawler Range Volcanics. The width of the anomaly is about 50 km, a similar size to the anomaly associated with the Willouran Trough, and it too has a central high between two lows. Selley (2000) also suggests that a pronounced gravity low beneath the Spencer Gulf is also related to Hiltaba Suite Granites. Finally, there is a weak gravity low over the Mt Painter Block (Slide 5), in which radiogenic Palaeoproterozoic to Mesoproterozoic granites and metamorphic rocks crop out (Coats and Blisset, 1971; Elburg et al., 2001). Sandiford and McLaren, (2002) suggest that the position of rifts may be influenced by the presence of crust weakened by high heat flow. The Hiltaba Suite Granites and the Mt Painter Block are enriched in radiogenic elements and are associated with high heat flows (Neumann et al., 2000). Hence, it is possible that the presence of hot low-density granites, of either the Hiltaba Suite Granites or basement similar to the Mt Painter Block, may have influenced the position of the Willouran Trough.

Slide 9 shows a cross-section from the interpreted geological model. The preferred model is that salt is not present as a broad blanket at depth and although diapirs are not shown in the cross-section (they do not crop out along the line of section), their presence along the Norwest Fault is accepted. The Curdimurka Subgroup thickens considerably at depth, in the hanging walls of the Norwest Fault and West Willouran Fault. The thickening is tectonic, and elsewhere the Curdimurka Subgroup is tectonically thinned.

From the cross-section, the broad features of the Willouran Trough are:

- The Norwest Fault is a first order fault on the western side of the trough,
- Normal Faults on the Torrens Hinge Zone probably became active during deposition of the Burra Group, with faults gradually stepping west with time.
- The eastern bounding fault has been obscured by later sedimentation
- The overall structure is graben generated on the hanging wall of a major northeast-dipping detachment, with the deepest part of the trough along the Norwest Fault.
- There is a central horst, which likely remained a basement high until some time during the deposition of the Curdimurka Subgroup.
- The Curdimurka Subgroup slightly over-steps the trough
- The Emeroo Subgroup of the Burra Group is thickest within the trough, but is present on the trough shoulders
- The Skillogalee Dolomite and the Myrtle Springs Formation are thickest within the trough but overstep the margins; the Myrtle Springs Formation oversteps the Skillogalee Dolomite.

The basement is not differentiated in this cross-section.

Basin Fill

Within the Willouran Range, three of the four basin phases of the Adelaide Fold Belt are exposed; the Callanna Group, the Burra Group and the Umberatana Group. The fourth and last basin phase, the Wilpena Group crops out either side of the Willouran Range. There is no doubt that the first three groups were deposited within the Willouran Trough but the lack of outcrop of the Wilpena Group sug-

gests that it was not deposited at all or was deposited and then eroded during the basin inversion in the Delamerian Orogeny. Slide 3 is a stratigraphic table for the Adelaide Fold Belt and Slide 10 is a geological map of the Willouran Range.

Arkaroola Subgroup

Diapiric breccias are mapped along the Norwest Fault, Bungarider Fault and the West Willouran Fault. There is also a diapiric breccia, the Breaden Hill Breccia mapped above the Curdimurka Subgroup and the Burra Group about 10 km south of Marree. A diapiric breccia is mapped at the intersection of the Norwest Fault and the South Hill Structure but work completed as part of this project suggests that the cause of brecciation in this area is not diapiric intrusion but is likely thrust-related. Other diapiric breccias are mapped along the southeastern edge, and north of the South Hill Structure, and together these breccias are the Witchelina Diapir. Within the diapiric breccias are blocks of mafic meta-volcanics and meta-limestone (the Black Knob Marble) that are assigned to the Arkaroola Subgroup. Also present are blocks of sandstone and dolomite but these are not diagnostic as they could be sourced from either the Arkaroola Subgroup or the Curdimurka Subgroup. Sandstone blocks could be sourced from a Paralana Quartzite equivalent carbonate blocks, including the Black Knob Marble, are equivalent to the Wywyana Formation and the mafic blocks are from the Noranda Volcanics, correlative to the Wooltana Volcanics. The source of the salt that formed the diapirs is a correlative of the Wywyana Formation.

Curdimurka Subgroup

The Curdimurka Subgroup crops out in a series of fault slices along the Norwest Fault, the Bungarider Fault and east of the West Willouran Fault. It is also present in the South Hill Structure and the Witchelina Diapir. Along the Norwest Fault, the Bungarider Fault and the South Hill Structure, only the Dome Sandstone is present, overlain by interbedded siltstone, sandstone and carbonates, which may correlate with the Dunns Mine Limestone. The stratigraphy above this level is entirely missing except east of the West Willouran Fault, where the stratigraphy has been tectonically dismembered. Only at the northern end of Witchelina Station is there a complete section of Curdimurka Subgroup. Within the Witchelina Diapir, the Curdimurka Subgroup is thickened by repetition of the Dome Sandstone, probably due to thrusting. East of the West Willouran Fault, the Curdimurka Subgroup is tectonically thinned beneath the Burra Group, but where the Burra Group is absent, above the Witchelina Diapir and the northern end of Witchelina Station, the Curdimurka Subgroup is thickened.

Burra Group

The Burra Group crops out in a series of east-facing slices between the major faults. Some authors (e.g., Belperio, 1990, Dyson, 2002) consider these slices to be sub-basins, having formed between rising salt walls. The favoured interpretation here is that the Burra Group outcrop is a series of thrust slices through a single basin. West of the Norwest Fault, the Burra Group is west facing, and thinned relative to east of the fault. In total, there is over 6000 m of Burra Group sediments within the Willouran Trough.

Umberatana Group

The Umberatana Group crops out adjacent to the Bungarider Fault and west of the West Willouran Fault, in small, fault-bounded basins. In these outcrops, the Umberatana Group is thinned, relative to the west of the Norwest Fault and east of the West Willouran Fault. The greatest thickness of Umberatana Group is east of the West Willouran Fault, where it is a minimum thickness of 8000 m (Preiss, 1987).

Curdimurka Subgroup

Understanding the Curdimurka Subgroup is important for three reasons;

- its sedimentology can assist in understanding the source of the salt in the Willouran Trough;
- the structure of the Curdimurka Subgroup can help decipher the development of the Willouran Trough;

- and in the context of this study, it is important to know where the Curdimurka Subgroup occurs within the basin stratigraphy.

The latter point can be dealt with quickly. Initially it was thought that the Curdimurka Subgroup may have been the basal unit of the Adelaide Fold Belt in the Willouran Trough, but as has been shown above, the Arkaroola Subgroup is present at depth. The question of the salt is dealt with in this section and the next and the structure of the Curdimurka Subgroup is discussed below.

The type section of the Curdimurka Subgroup occurs at the northern end of Witchelina Station. It is about 4000 m thick but the structural complexity of the area excludes the calculation of an exact true thickness. A stratigraphic section is shown in Slide 11. Mapping undertaken in the type area as part of this project is shown in Slide 12.

The Curdimurka Subgroup is a siltstone-dominated package, with two carbonate units, the Dunns Mine Limestone and the Hogan Dolomite, and a sandstone unit at its base, the Dome Sandstone. There are three black shale units (deposited below wave base), each over 80 m thick. A volcanic unit above the Dome Sandstone, the Rook Tuff has been dated at 802 ± 11 Ma (Fanning et al., 1986).

Evaporite pseudomorphs are common throughout the section, from the Dome Sandstone to the top of the Boorloo Siltstone. Halite and gypsum pseudomorphs have been identified and shortite has been reported, however, one of the occurrences of shortite has been identified in this study as scapolite. There is no evidence of thick salt deposits that might have been responsible for diapirism.

The lower contact of the Curdimurka Subgroup is everywhere tectonic. In the type area, the basal contact of the Curdimurka Subgroup is a fault, with northeast facing Dome Sandstone in contact with southwest facing Cooranna Formation or diapiric breccia. Elsewhere the lower contact is with upper units of the Burra Group.

The upper contact of the Curdimurka Subgroup is also tectonic. In the type area, north of the Breaden Hill Breccia, the Boorloo Siltstone is separated from the Umberatana Group by a diapiric breccia. A shear zone of variable width occurs along the contact, with the shearing occurring within the breccia and along the contact. Within the breccia, both the matrix and megaclasts are sheared (Slide 14). South of the Breaden Hill Breccia, the Boorloo Siltstone is in contact with the Burra Group. The contact is a shear zone, with shearing and brecciated zones from less than 5 m to greater than 200 m mapped (Slide 14). Here the brecciation is tectonic, with massive sandstones within the Burra Group being brecciated and inter-bedded siltstones and sandstones being sheared. Either side of the tectonic zone, bedding within the Boorloo Siltstone and the Burra Group is sub-parallel.

Salt and Callanna Group

There has been much work reported on diapirism in the Adelaide Fold Belt, with the source of the salt thought to be the Callanna Group (e.g., Dalgarno and Johnson, 1966; Mount, 1975; Lemon, 1985). Further evidence for this interpretation comes from the Willouran Trough, however the lithofacies of the Curdimurka Subgroup indicates that it was not a major source of the salt. Instead, the Curdimurka Subgroup is intruded by exotic diapiric breccias at several levels. Diagnostic clasts within the breccias comprise basic meta-volcanics (the Noranda Volcanics), clasts of Black Nob Marble, other large carbonate clasts that do not appear to be sourced from the Curdimurka Subgroup, and rare basement clasts including BIF and granite.

Along the western edge of the Curdimurka Subgroup type area, the Dome Sandstone has been brecciated along its entire length of outcrop. The brecciation has dismembered the Dome Sandstone into a series of blocks up to hundreds of metres across, some of which are conformable with the overlying stratigraphy, and other blocks that are bounded by and intruded by breccia. Between blocks, diapiric breccia has intruded up to and beyond the level of the Rook Tuff. In two localities the diapiric breccia has intruded to the top of the Dunns Mine Limestone and in one area, the brecciation intrudes to the base of Sandstone 1 of the Recovery Formation. Diapiric

breccia also occurs in the core of an anticline about 2 km southeast of Callanna Homestead. A sheet of diapiric breccia occurs at the contact between the Dunns Mine Limestone and the Recovery Formation, northwest of Dunns Mine. Breccia is mapped beneath Sandstone 1 of the Recovery Formation, but his may be part diapiric breccia, part tectonic breccia, the poor outcrop does not allow a definite conclusion, and the megaclasts present are not diagnostic. The final breccia, the Breaden Hill Breccia, occurs at the top of the Curdimurka Subgroup, beneath the Umberatana Group.

Field evidence shows that the timing of diapirism was active at about the time of initiation of the deposition of the Umberatana Group. Slide 22a shows clasts of tillite within a distinctive orange-weathering dolomite megaclast from the Breaden Hill Breccia, but Slide 22b shows a clast of the dolomite from within the tillite, indicating that the tillite had to be present when the diapir was forming but also the diapir had to be at the surface to be included within the tillite. Selley and Bull (2002) similarly showed that the breccias were emergent at the same time the Yudnamutana Subgroup was being deposited.

Salt tectonics played a role in the development of the Willouran Trough; the mobilisation of salt out of the trough along the marginal faults created space and the dissolution of salt, created space into which the Yudnamutana Subgroup was deposited. The area of the Willouran Trough underwent thin-skinned extension whereas outside of the Willouran Trough, thick-skinned extension dominated. As a result, the faults controlling deposition of the Umberatana Group within the area of the Willouran Trough are shallow angle listric faults, soling out into the Curdimurka Subgroup and the Arkaroola Subgroup and it is the effect of these shallow faults that give the Curdimurka Subgroup its distinctive deformation style.

Structure of the Curdimurka Subgroup

As has been reported previously (Mackay, 2002), the Curdimurka Subgroup has undergone three deformations; the first produced layer-parallel cleavages and recumbent folds; the second deformation produced close to tight upright folds, trending northwest–southeast with shallow plunges and the third deformation resulted in open folds, with steep plunges to the southwest and a widely spaced axial planar cleavage. However, the dominant structural style within the Curdimurka Subgroup is faulting. In outcrop, the major fault style appears to be strike slip but relative to bedding, the dominant fault styles are low angle normal and reverse faults. The apparent strike slip movement observed today is due to the rotation of horizontal structures to vertical during D_2.

At the outcrop scale thrusting is common, however mesoscopic thinning of the Curdimurka Subgroup indicates that major structures were extensional. Thrusts with movements of tens to hundreds of metres are present but these have formed as a response to local barriers on the normal fault systems.

Within the mapped area, there are several through-going normal fault systems. Slide 17shows the major fault systems. The upper-most system begins at the northern part of the area occurring at the top of the Boorloo Siltstone. As this fault system moves south, the fault cuts down through the Boorloo Siltstone, bringing the Burra Group into contact with the Cooranna Formation. Continuing south, the Cooranna Formation is cut out and the Burra Group is in contact with the Dunns Mine Limestone, indicating a loss of about 3000 m of stratigraphy.

The first outcrop of the next fault system occurs at the north end of the mapping area, with the Boorloo Siltstone in contact with the Recovery Formation. Moving to the south, the fault has cut down through the Boorloo Siltstone and Cooranna Formation, and finally the Hogan Dolomite, where it splits into two sections. The upper fault cuts up-section producing a series of south-directed thrusts that are developed within the Cooranna Formation. The lower fault continues along the base of the Hogan Dolomite, parallel to bedding until it cuts out the Hogan Dolomite at the southern end of its outcrop, meeting the upper fault once again, effectively boudinaging the Hogan Dolomite. Above the Hogan Dolomite, thrusting is the controlling mechanism in the Cooranna Formation. The south-directed thrusts are cut by north-directed reverse faults, indicating two direc-

tions of fault movement, a first south to southeast directed movement and a second, north to northwest directed movement; the south-directed transport having the largest movement. At the southern end of the Hogan Dolomite outcrop, the fault system cuts out the lower two thirds of the Curdimurka Subgroup, then moves parallel to bedding before it is truncated by the upper fault system.

Within the Recovery Formation, a series of bedding-parallel fault zones occur at the top and base of the sandstone units. Above Sandstone 2, decollement folds occur at the southern end of the Hogan Dolomite outcrop and in the north of the area. A series of small thrusts and reverse faults splay off the bedding-parallel faults, cutting up section in the siltstones, where the faults are marked by narrow breccia zones and over-turned synclines in the footwalls. The larger of the thrusts have a south-southwest transport direction. Below Sandstone 1 is a fault that has caused over-turning of bedding in the siltstone below, and is probably a thrust, with transport direction to the south-southwest. Along the line of this fault are a number of small, isolated carbonate blocks that are probably diapiric in origin. The faults when traced to the south act as normal faults, faulting out stratigraphy within the Recovery Formation, until all of the Recovery Formation has been removed.

In the northwest of the mapping area is a northwest-trending fault that brings southeast-facing Recovery Formation, Siltstone 2 against northwest facing Recovery Formation siltstones, probably also Siltstone 2. It is likely a faulted-out synclinal hinge associated with the anticline to the northeast.

The last major fault system occurs at the base of the Dome Sandstone, with northeast-facing Dome Sandstone is adjacent to southwest-facing Cooranna Formation, indicating that this fault is an anticline with the hinge faulted out. Within the fault zone is diapiric breccia and tectonic breccias. The Boorloo Siltstone is in contact with the Myrtle Springs Formation of the Burra Group, along an extension of the West Willouran Fault. Southwest of the fault is a syncline within the Burra Group and the present fault system orientation is attributed to D_2.

The dominant movement on the fault systems above the Recovery Formation is to the south or southeast, the same transport direction indicated by the F_1 recumbent folds. Faults with a reverse movement that is north to northwesterly-directed transport post-date the southerly transport faults, but the associated folds have steep plunges similar to F_1 fold plunges, so they predate D_2. These faults are considered to also be within D_1. The faulting within the Recovery Formation has transported directions to the south or southeast, as well as south-southwest transport directions, which indicates either inhomogeneous deformation during D_1, or possibly some thrusting during D_2. No conclusion on this is given here; it is still being addressed.

D_1 is the result of a vertical F^1. Ductile units such as the siltstone- and shale-rich Cooranna Formation, Boorloo Siltstone and Recovery Formation have deformed by flowing. The more brittle Dome Sandstone and Hogan Dolomite deformed in a brittle manner and have broken apart. As stress continued, the ductile layers eventually broke apart, forming the ramp and flat pattern of normal faulting observed. Thrusting within the Cooranna Formation was caused by the boudinage of Hogan Dolomite; as the ductile units flowed around the obstacle, the flow became turbulent and faults broke up-section, forming thrusts. Diapiric breccia flowed into the spaces created, particularly between the blocks of Dome Sandstone, and below the Recovery Formation. Strain was partitioned into layers, producing the layer-parallel deformation such as recumbent folds, thrusts, low-angle normal folds and locally, a layer-parallel cleavage. Slide 18 is a diagrammatic interpretation of the structure in the mapping area.

Deformation at the regional scale

What is seen at the local scale reflects the regional response to D_1. The Curdimurka Subgroup is a thick, siltstone dominant package; the Burra Group is mainly a clastic and carbonate package. Beneath the Curdimurka Subgroup, the Arkaroola Subgroup comprises the (relatively) low viscosity Wywyana Formation and the brittle Noranda Volcanics. A decollement likely formed between the Wywyana Formation and the Paralana Quartzite, decoupling

the Paralana Quartzite and basement from the sediments above the Paralana Quartzite.

Slide 20 shows the affect of D_1 at the regional scale. The ductile packages have responded to D_1 by flowing and the more brittle packages have broken apart. Hence, the Burra Group has behaved in a brittle manner, breaking apart into large tablets and the more ductile units have moved into the space created; the evaporitic Wywyana Formation has formed diapirs but the Curdimurka Subgroup has also thickened into the gaps between the tablets of Burra Group. Thickening of the Curdimurka Subgroup between the blocks of Burra Group has been balanced by its tectonic thinning beneath the Burra Group. Salt withdrawal and dissolution has accommodated much of the extension and created additional space for the deposition of the Umberatana Group. As a whole, the Willouran Trough has undergone thin-skinned extension during deposition of the Umberatana Group and the Yudnamutana Subgroup in particular. Thin-skinned extension results in large rotations of hanging wall blocks, which gives large the large-angle unconformities observed between the Burra Group and the Yudnamutana Subgroup (Selley and Bull, 2001) (Slide 23).

Outside the Willouran Trough, the extension has been thick-skinned. During basin inversion in the Delamerian Orogeny, D_2 for the Curdimurka Subgroup, the extensional faults have been reactivated as reverse faults, which gives rise to the differences in structural styles observed between the Willouran Trough area and the Torrens Hinge Zone and interpreted for the area to the east of the Willouran Trough. Folds within the area of the Willouran Trough have large amplitudes relative to their wavelengths whereas outside the D_2 folds have lower amplitudes and longer (relative) wavelengths (Slide 9).

Copper and the Willouran Trough

As has been noted by various authors, there is a link between diapiric breccias and the copper mineralisation within the northern Adelaide Fold Belt (Dyson, 2002; Selley, 2000) (Slide 25). The majority of copper occurrences are either within diapiric breccias or are in close proximity to the margins of the breccias. Occurrences in close proximity to breccias occur at several levels of the stratigraphy, including the Curdimurka Subgroup, the Tapley Hill Formation and the Bunyeroo Formation; the common factor being that the host lithology is a reduced siltstone or shale. Mineralisation within the breccias occurs within megaclasts, of which Blinman is the most notable example, or within the matrix.

Using the Zambian Copperbelt and the Kupferschiefer as the prime examples of stratiform mineralisation, within the Adelaide Fold Belt, the same level of stratigraphy does not outcrop except in a few places; around the margins of the Mt Painter Inlier and the Peak and Denison Inlier, northwest of the Willouran Trough. It may be that the copper occurrences observed shows that a copper mineralisation system (or systems) has been working. Mineralisation within breccia megaclasts may represent the primary mineralisation, the mineralised clasts having been ripped from the position of original deposition and transported by the movement of salt. Mineral occurrences at the margins of the diapirs and within the breccia matrix may represent the last gasps of that system; diapirism having broken the seal of the system, the evaporite layer. A second mechanism to explain the mineralisation at the margins of diapirs is, the salt walls create hydrothermal cells within the sediments above the salt layer; the size of deposits formed is limited by the size of the cell and this may explain the small size of the deposits. The presence of the mineralised megaclasts suggest that at depth, there is potential for copper mineralisation, not only within the Willouran Trough but wherever copper mineralisation has been noted adjacent to or within diapiric breccias.

Conclusion

To conclude, the evolution of the Willouran Trough is summarised in Slides 26 and 27.

Development of the Willouran Trough began with northeast–southwest extension at about 850 Ma. From outcrop information outside the margins of the trough, megaclasts within breccias and from interpretation of gravity data, a thick unit of sand-

stone, the Paralana Quartzite was deposited within the trough, followed by a thick evaporitic unit, the Wywyana Formation. Deposition of the Wywyana Formation was ended with the eruption of flood basalt, the Noranda Volcanics at about 827 Ma.

The Curdimurka Subgroup was deposited in the next phase of the Willouran Trough. At the base is about 1000 m of the Dome Sandstone and then followed about another 3000 m of mainly siltstone, with lesser carbonates and minor sandstone and black shale. The Curdimurka Subgroup contains evaporite pseudomorphs after gypsum, anhydrite and halite throughout and was deposited in the sag phase of the trough. It is probable that at this time, the basin was undergoing thermal relaxation after the eruption of the flood basalts. As a result, there is an absence of high-energy sediments (conglomerates and sedimentary breccias) and it may explain the large thickness of mainly shallow-water sediments that comprise the Curdimurka Subgroup.

At about 780 Ma, the next phase of the basin development began with the deposition of the Burra Group. The basal clastic units of the Burra Group were largely confined to the area of the trough, and although the Norwest Fault was still the dominant fault along the western edge of the trough, rifting had extended to the west of the Norwest Fault. Extension continued with the deposition of the Skillogalee Dolomite but during this stage, the basin went into the sag phase, which continued with deposition of the Myrtle Springs Formation.

At about 750 Ma, the next phase of rifting began with the deposition of the Yudnamutana Subgroup of the Umberatana Group. Within the Willouran Trough extension was thin-skinned, with salt tectonics and the silt-dominated Curdimurka Subgroup accommodating extension. Extension was occurred in two dimensions, with the Burra Group undergoing brittle failure, forming a chocolate block structure. Salt migration and dissolution created extra space within the trough, allowing a large thickness of the Yudnamutana Subgroup to be deposited. Outside the Willouran Trough, extension was thick-skinned, with the extensional faults soling out at depth into an east-dipping shallow normal fault, which controlled the extension. The controlling fault cropped out to the west of the Willouran Trough, along boundary between the Torrens Hinge Zone and the Stuart Shelf. It was during deposition of the Tapley Hill Formation that sedimentation stepped beyond the bounds of the rift for the first time.

Diapirism was active at the beginning of deposition of the Umberatana Group, the diapirs forming along the Willouran Trough margins and between blocks of Burra Group. It is possible that a copper mineralisation system was active at some time prior to diapirism but diapirism broke the seal to the system, allowing mineralising fluids to escape and form small, low-grade deposits wherever those fluids met a reduced environment.

Basin inversion during the Delamerian Orogeny reactivated the listric normal faults as reverse faults. Most of the Umberatana Group was eroded from the Willouran Trough, leaving the remnants that outcrop today. These remnants were originally deposited near the hinge points of the original half-grabens, hence the relatively thin packages observed.

References

Barrows, L and Fett J.D., 1985. A high-precision gravity survey in the Delaware Basin of southeastern New Mexico. Geophysics 50, 825 Ð 833.

Belperio, A.P., 1990. Palaeoenvironmental interpretation of the Late Proterozoic Skillogalee Dolomite in the Willouran Ranges, South Australia. In Jago, J.B. and Moore, P.S., The evolution of a late Precambrian - early Palaeozoic rift complex: the Adelaide Geosyncline. Geological Society of Australia, Special Publication 16, 85-104.

Coats, R.P., and Blisset, A.H., 1971. Regional and economic geology of the Mount Painter Province. Geological Survey of South Australia Bulletin 43.

Dalgarno, C.R and Johnson, J.E., 1968. Diapiric structures and late Precambrian-early Cambrian sedimentation in Flinders Ranges, South Australia. American Association of Petroleum Geologists Memoir 8, 301-314.

Dyson, I.A., 2002. Adelaidean sedimentation and the timing of salt tectonics in the east Willouran Ranges. 16th Australian Geological Convention, Adelaide South Australia. Geological Society of Australia Abstracts 17, 380.

Dyson, I.A., 2001. The diapir Ð base metal association in the northern Flinders Ranges. Mesa Journal 22, 37-43.

Elburg, M.A., Bons, P.D., Dougherty-Page, J., Janka, C.E., Neumann, N and Schaefer, B., 2001. Age and metasomatic alteration of the Mt Neill Granite at Nooldoonooldoona Waterhole, Mt Painter Inlier, South Australia. Australian Journal of Earth Sciences 48, 721-730.

Fanning. C.M., Ludwig, K.R., Forbes, B.G. and Preiss, W.V., 1986. Single and multiple grain U-Pb zircon analyses for the early Adelaidean Rook Tuff, Willouran Ranges, South Australia. In 8th Australian Geological Convention, Adelaide, 1986. Abstracts of the Geological Society of Australia 15, 71-72.

Gow, P.A., Wall, V.J. and Valenta, R.K., 1993. The regional geophysical response of the Stuart Shelf, South Australia. Exploration Geophysics 24, 513-520.

Kearey, P and Brooks, M., 1991. An introduction to geophysical

exploration (2nd edition). Blackwell Scientific Publications, Oxford. 254p.

Lemon, N.M., 1985. Physical modelling of sedimentation adjacent to diapers and comparison with late Precambrian Oratunga breccia body in central Flinders Ranges, South Australia. Bulletin of the American Society of Petroleum Geologists 69, 1327 Ð 1338.

Mackay, W.G., 2002. The structural history of the Curdimurka Subgroup, Willouran Range, South Australia. AMIRA / ARC Project 544. December 2002 Report.

Mount, T.J., 1975. Diapirs and diapirism in the Adelaide Geosyncline, South Australia. University of Adelaide Ph.D.thesis (unpublished).

Neumann, N., Sandiford, M. and Foden, J., 2000. Regional geochemistry and continental heat flow; implications for the origin of the South Australian heat flow anomaly. Earth and Planetary Science Letters, 183, 107-120.

Paul, E., Flottmann, T. and Sandiford, M., 1999. Structural geometry and controls on basement-involved deformation in the northern Flinders Ranges, Adelaide Fold Belt, South Australia. Australian Journal of Earth Sciences 46, 343 - 354.

Preiss, W.V., 1987. The Adelaide Geosyncline: Late Proterozoic stratigraphy, sedimentation, palaentology and tectonics. The Geological Survey of South Australia, Bulletin 53, 438p.

Priess, W.V., 1993. Neoproterozoic. In Drexel. J.F., Preiss, W.V. and Parker, A.J., (Eds). The Geology of South Australia, Volume 1; The Precambrian. Geological Survey of South Australia, Bulletin 54, 171-203.

Rowlands, N.J., Jarvis, D.M., Benade, D.R., Circosta, G. and Blight, P.G., 1981. S.A. stratiform copper project, EL. 461 Willouran Ranges. Fourth annual report on exploration activities (period 24.12.79–3.4.81). Utah Development Company Report No. 338 (unpublished).

Selley, D. and Bull, S., 2001. Basin architecture during deposition of the lower to middle Umberatana Group, Adelaide Fold Belt, South Australia; implications for Cu mineralisation. *In* P544 - Proterozoic sediment-hosted copper deposits. AMIRA / ARC Progress Report December 2001, 1-45.

Sandiford, M. and McLaren, S., 2002, Tectonic feedback and the ordering of heat producing elements within the continental lithosphere, *Earth and Planetary Science Letters,* 2002, 204, 133-150.

Selley, D., 2000. Proterozoic sediment hosted copper deposits. Geological framework and copper mineralisation of South Australia. AMIRA / ARC Research Project 544, December 2000 Meeting.

Wingate, M.T.D., Campbell, I.H., Compston, W. and Gibson, G.M., 1998. Ion microprobe U-Pb ages for Neoproterozoic basaltic magmatism in south-central Australia and its implications for the break-up of Rodinia. Precambrian Research 87, 135-159.

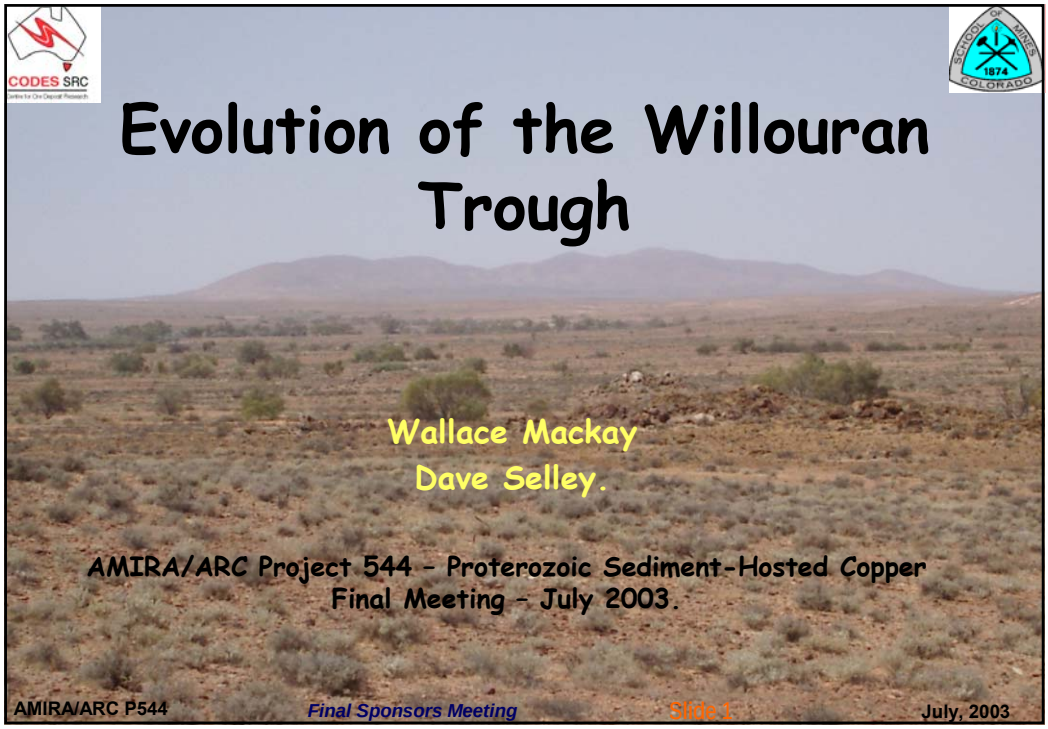
CODES SRC
SCHOOL OF MINES 1874 COLORADO
Evolution of the Willouran Trough
Wallace Mackay
Dave Selley.
AMIRA/ARC Project 544 – Proterozoic Sediment-Hosted Copper
Final Meeting – July 2003.
AMIRA/ARC P544
Final Sponsors Meeting
Slide 1
July, 2003

CODES SRC
SCHOOL OF MINES 1874 COLORADO
Introduction
• The Willouran Trough
• Stratigraphy of the Curdimurka Subgroup
• Structure of the Curdimurka Subgroup II
• Regional Structure
• Whither the copper?
• Conclusions
AMIRA/ARC P544
Final Sponsors Meeting
Slide 2
July, 2003

The Willouran Trough – three features that need explaining.

1. Thinning of CSG beneath Burra Group
2. Thickening of CSG where Burra Group absent
3. Breccia along margins of CSG and faults

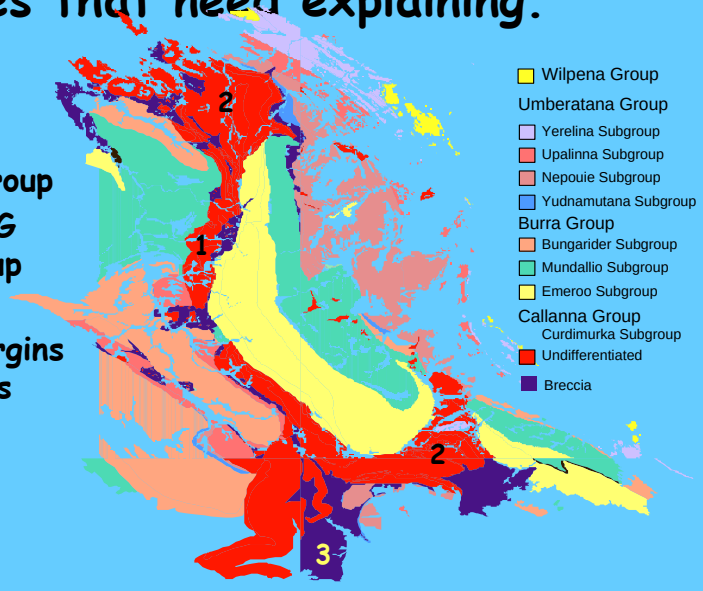

AMIRA/ARC P544 *Final Sponsors Meeting* Slide 3 July, 2003

Reminder of the Adelaide Fold Belt Stratigraphy

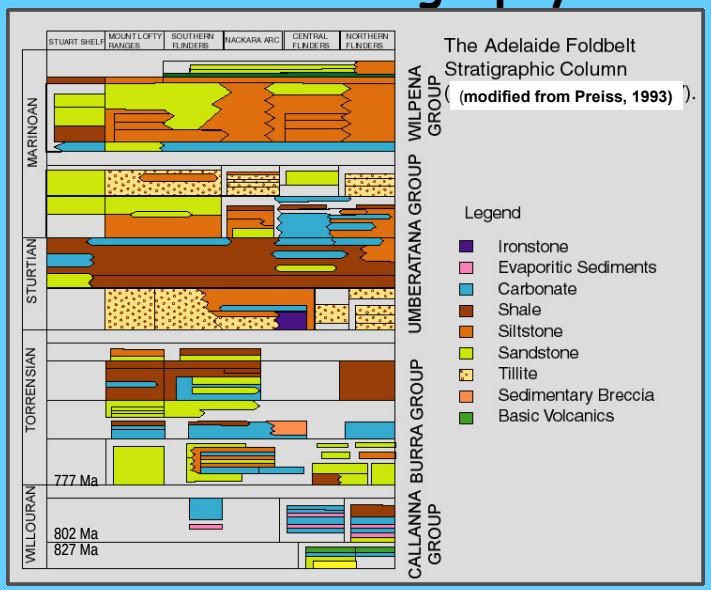

AMIRA/ARC P544 *Final Sponsors Meeting* Slide 4 July, 2003

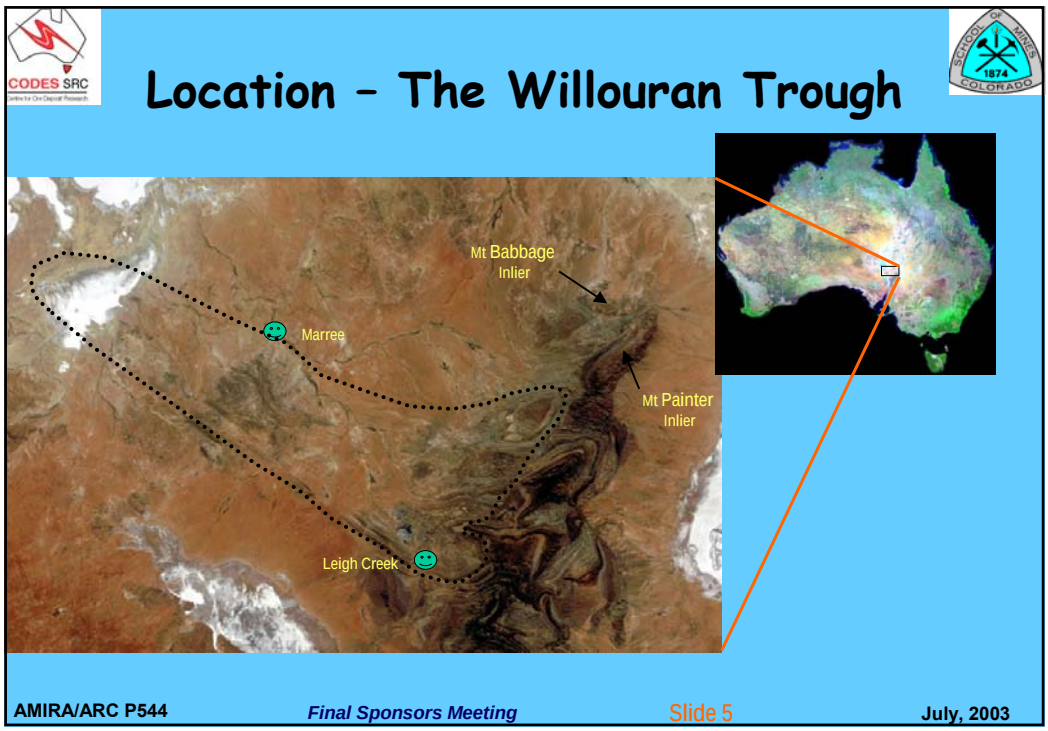
Location – The Willouran Trough
Mt Babbage Inlier
Marree
Mt Painter Inlier
Leigh Creek
AMIRA/ARC P544
Final Sponsors Meeting
Slide 5
July, 2003

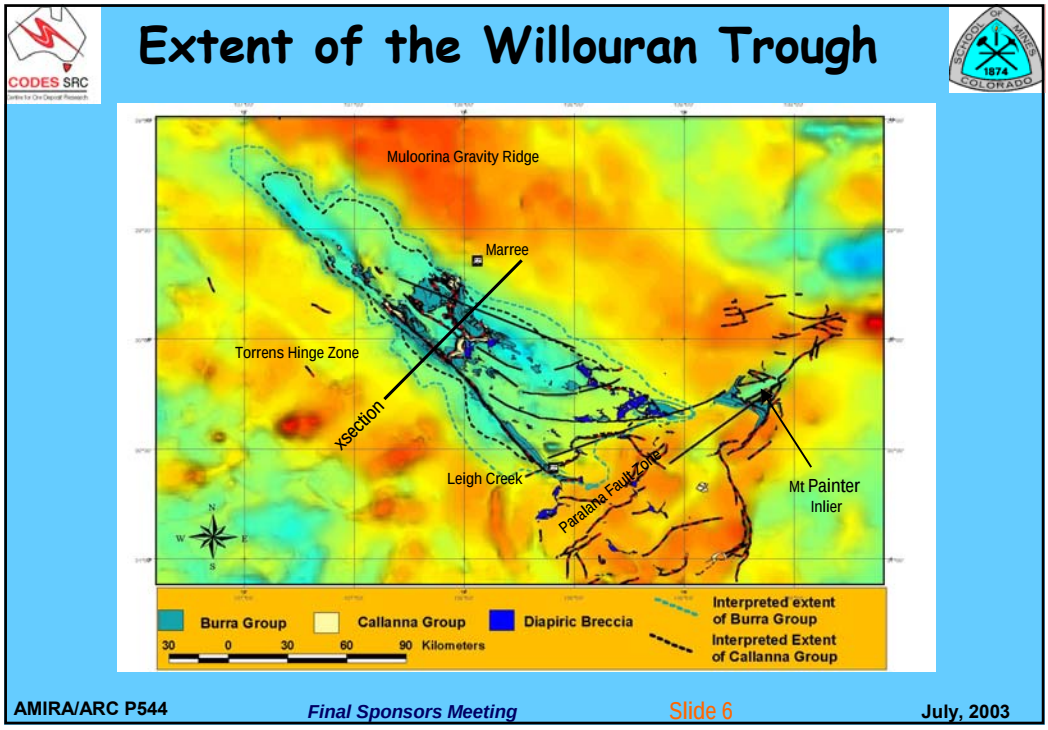
Extent of the Willouran Trough
Muloorina Gravity Ridge
Marree
Torrens Hinge Zone
xsection
Leigh Creek
Paralana Fault Zone
Mt Painter Inlier
Burra Group
Callanna Group
Diapiric Breccia
Interpreted extent of Burra Group
Interpreted Extent of Callanna Group
30 0 30 60 90 Kilometers
AMIRA/ARC P544
Final Sponsors Meeting
Slide 6
July, 2003

Distribution of Gravity Data

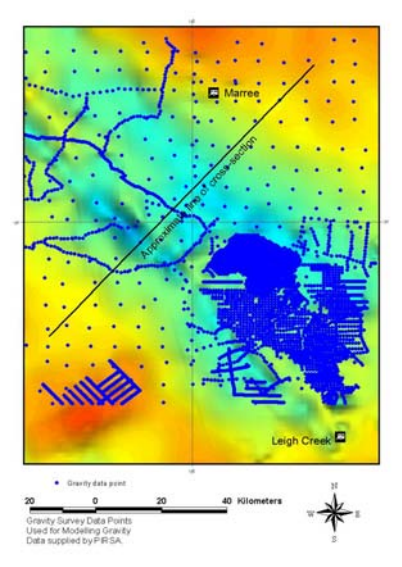

AMIRA/ARC P544 *Final Sponsors Meeting* Slide 7 July, 2003

Cross-section 1

Two alternatives: Salt and No Salt

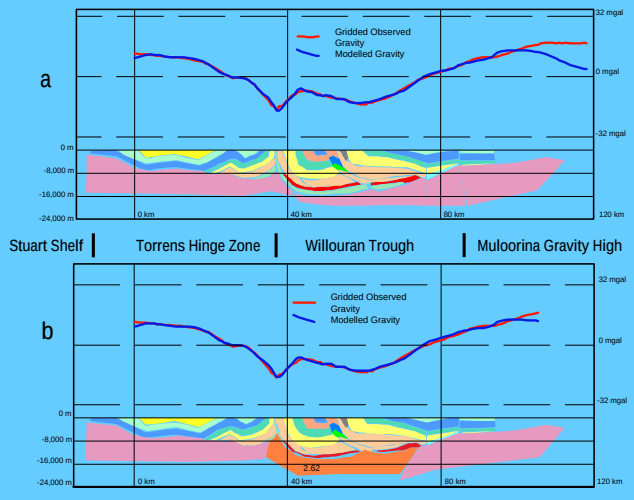

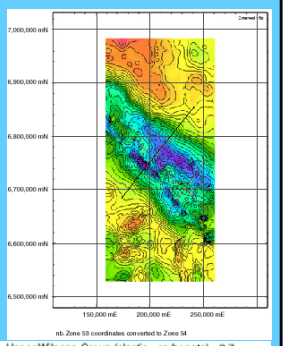

Upper Wilpena Group (clastic - carbonate) - 2.7
Lower Wilpena Group (clastic) - variable
Umberatana Group (siltstone) - 2.62
Myrtle Springs Formation (carbonate - siltstone) - 2.65
Skillogalee Dolomite (dolomite) 2.68 - 2.72
Emeroo Subgroup (sandstone) - 2.65
Mega-clast within breccia - 2.70
Curdimurka Subgroup (siltstone) - 2.58
Wooltana Volcanics (basalt) - 3.00
Wywyana Formation (evaporites) - 2.30
Hiltaba Suite Granite - 2.62
Other basement (granite - granodiorite) - 2.72

origin: 174,000 mE, 6,642,000 mN
azimuth 38.5°
regional: -20,348 mgal
background SG: 2.67 g/cm³

AMIRA/ARC P544 *Final Sponsors Meeting* Slide 8

Cross-Section of the Willouran Trough

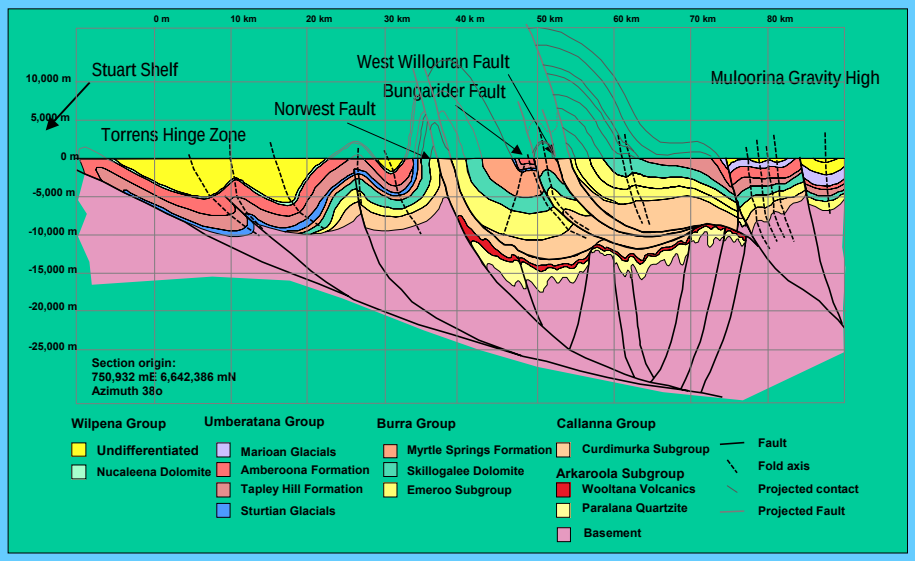

Geology of the Willouran Range

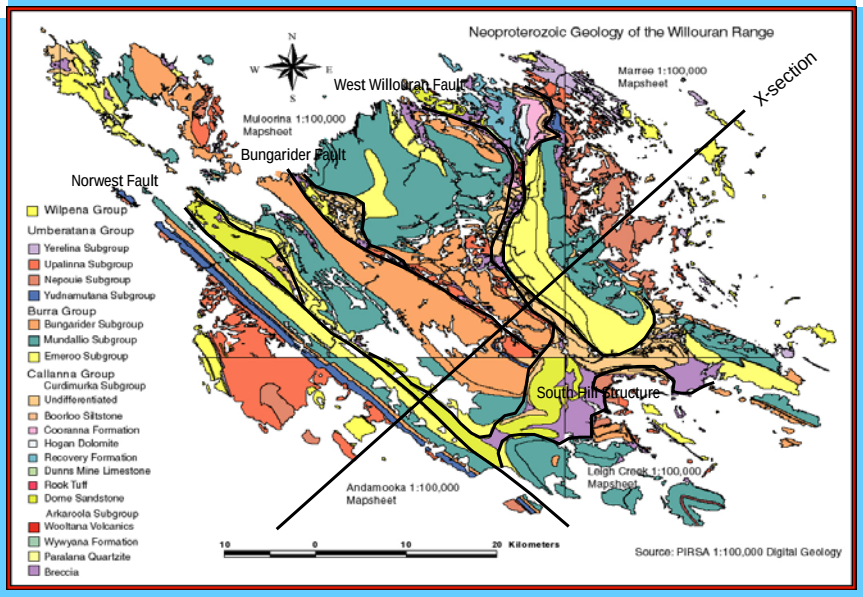

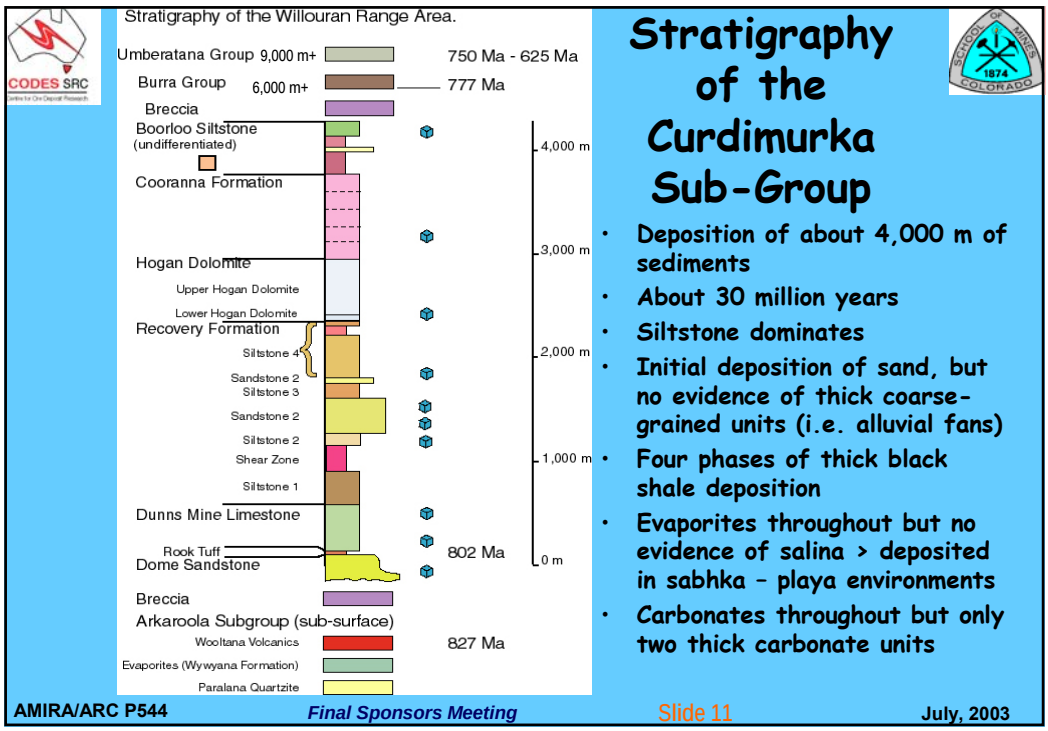
Stratigraphy of the Willouran Range Area.
Umberatana Group 9,000 m+
750 Ma - 625 Ma
Burra Group 6,000 m+
777 Ma
Breccia
Boorloo Siltstone (undifferentiated)
Cooranna Formation
Hogan Dolomite
Upper Hogan Dolomite
Lower Hogan Dolomite
Recovery Formation
Siltstone 4
Sandstone 2
Siltstone 3
Sandstone 2
Siltstone 2
Shear Zone
Siltstone 1
Dunns Mine Limestone
Rook Tuff
Dome Sandstone
802 Ma
Breccia
Arkaroola Subgroup (sub-surface)
Wooltana Volcanics
827 Ma
Evaporites (Wywyana Formation)
Paralana Quartzite
4,000 m
3,000 m
2,000 m
1,000 m
0 m
Stratigraphy of the Curdimurka Sub-Group
Deposition of about 4,000 m of sediments
About 30 million years
Siltstone dominates
Initial deposition of sand, but no evidence of thick coarse-grained units (i.e. alluvial fans)
Four phases of thick black shale deposition
Evaporites throughout but no evidence of salina > deposited in sabhka – playa environments
Carbonates throughout but only two thick carbonate units
AMIRA/ARC P544
Final Sponsors Meeting
Slide 11
July, 2003

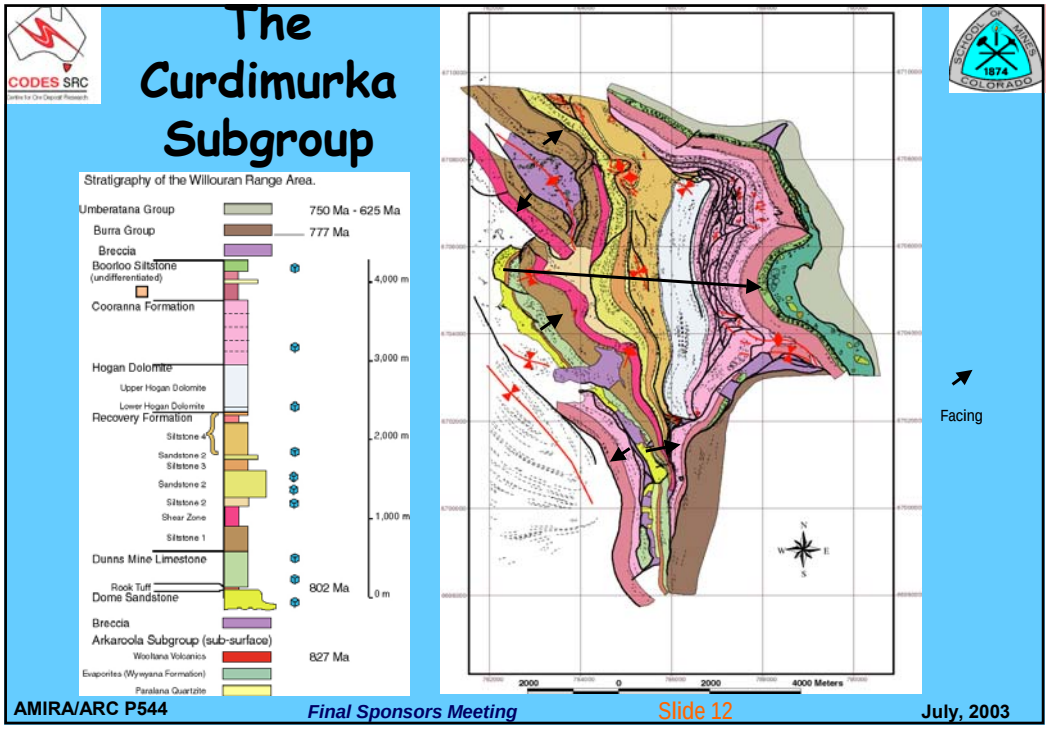
The Curdimurka Subgroup
Stratigraphy of the Willouran Range Area.
Umberatana Group
750 Ma - 625 Ma
Burra Group
777 Ma
Breccia
Boorloo Siltstone (undifferentiated)
Cooranna Formation
Hogan Dolomite
Upper Hogan Dolomite
Lower Hogan Dolomite
Recovery Formation
Siltstone 4
Sandstone 2
Siltstone 3
Sandstone 2
Siltstone 2
Shear Zone
Siltstone 1
Dunns Mine Limestone
Rook Tuff
Dome Sandstone
802 Ma
Breccia
Arkaroola Subgroup (sub-surface)
Wooltana Volcanics
827 Ma
Evaporites (Wywyana Formation)
Paralana Quartzite
4,000 m
3,000 m
2,000 m
1,000 m
0 m
Facing
2000
0
2000
4000 Meters
AMIRA/ARC P544
Final Sponsors Meeting
Slide 12
July, 2003

CSG Upper Contact

- Umberatana Group to the north
- Burra Group to the south
- Diapiric Breccia below the Umberatana
- Breccia and shear zone adjacent to the Burra Group
- Always a sheared contact
- Bedding across the contact is sub-parallel.

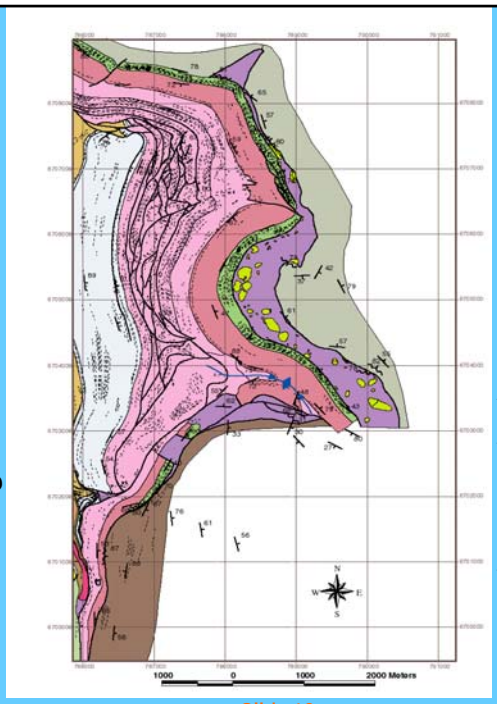

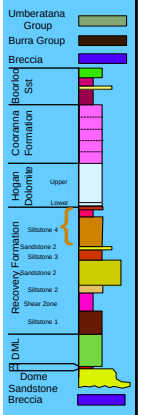

AMIRA/ARC P544 *Final Sponsors Meeting* Slide 13 July, 2003

Upper Contact

Sheared sandstone at the contact between the Umberatana Group and the diapiric breccia (right)

Cataclasite in the contact between the Burra Group and the Curdimurka Subgroup (below left)

Sheared interbedded siltstone and sandstone, in the contact between the Burra Group and the Curdimurka Subgroup (below right)

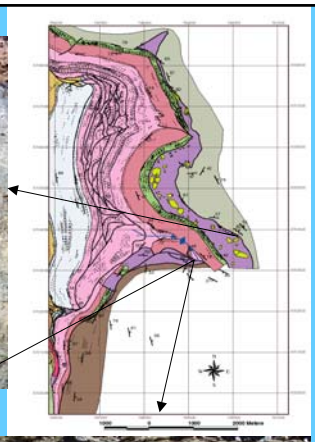

AMIRA/ARC P544 *Final Sponsors Meeting* Slide 14 July, 2003

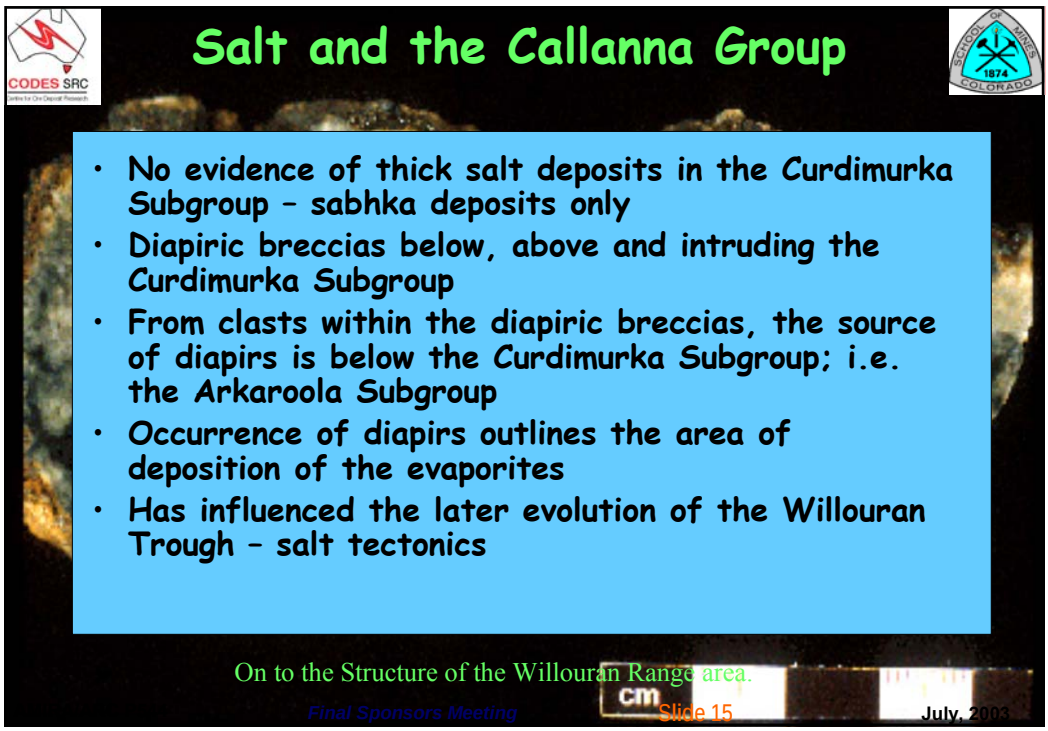
Salt and the Callanna Group
• No evidence of thick salt deposits in the Curdimurka Subgroup – sabhka deposits only
• Diapiric breccias below, above and intruding the Curdimurka Subgroup
• From clasts within the diapiric breccias, the source of diapirs is below the Curdimurka Subgroup; i.e. the Arkaroola Subgroup
• Occurrence of diapirs outlines the area of deposition of the evaporites
• Has influenced the later evolution of the Willouran Trough – salt tectonics
On to the Structure of the Willouran Range area.
Final Sponsors Meeting
Slide 15
July, 2003

A Reminder
Structure of the Curdimurka Subgroup - I
• 3 folding events have affected the Curdimurka Subgroup
• F1
– layer parallel
– Southeast – directed transport
– Confined to specific stratigraphic levels
• F2
– Dominant regional structure (Delamerian)
– Upright, non-cylindrical, tight to isoclinal
– Trend northwest – southeast
• F3
– Broad folds
– Plunge to southwest
Final Sponsors Meeting
Slide 16

Structure of the Curdimurka Subgroup ii

- Faulting is the main structural feature of the Curdimurka Subgroup
- Relative to bedding, faults are thrusts and low-angle normal faults
- In outcrop, these appear as strike-slip faults
- A few high angle reverse and normal faults
- One fault system may show both reverse and normal movement
- Lose 80% stratigraphic thickness
- D1

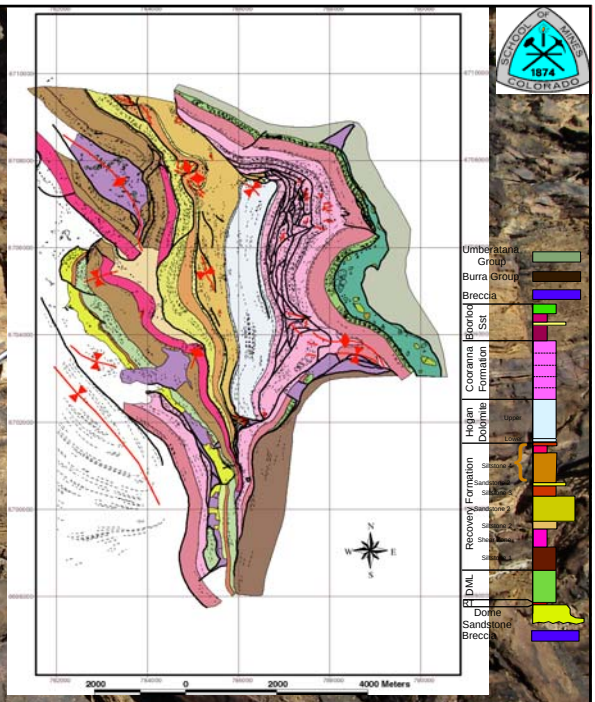

Interpretation

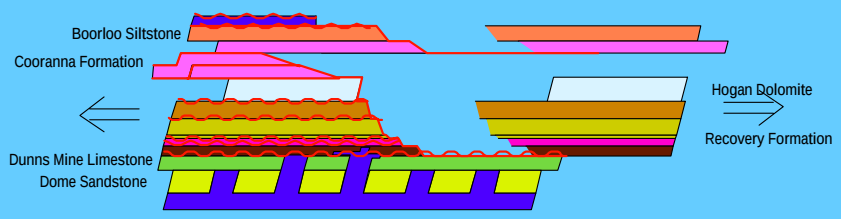

- Vertical σ1
- Ductile layers deform by flowing
- Brittle layers break apart
- Shear zones at boundaries between materials of different rheology
- Ductile layers eventually break

- Ramp and flat pattern of normal faulting
- Thrusting within Cooranna Formation caused by irregular flow over Hogan Dolomite
- Diapiric material flows between blocks of Dome Sandstone
- Gravity Spreading?

Summary – D1 and the Curdimurka Subgroup

- Partitioning of strain into layers
- Layer parallel deformation produces
  - Recumbent folds
  - Thrusts
  - Low-angle normal faults
  - Layer-parallel cleavage (locally)
- Sequence of events
  - Hogan Dolomite boudinaged
  - South to southeast directed movement
  - Northwest directed movement
- Results in the removal of thousands of metres of stratigraphy
- Overall extension, but local compression

AMIRA/ARC P544 *Final Sponsors Meeting* Slide 19 July, 2003

The Willouran Trough – three features that need explaining.

- Weight of Burra Gp squeezes CSG
- Burra Gp also being extended
- CSG thickens in absence of Burra Gp
- Salt withdrawal below CSG accommodates collapse, forms diapirs

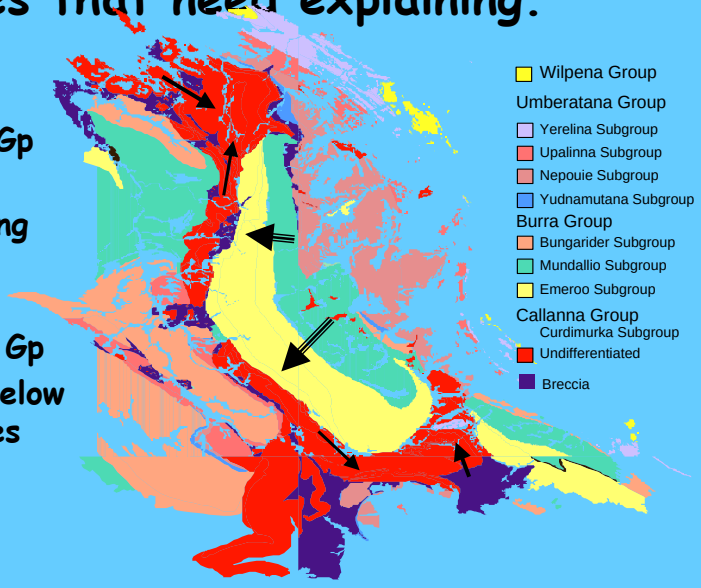

AMIRA/ARC P544 *Final Sponsors Meeting* Slide 20 July, 2003

Cross-Section of the Willouran Trough: NE – SW extension

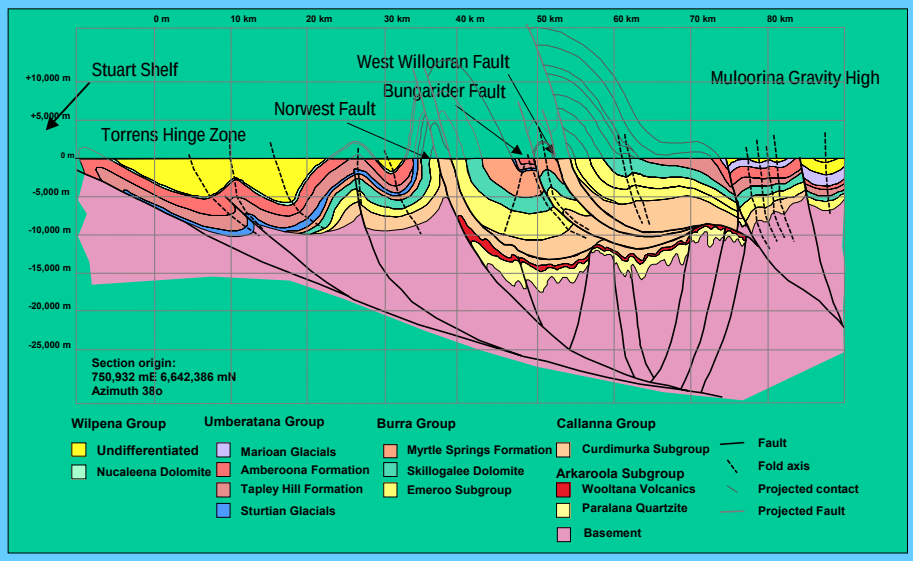

AMIRA/ARC P544 *Final Sponsors Meeting* Slide 21 July, 2003

Timing of Diapirism

Relationship between the diapiric breccia and the Umberatana Group

Tillite clasts within a carbonate clast, adjacent to the contact with the Umbertana Group (right and below)
Clast of distinctive orange-weathering carbonate from breccia, within a tillite. (below right)

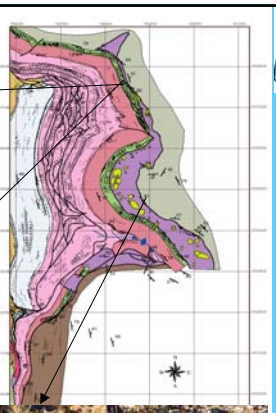

Slide 22a

Slide 22b

AMIRA/ARC P544 *Final Sponsors Meeting* Slide 22 July, 2003

D1 and the Umberatana Group
(Selley & Bull, 2001).

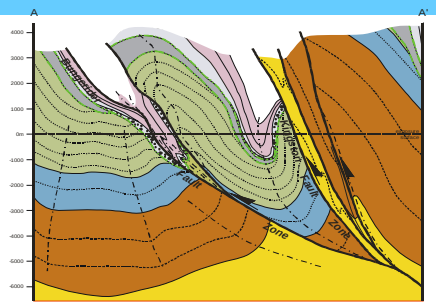

- SW & NE flanks of the syncline = respective footwall & hangingwall of shallow growth fault
- soles into detachment within evaporitic Callanna Gp
- megabreccias shed from highly rotated footwall

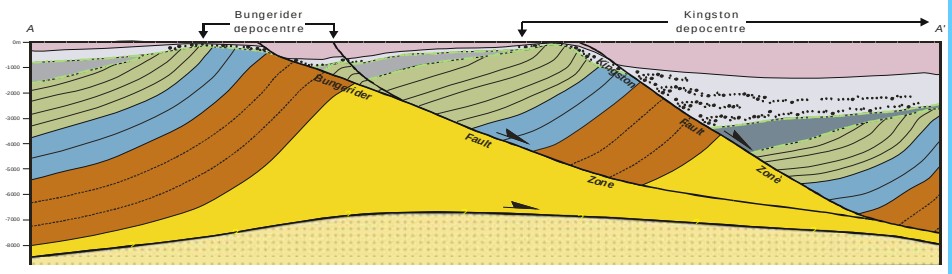

D1 Regionally

- Best observed within the Willouran Range
- Extension in two dimensions
  - Southeast – Northwest
  - Northeast – southwest
- Recorded by the deposition of the Umberatana Group in the Willouran Trough
- Recorded by diapirism at the margins of the Willouran Trough
- Facilitated by salt tectonics (salt withdrawal)
- Rodinia break-up

Whither the Copper?

- The copper is there (as occurrences to minor deposits)
- Association between diapiric breccias and copper
- Copper at many levels of stratigraphy from Arkaroola Subgroup to Wilpena Group
- Associated with reduced rocks

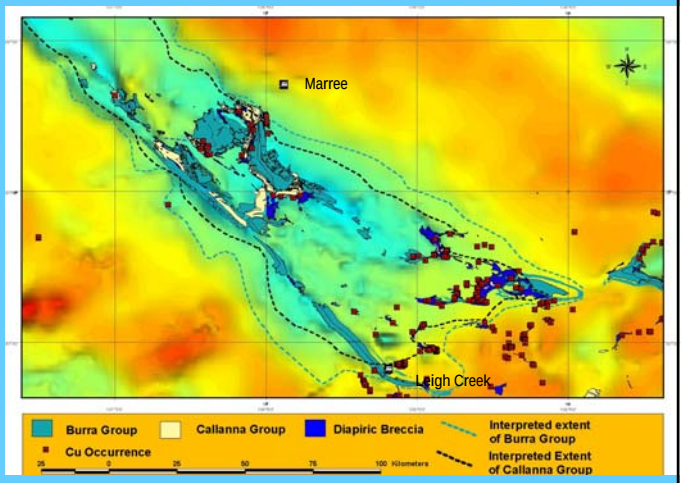

- Large stratiform deposits?
  - A mineralisation system has been working
  - Don't see the level of stratigraphy analogous to the Copperbelt and Kupferschiefer
  - What we see may be the last gasp of the system as diapirism breaks the seal?

AMIRA/ARC P544 *Final Sponsors Meeting* Slide 25 July, 2003

Evolution of the Willouran Trough Summary

2 - Deposition of the Curdimurka Subgroup in a sag basin (thermal relaxation?)

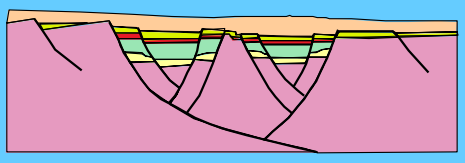

Callanna Group
Curdimurka Subgroup
Dome Sandstone

1 - Initial rifting and deposition of the Arkaroola Subgroup

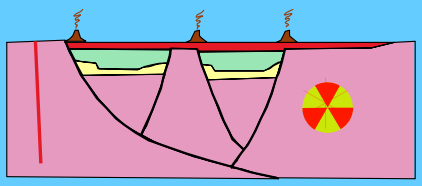

Arkaroola Subgroup
Wooltana Volcanics
Evaporites
Paralana Quartzite
Basement

AMIRA/ARC P544 *Final Sponsors Meeting* Slide 26 July, 2003

Evolution of the Willouran Trough Summary

4 – Rifting with deposition of the Yudnamutana SG and Tapley Hill Formation.
Salt withdrawal and dissolution
Rodinia Breakup

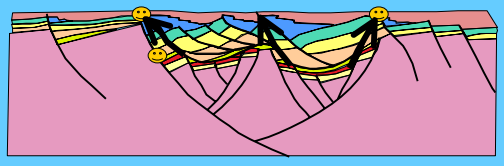

Umberatana Group
- Tapley Hill Formation
- Yudnamutana SG

Callanna Group
- Curdimurka Subgroup
- Dome Sandstone
- Arkaroola Subgroup
- Wooltana Volcanics
- Evaporites
- Paralana Quartzite
- Basement

3 - Renewed rifting, with deposition of the Emeroo Subgroup, then transition to sag phase and deposition of the Skillogalee Dolomite and Myrtle Springs Formation

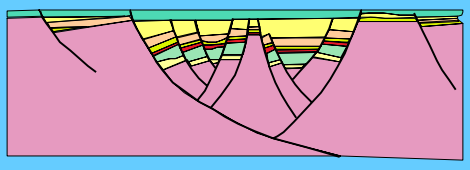

Burra Group
- Myrtle Springs Formation
- Skillogalee Dolomite
- Emeroo Subgroup

Salt movement

Cu mineralisation

AMIRA/ARC P544 *Final Sponsors Meeting* Slide 27 July, 2003

Conclusions – The Willouran Trough

- The Willouran Trough is a narrow depositional compartment, trending northwest – southeast, bounded to the west by the Norwest Fault and to the south by the Paralana Transfer Zone
- The eastern and northern boundaries are obscured by post-Burra Group sedimentation
- Sedimentation was confined to the trough (and trough shoulders) for ~100 Ma (~840 – 740 Ma)
- At the onset of deposition of the Umberatana Group and in particular the Tapley Hill Formation, sedimentation extended beyond the bounds of the trough

AMIRA/ARC P544 *Final Sponsors Meeting* Slide 28 July, 2003

Conclusions – Stratigraphy and Salt

- The Curdimurka Subgroup is a siltstone-dominated package, with evidence for evaporites being deposited in sabhka environments
- There is no evidence for the deposition of thick accumulations of salt within the Curdimurka Subgroup
- The Arkaroola Subgroup is the likely source of salt feeding diapirs within the Willouran Trough
- Salt movement was active at the beginning of deposition of the Umberatana Group

AMIRA/ARC P544 *Final Sponsors Meeting* Slide 29 July, 2003

Conclusions – D1

- D1 was extensional, creating space for the deposition of the Umberatana Group
- At the level of the Umberatana Group, D1 faults are low angle, with large rotation of the hanging wall block
- At the level of the Curdimurka Subgroup, D1 is seen as layer parallel deformation
- D1 results in the loss of stratigraphy of the Curdimurka Subgroup
- Salt tectonics has facilitated D1 within the Willouran Trough

AMIRA/ARC P544 *Final Sponsors Meeting* Slide 30 July, 2003

CODES SRC
The End
Final Sponsors Meeting
Slide 31

Architecture and evolution of the Yeneena Basin, Paterson Orogen, W.A.

Robert Scott
Centre for Ore Deposit Research

Summary

Neoproterozoic rocks of the Paterson Orogen are correlated with the basal Supersequence 1 of the Centralian Superbasin. The Yeneena Supergroup (Yeneena Basin, Paterson Orogen) is host to several significant mineral deposits and the region has long been considered to have potential for Zambian-style sediment-hosted copper deposits. However, recent PhD studies on the two major stratabound copper deposits in the Yeneena Basin (Nifty and Maroochydore), have both argued for a "late-stage" syn-deformational, syn-greenschist facies metamorphic origin for the deposits that contrasts with a well-established pre-metamorphic origin for the Zambian Copperbelt deposits.

The Yeneena Supergroup is interpreted to have been deposited near the margins of a failed intra-continental rift system. The gross tectono-stratigraphic development of the Yeneena Basin appears broadly similar to that recorded by Roan Group in Zambian Copperbelt. In both areas basal sequences are dominated by fluvial sandstone sequences with local development of conglomerates, particularly at sub-basin margins. During the latter stages of deposition of the basal sequence in both areas, there were abrupt increases in the rate of fault-controlled subsidence leading to the first significant marine incursion. Subsequent sedimentation (Upper Roan Group–Mwashia in ZCB; Broadhurst Formation and correlates in the Yeneena Basin) occurred in fluvial to shallow marine settings with widespread deposition of shales and carbonates. This phase of sedimentation was probably accompanied by a gradual decrease in rates of extension and possible transition to thermal sag phase subsidence. Substantial thicknesses of evaporite were deposited in the Upper Roan in the ZCB, but there is no evidence for thick accumulations of evaporites within the equivalent succession (e.g. Broadhurst Formation) in the Yeneena Basin.

Apotentially important difference between the evolution of the Yeneena Basin and Zambian Copperbelt is the much shorter time between sedimentation and basin inversion. The lower parts of the Katanga Supergroup in Zambia remained in a relatively stable setting, within a few kilometres of the Earth's surface for perhaps as much 300 m.y. In contrast, the Yeneena Supergroup was complexly folded and metamorphosed to mid- to upper greenschist facies, probably within 100 m.y. of deposition. This difference in post-depositional evolution may have been critical in determining patterns of basin-scale fluid migration during genesis of the copper deposits.

Introduction

Neoproterozoic sedimentary rocks of the Yeneena Basin are host to several significant mineral deposits and the region has long been considered to have potential for Zambian-style sediment-hosted copper deposits. The giant Telfer Cu–Au deposit in the eastern part of the Yeneena Basin, is a structurally-controlled, probably granite-related orogenic gold deposit with little similarity to the deposits of the Zambian Copperbelt (ZCB). However, the stratabound shale- and carbonate-hosted Nifty (148 Mt @ 1.3% Cu) and Maroochydore (140 Mt @ 0.5 % Cu) deposits were discovered using exploration models based on the then current understanding

(i.e. syn-genetic and syn-diagenetic genetic models) of the ZCB (e.g. Haines et al, 1993; Reed, 1996). While syn-genetic exploration models were important in the discovery of these deposits, subsequent PhD studies of both Nifty (Anderson, 1999) and Maroochydore (Reed, 1996) favoured a later syn-deformational, syn-orogenic timing for Cu-mineralisation.

The Yeneena Basin forms part of the Paterson Orogen, located immediately east of the Archaean Pilbara Craton (Figs 1, 2). Geological development of the Paterson Orogen, and its Neoproterozoic constituents in particular, are comparatively poorly understood. Stratigraphic relations between the constituent elements of the Yeneena Basin (i.e. Throssell and Lamil Groups, Isdell Formation) and their relationship to the Neoproterozoic Tarcunyah Group, exposed to the west and south of the Yeneena Basin along the southwestern margin of the Paterson Orogen (Fig. 2) are controversial (Scott, 2002). The relatively poor geological understanding of Neoproterozoic successions in the Paterson Orogen reflects the generally poor levels of exposure of these rocks and difficulties in dating and correlating units throughout the area. In addition, the remoteness and inhospitable climate of the region (on the western edge of the Great Sandy Desert) have contributed to the lack of detailed research in the area (Scott, 2002).

Previous detailed studies in the Yeneena Basing have been chiefly restricted to a series of unrelated Honours, MSc and PhD deposit studies. However, in recent times the Geological Survey of Western Australia (GSWA) has completed 1: 100,000 scale remapping of the central and northern portions of the Paterson Orogen. In view of the level of geological uncertainty about development of the region, and debate concerning the origin of the sediment-hosted stratabound copper deposits, the aim of the P544 research was to review and synthesis existing geological and geophysical data to improve constraints on:

- Neoproterozoic basin development, architecture and deformation history
- the timing and controls on development of the stratabound copper deposits of the region
- and, ultimately, compare the region with the Zambian Copperbelt.

This report focuses chiefly on the first of these objectives; the style and origin of the Copper deposits is discussed in a companion report (Scott, this volume).

Geological setting

The Paterson Orogen consists of three major elements: (1) the Palaeoproterozoic to Mesoproterozoic gneissic basement of the Rudall Complex, (2) the Neoproterozoic Yeneena Supergroup east of the Vine-Southeast-McKay fault zone (VSMFZ) and (3) the Neoproterozoic Tarcunyah Group (northwestern Officer Basin), west of the VSMFZ (Fig. 2). The Neoproterozoic cover rocks unconformably overlie or are faulted against the Rudall Complex. The geology and geological development of the basement rocks (Rudall Complex) is discussed in Scott (2002) and not repeated here.

The Yeneena Supergroup is interpreted to have been deposited in either a failed rift or a pull-apart basin system formed during strike-slip faulting (Williams, 1990; Hickman and Bagas, 1998; Williams and Bagas, 1999). It is divided into two main successions, the Throssell and Lamil Groups. The Throssell Group unconformably overlies basement along the NW-edge of the Rudall Complex. Exposures of the Throssell Group are restricted to the western half of the Yeneena Basin, west of the inferred NW-continuation of the Camel-Tabletop fault zone (Fig. 2). The Throssell Group is divided into a lower sandstone dominant package (Coolbro Sandstone, <100–4000 m thick) and an upward fining shale dominated package of interbedded sandstone, shale and carbonate (Broadhurst Formation, 2000 m). The Lamil Group is exposed in the eastern half of the Yeneena Basin (t of the inferred NW-continuation of the Camel-Tabletop fault zone, Fig. 2). There are no exposed contacts between the Throssell and Lamil Groups, however, the Lamil Group is generally interpreted to be younger. Its relationship to basement is obscured by younger cover sequences (Fig. 2). The Isdall Formation (Hickman and Clarke, 1994), which occurs east of, and in probable fault contact with the Throssell Group between the Goosewhacker and Maroochydore prospects (Fig. 2), was originally in-

terpreted to separate the Throssell and Lamil Groups is here shown included in the Lamil Group, in line with recent GSWA interpretations.

The Tarcunyah Group unconformably overlies the Archaean Pilbara Craton and Mesoproterozoic Bangemall Supergroup, and is in fault contact with the Throssell Group along the VSMFZ (Fig. 2). It consists of a monotonous sequence of sandstone, conglomerate with lesser siltstone and dolomite (Bagas et al., 1995; 1999; Williams and Bagas, 2000). The thin belt of gently to moderately dipping Tarcunyah Group strata unconformably overlies the eastern margin of the Pilbara Craton marks the western margin of the Paterson Orogen (Fig. 2). In this area, the Tarcunyah group is separated from the Yeneena Supergroup by the N- to NNW-trending Vines fault. The Tarcunyah Group is more extensively exposed further south where the belt swings southeastward (Fig. 2). In this region the Tarcunyah group is either in fault contact with or unconformably overlies the Rudall complex. Where the belt first swings southeastward, the Tarcunyah group is restricted the area south (footwall) of the NW-trending Southwest Thrust. Further to the southeast, where the Southwest Thrust links with the NW-trending McKay Fault, the Tarcunyah Group is exposed both to the north and south of fault system (Fig. 2). South of the present study area the Tarcunyah Group is unconformably overlain by younger gently-dipping to flat-lying sedimentary rocks of the Officer Basin (Williams and Bagas, 2000).

The age and tectono-stratigraphic context of the Tarcunyah Group are controversial (Goode and Hall, 1981; Scott, 2002). Stromatolites and acritachs from the basal Tarcunyah Group were interpreted to indicate an age of approximately 820 Ma (Grey and Stevens, 1997). However, the Tarcunyah Group is of lower metamorphic grade and much less deformed than Neoproterozoic rocks of the Yeneena Basin, a fact that led most GSWA geologists to conclude it was younger than the Yeneena Supergroup, and deposited during or after the middle Neoproterozoic (<750 Ma) Miles Orogeny (see Fig. 3). In contrast Goode and Hall (1981) argue for a gradational structural and metamorphic transition across the western margin of the Paterson Orogen. These authors note the broad lithological similarity between the Tarcunyah Group (their eastern Bangemall Basin succession) and rocks of the Yeneena Basin. Thus Goode and Hall (1981) argue the two Neoproterozoic successions are temporally correlative, with differences in structural style and grade of metamorphism simply reflecting differences in location with respect to the main belt of Neoproterozoic deformation (Figs 1, 2).

Recent GSWA (unpublished) analysis of detrital zircon populations from sedimentary rocks comprising the basal Tarcunyah Group and the Yeneena Basin succession provides important new constraints that in large part resolve the controversy surrounding the tectono-stratigraphic significance of the Neoproterozoic successions in the Paterson Orogen (L. Bagas, pers. comm. 2003). The Throssell and Lamil Groups contain similar detrital zircon populations with a major relative cumulative probability peak at ~1100 Ma, but probably including zircons as young as 800–900 Ma (L. Bagas, unpublished data). In contrast, detrital zircon ages from the basal Tarcunyah along the southwestern margin of the Paterson Orogen indicate a distinct provenance, with minimum zircon ages ~1000 Ma (L. Bagas, unpublished data). These new data indicate that the Tarcunyah Group is younger than 1000 Ma, and does not contain material reworked from the Yeneena Basin, following inversion in the Miles Orogeny (cf. earlier GSWA tectono-stratigraphic interpretations). The maximum age for the Tarcunyah Group is thus consistent with the fossil evidence (Grey and Stevens, 1997) and the interpretation by Goode and Hall (1981) that the group was deposited prior to the Miles Orogeny and is either temporally correlative or older than the Yeneena Supergroup (Fig. 3).

Both Neoproterozoic successions in the Paterson Orogen are now interpreted to form part of the ~800 Ma Supersequence 1 of the Centralian Superbasin (Fig. 3). Furthermore, the strong similarity of relative cumulative-probability distribution diagrams for zircon ages from the Throssell and Lamil groups suggests that these may represent broadly temporally equivalent successions (Fig. 4; L. Bagas, pers. comm. 2003). Difficulties in directly correlating units between the groups may reflect telescoping across the NW continuation across the Camel–Tabletop Fault Zone during either the Miles or younger Paterson orogenies (L. Bagas, pers. comm. 2003). The trace of

the Camel–Tabletop Fault Zone may also mark the location of a major intra-basinal growth fault active during deposition of the Yeneena Supergroup, but compartmentalising the basin into sub-basins with slightly different depositional histories (but very similar clastic sedimentary source areas). Revised Time–Space plots for the Paterson Orogen and stratigraphic correlations for the Yeneena Supergroup (Yeneena Basin) are presented in Figures 3 and 4 respectively (cf. Scott, 2002).

Yeneena Basin

Current GSWA interpretations of stratigraphic relations in the Yeneena Basin suggest the Yeneena Supergroup has a maximum exposed thickness of 6 to 8 km (Fig. 4). However due to generally poor exposure, the structural complexity of the region, and the difficulty in correlating units, this may significantly over-estimate (i.e. undetected stratigraphic repetitions) or under-estimate (erroneous correlations) the true thickness of the succession. A U-Pb SHRIMP age of 816±6 Ma for zircon (2 grains, 5 analyses) from the deformed mafic–intermediate Eva Well intrusion (Reed, 1996) possibly constrains the minimum age for the Throssell Group. However, although five age determinations on these grains were all within error of one another (Reed, 1996), $^{206}Pb/^{238}U$ and $^{207}Pb/^{235}U$ determinations for the individual analyses all plot above concordia casting some doubt on the reliability of the age (L. Bagas, pers. comm., 2003).

Coolbro Sandstone (basal Throssell Group)

The basal part of the Throssell Group, the Coolbro Sandstone, is interpreted to be up to 4 km thick in the northern exposed parts of the Paterson Orogen, and pinches out against the Rudall complex to the southeast (Fig. 2). On average it is about 2 km thick, and represented by a monotonous sandstone succession. Palaeocurrent data indicate a predominance of N- to NE-directed sediment transport away from the Rudall complex, however detritus clearly sourced from the Rudall Complex appears limited to isolated fanglomerates (e.g. Fig. 5) locally developed in basal Coolbro Sandstone along the northern margin of the Rudall Complex. Although the dominant lithology in the western part of the Rudall complex is K-feldspar megacryst orthogneiss Throssell Group sandstones are generally very quartz-rich (up to 98% quartz: Hickman and Clarke, 1994; Reed, 1996; Williams and Bagas, 1999).

Sediment dispersal patterns and thickness variations suggest the exposed Coolbro Sandstone was deposited near the edge of a major basin that deepened towards the north or northeast. If so, the areal extent of NE-directed (transverse) palaeocurrents suggests the Coolbro sandstone was deposited across the passively subsiding dip-slope of a major asymmetric half-graben, controlled by an extensional fault system further to the NE (Fig. 7). The overall lack of detritus from the Rudall Complex suggests in was either eroded to an area of low relief, or the younger sedimentary fill buried it, at an early stage in the development of the Yeneena Basin. Widespread syn-depositional slump folding is reported toward the top of the Coolbro sandstone suggesting an increase in fault-controlled subsidence prior to deposition of the Broadhurst Formation (Hickman and Clarke, 1994; Reed, 1996).

Broadhurst Formation and (?) correlative carbonate- and shale-dominated sequences of the Lamil Group

The Broadhurst Formation overlies the Coolbro Sandstone in the western part of the Yeneena Basin (Fig. 4). It is a 1–2 km thick upward fining succession of sandstone, shale and carbonate and minor conglomerate. Evaporite mineral casts (after gypsum, anhydrite and halite, all of probable diagenetic origin) are sporadically developed throughout finer grained units of the Broadhurst Formation (Reed, 1996; Anderson, 1999). However there is no evidence for the accumulation of thick evaporite sequences anywhere within the preserved stratigraphic section (Fig. 4).

Overall facies developed in the Broadhurst Formation are consistent with accelerated fault-controlled subsidence and an associated marine transgression with deposition in an increasingly euxinic low-energy shelf environment. Carbonaceous and dolomitic shales of the upper Broadhurst Formation approximately 1500 m stratigraphically above the basal contact with the underlying Coolbro Sandstone (Fig. 6; Reed, 1996) host the only known significant stratabound copper

deposits in the Paterson Orogen. Near the southern margin of the Yeneena Basin Reed (1996) recognised abrupt lateral facies changes in the basal part of the Broadhurst Formation. These were interpreted to reflect the continued influence of faults initiated during deposition of the upper part of Coolbro Sandstone (e.g. Hickman and Clarke, 1994) on local sediment dispersal patterns.

In the eastern Yeneena Basin, the transition from the sandstone-dominated Malu Formation to interbedded shale, siltstone and sandstone of the Telfer Member and the overlying carbonate-dominated Puntapunta Formation (Bagas, 2000) may record the same marine transgression / transition to lower energy depositional environments recorded by the Broadhurst Formation in the west (Fig. 4).

Structure and deformation history of the Yeneena Supergroup

Six deformation events are recognised in the Paterson Orogen, however, only the last four affect rocks of the Yeneena Supergroup (Fig. 3; Hickman and Clarke, 1994; Smithies and Bagas, 1997). The Yeneena Supergroup rocks underwent two phases of folding and fabric development in response to NE–SW directed compression (D_1–D_2 in the Yeneena Supergroup, or D_3–D_4 regionally, see Fig. 3) during the Miles Orogeny. The age of the Miles Orogeny is not well constrained. Age dating by Reed (1996) suggests a maximum age limit of 816±6 Ma (SHRIMP U-Pb zircon age) for the deformed Eva Well intrusion, although as noted previously, this age may not be reliable. Reed (1996) also obtained a 717±5 Ma $^{40}Ar/^{39}Ar$ age for syn-D_2 phlogopite from a Cu-bearing vein from the Maroochydore prospect. However Bagas et al. (2000; 2002) favour a younger age 680–630 Ma that is coeval with or predates widespread I-type plutonism in the Telfer area (eastern Yeneena Basin, Fig. 2).

Three samples from the Mount Crofton Granite, 20 km NW of Telfer, which cuts discordantly across folds and faults formed during the Miles Orogeny (Bagas, 2000), yielded concordant titanite SHRIMP U-Pb ages that range between 639±9 and 678±12 Ma. These ages are considered the more reliable constraints on the age of the plutonism than SHRIMP U-Pb zircon ages from the same samples that range from c. 600 to 630 Ma, but are affected by significant lead-loss due extreme radiation damage to the crystals (Dunphy in Bagas, 2000). Recently published $^{40}Ar/^{39}Ar$ ages for muscovite from the Coolbro Sandstone and adjacent Rudall complex yielded well-defined plateaux ages in the range 671–646 Ma, interpreted to reflecting cooling below ~350° during or after the Miles Orogeny (Durocher et al., 2003). Durocher (2003) considered these white mica $^{40}Ar/^{39}Ar$ ages to predate the main phase of granite plutonism, based on the younger but possibly erroneous c. 600 to 630 Ma zircon U-Pb ages for granites in the Telfer area. However, these ages are concordant with titanite SHRIMP U-Pb ages for the clearly post-orogenic Crofton granite, and thus may reflect a regional heating event at that time. Accordingly the minimum age for the main phase (D_2) of the Miles Orogeny is probably c. 680. A maximum age older than 717±5 Ma is implied by syn-kinematic phlogopite in the Maroochydore area (Reed, 1996) (Fig. 3).

D_1 produced local recumbent folds, thrusts and local development of a near bedding-parallel cleavage in the Throssell Group (Hickman and Clarke, 1994; Reed, 1996), while D_2 – the main deformation phase – produced open to tight, upright to overturned (towards the southwest) NW-trending folds, SW directed thrust faults and a pervasive slaty to crenulation cleavage (Goode and Hall, 1981; Hickman and Clarke, 1994; Reed, 1996). Greenschist facies metamorphism (prograde in the Yeneena Supergroup, retrograde in the Rudall Complex) accompanied the latter stages of deformation (D_2) during the Miles Orogeny (Hickman and Clarke, 1994; Bagas and Smithies, 1998).

D_3 (D_5 regionally) is poorly defined event or series of events (680–610 Ma Blake Movement: Williams, 1992; Bagas et al., 2000; 2002) responsible for local faulting and folding of variable style and orientation, principally affecting rocks of the Sunbeam Group (Tarcunyah Group correlate) along the northwestern margin of the Officer Basin (Williams and Bagas, 2000). In the area west of the Southwest Thrust (Fig. 2), the event is interpreted to be responsible for NE-trending folds, and NW-directed transport steep on reverse faults in the Tarcunyah and Sunbeam Groups

(Bagas et al., 1999; Williams and Bagas, 1999; 2000). This event preceded deposition of the Boondawari Formation, a glacigenic succession thought to correlate with the ~600 Ma Marinoan glaciation event (Williams, 1992).

Major deformation of the Tarcunyah Group is interpreted to have occurred during the Paterson Orogeny (Bagas and Smithies, 1998), the last significant phase of deformation to affect the region (regional D_6, D_4 in Neoproterozoic rocks of the Orogen). The NNE–SSW shortening during the Paterson Orogeny is younger than 610 Ma, based on the minimum depositional age of the Tarcunyah Group (Bagas and Smithies, 1998). Many of the major faults in the area cut the Tarcunyah Formation (Vines Fault, Southwest Thrust, McKay Fault, Marloo Fault; Fig. 2) and thus were either initiated or reactivated during the Paterson Orogeny (Bagas and Smithies, 1998; Williams and Bagas, 1999; 2000). The Paterson Orogeny is thus of apparently similar age and similar style to the 560–525 Ma Petermann Orogeny in central Australia (Bagas and Smithies, 1998; Bagas and Williams, 2000). Geophysical data indicate Petermann age structures in the Musgrave block continue beneath cover northwest into the Paterson Orogen, e.g. Warri gravity high (Fig. 1; Goode and Hall, 1981; Bagas and Smithies, 1998). These structures our now recognised as (regional) D_6 structures, in the Paterson Orogen, where they controlled deposition of the Disappointment Group (formerly Wells Foreland Basin Succession (Williams, 1992) of the upper Savory Group) in the area to the south (Williams and Bagas, 2000). The Disappointment Group post-dates the ~600 Ma Boondawari Formation and was apparently deposited in a foreland basin setting (Williams, 1992; Bagas et al., 1995).

Basin architecture and stratigraphic development: comparisons with the Katanga Supergroup in the Zambian Copperbelt

The Yeneena Supergroup is interpreted to have been deposited in either a failed intra-continental rift or a pull-apart basin system formed during strike-slip faulting (Williams, 1990; Hickman and Bagas, 1998; Williams and Bagas, 1999). The gross tectono-stratigraphic development of the Yeneena Basin appears broadly similar to that recorded by Roan Group in Zambian Copperbelt (e.g. Broughton; Selley et al., this volume). Not only do available age constraints permit the Roan Group (ZCB) and the Yeneena Supergroup to be of similar age, both appear to have been deposited in failed intra-continental rifts. In both areas basal sequences are dominated by fluvial sandstone sequences with local development of conglomerates at sub-basin margins (Fig. 7a). During the latter stages of deposition of the basal sequence in both areas, there were abrupt increases in the rate of fault-controlled subsidence leading to the first significant marine incursion (e.g. upward coarsening successions in the upper footwall succession of the Lower Roan in ZCB (Selley et al., this volume), slumping in the upper Coolbro Sandstone in the Yeneena Basin (Hickman and Clarke, 1994).

Subsequent sedimentation (Upper Roan Group –Mwashia in ZCB; Broadhurst Formation and correlates in the Yeneena Basin) occurred in fluvial to shallow marine settings with widespread deposition of shales and carbonates (Fig. 7b). This phase of sedimentation was accompanied by a gradual decrease in rates of extension and possible transition to thermal sag phase subsidence (Bull et al., this volume). However while substantial thicknesses of evaporite were apparently deposited in the Upper Roan in the ZCB (Broughton, this volume) there is no evidence for thick accumulations of evaporites anywhere within the Yeneena Basin. Only sporadically developed evaporite minerals (gypsum, anhydrite and halite) with displacive habit and of probable diagenetic origin occur in the Broadhurst Formation (Reed, 1996; Anderson, 1999).

In the ZCB, the total Neoproterozoic stratigraphic section (Katanga Supergroup), representing deposition over a period of up to 277 m.y. (<877–600 Ma), is only 5–6 km thick (Broughton; Bull et al., this volume). The lower part of the stratigraphic section in the Zambian Copperbelt (Roan Group ± Mwashia Group) is only 1.5–2.5 km thick compared to estimates of 3–7 km for the Yeneena Supergroup (N.B. the large variation in the estimated thickness of the Yeneena Supergroup is largely due to the variation (i.e. ~4 km) in thickness of the basal Coolbro Sandstone). Accordingly in positions close to the southern margin of the Yeneena

Basin the thickness of the Yeneena Supergroup and the lower part of the Katanga Supergroup in the ZCB, may be quite similar. However while stratabound copper deposits in the Copperbelt are localised at or below the stratigraphic level of the first significant marine transgression, whereas the only known significant stratabound copper deposits in the Paterson Orogen sit well above this position.

Another potentially important difference between the evolution of the Yeneena Basin and Zambian Copperbelt is the much shorter time between sedimentation and basin inversion. The syn- to post-Katangan deformation history of the ZCB is not fully resolved. However if the Kundelungu represents a generally conformable succession, no significant compressional deformation occurred prior to deposition of the Petit Conglomerate at c. 600 Ma. The major phase of deformation in the ZCB was during the Lufilian Orogeny, which probably peaked at ~500 Ma. Thus the lower parts of the Katanga Supergroup remained in a relatively stable setting, within a few kilometres of the Earth's surface for perhaps as much 300 m.y. In contrast, the Yeneena Supergroup was complexly folded and metamorphosed to mid- to upper greenschist facies, probably within 100 m.y. of deposition (Fig. 7c). This difference in post-depositional evolution may have been critical in determining patterns of basin-scale fluid migration during genesis of the copper deposits (Scott, this report).

References

Anderson, B., 1999, Structure, alteration and mineralisation of the Nifty Copper Deposit, Western Australia: Unpublished PhD Thesis, University of Tasmania, 225p.

Bagas, L., 2000, Geology of the Paterson 1:100,000 Sheet: Western Australia Geological Survey, 1:100,000 Geological Series Explanatory Notes, 20p.

Bagas, L., Comacho. A. and Nelson, D. R., 2002, Are the Neoproterozoic Lamil and Throssell Groups of the Paterson Orogen allochthonous?: Geological Survey of Western Australia Annual Review 2000–01, p. 45–52.

Bagas, L., Grey, K., Hocking, R. M. and Williams, I. R., 1999, Neoproterozoic successions of the northwestern Officer Basin: A reappraisal: Western Australia Geological Survey, Annual Review 1998–99, p. 39–44.

Bagas, L., Grey, K. and Williams, I. R., 1995, Reappraisal of the Paterson Orogen and Savory Basin: Western Australia Geological Survey, Annual Review 1994–95, p. 55–63.

Bagas, L. and Smithies, R. H., 1998, Geology of the Connaughton 1:100,000 Sheet: Western Australia Geological Survey, 1: 100,000 Geological Series Explanatory Notes, 38p.

Bagas, L., Williams, I. R., and Hickman, A. H., 2000, Rudall WA (2nd edition.): Geological Survey of Western Australia 1: 250,000 Geological Series Explanatory Notes.

Broughton, D., 2003, Stratigraphy of the Zambian Copperbelt: AMIRA P544 - Proterozoic Sediment Hosted Copper Deposits, Final Report, p. .

Bull, S. and the P544 Team, 2003, Comparison of Cu mineralised basins; the Zambian Copperbelt, the Polish Kupferschiefer, the Adelaide Fold Belt and the Yeneena Basin: AMIRA P544 - Proterozoic Sediment Hosted Copper Deposits, Final Report, p. .

Chin, R. J. and de Laeter, J. R., 1981, The relationship of new Rb-Sr isotopic dates from the Rudall Metamorphic Complex to the geology of the Paterson Province, Western Australia: Western Australia Geological Survey, Annual Report 1980, p. 80–87.

Durocher, K. E., Kyser, T. K., Marlatt, J., and Hanly, A., 2003, New 40Ar/39Ar ages from the central Paterson Orogen, Western Australia: Australian Journal of Earth Sciences, v. 50, 601–610.

Goode, A. D. T., 1981, Proterozoic geology of Western Australia, *in* Hunter, D. R. (ed.) Precambrian of the southern hemisphere: Developments in Precambrian Geology 2, Elsevier, Amsterdam, p. 105–203.

Goode, A. D. T. and Hall, W. D. M., 1981, The Middle Proterozoic eastern Bangemall Basin, Western Australia: Precambrian Research, v. 16, p. 11–29.

Grey, K and Stevens, M. K., 1997, Neoproterozoic palynomorphs of the Savory Sub-basin, Western Australia and their relevance to petroleum exploration: Western Australia Geological Survey, Annual Review 1996–97, p. 49–54.

Haines, D. W., Brooke, W. J. L., and Mazzoni, P.P., 1993, Application of conceptual models of sediment –hosted ore deposits in the discovery of the Nifty Copper and adjacent zinc–lead deposits, Yeneena Basin, Western Australia, *in* Kirkham, R.V., Sinclair, W. D., Thorpe, R. I. and Duke, J. M., (Eds.), Mineral deposit modelling: Geological association of Canada, Special Paper 40, p. 75–88.

Hickman, A. H. and Bagas, L., 1998, Geology of the Rudall 1: 100,000 Sheet: Western Australia Geological Survey, 1: 100,000 Geological Series Explanatory Notes, 30p.

Hickman, A. H. and Clarke, G. L., 1994, Geology of the Broadhurst 1:100,000 Sheet: Western Australia Geological Survey, 1: 100,000 Geological Series Explanatory Notes, 40p.

Reed, A., 1996, Structural, stratigraphic, and temporal setting of Neoproterozoic stratabound copper mineralisation at Maroochydore, Paterson Province, Western Australia: Unpublished PhD thesis, University of Western Australia, 289p.

Scott, R., 2002, Geological development and mineralisation in the Yeneena Basin – Paterson Orogen, W. A.: AMIRA P544 Proterozoic Sediment Hosted Copper Deposits, Annual Report, p. 13.1–13.18.

Scott, R., 2003, Alteration, geochemical and isotopic signatures of stratabound copper mineralisation in the Yeneena Basin, Paterson Orogen, W.A.: AMIRA P544 Proterozoic Sediment Hosted Copper Deposits, Final Report, p.

Selley, D., Bull, S., Croaker, M., Scott, R., Broughton, D. and Pollington, N., 2003 (a), Development of the Lower Roan basin system, western Kafue Anticline: AMIRA P544 Proterozoic Sediment Hosted Copper Deposits, Final Report, p.

Smithies, R. H. and Bagas, L., 1997, High-pressure amphibolite–granulite facies metamorphism in the Palaeoproterozoic Rudall Complex, central Western Australia: Precambrian Research, v. 83, p. 243–265.

Williams, I. R., 1990, Yeneena Basin, *in* Geology and mineral resources of Western Australia: Western Australia Geological Survey Memoir 3, p. 276–279.

Williams, I. R., 1992, Geology of the Savory Basin, Western Australia: Western Australia Geological Survey Bulletin, 141, 115 p.

Williams, I. R. and Bagas, L., 1999, Geology of the Throssell 1: 100,000 Sheet: Western Australia Geological Survey, 1: 100,000 Geological Series Explanatory Notes, 24p.

Williams, I. R. and Bagas, L., 2000, Geology of the Poisonbush 1:100,000 Sheet: Western Australia Geological Survey, 1: 100,000 Geological Series Explanatory Notes, 21p.

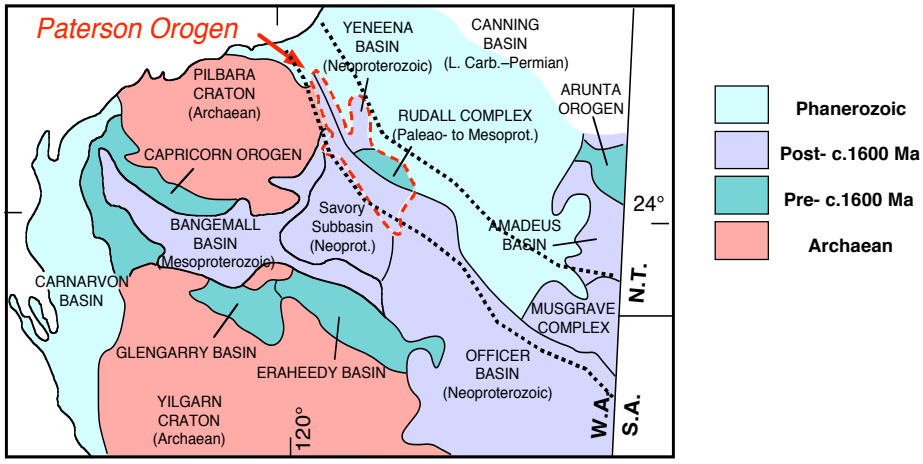

Figure 1. The Paterson Orogen is a 1200 km SE-trending belt of deformed Palaeo- to Neoproterozoic rocks at eastern margin of Pilbara Craton, central Western Australia. The domain delineated by the black dotted lines shows the continuation of the Warri gravity high, NW of the Musgrave Complex.

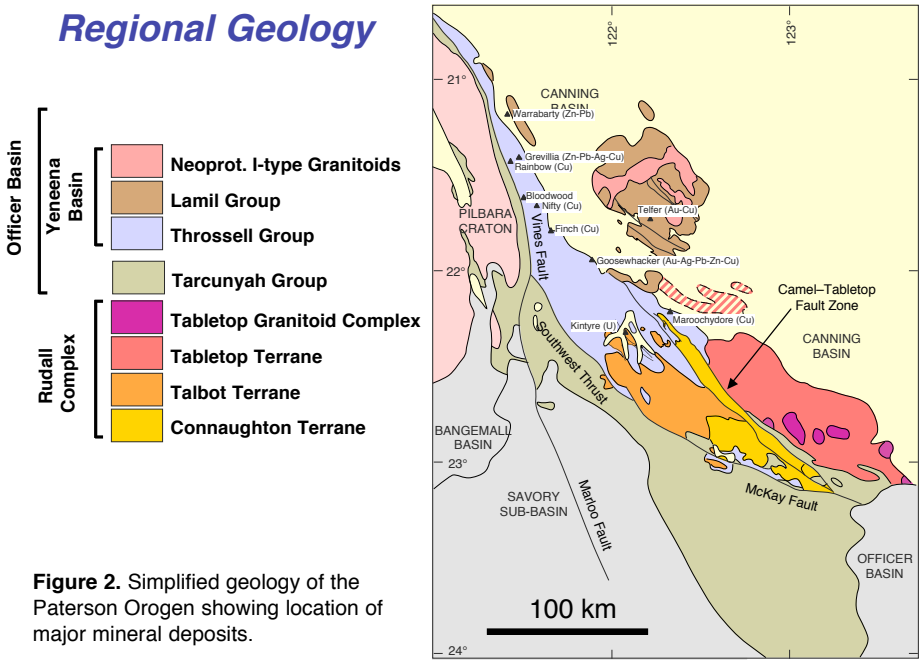

Figure 2. Simplified geology of the Paterson Orogen showing location of major mineral deposits.

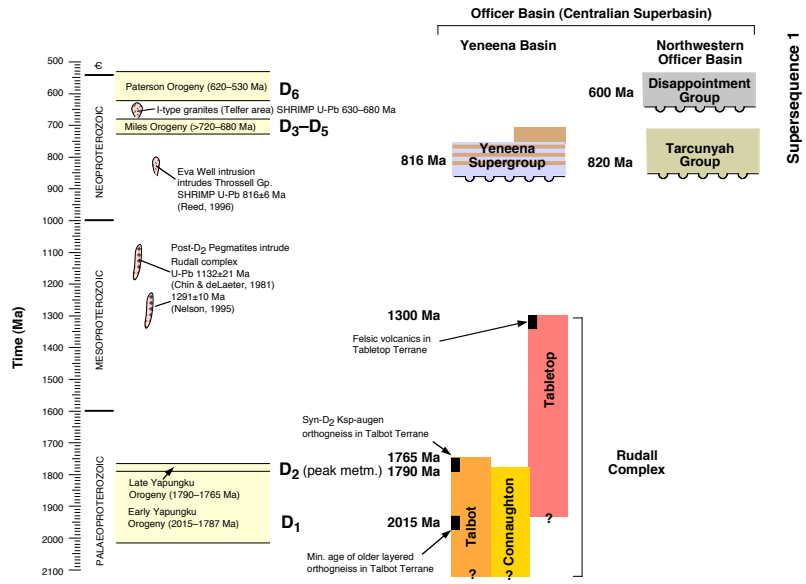

Figure 3. Temporal evolution of the Paterson Orogen.

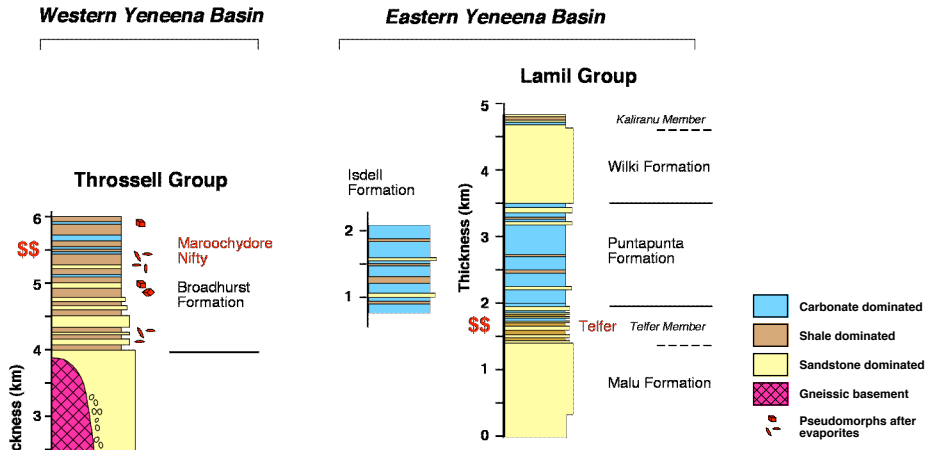

Figure 4. Interpreted stratigraphic relations between east and west Yeneena Basin. The Isdell Formation was originally interpreted to be younger than the Broadhurst Formation and older than Lamil Group, but all three may be correlative. Recent detrital zircon age dating suggests the Throssell and Lamil groups are of similar age, with lithological differences reflecting lateral facies changes telescoped across the continuation of the Camel–Tabletop F.Z.

Coolbro Sandstone

Figure 5. The Coolbro Sandstone is the basal fluvial/alluvial sequence of the Yeneena Basin. It thickens toward the N (or NE) and palaeocurrent indicators reveal a predominantly N- to NE-directed sediment dispersal pattern. Conglomerates such as that illustrated are rare, and largely restricted to the southern-most exposures of the unit where it pinches out against Palaeo- to Mesoproterozoic basement (Rudall Complex).

Broadhurst Formation

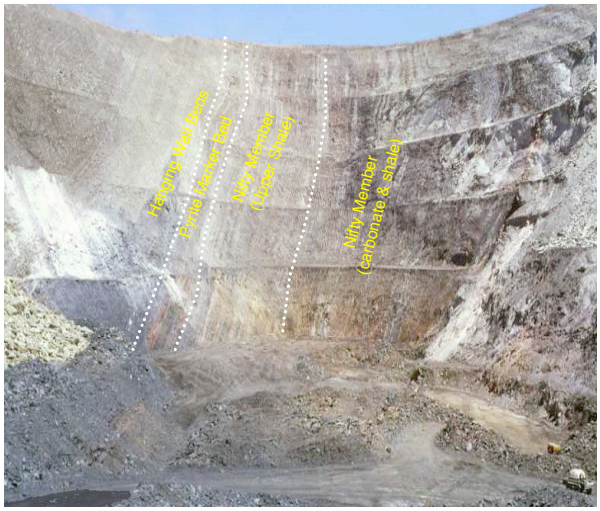

Figure 6. Medium to thinly bedded carbonaceous, dolomitic and sulfidic shale and carbonate in the upper Broadhurst Formation exposed in the Nifty open pit. Younging direction is towards the SW (left). Host rocks to the Nifty deposit are interpreted to be located c.1500 m above lowermost reduced shales near the base of the Broadhurst formation.

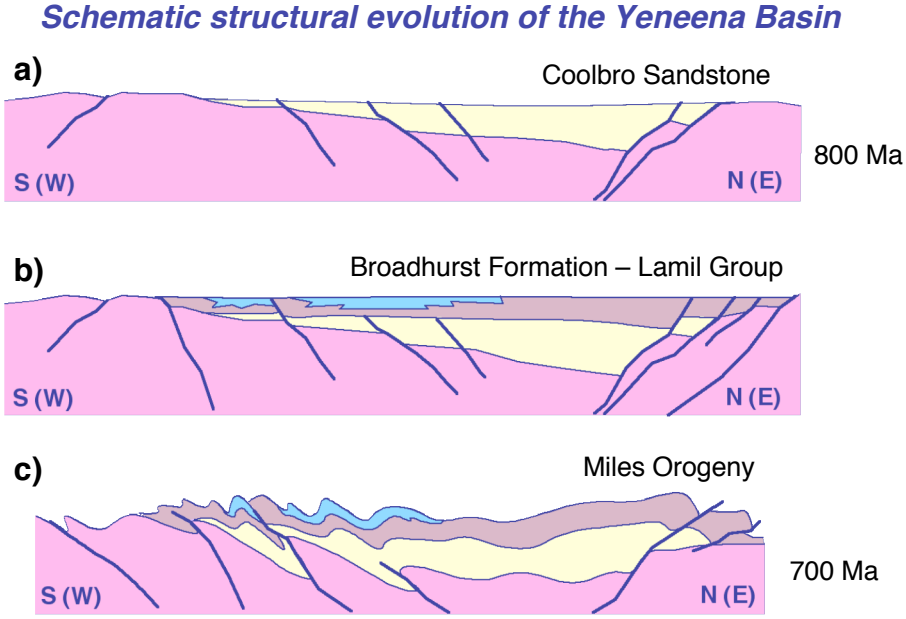

Figure 7. Schematic structural evolution of the Yeneena Basin.

Alteration history of the Roan

David Selley, Robert Scott, Mawson Croaker, David Broughton, Stuart Bull and Nicky Pollington
Centre for Ore Deposit Research, University of Tasmania

Abstract

Roan strata record a protracted history of fluid migration from early diagenesis to the latest stages of basin development. During initial burial, dense sulfate-rich brines descended from evaporitic strata contained largely above the level of the Ore Shale, to precipitate anhydrite and carbonate cements within coarse siliciclastic rocks of the Mindola Clastics Formation. Localised dissolution of these early diagenetic cements during subsequent hydrocarbon migration was important in terms of generating secondary porosity and permeability, but also providing a source of sulfur.

As Lower Roan strata were buried to depths of 2–3 km, hydrocarbons were generated from organic-rich facies of the Ore Shale (or equivalent strata outside the Copperbelt), and migrated to trap sites situated close to the upper contact of the Mindola Clastics Formation. Evidence for the former presence of hydrocarbons include (1) concentration of carbonaceous matter within host arenites at Mufulira, (2) localisation of arenite-hosted Cu-Co deposits within favourable hydrocarbon reservoirs, and (3) the association of high grade mineralisation with hydrothermal carbonate cements possessing distinctively 'light' $\delta^{13}C$ isotopic signatures. The necessary role of hydrocarbons in providing a reductant for the precipitation of Cu-Co sulfides from oxidised metal-bearing fluids militates against an early diagenetic age of mineralisation.

Potassic and subsequent albitic metasomatism provide the record of a protracted hydrothermal event that affected the entire Roan basin system. Brine generation occurred in response to dissolution of Upper Roan salt, which probably initiated during late diagenesis, but accelerated with the onset of Lufilian inversion. A broad stratigraphic partitioning of K-bearing phases into the Lower Roan and albite within Upper Roan strata, reflects the development of greater fracture-enhanced permeability at higher levels as the hydrothermal system waned. Early formed K-bearing phases and tourmaline were pervasively developed throughout consolidated siliciclastic units of all grainsizes, and suggest slow rates of fluid ingress, in part via replacement of argillaceous matter. Although albite is presently the dominant alteration phase within voluminous breccia bodies, evidence of pre-existing intense K-B metasomatism indicates that initial stages of fluid flow was also partly controlled by macroscopic zones of fracture permeability.

Most Copperbelt deposits display an intimate association of Cu-Co sulfides and metasomatic K-rich phases. Although an albite-ore association occurs in some cases, evidence can always be found for former K-B metasomatism, usually in the form of relict tourmaline needles contained with coarse-grained albite. These relationships suggest that metal introduction and 'classical' Copperbelt mineralisation occurred during early stages of hydrothermal evolution. However, the association of albite with structurally controlled Cu mineralisation at Kansanshi highlights the potential for alternative styles of 'late-stage' deposit formation.

Introduction

The topic of alteration was rarely an important consideration within much of the historical literature of the Zambian Copperbelt. This partly resulted from the application of favoured genetic models of the time, the syngenetic model in particular. Foremost in the lines of evidence against widespread alteration, was the perceived lack of permeability of the principal host stratum, the Ore Shale, during diagenesis or more advanced stages of burial (e.g., Mendelsohn,1989). If the basin were subjected to a widespread hydrothermal event, why would fluids have not been partitioned into coarsest-grained media, their passage recorded by alteration and mineralisation?

One of the earliest works to systematically tackle the problem of hydrothermal alteration was Darnley's (1960) petrographic and geochemical analysis of Lower Roan mineralisation. His detailed mineralogical descriptions highlighted the relationships of metasomatic feldspar (mainly potassium feldspar but also albite), sericite, tourmaline and carbonate, with many of the ore deposits. That this gangue assemblage is not dissimilar to the detrital components expected in a carbonate-bearing siliciclastic sequence of granitic provenance, certainly contributed to the underestimation of hydrothermal activity. If fact, much of the 'classical' ZCB stratigraphic nomenclature demonstrates that alteration phases were recognised, but that they were interpreted largely as primary sedimentary detritus. At Mufulira for example, the sub-arkosic protolith has been modified by feldspar destruction and/or addition of carbonaceous matter (Annels, 1979) to produce a spectrum of altered arenaceous units that have been variously described as 'quartzites', 'sericitic quartzites', and 'greywackes' (see also Scott et al., this volume B). By contrast, locally intense feldspathic metasomatism has led to the erroneous description of many sandstones as primary arkoses. The *Feldspathic Quartzite* (or TFQ) of Nchanga is perhaps the best known of these arkosic facies, and contains up to 50% microcline (McKinnon and Smitt, 1961).

This paper builds upon the results of previous P544 alteration studies (Bull & Selley, 2001; Selley & Cooke, 2001; Selley et al., 2002; Broughton, 2002), and incorporates conclusions from a number of detailed deposit-scale studies included in this volume (Bull & Selley; Selley & McGoldrick; Scott et al.; Broughton). In summarising the important elements of alteration from a petrographic perspective, the report prefaces a series of papers concerned with the affects of metamorphism on metasomatic mineral assemblages (Scott et al., this volume A), and litho-geochemical signatures of hydrothermal activity (Large et al, this volume A; Large et al., this volume B). The aims are three-fold:

- To demonstrate a systematic alteration paragenesis, applicable to the ZCB as a whole.
- To investigate which non-sulfide alteration assemblages possess spatial and/or temporal relations to ore.
- To provide constraints on the timing and scale of hydrothermal fluid activity.

Paragenesis and distribution of alteration assemblages

Through the affects of metamorphism, we have been able to recognise a broadly systematic paragenetic sequence of fluid input involving four distinct phases.

1. Early diagenetic SO_4 + Mg ± Ca addition.
2. Late diagenetic hydrocarbon generation.
3. Late diagenetic – syn-orogenic K + B + Cu ± Co addition.
4. Late diagenetic - syn-metamorphic Na ± Mg ± Ca addition.

Most importantly, the combined affects of these phases of fluid flow have resulted in alteration throughout the *entire* Roan sequence. However, alteration is generally most intense and complicated in terms of superposition of different phases within and as a halo to the Kitwe Formation (Slide 3). The distribution and petrographic characteristics of each alteration phase are presented in detail below.

Early diagenetic SO_4 + Mg ± Ca metasomatism

Anhydrite-carbonate cements are widely preserved within and above the level of the Ore Shale (Slide 4), where they are interpreted to have formed by the metamorphic recrystallisation of *in situ* (ie. largely syn-depositional) evaporitic components (Bull & Selley, this volume). In areas where this evaporite-related assemblage is particularly intense (e.g., Chambishi SE), the distribution of anhydrite and dolomite cements extends well into the 'footwall' sequences (ie. Mindola Clastics Formation: MCF), and even into basement granite (Slides 4, 5). As the facies associations of the MCF are incompatible with deposition within evaporitic environments, fluids responsible for precipitation of SO_4- and Mg-bearing cements are considered to have been exotic. The most likely origin of these constituents is evaporitic strata of the Rokana Evaporites Member. Due to the increasing stability of anhydrite with increasing temperature, descent of sulfate-rich brines must have occurred during the initial stages of burial, either via brine reflux and/or dehydration of gypsum (Bull & Selley, op cit.).

Although occluding porosity within "footwall" sandstones early in the basin's history, anhydrite was likely to have been unstable during subsequent alteration phases, thus playing important roles in terms of secondary porosity generation and providing a source of sulfur.

Late diagenetic hydrocarbon generation

Evidence for the former presence of hydrocarbons and its importance in terms of Cu mineralisation, was first presented in papers by Annels (1974 & 1979). His arguments were based upon the long recognised association of the stacked orebodies of Mufulira with carbonaceous arenites (known colloquially as 'greywackes'). Although Annels (op cit.) did not document the presence of pyrobitumen within the 'greywackes', nor did he conduct chemical analyses to demonstrate a hydrocarbon origin for the carbonaceous matter, he provided convincing evidence that there is no direct sedimentological control on the distribution of carbon. Most importantly, he recognised that the detrital framework of the 'greywackes' was identical to that of adjacent non-carbon bearing equivalents, and us such interpreted the carbonaceous component to represent alteration, rather than a primary sedimentary variant.

With the exception of carbonaceous matter at Mufulira, mineralogical evidence for hydrocarbon generation is sparse: ie. no pyrobitumen has been recognised to date. Arguments for the involvement of former hydrocarbons presented in previous P544 reports (e.g., Selley & Bull, 2001; Selley et al., 2002) have concentrated on aspects of basin/stratigraphic architecture and their links with ore body geometry, particularly for arenite-hosted Cu systems. Mineralogical evidence has been largely circumstantial, and has included:

1. The anomalously 'heavy' $\delta^{34}S$ isotopic signatures of sulfide phases at Chibuluma West, which led Selley & Cooke (2001) to postulate that sulfur was sourced from a 'sour gas' (H_2S) reservoir.
2. The association of sericitic alteration with arenite-hosted deposits (e.g., Mwambashi B, Mufulira) that may reflect acidic conditions resulting from oxidisation of hydrocarbons (Selley et al., 2002).
3. The association of sulfides with radiogenic heavy mineral bands (e.g., Slide 10), which may reflect local concentration of reductant by polymerised hydrocarbons within the thermal aureoles of radiogenic mineral phases (Scott, 2002; Selley & Cooke, 2001; Selley et al., 2002)

These lines of research have been expanded on within the final reporting period, the details of which are in accompanying papers in this volume. Summarised below are two principal lines of evidence of hydrocarbon generation, and its importance in the ore-forming process.

Basin and facies architecture of arenite-hosted deposits

Arenite-hosted ore bodies at Chibuluma West, Mwambashi B, Chambishi and Mufulira are each associated with distinctive stratigraphic and structural architectures that would have favoured hydrocarbon accumulation. Most importantly, the distribution of Cu ± Co mineralisation correlates strongly with restricted bodies of quality reservoir rock. Host strata comprise condensed sequences of relatively clean, argillite-poor sandstone, or less commonly conglom-

erate units, that occur within small transfer-related depocentres at the periphery of larger basin systems (Slide 8). Orebodies coincide with the most restricted portions of these depocentres, where coarse-grained host strata pinch-out both laterally and above crystalline basement, and below finer-grained units that transgress the host compartments.

Resultant vertical profiles through ore involve a characteristic coincidence of assay hangingwall with an abrupt geological contact separating host arenites from overlying less permeable strata (Slide 8). In most cases, the geological hangingwall comprises siltstone or argillaceous sandstone, however dolomite caps the B orebody at Mufulira. By contrast, ore bodies lack a well-defined geological footwall contact, with the primary textures and detrital composition of barren footwall strata being largely indistinguishable from those of the host unit.

The spatial relationships between facies architecture and ore distribution summarised above, are consistent with interaction of metal-bearing fluids with pre-existing hydrocarbons, trapped within a three-dimensional reservoir. This model also adequately explains the vertical partitioning of mineralisation within the uppermost portions of units with apparently homogenous compositional and textural characteristics.

Isotopic signature of carbonate gangue in arenite-hosted deposits

The most compelling line of mineralogical evidence for former hydrocarbons to come from our work is the isotopic composition of carbonate cements associated with arenite-hosted mineralisation. Best developed within the Mwambashi B deposit, this carbonate generation results in a pervasive bleaching at the hand specimen scale. In thin section, it occurs as discrete, coarse calcite grains that occupy space between detrital and metasomatic silicate grains (Slide 9). Although broadly increasing in intensity within the ore zone (see also Selley & McGoldrick, *this volume*), at thin section scale, the calcite alteration commonly displays an antithetic relationship with Cu-Co sulfides.

A profile of $\delta^{13}C$ isotopic values from a high grade intersection of the Mwambashi B deposit is shown in Slide 9. The intersection shows the characteristic partitioning of Cu mineralisation within the uppermost potion the arenaceous host, with abrupt transition to overlying Ore Shale. Furthermore, it demonstrates a remarkable coincidence of anomalously light $\delta^{13}C$ values with elevated Cu abundances. As the ore zone is approached from below, $\delta^{13}C$ values decrease from –6.9‰ to –23.6‰. Although hangingwall data are sparse, there is an apparent increase in $\delta^{13}C$ values relative to the ore zone, with a single sample from the barren Ore Shale measuring –11.5‰. These values contrast with those of ZCB sedimentary carbonate, which range –6 to +8‰, but are comparable with ore-related carbonate alteration from many of the Ore Shale-hosted systems (Large et al., this volume B).

Negative excursions in $\delta^{13}C$ values of carbonate on the scale recorded at Mwambashi B are best explained by the oxidisation of organic carbon to form CO_2. Although preservation of detrital or early diagenetic organic carbon is to be expected in the anoxically deposited Ore Shale, the same cannot be said for fluviatile sandstones. The most plausible explanation for concentration of organic carbon in such lithotypes is by the trapping of mobile hydrocarbons. This is again consistent with the observation that light in $\delta^{13}C$ signature occurs immediately below the impermeable seal in the Mwambashi B orebody (Slide 9). Further supporting this interpretation is the occurrence of calcite with light $\delta^{13}C$ values (~ –20‰) and coexisting pyrobitumen in association with strata-bound sediment-hosted (manto-type) Cu deposits of Chile (Zentilli et al., 1997; Wilson and Zentilli, 2003).

Carbonate cements associated with arenite-hosted mineralisation at Mufulira record similarly depleted $\delta^{13}C$ values (Scott et al., this volume B). However, rare carbonate cements within Chibuluma West orebody do not possess this distinctive signature, with $\delta^{13}C$ values ranging –7.7 to –2.9‰. Furthermore, these values are indistinguishable from those recorded by carbonate cements within the footwall and hangingwall units. The lack of a distinctive negative excursion in $\delta^{13}C$ values at Chibuluma West may indicate that hydrocarbons played a less significant role in ore genesis at this deposit (e.g., the active reductant was H_2S rather than hydrocarbon). Alternatively, the

moderately depleted values may record mixing of carbon sources: i.e., equilibration of 'light' organic carbon with 'heavier' carbon of early diagenetic, metasomatic or metamorphic origin. Supporting this interpretation is an anomalously high concentration of tremolite within the Chibuluma West orebody, which is likely to indicate the presence of an additional dolomitic component within the sandstone host prior to metamorphism.

Late diagenetic–syn-tectonic K + B + Cu ± Co addition

Distribution

Widespread potassium and boron metasomatism within Lower Roan strata was first demonstrated by Darnley (1960). His arguments were based on both petrographic and geochemical evidence, which included (1) paucity of detrital plagioclase relative to basement source rocks, (2) an associated increase of K_2O/Na_2O within most Lower Roan strata relative to basement, (3) abundance of non-detrital K-feldspar within both arenaceous and argillaceous lithotypes, (4) widespread growth of tourmaline as discrete prismatic grains, overgrowths on detrital tourmaline grains and as vein components, and (5) a six-fold 'enrichment' of B within Lower Roan strata relative to basement. Subsequent references to K-metasomatism and its importance in the Cu mineralising process include Sutton & Maynard (2002).

Our own studies have supported Darnley's conclusions, revealing the greatest intensity of K-metasomatism within rocks of the Kitwe Formation, but extending to various levels within the underlying Mindola Clastics Formation (Slide 12). As demonstrated in Scott et al. (this volume A), the formation of K-metasomatic phases was limited principally by the amount of available detrital Al (as Al remained immobile throughout alteration and metamorphism: Large et al., this volume A), and as such K-feldspar or its alteration/metamorphic products are most abundant within argillaceous lithofacies. Thus, the relative paucity of metasomatic K-feldspar within 'clean' non-argillaceous arenites of the Basal Quartzite Member is a result of detrital composition rather than lack of interaction with K-bearing hydrothermal fluids. An apparent decrease in the intensity of K-metasomatism within carbonate-dominated Upper Roan strata also relates in part to lithostratigraphic attributes. In addition, however, are the affects of subsequent Na-metasomatism, during which K-feldspar was largely replaced by albite.

As basement was not examined in detail in our studies, the degree to which K-bearing hydrothermal fluids infiltrated this level remains uncertain (Slide 12). Broughton (this volume) and Bull & Selley (this volume) have documented intense K-metasomatism within basement immediately below the basal Katangan unconformity. By contrast, Darnley's geochemical analyses of basement igneous rocks reveal less evidence pervasive alteration at depth, with abundances of both K_2O and Na_2O compatible with that of typical felsic plutonic rocks. Interestingly, however, his analyses of basement sedimentary rock reveal elevated K_2O/Na_2O values similar to those of many Lower Roan strata. Although little can be said conclusively without knowledge of the origin and lithological nature of Darnley's samples, his data raise the possibility of basement involvement, with partitioning of hydrothermal fluids within more permeable strata.

Textural and composition characteristics of K and B metasomatism

Intense K-alteration is manifested in many units at both meso- and macroscopic scales by a pervasive bleaching or honey-pink colouration accompanying the growth of metasomatic K-feldspar. Although usually developed within arenaceous lithotypes (Slides 13–18), particularly those contained within the Kitwe Formation (ie. hangingwall to the Ore Shale), intense bleaching may also occur within metasiltstones (Slide 26). The more typical dark grey to green colour of metasiltstones (Slide 19) has resulted from partial to complete replacement of metasomatic K-feldspar by anomalously K-enriched phlogopite during peak metamorphism (Large et al, this volume A; Scott et al, this volume A). Thus infiltration of K-bearing fluids occurred independently of original grainsize.

Grainscale textures associated with metasomatic K-feldspar growth are varied, and include (1) micro-crystalline to crypto-crystalline intergranular 'cements', (2) irregularly distributed coarse-grained aggregates, (3) highly domainal stratiform and less common layer-oblique concentrations, (4) over-

growths on detrital feldspar grains, and (5) pervasive replacement of aluminous phases in argillaceous facies (Slides 15, 17, 18, 19, 22). Fine-grained intergranular K-feldspar 'cements' are revealed in hand specimen by a chemical stain (Slides 14, 15). Although largely enclosing the detrital framework and giving the impression of infilling of primary pore space, in detail, metasomatic K-feldspar 'cements' overprint or cross-cut detrital grain boundaries. Examples of corroded margins of detrital quartz and infilling of intragranular microfractures by K-feldspar 'cements' are shown in Slide 16. These textural relationships reveal the fluid's capability of having generated reaction-enhanced permeability, thus removing the necessity for the introduction of hydrothermal fluids during early stages of sediment consolidation (cf. Darnley, 1960). Moreover, the highly domainal character of metasomatic K-feldspar distribution in some arenites, indicate that hydrothermal fluid infiltration was in part facilitated by micro-fracture controlled permeability (see also Bull & Selley, 2001). This processes is particularly evident in cases where narrow metasomatic seams form quasi-systematic planar arrays oriented at high angles to primary layering, requiring a high level of cohesion between framework grains of the host media (Slides 17, 22; also Selley and McGoldrick, this volume).

Metasomatic and detrital K-feldspar are further discriminated on compositional grounds. Electron-microprobe analyses of single grains from Mwambashi B, Chambishi, Mufulira and Ndola West have revealed subtle to extreme Ba enrichment within metasomatic grains relative to detrital grains, with less systematic enrichment of Sr, Ce and Cu (Sutton & Maynard, 2002; Scott et al., this volume B; Selley & McGoldrick, this volume). More conspicuous petrographically, is the common occurrence of fine, prismatic tourmaline crystals within metasomatic K-feldspar (Slide 18). It is unlikely that tourmaline simply records small-scale redistribution of B originally contained within the detrital clay fraction, as Darnley's (1960) analyses of B show greatest concentrations within arenaceous lithotypes: maximum B concentration of 0.14% in arenites verus 0.04% in argillites.

K-feldspar–Cu-sulfide association

In nearly all deposits studied, Cu-, Co- and to a lesser extent Fe-sulfides possess an intimate spatial association with K-feldspar (or its alteration/metamorphic products), suggesting that the K-bearing fluid was also responsible for the introduction of metals. Exceptions to this rule involve high grade portions of arenite-hosted deposits at Mufulira and Chibuluma. In these two cases, high grade ore is partly contained within conspicuously K-feldspar poor 'sericitic quartzites' (Darnley, 1960; Brandt et al., 1961; Annels, 1979). We interpret the formation of sericite to have occurred largely at the expense of K-feldspar due to local acidic conditions formed during oxidation of sour gas or hydrocarbons (e.g., Selley et al., 2002), a point that is expanded upon in Scott et al. (this volume B).

Examples of K-feldspar intergrown with sulfides from both arenite- and Ore Shale-hosted deposits are shown in Slides 21–23. At Ndola West, fine-grained, Fe-poor Cu sulfides occur randomly disseminated throughout a sub-arkosic host. Metasomatic K-feldspar also lacks a systematic distribution pattern, forming irregular aggregates at the margins of, or linking isolated sulfide grains (Slide 21). A similar textural association of metasomatic K-feldspar and chalcopyrite occurs within the argillite-hosted Konkola North deposit. Sulfide textures are characterised by randomly distributed grain aggregates containing irregular, coarse grains of K-feldspar, the latter being texturally distinct from the detrital framework of the enclosing metasiltstone (Slide 23).

By contrast, arenite-hosted mineralisation at Mwambashi B commonly involves domainal concentration of sulfides, approaching stratiform textures within higher grade portions of the deposit (Slide 22). However, detailed examination of the mineralised layers reveals that narrow sulfide concentrations often cross-cut bedding at low to high angles. The photomicrograph in Slide 22 contrasts the internal texture of a layer-oblique sulfide domain with adjacent 'wall rock'. It demonstrates strong partitioning of coarse-grained metasomatic K-feldspar within the sulfide domain, and associated obliteration of primary arenaceous textures. The sharp, planar margin of the K-feldspar–sulfide domain, coupled

with the lack of alteration and clear preservation of detrital textures in the adjacent 'wall rock' provide further evidence for introduction of hydrothermal fluids within well lithified media.

Late diagenetic–syn-metamorphic Na ± Mg ± Ca addition

Distribution

The principal mineral formed during this alteration phase is albite. Albite is most intensely developed within Upper Roan strata, while its distribution at lower stratigraphic levels is more erratic, where it is volumetrically subordinate to pre-existing K-feldspar (Slide 25). This broad stratigraphic partitioning of albite and K-feldspar is in accordance with a relative increase in Na_2O/K_2O values above the Upper Roan– Lower Roan contact (Broughton, this volume; Large et al., this volume A).

In general, the spatial distribution of albite coincides with zones of fracture-enhanced permeability. However, the processes responsible for brittle fracturing are varied and incompletely understood. Within the Upper Roan, the most important fracture zones relate to significant volumes of intraformational breccia (Slide 25), which are interpreted to have formed though processes of salt dissolution and withdrawal (Broughton, this volume). Although a component of tectonic fragmentation involved in breccia formation cannot be discounted, it is considered less likely as breccia bodies are largely discordant to enclosing stratigraphy and show little signs of having facilitated significant stratal dislocation. Concentration of such breccia bodies within the Upper Roan accounts in part for the broad partitioning of albitisation within higher stratigraphic levels.

Within the Lower Roan, intense albitisation also shows a broad spatial association with intraformational breccia bodies (Slide 25). Although texturally analogous to those bodies contained within the Upper Roan, these examples are volumetrically less significant and appear spatially related to gabbroic intrusions (e.g., Chibuluma West, Mwambashi B and Nkana West Limb). Fragmentation driven by salt withdrawal is untenable within lower stratigraphic intervals and most probably relates to either the gabbro emplacement process or utilisation of the rheological contrast between the gabbros and enclosing strata during subsequent tectonism. In favour of the latter process, is the common partitioning of albite within narrow, crudely stratabound cataclastic zones in coherent strata. The best example of this relationship occurs at Mwambashi B, where albitisation intensifies towards the Mindola Clastics Formation – lower Ore Shale contact, which decoupled, most probably at the onset of basin inversion (Selley & McGoldrick, this volume). Furthermore, in highly strained mineral deposits (e.g., Nkana and Chibuluma West), albite forms an important constituent of the ore assemblage (Selley & Cooke, 2001; Croaker & Selley, this volume).

Albite–K-feldspar relationships within Lower Roan strata

With the exception of an isolated occurrence within the Ndola West footwall (Scott, et al., this volume), albite consistently overprints metasomatic K-feldspar (Slides 26, 28). In general, albite is coarser grained, forming more prismatic crystals than pre-existing K-feldspar, however development of fine-grained albite pseudomorphs after micro-crystalline K-feldspar occurs locally within intensely altered argillaceous protoliths (Slide 27). In these latter cases, albite grains lack well-developed twinning and were identified only though the use of electron microprobe and whole rock geochemical techniques.

Albite is in many cases accompanied by, and occurs in apparent textural equilibrium with syn-metamorphic phlogopite and dolomite (Slides 27, 28). Although the necessary Mg, Ca and C to account for this assemblage were likely pre-existing as detrital constituents within dolomitic argillite facies, there are numerous examples where these elements were clearly absent prior to albitisation. For example, the siltstone precursor to albite-phlogopite assemblage in Slide 27 was manifestly lacking in available Mg, consisting largely of metasomatic K-feldspar with minor quartz and tourmaline. A similar relationship is shown in Slide 28, where an albite-phlogopite-dolomite domain, formed peripheral to a shear zone, clearly cross-cuts layering within a sub-arkose recording prior K-feldspar metasomatism. Thus Mg, and potentially Ca and C, were necessarily additional components of the sodic hydrothermal fluid.

Alteration assemblages within breccia facies

The alteration assemblage within breccia bodies distributed largely throughout the Upper Roan but extending locally to lower stratigraphic intervals, is very similar to that described above from more weakly deformed portions of the Lower Roan. Na, Mg and Ca bearing phases predominate the assemblage: ie. albite–phlogopite–dolomite and talc.

An example of a breccia unit formed peripheral to a gabbroic body and contained within Lower Roan strata is shown in Slides 29–32. Partitioning of late stage hydrothermal fluids within the breccia facies is indicated by an abrupt increase of Na_2O coupled with depletion of K_2O relative to less deformed enclosing strata. However, MgO enrichment is less obviously coupled with that of Na_2O, with elevated values being restricted to the lowermost portion of the breccia. The comparable abundances of MgO within the upper two thirds of the breccia and overlying Upper Roan metasediments imply that lithological precursors to brecciation involved a significant dolomitic component.

Preservation of primary sedimentary textures within the breccia is rare. The intensely Na-metasomatised base of breccia is associated with a massive plug of coarse-grained albite, with fragmental textures becoming apparent at higher levels (Slide 30). In situ fragmentation is indicated by the monomictic clast assemblage and crude jigsaw-fit texture. Although pervasively albitised, grainscale textures and mineral assemblages of the matrix and clasts are distinct, suggesting a multi-stage alteration history. Whereas the matrix comprises coarse, prismatic grains of twinned albite, phlogopite, talc and dolomite, the clasts are comparatively mica-poor, consisting of inclusion-rich felted masses of considerably finer-grained, untwinned albite (Slide 31). The internal texture of the clasts is very reminiscent of pseudomorphed metasomatic K-feldspar (cf. Slide 27), an interpretation that is supported by abundant tourmaline inclusions (Slide 32).

Albite–ore association

Although K-feldspar is the principal silicate alteration phase associated with Cu-Co mineralisation, late-stage albite occurs with varying abundances in a large number of the deposits studied, particularly those located in the Chambishi Basin (see also Selley & McGoldrick, this volume). The most extreme case is Chibuluma West, where albite is intimately associated with ore, whereas K-bearing phases are almost entirely absent. As with many other domains of intense albitisation, there is a close spatial relationship with breccia facies and gabbroic bodies, both of which are situated within the immediate hangingwall of the ore zone. Furthermore, there is clear evidence of structurally-controlled fluid ingress, with highly domainal albite-sulfide concentrations, oriented both parallel and oblique to primary layering (Slide 33; also Selley and Cooke, 2001).

Ore textures, sulfide compositions and parageneses are remarkably similar to those at the nearby Mwambashi B deposit (compare Slides 22, 33), however the distinct alteration assemblages are demonstrated clearly by a dramatic increase in Na_2O/K_2O at Chibuluma West (Slide 33). That potassium has been effectively stripped from the Chibuluma West ore during the sodic alteration event, is revealed at the grain-scale. Although albite presently occurs in apparent textural equilibrium within both Fe- and Cu-sulfides, a pre-existing phase of K + B metasomatism is recorded by abundant tourmaline crystals distributed along micro-fractures and relict grain margins preserved within the cores of coarse, optically-continuous albite grains (Slides 34, 35). These textures are analogous to the coarse albite clots that pseudomorph pre-existing intergranular metasomatic K-feldspar from the hangingwall of Chambishi SE ore shown in Slide 28.

Discussion and conclusions

Roan strata record a protracted history of fluid migration from early diagenesis to the latest stages of basin development. In the basin's early history, anhydrite and dolomite alteration was most probably associated with localised descent of relatively small volumes of dense, sulfate-saturated brines sourced from evaporitic strata above the level of the Ore Shale. Although unlikely to represent a major fluid flow event, precipitation of labile cements during early diagenesis was important in terms of supporting the detrital framework from the onset of burial (thus inhibiting compaction), but also allowing

for the generation of secondary reaction enhanced permeability and porosity as well as a sulfur source, during the subsequent mineralisation phase. The very fact that anhydrite remains preserved today, indicates that a widespread phase of early diagenetic silicification did not affect the Copperbelt.

Generation and trapping of hydrocarbons was also likely to have involved only small volumes of fluid and/or gas, derived from lower stratigraphic levels. The most probable source rocks were organic-rich facies within the Ore Shale, however additional contribution from thicker source units presumably located outside the ZCB is necessary to account for the significant hydrocarbon accumulation required at Mufulira. In addition to providing a reductant in otherwise organic-poor facies in arenite-hosted deposits, the former presence of hydrocarbons allows us to place a maximum time constraint on Cu-Co mineralisation. In order to have passed through the 80°-120°C 'oil window', source rocks must have been buried to depths of 2–3 km at least. This thickness of strata is roughly equivalent to the preserved stratigraphy between the Ore Shale and the Middle Kundelungu in the ZCB (Garlick, 1961; Annels, 1989). On the basis of the age of the global Marinoan glacial event (Petit Conglomerate – base of the Middle Kundelungu), maximum ages for hydrocarbon generation would range 700–600 Ma. However, if the original thickness of the Upper Roan involved a significant component of salt (now dissolved or remobilised), burial of source rocks to 3 km may have occurred closer to the end of Roan sedimentation (ie. ~740 Ma). As a final hypothesis, hydrocarbons may have been generated pyrolitically via local thermal input to the basin, such as the introduction of hot magma (e.g., Kontak & Sangster, 1998). The 740–760 Ma gabbro bodies that were emplaced mainly at the level of the Mwashia are possible candidates for this mechanism. Although the genesis of hydrocarbons is uncertain, their involvement in the ore forming process militates against an early diagenetic age of mineralisation.

Migration of hydrocarbons is also significant in that it had the potential to generate and maintain secondary permeability and porosity. This could have been achieved by the dissolution of early diagenetic anhydrite cements to form H_2S, or perhaps more importantly, by the dissolution of silicate phases. Surdam et al. (1989) argued that the formation of carboxylic acid anions through the breakdown of kerogens greatly increased the solubility of Al, thus promoting degradation of alumino-silicates and developing the necessary permeability for hydrocarbon migration. By contrast, if acidic fluids are buffered by more basic media (groundwaters or carbonates), organic acid-silica complexes may form, leading to dissolution of quartz (Bennett et al., 1991). Thus if organic acids were being generated along margins of the Ore Shale source media, upper and lower contacts may have remained permeable well into late diagenesis.

Potassic metasomatism and associated Cu-Co mineralisation heralded the onset of hydrothermal system that affected the entire Roan basin system. Addition of K and B to the system is compatible with an intrabasinal hypersaline brine, most probably sourced from dissolution of Upper Roan salt. That the fluid was clearly supersaturated with K may indicate the involvement of bittern brines, however similar compositions may have been achieved by interaction with arkosic basinal strata or perhaps K-rich basement rocks (see Kosiy et al., this volume).

Although evidence that fluid ingress was facilitated by grain-scale fracturing occurs at small number of deposits, this process alone cannot account for the pervasive nature of K-feldspar growth within even the finest-grained lithotypes. Furthermore, the intensity of K-metasomatism within 'hangingwall' strata indicates that fluids were not simply partitioned into an anomalously permeable aquifer system below the level of the Ore Shale. Instead, alteration textures recorded throughout most siliciclastic strata demand a protracted hydrothermal event, where the passage of fluids was influenced less by primary porosity and permeability, but rather by reaction-enhanced permeability in consolidated rock. Concentration of micro-crystalline K-feldspar within formerly silty facies as well as the matrix of 'dirty' arenites, the latter forming a broad halo to the Ore Shale, suggests that the detrital clay fraction was particularly susceptible to degradation in the presence of the potassic fluid. Combination of this process, with additional permeability generated through reaction of organic acids with detrital alumino-silicates and fracture-enhanced permeability at the margins of

the Ore Shale generated during tectonism, almost certainly contributed the focussing of metal-bearing fluids at this stratigraphic level.

The final stage of Na-, Mg- ± Ca-metasomatism is also consistent with passage of evaporite-sourced brines. Although albite precipitation postdates metasomatic K-feldspar in nearly all cases, the change in alteration assemblage may have been progressive, reflecting an evolving basin environment, rather than two unrelated hydrothermal events. A phase diagram depicting the relative stabilities of K-feldspar and albite in the context of variable temperature and Na/K is shown in Slide 38. It demonstrates that a fluid with moderate, but constant Na/K will precipitate K-feldspar and subsequent albite with increasing temperature. Supporting geochemical evidence for this process are the O-isotopic signatures of hydrothermal carbonate associated with K-feldspar and albite, which can be accounted for by precipitation from a common marine seawater at 120°–180°C and 350°C respectively (Large, et al., this volume B).

Increasing temperatures and the associated transition from K-feldspar to albite stability may have resulted from a number of different mechanisms: (1) intrabasinal thermal input related to gabbro emplacement, (2) increased burial during progressive sedimentation and basin growth, (3) increased burial due to structural thickening during basin inversion, or (4) passage of hydrothermal fluids through deep crustal levels along basement-tapping fault zones. Although there is a spatial relationship between albitic breccias with gabbroic bodies in some cases, this is comparatively rare, and certainly the voluminous Upper Roan breccia units on the eastern Kafue Anticline lack a systematic association with intrusive bodies. The gabbroic association may therefore relate to the rheological properties of these units, or more likely to the spatial, but not temporal coincidence of intrusions and subsequent fluid flow with major basin-bounding structures. Of the remaining alternatives, progressive burial related to structural thickening would appear most likely considering the widespread association of fracture-enhanced permeability and albitisation. Moreover, albitisation at the structurally-controlled Kansanshi copper deposit has been reliably dated at 514 Ma, an age which is rapidly approaching that of peak metamorphism.

The transition from widespread reaction-enhanced permeability associated with K-metasomatism to more domainal fracture-enhanced permeability characterised by albitisation most probably records progressive replacement of labile constituents and sealing-up of the system. The broad stratigraphic partitioning of potassic and sodic phases is therefore interpreted to reflect greater efficiency of fragmentation at higher levels during burial. Upward transition in structural style from high amplitude, upright folding involving Lower Roan strata, to recumbent folding and regional layer-parallel detachment surfaces at Mwashia levels has been documented by Broughton & Hitzman (2001). Development of sub-horizontal shear zones within evaporitic strata of the Upper Roan, would have greatly facilitated fluid flow, dissolution of salt and accompanying *in situ* fragmentation. Thus although the onset of brine-generation may well have preceded orogenesis, the process would have accelerated dramatically with tectonic decoupling of the stratigraphy close to the Mwashia–Upper Roan contact. Supporting the interpretation of fluid flow having been controlled by an evolving fracture system, is the evidence of intense K + B -metasomatism with breccia bodies as indicated by the replacive albitic textures and relict tourmaline crystals within clasts.

References

Annels, A. E., 1974. Some aspects of the stratiform ore deposits of the Zambian Copperbelt and their genetic significance. In: *Gisements stratiformes et provinces cupriferes*. Bartholome P. ed., pp. 235-254.

Annels, A., E., 1979. Mufulira greywackes and their associated sulfides. Institution of Mining and Metallurgy, Transactions, Section B: Applied Earth Science, vol.88, pp.15-23.

Annels, A. E., 1989. Ore genesis in the Zambian Copperbelt, with particular reference to the northern sector of the Chambishi Basin. In *Sediment-hosted Stratiform Copper Deposits*. Boyle, R., Brown., A., Jefferson, C., Jowett, E. & Kirkham, R. Eds. GAC Special Paper 36, pp. 427-452.

Bennett, P., Siegel, D., Hill, B., Glaser, P., 1991. Fate of silicate minerals in a peat bog. Geology (Boulder), vol.19, no.4, pp.328-331.

Brandt, R., Burton, C., Maree, S., Woakes, M., 1961. Mufulira. In: *The geology of the Northern Rhodesian Copperbelt*. Ed. Mendelsohn, F. pp. 411-461.

Broughton, D. & Hitzman, M., 2001. Progress report 2001. AMIRA P544 Progress Report, June 2001.

Broughton, D., 2002. Stratigraphy, regional alteration and mineralization patterns in the Zambian Copperbelt. AMIRA P544 Progress Report, Dec 2002. pp. 11.1-11.9.

Broughton, D., this volume. Stratigraphy, regional alteration and mineralisation of the Zambian Copperbelt.

Bull, S. & Selley, D., 2001. Geology of DDH NN 47, Chambishi Basin. AMIRA P544 Progress Report, June 2001.

Bull, S. & Selley, D., this volume. Chambishi basin studies; Chambishi SE Prospect.

Croaker, M. & Selley, D., this volume. Structural development and controls on Cu-Co mineralisation at Nkana-Mindola.

Darnley, A. G., 1960. Petrology of some Rhodesian Copperbelt Orebodies and associated rocks. Institution of Mining and Metallurgy, Transactions, Section B: Applied Earth Science, vol.638, no.69, pp.137-173.

Garlic, W., 1961. The Chambishi Nkana Basin. In: *The geology of the Northern Rhodesian Copperbelt*. Ed. Mendelsohn, F. pp. 281-297.

Kontak, D. & Sangster, D., 1998. Aqueous and liquid petroleum inclusions in barite from the Walton Deposit, Nova Scotia, Canada; a Carboniferous, carbonate-hosted Ba-Pb-Zn-Cu-Ag deposit. Economic Geology and the Bulletin of the Society of Economic Geologists, vol.93, no.6, pp.845-868.

Kosiy, L., Large, R., Yang, J., Bull, S., Selley, D., this volume. Numerical fluid flow, salinity and heat transfer modelling in the Zambian Copperbelt.

Large, R., McGoldrick, P., Bull, S., Scott, R., Selley, D. this volume A. Lithogeochemistry and Alteration Halos to Stratiform Copper Mineralisation in the Chambishi Basin, Zambian Copper Belt.

Large, R., Bull, S., Croaker, M., McGoldrick, P., Pollington, N., Scott, R., Selley, D., this volume B. Carbon and Oxygen Isotopic composition of Ore-Related and Sedimentary carbonates in the Roan, ZCB.

McKinnon, D. & Smitt, N., 1961. Nchanga. In: *The geology of the Northern Rhodesian Copperbelt*. Ed. Mendelsohn, F. pp. 235-275.

Mendelsohn, F., 1989. Central/southern African Ore Shale deposits. . In *Sediment-hosted Stratiform Copper Deposits*. Boyle, R., Brown., A., Jefferson, C., Jowett, E. & Kirkham, R. Eds. GAC Special Paper 36, pp. 453-470.

Scott, R., 2002. Stratigraphy, structure and copper mineralisation, Ndola West, Zambia. AMIRA P544 Progress Report, Dec 2002. pp. 10.1-10.33.

Scott, R., Berry, R., Selley, D., Bull, S., this volume A. Lufilian metamorphism in the Zambian Copperbelt: Implications for the interpretation of mineral assemblages and alteration paragenesis.

Scott, R., Selley, D., & Cooke, D., this volume B. Arenite-hosted copper mineralisation east of the Kafue Anticline: A comparison of tectono-stratigraphic, mineralogical, geochemical and C- and O-isotopic characteristics of small and large deposits.

Selley, D. & Bull, S., 2001. Stratigraphy and basin geometry at the Chibuluma West copper-cobalt deposit, Zambia. AMIRA P544 Progress Report, Dec 2001. pp. 101-132.

Selley, D. & Cooke, D., 2001. Mineral zonation and sulfur isotope systematics of the Chibuluma West copper-cobalt deposit, Zambia. AMIRA P544 Progress Report, Dec 2001. pp. 133-170.

Selley, D., Bull, S., Scott, R., Cooke, D., 2002. Chambishi Basin progress report 2: Basin geometry and its controls on mineralisation at Mwambashi B. AMIRA P544 Progress Report, Dec 2002. pp. 5.1-5.40.

Surdam, R., Crossey, L., Hagan, E., Heasler, H., 1989. Organic-inorganic and sandstone diagenesis. AAPG Bulletin, vol.73, no.1, pp.1-23.

Sutton, S. & Maynard, J., 2002. Fluid mixing model for the Zambian Copperbelt. 11th quadrennial IAGOD symposium and geocongress.

Wilson, N. & Zentilli, M., 2003. The role of organic matter in the genesis of the El Soldado volcanic-hosted manto-type Cu deposit, Chile. Economic Geology and the Bulletin of the Society of Economic Geologists, vol.94, no.7, pp.1115-1135.

Zentilli, M., Munizaga, F., Graves, M. C., Boric, R., Wilson, N., Mukhopadhyay, P. K., Snowdon, L. R. 1997. Hydrocarbon involvement in the genesis of ore deposits: an example in Cretaceous stratabound (Manto-type) copper deposits of Central Chile. International Geology Reviews, 39, 1-21.

Alteration History of the Roan:
a Summary of Textural Relationships

P544 Team

Slide 1

Alteration History

- Despite the effects of metamorphism, we are able to distinguish 4 *main* alteration events

Reflected in:
- Changes in bulk rock geochemistry
- Paragenetic relationships between mineral species

1. Early diagenetic SO4, Ca, Mg metasomsatism
   - *anhydrite - dolomite*
2. Late diagenetic hydrocarbon generation
3. Late Diagenetic – K, Cu, Co? +/- B metasomatism
   - *Kspar, sericite, Cu-Co sulphide, calcite*
4. Late Diagenetic - Na +/- Mg +/- Ca metasomatism
   - *Albite, dolomite, ?talc, ?phlogopite*

Slide 2

Distribution of Alteration Assemblages

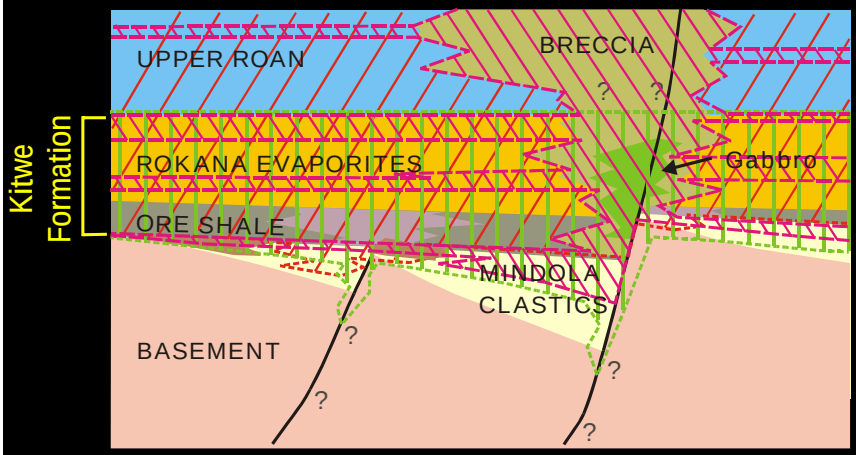

- Complex superposition of multiple alteration assemblages
- Intensity & complexity forms halo to Kitwe Formation

Slide 3

Early Diagenetic Anhydrite +/- Dolomite

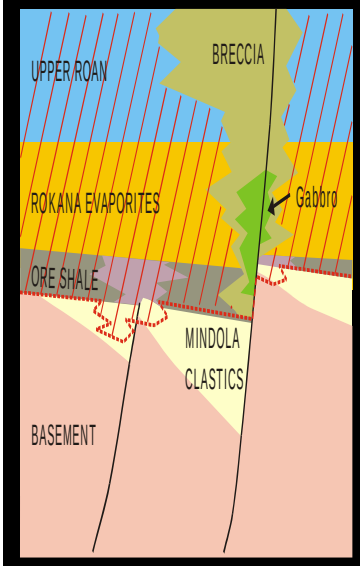

Distribution

- Insitu growth of anhydrite cements throughout Rokana Evaporites & upper portion of Ore Shale
  - primarily within fine-grained facies
- Cements persist locally into Mindola Clastics Formation (FW) and even Basement
  - where intensely developed in HW succession

Slide 4

Early Diagenetic Anhydrite+/- Carbonate

REM

- Muddy sandstones, microbial carbonates, displacive nodules in siltstones

MCF

- Recrystallised cements throughout clean sandstones
- Fluvial origin – inconsistent with playa facies

Slide 5

Early Diagenetic Anhydrite+/- Carbonate

Significance

- Descent of dense, early diagenetic sulphate rich brine
  - Brine reflux
  - Dehydration of insitu gypsum
- Early occlusion of pore space within FW sandstones
- Anhydrite potentially unstable during subsequent alteration
  - *Generation of secondary reaction enhanced permeability*
  - *Sulphur source*

Slide 6

Late Diagenetic Hydrocarbon Generation

- Least easily recognisable of all alteration phases in terms of mineral paragenesis
- No evidence of pyrobitumen
- Preservation of carbonaceous matter within mineralised "greywackes" at Mufulira (Annels, 1979)

Slide 7

Late Diagenetic Hydrocarbon Generation

Lines of evidence

1. Partitioning of arenite hosted mineralisation within lithological & geometric trap sites: *ie. coarse, clean, non-argillaceous or anhydrite-cemented media enclosed by 3-D seals*

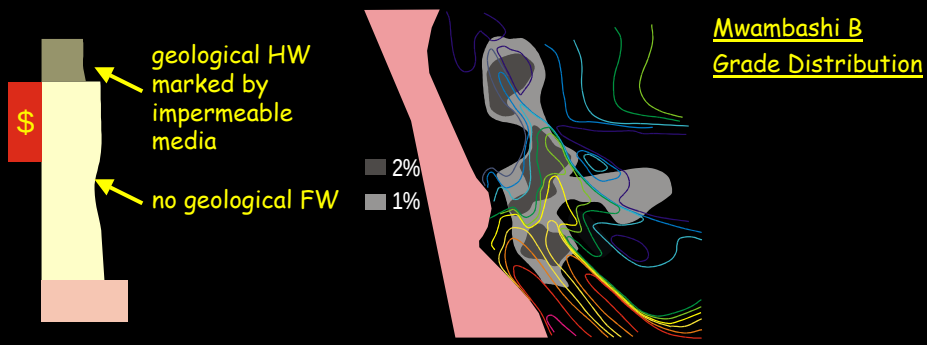

Slide 8

Late Diagenetic Hydrocarbon Generation

Lines of evidence

1. Partitioning of arenite hosted mineralisation within lithological & geometric trap sites: *ie. coarse, clean, non-argillaceous or anhydrite-cemented media enclosed by 3-D seals*
2. Calcite cements with strongly negative $\delta^{13}C$ isotopic signatures

- *requires oxidisation of organic carbon*

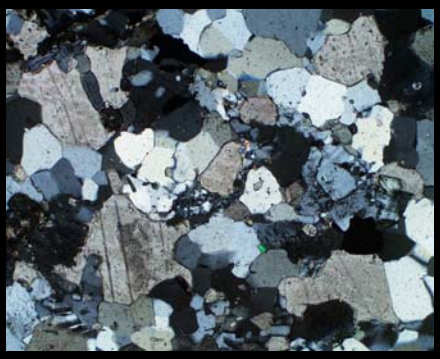

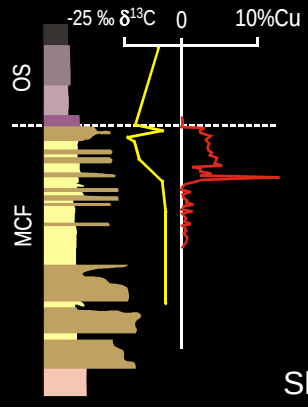

Slide 9

Late Diagenetic Hydrocarbon Generation

Lines of evidence

1. Partitioning of arenite hosted mineralisation within lithological & geometric trap sites: *ie. coarse, clean, non-argillaceous or anhydrite-cemented media enclosed by 3-D seals*
2. Calcite cements with strongly negative $\delta^{13}C$ isotopic signatures
3. Association of sulphides with radiogenic mineral phases: ie. monazite & zircon

- *thermally induced polymerization of hydrocarbons*

Monazite

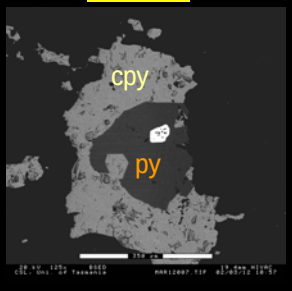

Huttonite

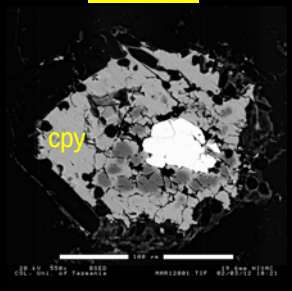

Slide 10

Late Diagenetic Hydrocarbon Generation

Lines of evidence

1. Partitioning of arenite hosted mineralisation within lithological & geometric trap sites: *ie. coarse, clean, non-argillaceous or anhydrite-cemented media enclosed by 3-D seals*
2. Calcite cements with strongly negative $\delta^{13}C$ isotopic signatures
3. Association of sulphides with radiogenic mineral phases: ie. monazite & zircon

- *thermally induced polymerization of hydrocarbons*

Significance

- Provides necessary reductant in otherwise reductant-poor media
- Provides constraint on timing of arenite-hosted Cu-mineralisation: ie. must be within "oil window"
  - burial to ~3km OR pyrolitic HC generation – gabbros, hydrothermal fluid?
- Has the potential to generate and maintain porosity via dissolution of anhydrite cements or alumino-silicates

Slide 11

K metasomatism

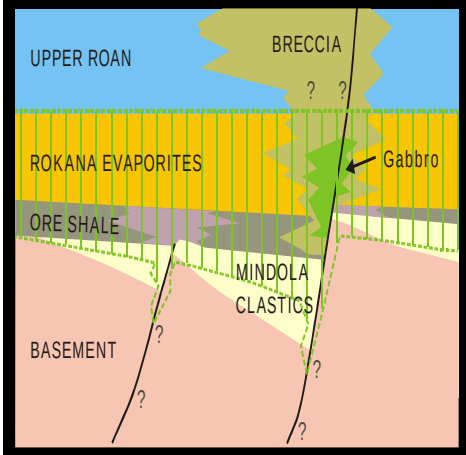

Distribution

- K metasomatism is concentrated within a halo to the Kitwe Formation
- Extends to varying levels into the Mindola Clastics Formation (ie. FW)
- Although most conspicuous within subarkosic protoliths, intensity of K-metasomatism is often developed independently of original grain-size

Slide 12

K metasomatism

Arenites

- Bleaching of sheet sands within Chambishi HW

Slide 13

K metasomatism

Arenites

- Clear preservation of detrital textures
- Pervasive intergranular kspar stain

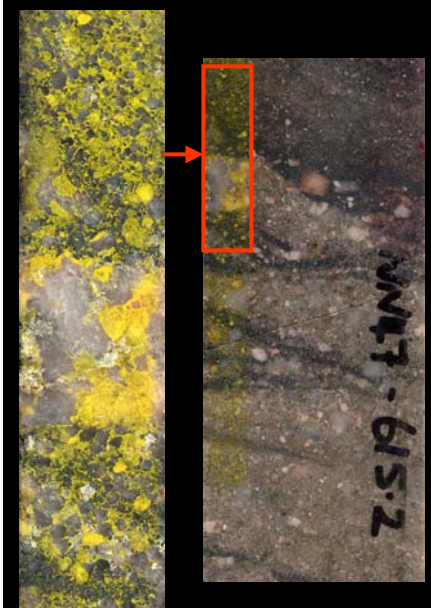

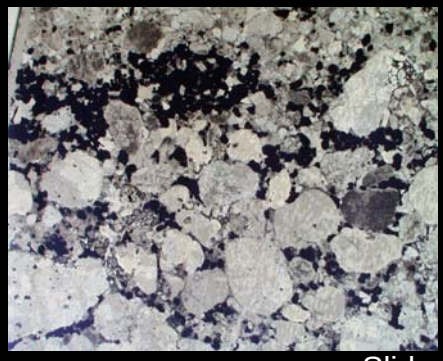

Slide 14

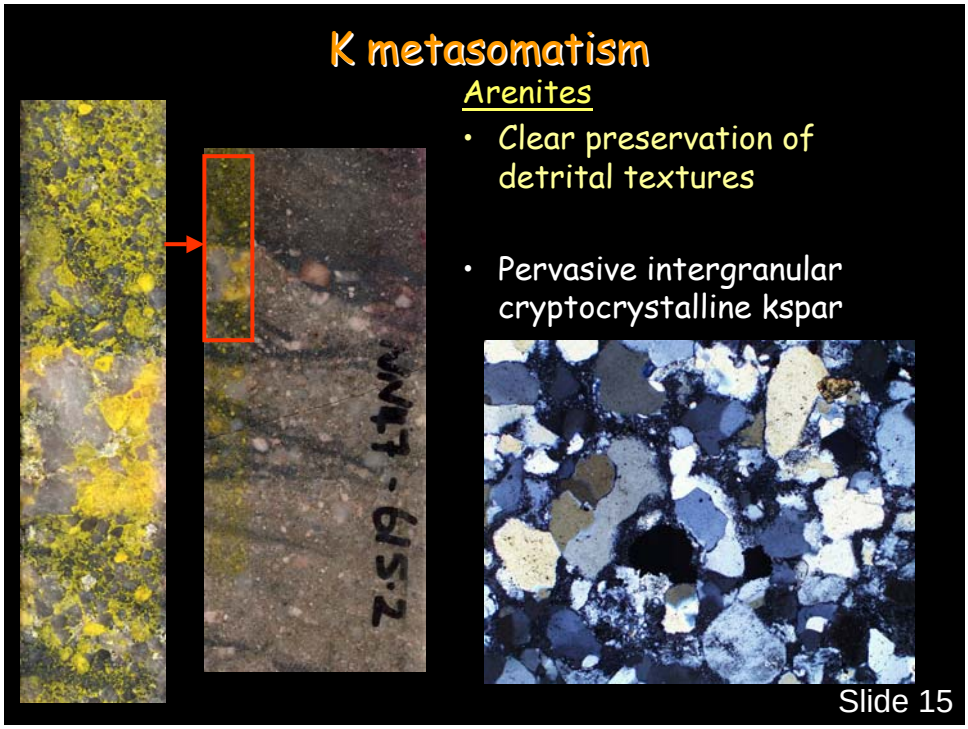
K metasomatism
Arenites
• Clear preservation of detrital textures
• Pervasive intergranular cryptocrystalline kspar
Slide 15

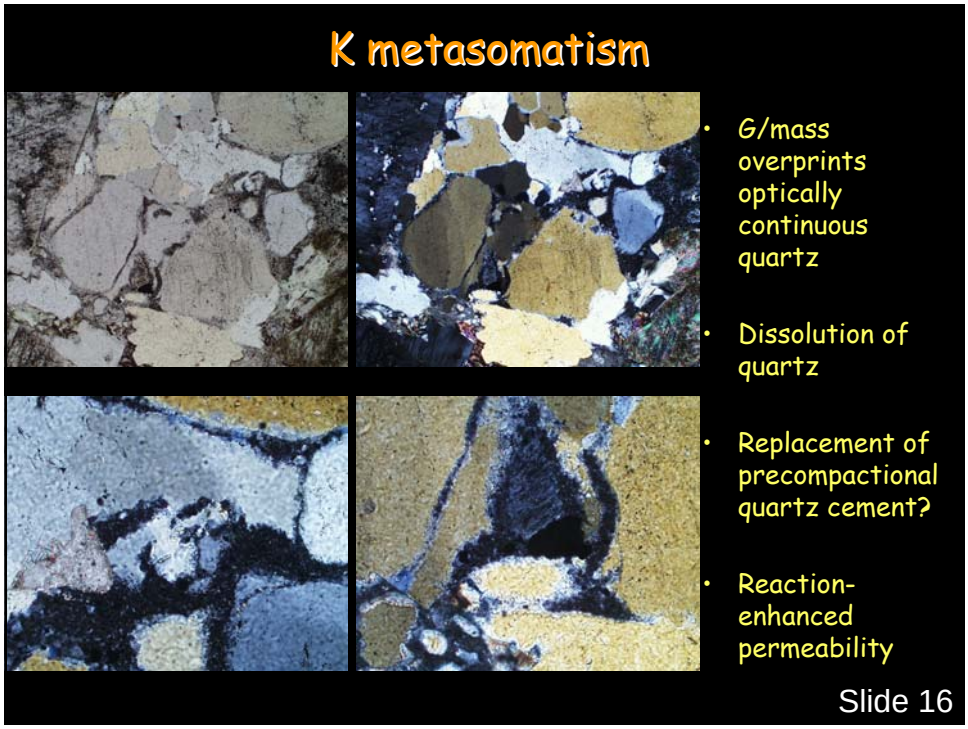
K metasomatism
• G/mass overprints optically continuous quartz
• Dissolution of quartz
• Replacement of precompactional quartz cement?
• Reaction-enhanced permeability
Slide 16

K metasomatism

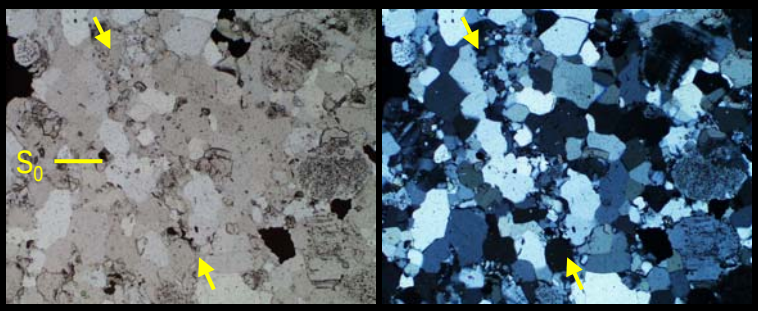

- Domainal kspar distribution
- Fine metasomatic kspar largely confined to planar layer-oblique seams
- High level of cohesion within host media
- Probable micro-fracture enhanced permeability

Slide 17

Late Diagenetic K metasomatism

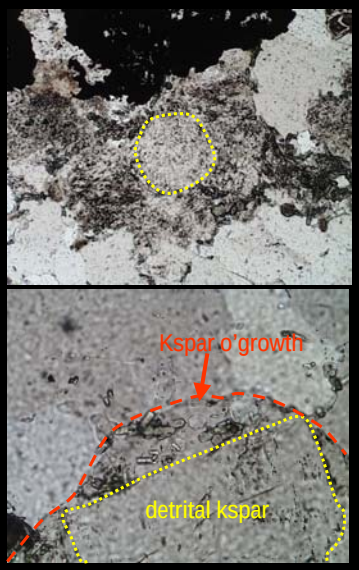

Kspar Composition

- Metasomatic kspar is distinguishable from detrital grains on compositional grounds
  - Ba, Sr, Na
- Common association of tourmaline within kspar overgrowths
  - particularly within the Mindola Clastics Formation
  - B is probable additional component of the K-bearing fluid

Slide 18

Late Diagenetic K metasomatism

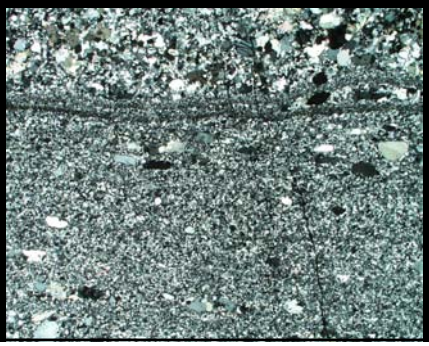

Siltstones

- Staining reveals pervasive kspar growth
- Common dark colour due to partial replacement of kspar by phlogopite during metamorphism
- Rare phlogopite-poor domains reveal cryptocrystalline kspar growth throughout fine media

Slide 19

Kspar-Cu Association

- In almost all cases, Cu-Co sulphides display an intimate spatial association with metasomatic Kspar *OR with alteration/metamorphic products of kspar*
  - *Important exception – high grade portion of the Mufulira "C" Orebody*
- However, the limits of intense K-metasomatism extend well outside those of mineralisation

Slide 20

Kspar-Cu Association

Arenite-hosted Deposits – Ndola West

- Patchy, disseminated Cu-sulphide – kspar aggregates
- kspar/qtz ratio (1:2-3)
  - detrital ~ 1:5

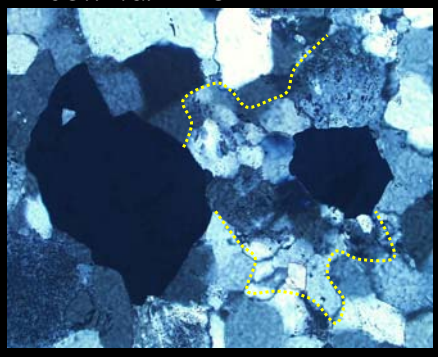

Slide 21

Kspar-Cu Association

Arenite-hosted Deposits – Mwambashi B

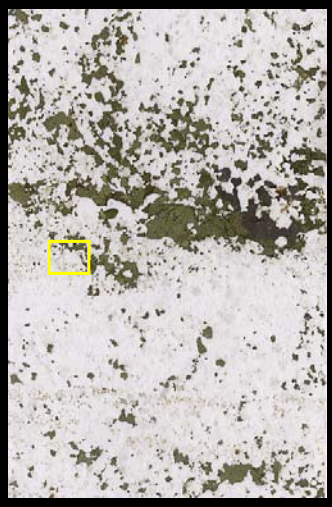

- Strong partitioning of kspar-carr-cpy into discrete domains
- Kspar/qtz ratio up to 1.8:1

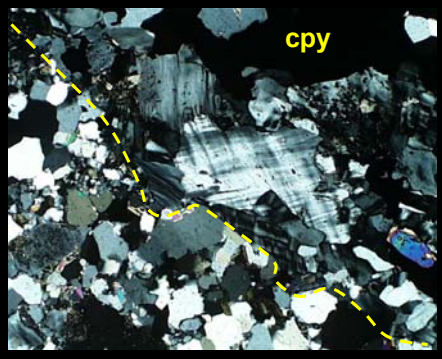

Slide 22

Kspar-Cu Association

Ore Shale-hosted Deposits – Konkola North

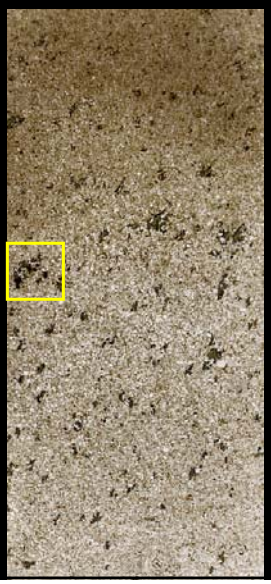

- Higher phyllosilicate component
- Disseminated sulphides
- Crude partitioning in coarser bands
- In detail, clotty intergrowth of Cu-sulphide & kspar

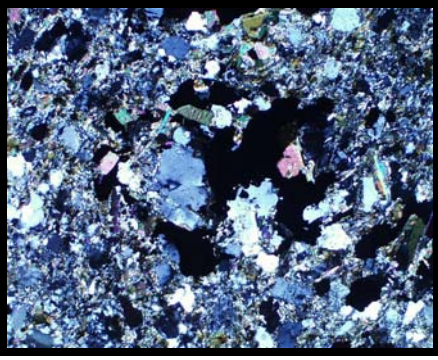

Slide 23

Sulphide Paragenesis

- Systematic sulphide paragenesis preserved throughout Chambishi Basin ore bodies

pyrite → carrollite → chalcopyrite - cpy +/- bn +/- cc

- Much of the early pyrite is cobaltiferous
  - Carrollite may represent a product of Co-pyrite consumption during precipitation of Cu
- Paragenesis does not hold at Nchanga & Konkola

Slide 24

Na +/- Mg +/- Ca Metasomatism

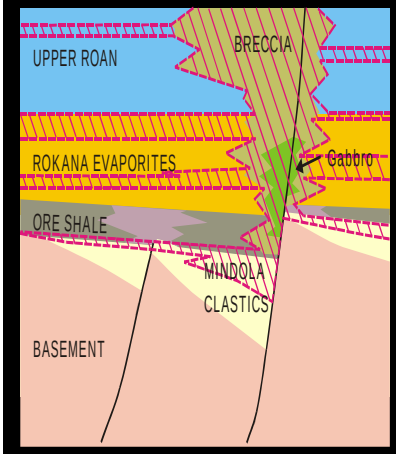

Distribution

- Intensely developed within fracture-induced breccia zones
- Dominant above the level of the Lower Roan, but locally extending to the Mindola Clastics Formation
  - mantle to gabbros – *"hydrid rock"*
- Discrete, crudely stratabound domains throughout Lower Roan
- In general, stratabound domains are narrower than K-metasomatic domains
  - Can follow same pathways (particularly where K-metasomatism is fracture controlled)
  - Often forms part of ore assemblage

Slide 25

Alteration fronts in Lower Roan (Chambishi HW)

- Extreme K-metasomatism
- Dark domain records Na-Mg metasomatism
  → Albite-phlogopite

Slide 26

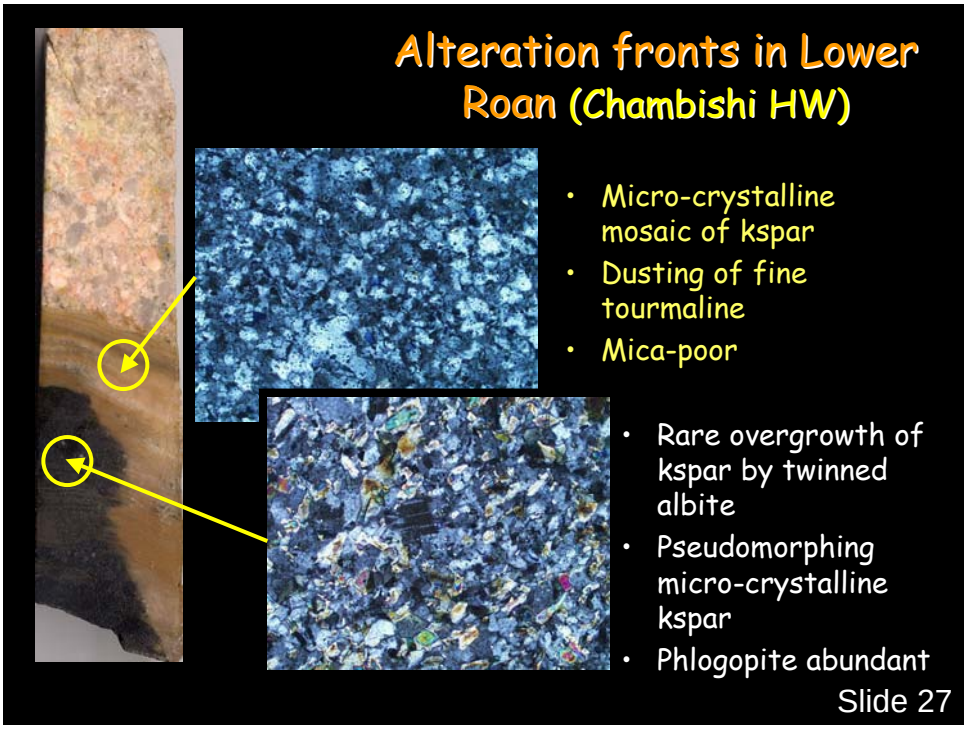
Alteration fronts in Lower Roan (Chambishi HW)
Micro-crystalline mosaic of kspar
Dusting of fine tourmaline
Mica-poor
Rare overgrowth of kspar by twinned albite
Pseudomorphing micro-crystalline kspar
Phlogopite abundant
Slide 27

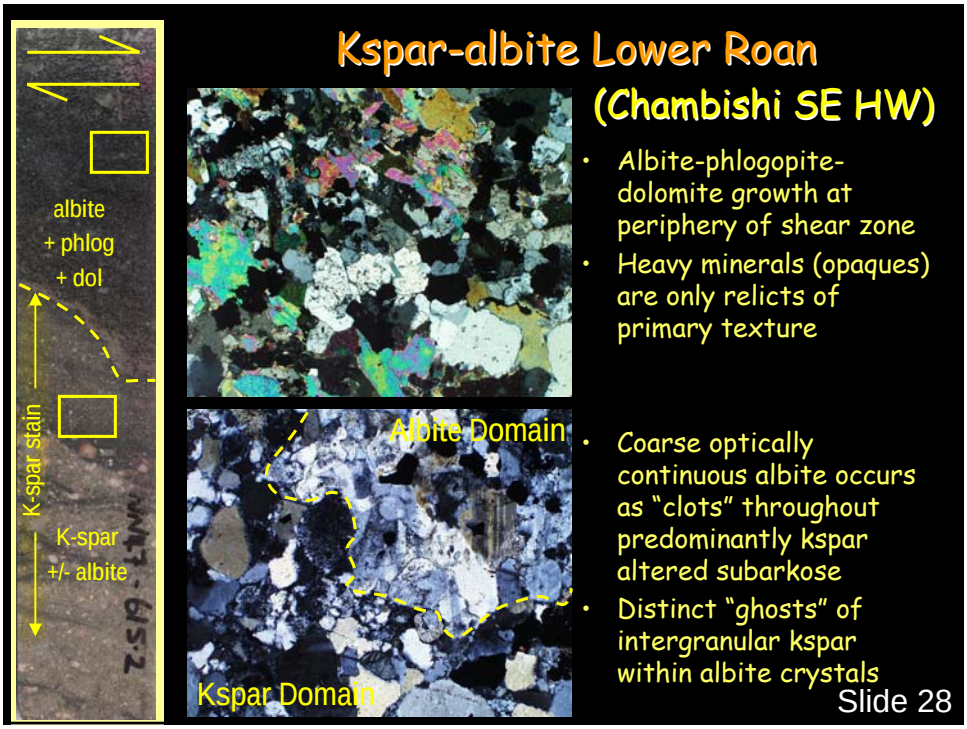
Kspar-albite Lower Roan (Chambishi SE HW)
albite + phlog + dol
K-spar stain
K-spar +/- albite
Albite Domain
Kspar Domain
Albite-phlogopite-dolomite growth at periphery of shear zone
Heavy minerals (opaques) are only relicts of primary texture
Coarse optically continuous albite occurs as "clots" throughout predominantly kspar altered subarkose
Distinct "ghosts" of intergranular kspar within albite crystals
Slide 28

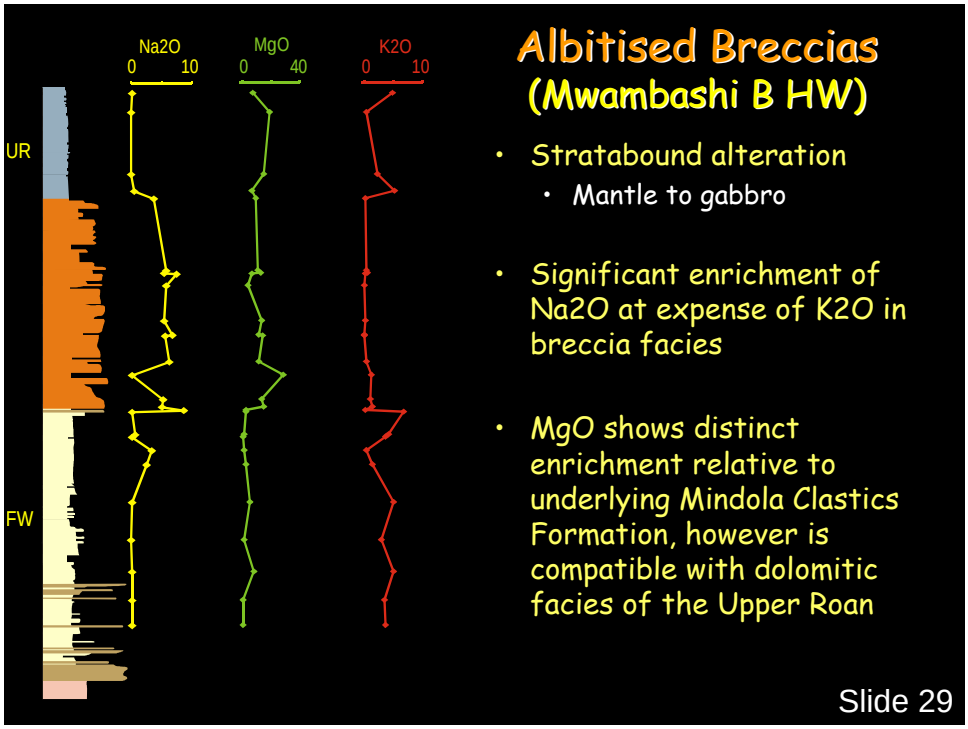
Na2O
0 10
MgO
0 40
K2O
0 10
UR
FW
Albitised Breccias
(Mwambashi B HW)
• Stratabound alteration
• Mantle to gabbro
• Significant enrichment of Na2O at expense of K2O in breccia facies
• MgO shows distinct enrichment relative to underlying Mindola Clastics Formation, however is compatible with dolomitic facies of the Upper Roan
Slide 29

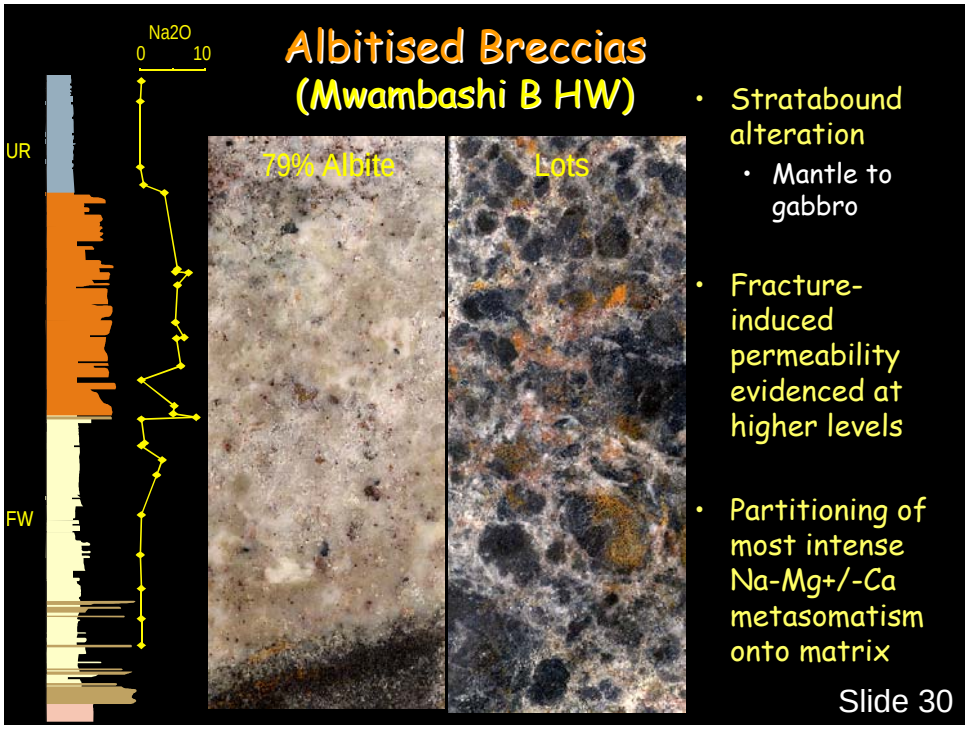
Na2O
0 10
UR
FW
Albitised Breccias
(Mwambashi B HW)
79% Albite
Lots
• Stratabound alteration
• Mantle to gabbro
• Fracture-induced permeability evidenced at higher levels
• Partitioning of most intense Na-Mg+/-Ca metasomatism onto matrix
Slide 30

Albitised Breccias (Mwambashi B HW)

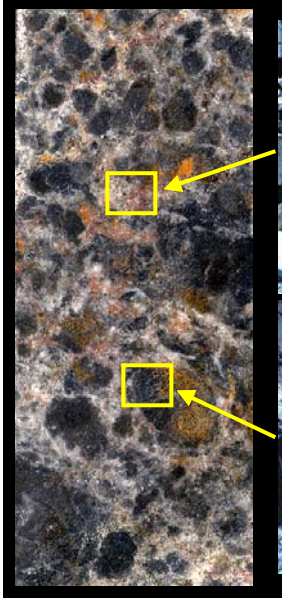

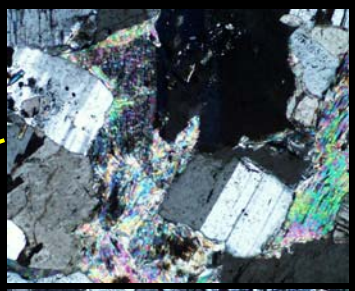

Matrix

- Coarse intergrowth of "clean" twinned albite, phlog, talc & dolomite

Clasts

- Felted masses of inclusion-rich, untwinned albite
- ?after kspar

Slide 31

Albitised Breccias (Mwambashi B HW)

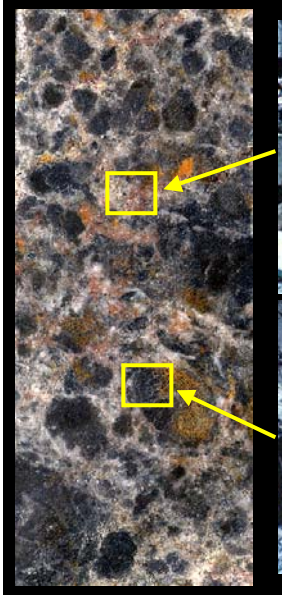

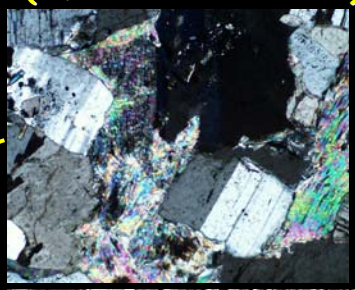

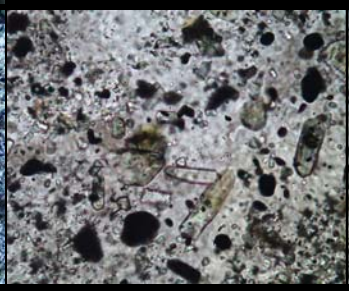

- Inclusions comprise tourmaline, rutile & phlog
- Compatible with K-metasomatism

Slide 32

Albite-Ore Association (Chibuluma West)

- Breccia complex positioned in immediate hangingwall of ore zone
- Sub-stratiform Cu-Fe-Co sulphide + albite association
- Texturally analogous to Mwambashi B
  - *but* Cu-Fe-Co sulphide + kspar
- Albite vs Kspar reflected in whole-rock geochemistry of respective ore zones
  - Chibuluma West av. 1.4% Na_2O, 0.14% K_2O
  - Mwambashi B av. 0.25% Na_2O, 4.0% K_2O
- K has been stripped from Chibuluma West

Slide 33

Albite-Ore Association (Chibuluma West)

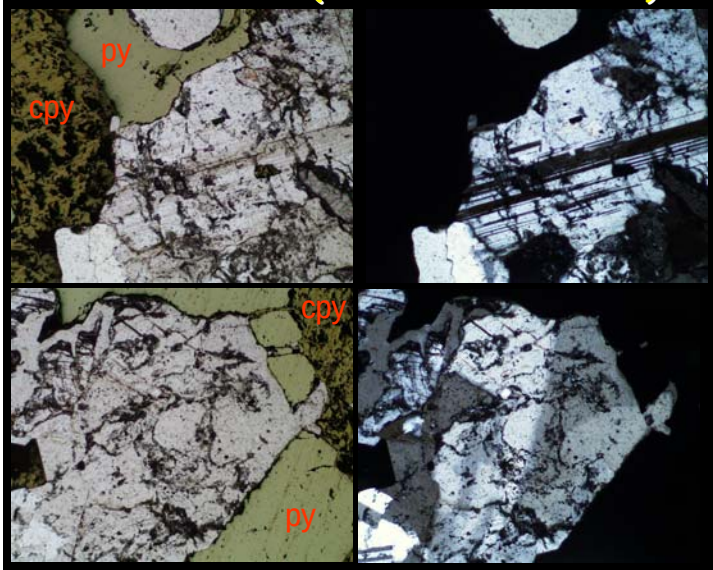

- Coarse optically continuous albite overprints pre-existing mineral assemblage
- Tourmaline along fractures and at margins of "ghost" grains reveals former K-metasomatic assemblage

Slide 34

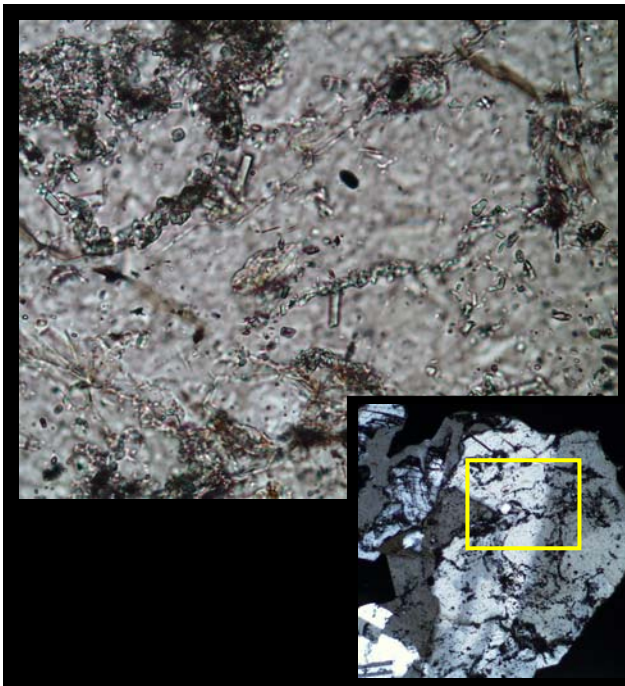

- Coarse optically continuous albite overprints pre-existing mineral assemblage
- Tourmaline along fractures and at margins of "ghost" grains reveals former K-metasomatic assemblage

Slide 36

Summary

- Complex alteration assemblages throughout the Roan record multistage fluid input
  - broadly consistent paragenetic relationships
  - assemblages are compatible with intra-basinally sourced brines
- Hydrocarbons provide constraints on timing of kspar – Cu-sulphide phase within arenite-hosted mineralisation at least
  - ie. must have been through "oil window"
  - consistent with fact that some arenite hosted deposits record fluid infiltration through cohesive media

Slide 37

Summary (cont.)

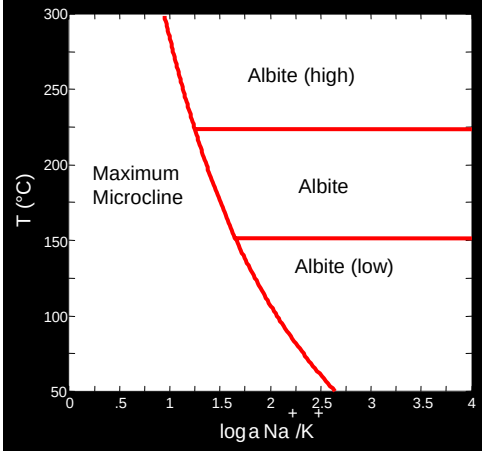

- K- & Na- metasomatic events are potentially genetically-related
- Transition between kspar & albite dependent on T and/or K/Na
- Concentration of albite within zones of potential high heat flow (ie. margin of gabbros) suggests T may be an important factor

Slide 38

Lufilian metamorphism in the Zambian Copperbelt: Implications for the interpretation of mineral assemblages and alteration paragenesis

Robert Scott, Ron Berry, David Selley and Stuart Bull
Centre for Ore Deposit Research, University of Tasmania

Summary

Rocks comprising the Roan Group in the Zambian Copperbelt (ZCB) were heated to temperatures in excess of 400°C (upper greenschist facies) during the Lufilian Orogeny. The main 'new' metamorphic mineral developed in the Lower Roan was phlogopite, which is generally abundant in all lithologies except very clean (i.e., little to no interstitial clay), well-sorted sandstones and massive primary carbonate units (Darnley, 1960; this study). The origins of phlogopite in the ZCB are somewhat controversial, with some favouring for a high-temperature metasomatic origin for at least some pf the phlogopite. However, regardless of differences in its distribution and textural character, phlogopite in the Lower Roan varies little in composition. The variations in phlogopite chemistry that are observed appear to mimic changes in bulk rock chemistry, consistent with a metamorphic origin for the mica.

The consistently high K_2O/Al_2O_3 ratio (generally >0.66) of Lower Roan phlogopite, and the development of Mg-rich phlogopite rather than biotite, indicate a precursor assemblage dominated by K-feldspar and Mg-rich chlorite, minerals formed during the earlier extensive K-metasomatism of the Lower Roan. K-feldspar generally forms part of the present (~peak metamorphic) mineral assemblage in the Lower Roan. Where K-feldspar is absent, and potentially completely consumed during prograde phlogopite development, the intensity of prior K-feldspar alteration and/or subsequent K-feldspar destruction due to subsequent alteration phases can be deduced from the composition (specifically the K_2O/Al_2O_3 ratio) and abundance of phlogopite. For fine-grained and very argillaceous lithologies (i.e., originally low to very low detrital K-feldspar contents), the whole rock K_2O/Al_2O_3 ratio (largely unaffected by metamorphism) can also be used to assess the extent of prior K-feldspar metasomatism. These relationships assume greater significance in the context of copper mineralisation, as the oxidised K-rich brines responsible for the widespread K-feldspar metasomatism most likely also transported copper. Furthermore, as micas appear more resistant to weathering and near-surface leaching than feldspars in the ZCB, biotite mineral chemistry provides a useful means of recognising prior K-feldspar metasomatism in moderately to strongly weathered rocks.

Introduction

Katangan series rocks of the Zambian Copperbelt were deformed and metamorphosed under greenschist facies conditions during the Lufilian Orogeny (Darnley, 1960; Fleischer et al., 1976). Although remobilisation of copper sulfides during this event is locally important (e.g., ore shoots at SOB, Nkana: Croaker, this volume), all major known copper deposits: (1) are stratabound or transgress stratigraphy at very low angles (2) occur within comparatively thin (generally <20 m) laterally extensive (km – tens of km) stratigraphic units or packages, and (3) are folded and cut by Lufilian-age folds, cleavage and faults. These relations demand copper mineralisation occurred prior to any significant folding of the Katangan succession, and certainly well before peak

metamorphic conditions were reached. Accordingly processes such as recrystallisation, dissolution, growth of new metamorphic minerals, and foliation development during the Lufilian Orogeny have the potential to mask or completely obliterate earlier mineral assemblages, textural and paragenetic relations. Yet it is precisely these earlier features that are most critical to understanding controls on copper distribution and associated patterns of hydrothermal alteration and ultimately for developing improved geological, geochemical and isotopic vectors to Cu deposits. Despite this, the effects of deformation and metamorphism are commonly overlooked in published literature on the Copperbelt, particularly that concerned with deposit genesis. In this report we examine the effects of Lufilian metamorphism and deformation on the Lower Roan, the maximum temperatures reached, and the extent to which earlier alteration assemblages, textural and paragenetic relations can be resolved.

Seeing through Lufilian deformation and metamorphism

Metamorphism and potentially associated processes (deformation, high-temperature metasomatism) can affect the composition, mineralogy and isotopic signature of rocks, hampering our ability to decipher their earlier history. In this report we chiefly consider compositional and mineralogical changes in the Roan resulting from the Lufilian deformation and metamorphism. Changes in the C- and O-stable isotopic signatures of carbonates as a result of metamorphism are discussed in Large et al. (a) (this volume).

Except for volatile-loss (principally through devolatilisation of hydrous minerals such as clays and micas) regional metamorphism is generally considered to be approximately isochemical on scales much larger than the grain size of the rock (i.e., centimetre to metre scale). However, where metamorphism is accompanied by deformation, cleavage development (particularly at greenschist facies conditions) may involve partial dissolution of specific minerals (e.g., quartz, carbonate) potentially resulting in apparent enrichments in less soluble constituents (e.g., Al, Ti, Fe). Material dissolved at high-stress grain contacts (i.e., pressure solution) may be either (1) re-deposited at adjacent low-stress sites (strain fringes), (2) precipitated locally in veins or strain fringes or (3) removed from the rock mass. Thus the extent to which pressure-solution modifies rock compositions during deformation and metamorphism depends not only the intensity of cleavage development, but on the original mineralogy of the rock and the scale of solute transport. Only where (1) deformation intensity is low, (2) the scale of solute transport is small, or (3) the original components removed from the rock are replaced (albeit in different sites, e.g., veins, strain fringes) by equivalent components sourced from adjacent material, should whole-rock geochemical patterns be almost completely unaffected by syn-deformational pressure-solution.

At greenschist facies and above, low average rock permeabilities act to focus large-scale, high-flux fluid flow into zones of intense cleavage development or networks of active shears and fractures. Accordingly these structures represent the principal sites for both high-temperature metasomatism and removal of solutes liberated by grain-scale dissolution. In rocks well removed from such syn-metamorphic fluid conduits it is reasonable to assume whole-rock geochemical patterns will reflect either original sedimentary compositions or their subsequent modification by diagenetic, hydrothermal, or near-surface leaching and weathering-related processes.

Although in weakly deformed rocks whole-rock geochemical patterns should be largely unaffected by Lufilian metamorphism, the mineralogy – and thus distribution of chemical constituents within the rock – may have been substantially modified. For example, during greenschist facies metamorphism, an arkosic sandstone that had previously been sericitised and then dolomitised, may develop the peak metamorphic assemblage quartz + phlogopite + dolomite + K-feldspar. The only 'new' metamorphic mineral is phlogopite, formed via the prograde decomposition of dolomite + sericite ± K-feldspar (with, in this case all sericite consumed by the reaction). Because phlogopite would either be in textural equilibrium with, or overprint, the dolomite, one could mistakenly conclude potassic alteration was synchronous with or post-dated carbonate alteration, and even that it occurred at peak metamorphic conditions. Furthermore, the chemical signature of

two separate alteration events; namely K introduced during sericitisation and Mg ± Fe introduced during dolomitisation are combined in a single metamorphic product, phlogopite.

Unravelling the pre-metamorphic diagenetic and alteration history of the Roan depends upon recognising the secondary minerals (and mineral assemblages), and their correct depositional (paragenetic) sequence, particularly with respect to the timing of copper introduction. In many cases, as demonstrated in the previous example, this may not be immediately obvious. However the formation of new minerals at the expense of pre-existing phases during metamorphism depends on a variety of factors including: (1) the stability of the original minerals at peak metamorphic conditions, (2) their distribution through the rock and (3) the bulk rock composition. If, in the previous example, large sericite-altered domains escaped dolomitisation or the sericitic alteration was far more intense, some sericite (perhaps recrystallised to the coarser grained equivalent, muscovite) could persist to upper greenschist facies conditions. Thus, whether or not alteration mineral assemblages (and textural relationships) survive metamorphism depends not only on the stability of the individual minerals at higher temperatures and pressures, but upon bulk rock composition, and the distribution and intensity of the alteration (i.e., whether a given alteration mineral is well in excess of, or isolated from, other reactive mineral phases).

In the previous two examples, differences in the peak metamorphic mineral assemblages simply reflect differences in the original proportion (and distribution) of the alteration minerals, sericite and dolomite. Although in the first example, the relative timing of K-metasomatism is uncertain, its existence may be inferred from either whole-rock geochemical data or an unusually high phlogopite content of the sample. However, having recognised early sericitisation in some samples, and that phlogopite formed at the expense of sericite during metamorphism, in the absence of evidence to the contrary, the distribution of both phlogopite and sericite reflects the original extent of K-metasomatism. Thus, particularly where rocks have undergone multiple phases of hydrothermal alteration prior to metamorphism, it is important to examine numerous thin sections in order to establish the true sequence of alteration events and to correctly interpret the origin of a particular geochemical signature.

Textural character and metamorphic grade of the Roan Group in the Copperbelt

The extent of metamorphic recrystallisation and the degree to which original sedimentary features are preserved within the Roan Group is highly variable across the Zambian Copperbelt. In some areas the rocks largely retain their original sedimentary character, and at least in hand specimen, display little textural evidence of modification by metamorphism. Elsewhere recrystallisation, metamorphic grain growth and foliation development have all but destroyed original features, and the rock has the textural character of high-grade schist (Slide 1). However these differences do not appear to reflect variations in peak metamorphic grade across the Copperbelt, as rocks of similar composition are generally characterised by the same mineral assemblage. Factors such as the intensity of deformation, the duration of heating, whether or not deformation outlasted heating, and the intensity of any prior hydrothermal alteration (i.e., pre-metamorphic textural and mineralogical modification) all contribute to differences in the appearance of originally similar rocks.

The mineralogy of Roan Group is relatively simple. Siliciclastics predominantly consist of quartz, feldspar and varying proportions of muscovite, phlogopite, carbonate (dolomite, calcite) and anhydrite, and more rarely, scapolite and tremolite. Haematite, rutile, tourmaline, and zircon are typical minor or accessory phases. Predominantly retrograde chlorite is developed locally. Carbonate-rich or originally carbonate-rich lithologies typically consist of dolomite (± calcite), talc and / or phlogopite and / or muscovite ± quartz ± anhydrite. The mineral assemblages developed in the Roan are consistent with mid- to upper greenschist facies metamorphism (e.g., Darnley, 1960; Fleischer et al., 1976). Specifically, in the Copperbelt, phlogopite is developed in all argillaceous lithologies and (prograde) chlorite is generally absent, tremolite (rather than hornblende) is the sole calc-silicate mineral and garnet is absent.

Textural relations suggest peak metamorphic temperatures were reached during deformation. Where present in foliated rocks, phlogopite is predominantly elongate and aligned in the dominant (S_1) schistosity (Slide 2a). Phlogopite generally shows only limited evidence of internal strain and is commonly developed in S_1 strain fringes adjacent to more competent (quartz and K-feldspar) grains (Slide 2b). These relations indicate phlogopite formed (and recrystallised) during the D_1 deformation. However, where S_1 is overprinted by a locally developed S_2 crenulation cleavage, phlogopite grains are folded, boudinaged and internally deformed (e.g., undulose extinction, kink-bands) or replaced by a chlorite–white mica assemblage (Slide 2c).

To improve constraints on maximum temperature reached during prograde metamorphism thermodynamic modelling of mineral stability as a function of pressure, temperature and bulk rock composition was conducted for two Lower Roan samples from Ndola West using Powell and Holland (1988) thermodynamic data and the calculation method of Connolly and Petrini (2002). One sample was of intensely K-feldspar altered, thinly bedded siltstone, sandstone and shale (Ndola Ore Shale, Sample number RJS-37) with the mineral assemblage phlogopite + K-feldspar + muscovite + quartz, the other was a quartz-rich argillaceous sandstone from the hanging wall formation (Sample number RJS-48). It contains quartz, abundant chlorite in addition to phlogopite and muscovite, but no K-feldspar. Phase diagrams calculated for the bulk compositions of these two samples indicate the observed mineral assemblages are first stabilised at temperatures above 400°C (Slide 3). The thermodynamic models also indicate both samples had the same mineralogy (quartz + K-feldspar + chlorite + muscovite + haematite) at temperatures <400°C. K-feldspar and chlorite are both consumed in the prograde development of phlogopite (see below). Thus the fact that K-feldspar, but not chlorite, persists to peak metamorphic conditions in the ore shale sample, while chlorite and not K-feldspar persists in the argillaceous sandstone, simply reflects the different relative abundances of these minerals in the lower temperature assemblages.

Phlogopite compositional variation in the Lower Roan

Despite strong evidence supporting a metamorphic origin for most of the phlogopite in the Roan Group, locally the distribution and character of phlogopite suggests development during high temperature hydrothermal alteration. In such cases, phlogopite aggregates (most commonly intergrown with either albite, carbonate, anhydrite and / or tourmaline) form semi-massive clots a few centimetres to over a metre in diameter. In addition, at many of the Cu-deposits phlogopite is concentrated in and around Cu-mineralised layers and may be intimately intergrown with both disseminated copper sulfides in the wall rock and coarser-grained sulfides in veins (Slide 4). These relations at Konkola led Broughton (2002) to suggest biotite [strictly, phlogopite] was co-precipitated with dolomite and copper sulfides, implying copper mineralisation was either the result of high temperature alteration or occurred at close to peak-metamorphic conditions.

To further evaluate the origin(s) of phlogopite in Lower Roan, electron microprobe data was obtained for phlogopite from a number of different stratigraphic levels (and in the immediately adjacent basement rocks). There were also differences in the grain-scale distribution and character (i.e., interstitial, porphyroblastic, clots) and mineralogical associations of the phlogopite (e.g., with or without sulfides, carbonate, etc) between samples. All bar one sample come from one of two areas on either side of the Kafue Anticline. At Chambishi SE, west of the Kafue Anticline, phlogopite from 10 different levels in drill hole NN48 was probed, representing ~300 m of Lower Roan stratigraphy (Slide 1). Phlogopite in basement granite, a few metres below the basal contact of the Lower Roan, was also probed (Slide 1). East of the Kafue Anticline, phlogopite from 12 Lower Roan samples, also representing ~300 m of stratigraphy, and two basement schist samples were probed (Slide 5a). An additional sample from west of the Kafue Anticline (drill hole DD72: hanging wall of the Chambishi deposit), in which an apparent phlogopite + albite alteration front overprints intensely K-feldspar metasomatised siltstone and sandstone, was also probed.

Microprobe analyses for phlogopite from both Chambishi SE and Ndola West show only minor variations in composition (Figs 6, 7). In all but one sample (from Ndola West) the Mg# (Mg# = Mg / (Mg + Fe) of the brown-pleochroic mica is >0.67 (average Mg# ~0.8) indicating it is phlogopite rather than biotite (Slide 6). This includes "biotite" in the granitic basement at Chambishi SE (a few metres below the basal contact of the Roan Group) that plots well outside the normal range of biotite in granite (Slide 6). Phlogopite from basement schists at Ndola West has a higher Mn and Cr content and somewhat lower Mg# (=0.68–0.70) but is otherwise similar to that in the Lower Roan.

At Ndola West, the Mg# of phlogopite is generally similar to whole rock values indicating it is the dominant iron and magnesium bearing mineral present in the rock (Slide 5b). However, in dolomitic rocks (specifically dolomite >> haematite + pyrite + bornite/chalcopyrite) the whole rock Mg# exceeds that of the phlogopite. Conversely, where other iron bearing phases (haematite + pyrite + bornite/chalcopyrite) are more abundant than dolomite, the phlogopite Mg# exceeds whole rock values (Slide 5b).

On both sides of the Kafue Anticline phlogopite has a relatively high K_2O/Al_2O_3 ratio (typically >0.66). At Ndola West, the K_2O/Al_2O_3 ratio of phlogopite invariably exceeds whole-rock values (Slide 5c), indicating whole-rock K_2O/Al_2O_3 values are of limited use in assessing the relative proportions of the principal potassic minerals, K-feldspar phlogopite and muscovite. Note that a K_2O/Al_2O_3 ratio of 0.66 would usually indicate a high proportion of K-feldspar ($K_2O/Al_2O_3 = 0.9$), as the micas muscovite, phengite, biotite, and phlogopite typically have K_2O/Al_2O_3 ratios in the range 0.3 – 0.5 (e.g., Deer et al., 1966).

Minor element concentrations in phlogopite are variable, both within and between samples. At Ndola West, phlogopite in the lower part of the footwall formation has elevated titanium and chlorine (Slide 5d), while phlogopite from a zone of intense acidic alteration in the lower part of the hanging wall formation (Scott, this volume), has notably has anomalously low Ti and elevated Na (Slide 5d and e). Zinc and manganese contents are erratic, although elevated values only occur in (but not in all) carbonate-bearing lithologies (Slide 5e). The highest *average* zinc content of phlogopite at Ndola West occurs at the level of the stratabound sandstone-hosted copper. However, the range in zinc content for individual grains at this level spans almost the entire observed range for phlogopite in the Lower Roan.

Probe data was also obtained for white micas and chlorite in some of the Ndola West samples. White mica compositions are consistently close to end-member muscovite, with only minor phengite substitution, while both prograde(?) and retrograde chlorite is Mg-rich and Fe-poor (Slide 7).

Discussion

Phlogopite in the Lower Roan: Metamorphic or metasomatic?

The limited compositional range of phlogopite from the Lower Roan (and the immediately underlying basement) is consistent with a high-temperature metasomatic origin, with the composition of phlogopite largely buffered by the hydrothermal fluid. This is also consistent with the development of phlogopite in Cu-bearing syn-metamorphic fibre veins (e.g., Konkola, Scott and Pollington, 2001) implying that both phlogopite and Cu-sulfides were precipitated at least locally precipitated at peak metamorphic conditions. However the Cu-bearing fibre veins appear restricted to, and much less widely developed than zones of stratabound disseminated copper sulfides. This implies copper in the fibre veins was remobilised from the adjacent wall rocks during metamorphism, and biotite growth therefore post-dates the original introduction of copper.

At Ndola West variations in major element chemistry of phlogopite throughout the Lower Roan (particularly K_2O/Al_2O_3 and Mg#) mimic variations in whole-rock chemistry. Specifically samples with the lowest whole-rock K_2O/Al_2O_3 contain phlogopite with the lowest K_2O/Al_2O_3 ratio, while phlogopite developed in relatively dolomite-rich rocks (higher Mg#) has a slightly higher Mg# (Slide 5). In addition Ti, Mn, Zn, Na, F and Cl contents in phlogopite vary

considerably. These relations suggest phlogopite compositions are rock-buffered, consistent with a metamorphic origin. Nonetheless, the almost exclusive development of Mg-rich phlogopite, rather than biotite, within a predominantly arkosic sequence (granitic and quartz-mica schist protoliths) is unusual. Phlogopite is generally restricted to marbles, calc-silicates and ultramafic rocks (Slide 6, Deer et al., 1966).

There are a number of possible explanations for the development of Mg-rich phlogopite in the Lower Roan. Although high fluorine contents exclude iron from the biotite (and phlogopite) lattice resulting in Mg-rich compositions (Mason, 1992; Chabu, 1995), the average fluorine content of phlogopite in the Lower Roan is too low to account for the observed Mg enrichment.

The average Mg# for Siliciclastics in the Lower Roan (e.g., Slide 5b) appears unusually high for sediments of largely granitic provenance, suggesting addition of Mg (or removal of Fe) at some stage prior to metamorphism. This suggests phlogopite development could reflect the widespread development of (diagenetic?) dolomitic cements and/or dolomitic alteration. Primary carbonates and zones of extensive dolomitic alteration occur within the Lower Roan at Ndola West (see Scott, this volume), and where carbonate is present, phlogopite is usually shifted to higher Mg# (Slide 5b). However, it seems unlikely that secondary carbonate was sufficiently uniformly distributed through the various lithologies of the Lower Roan, to explain such widespread development of phlogopite. In addition, sourcing the Mg in phlogopite from carbonate creates a mass balance problem, because in many areas (e.g., Konkola, Ndola West) there is essentially no calcium in the rock (other than that in dolomite), requiring the removal of enormous quantities of calcium during greenschist facies metamorphism.

A more likely explanation for the development of phlogopite is pre-existing Mg-rich chlorite, of probable hydrothermal origin, throughout the section. The very low solubility of aluminium in the oxidised brines responsible for K-feldspar metasomatism of the Lower Roan (Selley et al., this volume; Cooke, this volume) demands a local source for aluminium within the altered rocks. K-feldspar metasomatism was most intense in shales, argillaceous sandstones and siltstones, and did not affect primary carbonates and clean sandstones (Scott, this volume), suggesting detrital clay was the source of aluminium in the secondary K-feldspar. During K-feldspar metasomatism other constituents of the clay (e.g., Fe^{3+}>Fe^{2+}, Mg, Ca, Ti and excess Al not incorporated into K-feldspar) must have either been dissolved into solution or incorporated into new minerals (e.g., rutile, haematite and chlorite). At least for Fe, Ti and Al, which are all relatively insoluble in near-neutral fluids, the latter seems more likely.

Two factors appear to favour the development of Mg-rich chlorite during K-feldspar metasomatism. Firstly, assuming the oxidised brine had a composition similar to evolved seawater and contained appreciable Mg (e.g., Mg = 940 ppm, Mg/Fe ratio ~30 for the brine used in our geochemical modelling, Cooke, this volume) additional magnesium could have been added to the rock (as suggested by the elevated whole-rock Mg#). Secondly, either prior to, or as a result of, interaction with the oxidised brines, iron in the rock was largely oxidised to Fe^{3+}, permitting only limited substitution into chlorite).

Throughout the footwall succession and lower part of the ore formation at Ndola West, Mg-rich phlogopite generally coexists with, and is often roughly proportional to, lesser finely disseminated specular haematite (e.g., Slide 2b). Unless haematite formation reflects oxidation of Fe^{2+} during metamorphism (which seems unlikely), the oxidation state of iron during prior K-metasomatism would not have permitted significant substitution into 'hydrothermal chlorite'. Note, however, that the hanging wall succession at Ndola West locally contains up to 5% pyrite, yet phlogopite has a similar Mg# to that elsewhere and haematite is largely absent. Here, and at the level of the underlying copper mineralisation, development of Mg-rich phlogopite, rather than biotite, was apparently not solely due to a lack of Fe^{2+}, but reflects competition for Fe^{2+} with sulfides and (as elsewhere) minor addition of Mg to the rock during K-metasomatism.

This explanation for phlogopite development goes some way to explaining why phlogopite in the

apparently metasomatic clots and aggregates and the pervasive interstitial phlogopite have similar compositions. Both were derived from similar precursor (alteration) mineral assemblages dominated by K-feldspar and chlorite.

The phlogopite intergrown with copper sulfides or enriched in and adjacent to Cu-mineralised beds (e.g., Broughton, 2002) is compositionally similar to that elsewhere and therefore also likely to be of metamorphic origin. Copper was most likely transported in the oxidised brines responsible for metasomatic K-feldspar and Mg-chlorite, and deposited along with them wherever the brines encountered reduced sulfur reservoirs. Dolomite, which may also have been involved in phlogopite forming reactions (see below), was also be precipitated in proximity to sulfides. Thermo-chemical sulfate reduction (TSR) of anhydrite due to interaction with methane (and more complex hydrocarbons) is a locally important process producing both reduced sulfur (H_2S) — driving sulfide precipitation — and carbonate (Annels, 1974; Selley et al., this volume). Accordingly the phlogopite–copper sulfide association is most likely to reflect the original co-precipitation/spatial proximity of Cu-sulfides and phlogopite precursor mineral phases (K-feldspar, chlorite ± dolomite). In addition, Cu-sulfides in ore shales at Konkola and Ndola West are commonly preferentially developed within thin fine- to medium-grained sandstone interbeds, which may provide a more favourable microenvironment for early crystallisation of phlogopite during prograde metamorphism (see below).

Phlogopite chemistry: Implications for the interpretation of earlier hydrothermal alteration events

Secondary K-feldspar and Mg-rich chlorite formed during prior K-metasomatism are interpreted to be the principal phlogopite precursor phases in the Lower Roan. However there are numerous prograde metamorphic reactions that could possibly account for phlogopite development. Three generalised end-member reactions are given below. For simplicity (Mg, Fe) in carbonate, phlogopite and chlorite is represented by the Mg-end-member (see below).

Although these exact metamorphic reactions are unlikely to have occurred, they serve to illustrate two important points regarding phlogopite development in the Lower Roan. Firstly, in reactions 1 and 3, the Mg in phlogopite is provided by dolomite in the low temperature assemblage, and calcite (but not water) appears on the high temperature side of the reaction. At Ndola West, neither calcite (or any calcic phase other than dolomite) is observed in the Lower Roan, suggesting dolomite was of only local importance in phlogopite formation. In reactions 1 to 3, phlogopite has equal molar proportions of K_2O and Al_2O_3 (i.e., K_2O/Al_2O_3 (wt %) = 0.92, equivalent to that in K-feldspar). In nature, such high phlogopite K_2O/Al_2O_3 ratios are unlikely. However, unless another high-temperature aluminous phase is produced, K_2O/Al_2O_3 ratios >>0.3 (i.e., greater than that of muscovite) require the consumption of K-feldspar to form phlogopite. The K_2O/Al_2O_3 ratios for Lower Roan phlogopite probed in this study range from to 0.46–0.75.

$$3\ CaMg(CO_3)_2 + KAlSi_3O_8 + H_2O \Rightarrow KMg_3AlSi_3O_{10}(OH)_2 + 3\ CaCO_3 + 3\ CO_2 \quad [1]$$
dolomite K-feldspar phlogopite

$$6\ KAlSi_3O_8 + Mg_9Al_6Si_5O_{20}(OH)_{16} \Rightarrow 3\ KMg_3AlSi_3O_{10}(OH)_2 + 3\ KAl_3Si_3O_{10}(OH)_2 + 5\ SiO_2 + 2\ H_2O \quad [2]$$
K-feldspar chlorite phlogopite muscovite

$$3\ CaMg(CO_3)_2 + KAl_3Si_3O_{10}(OH)_2 \Rightarrow KMg_3AlSi_3O_{10}(OH)_2 + 3\ CaCO_3 + 3\ CO_2 + Al_2O_3 \quad [3]$$
dolomite muscovite phlogopite

The presence of corundum (Al_2O_3) on the high-temperature side of reaction 3 allows phlogopite with a high K_2O/Al_2O_3 ratio to form via a reaction not involving K-feldspar. However, this type of reaction does not account for the high K_2O/Al_2O_3 ratio of phlogopite in the Lower Roan. The only aluminous minerals other than phlogopite and K-feldspar are muscovite, chlorite, albite and scapolite. Albite and scapolite are either minor or absent throughout most of the Lower Roan section at Ndola West, and only rarely does chlorite form part of the prograde mineral assemblage.

Potentially more realistic phlogopite forming reactions in the Lower Roan are similar to that originally proposed by Mather (1970) for the formation of biotite in the Scottish Dalradian (see below).

Muscovite formed by these reactions has a lower K_2O/Al_2O_3 ratio than phengite or phengitic-muscovite in the low-temperature assemblage. However, unless a third aluminous phase is produced by the reaction, phengite and chlorite alone can not produce phlogopite with the high K_2O/Al_2O_3 ratios observed in the Lower Roan.

Thus the consistently high K_2O/Al_2O_3 ratio (typically 0.6–0.75) for phlogopite in the Lower Roan necessitates the involvement of K-feldspar in its formation. Furthermore, development of phlogopite rather than biotite suggests the consumption of a precursor Mg-rich chlorite. As discussed, the Mg-rich chlorite was probably also formed during interaction between the K-rich ore fluids and the original clay fraction in the rock. Thus the two main metasomatic minerals marking the passage of the oxidised ore fluid through the rock were progressively replaced by phlogopite (+ muscovite) during metamorphism. As metasomatic K-feldspar generally persists in the peak metamorphic assemblage, it must have either been considerably more abundant than chlorite ± phengite/muscovite ± dolomite in the low temperature assemblage or formed large clots (relative to the average grainsize) isolating it from these other reactive phases.

Where K-feldspar (± chlorite) was entirely consumed during prograde metamorphism, phlogopite abundance and its K_2O/Al_2O_3 ratio provides a good indication of K-feldspar abundance prior to metasomatism. Where K-feldspar was a minor constituent of muscovite- ± chlorite- ±carbonate-rich rock prior to metamorphism, and entirely consumed during prograde metamorphism (e.g., Sample number RJS-48, Slide 3b), phlogopite has a lower K_2O/Al_2O_3 ratio. Where K-feldspar was relatively abundant in the low-T mineral assemblage, but consumed during metamorphism phlogopite should have a relatively high K_2O/Al_2O_3 ratio (e.g., Ore Shale sample, NN48, Slide1).

Thus even where K-feldspar is no longer present in the rock, the K_2O/Al_2O_3 ratio of biotite (and to some extent the whole-rock K_2O/Al_2O_3 ratio) gives a good indication of the intensity of earlier K-feldspar metasomatism. Use of the whole-rock K_2O/Al_2O_3 ratio as an indicator of K-feldspar metasomatism is most reliable for finer grained or very argillaceous rocks, where detrital K-feldspar contents were likely to have been low (<10%).

$$\underset{\text{K-feldspar}}{4\ KAlSi_3O_8} + \underset{\text{chlorite (amesite)}}{Mg_8Al_8Si_4O_{20}(OH)_{16}} + \underset{\text{phengite}}{4\ KFe_{0.5}Mg_{0.5}AlSi_4O_{10}(OH)_2}$$
$$\Rightarrow \underset{\text{phlogopite}}{4\ KMg_{2.5}Fe_{0.5}AlSi_3O_{10}(OH)_2} + \underset{\text{muscovite}}{4\ KAl_3Si_3O_{10}(OH)_2} + 8\ SiO_2 + 4\ H_2O \qquad [4]$$

$$\underset{\text{K-feldspar}}{6\ KAlSi_3O_8} + \underset{\text{chlorite}}{2\ Mg_9Al_6Si_5O_{20}(OH)_{16}} + \underset{\text{phengite}}{9\ KFe_{0.5}Mg_{0.5}AlSi_4O_{10}(OH)_2}$$
$$\Rightarrow \underset{\text{phlogopite}}{9\ KMg_{2.5}Fe_{0.5}AlSi_3O_{10}(OH)_2} + \underset{\text{muscovite}}{6\ KAl_3Si_3O_{10}(OH)_2} + 19\ SiO_2 + 10\ H_2O \qquad [5]$$

Mica stability and the maximum temperature of metamorphism affecting the Lower Roan

At low grades of metamorphism in metasedimentary rocks the white micas formed are typically phengitic (i.e., appreciable (Mg, Fe^{2+})Si substitution for Al-Al in ideal muscovite), and biotite is generally restricted to relatively Al-poor metasedimentary rocks (meta-greywackes) (Miyashiro, 1973; Winkler, 1976). In more aluminous (pelitic) rocks, biotite (and phlogopite) development is initially suppressed as the mineral pair phengite–chlorite is stable to higher temperatures (Miyashiro, 1973; Vernon, 1976). With increasing grade of metamorphism extent of phengite substitution in muscovite decreases, and by amphibolite facies, muscovite in meta-pelites is typically close to the idealised composition (Miyashiro, 1973; Vernon, 1976). The decrease in phengite with increasing grade of metamorphism, allows biotite (or phlogopite) to form in rocks with a progressively wider range in bulk composition.

The early appearance of phlogopite in relatively Al-poor layers may help to explain apparent phlogopite enrichments around Cu-mineralised layers in the Ore Shale at Konkola and Ndola West, where copper sulfides are commonly enriched in thinly interbedded fine- to medium grained sandstone layers. While sulfide distribution probably reflects a porosity control on the distribution of reductants, the somewhat lower Al-content of the sandstone layer (compared to siltstone and shale layers) should favour early phlogopite development during metamorphism.

The presence of phlogopite in all Lower Roan lithologies except very clean sandstones (negligible Mg, Fe contents) and carbonates (negligible K, Al contents) suggests maximum temperatures during metamorphism were well above the biotite isograd. In addition, metamorphic white mica compositions at Ndola West approach end-member muscovite (Slide 7) as expected for micas crystallised at uppermost greenschist to amphibolite facies conditions (Miyashiro, 1973; Winkler, 1976). However, prior K-feldspar metasomatism of the Lower Roan probably shifted the chemistry of even the most Al-rich units (shales and siltstones) towards compositions that stabilise phlogopite at lower temperatures.

Nonetheless, thermodynamic modelling, using two samples with different bulk rock compositions from Ndola West, indicates peak metamorphic temperatures probably exceeded 400°C (Slide 3). As rocks of similar composition and appearance, west of the Kafue Anticline, have the same mineralogy, it is likely similar peak temperatures where experienced across this part of the Copperbelt (see also Fleischer et al., 1976).

Sulfide stability during metamorphism: Implications for the interpretation of sulfide textures

Peak metamorphic temperatures >400°C has implications for the interpretation of internal textural and compositional features of copper sulfides. At 400°C, the compositional range of bornite expands to include compositions slightly more Fe-rich than ideal bornite (Cu_5FeS_4) and Fe- S-poor compositions equivalent to chalcocite-digenite in lower temperature assemblages (Slide 8). Thus the complex bornite–'hypogene' chalcocite intergrowths observed at some deposits (e.g., Konkola, Scott and Pollington, 2001) are unlikely to be primary features, and probably reflect exsolution from a homogeneous Fe-, S-poor bornite phase stable at peak metamorphic temperatures. Intergrowths of bornite and chalcopyrite, with bornite>>chalcopyrite, could reflect exsolution an homogenous Fe-rich bornite stable at peak metamorphic conditions. Along the same lines, chalcopyrite>>bornite intergrowths may result from retrograde decomposition of 'intermediate solid solution' (iss). Although the iss compositional range does not quite encompass ideal chalcopyrite, at 400°C iss ranges from ~$Cu_5Fe_4S_7$ to $CuFe_2S_3$ (cubanite) (Slide 8, Craig and Scott, 1976), and thus could account for primary chalcopyrite–bornite mixtures with up to ~7% bornite.

Chalcopyrite, bornite and chalcocite all have limited compositional ranges at low temperature. As stratabound copper mineralisation predates Lufilian metamorphism, the present 'hypogene' chalcocite (digenite)–bornite and chalcopyrite–bornite intergrowths probably reflect original aggregates or intergrowths of these same minerals. While it is unlikely original sulfide textures are preserved, and trace element distributions may be strongly control-

led by element partitioning during exsolution, the presently observed 'hypogene' sulfides probably do reflect original mineralogies. As such mixtures of texturally identical chalcocite–purple bornite and orange-brown bornite ± chalcopyrite (e.g., Konkola (Scott and Pollington, 2001; Konkola North (Pollington, this volume), and Ndola West (Scott, this volume)) suggest disequilibrium conditions (S^{2-} availability changed progressively or fluctuated) during mineralisation.

Conclusions

Phlogopite (Mg# >0.67) is developed throughout the Lower Roan and interpreted to be (almost?) entirely of metamorphic origin. Although some hydrothermal phlogopite (associated with metasomatic albite) may be present locally, overall the minor observed phlogopite compositional variations mimic changes in bulk rock composition. Phlogopite crystallised during deformation and is one of the principal minerals defining the dominant S_1 foliation. Although intimately intergrown with copper sulfides at some deposits, phlogopite post-dates all but minor remobilisation of copper at peak metamorphic conditions. Thermodynamic modelling, using two samples with different bulk rock compositions from Ndola West, indicates peak metamorphic temperatures probably exceeded 400°C.

The development of Mg-rich phlogopite, rather than biotite, and the consistently high K_2O/Al_2O_3 ratio (generally >0.66) of phlogopite in the Lower Roan, is unusual considering the predominantly granitic source for the host package. Accordingly, phlogopite development during metamorphism is interpreted to reflect prior chemical modification of the succession by oxidised K-rich (and Cu-bearing) brines. Through oxidation and the addition of K (and to a lesser extent Mg?) potassic brines converted the original clay fraction throughout the succession into an assemblage of K-feldspar + Mg-chlorite (± sericite, quartz) + haematite + rutile + tourmaline. The K-feldspar, Mg-chlorite, phengitic-sericite formed during this alteration event, and to a lesser extent dolomite, were the main precursor minerals facilitating phlogopite growth at peak metamorphic conditions. Although K-feldspar was sufficiently abundant throughout most of the section, and persisted into the peak metamorphic assemblage, chlorite was generally consumed. The pre-existence of Mg-rich chlorite prior to metamorphism is implied by the development of Mg-rich phlogopite rather than biotite. At least at Ndola West, dolomite is precluded as a major source of Mg for phlogopite, because no calcic minerals (other than locally developed dolomite) form part of the prograde assemblage. The formation of Mg-rich chlorite during the earlier metasomatism is interpreted to reflect Mg contributions from both the potassic brines and the original clay fraction in the rock, as well as limited availability of Fe^{2+} under oxidised conditions (e.g., iron predominantly present as Fe^{3+} in haematite).

Although locally Lufilian metamorphism substantially modified alteration (and sulfide) mineral assemblages and textures, wherever alteration minerals were intensely developed, their preservation potential at peak metamorphic conditions was increased. The distinctive chemistry of phlogopite in the Lower Roan is interpreted to be a direct consequence of prior K-feldspar metasomatism. Even where metasomatic K-feldspar is no longer present (either through weathering, near-surface leaching, or where K-feldspar was entirely consumed during metamorphism) its earlier presence can be inferred from mica (i.e., phlogopite) chemistry and in particular high K_2O/Al_2O_3 ratios

Acknowledgments

David Steel and Fernando della Pasqua are thanked for their assistance with the electron microprobing of samples.

References

Annels, A. E., 1974, Some aspects of the stratiform ore deposits of the Zambian Copperbelt and their genetic significance, *in* Bartholomé, P., ed.: Gisements stratiformes et provinces cupifères, Société Géologique de Belgique, Liège, p. 235–254.

Broughton, D., 2002, Comparative study of drill cores from the Konkola North Orebody and barren gap: AMIRA P544 - Proterozoic Sediment Hosted Copper Deposits, Sponsors Meeting Presentations, May 2002. p. 16.1–16.18

Chabu, Mumba, 1995, The geochemistry of phlogopite and chlorite from the Kipushi Zn–Pb–Cu deposit, Shaba, Zaire: The Canadian Mineralogist, v. 33, p. 547–558.

Connolly, J. A. D. and Petrini, K., 2002, An automated strategy for calculation of phase diagram sections and retrieval of rock properties as a function of physical conditions: Journal of Metamorphic Geology, v. 20, p. 697-708.

Cooke, D. R., McGoldrick, P., Hitzman, M., Scott, R., and Selley, D., 2003, Geochemical modelling: Implications for mineralising processes in the Zambian Copperbelt, AMIRA P544 Proterozoic Sediment Hosted Copper Deposits, Final Report. This volume.

Craig, J. R. and Scott, S. D., 1976, Sulfide phase equilibria, *in* Ribbe P. H. (ed), Sulfide Mineralogy, Mineralogical Society of America, Reviews in Mineralogy Volume 1, p. CS-1–CS110.

Croaker, M., 2003, Structural development and controls on Cu-Co mineralisation, Nkana-Mindola, AMIRA P544 Proterozoic Sediment Hosted Copper Deposits, Final Report. This volume.

Darnley, A. G., 1960, Petrology of some Rhodesian Copperbelt orebodies and associated rocks: Transactions of the Institution of Mining and Metallurgy, v. 69, p. 137–173.

Deer, W. A., Howie, R. A., Zussman, J., 1966, An Introduction to the rock forming minerals, Longman, London, 528 p.

Fleischer, V. D., Garlick, W. G. and Haldane, R., 1976; The Geology of the Zambian Copper Belt, in Wolf, K. H. (ed), Handbook of strata-bound and stratiform deposits; II. Regional studies and specific deposits; Chapter 6, Cu, Zn, Pb and Ag Deposits. p. 223–243.

Hermann, W. and Berry, R. F., 2002, MINSQ – a least squares spreadsheet method for calculating mineral proportions from whole rock major element analyses: Geochemistry: Exploration, Environment, Analysis, v. 2, p. 361–368.

Large, R. R., Bull, S., Croaker, M., McGoldrick, P., Pollington, N., Scott, R., and Selley, D., 2003(a), Carbon and oxygen isotopic composition of ore-related and sedimentary carbonates in the Roan, Zambian Copperbelt, AMIRA P544 Proterozoic Sediment Hosted Copper Deposits, Final Report. This volume.

Large, R. R., McGoldrick, P., Bull, S., Scott, R. and Selley, D., 2003(b), Lithogeochemistry and halos to ore in the Chambishi Basin, AMIRA P544 Proterozoic Sediment Hosted Copper Deposits, Final Report. This volume.

Mason, R. A., 1992, Models of order and iron–fluorine avoidance in biotite: The Canadian Mineralogist, v. 30, p. 343–354.

Mather, J. D., 1970, The biotite isograd and the lower greenschist facies in the Dalradian rocks of Scotland, Journal of Petrology, v. 11, p. 64–86.

Miyashiro, A., 1973, Metamorphism and metamorphic belts, George Allen & Unwin, London, 492p.

Pollington, N., 2003, Sulphide mineral zonation and chemistry at Konkola North, AMIRA P544 Proterozoic Sediment Hosted Copper Deposits, Final Report. This volume.

Powell, R. and Holland, T. J. B., 1988, An internally consistent dataset with uncertainties and correlations; 3, Applications to geobarometry, worked examples and a computer program: Journal of Metamorphic Geology, v. 6, p.173-204.

Scott, R. J., 2003, Stratigraphy, alteration and copper mineralisation at Ndola West, AMIRA P544 Proterozoic Sediment Hosted Copper Deposits, Final Report. This volume.

Scott, R. J. and Pollington, N., 2001, Character, paragenesis and zonation of the copper ores at Konkola (Kirilabomwe), Zambia, AMIRA P544 Proterozoic Sediment Hosted Copper Deposits, Progress Report, p. 199–217.

Selley, D., Scott, R., Large, R., Croaker, M., Bull, S., Pollington, N., 2003, Alteration history of the Roan, AMIRA P544 Proterozoic Sediment Hosted Copper Deposits, Final Report. This volume.

Vernon, R. H., 1976, Metamorphic processes, George Allen & Unwin, London, 247p.

Winkler, H. G. F, 1976, *Petrogenesis of Metamorphic Rocks*: Springer-Verlag New York, 334p.

SLIDE 1.

(a) and **(b)** Photomicrographs (PPL and XPL, respectively) of coarse grained phlogopite in recrystallised Ore Shale (now dolomite + phlogopite + quartz + chalcopyrite schist), drill hole NN48, Chambishi SE. Although no K-feldspar is present, the high Mg# (=0.85) and K_2O/Al_2O_3 (=0.66) of phlogopite are interpreted to indicate derivation from a K-feldspar + Mg-chlorite precursor assemblage (see text).

(c) Graphic log of the Lower Roan in drill hole NN48. Dots indicate the locations of phlogopite-bearing samples probed in this study. Location of the Ore Shale sample illustrated in (a) and (b) is shown by the arrow.

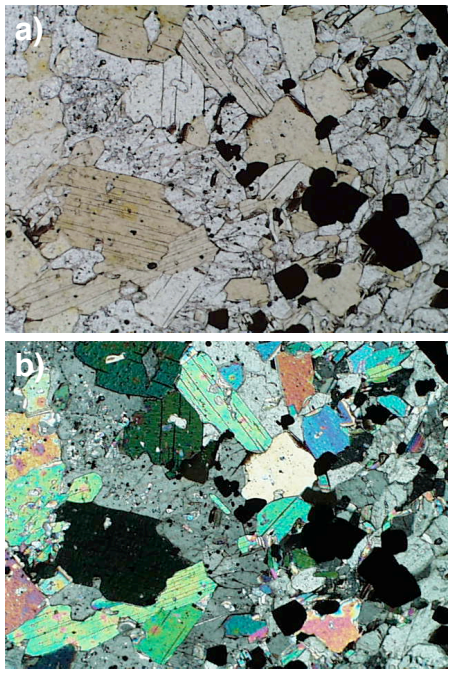

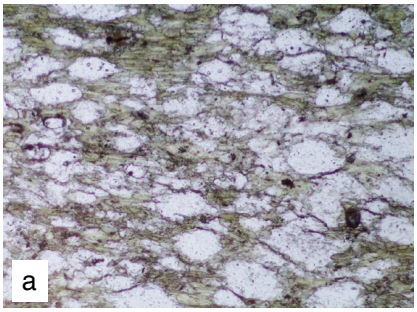

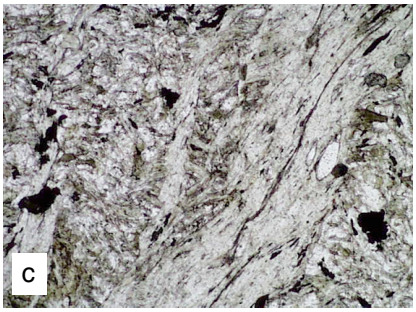

SLIDE 2. (a) Strongly-aligned interstitial phlogopite defining the S_1 fabric in an argillaceous sandstone, hanging wall formation, Lower Roan Ndola West. Sample KIT01DD004, 111.25 m, width of view 1.1 mm, PPL. **(b)** Syn-kinematic crystallisation of phlogopite within asymmetric strain fringes adjacent to large detrital feldspar grain, argillaceous sandstone, footwall formation, Note abundant disseminated haematite (elongate opaque (black) grains) aligned in the S_1 foliation. Ndola West. Sample KIT01DD002, 152.87 m, width of view 1.6 mm, PPL. **(c)** Phlogopite defining S_1 is folded and retrogressed to a chlorite + white mica assemblage within zones of the well developed S_2 crenulation cleavage. Sample KIT01DD002, 96.1 m, width of view 1.1 mm, PPL.

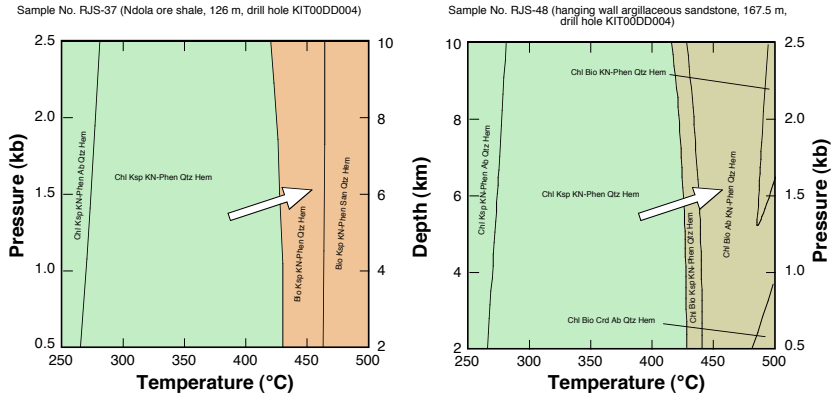

Whole-rock		*MINSQ mineral proportions*	
SiO_2	63.1 %	Quartz	23.4 %
Al_2O_3	15.6 %	K-feldspar	34.6 %
Fe_2O_3	3.6 %	Albite	1.2 %
MgO	4.4 %	Phlogopite	21.0 %
K_2O	9.8 %	Muscovite	17.3 %
LOI	2.4 %	Dolomite	0.5 %
		Haematite	1.5 %

Whole-rock		*MINSQ mineral proportions*	
SiO_2	78.0 %	Quartz	63.6 %
Al_2O_3	7.7 %	K-feldspar	3.8 %
Fe_2O_3	1.9 %	Albite	0.3 %
MgO	6.9 %	Phlogopite	10.9 %
K_2O	2.5 %	Muscovite	6.9 %
LOI	2.4 %	Chlorite	13.0 %
		Pyrite	1.4%

SLIDE 3. P-T mineral phase diagrams for specific bulk compositions (pseudosections) constructed for two Lower Roan samples from Ndola West. **(a)** Strongly K-feldspar altered Ndola ore shale. Whole-rock geochemical data and mineralogy of the sample (mineral proportions determined using MINSQ: Herrmann and Berry, 2002) given below. The observed assemblage corresponds to the biotite-in chlorite out isograd at ~425°C. **(b)** Strongly K-feldspar altered Ndola ore shale. Whole-rock geochemical data and mineral proportions indicated below section. The observed assemblage first appears at temperatures of 420–440°C.

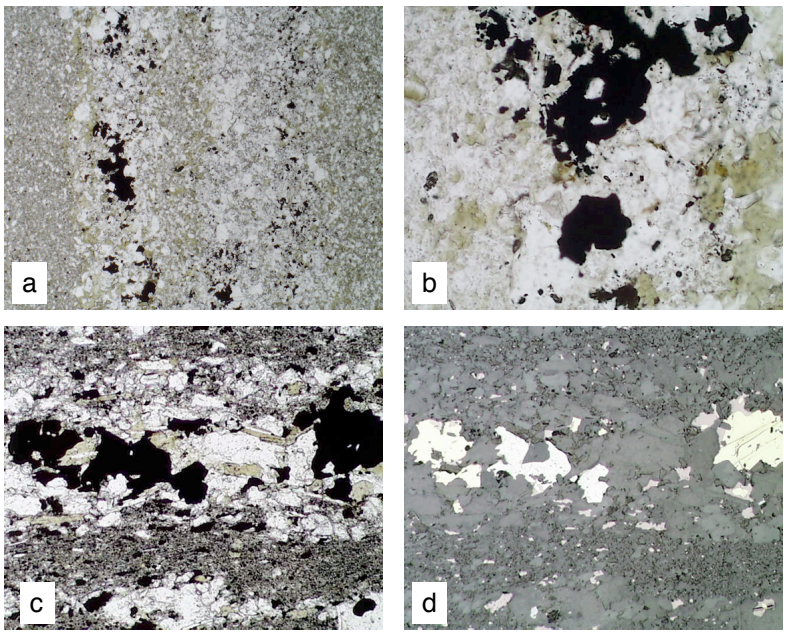

Figure 4. Phlogopite–Cu-sulfide spatial association within ore shale-hosted mineralisation at Ndola West and Konkola. **(a)** Phlogopite is coarser grained and more abundant adjacent to thin Cu-sulfide bearing sandstone interbeds within the Ndola ore shale. Sample from KIT01DD03, 171 m, width of view 4.4 mm, PPL. **(b)** Detail from thin Cu-mineralised sandstone bed. Sample from KIT01DD03, 171 m, width of view 0.55 mm, PPL. **(c)** and **(d)** Phlogopite intergrown with Cu-sulfides in thin sandstone bed from Ore Shale at Konkola. Sample from KLB145, 683.6 m, width of view 1.1 mm, PPL and REF.

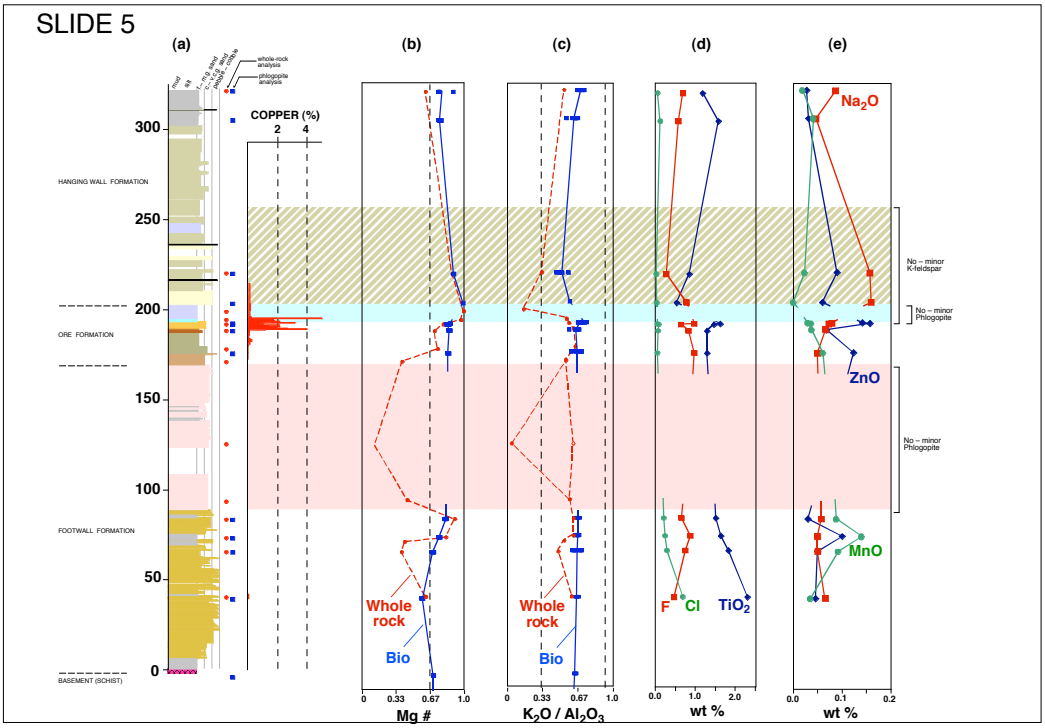

SLIDE 5. Electron microprobe data for phlogopite in the Lower Roan at Ndola West, plotted against a composite stratigraphic column (true thickness) for the area. **(a)** Composite stratigraphic section showing copper grade and sample locations. **(b)** Variation in Mg# for phlogopite (blue) and whole-rock (red). Whole-rock Mg# >0.67 generally reflect the presence of dolomite, and are reflected by slight increases in the phlogopite Mg#. Phlogopite Mg# is higher than whole-rock values for samples where the amount of iron in haematite, bornite–chalcopyrite or pyrite exceeds the amount of magnesium in dolomite. **(c)** Variation in K_2O/Al_2O_3 for phlogopite (blue) and whole-rock (red). Note that the K_2O/Al_2O_3 ratio of phlogopite unusually high (~0.67) and either equals or exceeds the corresponding whole-rock value. Fine grained (clay/mica-rich) units would normally be expected to have the lower whole-rock K_2O/Al_2O_3 ratios (little to no detrital K-feldspar) but the opposite relationship is observed here, indicating these units were the most intensely K-feldspar metasomatised. Note also that the anomalously low K_2O/Al_2O_3 ratio of the sample at the centre of the thick sandstone in the upper footwall formation (pink) is due to near-surface of feldspar. The K_2O/Al_2O_3 ratio for unweathered equivalents should be similar to or higher than that for the adjacent lithologically similar samples. For phlogopite-bearing units, the sample with the lowest whole-rock K_2O/Al_2O_3 ratio (from the zone of pre-metamorphic K-feldspar destruction in the lowermost hanging wall formation) also has phlogopite with the lowest K_2O/Al_2O_3 ratio. (d) Variations in average F, Cl, and Ti content of phlogopite. (e) Variations in average MnO, ZnO and Na_2O content of phlogopite.

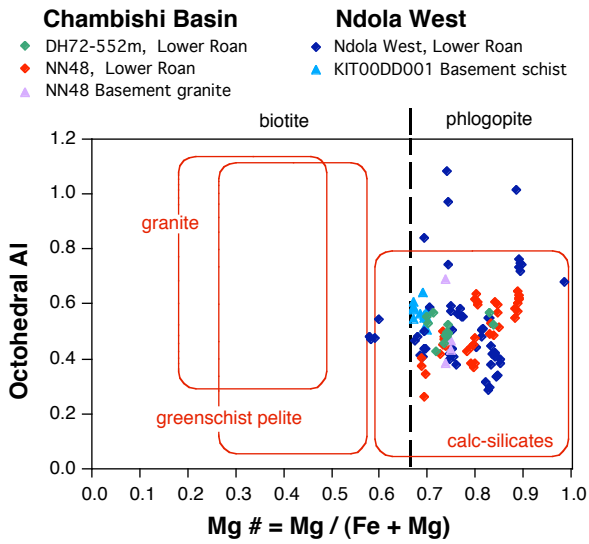

SLIDE 6. Mg# plotted against octahedral Al for all probed phlogopite/biotite from the Lower Roan. Only one sample (from Ndola West) contains biotite *sensu stricto*. Almost all of the data (including biotite from basement granite at Chambishi SE, plots in the field for calc-silicates.

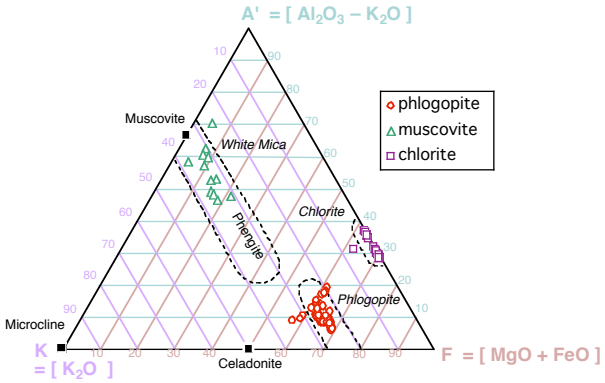

SLIDE 7. A'KF diagram for micas from the Lower Roan at Ndola West.

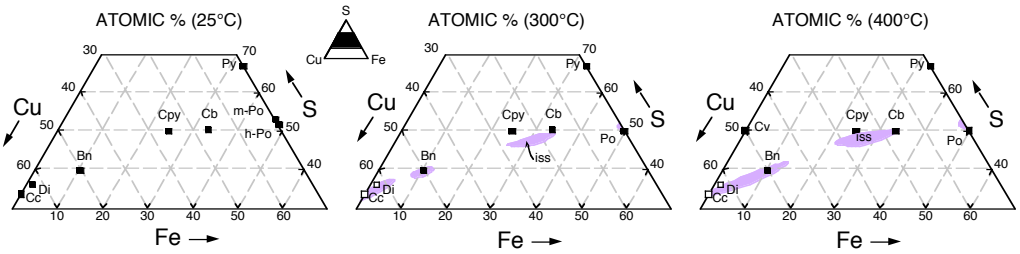

SLIDE 8. Schematic phase relations for the central portion of the Cu-Fe-S system. Bn = bornite, Cb = cubanite, Cc = chalcocite, Cpy = chalcopyrite, Di = digenite, m-Po = monoclinic pyrrhotite, h-Po = hexagonal pyrrhotite, and Py = pyrite. **(a)** At 25°C, Cu-Fe-S stable sulfide phases exhibit limited compositional variation. **(b)** At 300°C bornite and chalcocite-digenite exhibit expanded compositional ranges (purple shading). **(c)** At 400°C, the compositional range of bornite expands to include compositions equivalent to chalcocite-digenite in lower temperature assemblages. Compositional range of the intermediate solid solution (iss) phase is also expanded.

Introduction to Zambian Copperbelt geochemical and stable isotope studies

Peter McGoldrick
Centre for Ore Deposit Research, University of Tasmania

Introduction

One of the principal aims of our research was to apply modern high-quality multi-element geochemical and stable isotopic techniques to the investigation of the Zambian Copperbelt deposits.

It was anticipated that:

- host rock geochemical and stable isotope patterns may define halos or even vectors to ore
- that they would yield insight into ore-forming and/or alteration processes, and
- may allow another level of comparison between Zambian Copperbelt with prospective sequences elsewhere (Slide 9.1)

Early in the project it was decided to ignore the large body of historical geochemical data exists from all the Zambian Copperbelt mining operations. There were several reasons for this including:

- the largest data set came from monthly production and grade control assays, unfortunately these were routinely analysed for only a limited group of elements (often just total Cu, acid soluble Cu, Co, Ag, and Fe)
- a limited amount of multi-element data for Chambishi Basin deposits exists at the Kalulushi library; these data date from the 1970s and 1980s but a lack of quality control information precluded any assessment of the reliability of analyses, furthermore sample location information was often unsatisfactory
- despite many anecdotal comments to effect that 'large amounts of geochemical data do exist', only one contemporary multi-element data set was discovered by P544 researchers (from the Chambishi Deposit)

Sampling

In practise, two broad approaches have been used for this work. The first has been to sample a number of drill holes providing a broad stratigraphic interval including Lower Roan rocks. This yields information on the variations in rock geochemistry as ore positions are approached and in some instances laterally into more weakly mineralised parts of the Lower Roan sequences.

The second approach is more closely targeted at the level of mineralisation, and includes detailed studies of several deposits. Emphasis in these studies has been to recognise elements (other than Cu and Co) that form part of the 'ore association'.

To this end nearly 1000 new whole rock multi-element geochemical analyses and more than 360 new C and O isotope measurements were undertaken on material collected during the course of P544 geological investigations. It was decided from the outset that geochemical sampling would be guided by the detailed geological studies that formed the fundamental basis for all Zambian work in P544. This resulted in a strong focus in the Chambishi Basin, the Konkola area and at Zamanglo's Ndola West prospect. A limited sample set from the Mufulira deposit and samples from selected regional stratigraphic holes (Broughton, this report) were also investigated.

Techniques

Early in the project analyses were carried out at the University of Tasmania. Samples were shipped from Zambia and crushed and milled at the University in a low-contamination case-hardened carbon-steel mill. These samples were analysed by XRF for major and trace elements. Powdered samples were also sent to Becqueral (Sydney) for INAA for Au and a few trace (including some REE).

Later sample preparation was carried out in both Zambia and Tasmania. Unfortunately, the first Zambian batch (mainly from Konkola North and Nkana) were milled in a Ni-Cr steel mill and low level Ni, Cr (and possibly Mo and V) must be considered unreliable. Subsequent Zambian-prepared samples were crushed and milled at Alfred Knight's Kalulushi operations in low contamination carbon-steel mills. Later in the project all samples were analysed at ACME Laboratories Vancouver using a modification of their commercial '4A/4B' procedure. This involves separate alkali fusion and 3-acid sample digestions followed by a combination ICPOES and ICPMS finish. Sulfur and carbon were analysed separately by pyrolysis ('Leco'). University of Tasmania 'in house' standard rocks were included with the 'unknowns' submitted to both ACME and Becquerel. The results received for these indicate satisfactory accuracy for most elements for both laboratories.

The C and O isotope analyses were carried out at the Central Science Laboratory, University of Tasmania on both crushed whole rock samples and micro-drilled samples. The technique used is a modification of the procedure described by Charef and Sheppard (1984), and rocks containing a little as two or three percent carbonate yield satisfactory results. (Slide 9.2)

All samples were analysed for a diverse suite of elements which included all major elements, total C and total S, and the following trace elements: Ag, As, Ba, Bi, Cd, Co, Cr, Cs, Cu, Ga, Hf, Mo, Nb, Ni, Pb, Rb, Sb, Sc, Sn, Sr, Ta, Th, Tl, U, V, W, Y, Zn, Zr and REE. Due to poorer detection limits, not all these trace elements are reported for the samples analysed by XRF. Selected samples were analysed separately for Au, Pt, Pd (by ICPMS at ACME) and for organic and inorganic C (by pyrolysis at CSL, University of Tasmania).

Although of potential interest neither Hg, Se, Te nor B were analysed for, because separate specialised analytical procedures are required for the determination of these elements. (Slide 9.3)

Previous results

Zambian geochemical results had been presented previously at the sponsors meeting held in Golden last year, and reported in the 2002 P544 Annual Report. This work included major and trace element geochemistry for vertical section through Mwashia and Roan rocks from the Chambishi Basin (samples from drill holes RCB1A and RCB2). Major and trace element results for Ore Shale samples from several deposits (Nkana, Mindola, Konkola, Konkola North) and stratigraphic profiles of C and O isotopes for the hangingwall to the Ore Shale in RCB2 and few footwall samples from NN44X

A small set of organic C analyses were also discussed in Golden. (Slide 9.4)

This report

The chemostratigraphic work commenced on hangingwall samples from RBC2 has been extended through the Ore Shale and into the footwall position in this hole. Samples from a second hole (NN66, collared a few hundred metres east of RCB2 and lacking any significant mineralisation) have now been analysed for major and trace elements (Large, this report). Data from drill holes DH219 and MW107 from Mufulira and drill hole KLB 145 from Konkola are included in the database accompanying this report and will be further discussed in David Broughton's PhD. (Slide 9.5)

The geochemical data have also been important in quantifying the extent of alkali alteration (often Cu-related) in the Lower Roan rocks. Selley (this report) and Scott (this report) discuss results from

Mwambashi B deposit and Ndola W prospect, respectively.

The ore geochemical signatures work has now been extended to include several examples of both Ore Shale-hosted and arenite-hosted styles of Cu mineralisation. Deposits for which data are available include: Mwambashi B (Selley, this report), Ndola W and Mufulira (Scott, this report), Chibuluma W, Chambishi and Chambishi SE (McGoldrick et al., this report). (Slide 9.6)

For the C and O isotopes studies the RCB2 and NN66 profiles through the Ore Shale and into the footwall position were completed. In addition a large number of samples from the Lower Roan rocks at Chambishi SE prospect (including carbonate-rich 'barren gap' areas – Bull, this report) were also analysed. The existing Nkana data set was complemented with carbonates obtained by drilling paragentically well constrained samples. (Slide 9.7)

Databases

The appendix to this final report includes a series of spreadsheets containing all isotopic and geochemical data, together with sample locations (where possible), drill hole ID, rock names and limited mineralogy, stratigraphic unit and procedures performed. (Slide 9.8)

References

Charaf, A. and Sheppard, S.M.F., 1984, Carbon and oxygen isotope analysis of calcite or dolomite associated with organic matter, Isotope Geoscience, 2, 325-333.

CODES SRC

Introduction to ZCB Geochemistry

WHY?

- Host rock geochemical and stable isotope patterns may define halos or even vectors to ore
- They yield insight into ore-forming and/or alteration processes
- They allow another level of comparison between ZCB and prospective sequences elsewhere

CODES SRC

- About a thousand new multi-element geochemical analyses
- Most from ACME Vancouver (combination ICP-MS & OES), others from Tas Uni (XRF) and Becqueral (INAA)
- Quality control monitored using Tas Uni 'in house' standards
- Carbonate C/O isotopes measured on 365 samples (whole rock & drilled) at CSL, Tas Uni

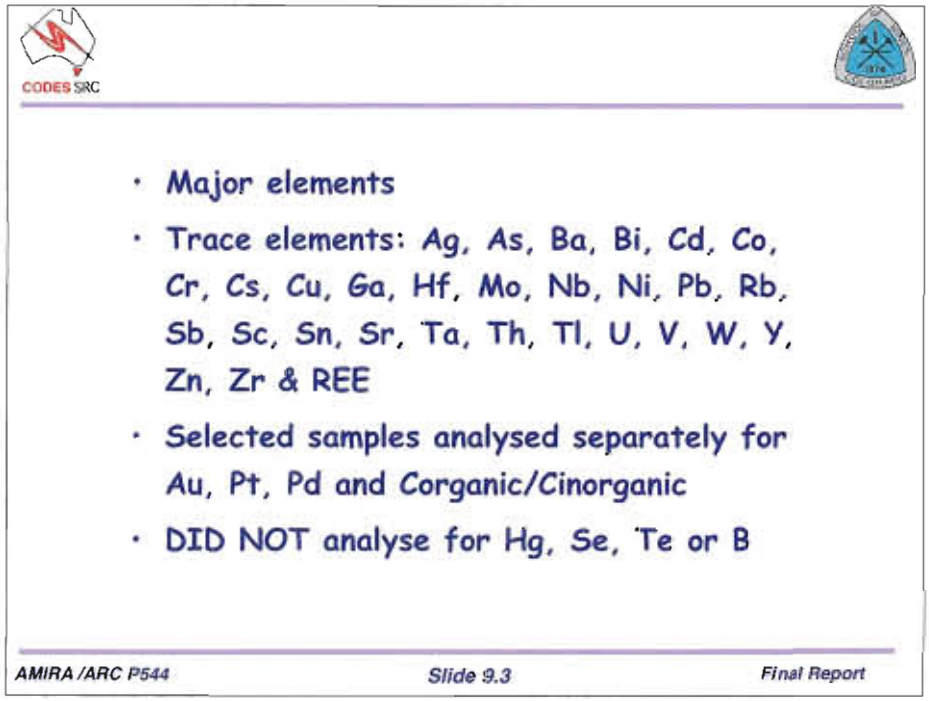
CODES SRC
• Major elements
• Trace elements: Ag, As, Ba, Bi, Cd, Co, Cr, Cs, Cu, Ga, Hf, Mo, Nb, Ni, Pb, Rb, Sb, Sc, Sn, Sr, Ta, Th, Tl, U, V, W, Y, Zn, Zr & REE
• Selected samples analysed separately for Au, Pt, Pd and Corganic/Cinorganic
• DID NOT analyse for Hg, Se, Te or B
AMIRA /ARC P544
Slide 9.3
Final Report

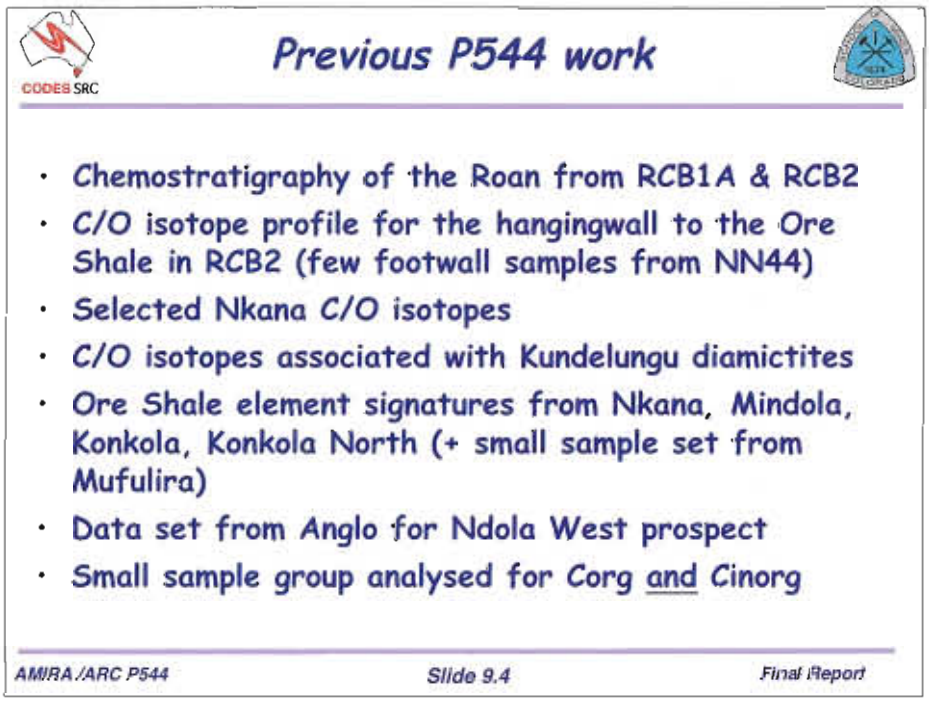
CODES SRC
Previous P544 work
• Chemostratigraphy of the Roan from RCB1A & RCB2
• C/O isotope profile for the hangingwall to the Ore Shale in RCB2 (few footwall samples from NN44)
• Selected Nkana C/O isotopes
• C/O isotopes associated with Kundelungu diamictites
• Ore Shale element signatures from Nkana, Mindola, Konkola, Konkola North (+ small sample set from Mufulira)
• Data set from Anglo for Ndola West prospect
• Small sample group analysed for Corg and Cinorg
AMIRA /ARC P544
Slide 9.4
Final Report

New work: chemostratigraphy

- Chemostratigraphy has been extended to a fence of holes from Chambishi South East deposit (includes RCB2) - Large: this meeting
- Drill holes DH219 & MW107 from Mufulira
- Drill hole KLB 145 from Konkola
- 16 samples from drill hole KIT01DD005 from Ndola W
- Major element chemistry has been used to gauge chemical effects of alkali alteration/metasomatism at Mwambashi B and Ndola West - Selley: this meeting; Scott: this meeting

AMIRA /ARC P544 Slide 9.5 Final Report

New work: ore signatures

- fence of holes from Mwambashi B
  - Selley/McGoldrick: this meeting
- 2 drill holes from Chambishi deposit
- 1 drill hole from Chibuluma
- Chambishi SE fences
- DH219, MW 107 Mufulira
  - McGoldrick: this meeting
- KLB145 Konkola
  - Broughton: this meeting

AMIRA /ARC P544 Slide 9.6 Final Report

New work: C/O isotopes

- Additional samples from Nkana: veins and whole rock
- Completed the RCB2 & NN66 profiles through the Ore Shale and into the footwall position
- Additional samples of Lower Roan rocks (incl. Ore Shale and 'barren gap' carbonates) from Chambishi SE fence
- Smaller number of samples from Ndola W and Mufulira
  - Large: this meeting

AMIRA /ARC P544 Slide 9.7 Final Report

Final Report

- A series of spreadsheets will be provided to sponsors containing all isotopic and geochemical data, together with sample locations, descriptions and procedures performed

AMIRA /ARC P544 Slide 9.8 Final Report

Lithogeochemistry and alteration halos to stratiform copper mineralisation in the Chambishi Basin, Zambian Copperbelt

Ross Large, Peter McGoldrick, Stuart Bull, Rob Scott and Dave Selley
Centre for Ore Deposit Research, University of Tasmania

Abstract

Lithogeochemical studies have been carried out on a series of drill holes in the Chambishi Basin in order to establish chemostratigraphic relationships and test for the presence of geochemical alteration halos or vectors that may be useful in exploration.

Ti/Zr ratio in the Roan sediments has been shown to be of use in stratigraphic correlation. There is a general increase in the Ti/Zr of siliclastic lithologies up-stratigraphy from the footwall clastics, which display the lowest values (5 to 17), to hangingwall Roan sediments (10 to 30), to the Mwashia with the highest values of 25 to 40. The gradual increase in Ti/Zr is interpreted to represent a change from felsic to mafic source areas passing from Lower Roan to Mwashia. The Ore Shale exhibits a diagnostic Ti/Zr signature; a systematic and rapid increase from base to top of 15 to 30, related to the rapid change from clastic to shale facies during 'ore shale' deposition.

A thick zone of stratiform potassic alteration encompasses the mineralised ore shale and enclosing Mindola Clastics. The potassic alteration halo is represented by enrichment of biotite and K-feldspar in the enclosing sediments, with whole rock K_2O values varying from 3.5 to 10 wt %. The K_2O/Al_2O_3 ratio is the best indicator of the potassic alteration zone, and provides a consistent vector to the "ore shale" over a distance of 200–400 m from the hanging wall side. Erratic Ba enrichment from 300 to 2000 ppm occurs throughout the potassic halo. The majority of Ba is present in K-feldspar, although free barite is present in some zones. A subtle cobalt halo occurs in the potassically altered clastics surrounding the ore shale, related to Co enrichment in disseminated pyrite and biotite.

A major zone of stratiform sodic alteration (albite–calcite) occurs in the Upper Roan siltstone–carbonate sequence overlying the ore-related potassic alteration zone. Na_2O values vary from 1.5 to 6.3 wt %, corresponding to a maximum of 60 wt % albite in the altered rock. The albite alteration varies up to 400 m thick and is centred on a stratabound carbonate breccia zone. Petrographic evidence indicates the albite alteration postdates the ore-related K-feldspar alteration. Thin zones of albite alteration also occur in the Mindola clastics in both the footwall and hanging wall to the Ore Shale.

Zinc is the only other element that may have potential exploration value as a hanging wall vector to mineralisation. In several drill holes Zn shows a subtle but systematic increase (10–60 ppm) toward the base of the Upper Roan, about 100 m above mineralised Ore Shale.

Introduction

Aims

- To determine the geochemical characteristics of the various sediment litho-facies in the Mwashia, Upper Roan and Lower Roan.
- To evaluate the presence of lithogeochemical halos or vectors to ore that may be useful for exploration

Sampling

Four drill holes in the Chambishi Basin were selected for this lithogeochemical study (Slide 3).

RCB1A: Intersected the Mwashia and Upper Roan siltstones and carbonates. Terminated in a gabbro intrusive and did not reach the mineralised stratigraphy (Slide 4). Forty samples were selected for lithogeochemistry from this hole

RCB2: Intersected the Upper Roan and Lower Roan stratigraphy including a highly mineralised section of "ore shale" averaging 2.7% Cu over 13.5 m. Sixty-six samples were collected and analysed over the interval from 250 to 1550 m down hole (Slides 4, 6, 8).

NN66: Intersected Upper Roan and Lower Roan stratigraphy including a narrow interval of very weakly mineralised 'ore shale' (maximum of 3000 ppm Cu) (Slides 5, 29). Forty-seven samples were collected and analysed over the interval 550–1152 m down hole.

NN48: Intersected Upper Roan and Lower Roan stratigraphy including the mineralised 'ore shale' (Slides 5, 40). Twenty-six samples were collected and analysed from 665 to 1054 m down hole.

Drill holes RCB2, NN66 and NN48 lie on a NNE section from the centre to the eastern edge of the Chambishi Basin (Slide 3). The stratigraphy and sedimentology of this section has been described by Bull (this volume).

Analytical techniques

Samples from RCB1A and the upper part of RCB2 were analysed for majors and traces by XRF at the University of Tasmania. Holes NN66, NN48 and the lower part of RCB2 were analysed by a combination of ICPMS and OES at the ACME Lab in Vancouver. Check analyses indicate that the results from the two labs are very comparable. The full tabulation of results are presented in a database on CD in the rear envelope of this volume.

Further information on the analytical techniques for this batch of samples and all other samples analysed as part of the AMIRA P554 project are provided by McGoldrick (this volume).

Previous work

The two previous significant studies of geochemistry of host rocks in the Zambian Copper Belt are Darnley (1960) and Moine et al. (1986). Both workers recognised the presence of potassium and sodium metasomatism in the Roan.

Lithostratigraphy

Stratigraphic units

The Lower Roan Clastics (FW Lower Roan) comprise basement-derived conglomerates and arkoses deposited in alluvial/fluvial environments. Rapid lateral facies variations attest to a strong structural control.

The Ore Shale is a carbonaceous siltstone–sandstone–dolomite that represents an abrupt transition to sub-wave-base conditions. The best Cu mineralisation is typically in the basal few metres of the unit.

The Rokana Evaporites (HW Lower Roan) are a cyclical succession of muddy sandstones siltstones and carbonates. Locally preserved primary evaporitic textures indicate deposition in a marginal sabkha setting. Lesser well-sorted sandstone (quartzite) intervals similar in character to the footwall clastics, the main example of which is termed the Nchanga or Glassy quartzite, attest to periodic progradation of braided fluvial aprons.

The Chambishi Dolomite is a microbial bioherm that has a coherent internal stratigraphy over large areas indicating it represents complete tectonic quiescence.

Shale with Grit (basal unit of Upper Roan) represents marginal marine siltstone deposition and the characteristic texture of crosscutting 'grit' dykes presumably represent substantial dewatering processes.

Upper Roan to Mwashia siltstones and carbonates represent continued marginal marine sedimentation in a range of environments from restricted (evaporitic salterns/salinas) to open marine sub-wave base conditions.

Chemostratigraphy

Classification of samples

Because of the vastly different geochemical attributes of clastic and chemical sediments the data set was divided into two groups based on carbonate content. The latter has been estimated using loss on ignition (LOI). Samples with greater than 20 wt % LOI have been grouped as carbonate-rich sediments, and those with less than or equal to 20 wt % LOI have been termed carbonate-poor sediments or siliclastics. The distinction between these two groups, for the Upper Roan in RCB2, is shown in Slides 7 and 8.

Ti/Zr ratios

A number of immobile element ratios, including Ti/Zr, V/Nb and Sc/Th, were tested to assess their potential to assist with stratigraphic correlations. Ti/Zr ratios proved to be the most useful in the siliciclastic group. The following is a summary of the Ti/Zr data:

- Overall Ti/Zr in the sediments shows significant variation that relates to sedimentary facies on the local (bed to bed) scale, and provenance on the unit or formation scale
- The 'ore shale' exhibits a systematic increase in Ti/Zr from the base to top with values from 15 to 30 (Slides 9, 38, 39, 43). The majority of ore shale samples fall in the Ti/Zr range 22 to 27 (Slide 10).
- Although somewhat erratic, there is a general increase in Ti/Zr up-stratigraphy (Slide 10) from footwall clastics (5 to 17), to Upper Roan (10 to 30) to the Mwashia (25 to 40). This suggests a gradual change in sediment provenance from felsic (granitic basement), to mafic sources.
- Due to their low immobile element contents, the carbonate-rich sediments show a very erratic pattern of Ti/Zr, and should not be used in chemostratigraphic assessment.

These data indicate that it is possible to use the Ti/Zr ratios of the Mwashia and Lower Roan to assist in stratigraphic correltations.

Cu–Co mineralisation

Copper

In this part of the Chambishi basin the copper mineralisation occurs as a narrow strabound chalcopyrite-bearing zone within the 'ore shale'. In all three drill holes (RCB2, NN66 and NN48) the best Cu grades are confined to the basal part of the ore shale (Slides 12, 29, 40).

Other points of note are:

- Background Cu values in the Lower Roan clastics and Upper Roan siltstones and carbonates typically vary from 1 to 20 ppm.
- There is no Cu halo in the hanging wall sediments above the 'ore shale'.
- There is a gradual drop-off in Cu values in the footwall clastics from values of 100s down to 10s ppm Cu over about 100 m in RCB2 (Slide 12).
- A second zone of anomalous Cu occurs in an Upper Roan dolomite-siltstone interval from 450 to 500 m in RCB2

Cobalt

Peak values of Co (200–500 ppm) correlate with the main Cu zones in the ore shale. However, compared with Cu which shows no hanging wall halo, each of the three drill holes (Slides 25, 32, 42) exhibit a distinct Co halo surrounding the Cu-ore zone.

Background Co values in the Roan sediments vary from 2 to 20 ppm, compared with a world mean of 10 ppm for black shales (Slide 25). In RCB2, Co values increase from values around 10 ppm upwards to 200 ppm over a distance of 200 m approaching the Cu-ore zone from the hanging wall side. In drill holes NN66 and NN48 the subtle Co halo extends about 100 m above and 100–150 m below the ore shale (Slides 32, 42).

Preliminary laser ablation ICPMS analyses of minerals in a sample from the Co halo (Slide 20) in RCB2

indicates that Co is present in pyrite (400–3500 ppm; mean 1480 ppm Co) and biotite (38–56 ppm; mean 48 ppm Co). One biohermal carbonate sample from the barren gap in Chambishi SE returned a Co analysis of 124 ppm, which is anomalously high for a primary unaltered carbonate.

Potassic alteration zone

Darnley (1960) described potassium and boron metasomatism associated with the copper orebodies. Selley et al. (this volume) has provided detailed petrographic descriptions of the extensive K-feldspar alteration of the ore shale and surrounding Mindola Clastics, and demonstrated a clear paragenetic relationship between K-feldspar alteration and copper mineralisation at a number of localities. Both Darnley (1960) and Selley et al. (this volume) recognised fine grained tormaline intergrown with the metasomatic K-felspar. This lithogeochemical study supports the petrographic observations of both Selley et al. (this volume) and Scott (this volume), and clearly demonstrates the widespread extent and stratigraphic nature of the potassic alteration.

K_2O patterns

Siltstones within the Mwashia and uppermost Roan vary from 0.2 to 5 wt% K_2O with a mean of 2.6 wt %. This compares with a world average shale mean of 3.2 wt % K_2O (McGoldrick, 2002). In contrast the siliclastics of the Lower Roan, in and surrounding the Cu orebodies, varies from 2 to 12 wt % K_2O (Slides 13, 30, 41). The average of 55 "ore shale" samples from the Chambishi Basin gave a value of 5.0 wt % K_2O, well above the world average shale of 3.2 wt %.

In RCB2 (Slide 13) elevated K_2O (> 3.2 wt %), occurs throughout the lower Roan from 900 to 1600 m down hole surrounding the ore zone. In NN66 (Slide 30), where no significant Cu ore was intersected, the potassic alteration zone still persists, but is thinner (850 to 1150 m down hole) and less intense.

In Slide 17 the MINSQ program (Herrmann and Berry, 2002) has been used to calculate down hole K-felspar percentages from the whole-rock geochemical data. This shows that the lower Roan sediments average about 15 wt % K-felspar, with intervals from 30 to 60 wt % K-felspar representing the intensely potassic altered zones.

A narrow zone of potassic alteration has also been identified by the geochemistry, in the Upper Roan at around 500 m in RCB2 (Slide 13). This corresponds with elevated Cu to 1000 ppm over the same interval.

K–Al relationship

The K_2O/Al_2O_3 ratio has proved to be the best way to define potassium alteration in the district (Slides 15, 16). This is because K-feldspar has the highest K_2O/Al_2O_3 ratio of all the aluminous minerals with a value around 0.9, compared with biotite (0.4), muscovite (0.3) and albite (0.0). From Slide 15 it is clear that the potassic altered sediments in the ore shale and Lower Roan have K_2O/Al_2O_3 values between 0.4 and 0.9, whereas the Upper Roan and Mwashia commonly display values less than 0.4.

In RCB2 (Slide 16), there is a general down hole increase in K_2O/Al_2O_3 ratio from 0.01 to 0.7 over a distance of 400 m approaching the mineralised ore shale. A very similar pattern is seen in NN66 (Slide 31). This ratio thus provides an excellent vector to the centre of the alteration system. However, it is not always a vector to ore, as some potassic alteration zones are not accompanied by ore-grade copper (e.g. NN66).

K–Cu relationship

The relationship between Cu and K_2O is displayed in Slide 18 using data from RCB2, NN66 and NN48. The graph shows that all samples with greater than 1000 ppm Cu have suffered potassic alteration, and all samples with less than 30 ppm Cu are strongly depleted in K_2O. However there is a large number of samples with elevated K_2O and low Cu which correspond to the zone of widespread stratiform potassic alteration surrounding the orebodies.

K–Co relationship

Anomalous Co, sited in pyrite and biotite, occurs throughout the potassic asltered sediments surrounding the Cu ore zones. This leads to the positive relationship between K_2O and Co shown in Slide 19.

K–Ba relationship

Down hole Ba plots (Slides 22, 33) show an erratic zone of Ba enrichment within and around the ore shale, corresponding with the zone of potassic alteration. For Ba values of less than 1200 ppm there is a positive relationship between Ba and K_2O (Slide 22), suggesting that the Ba is sited in K-feldspar. This relationship has been confirmed by microprobe analyses (Scott, this volume). For whole rock Ba levels greater than 1000 to 1200 ppm there is no correlation with K_2O, suggesting the presence of barite in these instances.

K–tourmaline relationship

Selley et al. (this volume) reports very fine grained tourmaline present throughout the potassic alteration zone. Although no boron analyses were undertaken in this study, we predict a geochemical correlation between K_2O and B throughout the potassic zone.

Sodic alteration zone

The down-hole geochemical plots for RCB2 and NN66 (Slides 23 and 34) indicate a stratiform zone of sodium metasomatism in the Upper Roan sediments overlying the potassic alteration zone. Na_2O values of 2 to 6 wt% occur over a thickness of 200 to 300 m, concentrated on zones of sedimentary breccia. This compares with world average shale values of 1.3 wt % Na_2O. Petrographic studies (Darnley, 1960; Selley et al., this volume) indicate the sodium enrichment is caused by albite alteration of the shales, carbonates and breccia zones. Irregular white zones of albite alteration, with up to 60 wt % albite, are present throughout the Upper Roan (Slide 24), particularly at the boundaries of mafic intrusives (e.g. RCB1A; 580 m). Good evidence, that the albite alteration postdates the K-feldspar alteration, has been provided by Darnley (1960) and Selley et al. (this volume).

Na_2O values throughout the ore shale are commonly in the range 0.1 to 1.0 wt %. Petrographic studies indicate that detrital albite is commonly replaced by K-feldspar throughout the ore shale and Lower Roan clastics within the potassic alteration zone.

Occasional narrow zones of Na_2O enrichment occur in the Lower Roan clastics (e.g. NN66; 1110 m). These correspond with albite alteration overprinting K-feldspar alteration, and represent a significant post-mineralisation fluid event.

Zinc distribution

Down hole Zn in RCB2 and NN66 shows generally very low values through the Lower Roan, including the ore shale, of typically less than 30 ppm (Slides 27, 35). However erratic values of >100 ppm are rarely present.

A subtle trend of increasing Zn values occurs, down stratigraphy, towards the base of the Upper Roan in both RCB2 and NN66. In the former, Zn increases from 1 ppm to over 30 ppm over 300 m from 800 to 1100 m down hole. In NN66, Zn increases from 5 ppm to 50 ppm over 250 m from 700 to 950 m down hole. The possibility exists that the Zn, although very subtle, represents a displaced vector pointing to the presence of mineralisation in the stratigraphically lower 'ore shale'. Further work is needed to test this possibility.

Conclusions and alteration model for exploration

An alteration model, based on the lithogeochemistry from RCB1A, RCB2, NN66 and NN48, is shown in Slide 44. The significant features of the model are outlined below:

- A zone of stratiform potassium feldspar alteration encompasses the ore shale and clastic Lower Roan

package. The potassic zone varies from 700 m thick surrounding the well-mineralised RCB2 ore zone, to 300 m thick surrounding the poorly mineralised NN66 intersection.

- The K_2O/Al_2O_3 and K_2O/Sc ratios are the best indicators of the potassic alteration zone.
- The K_2O/Al_2O_3 ratio increases systematically towards to 'ore shale' from the hanging wall side from values of <0.2 to >0.6. This represents a strong vector to the centre of the alteration system
- The potassic alteration halo is accompanied by elevated Co and Ba (and B?). Co is present in disseminated pyrite and phlogopite, Ba is present in K-feldspar and rarely barite, whereas B is present in tourmaline.
- A major zone of barren stratiform albite alteration occurs in the Upper Roan siltstone–carbonate sequence overlying the ore-related K-feldspar alteration zone. Paragenetic studies indicate the albite post-dates the K-feldspar alteration.
- The HW albite alteration is centred on a strata-bound carbonate breccia zone, which is interpreted by Broughton (this volume) to relate to a layer of salt dissolution in the Upper Roan.
- Immobile element ratio studies suggest that the Ti/Zr ratio may assist in stratigraphic correlations.
- The 'ore shale' exhibits a systematic increase in Ti/Zr from the base to top, with values from 15 to 30. The majority of ore shale samples fall in the Ti/Zr range 22 to 27.
- Although somewhat erratic, there is a general increase in Ti/Zr up-stratigraphy from footwall clastics (5 to 17), to Upper Roan (10 to 30) to the Mwashia (25 to 40). This suggests a gradual change in sediment provenance from felsic to mafic sources.

References

Darnley, A. G., 1960, Petrology of some Rhodesian Copperbelt Orebodies and associated rocks: Trans. Inst. Min. Metall., v. 69, p. 137–173.

Herrmann, W., and Berry, R. F., 2002, MINSQ – a least squares spreadsheet method for calculating mineral proportions from whole rock major element analyses: Geochemistry; Exploration, Environment, Analysis, v.2, p.361–368.

Moine, B., Guilloux, L., and Audeoud, D., 1986, Majoe element geochemistry of the host rocks in some sediment–hosted copper deposits; in Friedrich, G. H. (ed.) Geology and Metallogeny of Copper Deposits, Springer-Verlag, Berlin, 1986, p. 443–460.

McGoldrick, P. J., 2002, P544 AMIRA Meeting, Denver.

Lithogeochemistry and Halos to Ore in the Chambishi Basin

Peter McGoldrick, Stuart Bull, Rob Scott,
Dave Selley and Ross Large

AMIRA P544

Slide 1

Aims of lithogeochemical Research

- To evaluate the presence of lithogeochemical halos or vectors to Cu ore
- To determine the chemical characteristics of various alteration styles

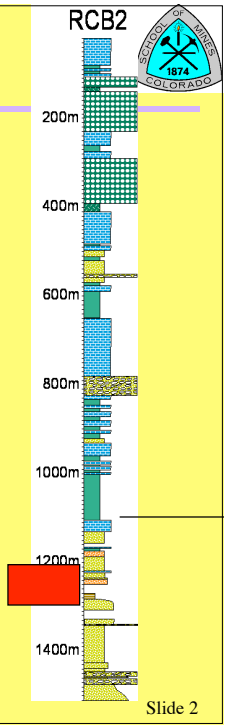

AMIRA P544

Slide 2

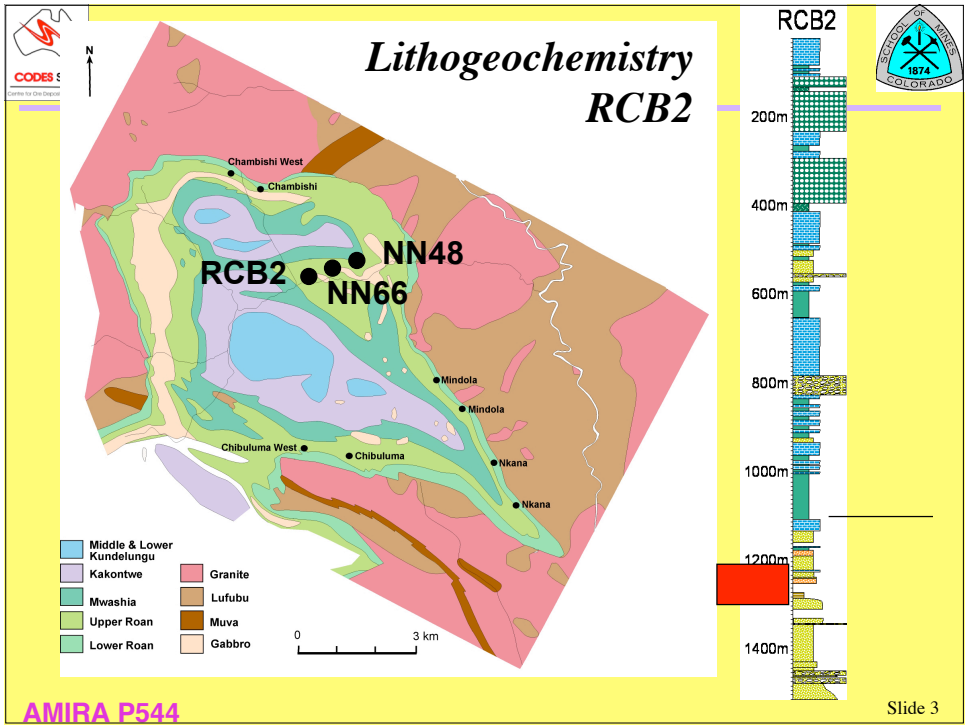
Lithogeochemistry
RCB2
N
Chambishi West
Chambishi
RCB2
NN48
NN66
Mindola
Mindola
Chibuluma West
Chibuluma
Nkana
Nkana
Middle & Lower Kundelungu
Kakontwe
Mwashia
Upper Roan
Lower Roan
Granite
Lufubu
Muva
Gabbro
0
3 km
RCB2
200m
400m
600m
800m
1000m
1200m
1400m
AMIRA P544
Slide 3

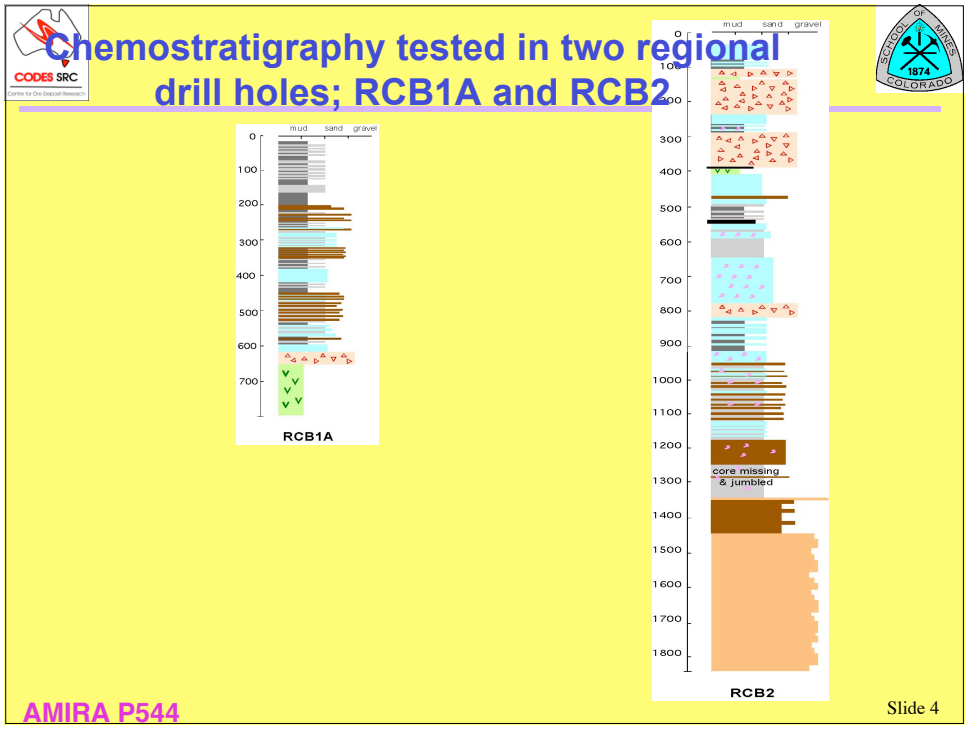
Chemostratigraphy tested in two regional drill holes; RCB1A and RCB2
mud
sand
gravel
RCB1A
RCB2
core missing & jumbled
AMIRA P544
Slide 4

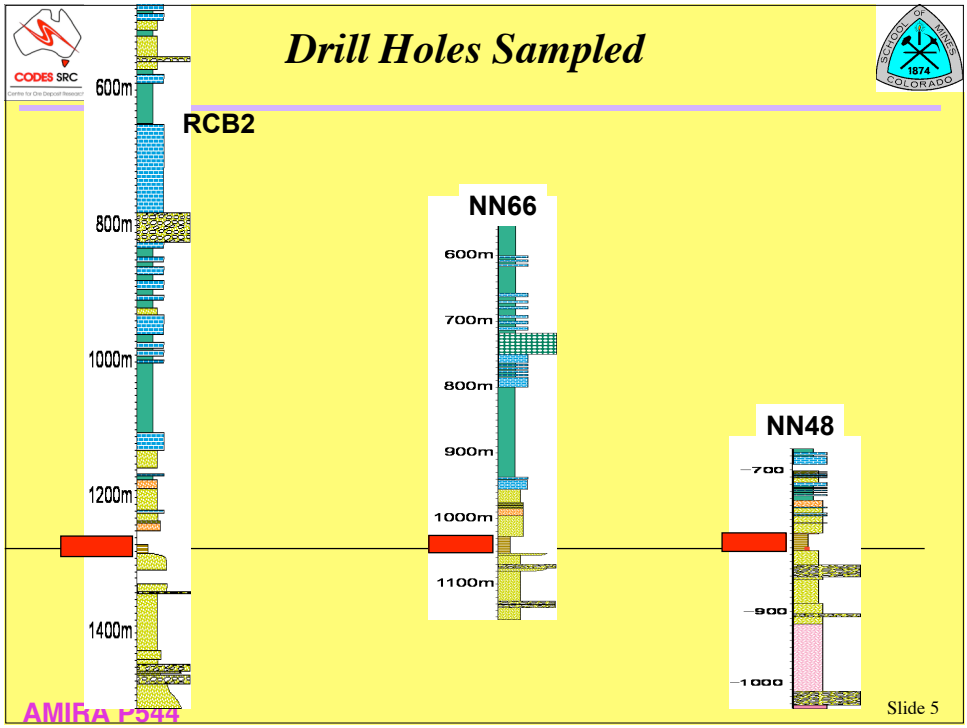
Drill Holes Sampled
CODES SRC
SCHOOL OF MINES 1874 COLORADO
RCB2
600m
800m
1000m
1200m
1400m
NN66
600m
700m
800m
900m
1000m
1100m
NN48
700
900
1000
AMIRA P544
Slide 5

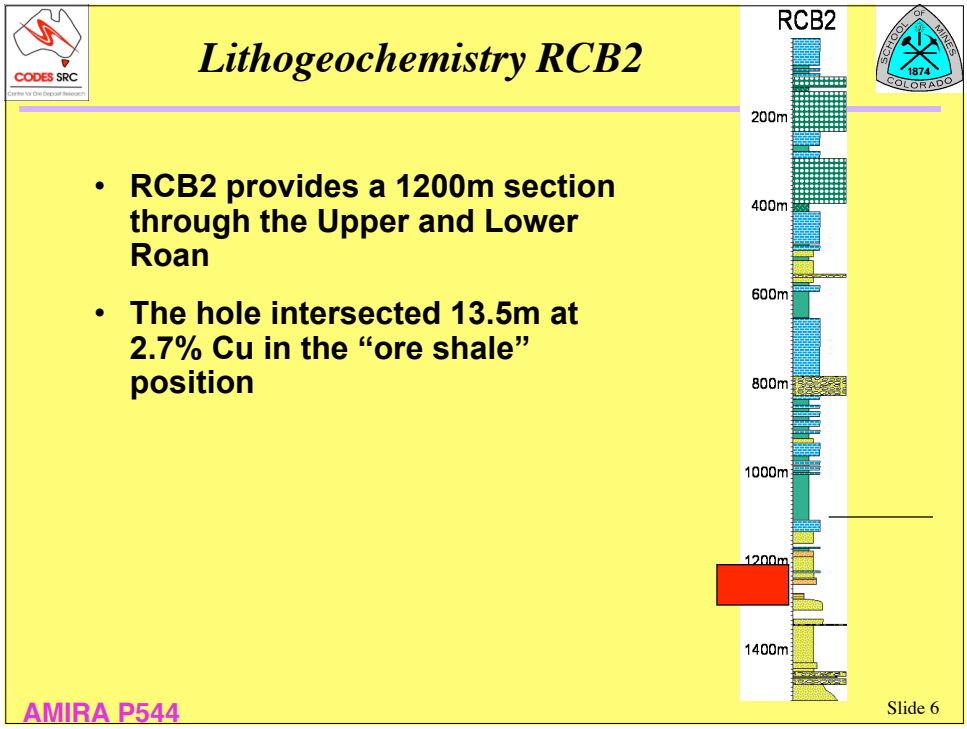
Lithogeochemistry RCB2
CODES SRC
SCHOOL OF MINES 1874 COLORADO
RCB2
200m
400m
600m
800m
1000m
1200m
1400m
• RCB2 provides a 1200m section through the Upper and Lower Roan
• The hole intersected 13.5m at 2.7% Cu in the “ore shale” position
AMIRA P544
Slide 6

RCB2: Carbonate Variation

- Data set split into two groups:
  - Siliciclastics, LOI < 20 wt%
  - Carbonates, LOI > 20 wt%
- Carbonate content increases systematically up stratigraphy through the Upper Roan above the Ore Shale.

AMIRA P544 Slide 7

Lithogeochemistry of Upper Roan in RCB2

Carbonate content

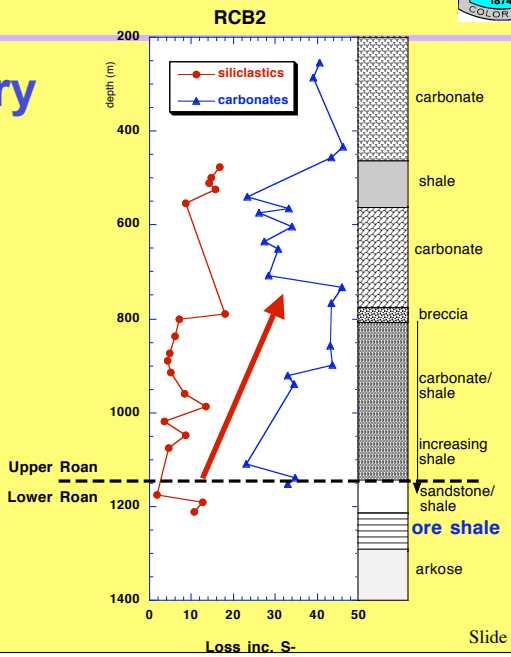

AMIRA P544 Slide 8

RCB2: Ti/Zr ratio

Ti/Zr ratio is variable within ore shale

Ti/Zr increases systematically from FW to HW in ore shale from 12 to 28

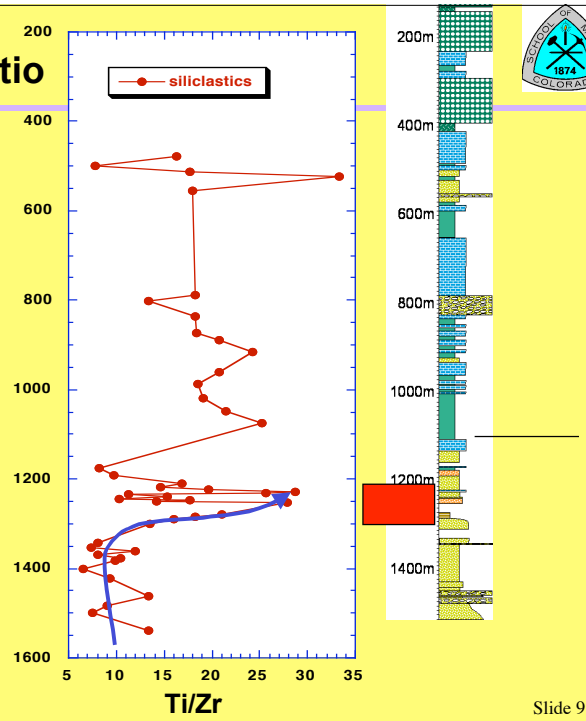

AMIRA P544

Slide 9

Ti/Zr Ratio Populations

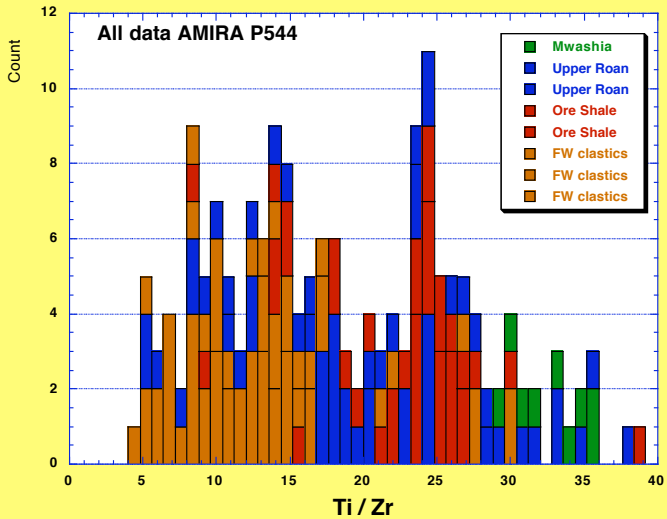

AMIRA P544

Slide 10

Ti - Zr patterns (all data)

- FW clastics have lowest values of Ti/Zr with most data in range 5 to 17 (due to granitic source)
- Ore Shale commonly has a tight distribution: Ti/Zr = 22-27; Ti < 0.8wt%, Zr < 200ppm
- Upper Roan siliciclastics are more variable: Ti/Zr = 10-30, two distributions are suggested by the data, mean Ti/Zr ~ 18 and 24
- Mwashia shales are more Ti-rich than Ore Shales, with Ti/Zr = 25 to 40 (suggesting a mafic source)

AMIRA P544 Slide 11

RCB2: COPPER

- Cu concentrated at base of ore shale
- Minor Cu mineralisation also in a thin HW shale unit
- No Cu halo in the overlying clastics or shales

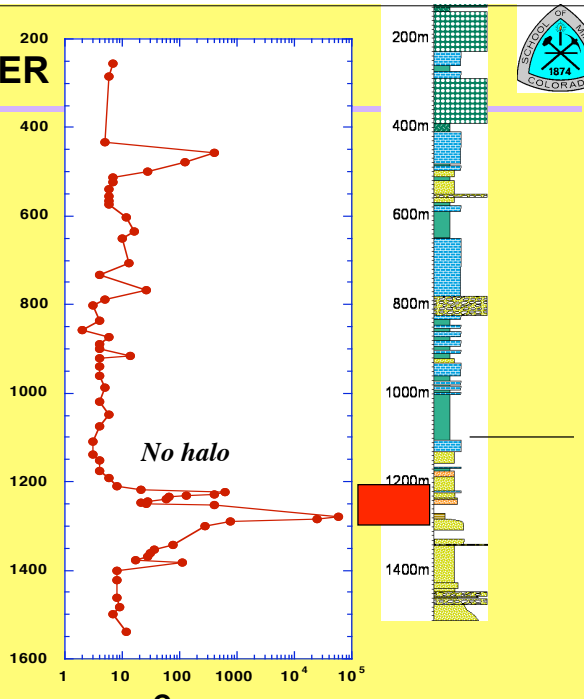

AMIRA P544 Slide 12

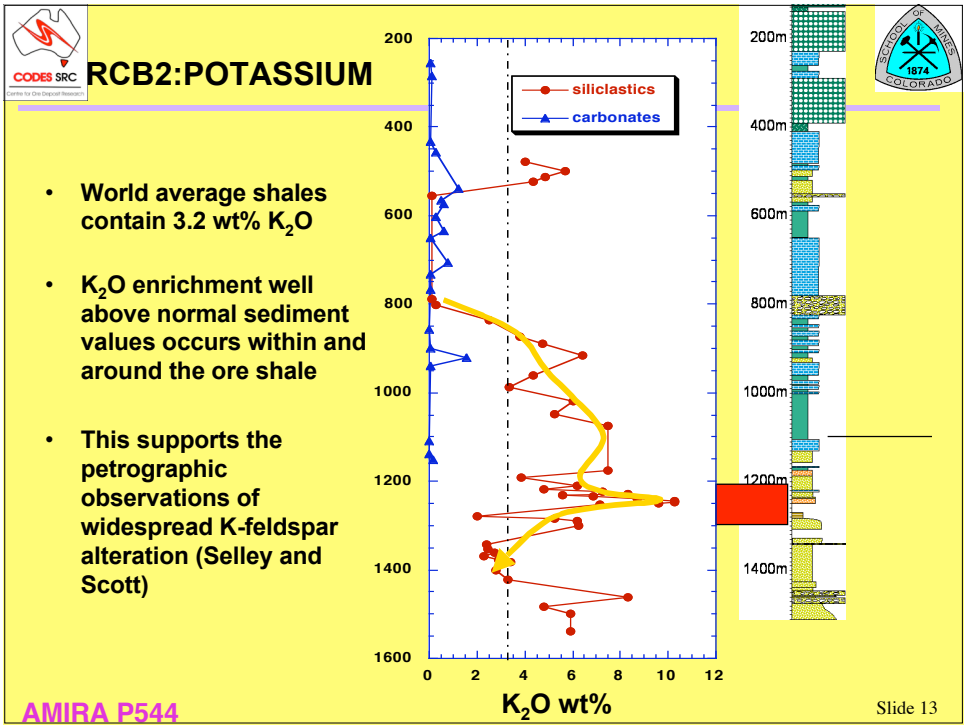
RCB2:POTASSIUM
• World average shales contain 3.2 wt% K_2O
• K_2O enrichment well above normal sediment values occurs within and around the ore shale
• This supports the petrographic observations of widespread K-feldspar alteration (Selley and Scott)
siliclastics
carbonates
200
400
600
800
1000
1200
1400
1600
0
2
4
6
8
10
12
K_2O wt%
200m
400m
600m
800m
1000m
1200m
1400m
AMIRA P544
Slide 13

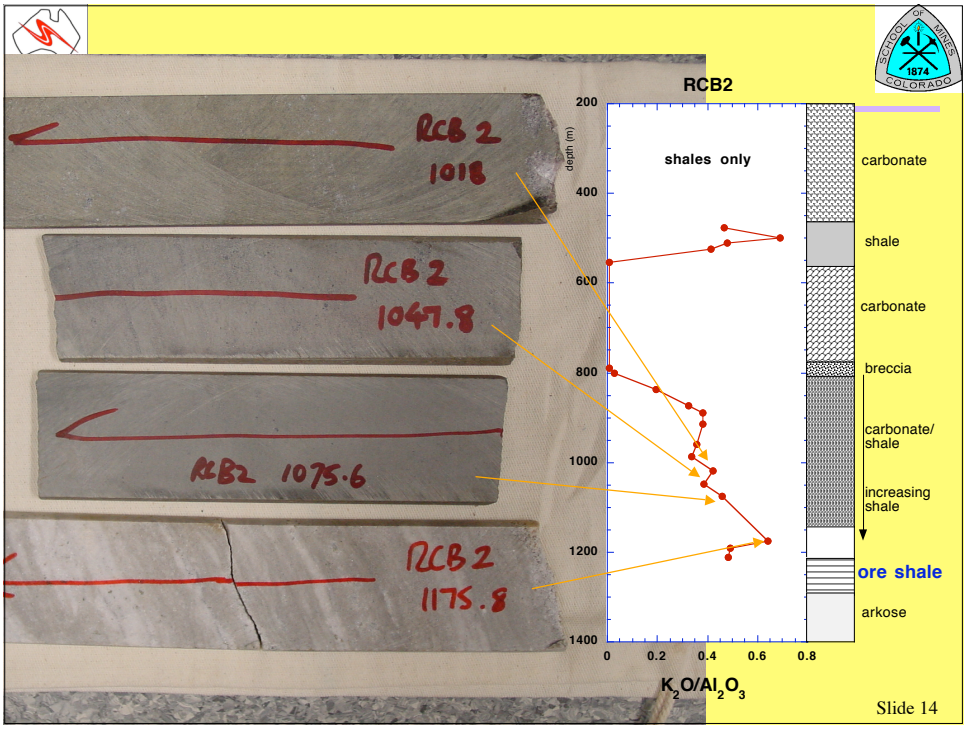
RCB2
RCB 2 1018
RCB 2 1047.8
RCB2 1075.6
RCB 2 1175.8
shales only
depth (m)
200
400
600
800
1000
1200
1400
0
0.2
0.4
0.6
0.8
K_2O/Al_2O_3
carbonate
shale
carbonate
breccia
carbonate/ shale
increasing shale
ore shale
arkose
Slide 14

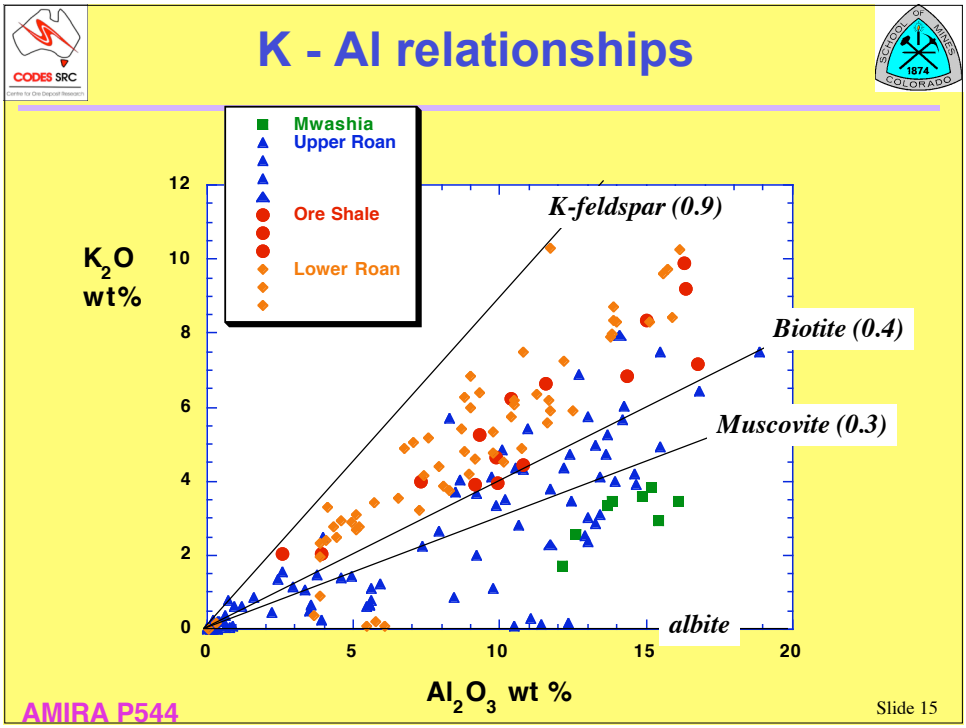
K - Al relationships
Mwashia
Upper Roan
Ore Shale
Lower Roan
K-feldspar (0.9)
Biotite (0.4)
Muscovite (0.3)
albite
K2O wt%
Al2O3 wt %
0
2
4
6
8
10
12
0
5
10
15
20
AMIRA P544
Slide 15

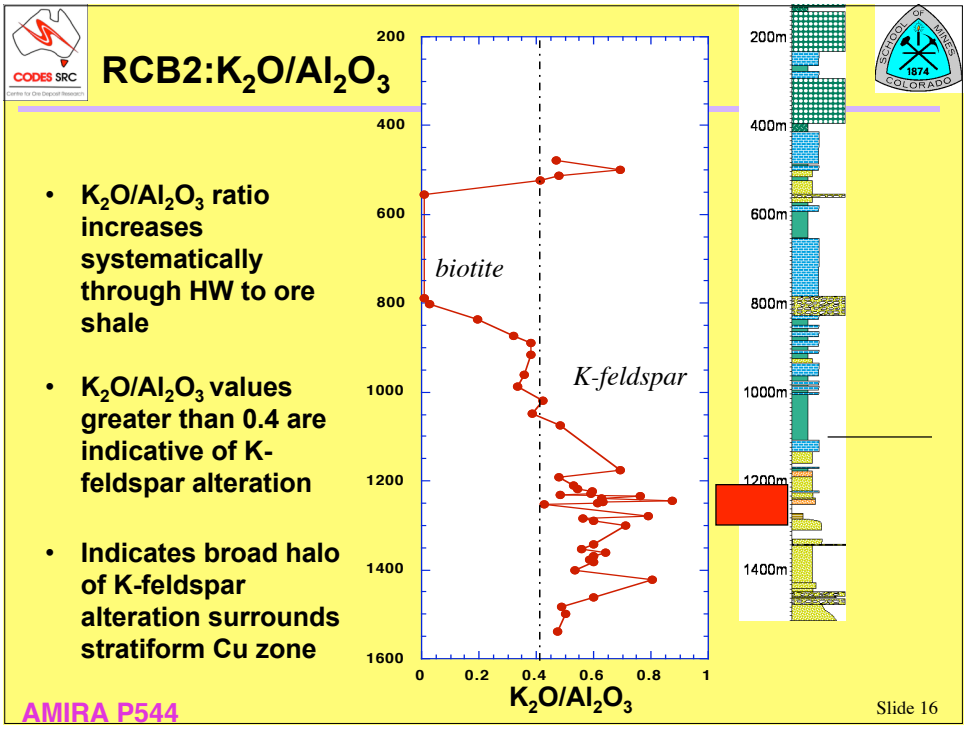
RCB2:K2O/Al2O3
K2O/Al2O3 ratio increases systematically through HW to ore shale
K2O/Al2O3 values greater than 0.4 are indicative of K-feldspar alteration
Indicates broad halo of K-feldspar alteration surrounds stratiform Cu zone
biotite
K-feldspar
200
400
600
800
1000
1200
1400
1600
0
0.2
0.4
0.6
0.8
1
K2O/Al2O3
200m
400m
600m
800m
1000m
1200m
1400m
AMIRA P544
Slide 16

K-feldspar wt%

- K-feldspar content is calculated from the whole-rock analysis by using the MINSQ computer program
- This confirms that K-feldspar alteration occurs in selected sedimentary units above and below the ore shale

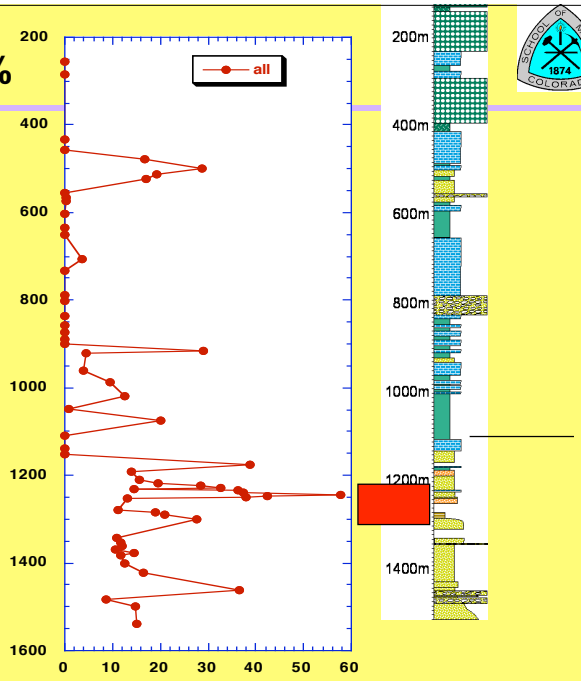

AMIRA P544

Slide 17

Cu - K_2O Relationships

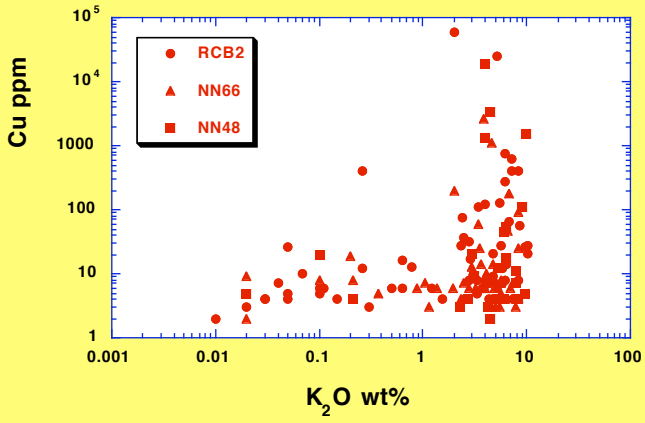

AMIRA P544

Slide 18

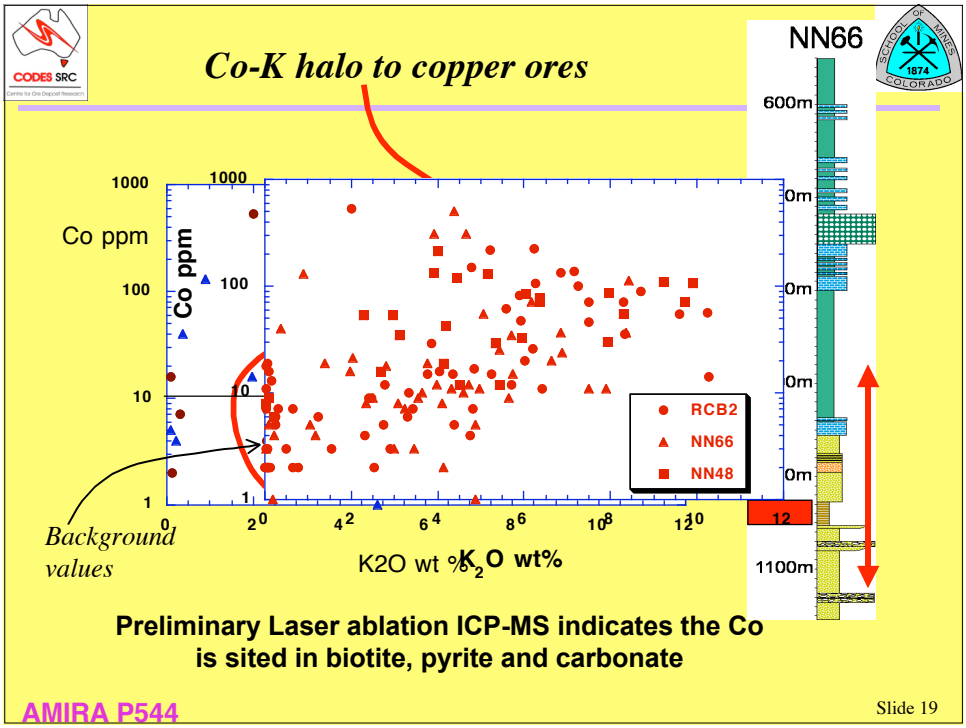

Preliminary Laser ablation ICP-MS indicates the Co is sited in biotite, pyrite and carbonate

AMIRA P544 Slide 19

Cobalt Host in Halo

- **Preliminary Laser Ablation analysis**

MINERAL	mean Co ppm	range
Pyrite (n=14)	1480	400 to 3500
Biotite (n=4)	48	38 to 56
Carbonate (n=5)	26	0.1 to 124
K-feldspar (n=6)	0.9	0.1 to 3.5

AMIRA P544 Slide 20

Two Pyrite Generations

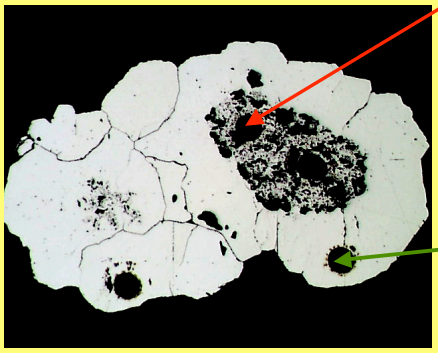

Early diagenetic pyrite
Co: 3507 ppm
Cu: 863 ppm
Pb: 1210 ppm
As: 1743 ppm

Later overgrowth pyrite
Co: 1175 ppm
Cu: 28 ppm
Pb: 29 ppm
As: 7 ppm

AMIRA P544

Slide 21

RCB2: BARIUM

- Ba shows erratic enrichment within and around the ore shale
- This corresponds to the zone of potassium enrichment
- Ba is principally in the K-feldspar

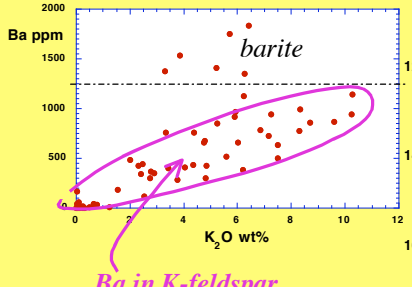

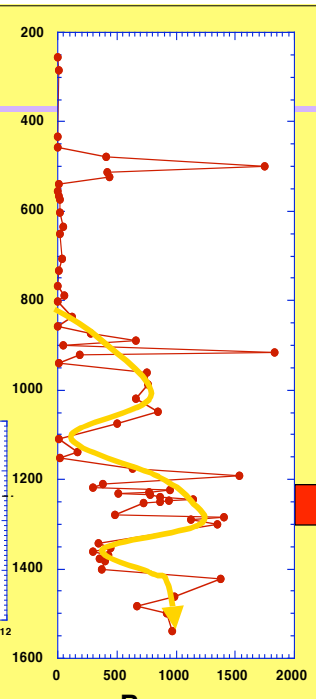

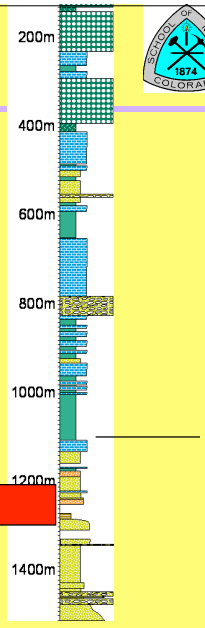

AMIRA P544

Slide 22

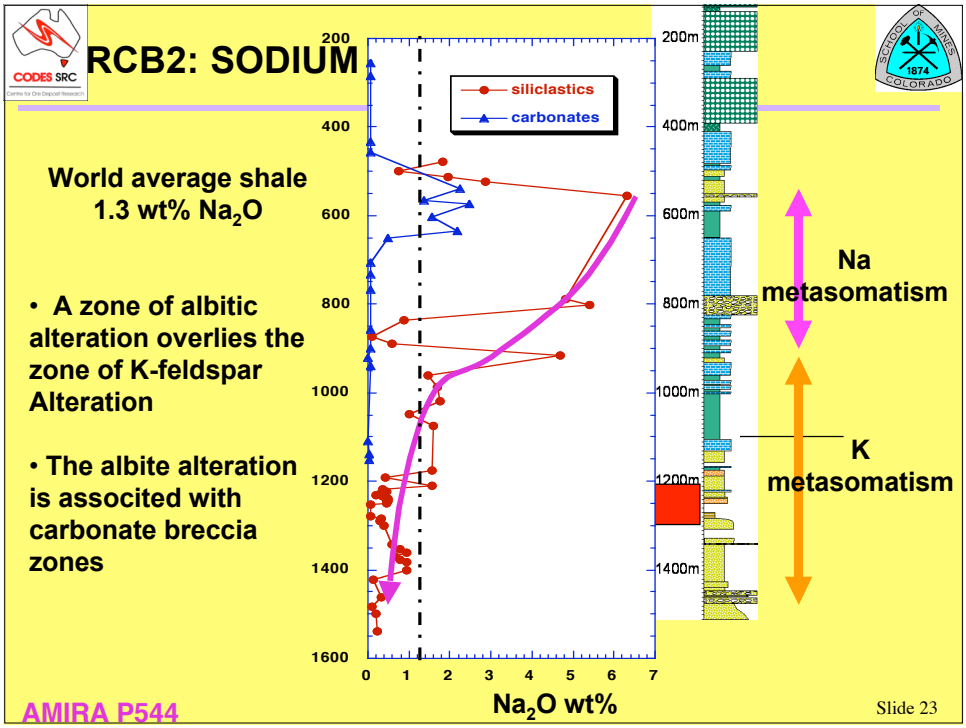
RCB2: SODIUM
siliclastics
carbonates
World average shale
1.3 wt% Na2O
• A zone of albitic alteration overlies the zone of K-feldspar Alteration
• The albite alteration is associted with carbonate breccia zones
Na metasomatism
K metasomatism
200
400
600
800
1000
1200
1400
1600
200m
400m
600m
800m
1000m
1200m
1400m
0 1 2 3 4 5 6 7
Na2O wt%
AMIRA P544
Slide 23

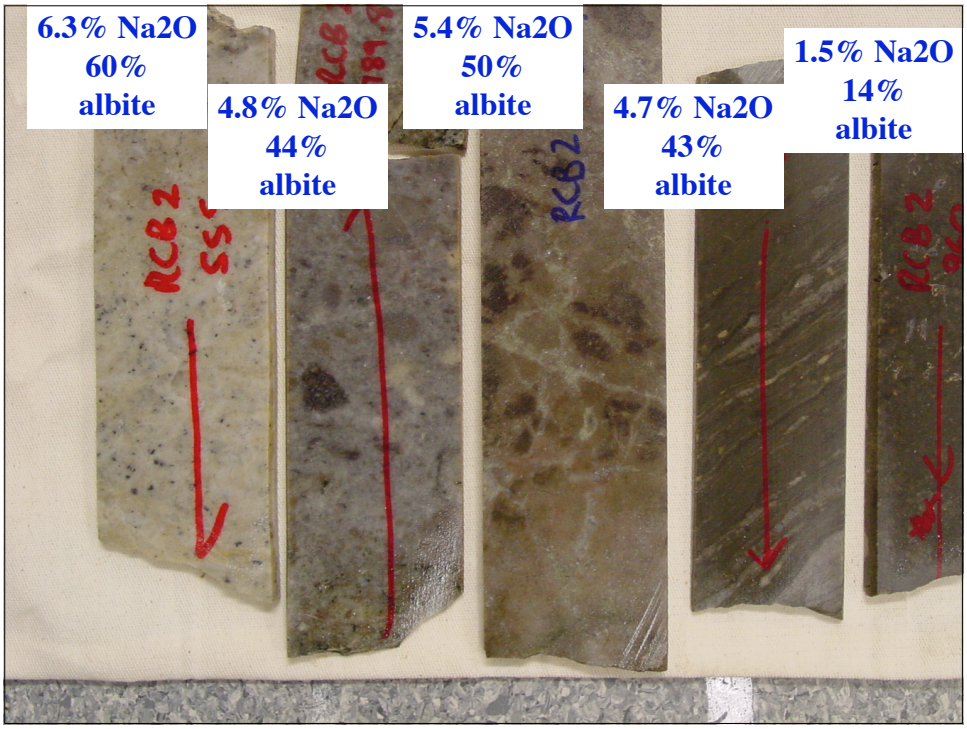
6.3% Na2O
60%
albite
4.8% Na2O
44%
albite
5.4% Na2O
50%
albite
4.7% Na2O
43%
albite
1.5% Na2O
14%
albite
RCB2

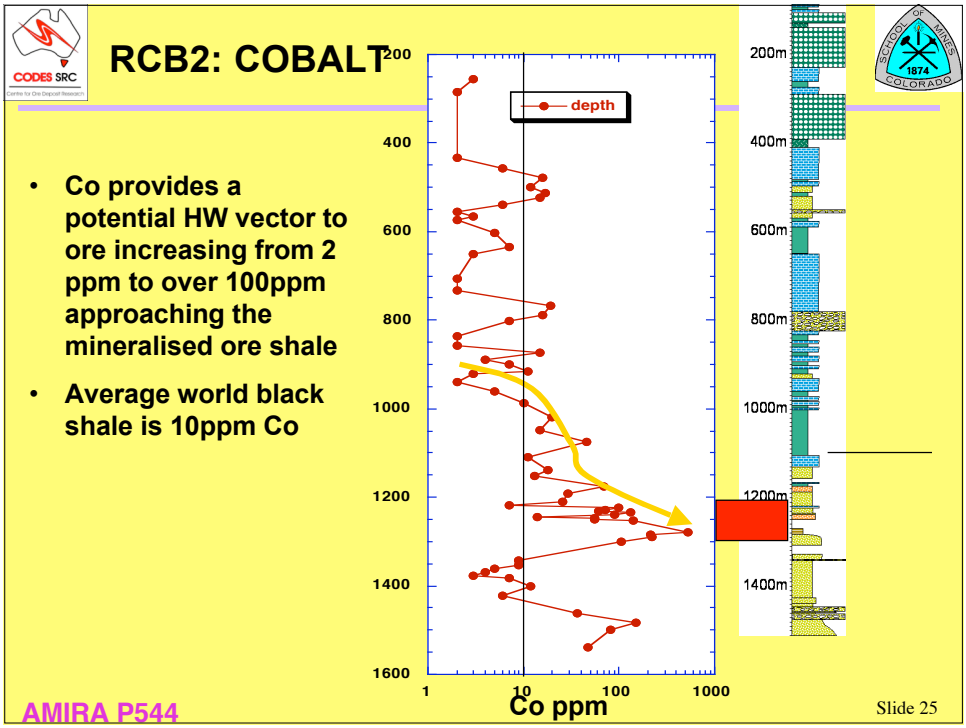
RCB2: COBALT
Co provides a potential HW vector to ore increasing from 2 ppm to over 100ppm approaching the mineralised ore shale
Average world black shale is 10ppm Co
depth
200
400
600
800
1000
1200
1400
1600
1
10
100
1000
Co ppm
200m
400m
600m
800m
1000m
1200m
1400m
AMIRA P544
Slide 25

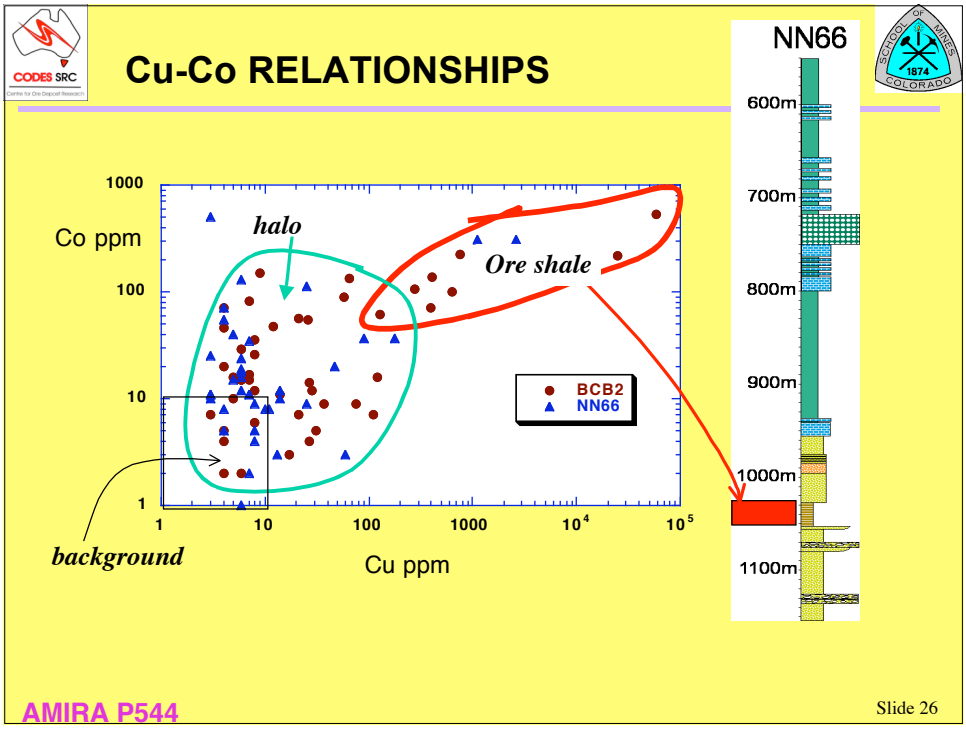
Cu-Co RELATIONSHIPS
NN66
1000
Co ppm
100
10
1
halo
Ore shale
BCB2
NN66
background
1
10
100
1000
10^4
10^5
Cu ppm
600m
700m
800m
900m
1000m
1100m
AMIRA P544
Slide 26

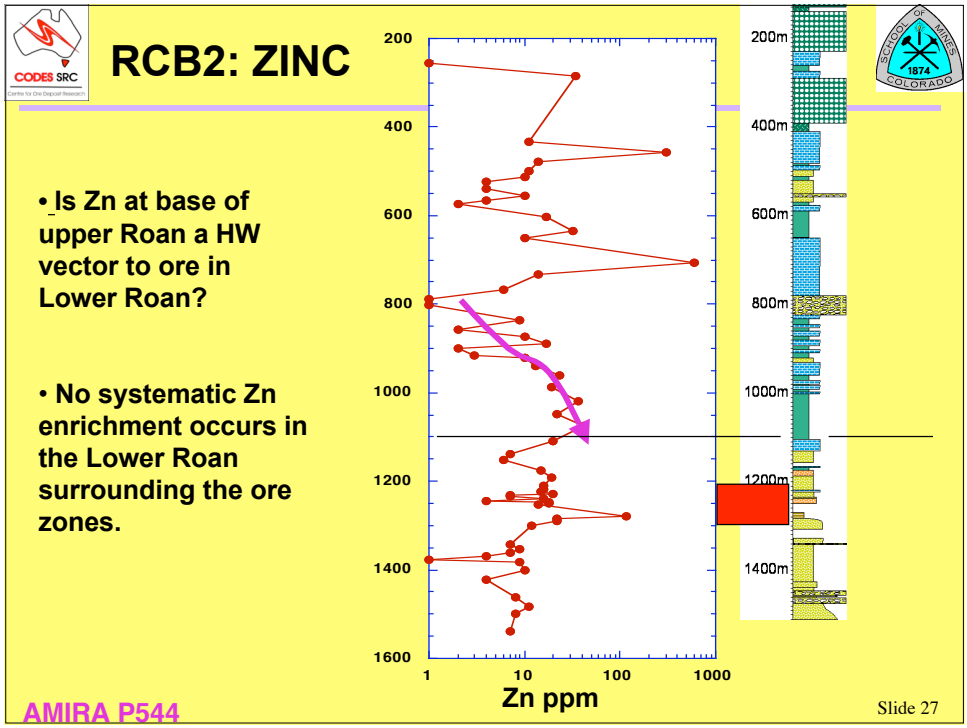
RCB2: ZINC
• Is Zn at base of upper Roan a HW vector to ore in Lower Roan?
• No systematic Zn enrichment occurs in the Lower Roan surrounding the ore zones.
200
400
600
800
1000
1200
1400
1600
1
10
100
1000
Zn ppm
200m
400m
600m
800m
1000m
1200m
1400m
AMIRA P544
Slide 27

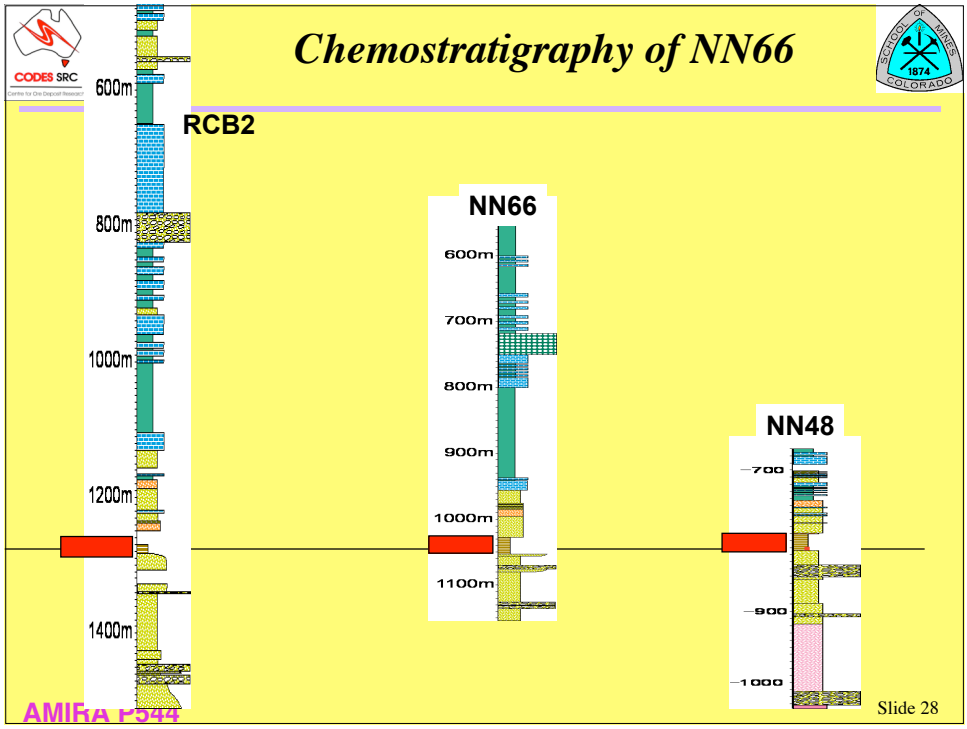
Chemostratigraphy of NN66
RCB2
600m
800m
1000m
1200m
1400m
NN66
600m
700m
800m
900m
1000m
1100m
NN48
700
900
1000
AMIRA P544
Slide 28

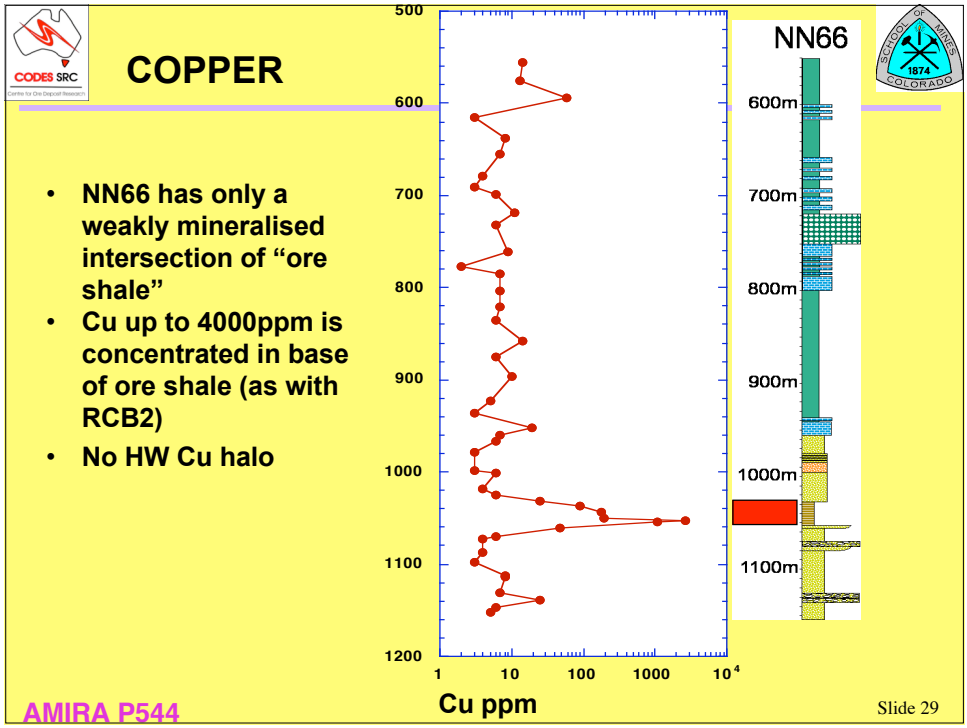
COPPER
• NN66 has only a weakly mineralised intersection of "ore shale"
• Cu up to 4000ppm is concentrated in base of ore shale (as with RCB2)
• No HW Cu halo
500
600
700
800
900
1000
1100
1200
1
10
100
1000
10 4
Cu ppm
NN66
600m
700m
800m
900m
1000m
1100m
AMIRA P544
Slide 29

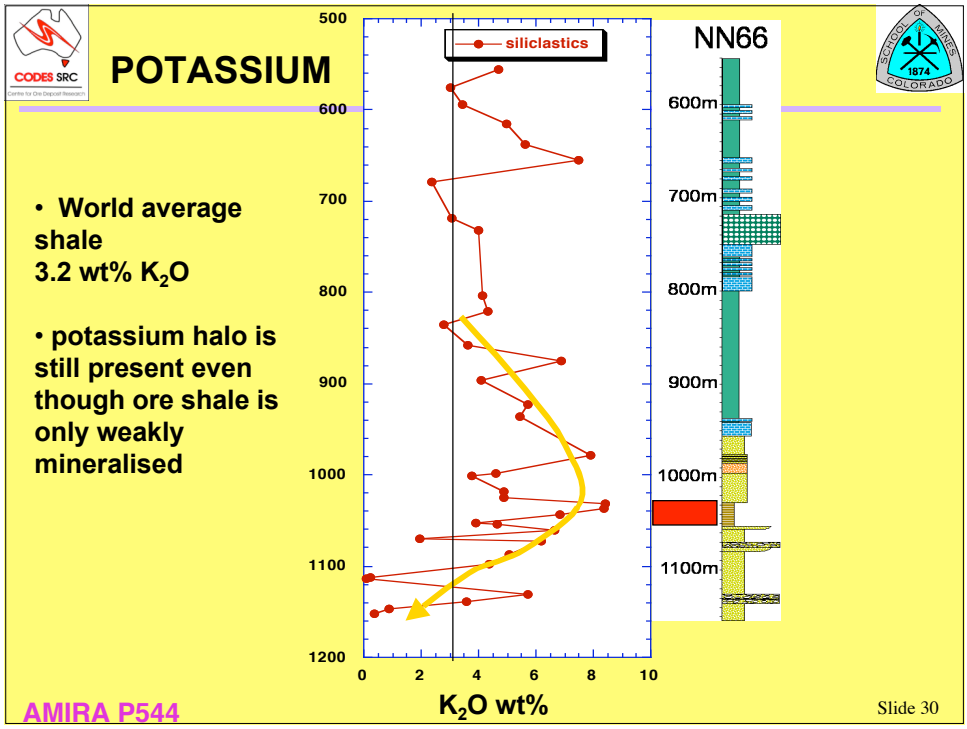
POTASSIUM
• World average shale 3.2 wt% K2O
• potassium halo is still present even though ore shale is only weakly mineralised
siliclastics
500
600
700
800
900
1000
1100
1200
0
2
4
6
8
10
K2O wt%
NN66
600m
700m
800m
900m
1000m
1100m
AMIRA P544
Slide 30

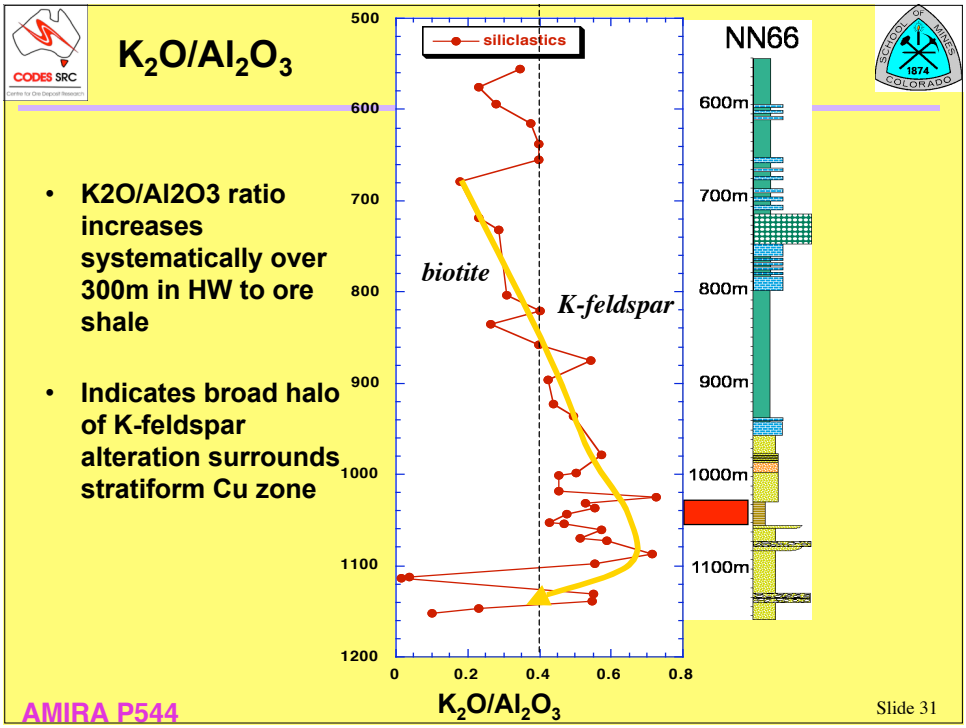
K_2O/Al_2O_3
• K2O/Al2O3 ratio increases systematically over 300m in HW to ore shale
• Indicates broad halo of K-feldspar alteration surrounds stratiform Cu zone
siliclastics
biotite
K-feldspar
NN66
600m
700m
800m
900m
1000m
1100m
500
600
700
800
900
1000
1100
1200
0
0.2
0.4
0.6
0.8
K_2O/Al_2O_3
AMIRA P544
Slide 31

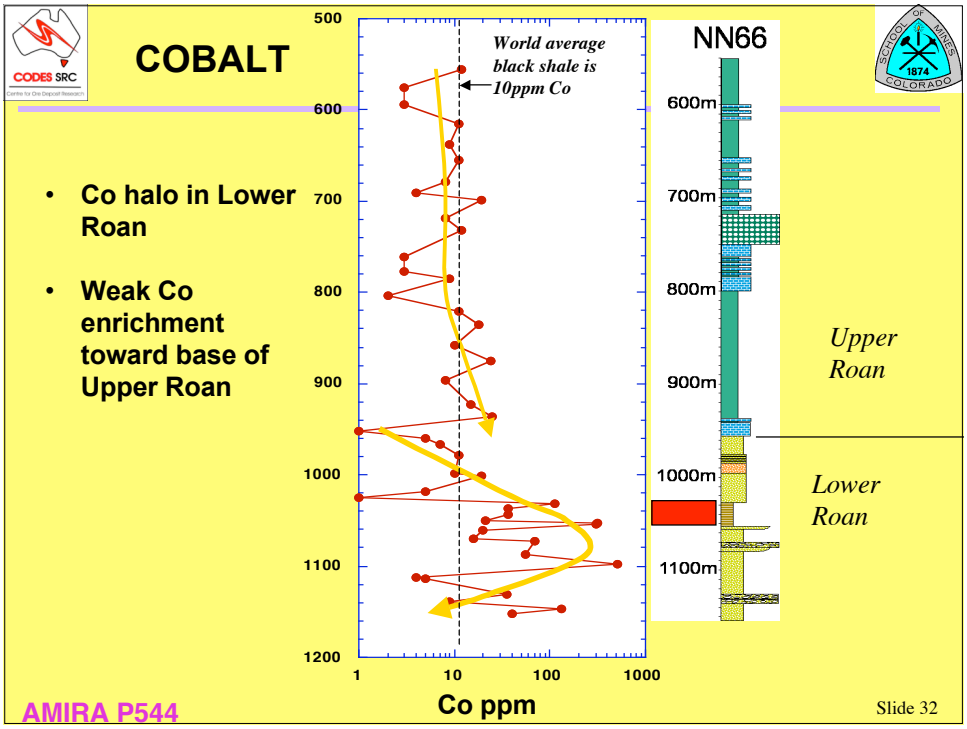
COBALT
• Co halo in Lower Roan
• Weak Co enrichment toward base of Upper Roan
World average black shale is 10ppm Co
NN66
600m
700m
800m
900m
1000m
1100m
Upper Roan
Lower Roan
500
600
700
800
900
1000
1100
1200
1
10
100
1000
Co ppm
AMIRA P544
Slide 32

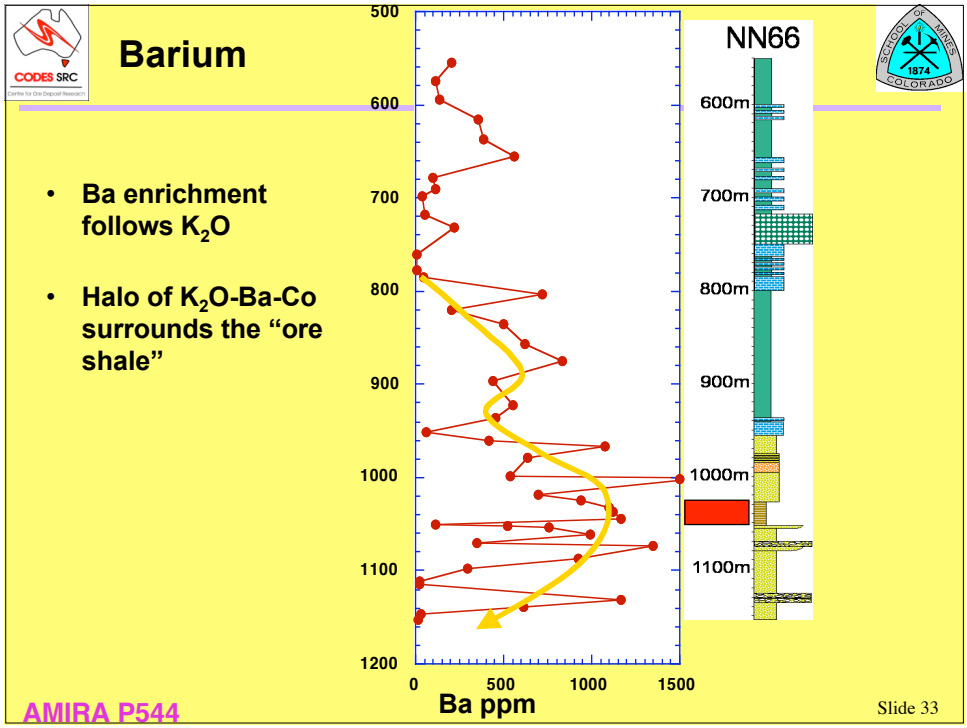
Barium
• Ba enrichment follows K_2O
• Halo of K_2O-Ba-Co surrounds the "ore shale"
NN66
500
600
700
800
900
1000
1100
1200
600m
700m
800m
900m
1000m
1100m
0
500
1000
1500
Ba ppm
AMIRA P544
Slide 33

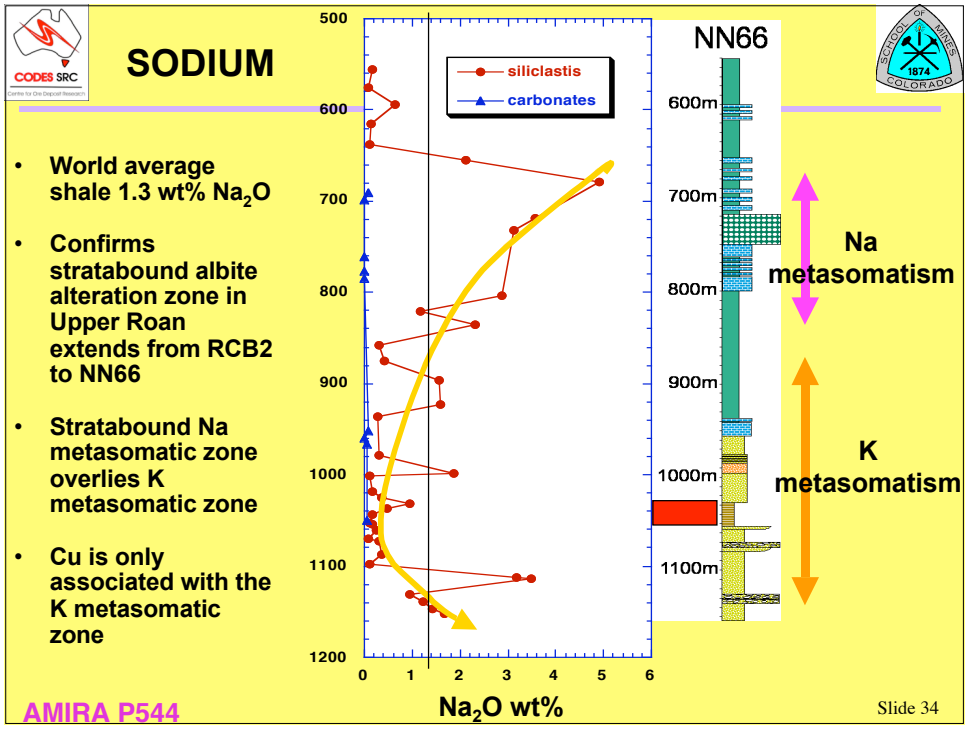
SODIUM
• World average shale 1.3 wt% Na_2O
• Confirms stratabound albite alteration zone in Upper Roan extends from RCB2 to NN66
• Stratabound Na metasomatic zone overlies K metasomatic zone
• Cu is only associated with the K metasomatic zone
siliclastis
carbonates
NN66
500
600
700
800
900
1000
1100
1200
600m
700m
800m
900m
1000m
1100m
Na metasomatism
K metasomatism
0
1
2
3
4
5
6
Na_2O wt%
AMIRA P544
Slide 34

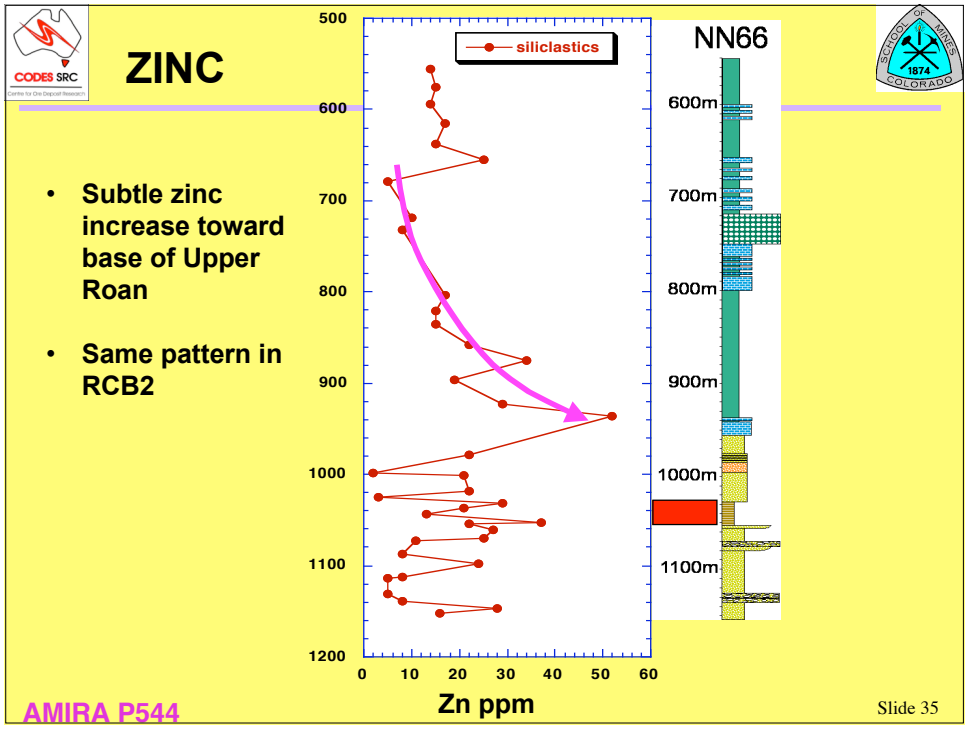
ZINC
Subtle zinc increase toward base of Upper Roan
Same pattern in RCB2
siliclastics
NN66
500
600
700
800
900
1000
1100
1200
600m
700m
800m
900m
1000m
1100m
0
10
20
30
40
50
60
Zn ppm
AMIRA P544
Slide 35

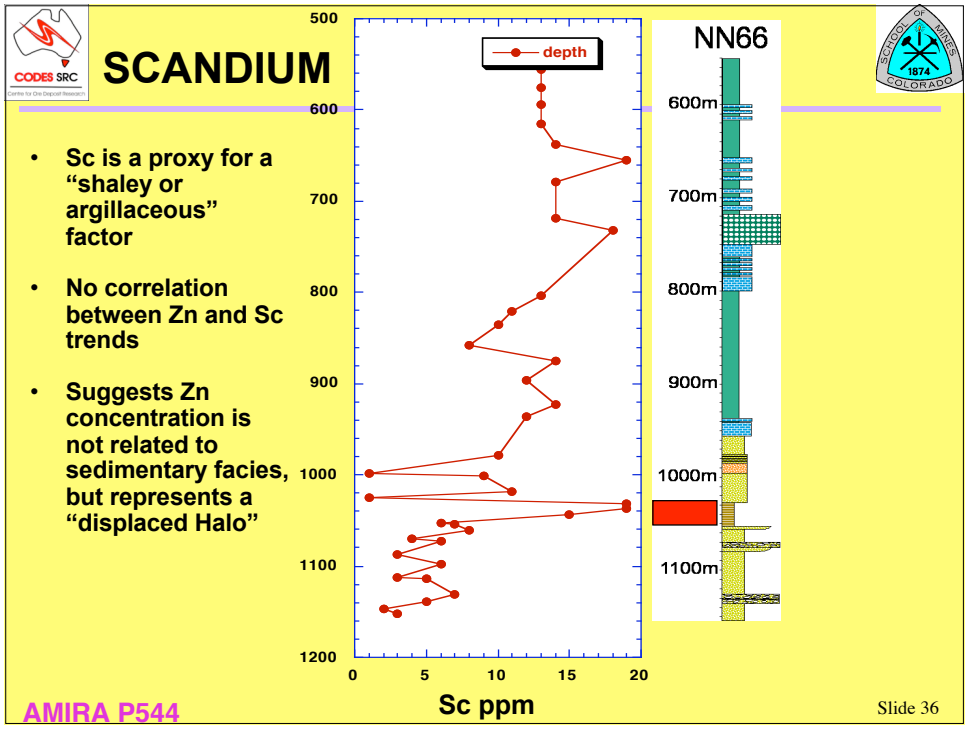
SCANDIUM
Sc is a proxy for a "shaley or argillaceous" factor
No correlation between Zn and Sc trends
Suggests Zn concentration is not related to sedimentary facies, but represents a "displaced Halo"
depth
NN66
500
600
700
800
900
1000
1100
1200
600m
700m
800m
900m
1000m
1100m
0
5
10
15
20
Sc ppm
AMIRA P544
Slide 36

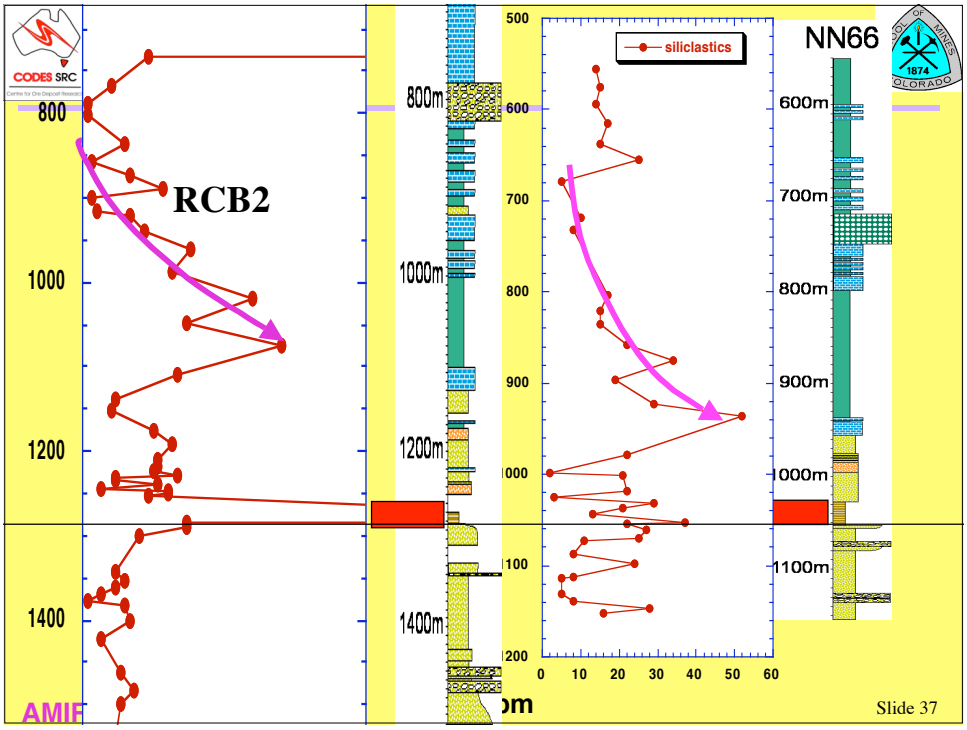
CODES SRC
RCB2
800
1000
1200
1400
800m
1000m
1200m
1400m
500
600
700
800
900
000
100
200
0 10 20 30 40 50 60
siliclastics
NN66
600m
700m
800m
900m
000m
1100m
Slide 37

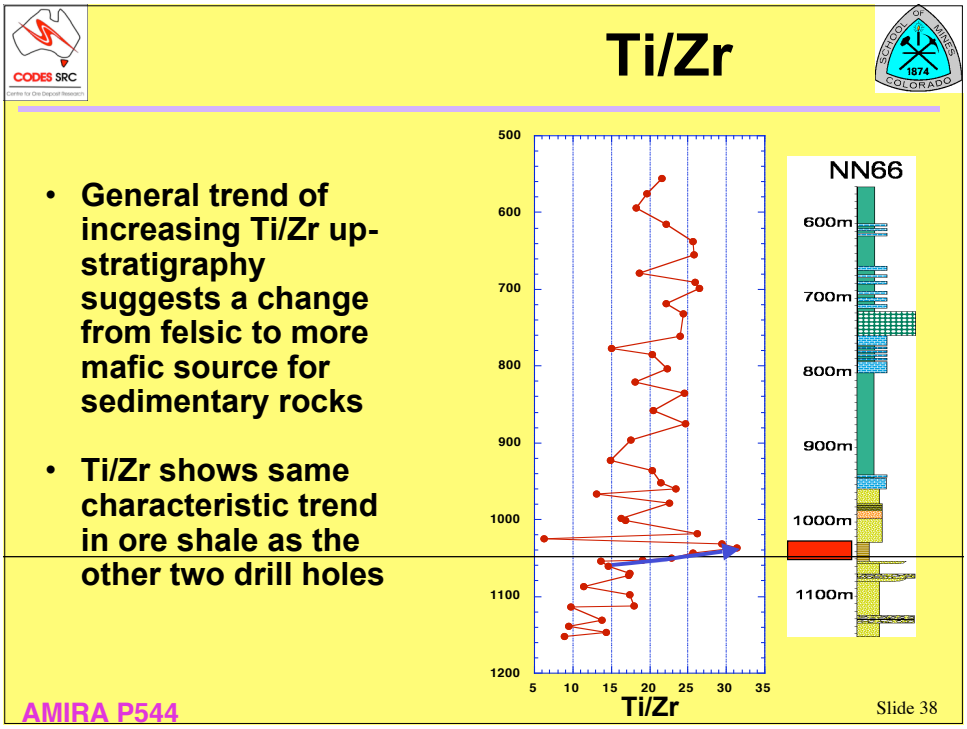
CODES SRC
Ti/Zr
• General trend of increasing Ti/Zr up-stratigraphy suggests a change from felsic to more mafic source for sedimentary rocks
• Ti/Zr shows same characteristic trend in ore shale as the other two drill holes
500
600
700
800
900
1000
1100
1200
5 10 15 20 25 30 35
Ti/Zr
NN66
600m
700m
800m
900m
1000m
1100m
AMIRA P544
Slide 38

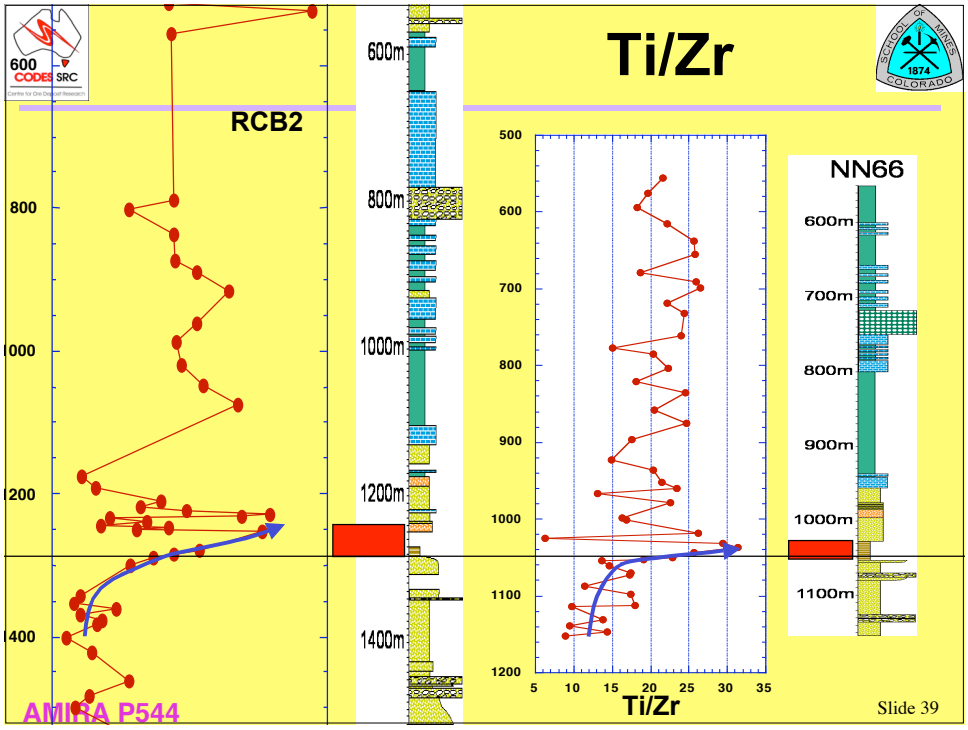
Ti/Zr
RCB2
600
800
1000
1200
1400
600m
800m
1000m
1200m
1400m
500
600
700
800
900
1000
1100
1200
5
10
15
20
25
30
35
Ti/Zr
NN66
600m
700m
800m
900m
1000m
1100m
AMIRA P544
Slide 39

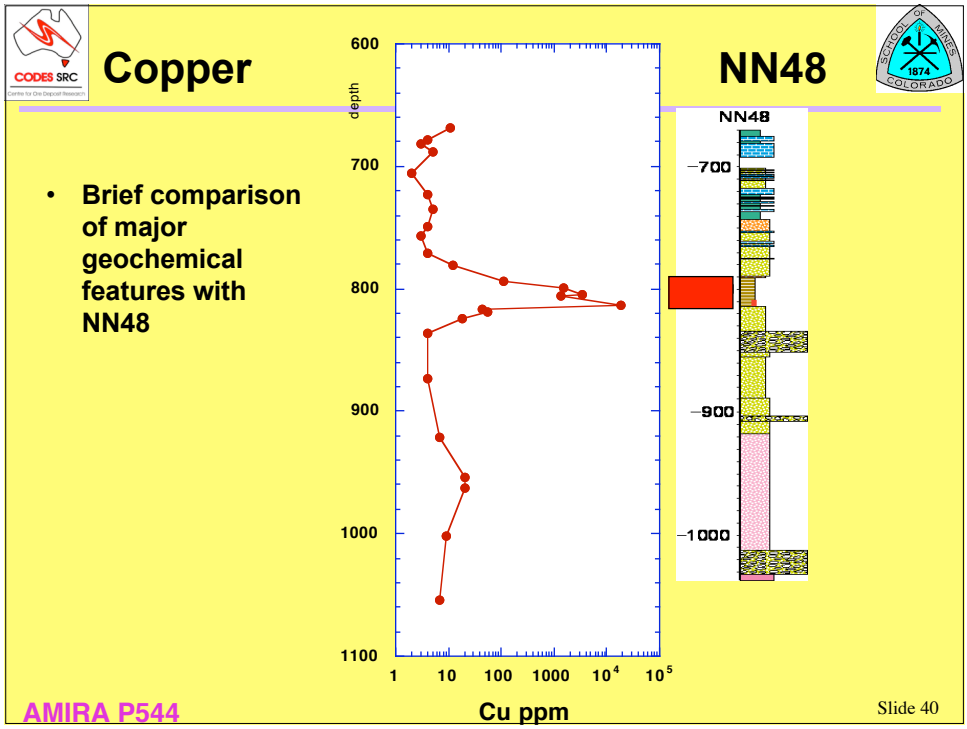
Copper
NN48
• Brief comparison of major geochemical features with NN48
depth
600
700
800
900
1000
1100
1
10
100
1000
10^4
10^5
Cu ppm
NN48
700
900
1000
AMIRA P544
Slide 40

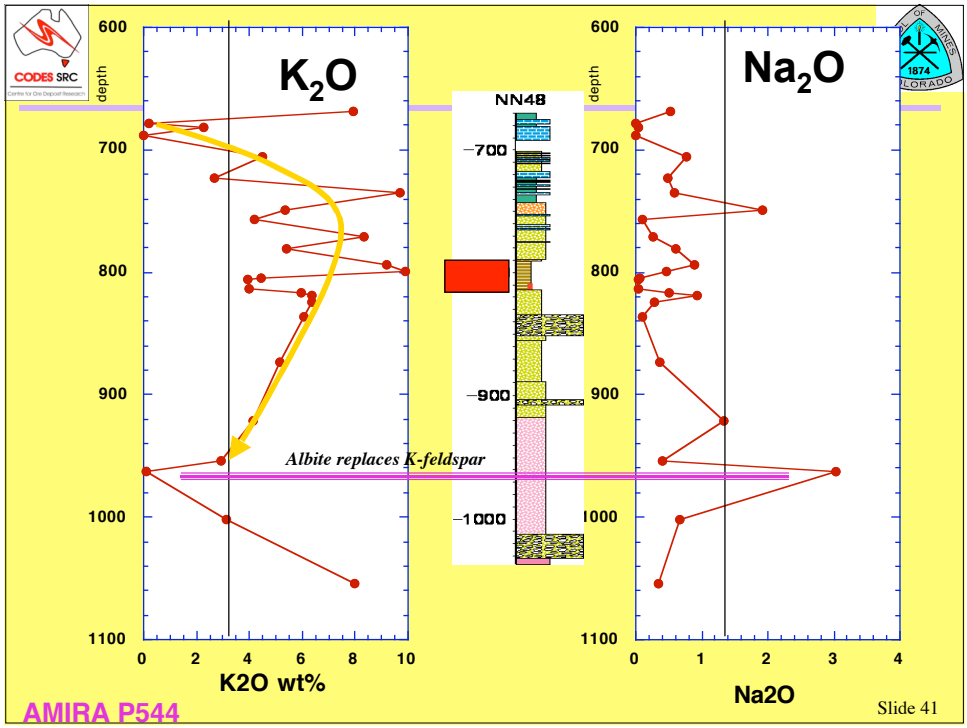
CODES SRC
K_2O
Na_2O
depth
600
700
800
900
1000
1100
NN48
-700
-900
-1000
Albite replaces K-feldspar
0
2
4
6
8
10
K2O wt%
0
1
2
3
4
Na2O
AMIRA P544
Slide 41

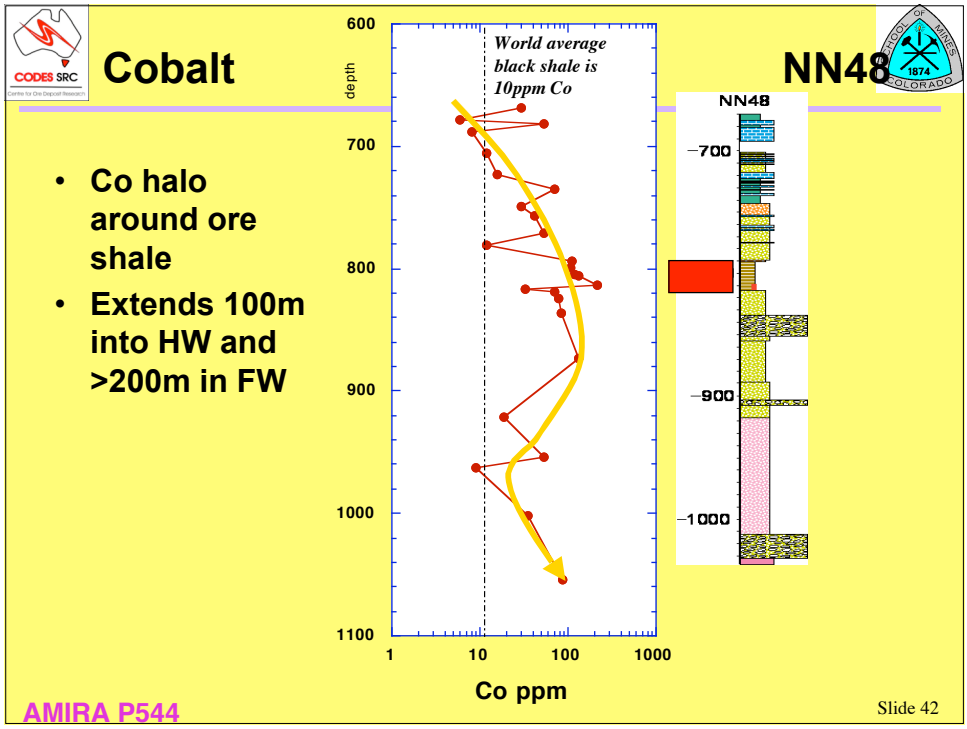
CODES SRC
Cobalt
NN48
• Co halo around ore shale
• Extends 100m into HW and >200m in FW
World average black shale is 10ppm Co
depth
600
700
800
900
1000
1100
NN48
-700
-900
-1000
1
10
100
1000
Co ppm
AMIRA P544
Slide 42

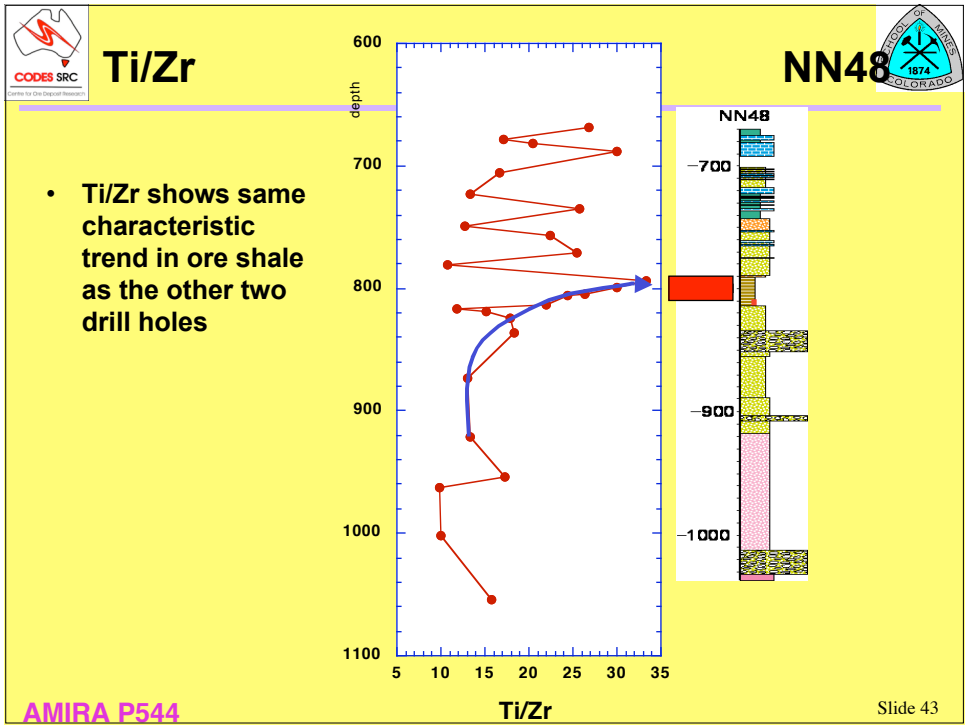
Ti/Zr
NN48
• Ti/Zr shows same characteristic trend in ore shale as the other two drill holes
depth
600
700
800
900
1000
1100
5
10
15
20
25
30
35
Ti/Zr
NN48
700
900
1000
AMIRA P544
Slide 43

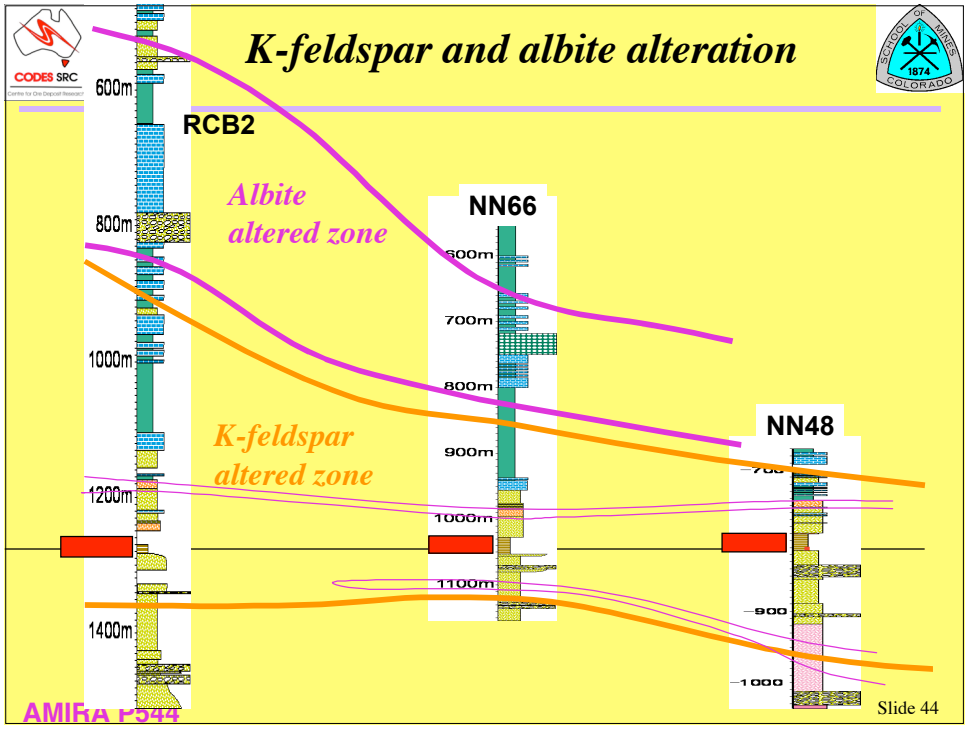
K-feldspar and albite alteration
RCB2
600m
800m
1000m
1200m
1400m
Albite altered zone
K-feldspar altered zone
NN66
600m
700m
800m
900m
1000m
1100m
NN48
900
1000
AMIRA P544
Slide 44

Regional Ore Shale K-metasomatism

- We need to see through the effects of source variability & sedimentary fractionation
  - Single lithotype
  - Single stratigraphic level
  - *Ore Shale*
  - *Chambishi Basin + Konkola*
- K-feldspar is a detrital phase in all lithotypes above shale grade
  - Isolate data with statistical heavy mineral anomalism (ie. Zr anomalism)

AMIRA P544

Slide 45

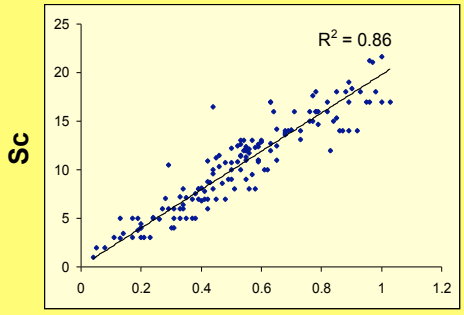

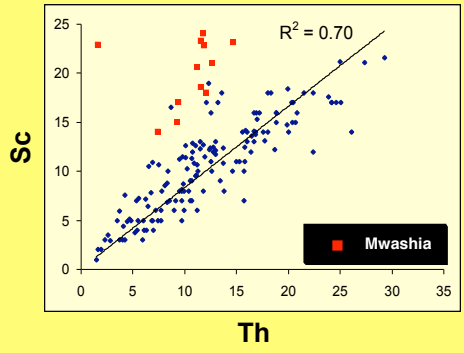

Source Variability

- Strong positive correlation of compatible elements indicates immobility during alteration
- Incompatible-compatible element ratios is most effective means of identifying source variation

Slide 46

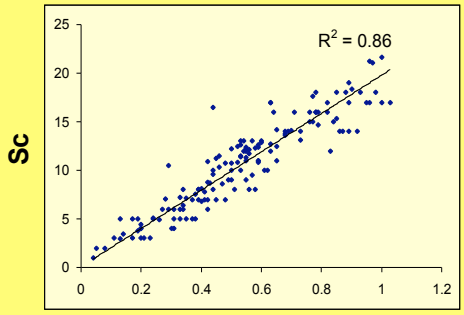

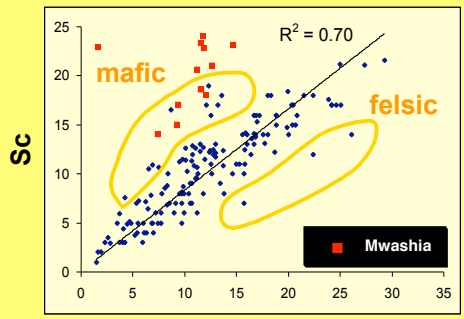

Source Variability

- Strong positive correlation of compatible elements indicates immobility during alteration
- Incompatible-compatible element ratios is most effective means of identifying source variation

Slide 47

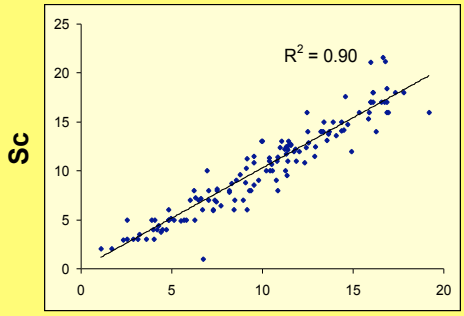

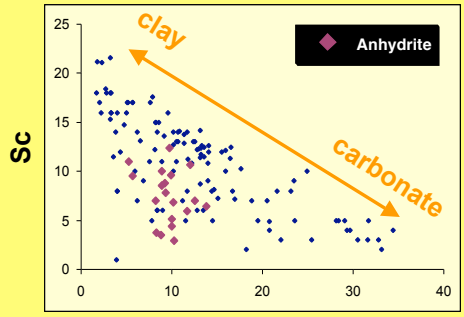

Sedimentary Fractionation

- Al_2O_3 is immobile
- Clay dominant detritus
- Statistically insignificant detrital white mica or kspar
- Detrital K in clays
- Mixing trend reflects carbonate dilution of clay component

Slide 48

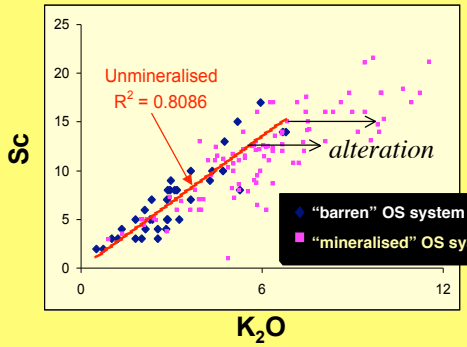

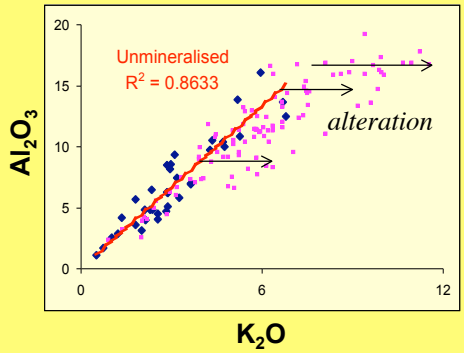

K Metasomatism

- Unmineralised Ore Shale systems display statistically low K_2O/Sc (~0.44×10^{-3}) & K_2O/Al_2O_3 (~0.45)
- Alteration indicies are potentially modified by K-destructive carbonate alteration

Slide 49

Lithogeochemical Conclusions for Chambishi SE

- Copper is concentrated in the base of the "Ore Shale" in the sandy facies
- No HW Cu halo occurs in any of the drill holes studied
- Cobalt is enriched in the ore shale (> 100 ppm Co)
- A halo of Co > 10 ppm surrounds the Cu ore, extending up to 100m into the HW and > 200m into the FW
- Within the halo, Co is present within pyrite (up to 3500 ppm) and biotite (up to 56 ppm)

AMIRA P544

Slide 50

Conclusions 2

- A zone of stratiform potassium feldspar alteration encompasses the ore shale and clastic package
- The K_2O/Al_2O_3 and K_2O/Sc ratios are the best indicators of the potassic alteration zone
- The K_2O/Al_2O_3 ratio increases systematically towards the ore shale from the HW side. This is a strong vector to "ore shale"
- Co and K_2O exhibit a linear correlation in the halo surrounding the copper ore

AMIRA P544 Slide 51

Conclusions 3

- A major zone of stratiform sodic alteration, expressed by albite, occurs in the upper Roan siltstone/carbonate sequence overlying the potassic alteration zone
- The HW albite alteration is centred on a stratabound carbonate-breccia zone
- Thin zones of albite alteration (replacing K-feldspar) may occur in the clastic package surrounding the ore shale

AMIRA P544 Slide 52

Conclusions 4

- Ti/Zr ratio can assist in stratigraphic correlations
- Ti/Zr exhibits a systematic increase from the base to the top of the ore shale, from 15 to 30. This is a distinguishing feature of the ore shale
- There is a general increase in Ti/Zr up-stratigraphy from FW Clastics (7-20), to Upper Roan (10-30), to Mwashia (25-40)
- This suggests a change from felsic to mafic sources for the sediments in the basin
- Other potential chemostratigraphic ratios are V/Nb and Sc/Th

AMIRA P544 Slide 53

Conclusions 5

- Zinc is depleted (< 30ppm) throughout the Cu ore and Co halo (however there may be erratic peaks)
- Zinc in the siliclastics increases stratigraphically downwards to the base of the Upper Roan. This may represent a displaced vector to ore in the Lower Roan (needs testing above barren 'ore shale')

AMIRA P544 Slide 54

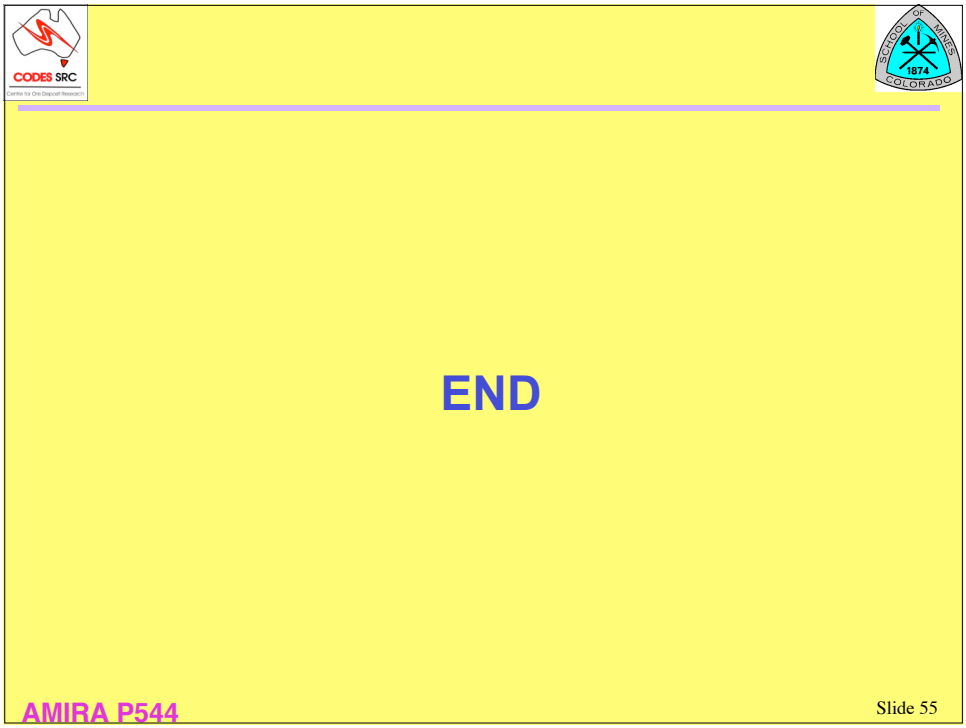
CODES SRC
END
AMIRA P544
Slide 55

Carbon and oxygen isotopic composition of ore-related and sedimentary carbonates in the Roan, ZCB

Ross Large, Stuart Bull, Mawson Croaker, Peter McGoldrick, Nicky Pollington, Rob Scott and Dave Selley
Centre for Ore Deposit Research, University of Tasmania

Summary

A comprehensive study of carbon and oxygen isotopes of various carbonate types throughout the sediments of the Zambian Copper Belt has shown a systematic relationship to copper mineralisation that should have significant application in mineral exploration.

A total of 369 samples have been analysed from the following localities: Mufulira (15), Nkana-Mindola (68), Ndola West (22), Mwambashi (56), Konkola North (24), Konkola (4), Chambishi (41), Chambishi SE (73), Chibuluma West (21), Chambishi Basin (25), Chingola (20). Sample types have included: cryptalgal carbonates, massive recrystallised sedimentary carbonate, dolomitic siltstones and sandstones, 'barren gap' carbonates, carbonate cement in ore shale and footwall clastics, carbonate nodules, patches and veins within ore shale, and veins in basement.

The following isotopic groups have been recognised:

1. Massive sedimentary carbonates in Upper Roan, cryptalgal carbonates and barren gap carbonates commonly exhibit a normal marine signature with $\delta^{13}C$ = +4 to –2‰ and $\delta^{18}O$ = 19 to 27‰.
2. Carbonate bearing siltstones which exhibit diagenetic and metamorphic alteration have a modified marine signature with $\delta^{13}C$ = +8 to –10‰ and $\delta^{18}O$ = 13 to 30‰.
3. Mineralised and altered "ore shale" shows strong coupled depletion in both carbon and oxygen isotopes, with $\delta^{13}C$ = –6 to –26‰ and $\delta^{18}O$ = 6 to 20‰.
4. Mineralised footwall clastics show less isotopic depletion than the ore shale, but are still very distinctive with majority of samples varying $\delta^{13}C$ = –3 to –11‰ and $\delta^{18}O$ = 8 to 23‰.

The strongly negative $\delta^{13}C$ values of carbonate in the ore shale and mineralised footwall clastics indicates the significant role of oxidation of organic carbon in the mineralising process. The fact that the relatively clean mineralised footwall clastics also show this negative carbon isotope shift suggests that organic reaction products migrated out of the shale into the permeable footwall clastics prior to mixing with the ore fluid, leading to redox reactions causing coupled oxidation of organic matter and reduction of sulfate to H_2S resulting in copper sulfide precipitation.

Modelling isotope exchange reactions for the carbonates, indicates that the fluid from which the ore shale carbonates precipitated had an isotopic composition of $\delta^{18}O$ = 0±3‰ and $\delta^{13}C$ = –15±1.5‰ at an assumed temperature of 120° to 180°C. This suggests the fluid had a predominantly marine origin with a high level of dissolved organic carbon.

What is significant for exploration, is that all major Cu-ore zones tested show a strong coupled carbon and oxygen isotope shift. Barren Gaps, on the other hand, exhibit no isotopic shift, indicating no significant passage of hydrothermal fluids or organic carbon oxidation reactions. The negative $\delta^{13}C$ isotopic halo surrounding the ore shale commonly corresponds with the subtle cobalt halo and zone of maximum potassic alteration previously defined. However there are exceptions, where late stage sodium metasomatism has caused re-equilibration of the isotope values accompanied by replacement

of K-feldspar by albite.

Introduction

A detailed study of carbon and oxygen isotopes in carbonates in and around the copper–cobalt deposits of the ZCB was undertaken to address the following questions:

- Do C and O isotopes in carbonate form a halo to ore. Can they be used as a vector to ore?
- Can C and O isotopes in carbonates assist in stratigraphic correlation in the district
- Can we use the C–O isotopes to gain information on the temperature of mineralisation, sources of fluids, or processes of sulfide deposition?

The only previously reported C–O isotope studies from the ZCB, were undertaken by Cunningham (1986; reported in Annels, 1989, fig. 11) and Sweeney and Binda (1989). The former study involved nine analyses of carbonates from the northeast Chambishi Basin. The study showed that two samples of reef dolomites have similar isotopic values to late Proterozoic marine dolomites, whereas samples of sub-concordant veins and carbonate nodules in the ore shale have distinctly lower values of both $\delta^{13}C$ and $\delta^{18}O$. Annels (1989) concluded that the very light $\delta^{13}C$ values in the nodules testify to the role of organic carbon in the replacement of very early diagenetic anhydrite by carbonate.

Sweeney and Binda (1989) reported that C–O isotopes of carbonate in ore shale samples has lower $\delta^{13}C$ and $\delta^{18}O$ values than footwall carbonates. They interpreted this to be due to the relative influence of seawater compared with meteoric water, during transgression (marine)–regression (meteoric) events, when diagenetic carbonates formed in the sediments.

Sampling and analysis

A total of 369 carbonate samples were analysed in this study. The location of samples were: Ndola West (22 samples), Mufulira (15 samples), Nkana–Mindola (68 samples), Mwambashi (56 samples), Konkola North (24 samples), Konkola (4 samples), Chambishi (41 samples), Chambishi SE (73 samples), Chambishi Basin regional drill hole - RCB1A (25 samples), Chibuluma West (21 samples), Chingola (20 samples).

Samples were grouped into the following sedimentary or mineralized carbonate facies:

- Carbonate bearing siltstones in Mwashia
- Massive sedimentary carbonate in Upper Roan
- Carbonate bearing siltstones in Upper Roan
- Massive sedimentary carbonate in Lower Roan (Kitwe Fm)
- Carbonate bearing siltstones in Lower Roan (Kitwe Fm)
- Barren gap cryptalgal carbonates (equivalent to "ore shale")
- Carbonate nodules, patches and veins in 'ore shale'
- Carbonate patches and veins in footwall Mindola Clastics
- Carbonate veins in basement

Isotope analyses were undertaken at the Central Science Laboratory, University of Tasmania, using the technique of McCrea (1950). The sediment samples varied in carbonate content from 20 to 95 wt %, determined by petrography and whole rock analysis. Results are expressed in the δ (‰) notation relative to standard mean ocean water (SMOW) for oxygen, and Pee Dee belemnite (PDB) for carbon. The precision of analyses for both C and O is ±0.2‰.

Results

C–O isotope chemostratigraphy

Three drill holes (RCB2, NN66 and RCB1A), which cover the full stratigraphic section of 1500m from the Mwashia down through the Upper and Lower Roan, were selected for chemostratigraphic analysis of carbon and oxygen isotope variation.

RCB2: Down hole isotopic data for RCB2 (Slide 6) shows that the Upper Roan sedimentary carbonates commonly vary from $\delta^{13}C = +5$ to –5‰ and $\delta^{18}O = 20$ to 30‰. These values are similar to normal marine Neoproterozoic carbonates which range from $\delta^{13}C$

= +10 to –5‰ and $\delta^{18}O$ = 19 to 26‰ (Jacobsen and Kaufman, 1999). However there is a major excursion to very low $\delta^{18}O$ values (around 5‰) in a zone of albitisation and brecciation at 790–900 m down hole.

In the Lower Roan sequence below 1100 m there is a strong coupled decrease in both $\delta^{13}C$ and $\delta^{18}O$ values surrounding the Cu-mineralised ore shale (Slide 6). In this zone $\delta^{13}C$ values decrease to as low as –20‰ and $\delta^{18}O$ values to 10‰. The decrease in $\delta^{18}O$ is more gradual when compared to the abrupt drop in $\delta^{13}C$ immediately surrounding and within the ore shale.

NN66: Samples from this hole cover a narrower stratigraphic range of 300 m at the base of the Upper Roan, and surrounding the ore shale (Slide 7). An identical pattern (to RCB2) of a strong coupled decrease in $\delta^{13}C$ and $\delta^{18}O$ in present in the Lower Roan surrounding the ore shale.

RCB1A: This hole intersects sedimentary carbonates in the Mwashia and Upper Roan. Samples in the Upper Roan carbonates show a similar pattern to RCB2 with $\delta^{13}C$ = +5 to –5‰ and $\delta^{18}O$ = 20 to 30‰ (Slide 8). There is a mild anomaly around 550 m down hole that may relate to increased diagenetic reactions. Of further interest is the change in $\delta^{13}C$ values of dolomitic siltstones in the Lower Mwashia, which show distinctly more negative values ($\delta^{13}C$ = –5 to –10‰) than the Upper Roan carbonates. Insufficient data is available to test if these lower $\delta^{13}C$ values are a feature of the Mwashia generally, or localised in this particular drill hole.

All data Groups

When the isotopic data from all localities is plotted together (Slide 10) it is apparent there is a trend across the C–O diagram from high $\delta^{13}C$ and $\delta^{18}O$ values (+5, +30), to low $\delta^{13}C$ and $\delta^{18}O$ values (–20, +10). The different carbonate facies will be considered separately.

a) Massive sedimentary carbonates and barren gap carbonates: Many of these samples show primary cryptalgal sedimentary textures, others are totally recyrstallised, but none show any evidence of hydrothermal alteration or mineralisation. The plotted isotope data shows a relatively tight cluster (Slide 11) with the majority of samples in the range $\delta^{13}C$ = –5 to +5‰ and $\delta^{18}O$ = 20 to 27‰, similar to Proterozoic marine carbonates.

b) Carbonate-bearing siltstones (Slide 12): These samples comprise dolomite bearing argillites. The C and O isotopes plot in a similar field to the massive sedimentary dolomites but show more spread, down to $\delta^{13}C$ = –10‰ and $\delta^{18}O$ = 12‰. The four samples with the lowest $\delta^{13}C$ values are within 150 m of the hangingwall of the ore shale and have probably been affected by hydrothermal alteration. If we ignore these samples, the diagonal spread of data to lower $\delta^{13}C$ and lower $\delta^{18}O$ values probably relates to mild diagenetic reactions in the siltstones by meteoric or evaporated seawater (Veizer, 1983; Large et al., 2001).

c) Carbonate nodules, patches and veins within the "ore shale" (Slide 13): These samples show far more negative $\delta^{13}C$ values and slightly lower $\delta^{18}O$ values (Slides 13, 15, 17). Weakly or non-mineralised shale (< 1000 ppm Cu) shows a trend in $\delta^{13}C$ values from +4‰ (in the sedimentary carbonate field) to –20‰ (in the ore-carbonate field). Ore shale samples with > 1000 ppm Cu plot within a field defined by $\delta^{13}C$ = –8 to –27‰ and $\delta^{18}O$ = 7 to 21‰ (Slide 13).

d) Carbonate nodules, patches and veins within the footwall clastics (Slides 15, 17): These samples dominantly show values of $\delta^{13}C$ = –5 to –10 (intermediate between barren sedimentary carbonate and ore shale carbonate (Slide 15). $\delta^{18}O$ values are widely variable from 8 to 32‰ across the field of all carbonates.

e) Veins in the basement: six samples collected from the basement gave $\delta^{13}C$ = –4 to –17‰ and $\delta^{18}O$ = 9 to 17‰. These values overlay the fields for the mineralised ore shale and footwall clastics.

Discussion and interpretation

The distinct difference between the isotopic field for the massive sedimentary carbonates and ore-related carbonates (Slide 13) could be due to a number of alternative process:

- Fluctuation in $\delta^{13}C$ in marine carbonates has been related to variations in the organic carbon cycle of the oceans, which is affected by sea level fluctuations, changes in burial of organic matter, outgassing of C species from the mantle, and, finally, climate change (Derry et al, 1992; Jacobsen and Kaufman, 1999; Frimmel et al., 2002). However fluctuations related to these processes are around $\delta^{13}C$ = +5 to –5‰, much less than the variations observed in our data.

- Fluid rock interaction between sedimentary carbonate and a medium to high temperature fluid (150° to 350 °C) can result in a coupled decrease in both $\delta^{13}C$ and $\delta^{18}O$ values passing from the un-altered carbonate host-rocks to the altered and mineralised carbonate within the ore zone. A typical example of this pattern is seen in the Irish style Zn–Pb–Ag deposits (Hitzman and Beatty, 1996) and from several MVT deposits (Taylor, 1987). However depletion trends are rarely greater than 5 to 8‰ $\delta^{13}C$ and up to a maximum of 10‰ $\delta^{18}O$ (Large et al., 2001). This is unlikely to explain the pattern of the ZCB data where depletion trends of up to 30‰ in $\delta^{13}C$, and 20‰ in $\delta^{18}O$ are recorded.

- Metamorphic volatilisation, decarbonation and contact metamorphism can all result in coupled depletions in $\delta^{13}C$ and $\delta^{18}O$ in carbonates. Field data and modelling in Valley (1986) indicates such depletions are commonly less than 10‰ in $\delta^{13}C$ compared with the 20 to 30‰ recorded here. Also, if this was the operative mechanism, the depletions should effect all the metamorphosed carbonates in the ZCB, not just the carbonates related to the ore shale and footwall clastics.

- Oxidation of organic matter to CO_2 which then becomes incorporated in diagenetic or hydrothermal carbonates can cause big negative shifts in $\delta^{13}C$ of up to –15 to –40‰ (Ohmoto and Golhaber, 1997; Rollinson, 1993). For example, Wilson et al. (2003) record variations in $\delta^{13}C$ values of gangue calcite from –4.2 to –20.2‰ at the El Soldado manto-type Cu deposit, Chile, which they ascribe to the oxidation of pyrobitumen by the mineralising fluids. These isotopic shifts are similar to those recorded in the ZCB (Slide 13), and thus organic matter oxidation, related to the mineralisation process, is likely to be the primary cause of isotopic variations in and around the ore zones.

Determination of ore uid isotopic composition

Using experimentally determined fractionation equations we can determine the mean C–O isotopic value of the ore fluid, from the mean value of mineralised carbonate-bearing ore shale. From Slide 18 the mean value of mineralised ore shale is $\delta^{13}C_{dol}$ = –12.5‰ and $\delta^{18}O_{dol}$ = +15.3‰. Using the fractionation equations shown below for dolomite–water and dolomite–$H_2CO_3^-$ it is possible to calculate the $\delta^{13}C$ and $\delta^{18}O$ values of the fluid.

$$\delta\,^{18}O_{dol} - \delta\,^{18}O_{fluid} = 3.23*10^6\,(T) - 3.29 \quad \ldots \text{Eqn 1}$$

(Land, 1983)

$$\delta\,^{13}C_{dol} - \delta\,^{13}C_{fluid} = 3.13(11.35*10^3/T) + 5.54*10^6/T^2 + \ldots\ldots \text{Eqn 2}$$

(Schwarcz et al., 1970; Ohmoto and Rye, 1979)

In order to calculate the isotopic fluid composition we first need to estimate the temperature of copper mineralization and carbonate deposition. Fluid inclusion data from Annels (1989, g. 10), suggests the most likely temperature of ore formation was around 120° to 180°C. Using this temperature, the calculated oxygen isotope value of the ore uid is $\delta\,^{18}O_{fluid}$ = –3 to +3‰ (Slide 19) and $\delta^{13}C_{fluid}$ = –13.5 to –16.5 ‰ (Slide 20).

The calculated $\delta\,^{18}O_{fluid}$ of around zero indicates a predominantly marine seawater source for the ore fluid. The very negative $\delta^{13}C_{fluid}$ value indicates that the oxidation of organic carbon has played a major role in carbonate precipitation in the ore shale.

Signi cance of $\delta^{13}C$ values of the footwall clastic orebodies

As noted earlier the ores in the footwall clastics have low $\delta^{13}C$ values overlapping with the ore shale-hosted mineralisation (Slide 15). However there is no obvious organic carbon within the footwall clastics that may have caused these low values. This suggests that either (a) all the organic carbon in the clastics was oxidised to CO_2 during the mineralising event,

or (b) the organic reductant was mobile (e.g. CH_4) and, although a key to the mineralising process, has since escaped the clastic package (Slide 16).

Possible controls on the variation in C and O isotopes

As shown in Slide 22 there is considerable variation in both C and O isotopes across the diagram. Some of the variation in the top right hand sector of the diagram is probably due to isotope exchange reactions at low temperatures during sediment diagenesis, as discussed previously, however the variations in the lower LHS of the diagram are likely to be due to variations in the hydrothermal processes related to mineralisation and metamorphism.

(a) Temperature variations: Using the fractionation equations between dolomite–water and dolomite–CO_2 it can be shown that fluid temperature variations can have a marked effect on the $\delta^{18}O$ values of hydrothermal carbonates, but a lesser effect on $\delta^{13}C$ values (e.g. Large et al., 2001, figs 15, 17). In Slide 23 it is shown that the spread in $\delta^{18}O$ values across the hydrothermal field of 30 to 5‰ could be caused by temperature fluctuations between 50° and 250°C.

(b) Variation in fluid source (or mixing of fluids): In addition to temperature, mixing of fluids from different sources, and with different $\delta^{18}O_{fluid}$ values, can also cause marked isotopic variation in the precipitated carbonate. As shown in Slide 24 a meteoric fluid will precipitate carbonates with $\delta^{18}O$ = 5 to 10‰, whereas an evolved-marine fluid will precipitate carbonates with $\delta^{18}O$ = 20 to 30‰. Mixing of two fluids represented by these end members will form carbonates with $\delta^{18}O$ across the full range from 5 to 30‰.

(c) Increasing organic oxidation : Whereas $\delta^{18}O$ values are affected mainly by temperature fluctuations and mixing of fluid from different sources, the big shifts in $\delta^{13}C$ observed in the ZCB hydrothermal carbonates most likely relate to the degree of organic matter oxidation. Mixing may have played a role, for example if one fluid was oxidised with no organic C, and the other was reduced and carrying organic C.

In summary, the variation in $\delta^{18}O$ and $\delta^{13}C$ values in the ore-related hydrothermal carbonates may be caused by a combination of three factors (a) temperature fluctuations, (b) mixing between marine and meteoric source fluids, and (c) degree of organic matter oxidation. Mixing of two fluids at the site of ore deposition was probably the most important process, with the temperature fluctuations and organic matter oxidation fluctuations directly related to the mixing process (Slides 25, 26).

Hangingwall albite–calcite alteration

Our lithogeochemical research discussed elsewhere in this volume (Large et al., 2003), has defined a zone of intense albite alteration associated with sedimentary breccias and gabbro intrusions in the Upper Roan, overlying the potassic alteration zone and related Cu–Co mineralization in the Lower Roan. Only four samples of carbonate associated with the albite alteration were analysed in this study. The data is plotted in Slide 28, where it is seen that the albite altered samples exhibit normal sedimentary carbon isotope values, but have very ^{18}O depleted oxygen isotope values. Two of the samples have the lowest $\delta^{18}O$ values measured in this study (4 –5‰). There are two possible explanations for these very oxygen depleted and albitised samples; a) they formed from meteoric fluids at low temperatures of around 150°C (Slide 28), or b) they formed from saline marine uids at much higher temperatures (around 350°C) during metamorphism (Slide 28). The former explanation is not favoured, as low salinity meteoric fluids are unlikely to cause albitisation. The latter explanation fits with the high temperature syn-metamorphic textural relations observed in the albite-calcite rocks.

Importantly, the normal marine $\delta^{13}C$ values in these breccias, indicates that the albite-calcite alteration event did not involve oxidation of organic carbon, or mixing with a second fluid carrying organic carbon (Slide 29).

$\delta^{18}O$ – $\delta^{13}C$ and K–Cu–Co relationships

The C–O isotope halo that surrounds the mineralised ore shale overlaps with the potassic alteration halo defined earlier in this volume (Large et al., 2003). The

plot of K_2O versus $\delta^{13}C_{carbonate}$ (Slide 30), shows that most samples with $\delta^{13}C < -5‰$ display elevated K_2O levels from 2 to 10 wt%. Conversely most samples with depleted K_2O values less than 1 wt % have elevated $\delta^{13}C > -10‰$ (Slide 30). These patterns strongly suggest that the fluid responsible for the K-felspar alteration and Cu mineralisation also caused the marked depletion in carbon (and oxygen) isotopes in the associated carbonate minerals.

The relationship of decreasing $\delta^{18}O$ and $\delta^{13}C$ with increasing Co displayed by Slides 32 and 33, indicates that the Co mineralisation is also related to the isotopic variation in and around the ore shale. The Co halo previously defined (Large et al., this volume) matches the outline of the C–O isotope halo.

The relationship between Cu and C–O isotopes (Slides 34, 35) is not as clearly defined as that for Co and the isotopes. This is because the isotopic halo is considerably broader in extent than the Cu mineralised zone. However the broad relationship holds, that the majority of samples with >100 ppm Cu have $\delta^{13}C < -5‰$, whereas most samples with <100 ppm have $\delta^{13}C > -5‰$.

Conclusions

- The 'Ore Shale' and mineralised FW clastics commonly exhibit strong coupled depletion of ^{13}C and ^{18}O compared to sedimentary carbonates.
- This suggests that mineralisation involved coupled oxidation of organic carbon to CO_2, reduction of sulphate to H_2S, and co-precipitation of carbonate and ore sulfides in a relatively closed environment.
- The variation in the C–O isotopic data suggest that the organic carbon oxidation was probably related to mixing of an oxidized ore fluid of ultimate marine derivation, with a more reduced, organic-bearing non-marine fluid resident in the ore-shale and footwall clastics.
- The lowest $\delta^{13}C$ values occur in mineralised ore shale, suggesting that maximum organic oxidation occurred in the ore shales.
- Light $\delta^{13}C$ values in highly mineralised 'clean' FW sandstones requires the introduction of an organic carbon source into the sandstones; probably organic-rich diagenetic fluids derived from the overlying organic-rich shales.
- HW massive carbonates and 'Barren Gap' carbonates have a normal marine isotope signature with no evidence of oxidation of organic carbon
- A tight halo of negative $\delta^{13}C$ surrounds most, but not all, Cu ore zones tested. A similar signature is given by some low grade (<1% Cu) ore shales (Slide 39).
- The $\delta^{13}C$ halo commonly corresponds with the Co halo and zone of maximum potassium metasomatism (however there are exceptions, where late stage Na-metasomatism has occurred) (Slide 39) .
- The oxygen isotope halo around the ore shale is commonly broader than the carbon isotope halo, and includes the complete Mindola Clastics package (Slide 39).
- Later Na metasomatism in the HW appears to be unrelated to organic oxidation, and has a higher $\delta^{13}C$ signature. It was caused by either a different (meteoric) fluid with a much lower oxygen isotope signature ($\delta^{18}O = -10‰$, $\delta^{13}C = -2‰$), or by a normal marine fluid at a significantly higher temperature (syn-metamorphic).

References

Annels, A.E., 1989, Ore genesis in the Zambian Copperbelt, with particular reference to the northern sector of the Chambishi Basin: Geological Association of Canada Special Paper, vol. 36, p. 427–452.

Cunningham, M.J., 1986, Copper-cobalt mineralization in the northern portion of the Chambishi Basin, Zambia, unpublished PhD research report, University College, Cardiff.

Derry, L.A., Kaufman, A.J., and Jacobsen, S.B., 1992, Sedimentary cycling in the Late Proterozoic: Evidence from stable and radiogenic isotopes: Geochem. Cosmochim. Acta, 56, p. 173–198.

Frimmel, H.E., Folling, P.G., and Eriksson, P.G., 2002, Neoproterozoic tectonic and climatic evolution recorded in the Gariep Belt, Namibia and South Africa: Basin Research, vol. 14, p. 55–67.

Hitzman, M.W., and Beaty, D.W., 1996, The Irish Zn-Pb-(Ba) Orefield, *in* Sangster, D.F., ed., Carbonate-Hosted Lead-Zinc Deposits: Society of Economic Geologists Special Publication 4, p. 112–143.

Jacobsen, S.B., and Kaufman, A.J., 1999, The Sr, C and O isotopic evolution of Neoproterozoic seawater: Chem. Geology, 161, p. 37–57.

Land, L.S., 1983, The application of stable isotopes to studies of the origin of dolomite and to problems of diagenesis of clastic sediments: Society of Economic

Palaeontologists and Mineralogists Short Course 10, p. 4, 1–4: 22.

Large, R. R., McGoldrick, P. J., Bull, S. W., Scott, R., and Selley, D.,(this volume), Lithogeochemistry and Alteration Halos to Stratiform Copper Mineralisation in the Chambishi Basin, Zambian Copper Belt: AMIRA P5444, Final Report, October, 2003.

Large, R.R., Bull, S.W., and Winefield, P.P., 2001, Carbon and Oxygen Isotope Halo in Carbonates Related to the McArthur River (HYC) Zn-Pb-Ag Deposit, North Australia: Implications for Sedimentation, Ore Genesis, and Mineral Exploration: Economic Geology, v. 96, p. 1567–1593.

McCrea, L.M., 1958, The isotope chemistry of carbonatates and a paleotemperature scale: Journal of Chemistry Physics, v. 18, p. 849–857.

Ohmoto, H., and Rye, R.O., 1979, Isotopes of Sulfur and Carbon, *in* Barnes, H.L., ed., Geochemistry of Hydrothermal Order Deposits – third edition: New York, Wiley, p. 509–567.

Ohmoto, H., and Goldhaber, M.B., 1997, Sulfur and carbon isotopes, *in* Barnes, H.L., ed., Geochemistry of Hydrothermal Order Deposits – third edition: New York, Wiley, p. 517–612.

Rollinson, H., 1993, Using Geochemical Data: Evaluation, Presentation and Interpretation: Longman, Essex, 352pp.

Schwarcz, H.P., Clayton, R.N., and Mayeda, T., 1970, Oxygen isotopic studies of calcareous and pelitic metamorphic rocks, New England: Geological Society of America Bulletin, vol. 81, no. 8, p. 2299–2315.

Sweeney, M. A., and Binda, P. L., 1989, The role of diagenesis in the formation of the Konkola Cu-Co orebody of the Zambian Copper Belt: Geological Association of Canada Special Paper, vol. 36, p. 499–518.

Taylor, B.E., 1987, Stable isotope geochemistry of ore-forming fluids, *in* Keyser, T.K., ed., Short Course in Stable Isotope Geochemistry of Low Temperature Fluids: Mineral Association Canada., v. 13, p. 337–445.

Valley, J.W., 1986, Stable isotope geochemistry of metamorphic rocks, *in* Valley, J.W., Taylor, H.P., and O'neil, J.R., eds., Stable Isotopes in High Temperature Geological Processes: Mineral Association of America Reviews in Mineralogy, v. 16, p. 445–490.

Viezer, J., 1983, Chemical diagenesis of carbonates: theory and application of trace element technique: Society of Economic Palaeontologists and Mineralogist Short Course 10, p. 3–1-3-100.

Wilson, N. S. F., Zentilli, M., Spiro, B., 2003, A sulfur, carbon, oxygen and strontium isotope study of the volcanic-hosted El Soldado manto-type copper deposit, Chile: the essential role of bacteria and petroleum: Economic Geology, v. 98, p. 163-174.

Carbon and Oxygen Isotopic Composition of Ore-Related and Sedimentary Carbonates in the Roan: Zambian Copperbelt

Stuart Bull, Mawson Croaker, Peter McGoldrick, Nicky Pollington, Rob Scott, Dave Selley and Ross Large

AMIRA P544

Aims of Study

- **To answer the following questions:**
- **Do C-O isotopes in carbonates form a halo to ore? Or can they be used as a vector to ore?**
- **Can C-O isotopes assist in stratigraphic correlations in the district?**
- **Can we use the isotopes to gain information on the temperature of mineralisation, sources of fluids, or processes of sulfide deposition?**

AMIRA P544

Sample Set: 369 samples

- Ndola West: 22 samples
- Mufulira: 15 samples
- Nkana - Mindola: 68 samples
- Mwambashi: 56 samples
- Konkola North : 24 samples
- Konkola: 4 samples
- Chambishi : 41 samples
- Chambishi SE: 73 samples
- Chambishi Basin regional drill hole - RCB1A 25 samples
- Chibuluma West; 21 samples
- Chingola: 20 samples

AMIRA P544

Stratigraphic groups

- Mwashia carbonate-bearing siltstones
- Upper Roan massive carbonates
- Upper Roan carbonate-bearing siltstones
- Kitwe Formation massive carbonates
- Kitwe Formation carbonate-bearing siltstones
- Copperbelt Orebody Member massive carbonates (barren gap)
- Copperbelt Orebody Member carbonate-bearing siltstones
- Mindola Clastics Formation sandstones (Footwall)
- Basement veins

AMIRA P544

Types of Carbonate Sampled

- Cryptalgal carbonates (rare)
- Massive recrystallised sedimentary dolomite/calcite
- Dolomitic siltstones and sandstones
- Carbonate cement in ore shale and "Footwall" clastics
- Carbonate nodules, patches and veins in ore shale and footwall clastics
- Veins in basement

AMIRA P544

RCB2: C-O Isotope Chemostratigraphy

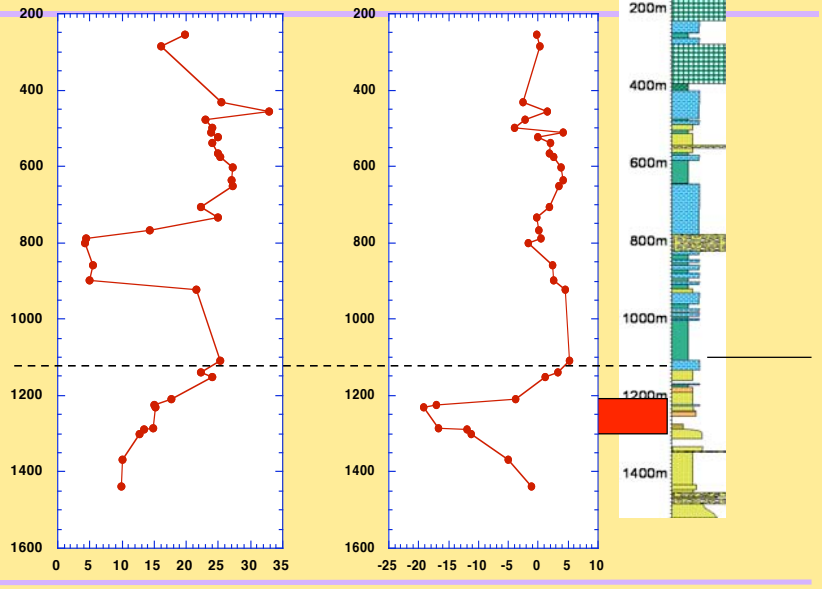

AMIRA P544 δ ^{18}O permil δ ^{13}C permil

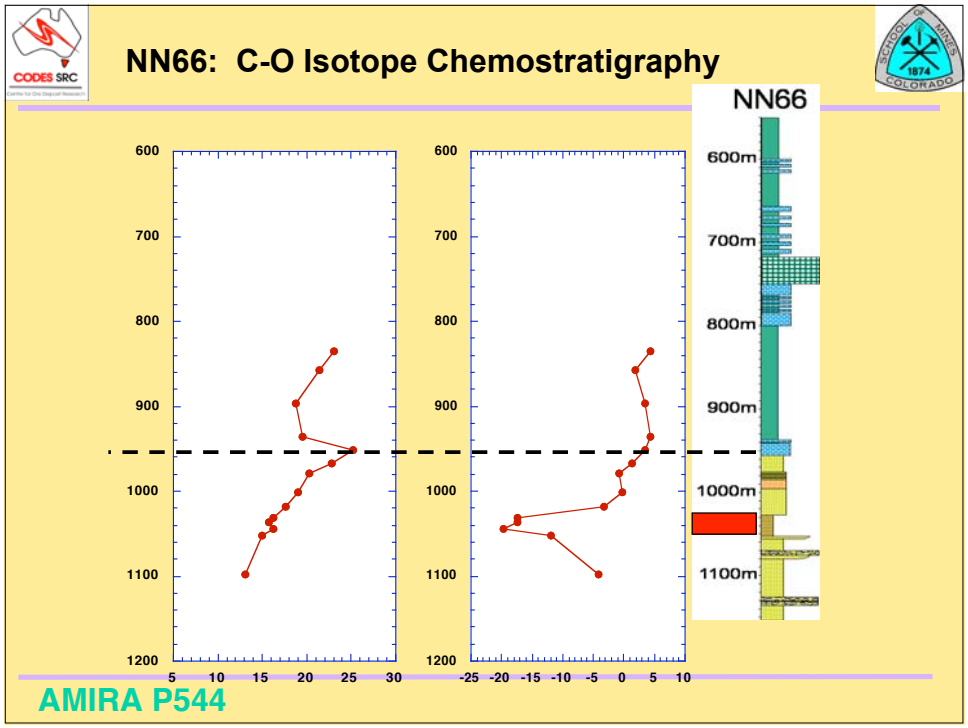
NN66: C-O Isotope Chemostratigraphy
NN66
600m
700m
800m
900m
1000m
1100m
600
700
800
900
1000
1100
1200
5 10 15 20 25 30
-25 -20 -15 -10 -5 0 5 10
AMIRA P544

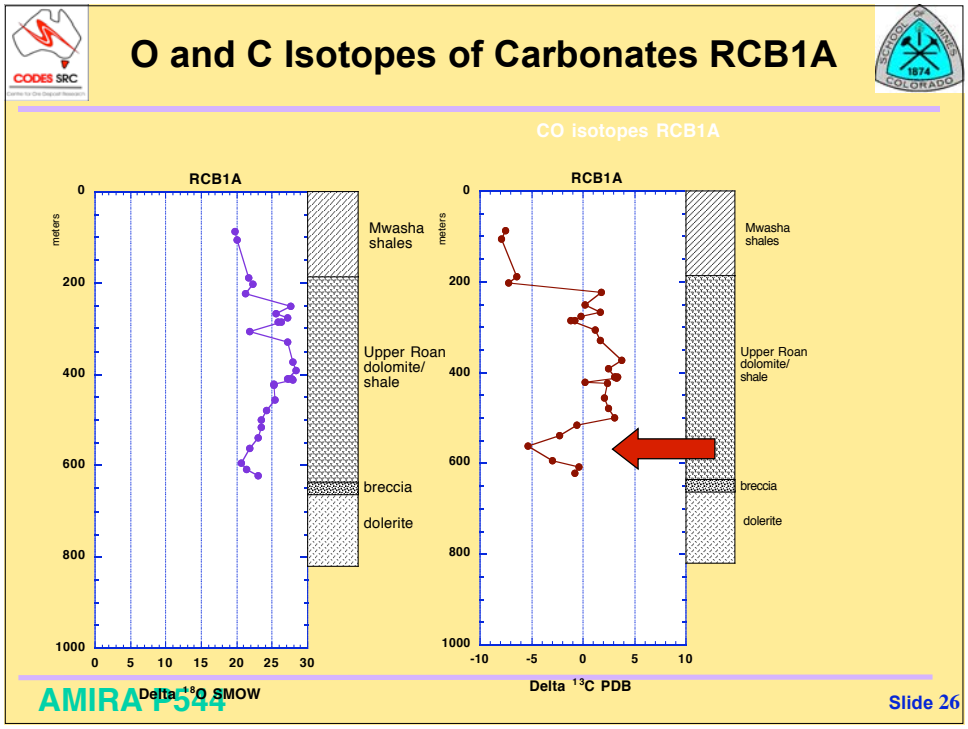
O and C Isotopes of Carbonates RCB1A
CO isotopes RCB1A
RCB1A
RCB1A
meters
0
200
400
600
800
1000
Mwasha shales
Upper Roan dolomite/ shale
breccia
dolerite
0 5 10 15 20 25 30
Delta -18O SMOW
-10 -5 0 5 10
Delta 13C PDB
AMIRA P544
Slide 26

Chemostratigraphy

- Both drill holes exhibit a strong C & O isotopic shift to lower values surrounding the "Ore Shale"
- The $\delta^{13}C$ shift is fairly abrupt, and centred directly on the ore shale
- The $\delta^{18}O$ shift is much broader and includes the complete Mindola Clastics package surrounding the ore shale
- The albite breccia alteration zone in the hanging wall shows a different isotopic pattern (strong $\delta^{18}O$ shift, but little $\delta^{13}C$ variation)

AMIRA P544

All Carbonate Isotope Data: n=365

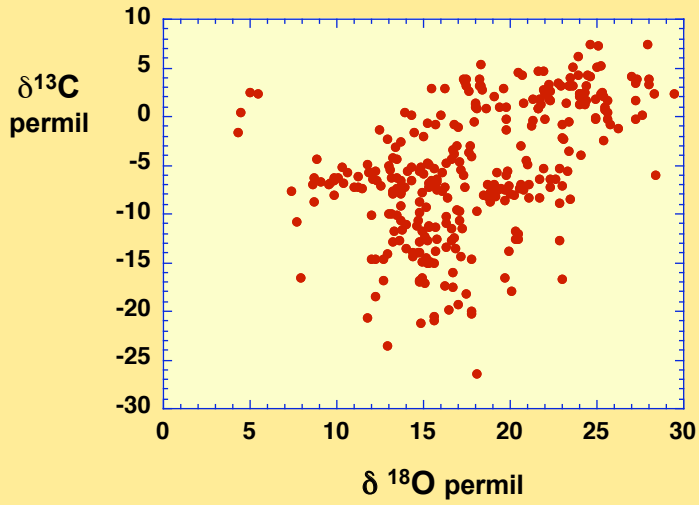

AMIRA P544

Massive sedimentary carbonates

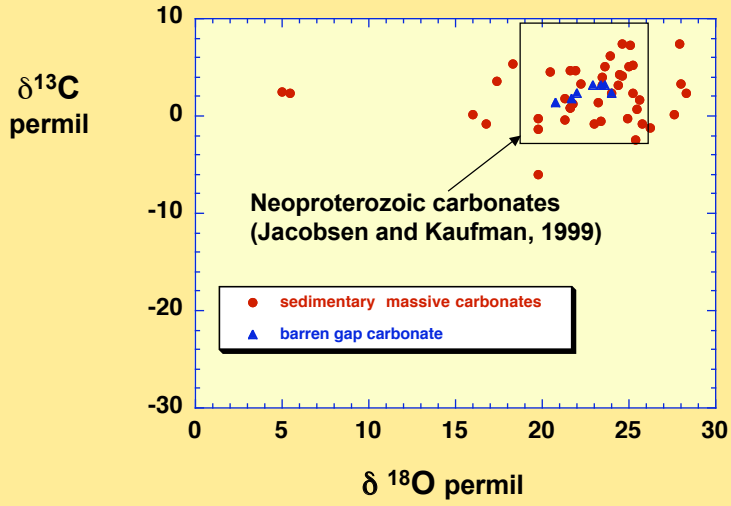

AMIRA P544

Hangingwall sedimentary carbonates

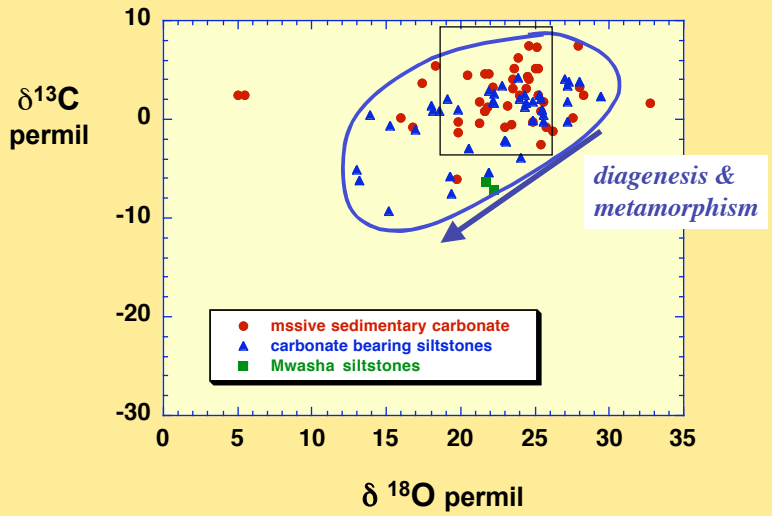

AMIRA P544

Ore Shales

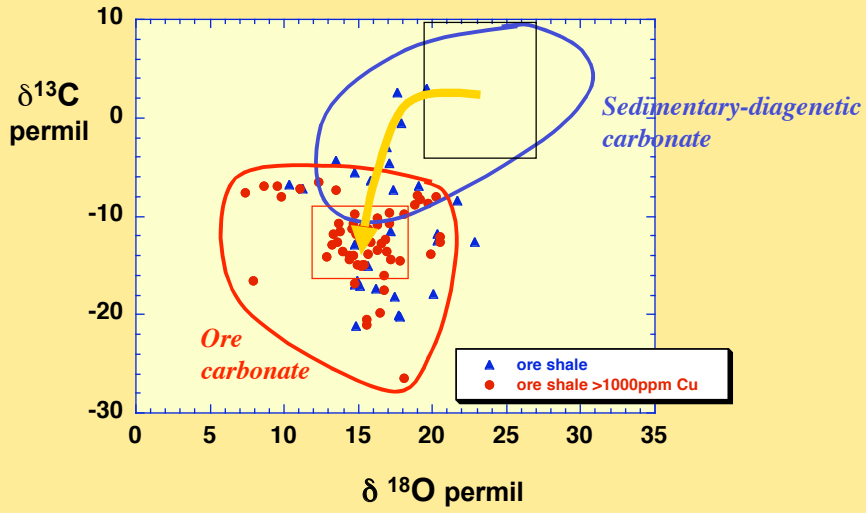

AMIRA P544

Possible causes of coupled C-O decrease

- High temperature of mineralisation - can cause the δ ^{18}O decrease, but not the highly negative shift in δ ^{13}C
- Metamorphic devolatilisation could cause the coupled trend, BUT should affect all the carbonates, not just the ore shale and "Footwall clastics"
- Oxidation of organic carbon to CO_2 which becomes incorporated in diagenetic and hydrothermal carbonates - can cause big negative shifts in δ ^{13}C, similar to those recorded in and around the ore shale- this is the most likely cause

AMIRA P544

Carbon isotope distribution

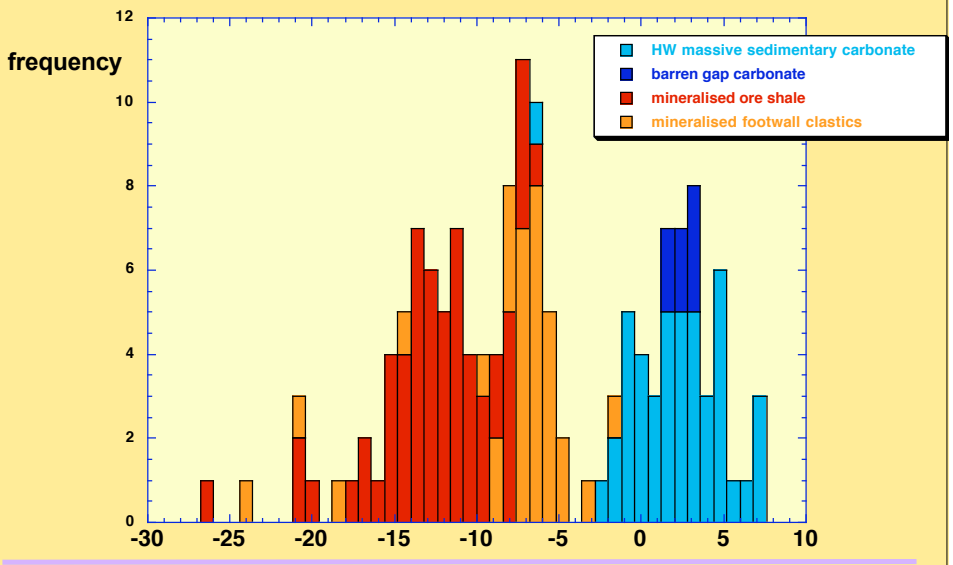

AMIRA P544

Carbon isotope distribution

- The negative $\delta^{13}C$ shift in the footwall clastics (-3 to -10 permil) indicates migration & oxidation of organic carbon within this unit.
- The greater $\delta^{13}C$ shift (-10 to -20) in the ore shale suggests this is the primary source of the organic carbon

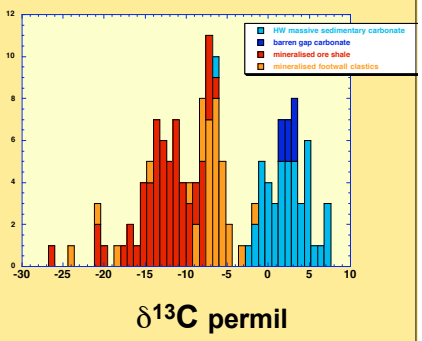

AMIRA P544

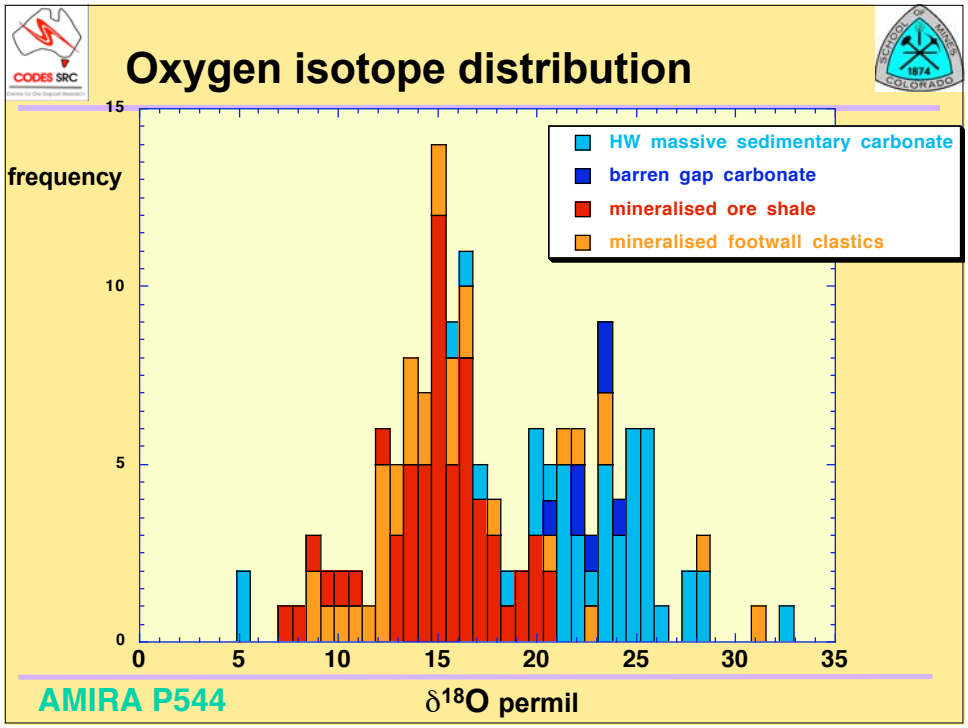
Oxygen isotope distribution
frequency
HW massive sedimentary carbonate
barren gap carbonate
mineralised ore shale
mineralised footwall clastics
0
5
10
15
0
5
10
15
20
25
30
35
AMIRA P544
δ18O permil

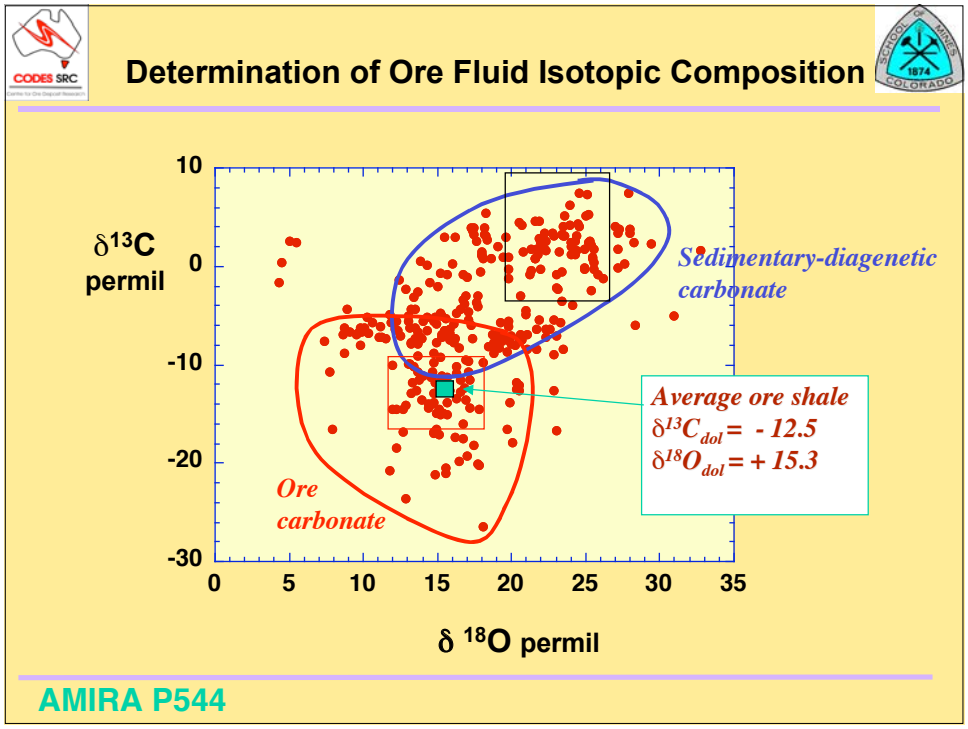
Determination of Ore Fluid Isotopic Composition
δ13C permil
10
0
-10
-20
-30
0
5
10
15
20
25
30
35
Sedimentary-diagenetic carbonate
Average ore shale
δ13Cdol = - 12.5
δ18Odol = + 15.3
Ore carbonate
δ 18O permil
AMIRA P544

Calculated oxygen isotope composition of ore fluid

Dolomite in mineralised ore shale averages $\delta^{18}O_{dol} = 15.3$ permil

Fractionation equation is $\delta^{18}O_{dol} - \delta^{18}O_{fluid} = 3.23*10^6 (273+T) - 3.29$

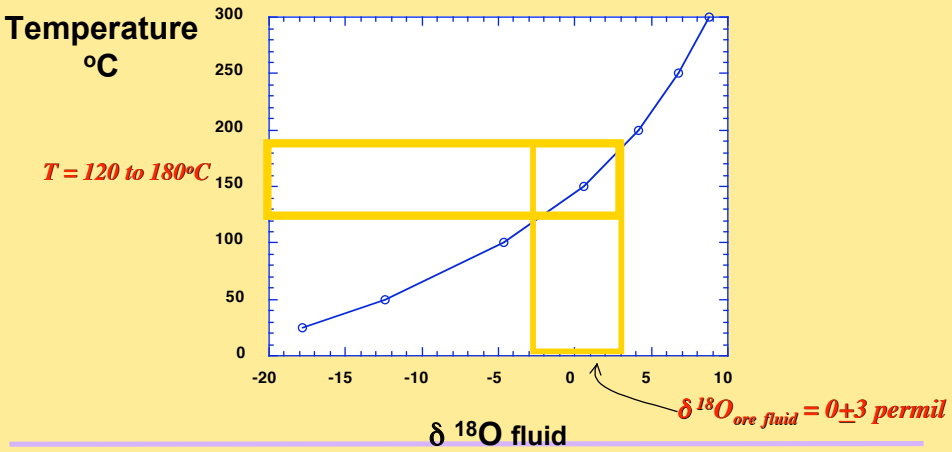

AMIRA P544

Calculated carbon isotope composition of ore fluid

Dolomite in mineralised ore shale averages $\delta^{13}C = -12.5$ permil

Fractionation equation is $\delta^{13}C_{dol} - \delta^{13}C_{fluid} = 3.13(11.35*10^3/T)+5.54*10^6/T^2+ \ldots..$

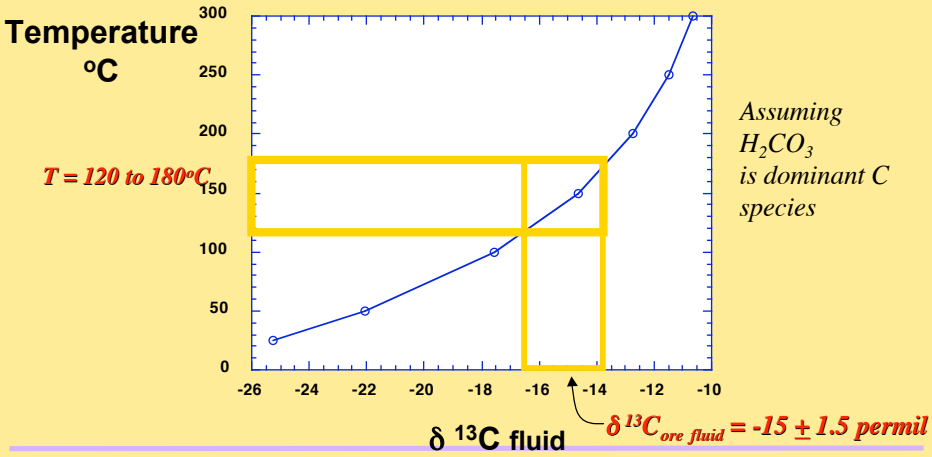

Assuming H_2CO_3 is dominant C species

AMIRA P544

Ore Fluid Isotopic Composition

- **Fluid $\delta^{18}O$ = 0±3 permil indicates a predominantly marine seawater source for the ore fluid, based on a hydrothermal temperature of 120 to 180°C**
- **Fluid $\delta^{13}C$ = -15 permil indicates oxidation of organic carbon has played a major role in carbonate development in the ore shale**

$$CH_4 + O_2 = CO_2 + H_2$$

→ *dolomite*

AMIRA P544

Controls on Variations in Isotopes

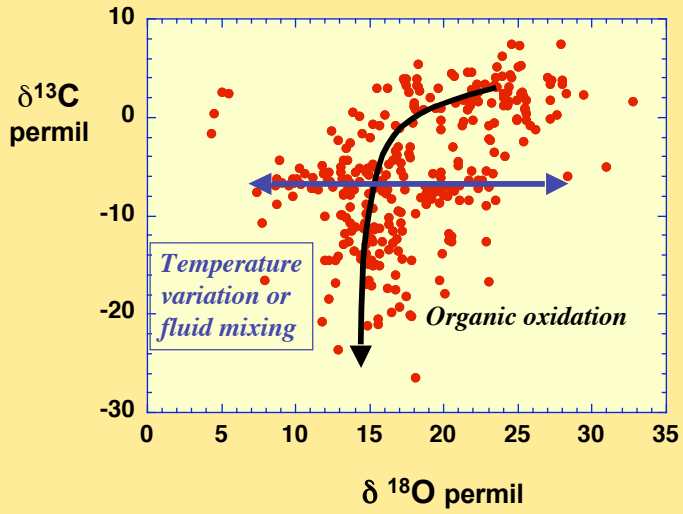

AMIRA P544

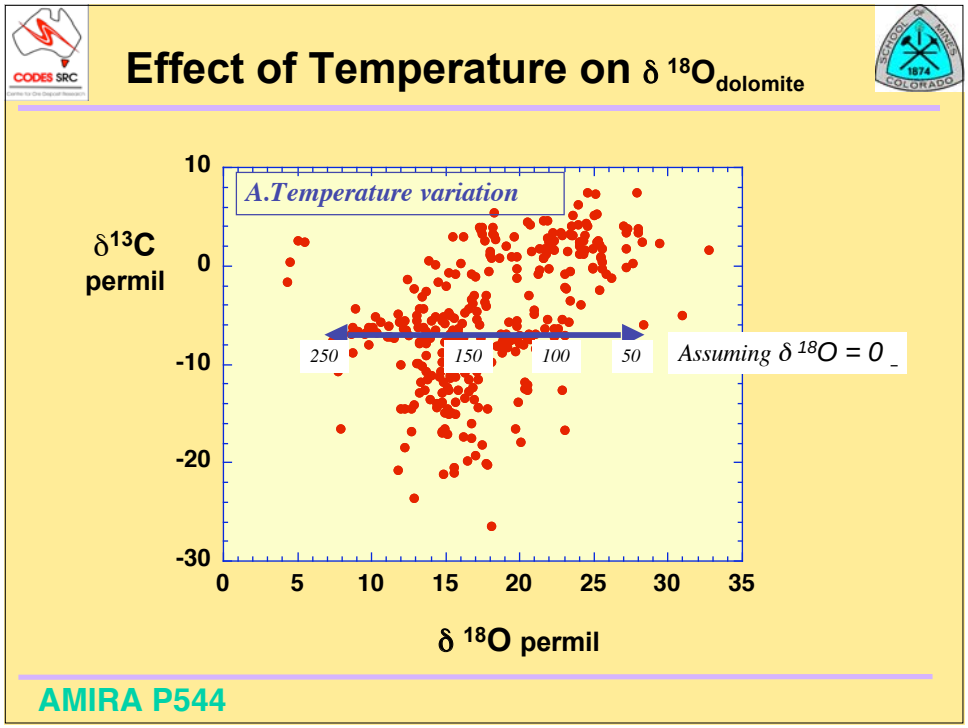
Effect of Temperature on δ 18O dolomite
A.Temperature variation
δ13C permil
δ 18O permil
250
150
100
50
Assuming δ 18O = 0
AMIRA P544

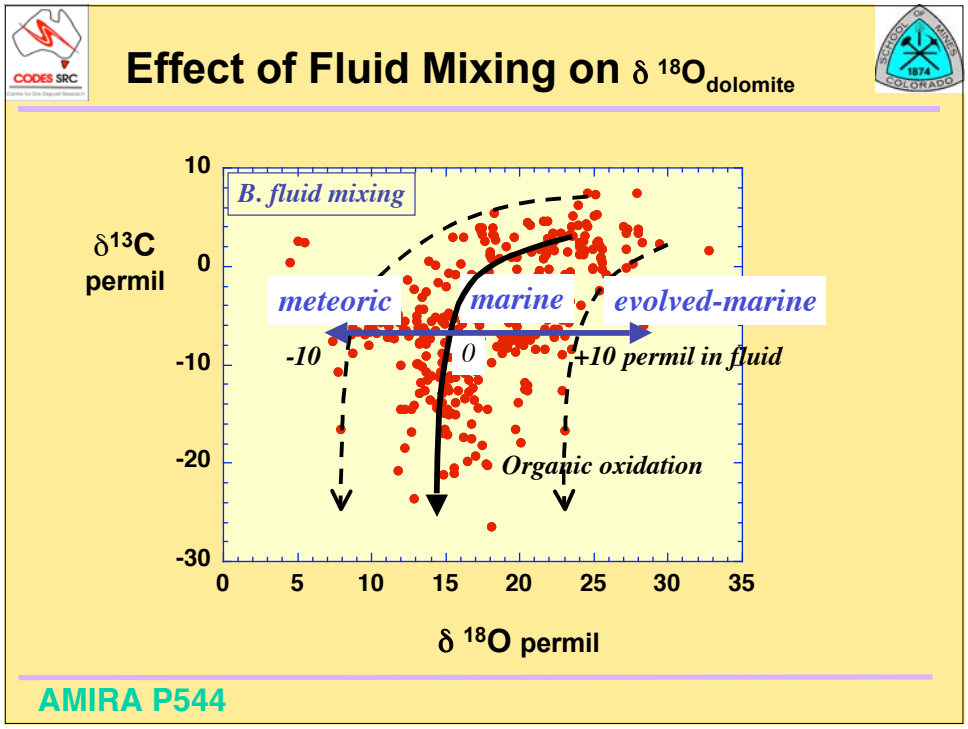
Effect of Fluid Mixing on δ 18O dolomite
B. fluid mixing
δ13C permil
δ 18O permil
meteoric
marine
evolved-marine
-10
0
+10 permil in fluid
Organic oxidation
AMIRA P544

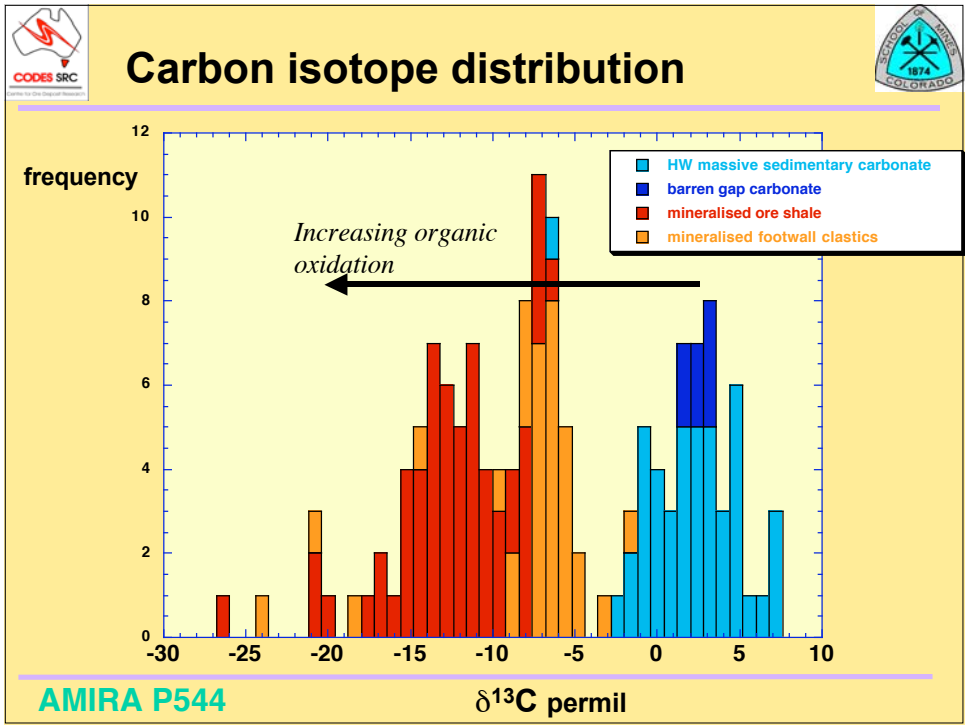
Carbon isotope distribution
frequency
HW massive sedimentary carbonate
barren gap carbonate
mineralised ore shale
mineralised footwall clastics
Increasing organic oxidation
AMIRA P544
δ13C permil

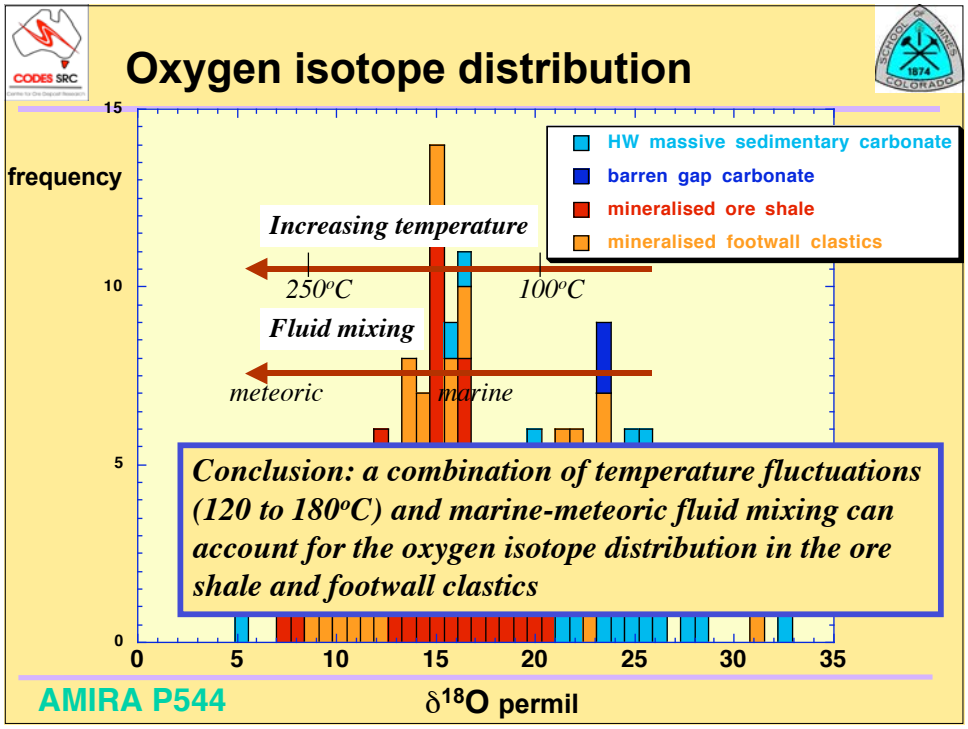
Oxygen isotope distribution
frequency
HW massive sedimentary carbonate
barren gap carbonate
mineralised ore shale
mineralised footwall clastics
Increasing temperature
250°C
100°C
Fluid mixing
meteoric
marine
Conclusion: a combination of temperature fluctuations (120 to 180°C) and marine-meteoric fluid mixing can account for the oxygen isotope distribution in the ore shale and footwall clastics
AMIRA P544
δ18O permil

All Carbonate Isotope Data: n=315

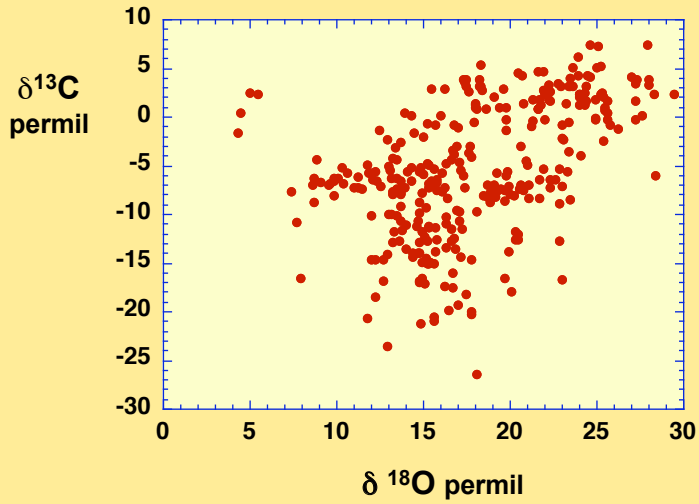

AMIRA P544

Hanging Wall Albite Alteration

Fluid isotopes

At 150°C (hydrothermal)
$\delta^{18}O_f$ = -10 permil
$\delta^{13}C_f$ = -2 permil

OR

At 350°C (metamorphic)
$\delta^{18}O_f$ = 0 permil
$\delta^{13}C_f$ = +2 permil

----> albite alteration does not involve organic oxidation

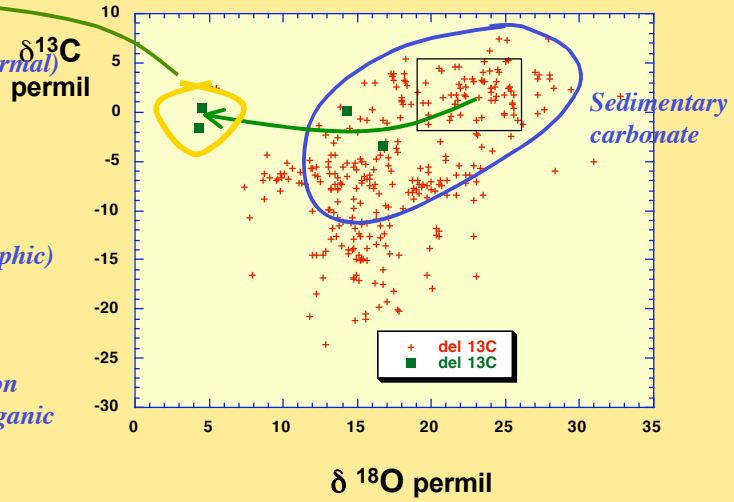

AMIRA P544

Sodium metasomatism

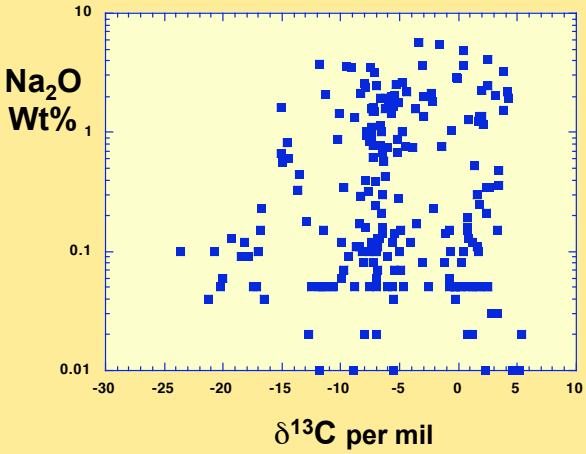

No clear correlation between $\delta^{13}C$ of carbonates and sodium metasomatism

AMIRA P544

Potassium metasomatism

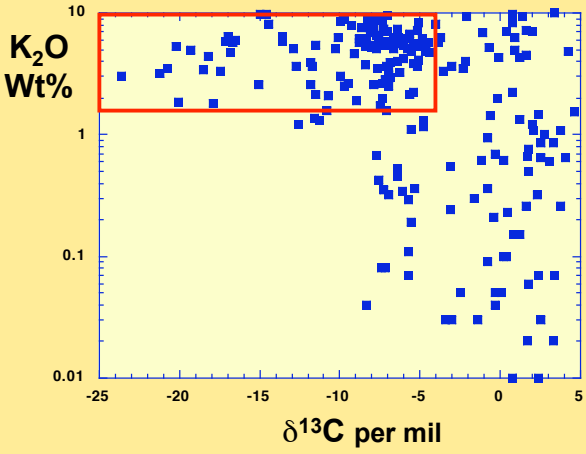

Ore shales and footwall clastics with low $\delta^{13}C$ values (< 4 per mil) exhibit clear potassium enrichment

AMIRA P544

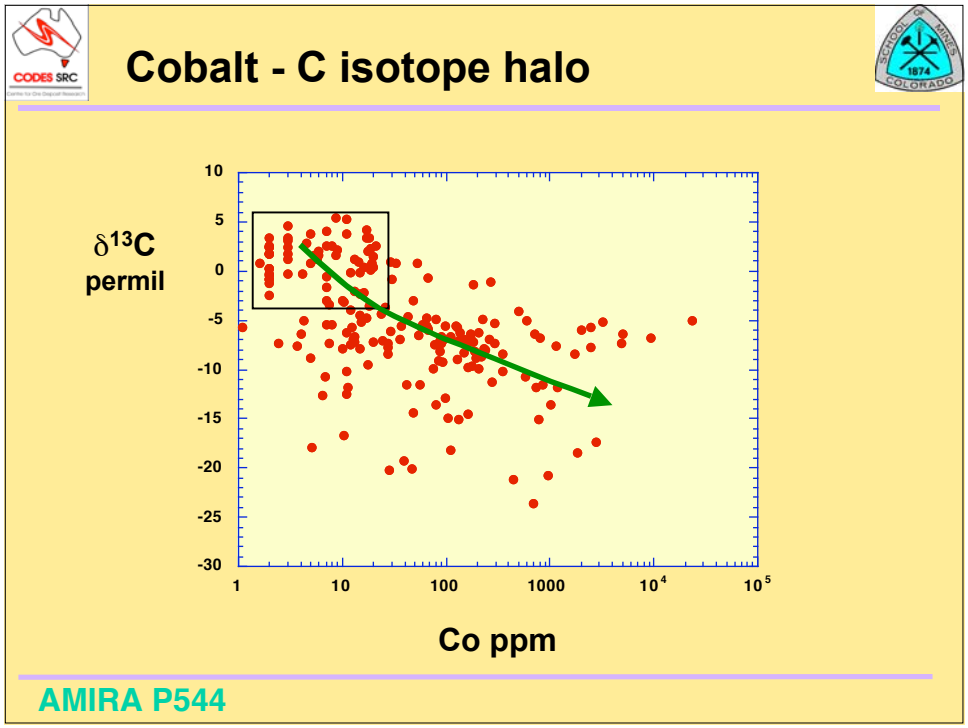
Cobalt - C isotope halo
δ13C permil
10
5
0
-5
-10
-15
-20
-25
-30
1
10
100
1000
10^4
10^5
Co ppm
AMIRA P544

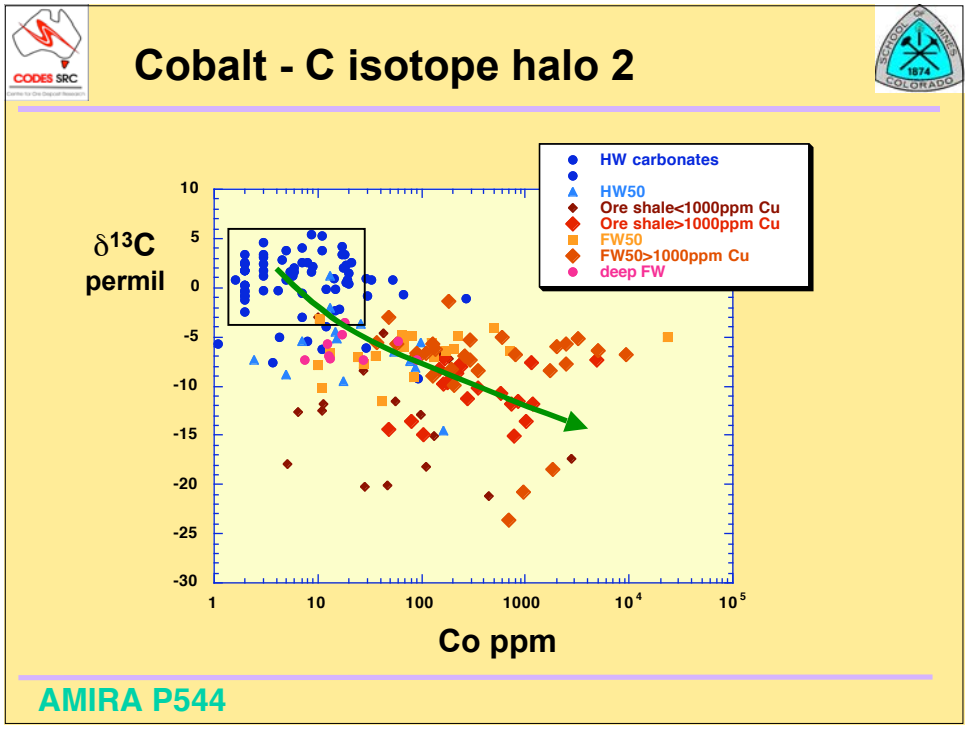
Cobalt - C isotope halo 2
HW carbonates
HW50
Ore shale<1000ppm Cu
Ore shale>1000ppm Cu
FW50
FW50>1000ppm Cu
deep FW
δ13C permil
10
5
0
-5
-10
-15
-20
-25
-30
1
10
100
1000
10^4
10^5
Co ppm
AMIRA P544

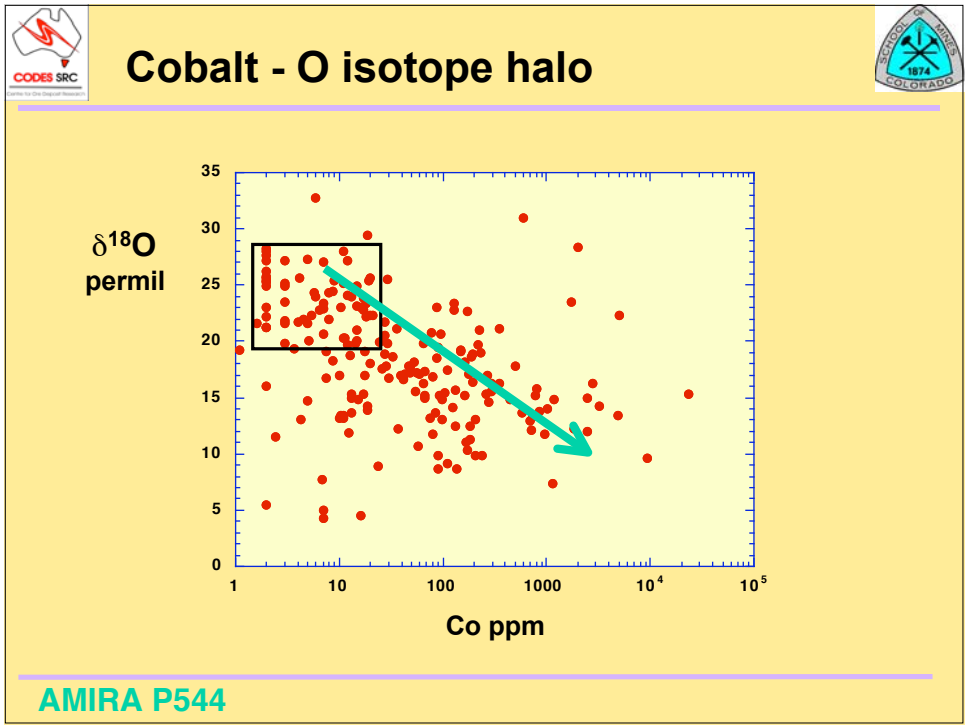
Cobalt - O isotope halo
δ18O permil
35
30
25
20
15
10
5
0
1
10
100
1000
10^4
10^5
Co ppm
AMIRA P544

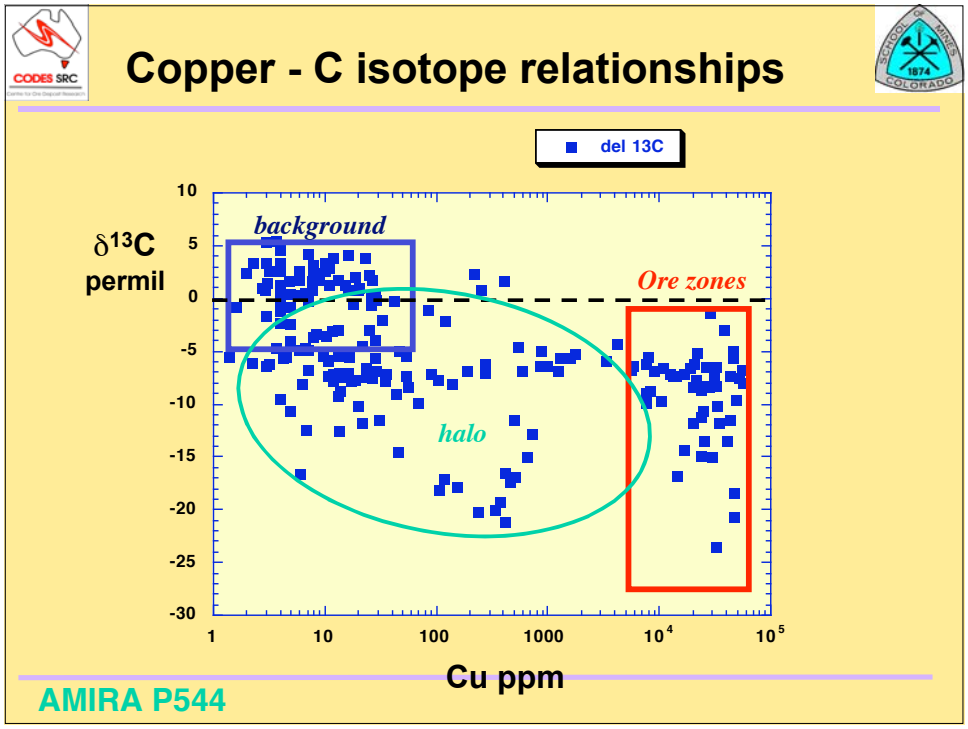
Copper - C isotope relationships
del 13C
δ13C permil
10
5
0
-5
-10
-15
-20
-25
-30
background
Ore zones
halo
1
10
100
1000
10^4
10^5
Cu ppm
AMIRA P544

Copper - C isotope relationships

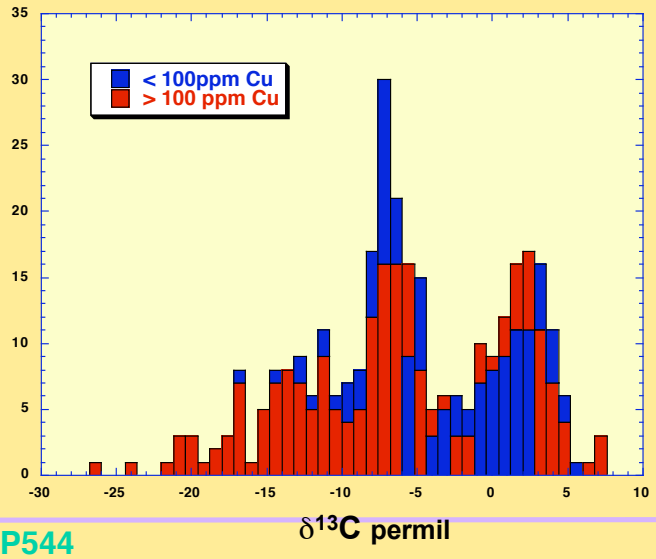

AMIRA P544

Conclusions on C isotopes

- **The "Ore Shale" and mineralised FW clastics commonly exhibit coupled depletion of ^{13}C and ^{18}O compared to sedimentary carbonates**
- **This suggests that mineralisation involved coupled oxidation of organic carbon to CO_2, reduction of sulphate to H_2S, and co-precipitation of carbonate and ore sulfides in a relatively closed environment**
- **The lowest $\delta^{13}C$ occurs in mineralised ore shale, suggesting that maximum organic oxidation occurred in the ore shales**
- **Light $\delta^{13}C$ values in highly mineralised "clean" FW sandstones requires the introduction of an exotic organic carbon source - HC**

AMIRA P544

Conclusions on C isotopes

- HW massive carbonates and "Barren Gap" carbonates have a normal marine isotope signature with no evidence of oxidation of organic carbon
- A tight halo of negative $\delta^{13}C$ surrounds most, but not all, Cu ore zones tested. A similar signature is given by some low grade (<1% Cu) ore shales
- The $\delta^{13}C$ halo commonly corresponds with the Co halo and zone of maximum potassium metasomatism (however there are exceptions, where late stage Na-metasomatism has occurred)
- Later Na metasomatism in the HW appears to be unrelated to organic oxidation, and has a higher $\delta^{13}C$ signature

AMIRA P544

Conclusions on O isotopes

- The oxygen isotope halo around the ore shale is commonly broader than the carbon isotope halo, and includes the complete Mindola Clastics package
- A combination of temperature and fluid mixing were probably the key controls on $\delta^{18}O$ values in alteration carbonates
- Variation in the $\delta^{18}O$ data is best explained by mineralisation occuring at T = 120 to 180°C due to mixing of evolved marine ore fluid with non marine hydrocarbon-rich formation waters
- Albite alteration in the HW was probably caused by a different (meteoric) fluid with a much lower oxygen isotope signature ($\delta^{18}O_f$ = -10 per mil, $\delta^{13}C_f$ = -2 per mil) OR at a higher temperature (syn-metamorphic)

AMIRA P544

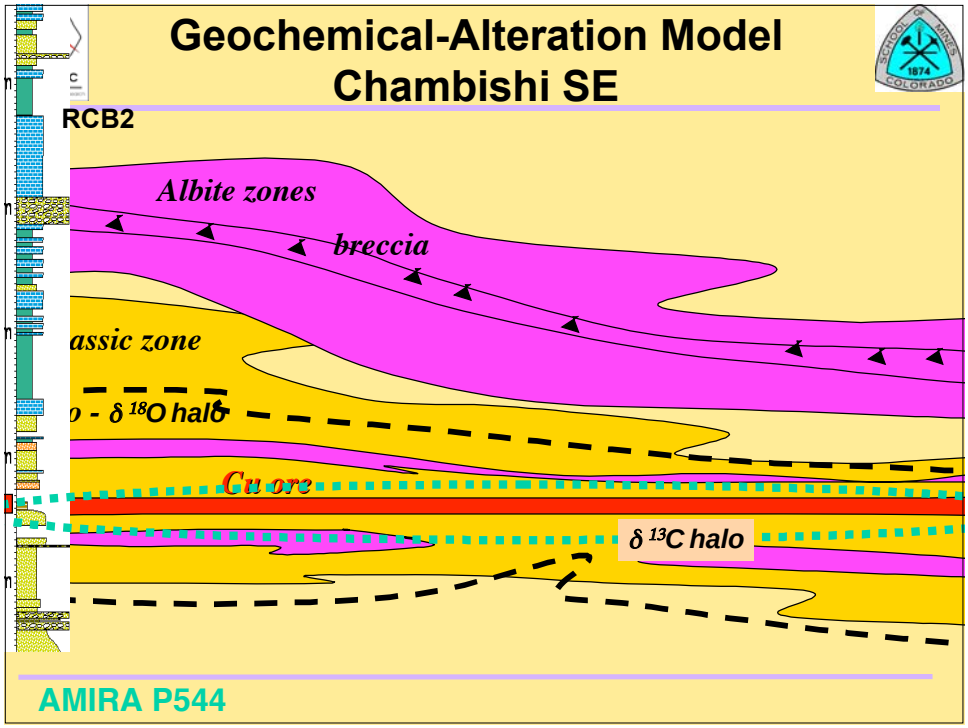
Geochemical-Alteration Model
Chambishi SE
RCB2
Albite zones
breccia
assic zone
δ 18O halo
Cu ore
δ 13C halo
AMIRA P544

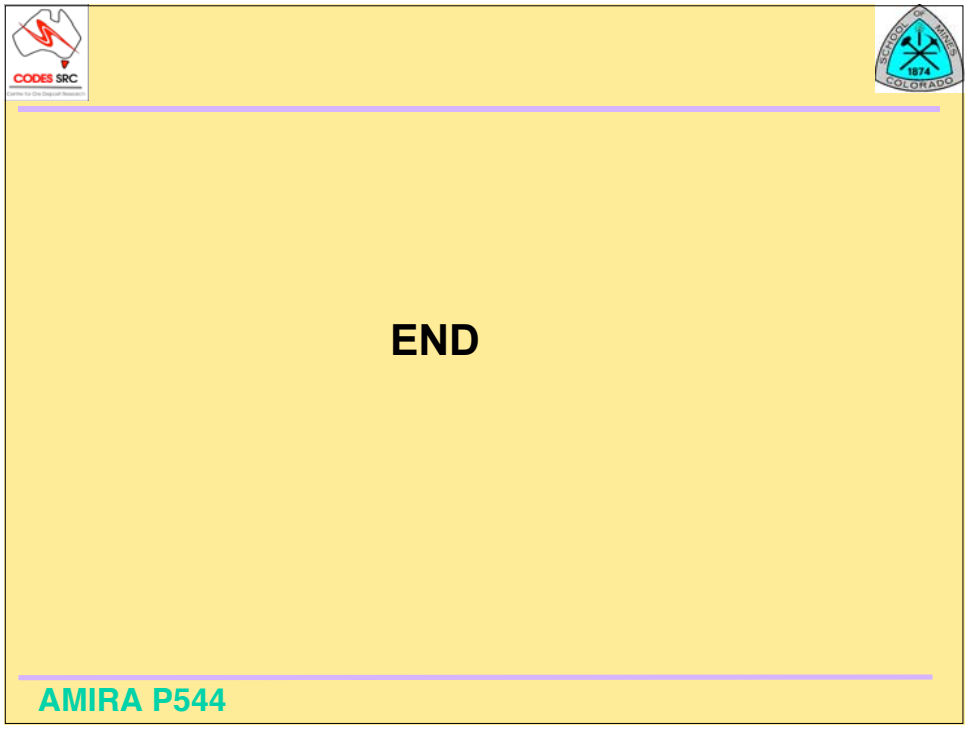
CODES SRC
END
AMIRA P544

Minor element geochemistry of Zambian Copperbelt deposits

Peter McGoldrick, Robert Scott, David Selley and *David Broughton
Centre for Ore Deposit Research, University of Tasmania
**Colorado School of Mines*

Summary

As well as Cu and Co, the ores of the Zambian Copperbelt contain, or are associated with, a group of other chalcophile elements: Ag, Bi, Mo, U, W, (locally Au, Pt, Pd), ± ?Ni ?V (in arenite deposits). This association is consistent with an oxidised metal transporting fluid (carrying Cu, Co, Ag, Bi, and U) interacting with organic reductant (possible source for Ni, V) or sour gas.

There may be a contribution of some 'organophile' elements (e.g., PGE, Au, V, Mo, Ni) from hydrocarbons in arenite-hosted deposits or original organic matter in the Ore Shale.

The lack of gradational halos of these metals (Co may be an exception; see Large et al., this volume), and their erratic distribution away from mineralisation suggests that ore fluids did not originate from a point source, rather, they were part of a complex regional fluid flow process operating over long periods of time. This has resulted in large volumes of altered rocks, but, because sulfide precipitation was reductant limited then chalcophile elements were mostly not fixed in oxidised, reductant-poor Lower Roan rocks. The 'spikey' chalcophile element patterns in parts of the Lower Roan host sequences may reflect an erratic and / or limited distribution of reductant at the time of introduction of the ore fluids.

For fresh rock lithogeochemical exploration Cu is still the best lateral 'vector' to ore, but in greenfields basins showing evidence for strong alkali alteration or saline diagenesis, then zones of 'spikey 'anomalous U, Mo, and Bi would give added encouragement.

Introduction

An important aim of our work was to systematically characterise minor and trace element geochemistry of a number of the Zambian Copperbelt (ZCB) deposits. Results from several 'Ore Shale' deposits (Nkana, Mindola, Konkola and Konkola North) were reported at sponsors' meetings last year and in the 2002 Annual Report (McGoldrick et al., 2002; Pollington and McGoldrick, 2002). New work reported here extends our coverage to the second important group of ZCB deposits,known collectively as 'arenite-hosted' deposits. These include 'footwall' orebodies in the Chambishi Basin (Mwambashi B and Chibuluma West) and, NE of the Kafue Anticline, the giant Mufulira deposit and the Ndola West prospect. Coverage of the Ore Shale-hosted deposits is extended to the Chambishi deposit and the Chambishi Southeast prospect. (Slide 12.3)

Arenite-hosted deposits 1 – Chambishi Basin

Mwambashi B

This is a small deposit on the western edge of the Chambishi Basin with a 1997 reported resource of 8.4 Mt at 2.63wt% Cu and 0.08wt% Co. (Slide 12.4) Ore-grade Cu is confined to arenites immediately below an essentially unmineralised siltstone unit at the Ore Shale stratigraphic position. There are pronounced lateral thickness changes and facies variations in the footwall rocks, including a dramatic thinning ('pinch-out') towards the N. The Cu orebody at

Mwambashi B corresponds closely to this pinch-out position. (Slide 12.5)

Complete details of the geology and geochemistry of the Mwambashi B orebody are presented elsewhere in the P544 Final Report (Selly, this volume), and only key geochemical observations are described here.

Geochemical data are from five drill holes that form part of a N-S fence extending nearly 5km S from just N of the footwall pinch-out position (Slide 12.6). Slides 12.7 through 12.9 are individual element plots depicting some of these results. Measured values for each sample are plotted relative to each drill-hole's distance from the pinch-out.

Copper is seen to increase abruptly in the footwall rocks within about 1500 m of the pinch-out, while high Co values are only reported from one hole. Strongly mineralised samples from the drill hole nearest the pinch-out are bornite-rich and Co-poor (Slide 12.7).

Among the other chalcophile elements, Mo, Bi and Ag are all variably enriched in the Cu-Co mineralised zone. Molybdenum and Bi values are highest in samples from the drill hole nearest the pinch-out (up to several tens of ppm), and data from the other holes suggest of a trend of increasing levels for both toward the pinch-out. High values of these elements correspond to chalcopyrite-carrolite rich ores. Anomalous Ag values of a few ppm are seen in many mineralised samples, with highest-Ag samples being bornite-rich. (Slide 12.8). Measurable amounts of Pt and Pd (few ppb to a few tens ppb) are also observed in samples from near the pinch-out.

Elevated Ba is a common feature of many ZCB deposits (see below, and Scott, this volume), with levels of several hundred to several thousand ppm Ba in their host rocks (Slide 12.9). By comparison, parts of Mwambashi B displays the most extreme Ba enrichment of any of the ZCB deposits examined thus far. Values of several weight percent Ba are seen in samples from close to the pinch-out. A sympathetic enrichment in Sr is also observed in these areas (Slide 12.9).

The significance of high Ba is discussed more fully in reports by Selley, Scott and McGoldrick, and Cooke, later in this volume. For Mwambashi B there are three possible explanations for the unusually high Ba:

- Ba, Sr and other large ion lithophile elements were concentrated at the site of subsequent K-feldspar and Cu sulfide precipitation; hydrocarbon concentration within a physical trap site would be a way of achieving this (see Scott, this volume)
- Ba and Sr may have been introduced with the oxidised (but low total S – see McGoldrick and Cooke, this volume) potassic Cu-mineralising fluids; again hydrocarbons and associated reduced aqueous fluids would allow Ba to build up to high concentrations which became incorporated into alteration phases as the hydrocarbons were consumed and K-feldspar and carbonate precipitated.
- the southernmost drill hole is in close proximity to a large gabbro intrusion, and samples are mainly albite-altered breccias that are very low in both Ba and Sr, and low in transition metals; the extreme Ba enrichment in the northern holes may relate to its re-distribution during this late sodic alteration event. (Slide 12.10)

In summary Mwambashi B shows (Slide 12.11):

- The same chalcophile element association as seen in the Ore Shale deposits.
- A distinct enrichment of chalcophiles, transition metals, Ba, Sr, (± Mo, Ce, Th) and other LILE towards the 'pinch-out'.
- Highest Pt, Pd (few ppb to tens of ppb) in 'pinch-out'.
- Evidence for leaching of transition metals adjacent to gabbroic bodies
- Pronounced Ba and Sr enrichment, that may be a record of former hydrocarbons at the ore trap site

Chibuluma West

This is a second example of a small, high-grade arenite-hosted deposit on the southern edge of the Chambishi Basin. It has been described in some detail in a previous P544 report by Selley et al. (2002). The Lower Roan at Chibuluma West is a condensed

sequence deposited on granite basement in a series of WNW trending depocentres. No 'Ore Shale' facies are recognised at this deposit. (Slides 12.12, 12.13).

Geochemical data are available for 37 samples from a single drill core (NS137) through a high grade part of the deposit (Slide 12.13). A series of down-hole element variation plots for the 30 m thick mineralised portion of NS137 are depicted on Slide 12.14 . Several observations can be made from these data, for instance, Co is 'de-coupled' from Cu, with high Co grades occurring for the most part only in the uppermost 10 m of the orebody (100s to 1000s ppm Co). High-grade Cu mineralisation (1–5 wt% Cu) is largely confined to the lower 20 m of the ore lens. Barium shows a range of two orders of magnitude (10s to 1000s ppm) with a systematic upwards increase through the ore lens, but the very low and very high values observed in the Mwambashi B system are not seen at Chibuluma W. Most samples from the Cu-rich part of the drill hole have anoma;lous Mo levels (several ppm to low 10s ppm Mo), and a subset of these samples have elevated Bi (few ppm to few 10s ppm Bi). Highly anomalous U levels (10s ppm cf <<5 ppm) are observed in samples from the footwall of the Cu-ore zone and a second group of samples in the upper third of the Cu zone.

Arenite-hosted deposits 2 — NE of the Kafue Anticline

Ndola West prospect

Ndola West is the subject of a major report elsewhere in this volume by Rob Scott, and only a few observations concerning Ba and some chalcophile metals are made here.

Multi-element analyses of 16 samples from two drill holes that together span about 300 m of Lower Roan stratigraphy were available. Two of these samples are from the Cu-mineralised interval in DDH KITOODD004 and contain percent levels of Cu, and both these samples are anomalous in Bi and Ag compared to hangingwall and footwall samples. Cobalt levels are mostly low (<10 ppm), and even in Co-rich samples do not reach the levels seen in the arenite-hosted deposits from the Chambishi Basin. A sample in the immediate footwall of the two high-Cu samples contains more than 100 ppm Co, as do a handful of samples about a 100 m stratigraphically below the Cu mineralisation (Slide 12.17).

Elevated Ba levels (100s to 1000s ppm) are present in all the Ndola West samples (Slide 12.18).

Mufulira (Slides 12.20, 12.21)

There was no systematic sampling for lithogeochemistry carried out at Mufulira for P544, however, new multi-element analyses were obtained for approximately 20 Cu-mineralised samples (>500 ppm Cu). Several underground samples collected by Rob Scott are discussed in detail elsewhere in this report, and thirteen samples are from surface drill-holes DH219 and MW107 used for David Broughton's stratigraphic study (see Broughton, this volume).

The samples show the Cu-Bi-Ag ore signature seen in the other ZCB deposits, but are relatively low in Co (few ppm to a few tens ppm), with some suggestion of an antithetic Cu-Co relationship.

Measurable Au (24 ppb) was present in a single Cu-Ag-Bi-rich underground sample, and Mo and Ni are low (< 55 ppm and <25 ppm respectively).

Elevated Ba is a feature of the Mufulira samples with most samples containing hundreds ppm, and one sample over 1200 ppm Ba.

Ore Shale deposits

The geochemical signature of mineralised and barren argillites from several Ore Shale-hosted deposits (Nkana, Mindola, Konkola and Konkola North) were presented at the P544 Golden meeting, and reported in the 2002 Annual Report (McGoldrick et al., 2002; Pollington and McGoldrick, 2002).

Important observations from this work include:

- that Cu, Co, Ag, Bi and Au (and possibly Mo) are 'ore-association' elements
- compared to 'average shale Cu is enriched 100 to 1000x, Ag up to100x, Co up to 50x, Bi up to 20x, Au between 1 and 10x

- U is anomalous in 'distal' samples at Nkana
- As, Sb, Ni, Pb, Tl and Zn in mineralised argillites are remarkably low (levels less than, or equal to 'average shale').

Work described here extends this study to the Chambishi SE deposit.

Chambishi SE

This deposit is a large, unexploited, Ore Shale-hosted system at the NE edge of the Chambishi Basin (Slide 12.22). It is the subject of two published descriptions (Annels, 1974; Fleischer, 1984) and was the focus of detailed sedimentological and tectono-stratigraphic investigations for P544 (see Bull et al., this volume). During detailed sedimentological logging earlier this year over 200 new samples were collected for multi-element whole rock geochemical analysis. A sub-set of these were the subject of C/O work reported in Bull (this volume) and Large et al. (this volume).

The deposits makes a particularly suitable case study for several reasons including:

- the existence of a large number of surface diamond drill cores.
- most of these cores extend to basement.
- relatively low-strain compared to other Chambishi Basin Ore Shale deposits such as Nkana and Chambishi.
- well documented gross sulfide mineral zonation SW to NE and down section of pyrite-pyrrhotite to pyrite-pyrrhotite-chalcopyrite to chalcopyrite (to bornite). (Fleischer, 1984)
- work in P544 has yielded a good understanding of the relationship between Lower Roan facies architecture and the distribution of high grade ore.

Samples of Ore Shale facies were available from a SW to NE fence of holes (Slide 12.23). NN66 (the SW drill hole) is the least mineralised hole on this fence, but still contains up to several thousand ppm Cu in Ore Shale samples (see Large et al., this volume, for a comprehensive discussion of vertical geochemical variations in this hole). The other three holes on this fence (NN48, NN45 and NN42) all contain a strongly Cu mineralised Ore Shale intersection (Slide 12.25). Assay data and our observations during sampling and logging indicate that Cu mineralisation is confined to the lower two thirds of the Ore Shale and the upper metre or so of the immediate footwall of the Ore Shale.

Drill-hole NN42 (Slides 12.26, 12.27) contains about 20 m of Ore Shale, including 16.3 m at 2.3% Cu. The high-Cu zone corresponds to a zone of high Co (several 100 to 1000s ppm). Several samples from the Cu zone are distinctly anomalous in Bi (few ppm to a few 10s ppm) and a single sample from the footwall contact is Mo-rich (437 ppm cf <<5 ppm in most samples). The Mo-rich sample also has more than 20 ppm U (cf 1 or 2 ppm U in most NN42 samples). Barium levels are eratic, but apparently elevated for tens of metres above and below the Ore Shale (100s and 1000s ppm Ba cf 10s ppm in upper samples).

Drill-hole NN48 (Slides 12.28, 12.29) has a thicker Ore Shale intersection (about 25 m) than NN42, but a thinner high-grade Cu zone (4.7 m at 2.1wt% Cu in the lower part the Ore Shale). Elevated V, Bi and Mo correspond closely with the Cu-rich part of this hole (Slide 12.28). By contrast, although elevated in the Ore Shale, As and Ni are highest in samples from the upper, less Cu-rich, but more pyritic, part of the Ore Shale (Slide 12.29).

To the NW of the main mineralised zone at Chambishi SE the Ore Shale pinches out to a laterally equivalent sandstone/conglomerate dominated facies. Samples from drill holes NN60 and NN69 from this area indicate that weakly anomalous Cu is still present at the Ore Shale position in both holes (1000s ppm in shaley samples from the inferred Ore Shale position in NN60 and 100s ppm in NN69 – Slide 12.30). Elevated Cu, Co, Bi, and Mo (and arguably U) are present at the Ore Shale position in NN60. In NN66, the most distal hole, Mo and U are elevated in several samples from the hangingwall, but not at the inferred Ore Shale position (which is marked by anomalous Cu, Co and Bi).

Discussion and conclusions

From the data described above, and in earlier reports, it can be seen that, as well as Cu and Co, both the arenite-hosted and the Ore Shale-hosted mineralisation types commonly contain elevated Ag, Bi and

Mo. Several other elements are enriched within, or close to, mineralisation, but their distributions are often 'spikey' and non-systematic. For example, some deposits have Au at 10s ppb abundances, and this Au will report from high-Cu samples, but not all high-Cu samples are Au-rich. Measureable Pt and Pd are present (few ppb to 10s ppb) in the Ba-rich 'pinchout' position of the Mwambashi B deposit, an area interpreted to be a former hydrocarbon accumulation (see also Selley, this volume).

Uranium levels are high in parts of some deposits, but samples with anomalous U (and Mo) also occur locally in otherwise barren sequences above and laterally away from ore positions (e.g., U in the west limb at Nkana (McGoldrick et al., 2002) and Mo and U in samples from Chambishi SE. footwall and distal positions.

Nickel and V, two chalcophile elements that can be highly enriched in some organic matter-rich shales, are not elevated in the Ore Shale deposits. In contrast, parts of the arenite deposits can be relatively enriched in both these elements, especially V (see below).

Although there is a general paucity of Zn and Pb in most Lower Roan rocks (see Large et al., this volume), relatively high values are seen in some parts of both Ore Shale and arenite-hosted deposits (up to several hundred ppm).

Systematic lateral and vertical sulfide mineral zonations have been described from Ore Shale deposits by previous workers. Our work at Chambishi SE shows some vertical trace element variations that reflect sulfide zonation, for instance the upper pyritic parts of the Ore Shale have high Ni and As, while high Bi, Ag and Mo are associated with the lower, Cu-rich, parts of the Ore Shale. We have not been able to distinguish systematic lateral chalcophile element variations in the Ore Shale deposits.

This complexity of element distribution patterns in both Ore Shale and arenite-hosted deposits is a manifestation of the interplay of multiple processes operating at several scales.

For instance, ore-forming fluids were not point sourced, but were part of a complex regional fluid flow that utilized aquifers over long periods of time throughout the Roan rocks. This resulted in large volumes of variably altered rocks (see Large et al. and Scott, this volume) but sulfide mineralisation only formed where sufficient reductant was available. As long as sufficient permeability and porosity was maintained (or created – see Scott, this volume) in carbonaceous facies of the Ore Shale, they would have been a trap for chalcophile metals carried in transient oxidised metal-transporting fluids. In the arenite-hosted deposits sulfide precipitation was promoted by interaction of ore-fluid with accumulated hydrocarbons and or sour gas. In order to precipitate ore-grade accumulations of sulfides , large amounts of reductant were needed. In contrast, some of the 'spikyness' in the element patterns may reflect an erratic distribution of small amounts of mobile reductants that were consumed to fix small amounts of the ore-related chalcophile elements.

Additional complexity for some elements, for instance V, Ni, Mo and some PGE, may reflect their proclivity for accumulating in organic-rich shales and hydrocarbons (e.g., Coveny et al., 1992; Mossman, 1999). Hence, not all ore-associated chalcophile metals need be sourced from the Cu-transporting fluids.

Finally, a third source for some trace metals in the Ore Shale deposits may be Fe sulfides formed during early burial and diagenesis. These sulfides have the ability to scavenge and concentrate a range of chalcophile metals from ambient pore waters. The upper part of the Ore Shale often contains pyrite interpreted to form this way (Annels, 1974). Hence, some component of the chalcophile metals in pyritic Ore Shale may have accumulated prior to the introduction of the main ore-forming fluids, and the chemistry of pyritic ores may reflect this process.

References

Annels, A. E. (1974). Some aspects of the stratiform ore deposits of the Zambian copperbelt and their genetic significance. Gismentes Stratiformes et Provinces Cupriferes. J. P. Bartholome. Liege, La Societe Geologique de Belgique.

Fleischer, V. D. (1984). Discovery, geology and genesis of copper-cobalt mineralization at Chambishi Southeast prospect, Zambia. Precambrian Research **25**: 119-133.

McGoldrick, P., M. Croaker, et al. (2002). Zambian Copperbelt chemistry II: 'Ore Shale' geochemistry.

AMIRA / ARC P544 Proterozoic Sedimentary Copper Deposits Annual Report: 2.1-2.24.

Pollington, N. and P. McGoldrick (2002). Konkola North geochemistry: preliminary observations. AMIRA / ARC P544 Proterozoic Sedimentary Copper Deposits Annual Report: 3.1-3.8.

Selley, D., S. Bull, R. Scott and D. Cooke (2002). Chambishi Basin progress report 2: Basin geometry and its control on mineralisation at Mwambashi B. AMIRA / ARC P544 Proterozoic Sedimentary Copper Deposits Annual Report: 5.1-5.40.

Minor elements in Zambian Copperbelt deposits

Peter McGoldrick, David Selley,
Rob Scott, Dave Broughton

Minor elements: introduction

- previous results for Ore Shale deposits (Nkana-Mindola, Konkola) presented in 2002 Annual report and at Golden meeting
- now broadened to include additional Ore Shale deposits & arenite-hosted deposits

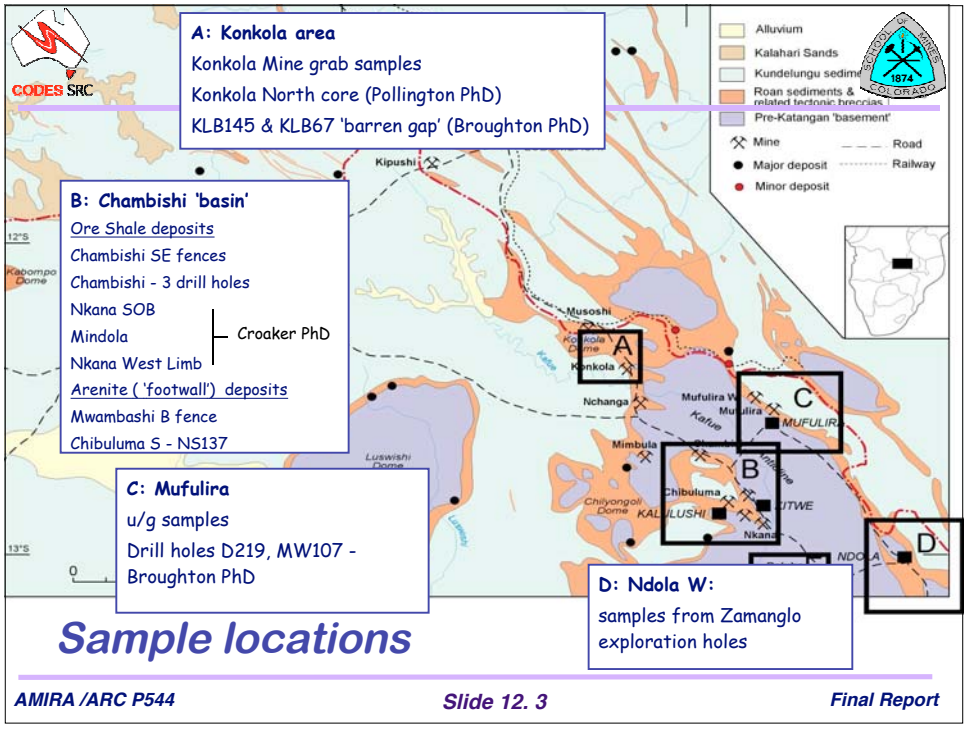
A: Konkola area
Konkola Mine grab samples
Konkola North core (Pollington PhD)
KLB145 & KLB67 'barren gap' (Broughton PhD)
B: Chambishi 'basin'
Ore Shale deposits
Chambishi SE fences
Chambishi - 3 drill holes
Nkana SOB
Mindola
Nkana West Limb
Croaker PhD
Arenite ('footwall') deposits
Mwambashi B fence
Chibuluma S - NS137
C: Mufulira
u/g samples
Drill holes D219, MW107 - Broughton PhD
D: Ndola W:
samples from Zamanglo exploration holes
Alluvium
Kalahari Sands
Kundelungu sediments
Roan sediments & related tectonic breccias
Pre-Katangan 'basement'
Mine
Road
Major deposit
Railway
Minor deposit
Kipushi
Musoshi
Konkola
Nchanga
Mufulira
Mimbula
Chibuluma
Nkana
Ndola
A
B
C
D
12°S
13°S
Sample locations
AMIRA /ARC P544
Slide 12. 3
Final Report

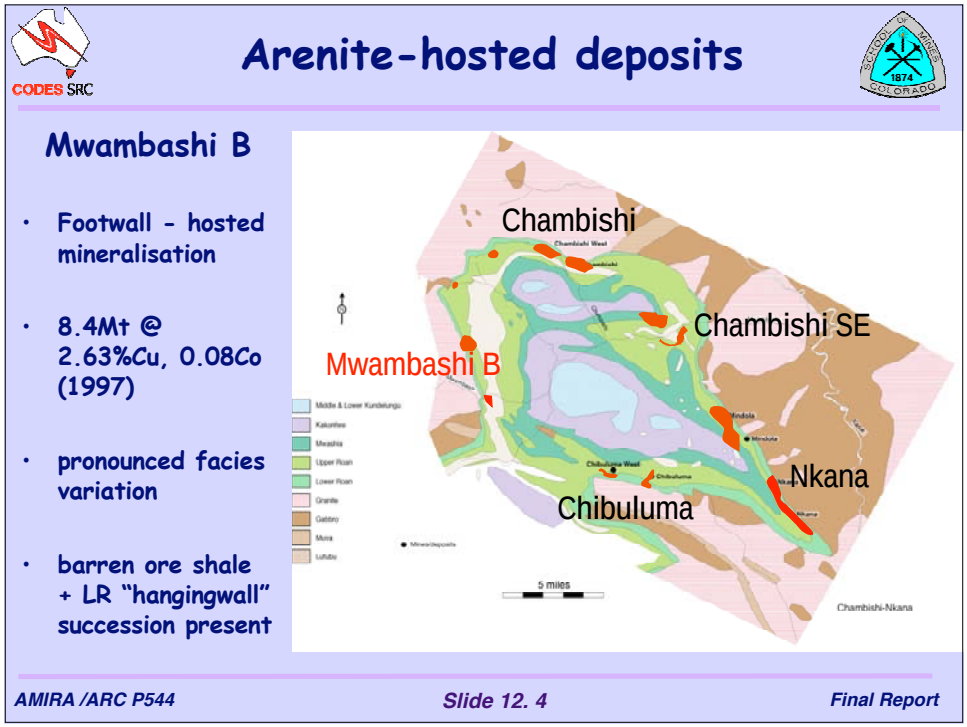
Arenite-hosted deposits
Mwambashi B
Footwall - hosted mineralisation
8.4Mt @ 2.63%Cu, 0.08Co (1997)
pronounced facies variation
barren ore shale + LR "hangingwall" succession present
Chambishi
Chambishi SE
Mwambashi B
Nkana
Chibuluma
5 miles
Chambishi-Nkana
AMIRA /ARC P544
Slide 12. 4
Final Report

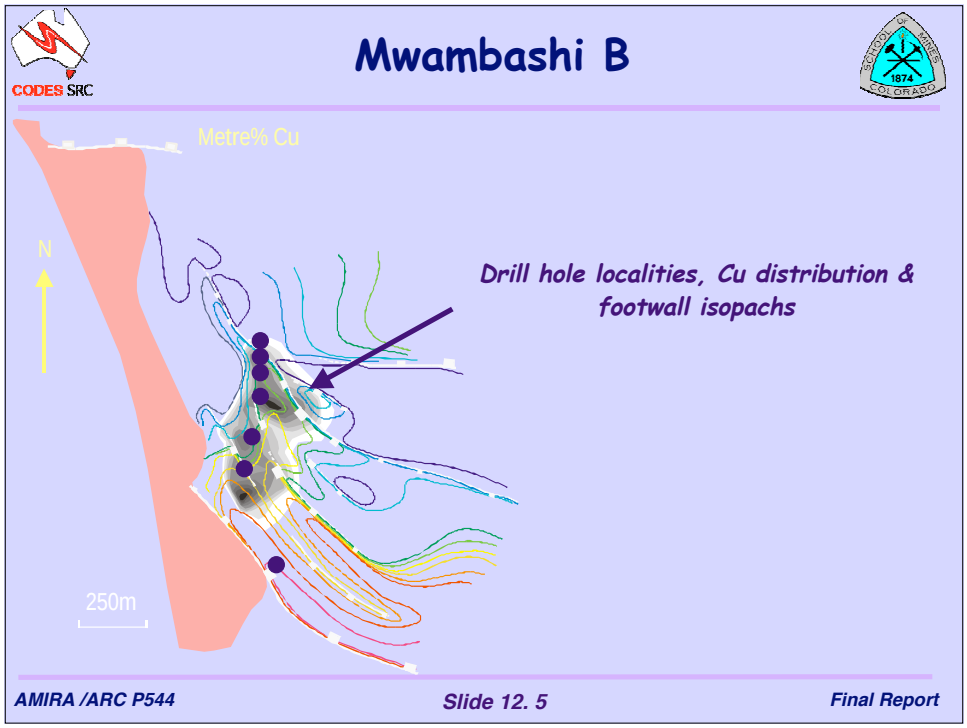
CODES SRC
Mwambashi B
Metre% Cu
N
Drill hole localities, Cu distribution & footwall isopachs
250m
AMIRA /ARC P544
Slide 12. 5
Final Report

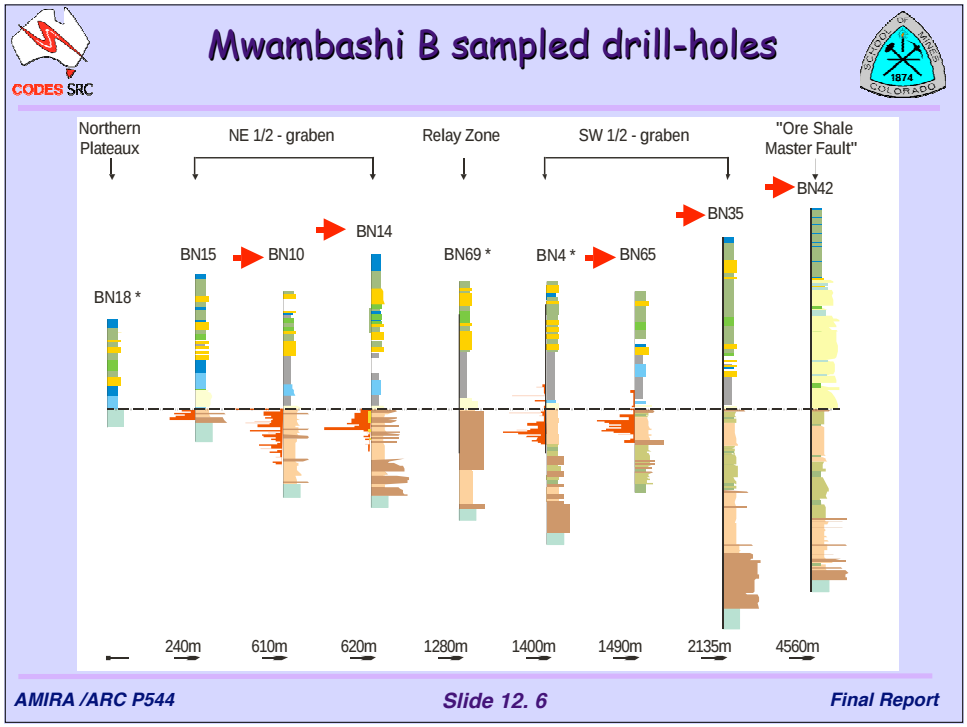
CODES SRC
Mwambashi B sampled drill-holes
Northern Plateaux
NE 1/2 - graben
Relay Zone
SW 1/2 - graben
"Ore Shale Master Fault"
BN18 *
BN15
BN10
BN14
BN69 *
BN4 *
BN65
BN35
BN42
240m
610m
620m
1280m
1400m
1490m
2135m
4560m
AMIRA /ARC P544
Slide 12. 6
Final Report

Cu-Co

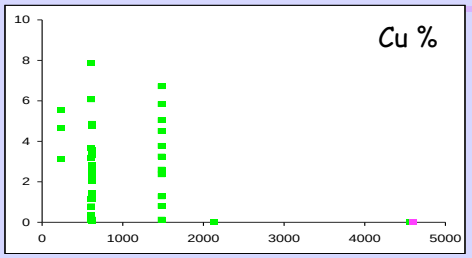

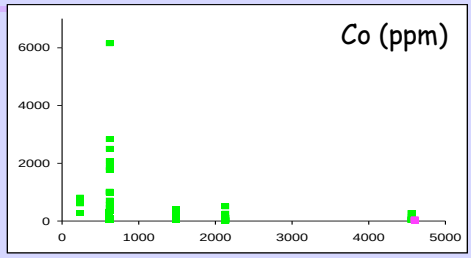

- Cu increases abruptly within 1500m of pinch-out
- Co is more restricted to areas preserving significant calcite cement with anomalously light $\delta^{13}C$ values
- Marginal Co-poor intersection is bornite rich

Other Chalcophiles

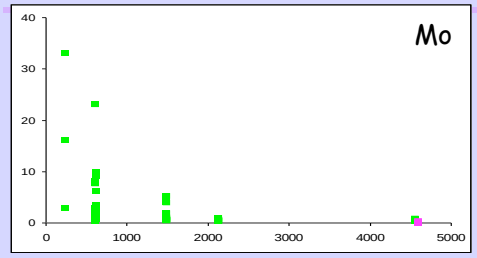

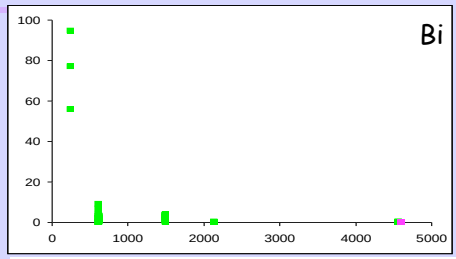

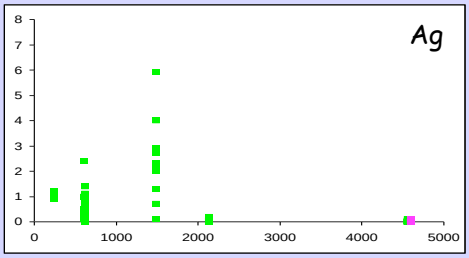

- Marked enrichment of Mo, Bi & Ag within Cu zone
- Ag highest within marginal bornite-rich intersection
- Mo & Bi highest within cpy-carr rich zones & show extreme enrichment within "pinch-out"

Ba & Sr

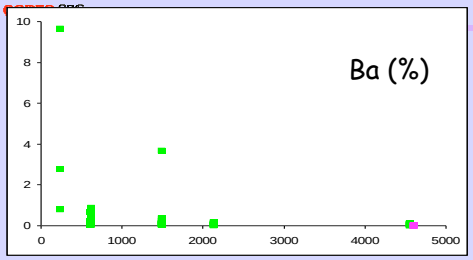

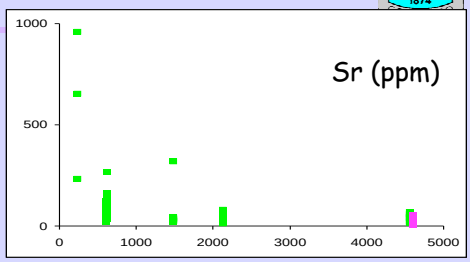

- Ba & Sr increase within ore zone
- Extreme enrichment in "pinch-out"
- Ba >9% - near 2 orders of magnitude greater than most Ore Shale hosted deposits

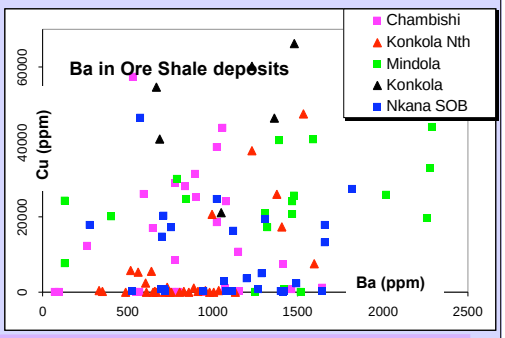

Significance of Ba at Mwambashi B

- 3 possible explanations for Ba distribution:
  - (Early) diagenetic, pre-Kspar, concentration of Ba, & Sr
    - *Consistent with hydrocarbon concentration within physical trap site*
  - Ba & Sr introduced with K-Cu phase
    - *Concentrated by interaction with hydrocarbons*
    - *Very high amounts fixed at site of abrupt redox change*
  - Ba & Sr are mobilised by Na-alteration, and deposited with (later generation) Kspar on a cooling trend

Mwambashi B: main conclusions

- Distinct enrichment of chalcophiles, transition metals, Ba, Sr, (+/- Mo, Ce, Th) & other LILE towards the "pinch-out"
- Highest Pt, Pd (few ppb tens of ppb) in "pinch-out"
- Same chalcophile association as seen in the Ore Shale deposits
- Evidence for leaching of transition metals adjacent to gabbroic bodies
- Ba-Sr enrichment, may record a hydrocarbon signature

Arenite-hosted deposits (con)

Chibuluma West

- Small, high grade arenite-hosted deposit
- Condensed Lower Roan package deposited in WNW-trending depocentres on granite basement
- No Ore Shale present

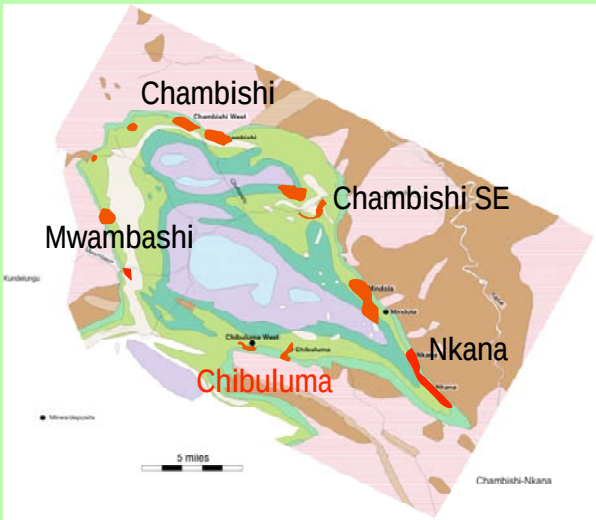

Chibuluma West

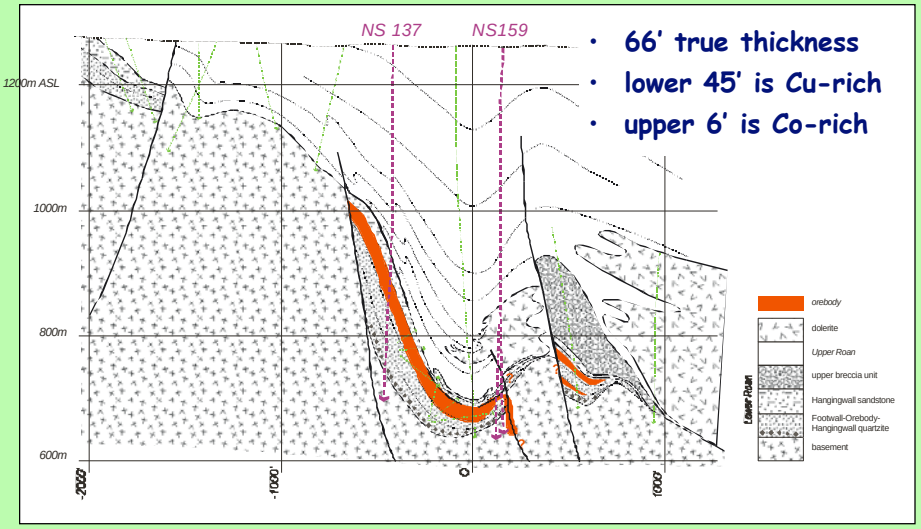

- 66' true thickness
- lower 45' is Cu-rich
- upper 6' is Co-rich

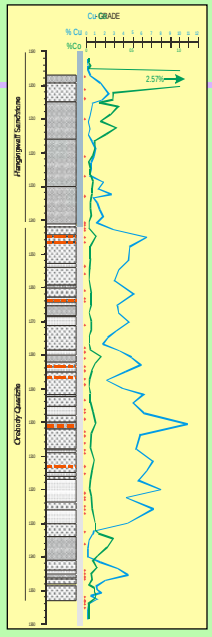

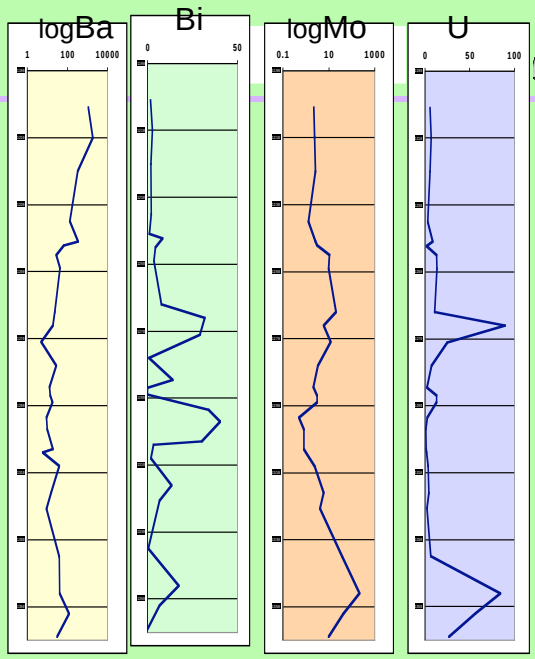

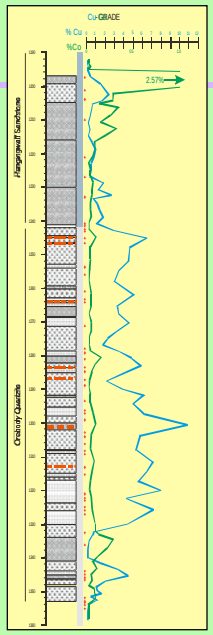

Chib W - NS137

Summary

- wide range in Ba with highs associated with the Co zone
- Bi and Mo associated with the Cu-rich areas, but fewer samples with high Bi
- U 'spikes' in two levels in the hole
  - One in the f/w to the Cu zone
  - Second in the upper third of the Cu zone

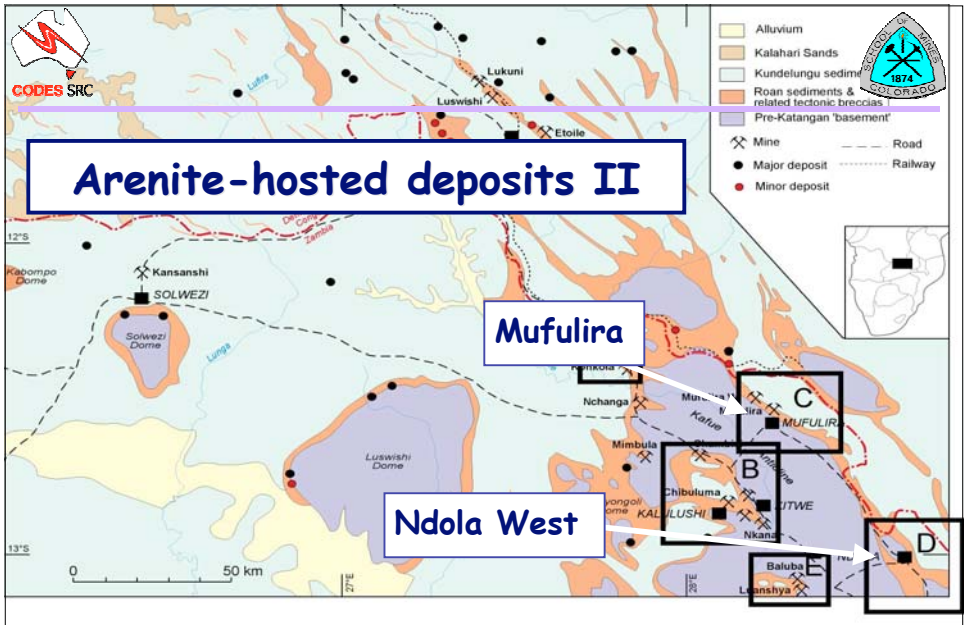

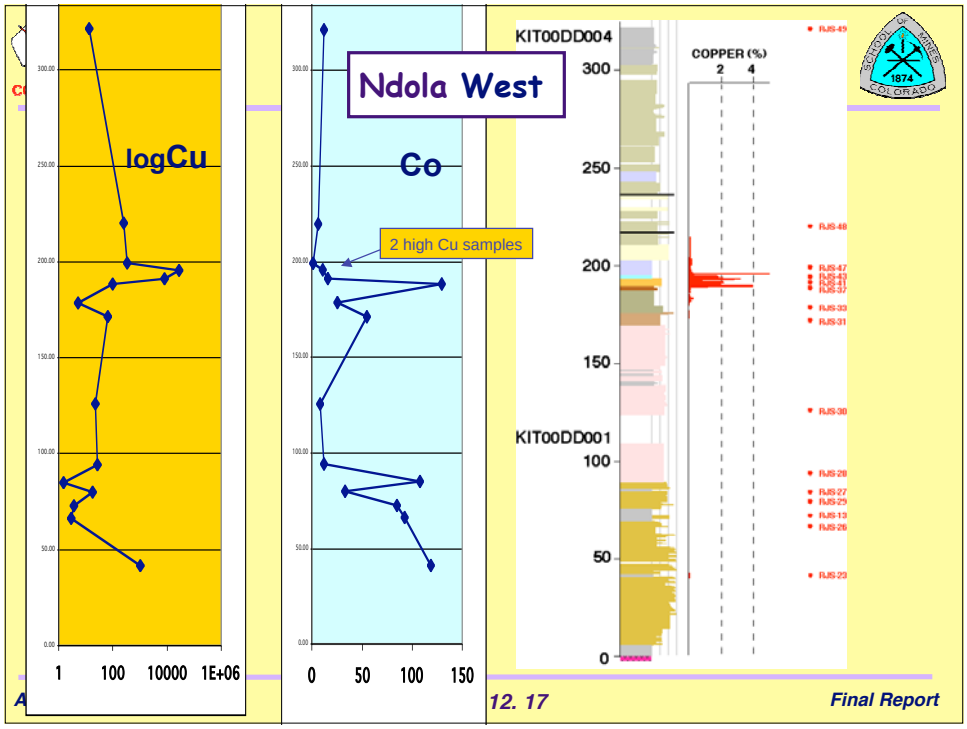
Ndola West
logCu
Co
2 high Cu samples
KIT00DD004
KIT00DD001
COPPER (%)
1 100 10000 1E+06
0 50 100 150
0 50 100 150 200 250 300
12. 17
Final Report

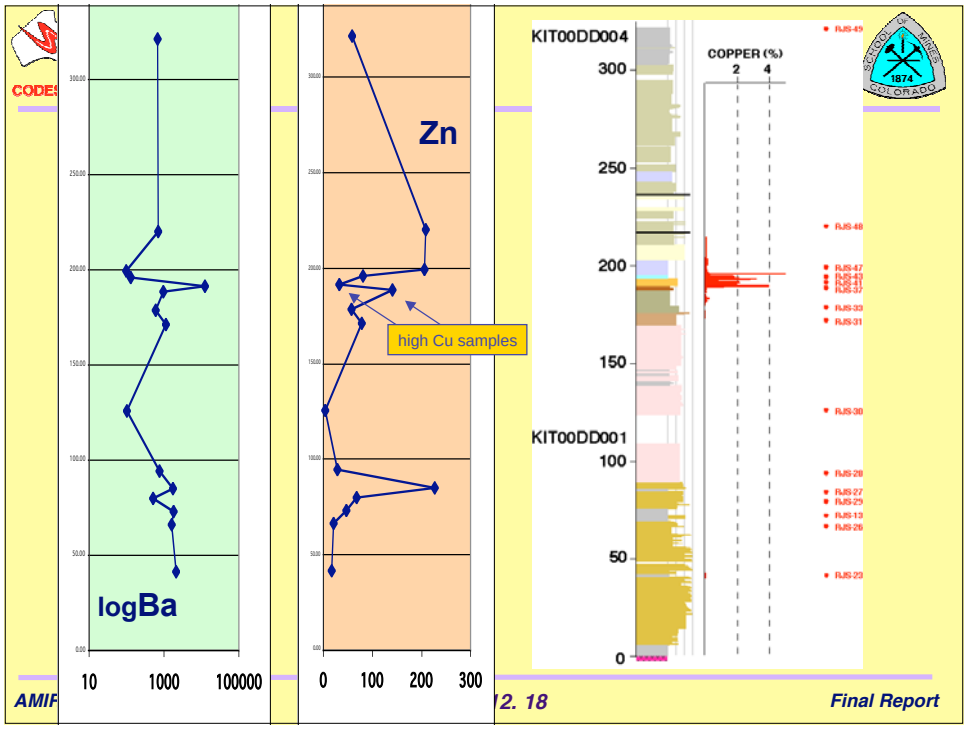
logBa
Zn
high Cu samples
KIT00DD004
KIT00DD001
COPPER (%)
10 1000 100000
0 100 200 300
0 50 100 150 200 250 300
12. 18
Final Report

Ndola West

Summary

- Cu and Co partly decoupled
- elevated Ba throughout
- moderate Zn displaced into the hangingwall and ?footwall of the Cu
- elevated Bi and Ag in a couple of the high-Cu samples
- no anomalous Mo

Mufulira

- No systematic sampling, however approximately twenty Cu-mineralised samples available
- 7 underground grab samples and mill feeds collected by Rob Scott
- 13 samples from stratigraphic DH219 (one from MW107) with >500 ppm Cu - collected by David Broughton

Mufulira

- The samples show a Cu-Bi-Ag association, but are relatively low in Co (few ppm to a few tens ppm), with some suggestion of an antithetic Cu-Co relationship
- Measurable Au (24 ppb) was present in a single Cu-Ag-Bi-rich underground sample
- Mo and Ni are low (up to 55 ppm and 25 ppm respectively
- Maximum Ba is 1226 ppm, with most samples in the range tens to hundreds ppm
- Zn and Pb are low (few ppm to few tens ppm)

Ore Shale deposits: Chambishi Basin

- Nkana-Mindola
  - Results for Ore Shale presented in Golden
  - Also Croaker PhD

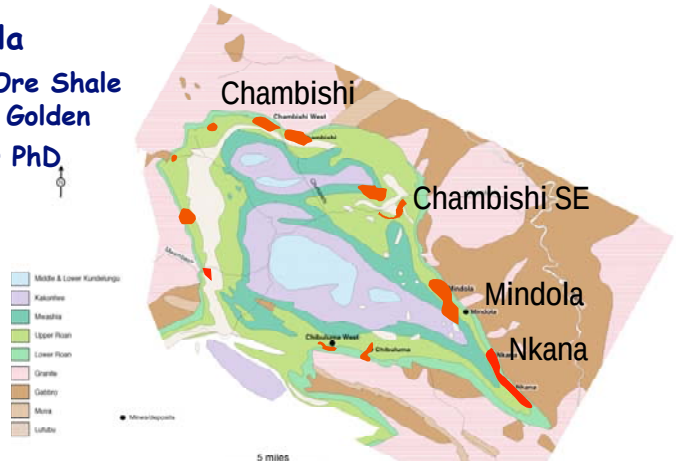

- New work here for Chambishi SE

Chambishi SE

- Large Ore Shale hosted system
- Gross lateral and vertical mineral zonation (py-po>py-po-cpy>cpy(>bn) SW > NE & down section (Fleischer, 1984)

SW to NE fence across high-grade zone & includes unmineralised (NN66), high-grade (NN42&45) and basement high (NN47)

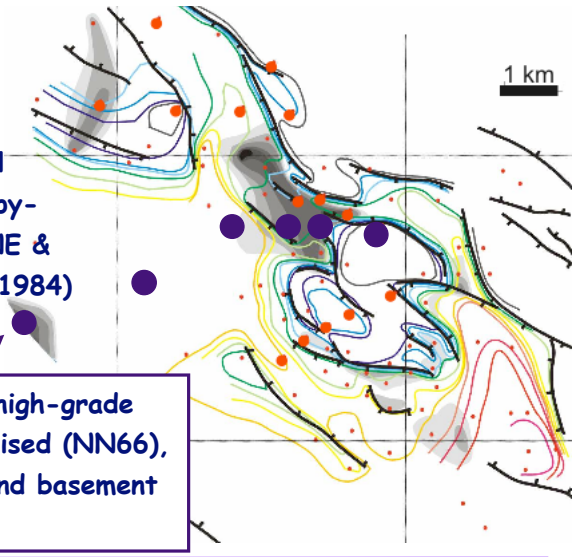

AMIRA /ARC P544 Slide 12. 23 Final Report

Chambishi SE

+ 2 'barren' holes (NN60 & 69) were OS pinches outs to the NW (becomes biotitic sandstone within a coarse-grained apron of well-sorted evaporitic sandstone and conglomerate)

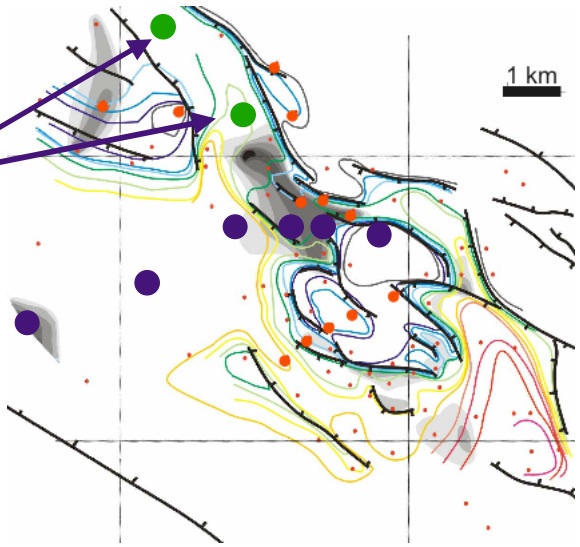

AMIRA /ARC P544 Slide 12. 24 Final Report

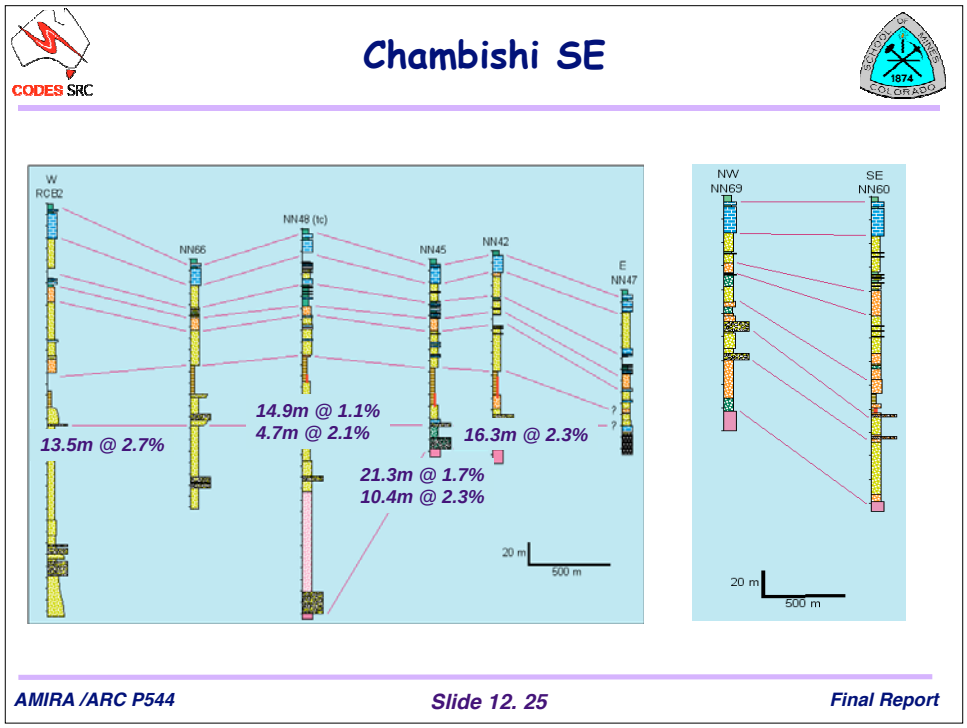
CODES SRC
Chambishi SE
W
RCB2
NN66
NN48 (tc)
NN45
NN42
E
NN47
13.5m @ 2.7%
14.9m @ 1.1%
4.7m @ 2.1%
21.3m @ 1.7%
10.4m @ 2.3%
16.3m @ 2.3%
20 m
500 m
NW
NN69
SE
NN60
20 m
500 m
AMIRA /ARC P544
Slide 12. 25
Final Report

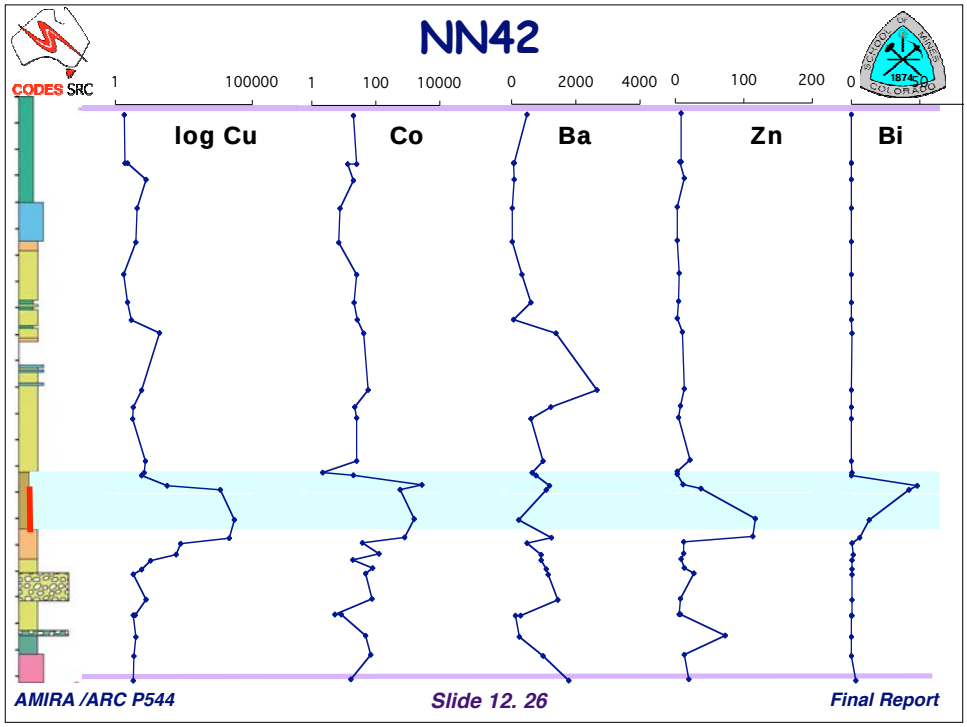
CODES SRC
NN42
1
100000
1
100
10000
0
2000
4000
0
100
200
0
log Cu
Co
Ba
Zn
Bi
AMIRA /ARC P544
Slide 12. 26
Final Report

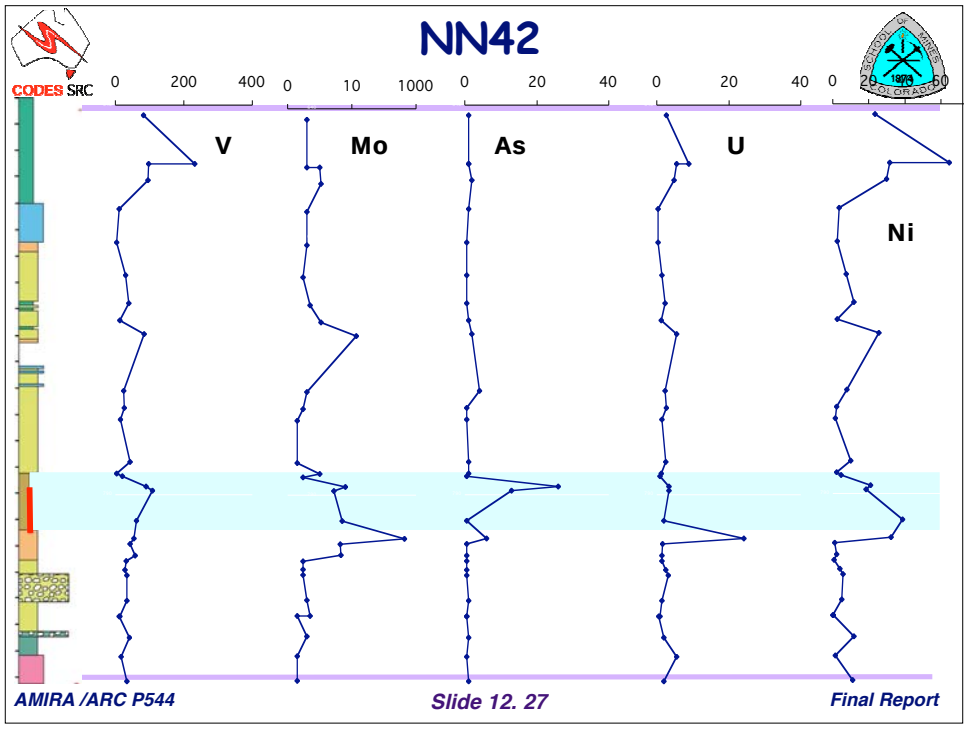
NN42
CODES SRC
0
200
400
0
10
1000
0
20
40
0
20
40
0
20
50
V
Mo
As
U
Ni
AMIRA /ARC P544
Slide 12. 27
Final Report

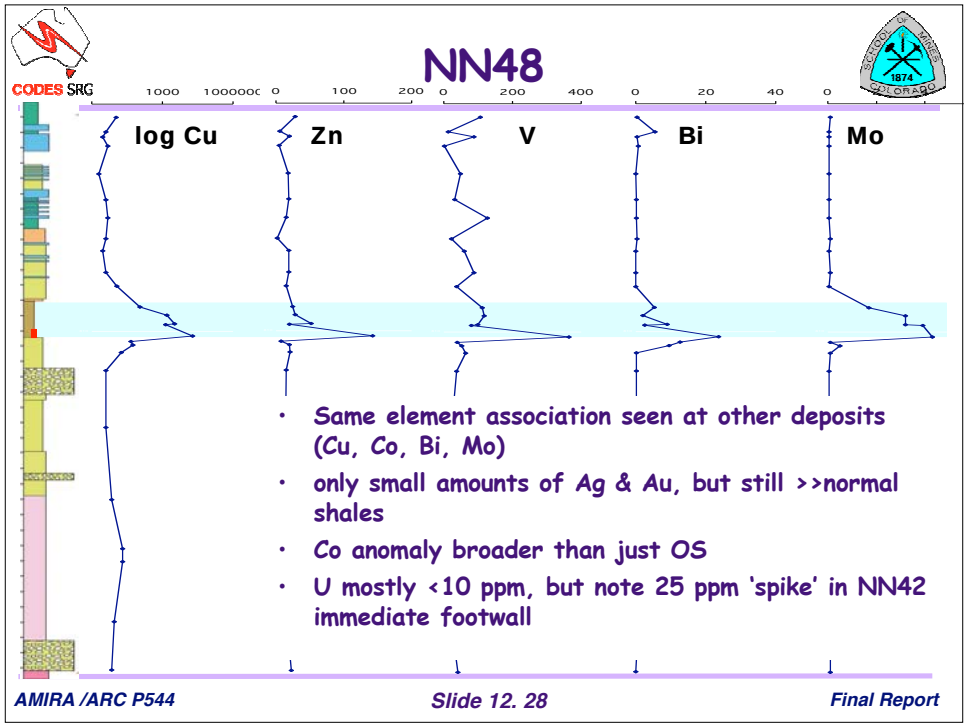
NN48
CODES SRC
1000
1000000
0
100
200
0
200
400
0
20
40
0
log Cu
Zn
V
Bi
Mo
• Same element association seen at other deposits (Cu, Co, Bi, Mo)
• only small amounts of Ag & Au, but still >>normal shales
• Co anomaly broader than just OS
• U mostly <10 ppm, but note 25 ppm 'spike' in NN42 immediate footwall
AMIRA /ARC P544
Slide 12. 28
Final Report

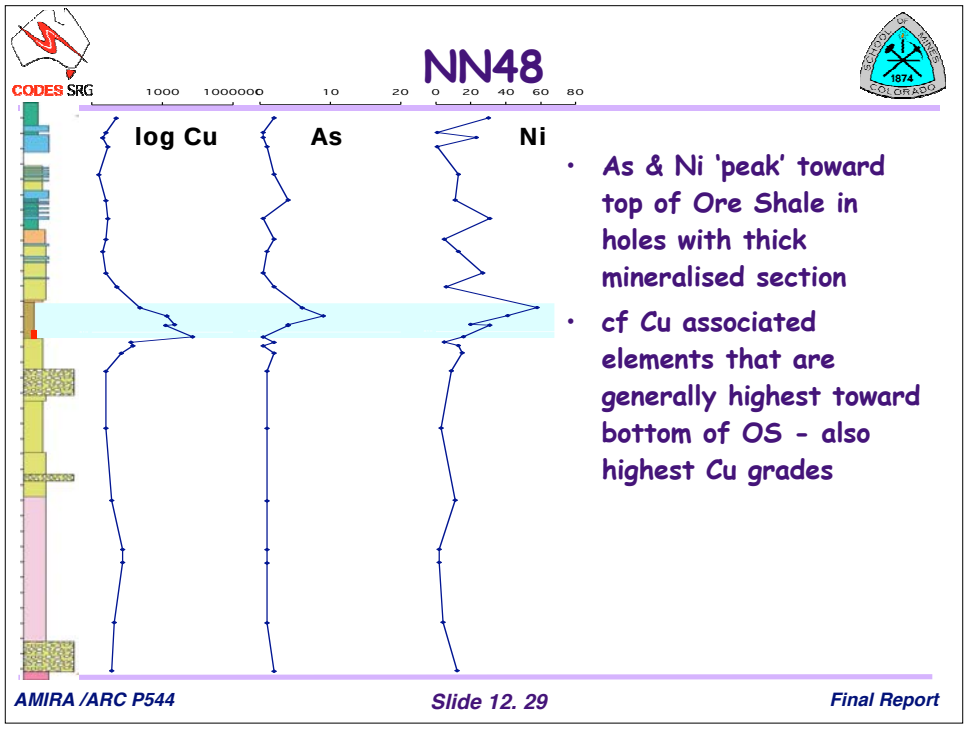
CODES SRG
NN48
1000
1000000
10
20
0
20
40
60
80
log Cu
As
Ni
• As & Ni 'peak' toward top of Ore Shale in holes with thick mineralised section
• cf Cu associated elements that are generally highest toward bottom of OS - also highest Cu grades
AMIRA /ARC P544
Slide 12. 29
Final Report

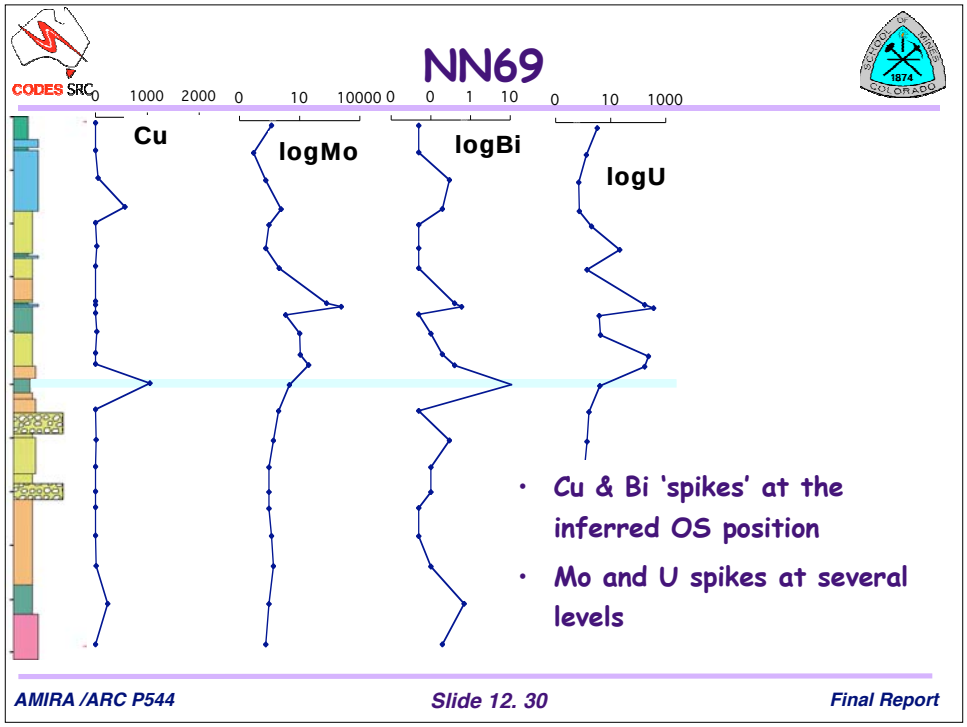
CODES SRC
NN69
0
1000
2000
0
10
10000
0
0
1
10
0
10
1000
Cu
logMo
logBi
logU
• Cu & Bi 'spikes' at the inferred OS position
• Mo and U spikes at several levels
AMIRA /ARC P544
Slide 12. 30
Final Report

Main conclusions

·(as well as Cu and Co) ZCB ores contain, or are associated with, a group of other chalcophile elements:

Ag, Bi, Mo, U, W,(locally Au, Pt, Pd), ± ?Ni ?V

»»» *OXIDISED FLUID*

·Zn and Pb are (mostly) low in the ores

·in detail, minor element distribution is complex, but patterns are recognisable in smaller and/or less deformed deposits e.g., laterally at Mwambashi B, vertically at Chambishi SE

·some elements 'kick' sporadically away from the areas of mineralisation e.g., Mo, U

Main conclusions (con)

- chalcophile element patterns are a manifestation of the interplay of multiple processes operating at several scales
- ore-forming fluids were not point-sourced, but part of a complex regional fluid flow operating over long periods of time

HENCE

- large volumes of altered rocks,

BUT

- because sulfide precipitation was reductant limited then chalcophile elements were not fixed in oxidised Roan rocks

  (rocks that have otherwise been strongly altered by transient (?ore) fluids)

- Co may be an exception

  (e.g., 'barren gap' & h/w samples with anomalous Co)

Main conclusions (con)

- (permeable) carbonaceous Ore Shale facies were a good trap for chalcophile metals
- arenite facies of the Roan needed 'mobile' reductants to trap chalcophile metals
- 'spikey' chalcophile element patterns may reflect an erratic and/or limited distribution of reductant
- ore-associated metals that display 'organophile' behaviour (e.g., V, Ni, Mo, Au, PGE, ?Bi,) may have a different source to chalcophile metals introduced by the Cu fluid(s)
- ores may have a contribution of trace metals inherited from early diagenetic Fe sulfides

Summary

• Cu, Co, Ag, Bi and Au & Mo are 'ore-association' elements:

cf 'average shale':

Cu - 100 to 1000x, Ag - ?100, Co - 50, Bi - ?20, Au - 1 to 10

•There may be a contribution of some 'organophile' elements (PGE, Au, V, Mo ???others) from hydrocarbons in arenite deposits or original organic matter in the Ore Shale, but hard to quantify

• U can be anomalous near ore, but also elevated in 'distal' samples; spikes rather than a smooth halo

•Cu is still the best 'vector' to ore, but in a greenfields areas 'spikey' U, Mo, and Bi would give added encouragement

•BIG & (probably) LONG LIVED pervasive hydrothermal system, so halos are BIG

Controls on mineral zones at Konkola mine

David Broughton
Colorado School of Mines

The Konkola (Kirilabombwe) mine in the northernmost Zambian Copperbelt consists of a single orebody mined from two shafts, #1 (South) and #2 (North). The shafts are separated by a barren gap which was originally thought to define separate north and south orebodies, however these proved to be continuous at depth (Slides 3, 4). Compilation of existing drill hole data and selected logging of available core allows a re-evaluation of the stratigraphic and structural setting of the mineralisation, and of the Cu and Co mineral zones within the deposit.

The majority of the Konkola deposit occurs between two major NNW trending faults, the Kawiri-Lubengele to the north, and the Fitwaola to the south (Slide 4). East of the deposit along these faults, the footwall formations to the ore shale are metres to tens of metres thick, and in places the ore shale sits on the basement. Along the Kawiri-Lubengele fault, and in the barren gap, the ore shale is commonly sandier than in the deposit area (where it is predominantly siltstone), and mineralisation is weak or absent. In the Konkola mine area, however, the footwall succession is approximately 450 m thick. This suggests that the deposit area represents a graben, whereas the areas to the east are basement highs.

In the mine area, the ore shale is immediately underlain by a metres-thick footwall conglomerate, which locally carries ore (Slides 5, 6). The distribution of the conglomerate, and its thickness variations, suggest the presence of NNW and NE faults active prior to ore shale sedimentation (Slide 5). The limits of the footwall conglomerate coincide reasonably well with the limits of economic mineralisation, particularly in the barren gap, along the Fitwaola fault, and at the northwestern edge of the mineralisation (pyritic fringe in Slide 7). Note that the northern edge of the barren gap and the eastern edge of the North orebody are on the same NE structural trend, which defines the eastern limit of economic mineralisation in the northern part of the Konkola mine. The distribution of economic mineralisation within the footwall conglomerate is shown in Slide 6, and again demonstrates NE and NW structural control.

The distribution of mineral zones at Konkola shows a systematic relationship to the NE and NNW faults (Slides 7, 9, 10). The barren gap represents an uplifted block where the ore shale is sandy and lacks carbonate, the footwall conglomerate is absent, Cu-Co mineralisation is weak or absent, and hematite is present. To the northwest and perpendicular to the NE boundary of the barren gap, there is a moderately developed mineral zoning from proximal bornite-dominant to more distal bornite-chalcopyrite to pyrite at the northwest margin of the orebody (Slide 7). Along the crest of the Kirilabombwe Anticline, this pattern is disrupted by secondary malachite mineralisation related to anticlinal fractures. Thus, the two bornite-dominant zones on either side of the anticline were probably continuous prior to the effects of weathering. The lateral zoning matches that expected from a simple redox control on mineralisation, with oxidising metalliferous fluids precipitating copper-rich to copper-poor sulfides in a progressive fashion as they moved laterally away from a fault- and lithologically-controlled redox boundary.

The distribution of mineralisation also can be examined in section parallel to the zoning (Slides 9, 10). Close to the redox boundary, copper mineralisation

is confined to the middle portion (carbonate-bearing C and D facies) of the ore shale (siltstone), and often the copper grades increase upwards toward the top of the ore zone. In a model whereby mineralisation occurs via oxidation of organic carbon, and produces ore-related (and isotopically light) carbonate, this would suggest that organic carbon was restricted to the uppermost facies of the siltstone. A similar mechanism is interpreted at the Musoshi ore shale deposit, some 15 km to the northwest. There, the base of mineralisation also occurs above the base of the siltstone, immediately above a visible redox boundary between red hematitic and grey reduced siltstone (Lefebvre and Tshiauka, 1986). Vertical zoning is in general poorly developed at Konkola, perhaps because the reductant ore shale horizon is both overlain and underlain by oxidised hematitic sandstones and conglomerates. However, in the western part of the drill section some of the ore intersections pass upwards through a zoned bornite–chalcopyrite–pyrite sequence, similar to that seen along strike.

In the western half of the drill section, mineralisation commonly occurs throughout the ore shale and footwall, and locally in the hangingwall. In part this appears due to secondary (supergene) redistribution, as the footwall ore is composed primarily of chalcocite-malachite. There may also be other, more localised structural controls, as is suggested by the plan distribution of footwall copper mineralisation, and cobalt mineralisation (Slides 6, 8).

Cobalt mineralisation is unequally distributed throughout the deposit, forming high-grade zones apparently related to structures (Slide 8). A high-grade (>10% Co) zone parallels the Fitwaola fault, and is approximately coincident with a zone of NNW trending folds at the south end of the ore-body, related to the fault. A second, NE-trending, high-grade zone occurs in the west-central part of the deposit, and parallels the southeastern limit of the footwall mineralisation. A third zone occurs in the vicinity of the Lubengele fault. The distribution of cobalt mineralisation does not vary systematically with that of copper, suggesting the possibility of a different precipitation mechanism and/or temporal control. An example of this is seen in drill hole KLB145, where carrollite is dominant in subvertical sulfide–dolomite veins.

These findings indicate that exploration for and within copper systems will be aided by targeting basin-controlling faults, defined by across-fault changes in sediment thickness and lithology, and by mapping the relative distribution of hematitic, pyritic and Cu-sulfide mineralisation. These faults can be readily recognised despite significant modification during penetrative deformation.

Reference

Lefebvre, J.J. and Tshiauka, T., 1986. Le Groupe de Mines a Lubembe, Shaba, Zaire. Annales de la Societe geologique de Belgique, T. 109, pp. 557-571.

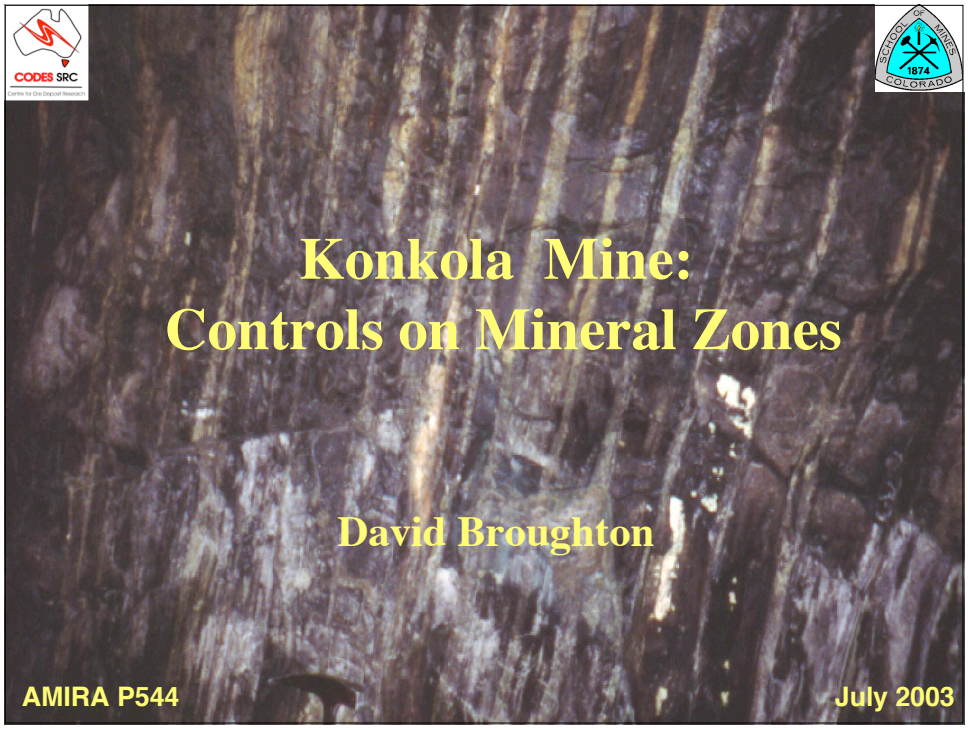
CODES SRC
SCHOOL OF MINES
1874
COLORADO
Konkola Mine:
Controls on Mineral Zones
David Broughton
AMIRA P544
July 2003

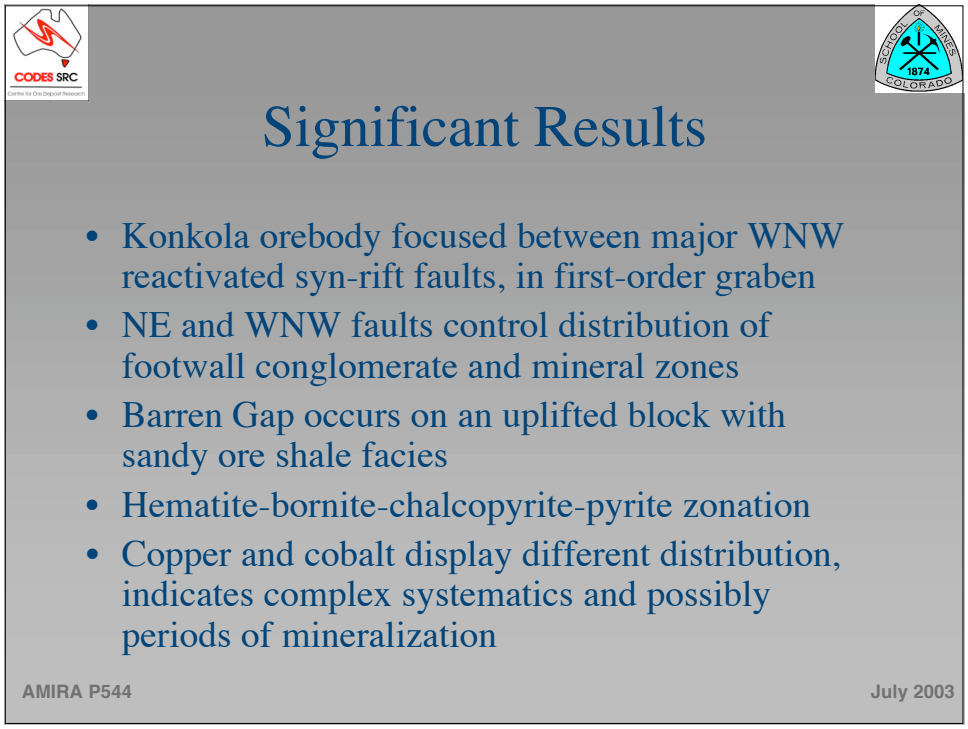
CODES SRC
SCHOOL OF MINES
1874
COLORADO
Significant Results
• Konkola orebody focused between major WNW reactivated syn-rift faults, in first-order graben
• NE and WNW faults control distribution of footwall conglomerate and mineral zones
• Barren Gap occurs on an uplifted block with sandy ore shale facies
• Hematite-bornite-chalcopyrite-pyrite zonation
• Copper and cobalt display different distribution, indicates complex systematics and possibly periods of mineralization
AMIRA P544
July 2003

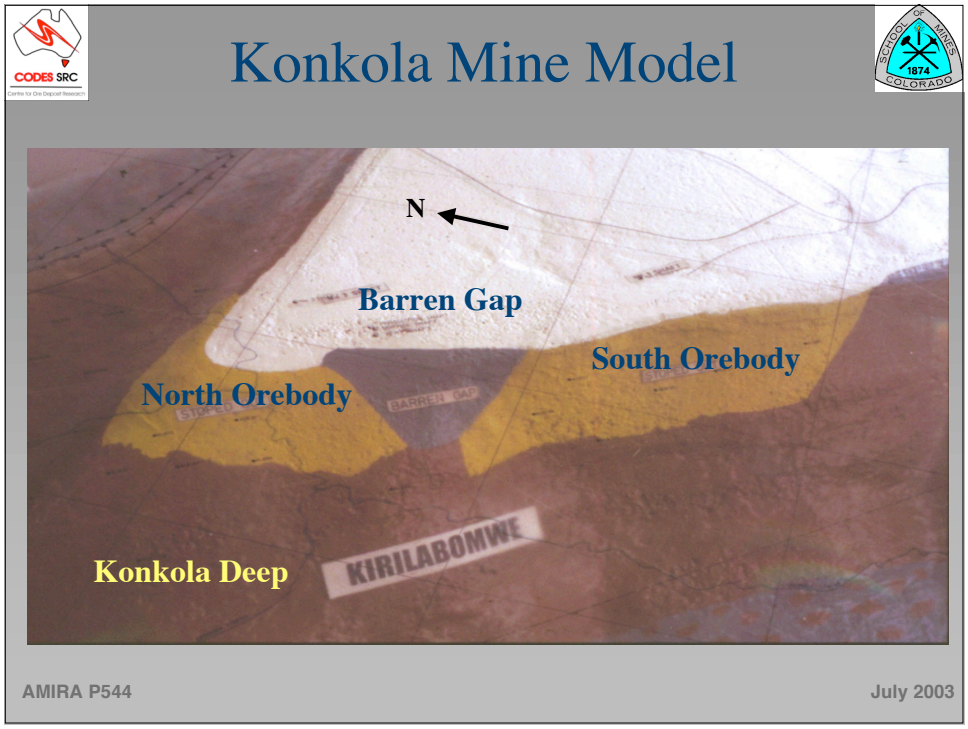
Konkola Mine Model
N
Barren Gap
South Orebody
North Orebody
Konkola Deep
KIRILABOMWE
AMIRA P544
July 2003

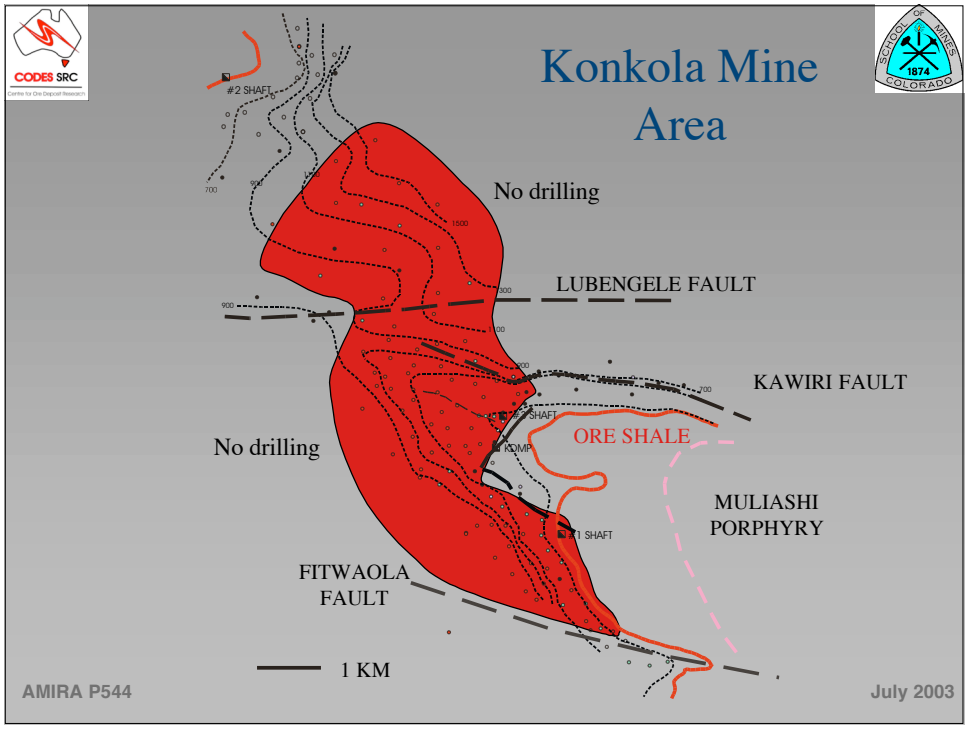
Konkola Mine Area
#2 SHAFT
No drilling
LUBENGELE FAULT
KAWIRI FAULT
ORE SHALE
No drilling
MULIASHI PORPHYRY
FITWAOLA FAULT
1 KM
AMIRA P544
July 2003

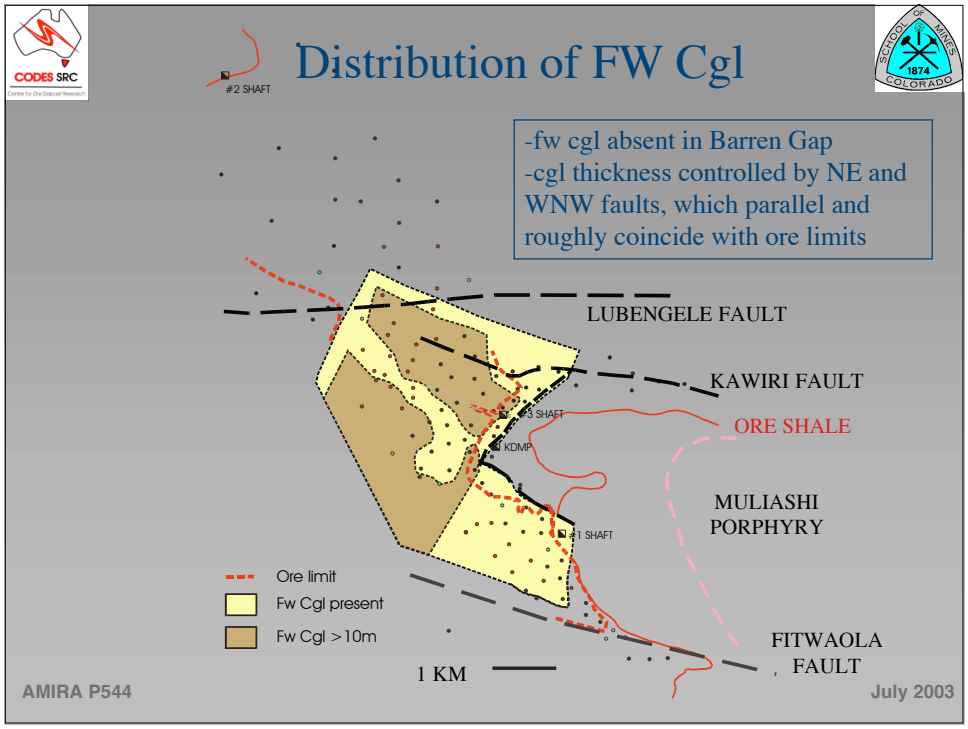
Distribution of FW Cgl
#2 SHAFT
-fw cgl absent in Barren Gap
-cgl thickness controlled by NE and WNW faults, which parallel and roughly coincide with ore limits
LUBENGELE FAULT
KAWIRI FAULT
ORE SHALE
MULIASHI PORPHYRY
FITWAOLA FAULT
#3 SHAFT
KDMP
#1 SHAFT
Ore limit
Fw Cgl present
Fw Cgl >10m
1 KM
AMIRA P544
July 2003

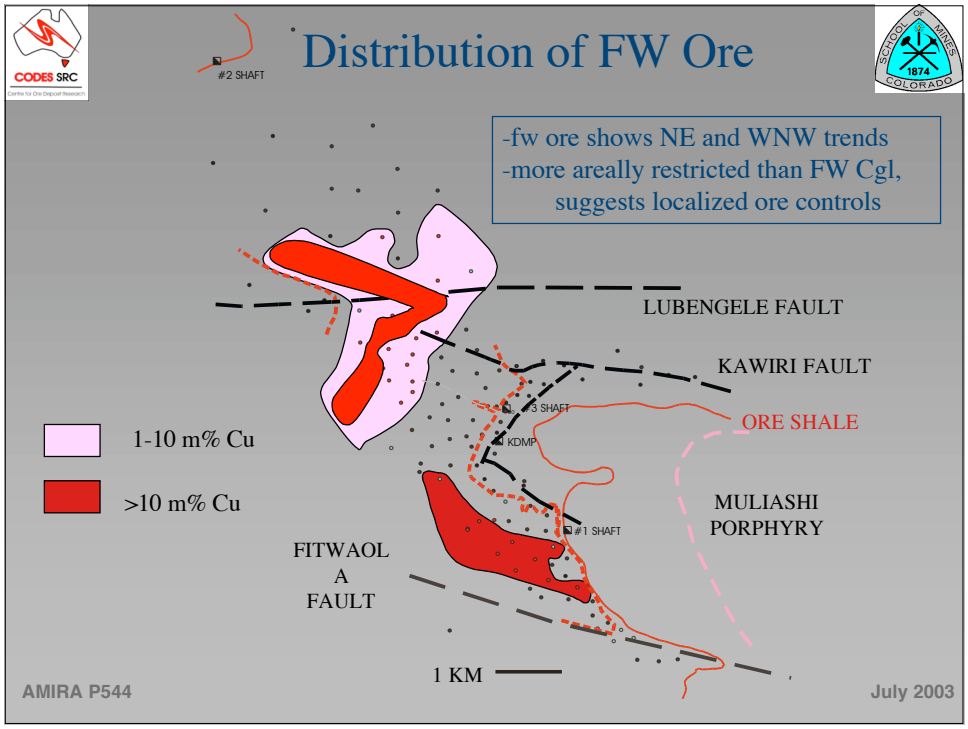
Distribution of FW Ore
#2 SHAFT
-fw ore shows NE and WNW trends
-more areally restricted than FW Cgl, suggests localized ore controls
LUBENGELE FAULT
KAWIRI FAULT
ORE SHALE
MULIASHI PORPHYRY
FITWAOLA FAULT
#3 SHAFT
KDMP
#1 SHAFT
1-10 m% Cu
>10 m% Cu
1 KM
AMIRA P544
July 2003

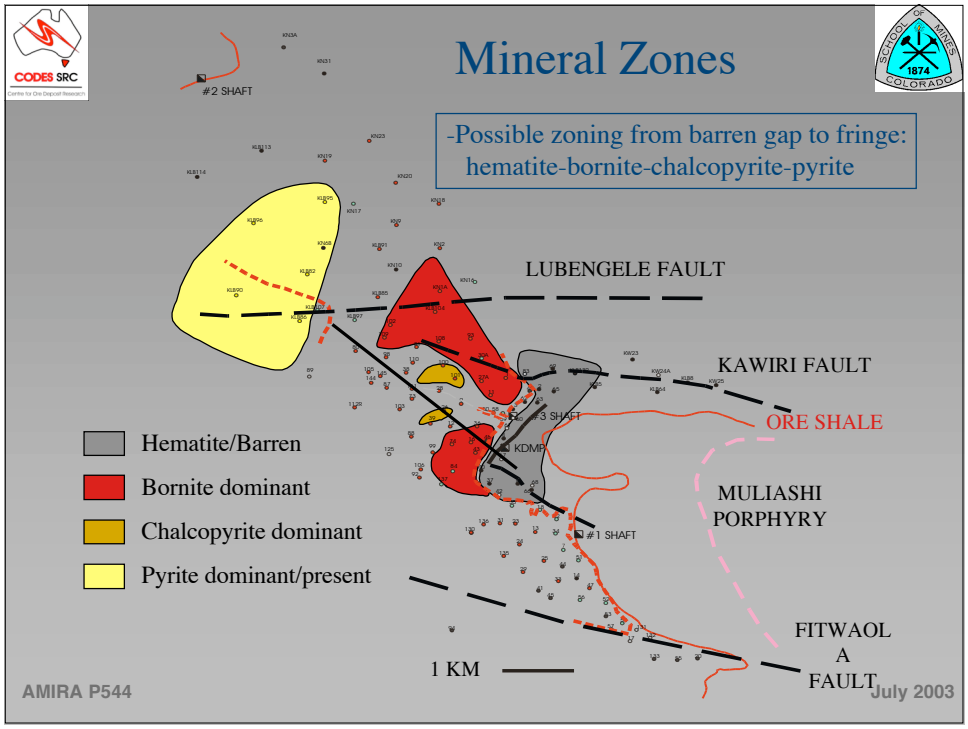
Mineral Zones
-Possible zoning from barren gap to fringe:
hematite-bornite-chalcopyrite-pyrite
#2 SHAFT
LUBENGELE FAULT
KAWIRI FAULT
ORE SHALE
#3 SHAFT
KDMP
#1 SHAFT
MULIASHI
PORPHYRY
FITWAOL
A
FAULT
Hematite/Barren
Bornite dominant
Chalcopyrite dominant
Pyrite dominant/present
1 KM
AMIRA P544
July 2003

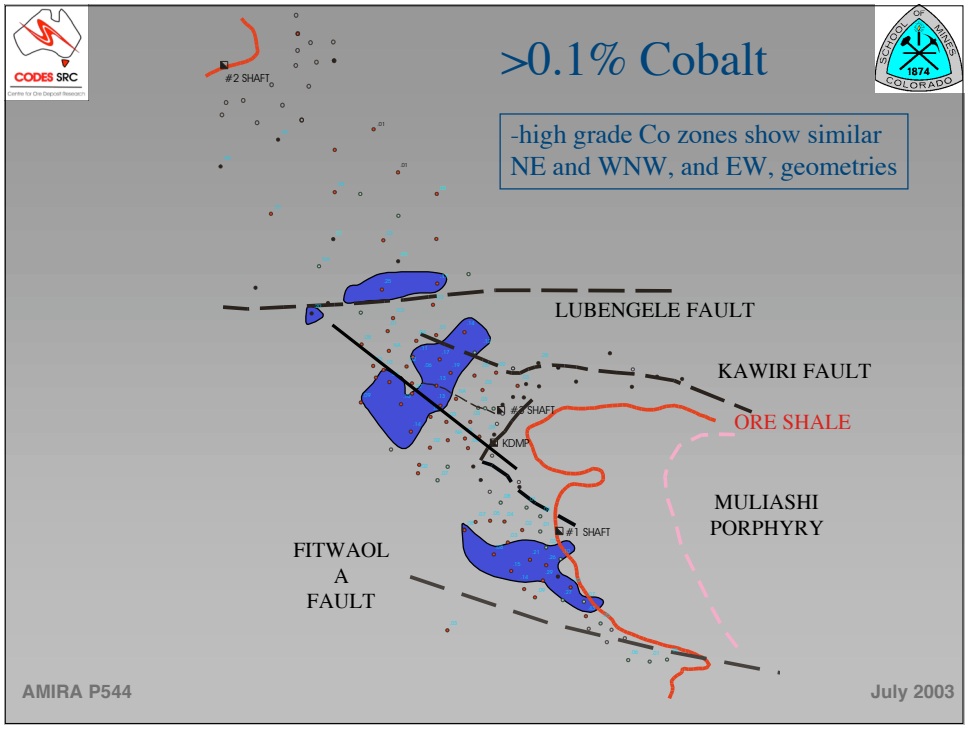
>0.1% Cobalt
-high grade Co zones show similar
NE and WNW, and EW, geometries
#2 SHAFT
LUBENGELE FAULT
KAWIRI FAULT
ORE SHALE
#3 SHAFT
KDMP
#1 SHAFT
MULIASHI
PORPHYRY
FITWAOL
A
FAULT
AMIRA P544
July 2003

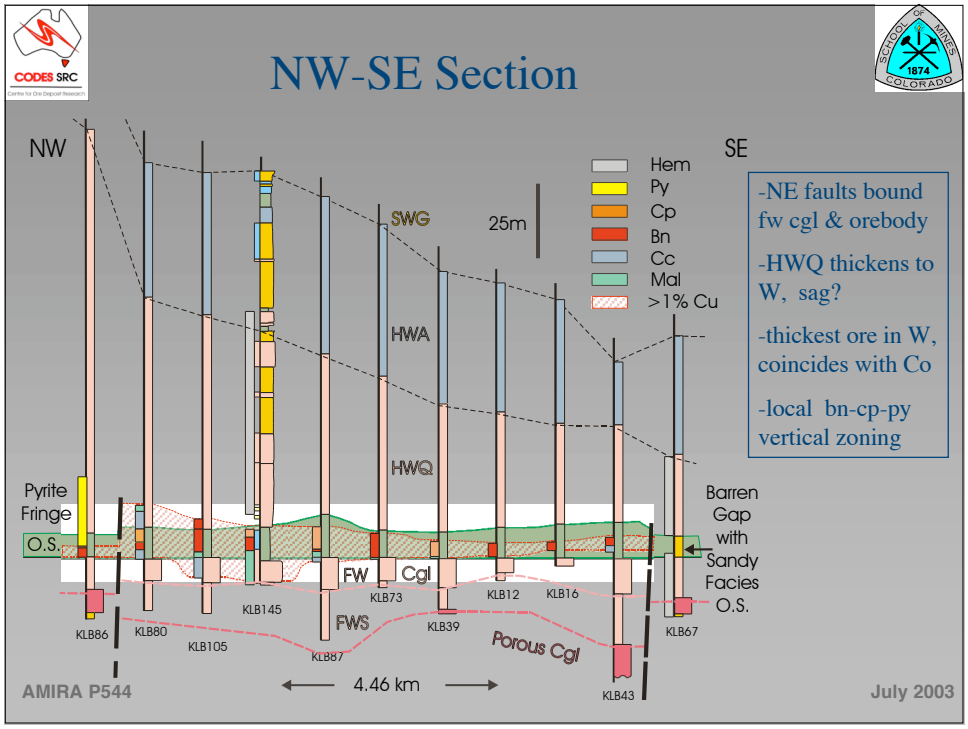
NW-SE Section
CODES SRC
NW
SE
Hem
Py
Cp
Bn
Cc
Mal
>1% Cu
SWG
25m
HWA
HWQ
-NE faults bound fw cgl & orebody
-HWQ thickens to W, sag?
-thickest ore in W, coincides with Co
-local bn-cp-py vertical zoning
Pyrite Fringe
O.S.
FW
Cgl
FWS
Porous Cgl
Barren Gap with Sandy Facies O.S.
KLB86
KLB80
KLB105
KLB145
KLB87
KLB73
KLB39
KLB12
KLB16
KLB67
KLB43
4.46 km
AMIRA P544
July 2003

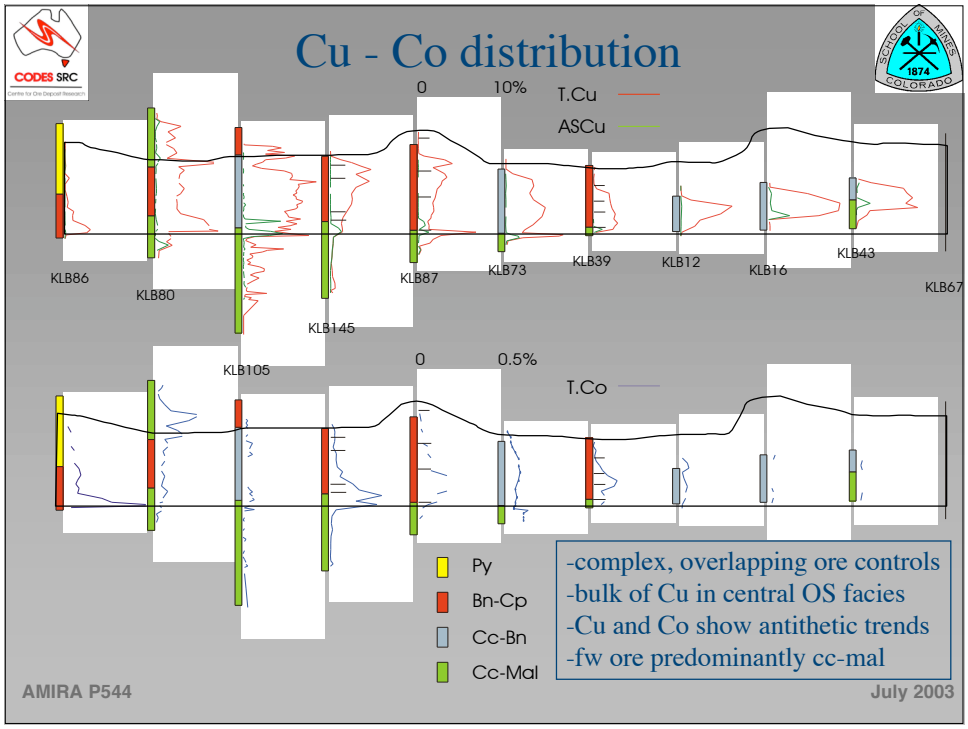
Cu - Co distribution
CODES SRC
0
10%
T.Cu
ASCu
KLB86
KLB80
KLB105
KLB145
KLB887
KLB73
KLB39
KLB12
KLB16
KLB43
KLB67
0
0.5%
T.Co
Py
Bn-Cp
Cc-Bn
Cc-Mal
-complex, overlapping ore controls
-bulk of Cu in central OS facies
-Cu and Co show antithetic trends
-fw ore predominantly cc-mal
AMIRA P544
July 2003

Conclusions

-WNW and NE faults control pre-, and to some extent post- Ore Shale sedimentation, are reactivated during Lufilian deformation

-Barren gap occurs on basement high, with sandy Ore Shale facies

-Cu and Co mineralization is controlled by NE and WNW faults

-Available data suggests presence of vertical and lateral hematite-bornite-chalcopyrite-pyrite zoning, but zones are locally complex

-Highest primary Cu grades commonly occur in the middle and upper part of the Ore Shale

-High grade Co zones show NE trends, but in detail high Co often not related to high grade Cu, suggesting different mechanisms or timing

AMIRA P544 July 2003

Sulfide mineral zonation and chemistry at Konkola North

Nicky Pollington and Rob Scott
Centre for Ore Deposit Research, University of Tasmania

Introduction and rationale

Slide 3: The overall aims for the PhD project are to elucidate the sedimentology, mineral paragenesis and geochemistry of the Konkola North deposit. In order to do this a number of specific aims were defined, one of which was to understand the sulfide mineral paragenesis and zoning, with particular reference to chalcocite, and determine a criteria for distinguishing hypogene and supergene chalcocite.

This report aims: to document the distribution of mineralisation vertically and horizontally within the ore shale, to geochemically characterise the different mineralised zones and to use LA-ICPMS trace element geochemistry and textural observations to distinguish mineral zones and supergene from hypogene chalcocite.

Slide 4: The mineral distribution is important because it has been used in the past in the Copperbelt and other sediment hosted mineral deposits to support genetic models for the emplacement for the ore. According to the syngenetic theory the zoning was produced as a result of proximity to the paleoshoreline with chalcocite deposited first in the shallowest and most oxidised waters and pyrite in the deepest and least oxidised (Garlick 1976).

The diagenetic interpretation is that the gradual infiltration of oxic metalliferous brines originating from evaporites extracted the ore metals from underlying redbed aquifers and then deposited them into reduced sediments (Kirkham 1989). This gradual infiltration results in different sulfide phases being deposited in overlapping zones upward and outward from the initial infiltration site. The zoning generally described for this type of deposit is hematite –chalcocite–chalcopyrite+bornite –sphalerite+galena–pyrite (Kirkham 1989).

Research plan

Slide 5: Detailed investigation of the sulfide distribution was carried out with thorough logging, thin section work and interpretation of wholerock geochemistry. This work highlighted the zoning and the gross distribution of the various sulfide phases and was then used to select appropriate samples which covered all the mineral zones and associations. First pass investigation of major element and limited trace element variations was carried out using the electron microprobe and the results from this were used to target the samples for further investigation using the LA-ICPMS.

Mineral distribution at Konkola North

Slide 6: Throughout the Konkola North deposit the mineralisation is confined to the ore shale apart from where it has been remobilised and supergene minerals are present in either the immediate footwall or hangingwall. The ore shale can vary from 2 to 15 metres thick and is on average 6 metres. There are three main mineralised zones, which for the purpose of this study have been termed – East, South and Far South.

Slide 7: In the East zone (also termed the Bornite – Chalcocite zone) the ore shale is a dark grey fine

silt with abundant specular haematite throughout and no leaching or iron and manganese staining present. In this area the sulfides are predominantly chalcocite and bornite, which is generally pink to purple, and rare malachite is present. Mineralisation tends to start 1–2 m above the footwall contact and wholerock geochemistry shows that sulfur is low throughout.

Slide 8: In the South or Chalcopyrite – Pyrite zone, the ore shale is commonly leached and abundant iron and manganese oxides are concentrated on fractures and the footwall contact. The mineralisation consists of chalcopyrite, pyrite and brown bornite in order of abundance and minor chalcocite is also present. Outside the oxidised zones the copper to sulfur ratio is generally one to one. On the edges of these zones and particularly the footwall contact, copper is significantly enriched and sulfur is depleted. Mineralisation almost always starts immediately on the footwall contact.

Slide 9: The Far South or Cobalt zone is significantly leached and there are abundant iron and manganese oxides throughout the ore shale. The sulfide minerals present are chalcopyrite, bornite and chalcocite, with secondary malachite, pseudomalachite ($Cu_5(PO_4)_2(OH)_4$), wad (manganese oxides with cobalt) and native copper also being common. Consequently the copper and sulfur distribution is variable throughout the ore shale. Cobalt is present in the far south, mostly associated with the wad and can be up to 0.5%.

Sul de chemistry

Slide 10: The trace element compositions of sulfides is determined by the physicochemical conditions of the ore fluid at the time of mineral deposition and thus can be used diagnostically to clarify different generations of mineralising events, Loftus-Hills and Solomon (1967) and Griffen et al (1991). Thus the trace element characteristics can be used to help understand the distribution of the sulfides when a number are present and the paragenetic history is not obvious. With this in mind the first step in this study is to determine the trace element characteristics of all the main sulfides present which define the mineral zones at Konkola North. The techniques used to address this problem include the electron microprobe and Laser Ablation ICPMS.

Slide 11: The electron microprobe housed in the Central Science Laboratory at the University of Tasmania has very high spatial resolution is non destructive and was used in this study to analyse for S, Fe, Co, Ni, Cu, As, Se, Ag, Ba, Pb and Bi. The LA-ICPMS facility housed in the School of Earth Sciences at the University of Tasmania was used to measure Ti, V, Mn, Fe, Co, Ni, Zn, Ge, As, Se, Zr, Mo, Pd, Ag, Cd, Sn, Sb, Te, La, Pt, Au, Hg, Pb^{204}, Tl, Pb^{206}, Pb^{207}, Pb^{208}, Bi, Th. This destructive technique provides high spatial resolution and very low detection limits which can be sub-ppm, dependent on spot size and calculated for every sample. Copper was used as the internal standard as it was already known from the microprobe data and the results were quantified by reference to a synthetic in house standard.

Slide 12: An example of the 90-second spectra resulting from the laser ablation technique is shown in Slide 12. This is the result of a line from the edge of the sulfide grain shown, moving from the chalcocite on the edge through the bornite and ending in the chalcopyrite in the centre. It can be seen quite clearly where the different minerals were encountered and particularly how Pb, Bi, Fe and Ag vary within each mineral. Also a feeling for how the destructive nature of the ablation technique can be dealt with in terms of understanding when and if the primary sulfide target has been burnt through and contamination with surrounding material and / or other sulfides has occurred. Because this is very easily observed, only the data relevant to the target sulfide can be separated from the contamination by restricting the time frame over which the statistics are carried out. Inclusions can also be dealt with in this way as they are equally as obvious.

Slides 13 and 14: The three main sulfide types which are present in the deposit are chalcopyrite, bornite and chalcocite. Pyrite is not abundant and, as only a small dataset has been compiled so far the information has not been included in this report. In order to compare the trace elements between the sulfides they have been plotted against Fe in scatterplots and a number

of systematic variations are evident, particularly with Ag, Pb, Bi, Zn and Sn. Chalcopyrite is distinguished by low average Ag (0.4 ppm), Bi (1.1 ppm) and Pb (5.5 ppm), high Sn (7.5 ppm) and variable Zn. Bornite has high Bi (212 ppm), medium Ag (9.1 ppm) and Pb (30.4 ppm), and low Sn. Chalcocite is more variable and tends to have two or three populations evident, and hence a more detailed investigation of the chalcocite group is required.

Detailed investigation of variations within each sulfide group was then carried out.

Slide 15: Chalcopyrite is relatively consistent both texturally and in most trace element contents apart from Zn which is higher in the samples closer to the East zone. This has not been fully tested as yet with data only covering five holes. Further systematic sampling of holes in a fence through the deposit will be carried out to test if this zoning is real.

Slide 16: Bornite has one distinct textural variation within the deposit, when it is associated with chalcocite it is pink to purple and when associated with chalcopyrite it is brown. The trace element variations between these have also not been fully tested as intergrowths are very fine and many of the analyses done to date are not clean and detection limits are low. Although there is a variation in the copper content, 63–65% in the pink and 58–61% in the brown. Pb and As also appear to vary with the pink bornite containing 21.2–199 ppm Pb 2.8–33 ppm As and the brown bornite containing 0.2–10 ppm Pb and 0.4–13.9 ppm As.

Slide 17: Peak metamorphic temperatures >400°C have implications for the interpretation of internal textural and compositional features of the copper sulfides. Importantly complex intergrowths of bornite and chalcocite are exsolution features formed during cooling following peak metamorphism. At 400°C, bornite displays complete solid solution between compositions approximating ideal bornite (Cu_5FeS_4) and S-, Fe-poor compositions similar to chalcocite-digenite in low temperature assemblages. Bornite has a limited compositional range at low temperature implying grains which exsolved chalcocite-digenite following metamorphism were originally represented by chalcocite + bornite aggregates. Although primary grain textures are unlikely to be preserved, sulfide assemblages with intermixed texturally identical chalcocite-purple bornite and orange-brown bornite ± chalcopyrite or chalcopyrite must reflect original disequilibrium assemblage in which S^{2-} availability changed progressively or fluctuated during mineralisation.

Chalcocite is quite variable in both textural associations and trace element characteristics. Three groups are described on textural associations: (1) rimmed by haematite (Slide 18), (2) intermixed with bornite (Slide 19) and (3) 'others' which includes chalcocite with no other associated minerals visible, those with chalcopyrite cores and those which are rimming chalcopyrite, bornite or both (Slide 20). The chalcocite which is clearly associated with haematite is significantly enriched in silver, on average 30 ppm. The chalcocite which is intimately associated with bornite is significantly enriched in Pb (80 ppm), Bi (103 ppm), Fe (0.5%) and to a lesser extent Ni (2.3 ppm). The third group is obviously a combination of a number of different chalcocites and the trace elements were investigated further to see if any of them had similar enrichments as the known trace element associations. The Ag and Bi data were plotted (Slide 21) and a number of groups within this were clearly evident. A high Ag group which is interpreted to belong to the first group and be supergene in origin. The other which is high in Bi is interpreted to be part of the second group — exsolution from bornite and the process has gone to completion and all the parent bornite has been completely exsolved. Once these samples have been removed from the dataset to investigate further variations within the remaining chalcocites without any obvious textural associations two groups immediately stand out. What these variations indicate is not obvious so far and further work will be carried out on these.

Discussion

In Konkola North the three main sulfides present have distinctly different trace element characteristics. Chalcopyrite is distinguished by low Ag, Bi and Pb and high Sn. Based on a small sample set, Zn appears to have a systematic variation in relation to where in the deposit it is sampled. Two different bornite phases

are present which can be determined by colour and trace element characteristics. One phase is brown/orange and has slightly lower Fe, Pb and As content than the other which can be either pink or purple. Chalcocite exhibits a number of textural variations and trace element characteristics, the most obvious of which is associated with haematite and malachite and significantly enriched in Ag. These are all found in weathered and leached rocks and are clearly of supergene origin. The haematite rims are classic examples of the low acid nature of the oxidised fluid as the Fe has only undergone local transport once liberated from the original bornite and chalcopyrite (Anderson 1982, Clark et al. 2001). There are also a number which have the high Ag content but do not have the haematite association and thus are also interpreted to be supergene in origin however the fluids are more acidic and thus able to transport the Fe further from the site of oxidation. Thus meteoric oxidation processes have produced two secondary chalcocite phases reflecting differences in supergene fluid acidity.

Future directions

The future directions for this study include further LA-ICPMS analyses in order to increase the dataset and test the observations made so far. Once the dataset is complete the three main questions which will be addressed are:

- What is the fluid chemistry required to transport and concentrate the trace elements which define the different sulfide phases?
- Can the trace element characteristics of the primary sulfide phases be used to determine where in the deposit you are?
- Compare to other well known supergene environments – Is there a common set of elements which are concentrated in supergene chalcocite or is it deposit specific?

References

Anderson (1982) Characteristics of Leached Capping and Techniques of Appraisal. In S.R. Titely (ed) Advances in the geology of the porphyry copper deposits, south west North America, Tuscon: The University of Arizona Press

Clarke, Gemmell, Norman and Hespe (2001) Textural and geochemical distinction between supergene and hypogene Cu sulfide phases at the Mammoth copper deposit, Queensland, Australia, Mineral deposits at the beginning of the 21st Century.

Griffin, Ashley, Ryan, Sie and Sutter (1991) Pyrite geochemistry in the North Arm epithermal Ag-Au deposit, Queensland, Australia; a proton-microprobe study. The Canadian Mineralogist. 29, 185-198

Loftus-Hills and Solomon (1967), Cobalt, nickel and selenium in sulfides as an indicator of ore genesis. Mineralium Deposita, 2, 228-242.

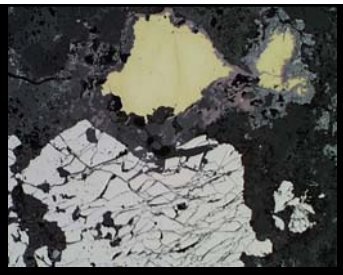

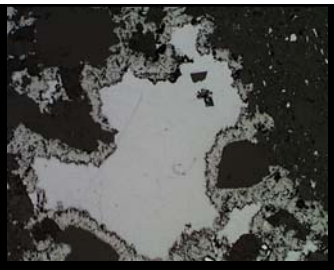

Sulphide Mineral Zonation and Chemistry at Konkola North

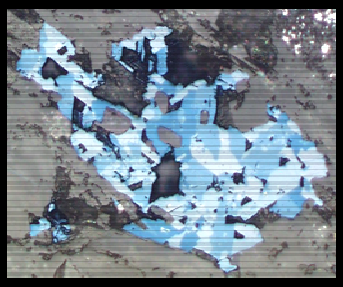

Nicky Pollington
& Rob Scott

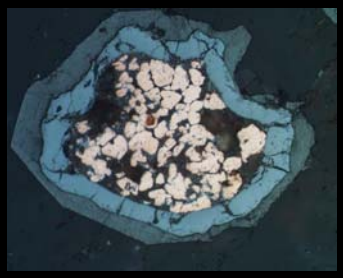

AMIRA/ARC P544 *Final Sponsors Meeting* *July 2003*

Observations

- The three main sulphides at Konkola North have distinctly different trace element characteristics
- Two different bornite phases are present with trace element variations between them
- Co-existing Cc-Bn and Cpy-Bn sulphide assemblage reflects original disequilibrium sulphide assemblage. However internal sulphide textures probably just reflect exsolution during cooling following peak metamorphism
- Meteoric oxidation processes have produced two secondary Cc phases reflecting differences in supergene fluid acidity
- In Konkola North trace elements can be used to distinguish hypogene and supergene chalcocite phases in the absence of textural evidence

AMIRA/ARC P544 *Final Sponsors Meeting* *July 2003*

PhD Project

Overall aims : to elucidate the sedimentology, mineral paragenesis and geochemistry of the Konkola North Copper deposit, Zambia

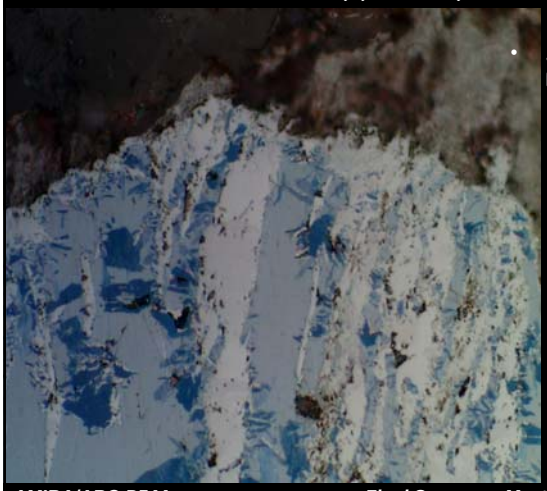

- Specific aims relevant to this report:
  - Document the distribution of mineralisation vertically and horizontally within the ore shale
  - Geochemically characterise different mineralised zones
  - LA ICPMS geochemistry and textural observations to distinguish mineral zones and supergene from hypogene Cc

AMIRA/ARC P544 *Final Sponsors Meeting* *July 2003*

Why is mineral distribution important?

Used in the past to support genetic models for the Copperbelt

Syngenetic - primary depositional characteristics due to proximity to palaeoshoreline, Cc - shallow through to Py - deep (Garlick)

Diagenetic - a result of redox variations as oxic metalliferous brines infiltrate reduced sediments (Kirkham)

Zoning generally described in sediment hosted deposits

Hm – Cc – Cpy+Bn – Sp+Gn - Py

AMIRA/ARC P544 *Final Sponsors Meeting* *July 2003*

Research Plan

Detailed investigation of the variation in sulphide distributions throughout Konkola North from logging, thin section work and interpretation of wholerock geochemistry

Careful selection of samples which cover all the mineralised zones and associations

Testing firstly with Probe for major (and some minor) element compositions

LA ICPMS of specifically targeted sulphides

What is the mineral distribution at Konkola North

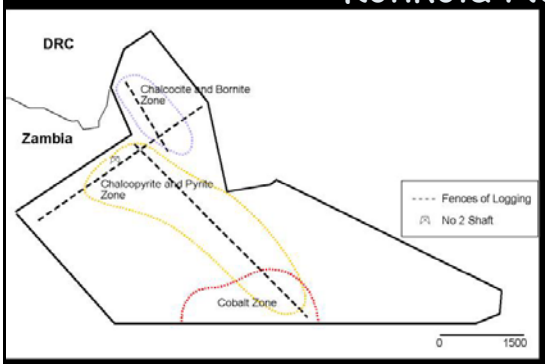

- East - Chalcocite and Bornite (rare malachite)
- South – Pyrite, Chalcopyrite and Bornite (malachite and chalcocite associated with oxidised fractures)
- Far south – Chalcopyrite and abundant secondary minerals
  - malachite
  - pseudomalachite ($Cu_5(PO_4)_2(OH)_4$)
  - Wad (Mn Oxides with Cobalt)

AMIRA/ARC P544 *Final Sponsors Meeting* *July 2003*

Bn - Cc Zone

- Dark grey, fine silts
- No leaching or iron oxides
- Cc and Bn (pink/purple)
- Specular Hm and red Hm stain throughout
- Mineralisation tends to start 1-2m above footwall contact
- S low overall

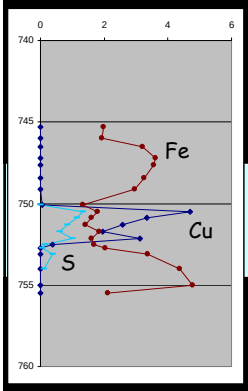

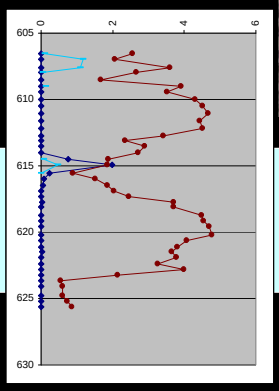

AMIRA/ARC P544 Final Sponsors Meeting July 2003

Cpy – Py Zone

- Iron oxides and leaching concentrated on fractures and footwall contact
- Cpy and Py dominant, Bn (brown) common, Cc present
- Cu and S 1:1 apart from some holes where in contact with the footwall aquifer where Mal and other supergene minerals are common
- Mineralisation starts immediately on the contact with footwall

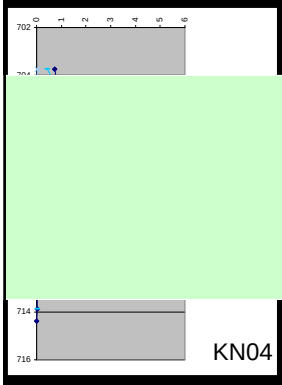

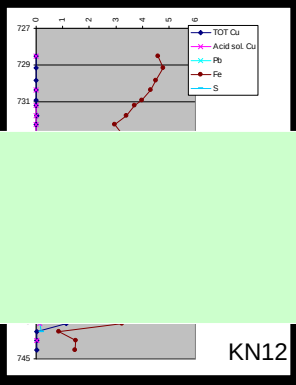

AMIRA/ARC P544 Final Sponsors Meeting July 2003

Co Zone

- Entire ore shale leached
- Common copper oxides in footwall
- Chalcocite, wad, pseudomalachite and native copper common throughout
- Cu and S distribution variable throughout the ore shale
- Co present (up to 0.5%), enriched on contact and in footwall – associated with Wad

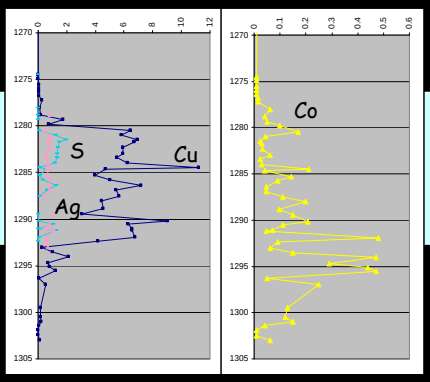

AMIRA/ARC P544 Final Sponsors Meeting July 2003

Sulphide Chemistry

- Loftus-Hills and Solomon (1967) and Griffen et al (1991)
  - trace element compositions of sulphides is determined by the physicochemical conditions of the ore fluid at the time of mineral deposition and thus can be used diagnostically to clarify different generations of mineralising events
- An understanding of the trace element characteristics of all sulphides present is important

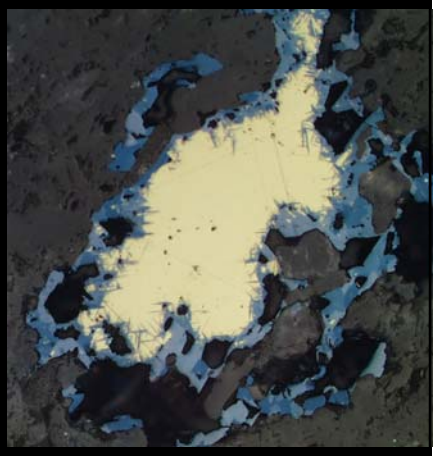

AMIRA/ARC P544 Final Sponsors Meeting July 2003

Sulphide Chemistry - Analytical Techniques

- Electron Microprobe
  - •Very high spatial resolution
  - •Detection limits -100's of ppm
  - – S Fe Co Ni Cu Zn As Se
    Ag Ba Au Pb Bi
  - –Non destructive

- Laser Ablation ICPMS
  - – High spatial resolution (20 – 200um)
  - – Low detection limits (sub ppm – dependent on spot size)
  - – Ti V Mn Fe Co Ni Zn Ge
    As Se Zr Mo Pd Ag Cd Sn
    Sb Te La Pt Au Hg Pb204 Tl
    Pb206 Pb207 Pb208 Bi Th U
  - – Cu used as internal standard (known accurately from probe)
  - – Quantified by reference to a synthetic in house standard
  - – Destructive

AMIRA/ARC P544 *Final Sponsors Meeting* *July 2003*

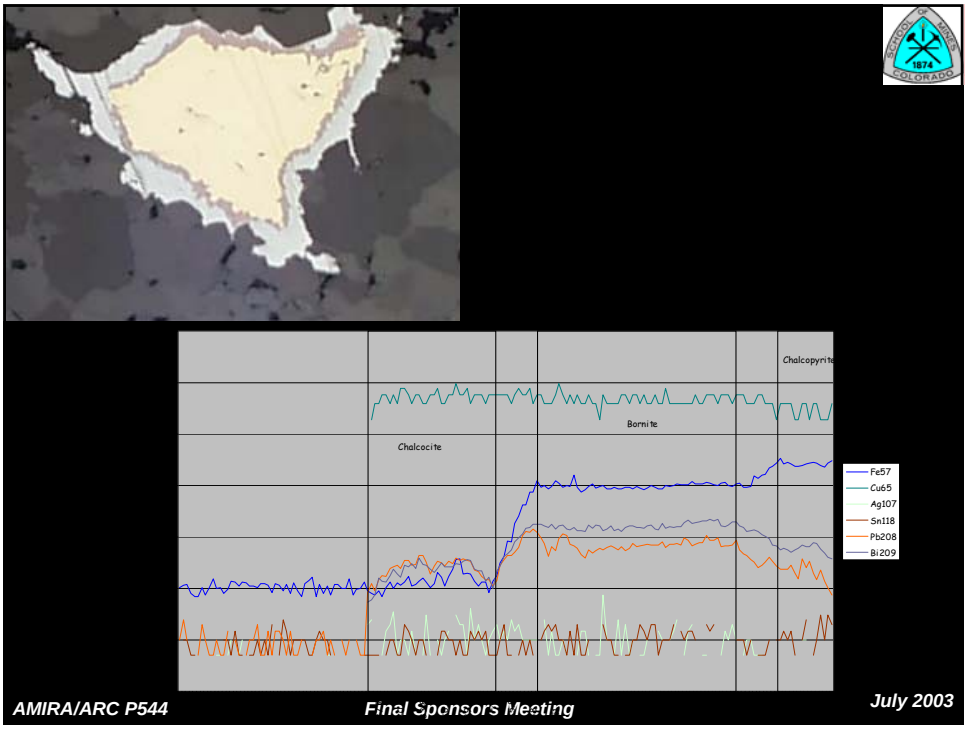

AMIRA/ARC P544 *Final Sponsors Meeting* *July 2003*

Trace element characteristics of common sulphides in Konkola North compared to Fe

Ag

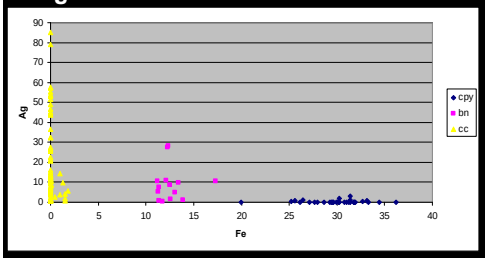

Bi

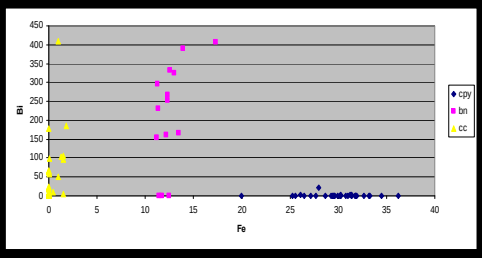

Pb

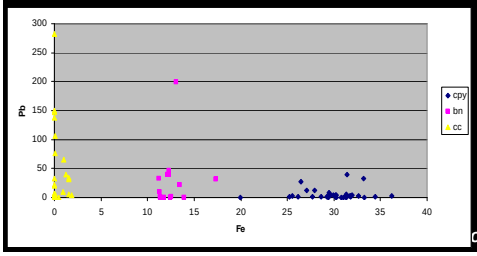

Sn

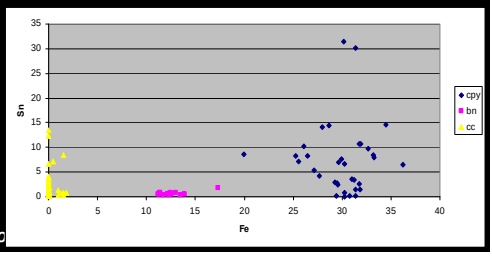

Trace element characteristics of common sulphides in Konkola North compared to Fe

Zn

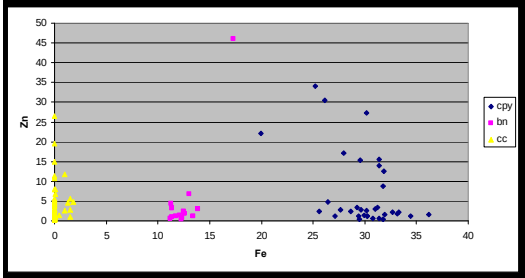

Trace element compositions vary between Cpy, Bn and Cc

In particular – Ag, Pb, Bi, Zn, Sn

Cc commonly has two (sometimes three) distinct groupings

AMIRA/ARC P544 *Final Sponsors Meeting* *July 2003*

Chalcopyrite

- Texturally and geochemically similar throughout Konkola north
- Moderately enriched in Sn (7-30ppm)
- Zn increases towards the Bn zone

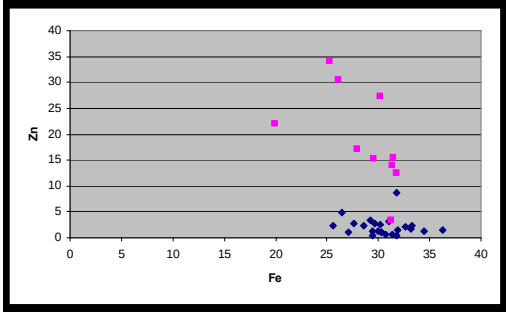

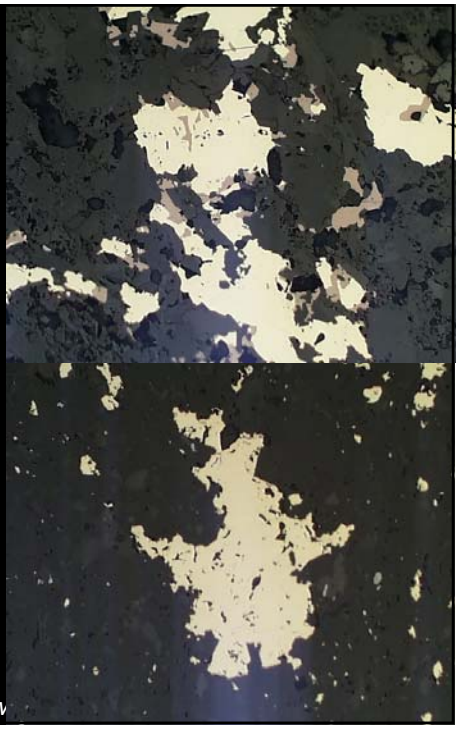

AMIRA/ARC P544 Final Sponsors M

Bornite

- Two different bornites observed
  - Associated with Cpy – brown/orange
  - Associated with Cc – purple/pink

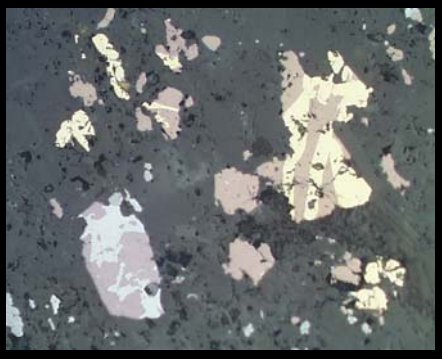

	Purple	Brown
Cu	63-65 %	58-61 %
Pb	21.2-199ppm	0.2 – 10ppm
As	2.8 – 33ppm	0.4 – 13.9ppm

AMIRA/ARC P544 Final Sponsors Meeting July 2003

Cu-Fe-S stability during metamorphism

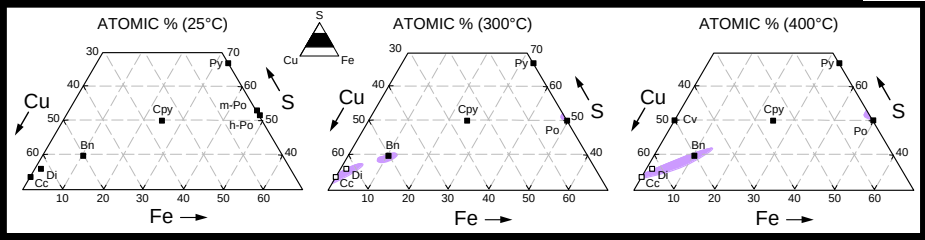

- At peak metamorphic conditions (T > 350-400°C) bornite solid solution spans the original compositional range Cc-Bn
  - Cc-Bn grains represented by homogeneous Bn at peak metamorphic conditions
  - Complex Cc-Bn intergrowths reflect exsolution of Cc-Di during cooling
- Variable Fe, S content of Bn grains at peak metamorphic conditions preserves original disequilibrium (Cc+Bn, Bn+Cpy) assemblages

AMIRA/ARC P544 *Final Sponsors Meeting* *July 2003*

Chalcocite

Coarse grains rimmed by haematite and Malachite

Significantly enriched in Ag (30ppm)

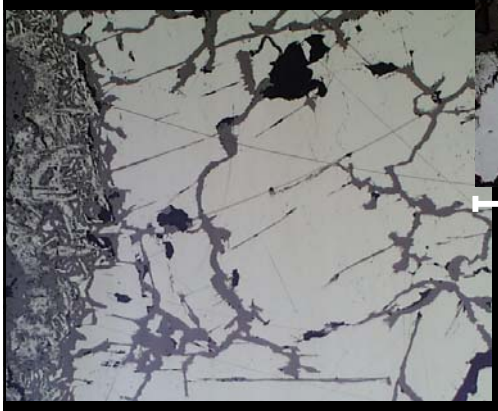

AMIRA/ARC P544 *Final Sponsors Meeting* *July 2003*

Chalcocite

Associated with (pink/purple) bornite

Significantly enriched in

Fe	0.5%
Pb	80ppm
Bi	103ppm
(Ni)	2.3ppm

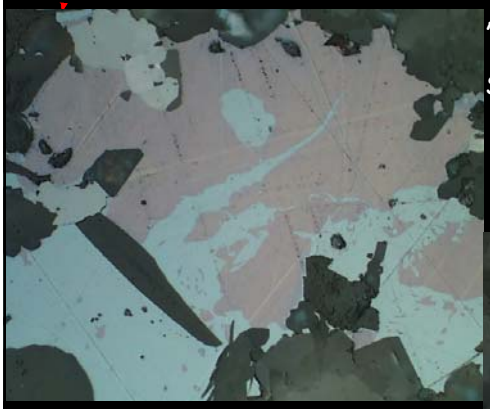

0.22mm

AMIRA/ARC P544 Final Sponsors Meeting July 2003

Chalcocite

Others

- Without Cpy core or Hm rim and/or Mal association how do you tell if a Cc in isolation is one which has exsolved from Bn or completely replaced Cpy or is related to later supergene fluids

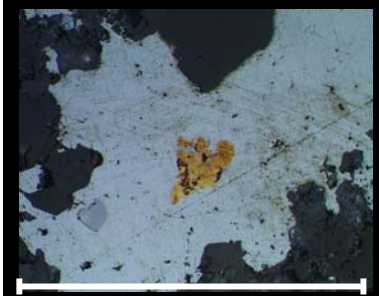

0.22mm

AMIRA/ARC P544 Final Sponsors Meeting July 2003

"Others" Chalcocite

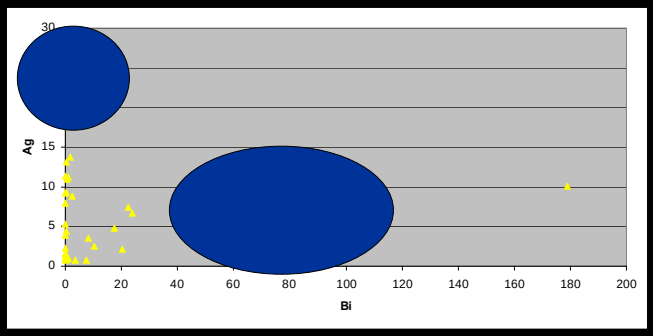

Chalcocites without any textural evidence to help identification – "others"

three groups – Hi Ag - Supergene
Hi Bi - exsolved from Bn
?? Can this group be separated further?

Future directions

•Investigate the fluid chemistry required to transport and concentrate the trace elements which define the different sulphide phases

•Can the trace element characteristics of the primary sulphide phases be used to determine where in the deposit you are?

•Compare to other well known supergene environments – Is there a common set of elements which are concentrated in supergene chalcocite or is it deposit specific?

Mwambashi B: Keys to arenite-hosted Cu–Co mineralisation

David Selley & Robert Scott
Centre for Ore Deposit Research, University of Tasmania

Abstract

Cu-Co mineralisation at Mwambashi B records the important interplay between basin architecture, hydrocarbon accumulation and influx of metal-bearing potassic fluids. A close association of sulfides, K-feldspar and calcite with anomalously light $\delta^{13}C$ values, indicates ore formation within a former hydrocarbon reservoir. Hydrothermal fluids were introduced along a laterally extensive pathway within coarse-grained strata at the top of the Mindola Clastics Formation (MCF). Permeability at this level was enhanced by dissolution of detrital quartz and clay components, however micro-fracturing related to tectonic decoupling at the base of the Ore Shale, was also significant. Post-mineralisation sodic fluids were partitioned within discrete fracture zones near the MCF–Ore Shale contact, and were potentially introduced via a high level breccia zone at the southern end of the system.

Introduction

Mwambashi B is a small footwall-hosted Cu-Co deposit located on the western flank of the Chambishi Basin (Slide 2). Mineralisation is positioned within a narrow, transfer-related trough, containing a highly condensed section of the Mindola Clastics Formation (MCF). The immediately overlying Ore Shale is weathered but otherwise well preserved (although commonly sheared at its base), dolomitic to carbonaceous, but effectively barren. Although small, the deposit provides valuable insight into the processes of mineralisation, as the "edges" of the system are clearly defined. It is possible therefore, to examine the relationships between lateral variations in facies architecture and basin geometry, silicate and carbonate alteration, and sulfide distribution.

Basin development and ore distribution

A detailed account of facies architecture and its relationship to basin development was presented in Selley et al. (2002). Below is a summary of salient aspects relating to the distribution of ore.

Thickness and facies variation of the MCF define a NW-trending, asymmetric half graben, controlled by a growth fault at the southern end of the deposit (Slide 3). Strata thin progressively to the northeast, except in the central part of the deposit, where displacement along an array of NNW-trending linkage or transfer faults resulted in the development of a narrow, weakly subsident trough. Displacement on the main linkage structure dissipated rapidly to the NNW, where the associated trough narrows and contains coarse-grained fanglomerate units that ultimately pinch-out onto an emergent basement bock (Slides 3, 5).

The local fault system became inactive following deposition of the MCF, with predominantly fine-grained marginal marine facies of the Ore Shale and Rokana Evaporites Member forming a transgressive blanket to underlying basin compartments (Slides 3, 5). Over most of the deposit, the Ore Shale is represented by subaqueously deposited siltstone with variable dolomitic component, the latter increasing above the position of the MCF pinch-out where sub-emergent depositional conditions persisted (Slide 5).

Approximately 5km south of the deposit, a polylithic breccia facies that in part forms a carapace to a gabbroic body, occurs at the level of the Ore Shale and its immediate hangingwall (Slide 5). Although considered to have been of sedimentary origin by Selley et al. (2002), we now interpret the breccia to have formed by a process involving *in situ* fragmentation. This interpretation is based partly on the textural characteristics of the breccia, which include local jigsaw fit clast arrangement. Moreover, the breccia forms the locus of intense albitic alteration (see also Selley et al., this volume), and as such closely resembles voluminous Upper Roan breccia facies, considered to have formed via dissolution or evacuation of salt (Broughton, this volume). Whether a similar mechanism can account for the Mwambashi B breccia unit is uncertain, as there is little evidence of former accumulation of thick salt within the Lower Roan. Alternatively, decoupling at the base of the Ore Shale during subsequent extension, or possibly inversion, may have resulted in tectonic removal of higher levels of the Lower Roan and juxtaposition of brecciated Upper Roan strata with an intact sequence of MCF. Although intense alteration at the base of the breccia has obscured the true nature of the contact, evidence for shearing along the MCF–Ore Shale contact is widespread within the deposit area. It will be demonstrated in following sections that this decoupling event was important in terms of directing hydrothermal fluid flow.

Distribution of mineralisation

Distribution of Cu mineralisation within the context of the basin framework is shown in Slide 4. Highest grades coincide broadly with the northeastern fringe of the main half graben, but are most strongly partitioned within the central transfer-related trough, particularly near pinch-out positions of the MCF. This relationship is further demonstrated in a longitudinal ore section positioned along the axis of the trough (Slide 5), which highlights concentration of Cu-grade within the uppermost portion of anomalously condensed and coarse grained MCF. At the southern end of the trough, where accommodation development was greater, mineralisation is confined to a relatively 'clean' subarkosic unit, enclosed by more argillaceous strata (BN4 and BN65 in Slide 5).

Metal distribution along the axis of the trough is crudely systematic. Highest Co grades are concentrated towards the pinch-out, with Cu mineralisation extending a further 1000 m to the south (Slide 6). In terms of Cu-sulfide composition, there is a broad zonation from chalcopyrite-dominated ore within central and northern parts of the deposit, to a bornite-dominated assemblage at the southern margin. This transition is reflected by increased Ag abundances within the bornite-rich fringe (Slide 6).

Textural character of ore

Ore textures are broadly compatible with those from the arenite-hosted Chibuluma West deposit (Selley and Cooke, 2001). Sulfides are typically coarse-grained, occurring as irregular disseminations throughout poorly structured sandstone and conglomerate, but approaching stratiform textures within parallel- and cross-stratified subarkose (Slides 8, 15, 20). Sulfide concentration within narrow, discontinuous seams oriented at moderate to high angles to primary layering is a less common, yet conspicuous texture (Slide 15).

Principal non-sulfide alteration phases include K-feldspar, tourmaline, albite and calcite. Of these, K-feldspar displays the most consistent intimate textural association with sulfides, its abundance increasing progressively toward the top of the MCF. This vertical zonation in K-feldspar metasomatism corresponds in part to a similar enrichment of detrital clay component, and hence available Al_2O_3, in the uppermost portion of the MCF. However, also paralleling the variation in K-feldspar abundance is a progressive increase in grain-scale deformation textures toward the MCF-Ore Shale contact.

Base of Ore

Low grade mineralisation at the base of ore is characterised by sparsely disseminated sulfides and rare stratiform concentrations (Slide 8). Associated metasomatic K-feldspar is similarly partitioned within the stratiform sulfide bands, but also occurs along microfracture arrays oriented oblique to bedding (Slide 9). It is distinguished petrographically from detrital K-feldspar by its less regular distribution throughout

the sandstone framework, lack of rounded habit and abundance of interstitial tourmaline needles (Slides 10, 12). Evidence of fracture-controlled fluid ingress includes development of systematic microfracture arrays along the margins of layer-parallel sulfide – K-feldspar – tourmaline seams (Slide 11), but more convincingly by concentration of tourmaline along layer-oblique microfractures that propagate through detrital grains (Slide 13).

Although the domainal distribution of alteration phases supports our interpretation of micro-fracture enhanced permeability, there is no evidence of open space vein fill. Generation of pore space was facilitated by replacement of detrital aluminous phases, principally clay within heavy mineral bands, but also by replacement of quartz (Slide 14).

Central ore position

The domainal distribution of sulfides and associated K-feldspar is most apparent within well-stratified subarkose from the central ore position (Slide 15). Sulfide concentrations generally mimic primary layering, but also form diffuse, to sharply-bounded, systematic layer-oblique and orthogonal arrays ranging 1-10mm in width. Internally, both layer-parallel and oblique sulfide domains are distinguished from enclosing strata by partial to complete destruction of detrital textures accompanying the growth of coarse microcline (Slides 16-19).

Calcite also becomes a conspicuous phase at this level of ore, however in detail, it displays an antithetic relationship with sulfides and metasomatic K-feldspar. It occurs primarily within less altered inter-sulfide domains as coarse crystal aggregates, randomly distributed throughout the sandstone framework (Slide 19).

Evidence of elevated intragranular strain with sulfide – K-feldspar domains is generally weak, but includes bent twin lamellae and regular shear band arrays (Slide 18). Supporting an interpretation that this phase of shear band development was broadly coeval with hydrothermal fluid input is the similar orientation of systematic sulfide – K-feldspar seams at the periphery of layer-parallel domains (Slide 18). However, the most convincing lines of evidence of fracture-enhanced permeability are (1) the abrupt margins of altered domains, demanding a high level of intergranular cohesion at the time of fluid input, and (2) the development of systematic, cross-cutting sulfide domains, which are interpreted as tensile fracture arrays formed between layer-parallel shears.

Upper ore position

The uppermost portion of the MCF is generally conglomeratic and lacks the coherent stratification preserved at lower levels. Increased strain as the Ore Shale contact is approached from below is indicated by widespread cataclastic textures. Grain breakage is particularly common at the periphery of rigid granite clasts, but is also concentrated within layer sub-parallel domains (Slide 20). The grain-scale distribution of sulfides and K-feldspar is less systematic at the top of ore, but displays crude partitioning within these zones of elevated strain (Slides 20, 21).

Accompanying increased cataclastic flow, is the sudden appearance of albite as a dominant phase within the ore assemblage. Although intimately associated with sulfides, albite displays consistent overprinting relationships with pre-existing K-feldspar (Slide 22). Local recrystallisation of sulfides during albite growth is demonstrated by planar, non-corrosive contacts between these phases, as well as the inclusion of small sulfide grains within the albitised portions of K-feldspar (Slide 22).

Deposit-scale alteration patterns

The broader distribution of alteration phases within and at the periphery of ore, has been determined using whole rock geochemical data from a selected group of drill holes positioned along the axis of the transfer-related trough (Slide 24). In order to quantify the degree of metasomatism however, variability of protolith composition relating to provenance and sedimentary fractionation processes must be considered first. The affects of provenance are unlikely to be significant for the MCF at least, as petrographic data reveal that detritus was proximally derived from a uniform granitic source area. However, variation

in the relative proportions of the principal detrital components (i.e., quartz, K-feldspar and clay) within different sedimentary lithotypes will have had a considerable affect on original K_2O content in particular. In order to minimise these affects, quantitative analysis of K-metasomatism has been restricted to argillite-poor, subarkosic protoliths, which account for a significant portion of the MCF, including the main host stratum (Slide 24). Affects of sedimentary fraction are less considerable for determining the degree of Na-metasomatism, as the Na content of granitic source rocks appears insignificant (Na_2O <0.2%). Thus, absolute abundance of Na_2O is interpreted to relate principally to that of metasomatic albite.

The relative abundances of the principal non-sulfide alteration phases, i.e., K-feldspar, albite and calcite, were determined using the MINSQ program, which expresses whole-rock geochemical data as absolute mineral proportions.

Na-metasomatism

Although albite is the paragenetically youngest alteration phase, its distribution will be dealt with first as it is the easiest to determine from whole rock data, but as it also has a considerable masking effect on the distribution of earlier K-metasomatism.

Albite abundance increases progressively from a background value of less than 1% to a maximum of 79% as the MCF–Ore Shale contact is approached from below (Slide 25). However, there is significant lateral variation in both intensity of albitisation and the depth to which it extends below the contact. Where associated with ore positioned close to the MCF pinch-out, Na-metasomatism is restricted to a narrow halo, extending less than 2m either side of the contact, with a maximum albite component of only 8%. These values increase progressively through the southern periphery of ore and into barren strata. Highest albite abundances occur within and below the hangingwall breccia facies situated 4.5km south of the MCF pinch-out position, implying that this zone of enhanced fracture-induced permeability was a major input point for sodic fluids (Slides 25 and 28).

K-metasomatism

The potassium content of subarkosic units contained within both mineralised and barren portions of the MCF become highly erratic within a 70′ thick zone immediately below base of the Ore Shale (Slide 26). Petrographically least altered samples occur below this zone and provide a constraint on original detrital compositions: i.e., ~3% K_2O and a K-feldspar:quartz ratio of ~0.2. Altered samples with lower values for these parameters have been affected by K-feldspar destruction during sodic metasomatism. Removal of these samples reveals a progressive increase in K-metasomatism towards the Ore Shale contact (Slide 27). This trend is best demonstrated in K-feldspar: quartz ratio, which exceeds a two-fold enrichment within mineralised samples. Absolute K_2O values are less informative as K-metasomatism is accompanied by significant CaO enrichment (related to hydrothermal calcite) in some samples. Although more difficult to establish in southern barren holes due to the deeper penetration of sodic fluids in these regions, a single albite-poor sample records moderate potassium enrichment approximately 60′ below the Ore Shale. These data support the petrographic relationship of metasomatic K-feldspar and sulfides, but indicate that input of potassic fluids were likely widespread near the top of the MCF, and extended well beyond the limits of ore (Slide 28). Limited fluid ingress within the Ore Shale is indicated by low K_2O/Al_2O_3 values at this level (average 0.5), relative to mineralised Ore Shale samples from Nkana-Mindola and Konkola North (0.69 and 0.59 respectively).

Hydrothermal calcite

Of all the non-sulfide alteration phases, calcite displays the closest spatial association with ore. Although there is no systematic relationship between calcite abundance and Cu-grade, there is a broad partitioning of interstitial carbonate cements within the mineralised pinch-out position (Slide 30). Only at the southern periphery of ore is there no calcite associated with high grade mineralisation (BN65).

Textural and compositional characteristics of the carbonate cements are variable. Within ‘clean’ sub-

arkoses, calcite forms the dominant phase, occurring as coarse, prismatic crystals scattered throughout the detrital framework (Slide 31). Near the upper ore contact, where strain, argillaceous content and albitic alteration all increase, carbonate cements include both dolomite and calcite. Carbonate grains have a considerably 'dirtier' appearance and commonly display overprinting relationships with K-feldspar.

Whole rock C-O isotope analyses of carbonates reveal a broad depletion of $\delta^{13}C$ values within the mineralised pinch-out position of the MCF (Slide 32). Within the ore zone, lightest $\delta^{13}C$ values were obtained from high grade samples containing abundant 'clean' prismatic calcite (–25 to –17‰), with abrupt increase to ~ –7 to –10‰ for carbonate cements positioned at the base of mineralisation, or associated with albitic and/or argillaceous strata. Heaviest values were recorded from barren strata situated below the albitic breccia facies, 4.5km south of the pinch-out position (–3 to –7‰).

The distinctive strongly negative $\delta^{13}C$ signature of ore-related calcite is compatible with C-O isotopic data from other arenite- and Ore Shale-hosted deposits, and is best explained by incorporation of CO_2 in hydrothermal carbonate via the oxidation of organic matter (Large et al., this volume). As the fluviatile subarkosic host at Mwambashi B was unlikely to contain a significant component of detrital organic carbon, contribution from a late diagenetic hydrocarbon-rich fluid or gas is most plausible. Providing good support for this interpretation is the strong partitioning of calcite (and sulfides) within a clean, favourable reservoir rock, contained within a confined 3-D seal.

Trends toward heavier $\delta^{13}C$ values are interpreted to relate to either lack of an organic component, or mixing of carbon sources. The association of increasing $\delta^{13}C$ within albitic zones near the top of the MCF, could be interpreted to indicate re-equilibration of organically-derived carbon with slightly heavier carbon sourced from the Na-rich fluid. More likely however, is interaction with early diagenetic dolomitic cements, related to descent of dense evaporitic brines sourced from the overlying Rokana Evaporites Member (Bull and Selley, this volume).

Discussion and conclusions

Mwambashi B demonstrates the essential and interrelated roles of basin architecture, hydrocarbon accumulation and infiltration of metal-bearing potassic fluids in the genesis of arenite-hosted Cu deposits. The most important aspect of basin architecture was the accumulation of 'clean', anomalously coarse-grained lithofacies with a confined depocentre. Enclosure of this package by crystalline basement at its base and margins, and by argillaceous/dolomitic facies of the Ore Shale at its top, provided an effective physical trap for migrating hydrocarbons. Former presence of an organic carbon-bearing fluid or gas within the trap site is indicated by calcite cements with an anomalously light $\delta^{13}C$ signature.

The broad correspondence of Cu mineralisation with organically-derived calcite and metasomatic K-feldspar suggests that sulfides formed via reduction of potassic, metal bearing brines within the hydrocarbon trap site. However, the source of sulfur in this system remains uncertain. In contrast to the giant arenite-hosted system at Mufulira, where there remains a significant anhydrite component peripheral to high grade ore (Scott et al., this volume), there is a distinct paucity of anhydrite within either mineralised or barren portions of the host stratigraphy at Mwambashi B. Either anhydrite was not originally present, or was in such small or localised abundance that it became entirely consumed during the mineralising process. Providing support for the latter is the crude zonation from chalcopyrite-dominated ore within central part of the system to bornite-dominated ore at the southern periphery, suggesting that sulfur availability was limited away from the pinch-out position. This apparent concentration of sulfur close to pinch-out may have resulted from funnelling of early diagenetic sulfate rich brines, derived from more evaporitic portions of the stratigraphy located above the basement high (Selley et al., 2002; Bull and Selley, this volume). Alternatively, migrating hydrocarbons may have contained an additional, exotic component of H_2S. Regardless of which of these two scenarios is correct, the limited sulfur availability at Mwambashi B accounts in part at least for the small size of the mineralised system.

Influx of potassic fluids was directed along a zone of enhanced permeability within the uppermost portion of the MCF. Unlike most other deposits in the Copperbelt, the Ore Shale remained largely impervious to this hydrothermal fluid, as indicated by its low Al_2O_3/K_2O contents. Partitioning of fluids within subarkosic lithofacies may have been facilitated at early stages by porosity and permeability either preserved or generated throughout the migration and accumulation of hydrocarbons. The random distribution of intergranular calcite cements formed from the oxidation of hydrocarbons supports this interpretation. However, the more domainal distribution of both K-feldspar and sulfides, their association with microfracture arrays and corroded contacts with detrital quartz, implies rapid loss of primary permeability and the onset of both fracture and reaction enhanced permeability.

Microfracturing increased in intensity towards the upper portion of the MCF in response to tectonic decoupling at the base of the Ore Shale. Displacements on this contact were very minor in the region of the deposit, but were potentially significant to the south, where brecciated strata typical of the Upper Roan lie directly on an intact MCF succession. Post-mineralisation sodic hydrothermal fluids were directed along zones of fracture-enhanced permeability, both within the breccia and cataclastic zones extending into the underlying MCF. As the deposit is approached from the south, albitisation was focussed into a progressively narrower damage zone located at the MCF–Ore Shale interface.

References

Broughton, D., this volume. Stratigraphy, regional alteration and mineralisation of the Zambian Copperbelt.

Bull, S. and Selley, D., this volume. Chambishi basin studies; Chambishi SE Prospect.

Large, R., Bull, S., Croaker, M., McGoldrick, P., Pollington, N., Scott, R., Selley, D., this volume. Carbon and Oxygen Isotopic composition of Ore-Related and Sedimentary carbonates in the Roan, ZCB.

Scott, R., Selley, D., and Cooke, D., this volume. Arenite-hosted copper mineralisation east of the Kafue Anticline: A comparison of tectono-stratigraphic, mineralogical, geochemical and C- and O-isotopic characteristics of small and large deposits.

Selley, D. and Cooke, D., 2001. Mineral zonation and sulfur isotope systematics of the Chibuluma West copper-cobalt deposit, Zambia. AMIRA P544 Progress Report, Dec 2001. pp. 133-170.

Selley, D., Bull, S., Scott, R., Cooke, D., 2002. Chambishi Basin progress report 2: Basin geometry and its controls on mineralisation at Mwambashi B. AMIRA P544 Progress Report, Dec 2002. pp. 5.1-5.40.

Selley, D., Scott, R., Croaker, M., Broughton, D., Bull, S. and Pollington, N., this volume. Alteration history of the Roan.

Mwambashi B

Keys to Arenite-Hosted Mineralisation

Slide 1

Mwambashi B

- 8.4Mt @ 2.6% Cu & 0.08% Co
- Arenite (FW) hosted
- "Edges" of the system are clearly defined
- Opportunity to examine vertical and lateral variation in alteration
- Relationship to basin architecture

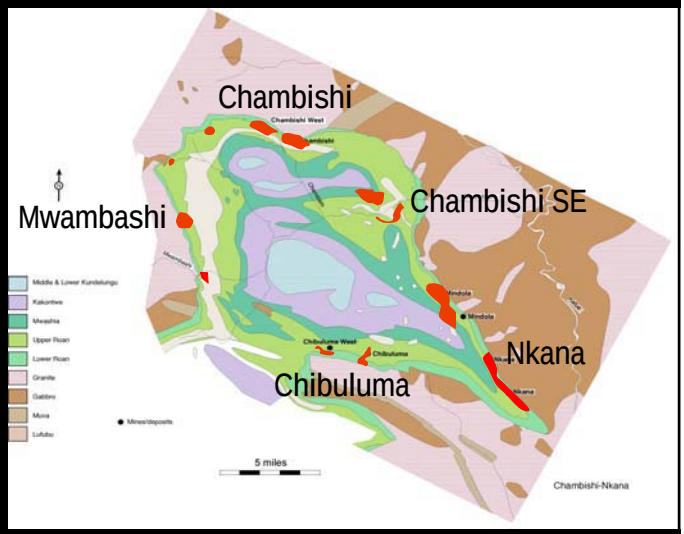

Slide 2

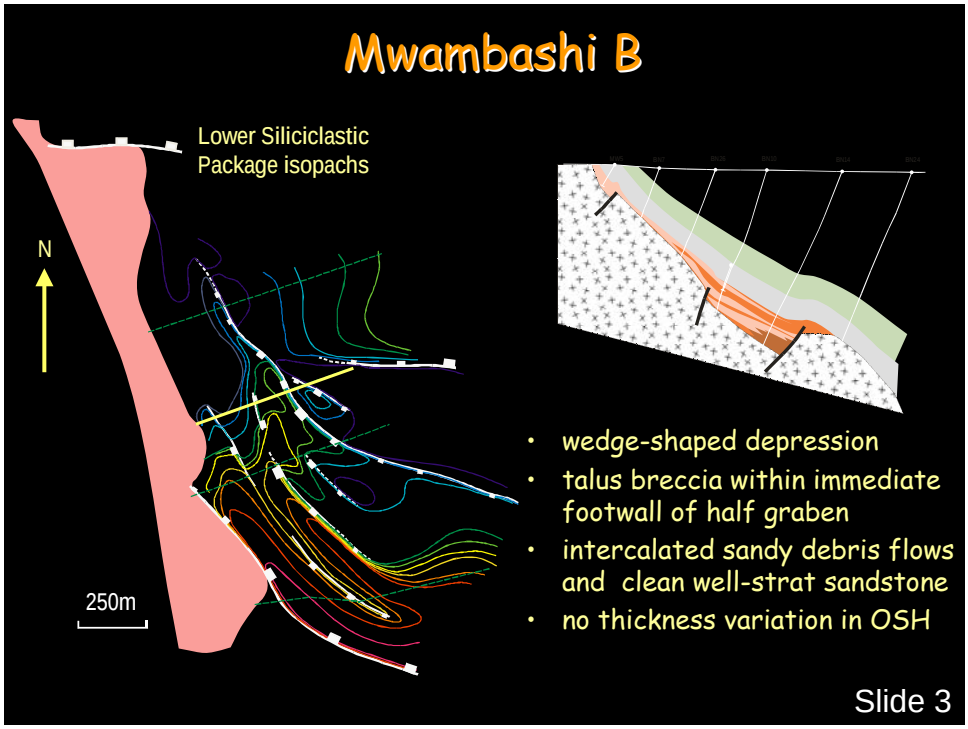
Mwambashi B
Lower Siliciclastic Package isopachs
N
250m
wedge-shaped depression
talus breccia within immediate footwall of half graben
intercalated sandy debris flows and clean well-strat sandstone
no thickness variation in OSH
Slide 3

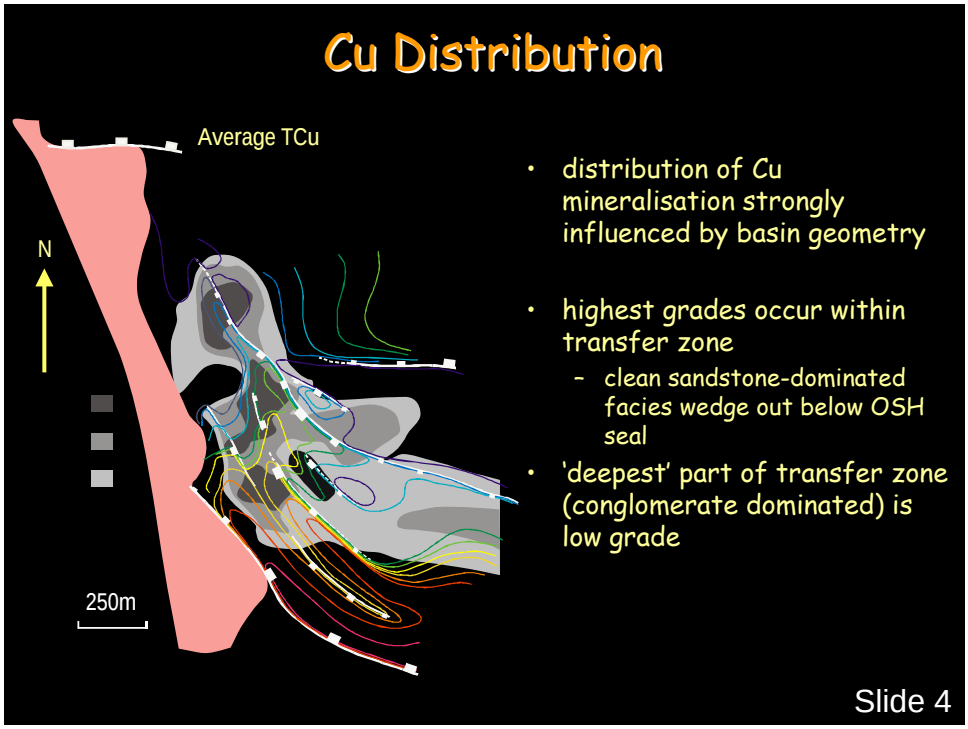
Cu Distribution
Average TCu
N
250m
distribution of Cu mineralisation strongly influenced by basin geometry
highest grades occur within transfer zone
- clean sandstone-dominated facies wedge out below OSH seal
'deepest' part of transfer zone (conglomerate dominated) is low grade
Slide 4

Long Section

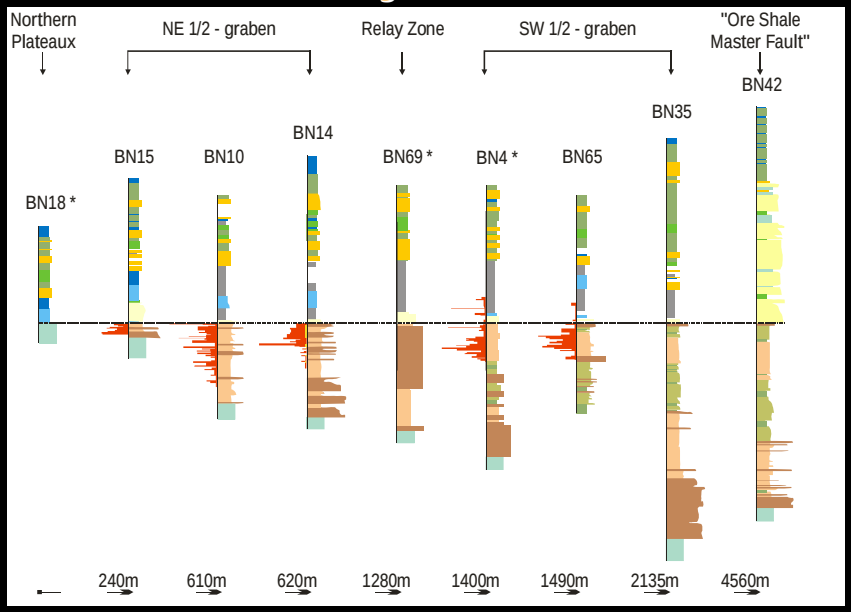

Slide 5

Cu-Co

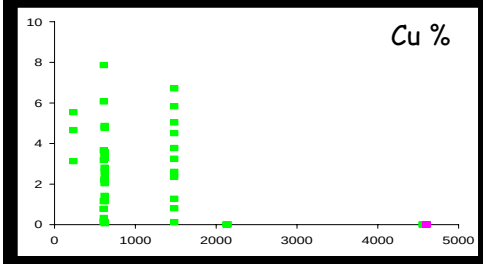

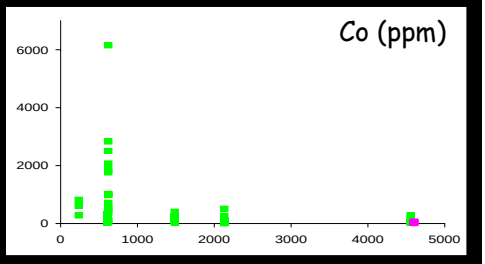

- Cu increases abruptly within 1500m of pinch-out
- Co is more restricted
- Marginal Co-poor intersection is bornite rich and coincides with elevated Ag

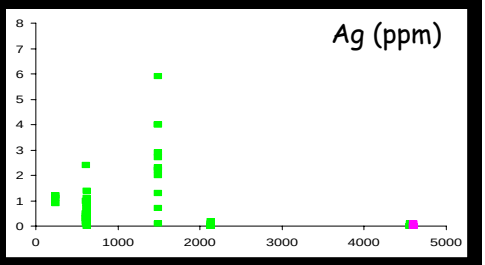

Slide 6

Textural Character of Alteration & Mineralisation

- Alteration phases are very similar to detrital phases
  - Sub-arkoses – qtz-kspar-heavies (incl. tourmaline)
  - Alteration – qtz-kspar-tourmaline-haem-calcite
  - Subsequent albite-biotite-calcite-chlorite
- Metasomatism vs sedimentary fractionation
  - eg. does variable K_2O content reflect K-metasomatism or increased detrital feldspar/quartz ratio (ie. provenance, source weathering, transport mechanism – granite clasts)
- Disseminated – very rarely vein hosted
  - Difficult establishing paragenetic sequence
  - Rocks are metamorphosed - recrystallised
  - Difficult to distinguish between early diagenetic and post-lithification fluid infiltration
  - Diagenetic textures are lost through multistage metasomatism and metamorphic recrystallisation
  - Recrystallisation of sulphides and alteration phases during deformation
  - Textural relationships are ambiguous

Slide 7

Base of Ore (~1.8% Cu)

- Excellent preservation of original sub-arkosic sandstone composition and texture
  - Mica and carbonate content low
  - Strain low
- Sulphides (secondary cc, haem, mal) concentrated locally in discrete S0 sub-parallel seams

Slide 8

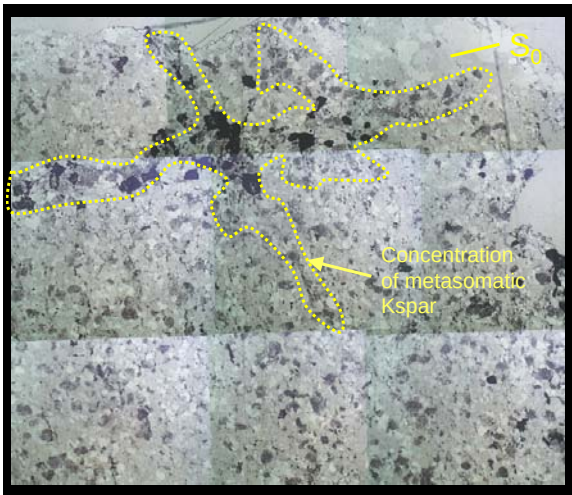

Kspar Metasomatism

- Generally even distribution of K-spar (dusty grey phase)
- Subtle increase in kspar where in association with sulphides
- Concentration of kspar in narrow layer-parallel and NW-SE fracture seams

Slide 9

Kspar Metasomatism

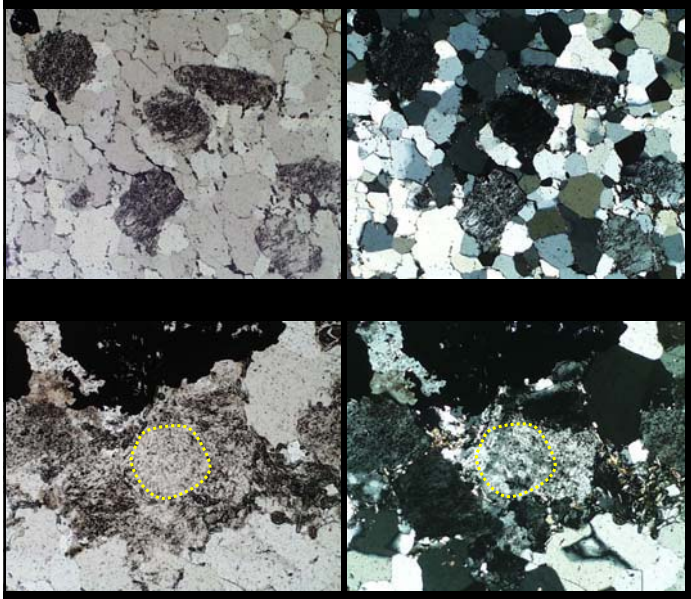

Sulphide Poor

- Rounded detrital grains set in quartz aggregate
- Minor tourm at grain edges

Sulphide Rich

- Optically continuous K-spar overgrowths on detrital cores
- Tourmaline concentrates in and at fringes overgrowths

Slide 10

Fracture Induced Permeability

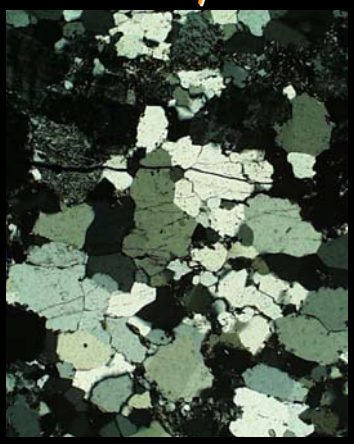

- Healed micro-fractures parallel margin of kspar-tourm-sulphide band
- Density of micro-fractures decrease rapidly from margin
- No clear evidence of syn-metasomatic breakage – but indicates history of fragmentation

Slide 11

Fracture Induced Permeability

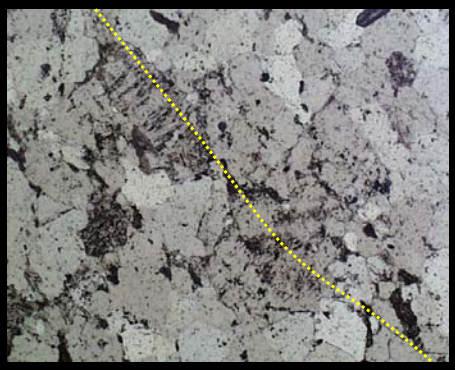

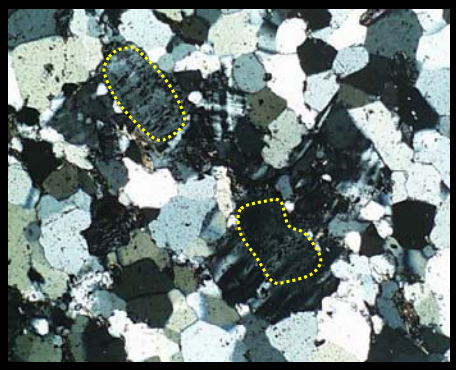

- Similar textural relationships to layer-parallel band
- Only Kspar overgrowths contain tourmaline inclusions
- Significant increase in tourmaline abundance in fracture seam
- Fine intergrowth of feldspar-qtz-tourm along NW-SE seams in "wall rock"

Slide 12

Fracture Induced Permeability

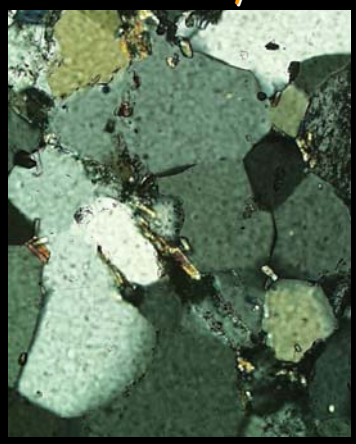

- Unequivocal through-going intragranular microfractures
- Tourmaline concentrated within fracture and along grain boundaries
- Tourmaline lying along intragranular fractures
- High degree of consolidation during influx of B-bearing fluids
  - By association, also precipitation of kspar and sulphides

Slide 13

Dissolution Enhanced Porosity

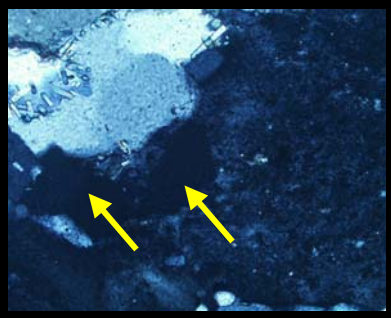

- Kspar enclosing optically continuous, corroded fragments of quartz
- Porosity generated in part at least via dissolution of quartz

Slide 14

High Grade Ore (~4.8% Cu)

- Sulphides: cpy overgrowing carr – invariable paragenesis
- Very coherent stratification, near stratiform sulphide distribution
- Possible textural destruction in Cu-rich domain
- Detail shows concentration of sulphides in layer-parallel bands, but also in oblique and sub-orthogonal bands
- *Characteristic domainal distribution*
- Calcite becomes a conspicuous alteration phase

Slide 15

Sulphide Domains

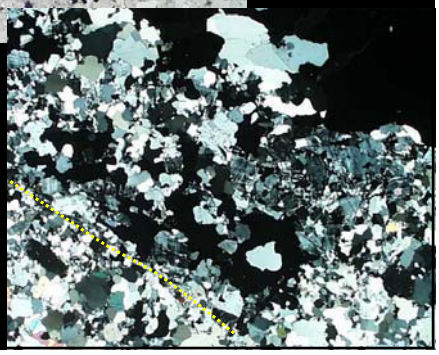

- Pervasive kspar-qtz throughout main sulphide domain
- Abrupt planar margin
- Qtz (detrital), calcite minor kspar and cpy throughout "wall rock"

Slide 16

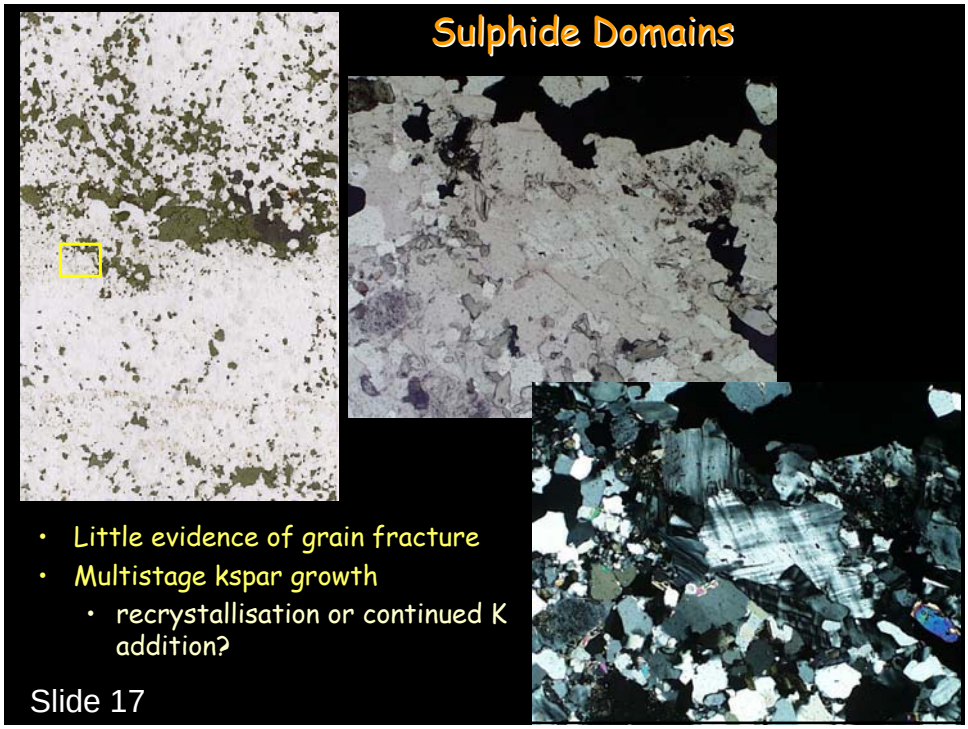
Sulphide Domains
• Little evidence of grain fracture
• Multistage kspar growth
• recrystallisation or continued K addition?
Slide 17

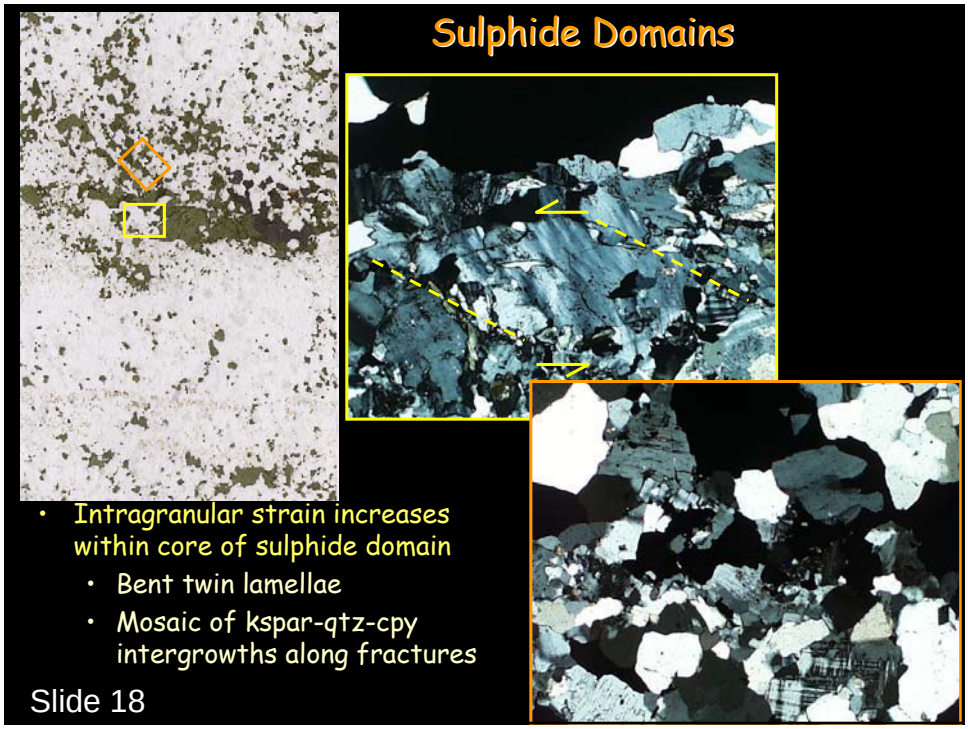
Sulphide Domains
• Intragranular strain increases within core of sulphide domain
• Bent twin lamellae
• Mosaic of kspar-qtz-cpy intergrowths along fractures
Slide 18

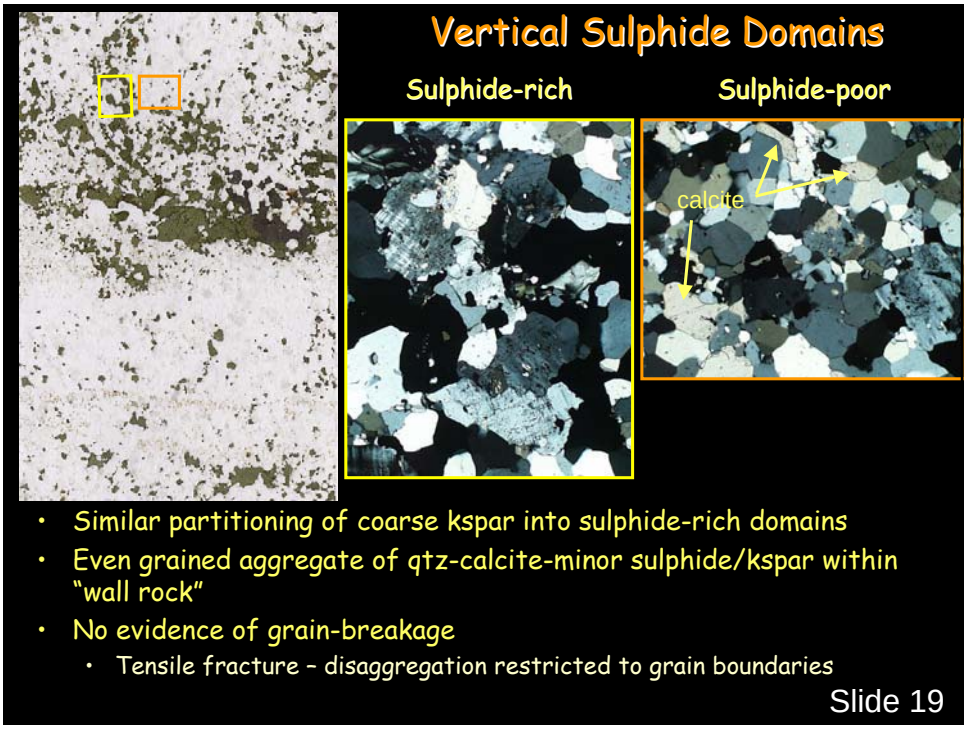
Vertical Sulphide Domains
Sulphide-rich
Sulphide-poor
calcite
• Similar partitioning of coarse kspar into sulphide-rich domains
• Even grained aggregate of qtz-calcite-minor sulphide/kspar within "wall rock"
• No evidence of grain-breakage
• Tensile fracture – disaggregation restricted to grain boundaries
Slide 19

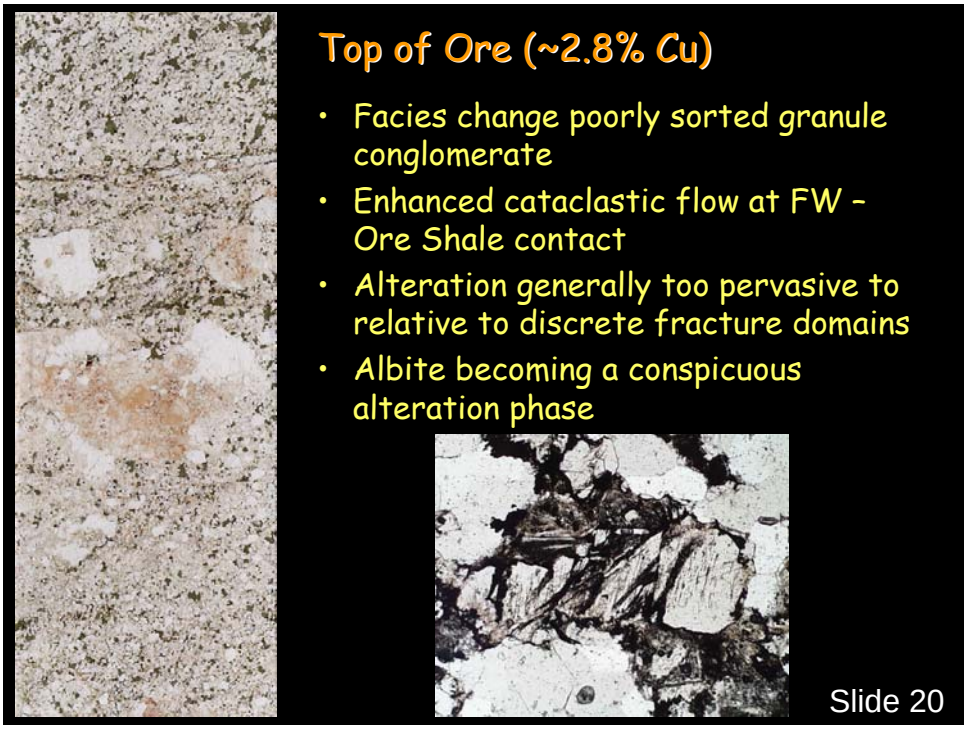
Top of Ore (~2.8% Cu)
• Facies change poorly sorted granule conglomerate
• Enhanced cataclastic flow at FW – Ore Shale contact
• Alteration generally too pervasive to relative to discrete fracture domains
• Albite becoming a conspicuous alteration phase
Slide 20

Top of Ore (~2.8% Cu)
• Crude and un-convincing enrichment of kspar in main fracture seam
Slide 21

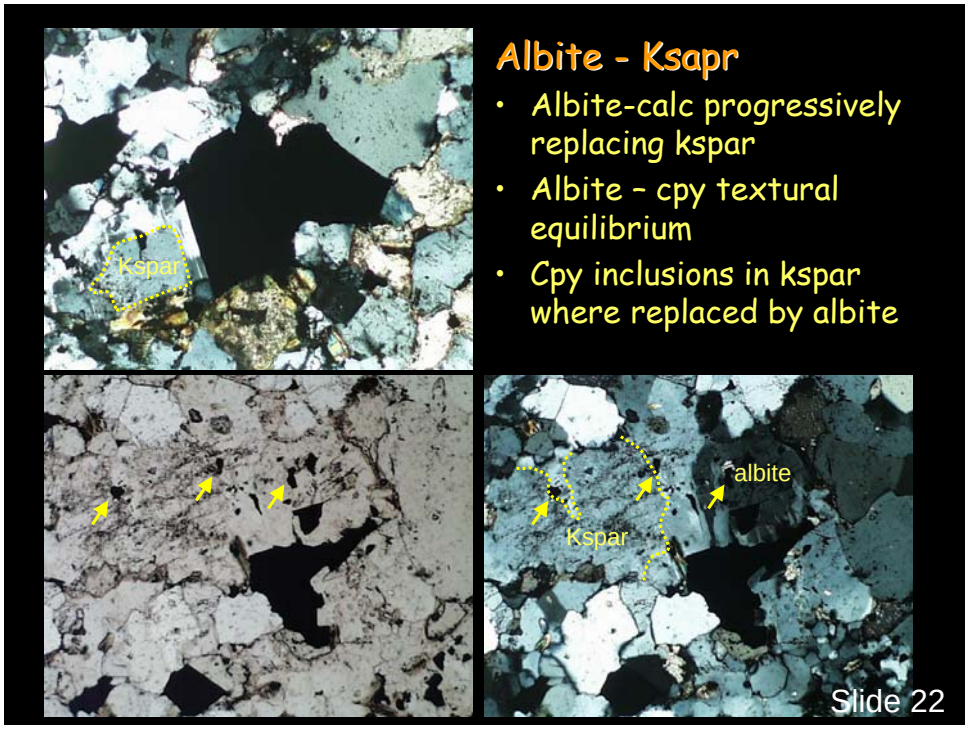
Albite - Ksapr
• Albite-calc progressively replacing kspar
• Albite – cpy textural equilibrium
• Cpy inclusions in kspar where replaced by albite
Kspar
albite
Kspar
Slide 22

Textural Relationships

- Media were sufficiently cohesive to allow formation of systematic fluid pathways
- Evidence of cataclastic flow increases towards the Ore Shale contact (top of ore)
- Infiltration of ?evolving fluids (ie. K to Na metasomatism)

Slide 23

Lithogeochemical Sampling

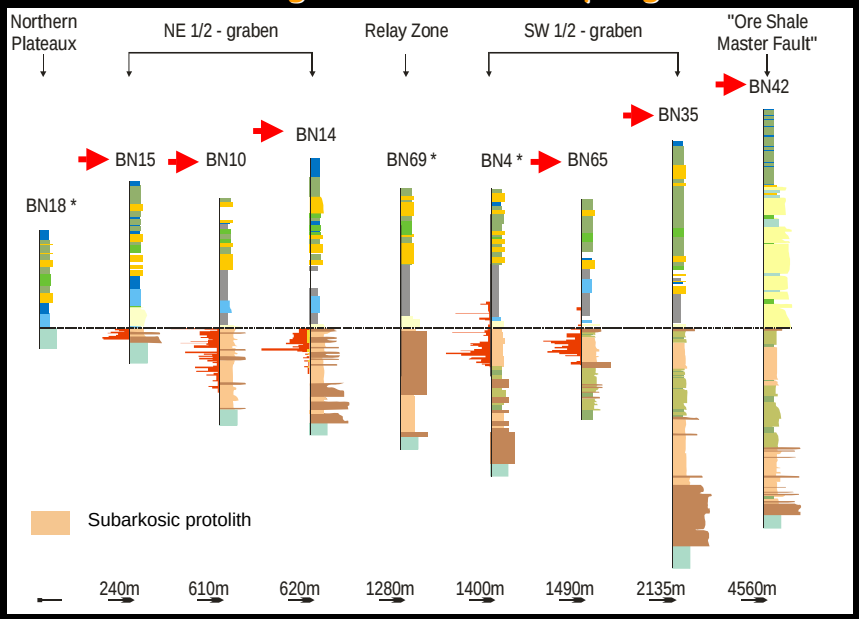

Slide 24

Albite Distribution

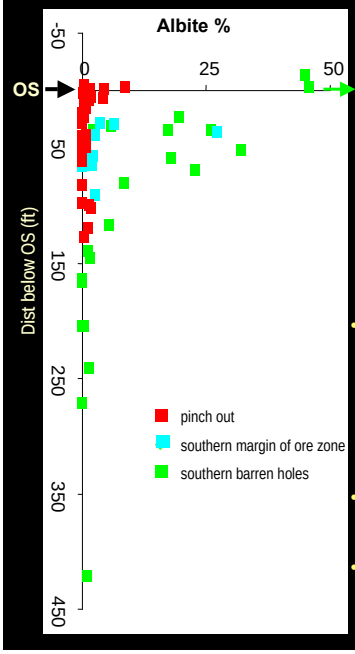

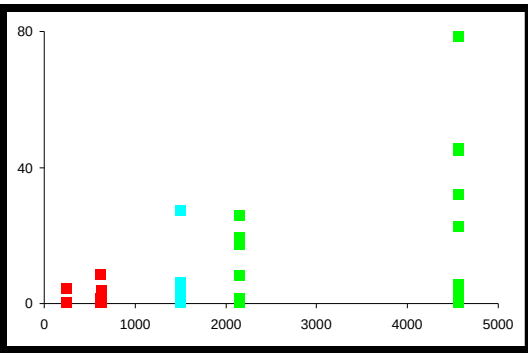

- Nearly all albite is considered metasomatic
  - Granite: 34% qtz, 26% kspar 1% albite
  - Qtz-feldspar ratio increased by ~300% during depositional process
  - Detrital albite ~0.3%
- Increase in albite towards OS contact in all drill holes
- Albitic metasomatism increases southward to wards HW breccia unit

Slide 25

K Metasomatism

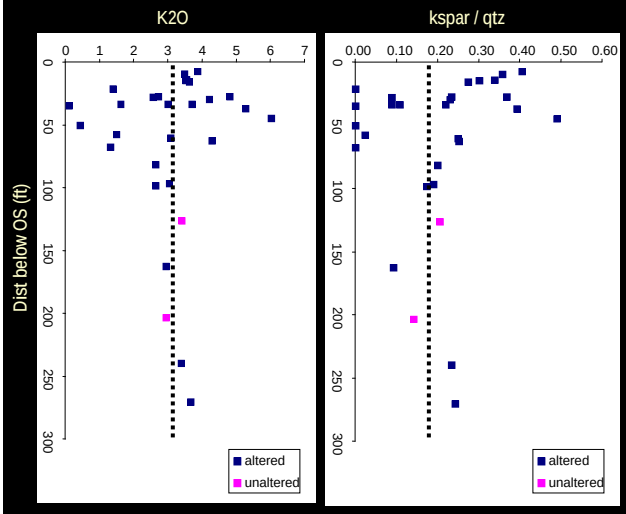

- Facies type = clean sub-arkose
- Unaltered sandstone ~3%K2O or ~0.2Kspar/qtz
- Clear mobility of K within ~70' of Ore Shale contact
- K Depletion relates to late stage Na metasomatism

Slide 26

K Metasomatism

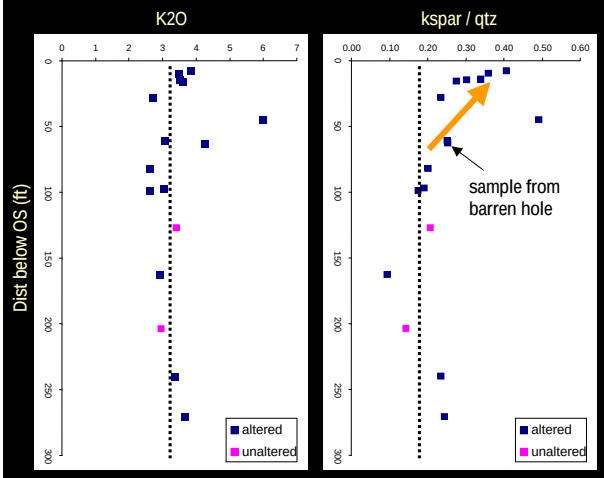

- samples <1.5% albite
- K/Q reveals progressive increase in K metasomatism towards OS contact
  - 100% increase
- Less clear in terms of K2O
  - High K/Q rocks contain nearly 20% calcite + significant Cu (ie. dilution of absolute K_2O)

- Although difficult to see through subsequent Na metasomatism distal to ore – K metasomatism appears to be partitioned within a blanket immediately below the Ore Shale = *lateral fluid flow*

Slide 27

Feldspar distribution within subarkosic protoliths and hangingwall breccia facies

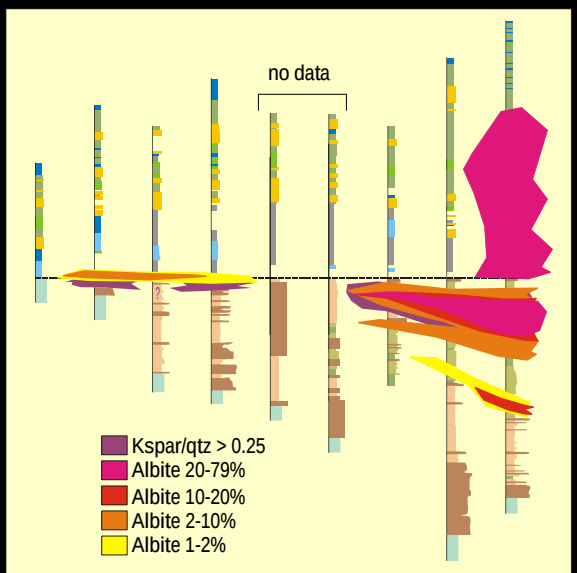

kspar from subarkose only: albite from entire FW + breccia

- Feldspar metasomatism partitioned into upper portion of FW
- Albitic metasomatism increases in intensity away from pinch-out + below HW breccia
  - Replacement of pre-existing kspar?
- Vertical transition from kspar to albite at OS contact in pinch-out

Slide 28

K vs Cu

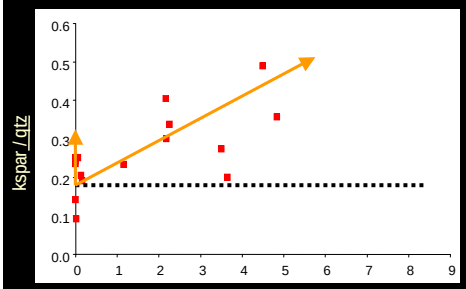

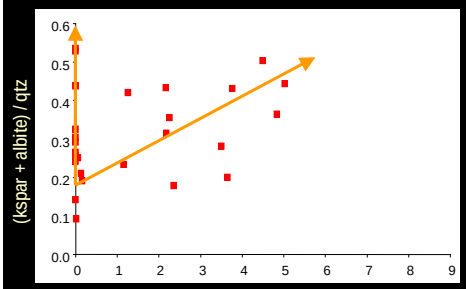

- Two crude populations
  - Positive correlation of K with Cu
  - K varying independently of Cu
- K/Q plot heavily biased towards albite poor zones in main part of ore zone
  - (K+A)/Q may be a proxy for original metasomatic kspar component in distal albitic zones
- Feldspar alteration alone does not account for Cu

Slide 29

Calcite vs Cu

- Holes closest to pinch-out showing broad spatial association of calcite with Cu
- Increase toward OS contact
- Poor correlation in detail
  - ie. Cu vs calcite

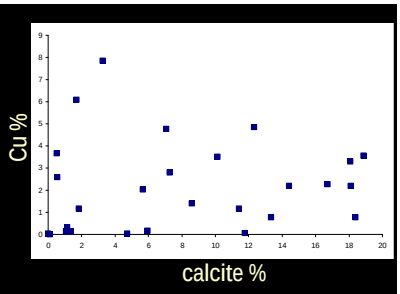

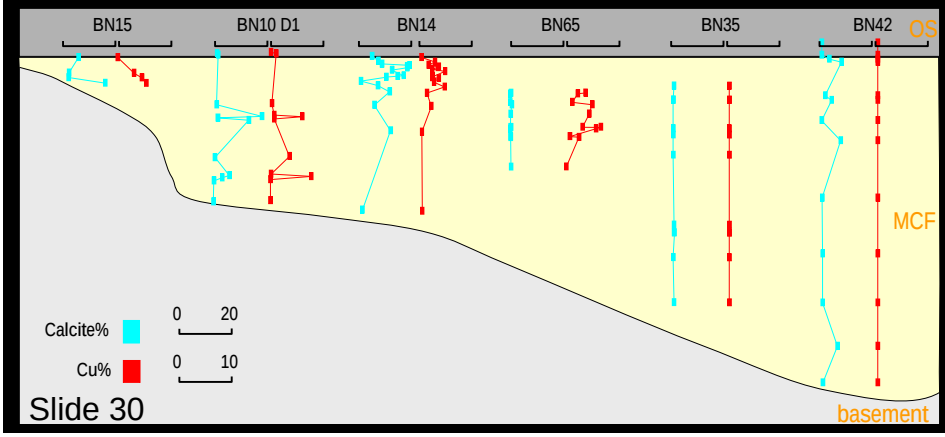

Slide 30

Calcite vs Cu

- Holes closest to pinch-out showing broad spatial association of calcite with Cu
- Increase toward OS contact
- Poor correlation in detail
  - ie. Cu vs calcite

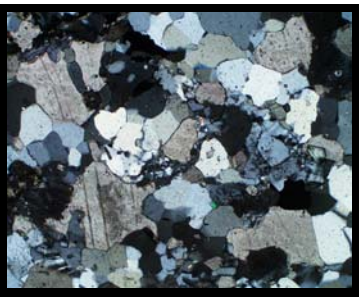

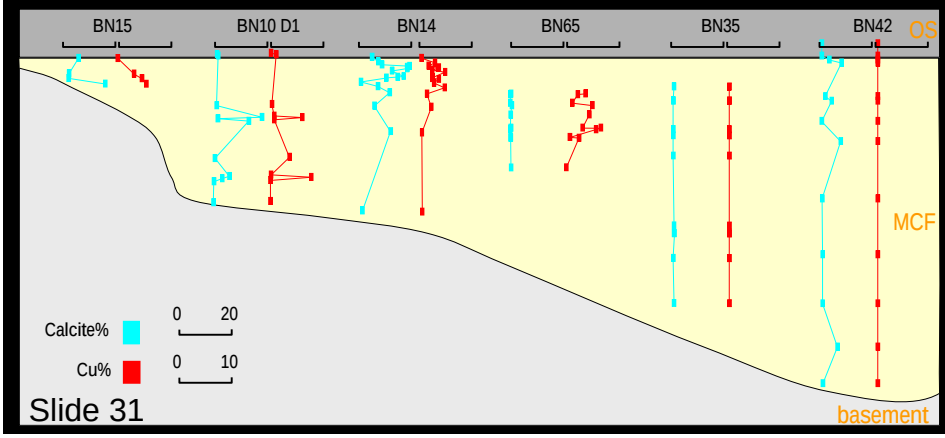

Slide 31

δ13C vs Cu

Slide 32

- Strongly depleted dC13 within pinch-out - *Organic C signature*
  - largely contained within FW, but extending into Ore Shale
  - most depleted values (-25 permil) correlate with highest Cu grades
- δC13 values within peripheral hole averages -5.4 permil - *diagenetic*
- Paucity of carbonate at margin of ore (BN65) may reflect limited organic carbon component
  - Bornite dominant – limited sulphur available?

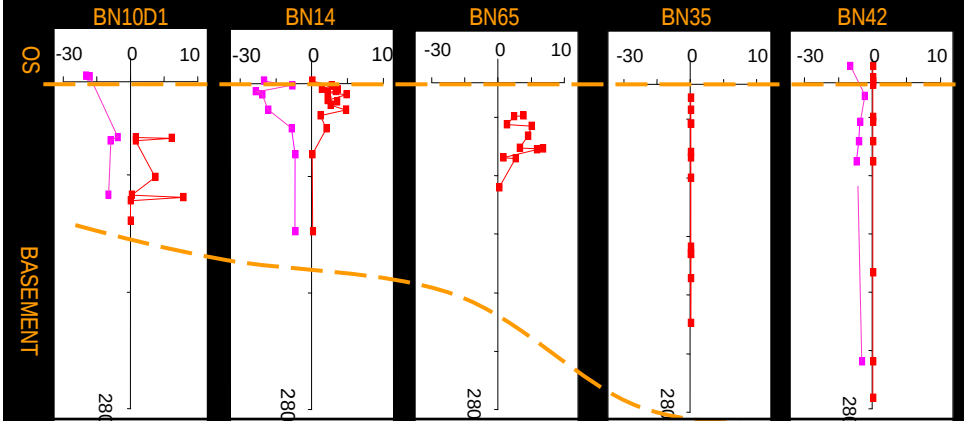

Stratigraphy, alteration history and copper mineralisation at Ndola West, Zambian Copperbelt

Robert Scott
Centre for Ore Deposit Research, University of Tasmania

Summary

The Ndola West prospect, east of the Kafue Anticline hosts low-grade stratabound copper mineralisation within relatively clean arkosic sandstone at the same stratigraphic level as the B-Orebody at Mufulira. The Lower Roan stratigraphy at Ndola West records a similar history of early basin development to that in the Chambishi Basin, west of the Kafue Anticline. A direct facies and stratigraphic equivalent of the Ore Shale is also present, but is itself only weakly mineralised locally, and underlies the main mineralised horizon. Despite of the fact, and perhaps because, it is a weakly mineralised system, a number of features that give unique insight into the copper mineralisation process, are relatively well preserved at the Ndola West. Although it records a complex history of hydrothermal alteration, and parts of the succession are as strongly K-feldspar altered as any in the Lower Roan (reflecting prolonged interaction with the K-rich ore fluid), Cu-mineralisation is weakly developed. This is interpreted to reflect a lack of existing sulfur sources in and around the rocks that host the mineralisation, and perhaps more importantly, a lack of significant accumulations of organic-derived reductants. Sulfur is interpreted to have been introduced into the small hydrocarbon reservoirs (that now host the low-grade stratabound disseminated Cu-mineralisation) as SO_4^{2-} in the oxidised ore fluid. Interaction with the hydrocarbons eventually led to the generation of reduced sulfur, via thermochemical sulfate reduction, driving sulfide precipitation. The process was evidently sluggish with initial fluid mixing at the trap sites being characterised by barite precipitation (Ba introduced with the hydrocarbons), and the partitioning of copper into silicates as well as (or instead of!) sulfides. Once hydrocarbon reserves were depleted by oxidation reactions, no further sulfide deposition occurred. The inferred low sulfur, low organic-derived reductant system is characterised by a sulfur-poor primary sulfide assemblage dominated by a chalcocite and bornite (chalcopyrite, and particularly pyrite are very rare), and carbonate in and around the ore horizon lacks the strongly negative $\delta^{13}C$ signature that is typical of well mineralised systems (both shale- and arenite-hosted) elsewhere in the Copperbelt and indicates significant incorporation of oxidised light organic-derived carbon.

Introduction

Ndola West is a stratabound copper prospect in the Lower Roan on the NE flank of the Kafue Anticline, approximately 8 km west of Ndola township, and 60 km SE (more-or-less along strike) of Mufulira (Fig. 1). In this area the Lower Roan is folded into a tight syncline (Ndola syncline), flanked by basement rocks (Lufubu Schist and lesser granite). Anglo American tested a stratabound copper target with a series of diamond drill holes between 2000 and 2001, defining a low-grade resource with excellent lateral continuity (>1.4 km) and consistent grade on the NE limb of the syncline. The main Cu-mineralised horizon is however, relatively thin, and the currently defined portion of the mineralising system is sub-economic. This report is based on detailed sedimentary and structural logging and thin section petrography of most of the recent drill holes, including all five (plus two deflections) that intersected copper sulfides. In addition carbonate stable isotope data was obtained from 18 samples from six drill holes, and whole-rock geochemical data for 15 samples from KIT00DD001

and KIT00DD004. Summaries of key petrographic, isotopic and geochemical features are shown plotted against a representative stratigraphic log for the NE limb of the Ndola syncline (Fig. 2, based on logs for drill holes KIT00DD001 and KIT00DD004).

Previous reports on P544 research at Ndola West can be found in Scott (2002a; 2002b; 2002c). These reports were based primarily on core-based observations (e.g., stratigraphy, stratigraphic correlations, depositional environment) and provide only general descriptions of petrography and alteration history, and speculations on the timing and controls on copper deposition. These latter aspects are discussed in more detail here. Scott (2002c) includes interpretive geological sections for each of the drill holes logged as part of this study. In this report, drill hole data is instead presented as detailed stratigraphic logs showing interpreted stratigraphic correlations between drill holes (Figs 3, 4).

The P544 work at Ndola West was part of a broader study into the controls on and distribution of arenite-hosted copper deposits NE of the Kafue anticline. The aim of this report, therefore, is to thoroughly document the stratigraphy, stratigraphic (basin) development, copper mineralisation and alteration history at Ndola West. Genetic considerations are discussed more fully in a companion paper, which compares features of the Ndola West and Mufulira systems (Scott et al. (b), 2003).

Stratigraphy and stratigraphic correlations

Figure 2 is a representative stratigraphic column for the NE-limb of the Ndola Syncline, based on Anglo American's recent diamond drilling at Ndola West. The succession is subdivided into three main packages; namely the footwall, ore and hanging wall formations. Except for the lower part of the footwall formation, the stratigraphy intersected in all of the recent drilling at Ndola West appears relatively consistent (e.g., consistent over 1400 m along strike on the NE-limb of the Ndola Syncline (Fig. 3), and across the axis of the syncline, representing an original distance, orthogonal to strike, of at least 2 km). However stratigraphic relations on the more structurally complex SW-limb of the Ndola syncline are more difficult to interpret (i.e., drill holes KIT01DD001 and KIT01DD002) and the section is less completely sampled by these drill holes (Fig. 4). The major difference in stratigraphy across the syncline is the presence of a >30 m thick package of green-grey argillaceous sandstone and shale, not present in the NE, underlying the pink arkosic sandstone (upper footwall formation) on the SW-limb of the syncline (Fig. 4).

Only the upper part of the Ndola West ore formation is significantly mineralised, however the entire package is interpreted to represent a distinct stage in basin development, and is distinguished on that basis. This terminology also aids comparison with the mine stratigraphy at Mufulira, as the basal unit of the ore formation at Ndola West is interpreted to be stratigraphically equivalent to the C-Orebody, and thus the base of the Ore Formation at Mufulira (Fig. 5, see below).

Footwall formation

The lower 80–90 m of the Ndola West footwall formation are dominated by moderately- to well-stratified, poorly-sorted argillaceous coarse clastics (coarse grained sandstone, pebbly to conglomeratic sandstone and minor conglomerate, all of sub-arkosic to arkosic composition) and lesser intercalated siltstone and shale (Fig 2; Scott, 2002c). Small-scale stratification and cross-stratification throughout the section suggests that although poorly sorted, the conglomerates and conglomeratic sandstones were mostly deposited by streams rather than mass flows. The dominantly argillaceous character of the sequence and abundance of sub-angular to angular clasts within the coarser detritus implies limited transport distances and little attendant winnowing out of fines. The internal sedimentary character of the coarse clastic succession, coupled with the apparent lack of significant debris flow deposits or clast-supported conglomerates suggests deposition occurred within the mid- to distal parts of an alluvial fan or fan system. The pronounced upward coarsening over the basal 20–30 m (true thickness) of the succession, and more poorly defined upward fining and upward coarsening cycles (over 5–10 m intervals) throughout the remainder of the succession (Fig. 2) are consistent with an episodically prograding fan (system),

in response to faulting at the (sub-)basin margins. The poor correlation, in detail, of units comprising the lower footwall succession between drill holes KIT00DD001, KIT00DD003 and KIT01DD002 (Figs 3 and 4) suggests significant lateral facies changes occur over hundreds of metres within this part of the sequence, consistent with deposition from a series of overlapping small alluvial fans.

Although comprising less than 10% of the total succession, shale/siltstone dominated horizons up to several metres thick occur throughout much of the lower part of the footwall formation (Fig. 2). However, as there are no significant changes in the character or composition of the intervening coarser grained sediments, the finer grained horizons are interpreted to represent internal facies variations within the alluvial fan(s) (e.g., fines deposited downstream of longitudinal bars or within abandoned channels), rather than reflecting episodic changes in sedimentary setting. Preservation of finer grained material indicates little reworking after deposition consistent with rapid sediment accumulation within the fans.

In contrast to the relatively argillaceous, poorly sorted character of the lower part of the footwall formation at Ndola West, the upper part consists of generally well sorted, clean (i.e., very little mica after original clay) pale pink to cream arkosic sandstone (Figs 2–4; Scott, 2002c). Both quartz and feldspar grains tend to be well rounded. The unit is relatively massive and internal stratification is principally defined by accumulations of iron oxides (specular haematite) along heavy mineral bands (zircon, tourmaline, rutile) defining bedding and ripple/dune foresets. More rarely stratification is defined by abrupt grainsize variations (e.g., pebbly interbeds) within the arkose. No single drill hole passes through the entire unit (Figs 3, 4), so its total thickness is unknown. Nearly overlapping intersections in drill holes KIT00DD001 and KIT00DD004 on the NE-limb of the Ndola syncline suggest the arkose (including minor interbeds of grey siltstone) is 60–80 m thick (Fig. 2). On the SW-limb of the syncline, >70 m (true thickness) of pink arkosic sandstone and interbedded siltstone (two units ~10 and 15 m thick, respectively) occurs in the top of KIT01DD001. The (1) lack of an interstitial clay component and high degree of sorting and rounding, (2) widely developed small-scale cross-stratification and (3) lateral continuity in two dimensions suggest the pink arkosic sandstone represents a wide braided river system–alluvial plain (braid-plain) deposit. The finer grainsize, lack of interstitial clay and well sorted nature of the sandstones suggests they were deposited by longer path-length drainage systems than the lower part of the footwall formation (e.g., better sorting and rounding due to greater transport distances and reworking). The abrupt nature of the transition suggests it reflects onlap of a long-path length axial drainage system onto shorter path-length (orthogonal) drainage systems developed at the original basin margins (Fig. 6). This change may be due to either widening of the sub-basin due to ongoing extension or denudation of topography at the sub-basin margins.

The thickness (>180 m) and lateral continuity of units in at least the upper part of the footwall formation, and absence of fault proximal facies associations (e.g., talus, debris flows) suggests the Ndola West area was located at some distance from the sub-basin margin, during the initial stage of Lower Roan sedimentation. As facies changes in the footwall formation are more profound across the Ndola West synform, than along strike on either limb, it is likely syn-depositional faults that controlled initial sub-basin development trended NW–SE in this area. The implications of early sub-basin geometry are discussed more fully in the companion report to this paper (Scott et al. (b); 2003).

Ore formation

The Ndola West ore formation conformably overlies the footwall formation. On the NE-limb of the Ndola syncline the ore formation thins towards the north-west, from a maximum thickness of 35 m to >40 m in KIT00DD004 and KIT01DD005, respectively, to about 17 m in KIT01DD004 (Fig. 7). The very thin ore formation in KIT01DD004, however, is partly the result of excision of stratigraphy by later faulting. Due to unforeseen structural complexities prior to drilling, the ore formation is not well sampled by the two drill holes on the SW-limb of the Ndola syncline (Fig. 4). The transition from the footwall formation to the ore formation is marked by both gradual and abrupt changes in the colour, clay (now mica) and

carbonate content of the sandstones. The arkosic sandstone-dominated package at the base of the ore formation (transition unit, 2–7 m thick, Fig. 7) is orange to grey, and much more argillaceous (discontinuous wispy pale grey to buff shale interbeds are a typical feature of the transition unit) and locally more carbonate rich than sandstones in the upper part of the footwall formation. Stratification defined by heavy mineral/haematite is less common and more diffuse in all units above the footwall formation.

Significant lateral facies changes between drill holes are evident in the transition unit. In KIT01DD002 and KIT01DD003 the transition unit fines upward from a basal conglomerate/conglomeratic sandstone that is slightly to significantly coarser grained than the underlying pink arkose (Figs 3, 4). Elsewhere the basal transition unit is finer grained than, or of similar grain size to, the underlying arkose. In drill holes KIT00DD004 and KIT01DD004 the transition unit coarsens upward from fine to medium grained sandstone at the base to conglomeratic sandstone at the top (Fig. 3). The abrupt lateral facies changes and poorly sorted, argillaceous character of the transition unit suggest a return to a depositional setting similar to that which prevailed during deposition of the lower part of the footwall formation. Accordingly, deposition of this unit is interpreted to signify either (1) renewed or accelerated slip on basin bounding faults or (2) development of new fault systems in response to a change in the stress regime.

A conglomeratic sandstone at the top of the transition unit in KIT01DD004 contains numerous randomly oriented <1 cm long millet-seed shaped features, that overgrow the now silicified sandstone framework, and are interpreted to reflect diagenetic overgrowths gypsum (Fig. 8a). If so, they represent the only evaporite minerals (either primary or secondary) observed in the Lower Roan at Ndola West. The sandstone matrix surrounding the silicified gypsum casts is porous and stained by iron oxide. It contains rare sub-mm rhombic pits suggesting dissolution of (Fe-bearing?) carbonate cements and overgrowths. These features do not occur within the gypsum casts, suggesting the carbonate cements formed after gypsum. Dissolution of the gypsum and subsequent infilling by silica predates dissolution of the carbonate which is likely to have occurred in recent times. Detrital K-feldspar grains rimmed by thin discontinuous K-feldspar overgrowths occur in both silicified gypsum casts and the surrounding matrix. This indicates the feldspar overgrowths formed prior quartz precipitation in the gypsum castes and probably before either the gypsum or carbonate cements, and thus represent the earliest diagenetic features evident in the rocks.

Overlying the transition unit is a massive to very poorly stratified package of poorly sorted argillaceous sandstone (Fig. 7). On the northeastern limb of the Ndola Syncline, most of this unit is moderately to strongly carbonate altered (Scott, 2002c). Carbonate (dolomite) occurs within thin veins, in vein haloes, and as irregular patches randomly distributed throughout the rock. In KIT01DD005, carbonate-fill hydraulic breccias occur within the lower part of the unit. Carbonate veins and alteration are overprinted by the S_1 cleavage, which is well developed in this unit as it contains a high proportion of relatively weak soft minerals (dolomite, phlogopite, sericite and haematite). The carbonate veins are generally inclined at a low-angle to the cleavage, but intensely folded veinlets at high angles to the cleavage also occur (Fig. 8b, c). Some carbonate-altered domains possibly reflect preferential replacement of originally coarser grained beds (now inclined at a low angle to cleavage). The argillaceous sandstone commonly approaches 'shale-with-grit' texture, with irregularly shaped patches containing 'out-sized' (<1–2 mm) clasts of quartz and feldspar within a dark argillaceous medium to fine grained sand matrix. In hand specimen, the outsized clasts are most obvious in carbonate-altered domains where the matrix is paler in colour. The patchy carbonate alteration often appears to be localised in domains with a high proportion of coarser grains, however the outsized sand grains occur in both carbonate and non-carbonate altered domains. The high original clay content and poorly sorted and stratified nature of this unit suggests rapid deposition from sediment-rich slurries. Reworking due to de-watering may have also contributed to the poor sedimentary textural preservation within this unit.

A thin (2–5 m) well stratified, medium to thinly bedded package of shale, siltstone and fine-grained sandstone overlies the massive, poorly sorted

argillaceous sandstone (Fig. 7). Many sandstone beds are normally graded, consistent with deposition from turbidity currents, indicating deposition in a relatively deep (sub-wave base), generally quiet water setting (Scott, 2002c). The sedimentary characteristics are very similar to those of the upper part of the Ore Shale at Konkola (i.e., Ore Shale units C to E), and it is interpreted to reflect the same stage/event in basin development (see Selley et al. (a), 2003). The sedimentary progression recorded by the lower three units of the Ndola ore formation is interpreted to reflect accelerated fault-controlled basin subsidence, resulting in, by 'ore shale'-time, the deepest water conditions that existed during deposition of the Lower Roan. For this reason, and the fact that it locally hosts minor 'Konkola-style' Cu mineralisation, the thinly bedded turbidite unit is herein termed the Ndola ore shale. Like the underlying argillaceous sandstone, it is variably carbonate altered. However, carbonate alteration in the Ndola ore shale is strongly stratabound, and is preferentially developed in sandstone layers. Some of the thicker sandstone layers (up to 10s of centimetres) near the base of the unit, are so intensely carbonate altered as to be readily confused with primary carbonate.

The Ndola ore shale is abruptly to gradationally overlain by medium to coarse grained, relatively clean arkosic to sub-arkosic sandstone (Figs 2, 7). The lower part of this unit is typically finer grained and moderately to well stratified, while the upper part is more commonly medium to coarse grained (locally conglomeratic, e.g., KIT00DD004 Deflections 1 and 2) and poorly stratified to massive. This unit is the main host of the disseminated copper mineralisation at Ndola West.

The mineralised arkose is in turn overlain by massive to stratified dolomite. The dolomite contains minor quartz, variable talc (± phlogopite) as well as minor sulfides (pyrite, chalcopyrite, bornite) over the lower few meters, but is otherwise relatively pure. $\delta^{13}C$ values (6.1–7.5‰) for less deformed dolomite samples are the heaviest of any carbonates analysed from the Copperbelt during P544 (Fig. 2b). This signature is interpreted to reflect minor diagenetic or metamorphic modification of original sedimentary carbonate (see below). The thickness of the carbonate between drill holes is extremely variable, although this is probably largely due to shearing (and replacement by up to 6 m (true thickness) of talc schist) along the upper (stratigraphic) contact (Figs 3, 7). The maximum true thickness of the dolomite in the Anglo American drill holes is about 10 m, in KIT01DD005, where it is overlain by a further 5 m (true thickness) of talc schist (Fig. 7). Dolomite is absent in KIT01DD004, where the equivalent stratigraphic position is represented by 2.5 m of talc schist (Figs 3, 7). In other drill holes on the NE-limb of the syncline the combined thickness of the dolomite and talc schist is about 8–10 m. Collectively the dolomite and talc schist form the uppermost unit of the Ndola ore formation (as defined here). However, the range in thickness of units above and below the talc schist, as well as the schist itself, suggest it marks a fault zone that cuts across stratigraphy at a low angle.

The sedimentary progression recorded by units immediately overlying the Ndola ore shale indicates a gradual return to shallower water conditions, following the earlier marine transgression. The relatively clean and massive sandstone that hosts most of the copper sulfide mineralisation was presumably deposited in a moderate to high-energy shallow marine (to fluvial?) environment. The paucity of clastic material in the overlying dolomite, however, suggests either a less energetic environment or that the dolomite was deposited upon a slight topographic high, perched above the level of significant clastic input. The apparent areal extent of the dolomite (similar to the underlying sandstones), suggests the former may be more likely.

Hanging wall formation

On both limbs of the Ndola syncline the talc schist is overlain by a distinctive cream-coloured coarse grained porous sandstone. The unit is massive to poorly stratified and normally graded in some drill holes (Fig. 3). The sandstone is (white-)mica-rich and lacks feldspar, although it was almost certainly sub-arkosic to arkosic originally. Another distinctive feature of the porous sandstone is the presence of sparse cubes to 3 mm of pyrite (now variably oxidised and in some holes may only be recognised as large rusty spots scattered through the sandstone; Scott, 2002c). Pyrite is not observed in any of the stratigraphically lower sandstones.

Detailed subdivision and correlation of the remainder of the intersected hanging wall sequence above the porous sandstone marker is not possible (Fig. 3). This sequence is dominated by monotonous fine to medium grained massive green-grey argillaceous sandstones, often with patchy white to green-grey colour banding, and lesser (cross-cutting?) talc schist bands. The entire hanging wall formation is typically more strongly foliated and more deeply weathered than either the footwall or ore formations. As a result primary textures (including bedding) are for the most part poorly preserved. The upper 10–20 m of the stratigraphic section intersected in KIT00DD004 is thinly bedded, and locally contains abundant (>5%) finely disseminated pyrite. Similar material occurs in KIT01DD004, but it is not known whether this unit correlates with that in KIT00DD004.

Poor preservation of primary textures within the hanging wall formation make reliable interpretations of the environment of deposition difficult. Overall the character of the hanging wall sediments appears most similar to the relatively massive, poorly sorted argillaceous sandstone in the lower part of the ore formation, and a similar environment of deposition appears likely.

Regional correlations

Comparison with the Lower Roan stratigraphy at Mufulira, suggests the carbonate unit capping the Ndola Ore Formation is stratigraphically equivalent to the Lower Dolomite (Mufulira Ore Formation) overlying the B-Orebody (Fig. 5). On this basis, the Ndola ore shale most likely correlates with the dolomite–dolomitic siltstone–shale package (including the basal 'Mudseam') capping the C-Orebody at Mufulira (Fig. 5). The Mudseam and overlying shale-bearing package is the first significant and laterally extensive package of fine-grained sediments in the Lower Roan at Mufulira. Thus the main copper-mineralised sandstone at Ndola West is probably stratigraphically equivalent to the B-Orebody at Mufulira (Fig. 5). As noted previously the Ndola ore shale and its probable correlate the 'Mudseam' at Mufulira are interpreted to reflect the same stage / event in regional basin development as the Ore Shale to the west of the Kafue Anticline.

In previous interpretations of the Ndola area the argillaceous sandstone package above the mineralised horizon (i.e., the dolomite (±talc schist) and hanging wall formation) is correlated with the Upper Roan. However, the hanging wall formation at Ndola West does not contain dolomite, which is the dominant lithology in the Upper Roan at Mufulira. The thin bands talc schist in the hanging wall formation at Ndola West may be the sheared and metasomatised remnants of original dolomite layers. However these cannot be correlated as bedding-parallel units between drill holes, suggesting instead that they occupy faults and shears oblique to bedding. The hanging wall formation at Ndola West appears to correlate more closely with the Hanging Wall Formation (immediately above the Ore Formation) at Mufulira. Accordingly entire Katangan succession at Ndola West is here interpreted as part of the Lower Roan (Fig. 5).

Copper distribution and character

At Ndola West, stratabound copper mineralisation occurred at two levels in the Lower Roan (Scott, 2002c). The upper-most (main) copper accumulation is hosted by the relatively clean arkosic sandstone within the ore formation. Copper sulfides also extend into the lower few meters of the overlying dolomite and occur sporadically (principally within thin sandstone interbeds) through the underlying fine grained turbiditic ore shale. The maximum true width of the mineralised interval is about 10 m. Fine to very fine-grained chalcocite and bornite with interstitial to replacive habit, are the principal copper minerals. Chalcocite occurs as both complex intergrowths with bornite (post-metamorphic exsolution textures, but composite grains probably reflecting original chalcocite–bornite intergrowths), and as a secondary replacement of bornite ± chalcopyrite. Except where remobilised by supergene fluids, the copper sulfides are fairly uniformly disseminated throughout the host arkose.

Copper mineralisation in the Ndola ore shale occurs within thin (2–20 mm) sandstone interbeds, and locally as sparse irregular clots and disseminations extending into the overlying finer grained sediments. In sandstone beds greater than a few millimetres

thick, copper sulfides if present, are commonly restricted to the basal 1–2 mm of the bed). Chalcocite (both intergrown with bornite and secondary) is the principal copper mineral within the ore shale.

The copper sulfides also occur within a thinly bedded package of sandstone, siltstone and shale in the footwall formation, approximately 40 m above the base of the Lower Roan (Fig 2). Cu-sulfides at this stratigraphic level were only intersected in DD00KIT001. No anomalous copper values occur in KIT00DD003, which also intersects the lower part of the footwall formation. Due to the difficulty in correlating units in the lower part of the footwall between KIT00DD001 and KIT00DD003 (Fig. 3), it is unclear whether KIT00DD003 intersects the stratigraphic equivalent of the lower mineralised horizon. The lower mineralised horizon occurs midway through the lower, coarser grained part of the footwall formation. Except for the basal package of interbedded siltstone and sandstone, the lower Cu-mineralised horizon represents the first significant accumulation of fine-grained rocks in the Lower Roan. However, unlike the overlying Ndola ore shale, these sediments are not obviously turbiditic in character. Furthermore, as previously noted, the units above and below this horizon are very similar, suggesting deposition of the finer grained package does not reflect a significant change in basin configuration (cf. Ndola ore shale). The grainsize and distribution of copper sulfides in the lower mineralised horizon is similar to that within mineralised parts of the ore shale, being very fine grained, of interstitial to replacive habit and largely restricted to sandstone interbeds (commonly at layer interfaces with siltstone and shale). The mineralogy is different however, with chalcopyrite (>>bornite) the dominant sulfide. Secondary chalcocite rims some chalcopyrite and bornite grains.

Mineralogy/alteration: Assemblages, geochemical and isotopic signature, distribution and paragenesis

Almost the entire stratigraphic section at Ndola West was affected to some degree by hydrothermal alteration (Figs 2, 3). A number of alteration events can be recognised at Ndola West, although volumetrically the most significant are K-feldspar, carbonate and acidic (K-feldspar destructive) alteration. Based on the evidence outlined below, both carbonate and acidic alteration are interpreted to post-date the main phase of K-feldspar metasomatism. However, as carbonate and acid alteration affect different levels of the stratigraphy, their respective timings are uncertain. All phases of hydrothermal alteration pre-date mid- to upper greenschist facies metamorphism during the Lufilian Orogeny and as a result, the mineral assemblages (and compositions) observed today do not necessarily reflect those at the time of hydrothermal alteration (Scott et al. (a), 2003). Modification and/or re-equilibration of mineral textures and compositions during metamorphism complicates the task of determining the original alteration paragenesis. Furthermore, in some cases the textural modification during metamorphism also makes it impossible to confidently distinguish mineralogical changes related to diagenesis (e.g., quartz or carbonate cements) from those due to later, higher temperature hydrothermal alteration.

The effects of weathering and groundwater leaching also mask the original extent of the various alteration assemblages and leaching that has resulted in the preferential removal or modification (e.g., clay development) of earlier constituents of the rock. Much of the core is pitted with numerous irregular mm- to cm-sized cavities, often coated with iron-oxides (limonite–goethite), The cavities are commonly elongate and roughly aligned in the main cleavage, indicating removal of a patchily developed pre-metamorphic alteration mineral or cement. In many instances leached and pitted core is transitional into fresher rock containing patchily developed dolomite cements and veins, suggesting pits reflect the removal of carbonate. Fe-oxide coatings probably reflect residual iron from the carbonate while the more soluble calcium and magnesium were removed. Although anhydrite was not observed in any of the drill holes, its former presence in pitted sections of core cannot be discounted.

An appreciation of mineralogical changes due to diagenetic hydrothermal alteration requires some understanding of likely original composition and mineralogy of the rocks. Almost the entire Lower Roan section at Ndola West consists of sub-arkosic

to arkosic sandstone with lesser conglomeratic sandstone, siltstone and shale. Definite primary carbonate only occurs at one level in the stratigraphy, capping the ore formation, and there is no evidence of prior accumulations of evaporites within this part of the stratigraphic section. The original composition of the clastic component of the sandstones indicates derivation from a granitic source (cf. local basement which is predominantly meta-quartzite and quartz-mica schist that forms basement in KIT00DD001) and this does not appear to vary significantly throughout the section. The main *primary* compositional difference between the sandstones throughout the section is in the amount of interstitial clay (now mica), which ranges from ~0% to >30%. In the least altered 'clean' arkoses, detrital feldspar (almost entirely microcline) accounts for ~15–20% of sand-sized grains and quartz the rest. However, accessory phases specular haematite, tourmaline, zircon and rutile are locally concentrated in heavy mineral rich bands. The original feldspar content of argillaceous sandstones must have been < 15% due to the larger proportion of clays and detrital micas. The original feldspar content of clastic sediments should also decrease with decreasing grainsize due to preferential breakdown of feldspar (compared to quartz) during weathering and sediment transport. Thus the detrital feldspar content of siltstones was probably <10%, while for true shales it should have been negligible.

K-feldspar alteration

Secondary K-feldspar is widespread at Ndola West, but it is not all of the same age. Secondary K-feldspar occurs as (1) thin, generally discontinuous overgrowths on detrital feldspar grains in relatively clean (interstitial mica / clay-poor sandstones), (2) semi-pervasive to pervasive micro- to crypto-crystalline replacement of (±interstitial) clay in shales, and argillaceous siltstones and sandstones, (3) fine to medium grained intergrowths with barite and copper sulfides within mineralised horizons and (4) locally within 'late-stage' quartz ± K-feldspar (± haematite or Cu-sulfide) veins in the ore and footwall formations.

(1) K-feldspar overgrowths

Units affected: Clean arkosic sandstones and conglomeratic sandstones.
Probable timing: Early diagenetic, pre-Cu mineralisation.

Evidence for timing: Barite that apparently pre-dates copper introduction in the Cu-mineralised arkose overgrows detrital feldspar with overgrowths (e.g., sample 01-DD3-7). In mineralised units overgrowths never encase Cu-sulfides. Sample 01-DD4-10 preserves millet seed shaped domains of quartz cemented arkosic sandstone (Fig. 8a). The original inter-granular porosity in the surrounding material was apparently cemented by dolomitic carbonate. The distribution indicates the quartz cement was precipitated following the dissolution of gypsum, but while carbonate cement was largely intact. While quartz cement is restricted to gypsum casts, feldspar overgrowths occur in both the formerly gypsum-encased domains and the surrounding (formerly carbonate cemented) arkosic sandstone.

Significance: Overgrowths depleted in Na and Ba relative to detrital grains. Suggests interaction with pore / ground waters may have enriched basinal fluids in these elements.

The thin K-feldspar overgrowths on detrital grains (Fig. 9a–c) are interpreted to be diagenetic in origin, formed as a result of dissolution-precipitation reactions transferring material away from higher stress grain-grain contacts during compaction. Both optically continuous and optically discontinuous overgrowths (with respect to the host grain) occur. Electron microprobe data shows the overgrowths are consistently lower in Na ± Ba than the detrital K-feldspar (Fig. 10).

(2) Fine grained interstitial secondary K-feldspar

Units affected: All argillaceous sandstones and conglomeratic sandstones, siltstones and shales. Absent in 'clean' sandstones (Figs 2, 3).

Probable timing: Late diagenetic to early syn-D_1. Coeval with Cu-mineralisation.

Evidence for timing: Pre-dates carbonate and acidic (K-feldspar destructive) alteration. Necessary existence of clay or low-grade mica precursor in K-feldspar metasomatised rocks suggests alteration occurred prior to low-grade metamorphism (Scott et al. (a) 2003).

Significance: Pervasive development and lack of evidence for fracture-control on distribution or intensity of K-feldspar alteration suggests gradual fluid infiltration by reaction-enhanced permeability through reaction with clay. Lack of associated veins suggests fluid infiltration occurred at relatively low fluid pressures ($P_f < \sigma_3 + T$, where P_f is the fluid pressure, σ_3 is the least compressive stress, and T is the tensile strength of the rock; cf. later-stage quartz–K-feldspar veins).

Semi-pervasive to pervasive micro- to crypto-crystalline K-feldspar is the most widespread form of secondary K-feldspar at Ndola West, and is volumetrically the most significant alteration affecting the Lower Roan (Fig. 9d, e). K-feldspar alteration affected the entire stratigraphic section except for the thick pink heavy mineral stratified sandstone at the top of the footwall formation and the dolomite that caps the ore formation (Figs 2–4). On the NE-limb of the Ndola Syncline, however, there is a laterally extensive zone of K-feldspar destruction immediately above the ore formation that extends at least 50 m into the hanging wall (Fig. 3). Pockets of K-feldspar metasomatised rocks occur within this zone, and rocks at the same stratigraphic position on the SW-limb of the syncline are strongly K-feldspar metasomatised suggesting the K-feldspar-destructive alteration postdates K-feldspar metasomatism (see below).

Due to the generally very fine grainsize of the secondary K-feldspar (difficult to distinguish from quartz in thin section) the intensity of K-feldspar metasomatism can only be assessed using wholerock geochemical data or by staining samples for K-feldspar. Wholerock geochemical data was obtained for 15 samples at Ndola West, and the K-feldspar contents of these samples (Fig. 2) were estimated using the MINSQ program (Herrmann and Berry, 2002). Fifty-six samples (including 11 of samples with wholerock geochemical data) were stained for K-feldspar (Fig. 3). Correlation of the intensity of K-feldspar stain with MINSQ estimates for K-feldspar content suggests the most strongly K-feldspar metasomatised rocks, shales and siltstones, typically contain 30% secondary K-feldspar. In clean arkosic sandstones, the proportion of detrital K-feldspar to quartz is typically 1:4–5 (Fig. 9a–c), i.e., Ksp/(Ksp+Qtz) = 17–20%. Assuming this to represent the maximum ratio of K-feldspar to quartz in sandstones, the extent of K-feldspar metasomatism in (argillaceous) sandstones was assessed using MINSQ estimates of K-feldspar and quartz content based on wholerock geochemical data. This indicates most argillaceous sandstones in the Lower Roan at Ndola West have K-feldspar contents that are 50–100% higher than can be explained by detrital components (Fig. 2).

In addition to providing semi-quantitative constraints on the K-feldspar content of samples, staining also reveals the grain-scale distribution of K-feldspar. None of the 56 samples stained as part of this study revealed any fracture control (at any scale) on the intensity of K-feldspar alteration, implying fluid access was via either residual permeability (relict primary porosity), secondary porosity or reaction-enhanced permeability. In fact, the fundamental control on the distribution of secondary K-feldspar appears be the initial clay content of the sediments. Clean sandstones, such as those in the upper part of the footwall lack K-feldspar alteration, while the matrix of argillaceous sandstones may show similar intensities of K-feldspar alteration to siltstones and shales (NB. total K_2O contents of sandstones are lower due to greater proportion of detrital quartz). The lithologic control on the distribution of K-feldspar alteration is readily explained by the low solubility of aluminium in low temperature, acidic to near-neutral oxidised fluids (Cooke, 2003). As the K-rich fluids could not transport significant concentrations of Al, Al in the secondary K-feldspar must have been sourced from an existing Al-bearing phase, namely the clays and low-grade micas already present in the rock. Conversion of clays to a K-feldspar ± mica assemblage (see Scott et al. (a) 2003) probably created secondary porosity that would have promoted further fluid infiltration. In the clean arkosic sandstones, detrital K-feldspar is the only significant Al-bearing phase so the rock was non-reactive. If the clean sandstones were well compacted or cemented at the time of K-feldspar

metasomatism, they may have been impermeable to the K-rich fluids. Due to the lack of clay in the dolomite capping the ore formation, it was also unaffected by (and impermeable to?) the K-feldspar metasomatism.

As K-feldspar metasomatism at Ndola West was facilitated by reaction-enhanced permeability, the pervasive nature of the alteration can not be taken as evidence that the rocks were either relatively porous or poorly lithified at that time. However, if Al was principally sourced from clays, K-feldspar alteration must have occurred prior to low-grade metamorphism. Scott et al. (a, 2003) speculate on the other mineralogical changes that accompanied K-feldspar metasomatism, based on considerations of element mobility and the composition and likely precursors minerals of metamorphic micas. It is likely that Mg-chlorite, sericite, haematite and rutile (TiO_2) were precipitated along with K-feldspar in areas where no organic-derived reductants (hydrocarbons, sour gas) were present. Copper sulfides ± pyrite were deposited instead of haematite where reductants were present. Tourmaline is also commonly developed/enriched in K-feldspar altered rocks (e.g., Darnley, 1960; Selley et al. (b), 2003). As Ti and Al were immobile during K-metasomatism (Large et al. (a), 2003), and Fe is relatively insoluble in near-neutral fluids the hydrothermal mineral assemblage principally reflects the addition of K and Mg from the brines. The origin of boron in tourmaline $[Na(Mg,Fe)_3Al_6Si_6O_{18}(BO_3)_3(OH,F)_4]$ is more problematic, and may have been either derived from clay or exotically sourced.

(3) K-feldspar intergrowths with barite and Cu-sulfides

Units affected: Restricted to the Cu-mineralised arkose, but preservation variable (weathering, retrograde metamorphism +/-carbonate alteration). Generally barite ± K-feldspar aggregates are at least partially replaced by felted masses of fine-grained mica, quartz and Fe-oxides.

Probable timing: Late diagenetic to pre-metamorphic, syn- to post-oil window. Barite predates carbonate alteration.

Evidence for timing: Chalcopyrite and bornite rim or partially replace barite in the mineralised arkose. Dolomite and chlorite commonly partially replace barite.

Significance: The restriction of barite to the main mineralised unit suggests Ba (an organophile) was most likely transported with the hydrocarbons (or associated organic acids) as this is the only other phase (other than copper) that was restricted to this specific horizon. Barite was subsequently precipitated due interaction with the Cu-bearing oxidised K-rich brines provided they contained sufficient SO_4^{2-}. The intergrowths of barite and K-feldspar thus reflect coupled mixing between oxidised and reduced (i.e., hydrocarbons) fluids and reaction with interstitial clay. Alternately 10s–100 ppm of Ba can be transported in oxidised fluids with low (~100 ppm) sulfate concentrations (McGoldrick, 2003). However it is difficult to explain why an oxidised fluid carrying Ba, Cu and SO_4^{2-} would first deposit barite and then sulfides upon entering a reduced and potentially more acidic trap site (both of which should Ba more soluble).

Within the main mineralised arkose some K-feldspar, interpreted to be secondary, is both (1) intergrown with or encased by barite (Fig. 11a, b) and (2) concentrated around or intergrown with copper sulfides (Fig. 11c). Although some feldspar grains in these aggregates may be detrital, or at least have detrital cores, others have unabraded euhedral grain boundaries (distinct from anhedral diagenetic overgrowths) in contact with either barite or copper sulfides suggesting a secondary origin. Electron microprobe data for some of these grains reveals anomalously high Ba or Cu contents relative to detrital K-feldspar (and diagenetic overgrowths), consistent with the inferred secondary origin (Fig. 10).

K-feldspar–barite intergrowths are restricted to Cu-mineralised arkose of the ore formation (see also Fig. 2c), and appear best developed in the lower part of the unit. In thin-section there is no consistent spatial relationship between barite and copper sulfides. Where the two are in contact copper sulfides either rim or (only? in the case of chalcopyrite) partially replace barite (Fig. 11e, f).

The origin of barite at Ndola West is somewhat enigmatic as barium can be transported in both reduced fluids (e.g., hydrocarbons ± sour gas) and oxidised fluids that are low in SO_4^{2-} (Cooke et al., 2000). Barium solubility also increases with either increasing salinity or decreasing pH (Cooke et al., 2000). Barite precipitation is most likely to occur as a result of either an increase in pH of a highly acidic fluid or an increase in SO_4^{2-}. At Ndola West there is little evidence to suggest pre-existing diagenetic sulfate (anhydrite) anywhere in the section, and pyrite does not occur below the level of the dolomite capping the ore formation. Thus there was no obvious local source of sulfur (other than potential accumulations of sour gas (H_2S) within the hydrocarbon trap) to account for the sulfur in the Cu-sulfides and barite. If the Ba was introduced in oxidised fluid, precipitation of barite precludes the existence of significant H_2S at the trap site as this would precipitate copper sulfides and increase Ba solubility. This leaves the oxidised ore fluid (Cu-bearing K-rich brine) as the most plausible source for the sulfur. However if the oxidised fluid carried Ba, Cu and SO_4^{2-} it is difficult to explain the observed timing relationship between barite and Cu-sulfides. Overprinting relations between these minerals indicate a progressive decrease in the SO_4^{2-}/S^{2-} following interaction with the hydrocarbons. This is readily explained by progressive thermochemical reduction of ore fluid sulfate by the hydrocarbons. Accordingly the solubility of Ba in the hydrocarbon reservoir would be at a minimum (i.e., most likely to precipitate barite) during the initial stages of interaction with the oxidised fluid, before significant sulfate reduction occurred. In contrast, the solubility of any Ba in the oxidised fluid would be at a minimum *prior* to interaction with the hydrocarbon reservoir.

(4) 'Late' quartz–K-feldspar fibre veins

Units affected: Restricted to relatively brittle (quartz-rich) units, particularly in the upper part of footwall and lower ore formation and within the Cu-mineralised arkose of the ore formation.

Probable timing: Pre- to syn-D_1, post-stratabound disseminated copper mineralisation.

Evidence for timing: Where the veins occur in Cu-mineralised rocks, disseminated sulfides are leached in vein haloes (up to a few centimetres wide) and apparently re-deposited as coarser grained aggregates within the veins. Fibrous character indicates the veins formed by episodic, incremental opening during deformation. Veins are weakly overprinted by the S_1 cleavage, but not significantly folded. Veins are oriented at a high-angle to S_1, but mineral fibres are generally elongate sub-parallel to S_1, suggesting they formed during the same deformation event.

Significance: Veins are oriented at a high angle to steeply inclined drill holes and cleavage and are thus gently dipping. Vein fibres are oriented perpendicular to the vein walls, consistent with extensional opening during horizontal compression, when the condition $P_f = \sigma_3 + T \approx \sigma_v + T$ was met (NB. σ_3 is equal to σ_v the lithostatic pressure, during horizontal compression). Within the mineralised arkose the veins contain copper sulfides leached from the immediately adjacent wall rocks. Elsewhere the veins contain haematite. These relations suggest vein mineralogy reflects local wall rock composition.

Quartz ± K-feldspar ± haematite veins ranging from <1 cm to 5 cm wide, and oriented at high angles to bedding occur throughout much of the footwall but are best developed towards the top of the clean arkosic sandstone and in the overlying 'transition unit' at the base of the ore formation. Similar quartz ± K-feldspar ± Cu-sulfide veins occur within the Cu-mineralised arkose of the ore formation (Fig. 9e). Accordingly veins appear to be preferentially developed in relatively well silicified or quartz-rich units (clean sandstones) adjacent to more mica-rich units, suggesting a strong rheological control on vein distribution. Vein-fill ranges from fibrous to coarse crystalline, and where developed fibres are perpendicular to vein margins indicating purely extensional opening.

The veins are invariably oriented at high-angles to bedding, cleavage (S_1) and the core axis in drill holes on the NE-limb of the Ndola syncline, and thus have moderate to gentle westerly dips. The veins are overprinted by S_1, but much less intensely deformed than the carbonate veins that occur throughout much of the lower part of the ore formation (see below). The difference in intensity of deformation may however simply reflect the greater competency of the

quartz–K-feldspar veins and their host rocks, rather than or in addition to a difference in age. Although overprinted by S_1, fibres in the quartz ± K-feldspar veins are generally oriented at a low angle to the foliation suggesting the veins may have formed during the latter stages of the D_1 deformation event.

The mineralogy of the veins appears to closely reflect that of the host rocks. Veins cutting the footwall formation generally have fibres or crystals of haematite in addition to quartz and K-feldspar. In contrast, veins cutting the mineralised arkose contain copper sulfides (chalcopyrite, bornite and (secondary) chalcocite) rather than haematite (Fig. 12a–c). Copper in the veins was apparently stripped from the immediately adjacent wall rocks, which are devoid of disseminated Cu-sulfides within a few centimetres of the veins (Fig. 12a). Chalcopyrite is proportionally more abundant within the vein sulfide assemblage compared to the primary chalcocite–bornite dominated disseminated sulfide assemblage in the wallrocks. Within the ore formation, barite is also a minor constituent of the quartz ± K-feldspar veins and their surrounding alteration haloes (extending up to 10 cm from the veins). Barite occurs in association with fibre veins up to 20 m stratigraphically below the level containing the only significant (stratabound) barite accumulations (i.e., the Cu-mineralised arkose). Vein-hosted barite is partially replaced by chalcopyrite and bornite in the mineralised arkose (Fig. 12d, e), apparently repeating the paragenetic relationship between the earlier generation of these mineral phases in the wall rocks. Reduction of vein sulfate (barite) during episodic fluid exchange between the veins and the wall ocks, may have provided additional S^{2-} which promoted chalcopyrite–bornite precipitation within the veins (rather than the typical wall rock bornite–chalcocite assemblage).

Albite alteration

Units affected: Cu-mineralised thin sandstone interbeds within Ndola ore shale, pyritic siltstone sandstone in the hanging wall formation, and possibly at the level of the lower Cu-mineralised horizon in the footwall formation.

Probable timing: Syn-Cu mineralisation, pre- to syn-K-feldspar alteration.

Evidence for timing: Albite is restricted to sites of copper sulfide deposition, and the two phases (+ secondary quartz) are intimately intergrown. Albite also contains minor amounts of copper (up to 0.5 wt % Cu) either in solid-solution or as very fine-grained inclusions. Timing relations with K-feldspar are more equivocal but the fact that there are sharp boundaries and no overprinting between domains of albite (+Cu) and K-feldspar deposition, and that K-feldspar alteration completely envelopes domains of albitic alteration suggests albite either pre-dates or was synchronously precipitated with K-feldspar.

Significance: The strong coupling between albite and copper sulfides in the Ndola ore shale suggests either a change in the state of fluid led both to precipitate, or precipitation of one phase resulted in precipitation of the other. It is considered most likely that the albite-copper precipitation was broadly synchronous with K-feldspar metasomatism. A possible scenario involves interaction between the K-rich oxidised ore fluid and small pockets of residual hydrocarbon- or organic acid-charged saline brine (principally residing within the more porous thin sandstone interbeds). As a result fluid mixing increases in the Na/K and H_2S/SO_4^{2-} ratios of the Cu- and SO_4^{2-}-bearing ore fluid changed sufficiently to precipitate albite (plus quartz) instead of K-feldspar and, once thermochemical reduction of ore fluid sulfate was well underway (see above), copper sulfides.

At Ndola West, sodium is slightly elevated at the three stratigraphic levels in the Lower Roan with appreciable sulfide enrichments; namely: (1) the lower Cu-mineralised horizon in the footwall, (2) the Ndola Ore shale and overlying Cu-mineralised arkose, and (3) pyritic siltstone and shale in the hanging wall formation (Fig. 2). Minor albite probably accounts for the elevated sodium in both the ore and hanging wall formations, however at the level of the Cu-mineralised horizon in the footwall, sodium is principally contained in scapolite ($Na_4Al_3Si_9O_{24}Cl$). At this level millimetre-sized scapolite porphyroblasts with a strong crystallographic preferred orientation occur principally within shale beds, where they overgrow

S_1 and are locally intergrown with chalcopyrite. A weak S_2 crenulation overprints the scapolite porphyroblasts. These relations indicate scapolite probably grew at peak metamorphic conditions syn- to post-S_1 development and syn- to post-copper introduction (Scott, 2002c). The fact that scapolite is preferentially developed in shale layers, which should have been less permeable than surrounding layers under greenschist facies metamorphic conditions, suggests sodium enrichment occurred prior to metamorphism. Biotite from this stratigraphic level has elevated Cl. (relative to phlogopite elsewhere in the Lower Roan section at Ndola, Scott et al. (a), 2003), suggesting these rocks were impregnated with NaCl or highly saline pore water prior to metamorphism.

Four wholerock geochemical samples from the ore formation show a small increase in Na content towards the mineralised arkose, which contains 0.34 wt % Na_2O, or <4 wt % albite (Fig. 2). Textural relations within the arkose, particularly between copper sulfides and albite, are generally not definitive, however some albite appears to replace K-feldspar. In the underlying Ndola ore shale, although overall the albite content is <1–2 %, it is intimately associated with the copper sulfides (Figs 13, 14). Where the Ndola ore shale is mineralised very fine-grained copper sulfides are preferentially developed in thin fine-grained sandstone interbeds or form irregular clots and disseminations in the adjacent siltstone layers. Although the ore shale is for the most part uniformly enriched in secondary K-feldspar the sulfide clots are intimately intergrown with microcrystalline albite and quartz but not K-feldspar (Figs 13, 14). Albite only occurs where copper sulfides are developed; barren but otherwise identical ore shale is pervasively K-feldspar metasomatised throughout. Boundaries between albite and K-feldspar altered domains are invariably sharp with no obvious overprinting relationships between K-feldspar and albite (Fig. 13). However as albite-altered domains are enveloped by K-feldspar alteration it seems most likely that albite (+ Cu-sulfides) were deposited either prior to or synchronously with the secondary K-feldspar.

In detail, copper sulfides in the Ndola ore shale are both enveloped by, and finely disseminated through the microcrystalline aggregates of albite and quartz (Fig. 13d, e). Some coarser grained sulfides contain euhedral inclusions of hydrothermal quartz (Fig. 14a–c). Probe data indicates secondary quartz and albite commonly contain small amounts of copper (e.g., 0.3 wt % Cu: average of 10 albite analyses: Fig. 14d, and 0.9 wt % Cu: average of 8 quartz analyses: Fig. 14e). However, in only one of the 17 grains with Cu above detection is the copper content likely to be explained by a sulfide inclusion (Fig. 14e). In general, sulfur concentrations are below detection. Although the electron microprobe beam penetrates a few microns below the polished surface of quartz and feldspar grains, emissions from lighter elements comprising 'buried' inclusions may be absorbed by the host mineral, and not detected. Accordingly the failure to detect sulfur (atomic weight 32.06) along with copper (atomic weight 63.55) does not necessarily discount the possibility that copper occurs as minute sulfide inclusions. However within the quartz grains, where such high copper contents can only be explained by inclusions, aluminium contents (atomic weight 26.98, slightly lighter than sulfur) are generally above detection and display a crude sympathetic variation with copper (Fig. 14e). One quartz grain contains an inclusion that is large enough to resolve optically. It is a pale green translucent mineral (Fig. 14c), and assuming it to be the source of the Cu and Al, it is likely to be chrysocolla ($(Cu, Al)_2H_2Si_2O_5(OH)_4.nH_2O$). The origin of the elevated copper in the albite is less certain because the aluminium content does not help distinguish between copper bearing inclusions and copper incorporated into the feldspar lattice.

Paragenetic relations in the Ndola ore shale have several important implications for controls on copper precipitation. The strong coupling between albite and copper sulfides indicates that either a change in the state of fluid led both to precipitate, or the precipitation of one phase resulted in precipitation of the other. This is in contrast to the relationship between secondary K-feldspar and copper sulfides elsewhere in the Copperbelt. While copper was most likely transported in the oxidised K-rich brines (Selley et al.; Large et al.; Cooke; 2003), K-feldspar deposition did not affect the stability of copper complexes as K-feldspar was deposited either with or without copper sulfides. Given (1) the overall intensity of K-feldspar metasomatism in the Ndola ore shale, (2) sharp boundaries and lack of

overprinting between domains of albite (+Cu) and K-feldspar deposition, and (3) the evidence that copper was transported in the K-rich brines, it is considered most likely that a precursor phase at the eventual sites of copper deposition, increased the Na/K and H_2S/SO_4^{2-} ratios of the Cu- and SO_4^{2-}-bearing ore fluid to the extent that albite + quartz + copper sulfides were deposited instead of K-feldspar. The most likely candidate would thus appear to be a residual, highly saline hydrocarbon- (or organic acid?)-charged brine locally within and adjacent to the thin sandy interbeds. Although the change from microcline/albite stability is also controlled by temperature (with higher temperatures favouring albite precipitation), it is difficult to envisage how temperature variations could explain the observed distribution of albite and sulfides.

The fact that euhedral quartz crystals (± albite), which formed synchronously with or prior to sulfide precipitation, contain copper-bearing (?)silicate minerals and that copper also substituted into the feldspar crystal lattice suggests (1) that availability of reduced sulfur, at least initially, was limited and (2) that copper precipitation was not solely driven by reaction with sulfide ions. Progressive thermochemical reduction of small amounts of sulfate in the ore fluid (due to interaction with the small pockets of hydrocarbon) to produce S^{2-} is considered the most likely explanation for the change from Cu in silicates to sulfides

Carbonate alteration

Units affected: Ore formation (particularly the massive poorly sorted arkose) and locally throughout the footwall (typically finer grained units). However, the numerous mm- to cm-sized dissolution cavities developed in the footwall sandstones suggest patchy to pervasive carbonate cements were once much more extensive. No carbonate occurs in the hanging wall formation, although as the core at this level is much more leached / weathered and carbonate preservation potential is much lower. In the poorly sorted argillaceous sandstone of the ore formation, carbonate alteration was accompanied by the local development of veins and hydraulic breccias. In the overlying Ndola ore shale, carbonate is strongly partitioned into sandstone layers.

Probable timing: Pre-D_1, post-K-feldspar metasomatism.

Evidence for timing: Carbonate grains strongly aligned in the S_1 fabric and S_1 axial planar to tightly folded carbonate veinlets in the lower part of the ore formation. Carbonate alteration appears to overprint both disseminated copper sulfides and the pervasive K-feldspar metasomatism. However, the effects of metamorphism commonly mask earlier textural (and thus paragenetic) relations. In the mineralised arkose the normally uniformly disseminated copper sulfides (±interstitial secondary K-feldspar) are less abundant and more patchily developed in the strongly carbonate altered rocks. More pronounced structural and lithological controls on the distribution of carbonate alteration suggest the rocks were potentially more lithified than appears the case for the pervasive K-feldspar metasomatism.

Significance: Carbonate alteration is best developed in the units underlying the mineralised arkose, but no clear genetic association with Cu-sulfides is evident. The carbon isotopic signature of the carbonate (Fig. 2) is not strongly shifted to the highly negative values (e.g., $\delta^{13}C < -15$ ‰) indicative of 'ore stage' oxidation of light organic-derived carbon (see Large et al. (b), 2003).

Carbonate (dolomite) alteration is well developed at several levels in the stratigraphy, but principally within the ore formation. Although the most intensely carbonate altered rocks occur in the immediate stratigraphic footwall of the main Cu-mineralised horizon (which is also variably carbonate altered), no genetic relationship between the copper deposition and carbonate alteration is apparent.

There is a crude antithetic relationship between the distribution of disseminated sulfides and patchy carbonate-altered domains in the mineralised arkose. In the Ndola ore shale carbonate alteration is preferentially developed in the coarser grained layers (fine to medium grained sandstone) and spottily developed in adjacent siltstone layers. Because Cu-sulfides are also preferentially developed in these layers there is locally a strong spatial correlation between the two (Fig. 13a). However Cu-sulfides also occur in non-carbonate altered beds, and vice versa.

Some sandstone layers (particularly near the base of the ore shale in KIT01DD005) are so pervasively metasomatised as to be readily mistaken for primary carbonates. However the C-isotopic signature of carbonate in these beds is generally similar to the clearly metasomatic carbonate in the underlying argillaceous sandstone (Fig. 2b).

The argillaceous sandstone in the ore formation is the most intensely and consistently carbonate altered unit in the Lower Roan, with carbonate veins and carbonate-cemented hydraulic breccias locally well developed (Figs 2b, 8b, c, see also Scott 2002). Weakly carbonate altered parts of this unit now have the metamorphic mineral assemblage: quartz + phlogopite + K-feldspar + carbonate + up to 5% finely disseminated haematite. With increasing intensity of carbonate alteration first K-feldspar, then haematite, quartz and finally phlogopite are progressively removed from the resultant metamorphic assemblage. The most intensely carbonate altered units now contain >80% dolomite, with minor quartz and phlogopite.

Three to 8 mm thick elongate carbonate-rich 'vein-like' bands or layers with narrow phlogopite rich selvedges occur within the argillaceous sandstone. These features are typically oriented at a low angle to the S_1 foliation (generally well developed in this unit due to the abundance of dolomite and mica). Although the intensity of deformation is such that original grain textures are not preserved, many of these bands contain higher concentrations of medium- to coarse-grained detrital quartz (± K-feldspar) grains than the adjacent phlogopite-rich domains. This suggests that rather than veins, many of these features are relict thin sandy interbeds, that were preferentially carbonate altered because they were more porous than their surroundings.

Acid (K-feldspar destructive) alteration

Units affected: Lower part of the hanging wall formation and *possibly* within the upper part of the Cu-mineralised arkose of the ore formation. In drill holes on the NE limb of the Ndola syncline, the zone of K-feldspar destruction extends from the porous sandstone marker immediately above the ore formation at least 50 m into the hanging wall. Relict pockets of K-feldspar-bearing argillaceous sandstone occur within this zone (Fig. 3), and rocks at the same stratigraphic level on the SW-limb of the syncline both retain detrital K-feldspar and are strongly K-feldspar metasomatised. The porous sandstone marker (basal hanging wall formation) is acid altered on both sides of the Ndola synform.

Probable timing: Pre-D_1, post-K-feldspar metasomatism.

Evidence for timing: K_2O/Al_2O_3 ratio of syn-D_1 phlogopite from acid altered zones is much lower than that elsewhere in the section (Fig. 2), implying a low K-feldspar content prior to metamorphism (Scott et al. (a), 2003). Relict(?) pockets of K-feldspar-metasomatised rocks within the acid altered zone on the NE-limb of the syncline suggest acid alteration post-dates K-feldspar metasomatism (Fig. 3). Fine-grained needles of tourmaline (locally up to 1–2% of the rock) throughout the acid altered zone may be a product of that alteration. However the tourmaline is similar to that deposited in association with the K-feldspar alteration and could provide further evidence these rocks were K-feldspar metasomatised prior to acid alteration.

Significance: K-feldspar destruction and preservation of a quartz + phlogopite sericite + ± chlorite + tourmaline ± pyrite assemblage indicates alteration by acidic fluids. Elsewhere in the Copperbelt it has been argued acidic alteration is spatially and genetically associated with copper mineralisation in some (formerly arkosic) sandstones (Darnley, 1960; Scott et al. (b), 2003). Scott et al. (b) (2003) interpret acid alteration to result from mixing between the oxidised ore fluids and sour gas (H_2S)-rich hydrocarbon reservoirs to produce sulfuric acid. As such the acid originates at the site of ore deposition. The lateral extent of acid alteration (away from the immediate ore environment) should reflect the volume and strength of acid produced (proportional to the size of the sour gas reservoir) and the mineralogy of rocks along the outflow path. If K-feldspar and carbonate are plentiful 'downstream' of the original sour gas reservoirs, acid pore fluids may be rapidly neutralising through reaction with the rock (restricting acid alteration to the near ore environment). Alternately zones of acid alteration of feldspar might be quite extensive

where the 'outflow' is confined to a relatively narrow aquifer, and/or carbonate the carbonate content of the rock is minor. If the latter explains the zone of acid alteration at Ndola West, it apparently formed down-stream of a major Cu deposit.

K-feldspar is generally absent in rocks in the lower part of the hanging wall formation on both limbs of the Ndola syncline (Fig. 2a). The porous sandstone marker at the base of the hanging wall formation consists of recrystallised originally well sorted quartz grains in a strongly foliated matrix of fine grained very pale brown to colourless mica (muscovite + phlogopite ± chlorite assemblage) and tourmaline (Fig. 15a–d). The sandstone lacks haematite, but contains sparse cubes of pyrite (mostly altered to limonite-goethite) up to 5 mm across (Fig. 15a). The distinctive mineralogy of this unit (all stratigraphically lower sandstones are sub-arkosic to arkosic, and are mostly haematitic) is not due to an abrupt change in sedimentary provenance, but acidic alteration. On the NE-limb of the Ndola syncline, the zone of K-feldspar destruction extends ~50 m (true thickness) into the hanging wall formation, and only small pockets of K-feldspar-bearing sandstone persist (Fig. 3). On the SW-limb of the Ndola syncline, acidic alteration appears largely restricted to the porous sandstone marker, as the overlying argillaceous sandstone contains both detrital and abundant interstitial metasomatic K-feldspar (Fig. 4).

Metamorphic modelling using wholerock geochemical data for sample RJS-48 (acid altered zone, 167.5 m KIT00DD004) suggests K-feldspar was present as a minor constituent of the rock at temperatures below 400°C, but was consumed by reaction with sericite and chlorite at peak metamorphic conditions (Scott et al. (a); 2003). Although bulk rock composition (and thus the results of the metamorphic modelling) may have been affected by post-metamorphic K-loss, phlogopite compositions from the acid altered zone also suggest K-feldspar destruction predated metamorphism. Phlogopite from the acid altered zone has a lower K_2O/Al_2O_3 ratio (0.52–0.58) than that elsewhere in the stratigraphy (i.e., K_2O/Al_2O_3: 0.63–0.72 (av. = 0.66) implying little K-feldspar was present in the rock prior to greenschist facies metamorphism (see Scott et al. (a), 2003, for further discussion).

Elsewhere in the Copperbelt, acidic alteration is both spatially and genetically associated with copper mineralisation, e.g., sericitic alteration of ore shale cap to footwall mineralisation at Mwambashi B (Selley et al. (b); (c), 2003), sericitic ± carbonaceous Orebody quartzites at Mufulira: (Darnley, 1960; Scott et al. (b), 2003) and Chibuluma (Darnley, 1960). Scott et al. (b) (2003) interpret acid alteration to result from mixing between the oxidised (ore) fluids and sour gas (H_2S)-rich hydrocarbon reservoirs to produce sulfuric acid, and as such, this style of alteration may be a direct indicator of the ore formation process. The volume of acid (and acid altered rocks) produced should reflect the size of the sour gas reservoir, and thus the size of the reductive trap for copper transported by the oxidised fluids. If the zone of acid alteration on the NE-limb of the Ndola syncline reflects the subsequent passage of the 'spent' ore fluid, the amount of acid involved suggests the associated copper deposit could be very large indeed.

It is unlikely that acid alteration in the hanging wall formation is directly related to the currently defined Cu-mineralisation at Ndola West. Wholerock geochemical data and samples stained for K-feldspar from the NW-limb of the Ndola syncline show a pronounced decrease in K-feldspar content (to <10 %) up-section through the main mineralised arkose (Fig. 2). The apparent K-feldspar destruction could be partly due to acid generated during Cu-mineralisation. However, petrographic examination of the mineralised arkose shows that altered K-feldspar is generally replaced by carbonate or quartz and more rarely by sericite or albite. Thus K-feldspar destruction does not appear to be solely, or even principally, due to acid attack. Unless formed during later alteration, common to abundant interstitial carbonate within the mineralised arkose should have neutralised any acid generated through the interaction between H_2S and the oxidised ore fluid.

Discussion and conclusions

Although rocks at Ndola West are for the most

part moderately to strongly deformed and strongly altered, the apparently less intense nature of the Cu-mineralising system has resulted in preservation of many features and paragenetic relationships that provide important insights into the evolution of the system. Like correlative rocks west of the Kafue anticline, the Lower Roan at Ndola West records a complex history of both diagenetic and hydrothermal alteration. All argillaceous rocks (i.e., argillaceous sandstones, conglomerates, siltstones and shales) in the Lower Roan were moderately to strongly K-feldspar metasomatised in the earliest significant phase of hydrothermal alteration. Circulating basin brines that interacted with the carbonate and (originally) evaporate-dominated Upper Roan (not preserved at Ndola West) are likely to have been strongly enriched in K, Na, Mg and Ca. Fluid modelling (Koziy et al., 2003), suggests such brines should have descended significant depths into the basement, before gradually heating and rising back into the Katangan cover sequences due to increased buoyancy. Interpreted albite deposition along higher temperature portions of the flow path (principally faults and shear zones) may have increased the K/Na ratio to the extent that K-feldspar became the stable feldspar phase at lower temperature (i.e., subsequent fluid interaction with at least shallow levels of the basement and the Lower Roan) (Koziy et al., 2003).

Element mobility considerations (i.e., Ti, Al, Fe al ~immobile) and the restriction of K-feldspar metasomatism to argillaceous rocks indicate that in the Lower Roan the K- and probably Mg-rich enriched brines reacted with clays (and low-grade micas) to form a K-feldspar > Mg-chlorite ± sericite ± haematite + rutile ± tourmaline alteration in argillaceous rocks. Primary controls on the abundance of secondary K-feldspar in the Lower Roan at Ndola West are thus initial clay content of the sediments and duration and intensity of interaction with the K-rich brines. However, subsequent carbonate alteration, albitisation (present(?) but weakly developed in the Lower Roan at Ndola West) and upper greenschist facies metamorphism all affected the stability of K-feldspar and thus its abundance in the rocks today (Selley et al.; Scott et al. (a), 2003). The marked up section decrease in K-feldspar abundance through the Cu-mineralised arkose at Ndola West may reflect any, or more likely a combination of these controls.

P544 research at Konkola, Konkola North and within the Chambishi Basin demonstrates copper was most likely stripped from the Katangan and basement rocks and transported in the K-rich brines (Selley et al., Large et al. (a), Koziy et al., 2003). Copper was deposited where the brines encountered reduced host-rock successions (e.g., 'oil shales': Ore Shale deposits, and hydrocarbon ± sour gas reservoirs in arenaceous host rocks). In reduced argillaceous rocks, instead of haematite, pyrite and copper sulfides were deposited along with K-metasomatic assemblages. A variety of potential sulfur sources (diagenetic anhydrite and pyrite (e.g., Annels, 1974); ore fluid sulfate (McGowan et al., 2002; McGoldrick, 2003) and sour gas reservoirs (Scott et al. (b), 2003) may have contributed to the precipitation of copper sulfides in the Lower Roan. However, with the exception of sour-gas accumulations related to thermal cracking of crude oil (Machel, 1989), thermochemical sulfate reduction (TSR) is strongly implicated as a critical process in providing the reduced sulfur to drive sulfide precipitation (Annels, 1974; McGoldrick, 2003). Collectively these relations (clay-rich precursor assemblage, TSR) suggest pervasive K-feldspar metasomatism occurred prior to significant metamorphism of the rocks (i.e., T<200°C), but above temperatures necessary for hydrocarbon generation and TSR (T > 140–150°C).

The interpreted progression from (1) widespread pervasive K-feldspar metasomatism (with no associated veining), to (2) the more restricted fracture-, vein- and lithologically-controlled carbonate alteration and finally (3) localised development of quartz ± K-feldspar fibre veins is interpreted to reflect changes in fluid composition and flow path architecture during progressive burial (and deformation) of the Roan succession. Textural and overprinting relations clearly indicate K-feldspar metasomatism, disseminated Cu-sulfides and carbonate veining and alteration all pre-date significant deformation of the host sequence. Where they cut previously Cu-mineralised rocks, the late K-feldspar veins display similar mineral paragenesis to the earlier phase of K-feldspar metasomatism and associated (localised) copper deposition (i.e., early quartz + K-feldspar + barite, with subsequent replacement of barite by Cu-sulfides). However overprinting relations, internal

textural features and the orientation of the veins all indicate they formed at a relatively late stage during the Lufilian deformation.

Controls on copper deposition at Ndola West

Most of the Lower Roan at Ndola West is moderately to intensely K-feldspar metasomatised indicating significant interaction with the ore fluid. In contrast copper (transported in the K-rich brines) is restricted to discrete, relatively narrow horizons. Decoupling between deposition of secondary K-feldspar and copper sulfides reflects the limited availability of reduced sulfur (reservoirs) throughout the succession. At Ndola West sulfur sources were apparently limited as anhydrite is not present in the section and there is no evidence for diagenetic pyrite in either the ore or footwall formations. The possibility of prior sour gas accumulations within the hydrocarbon-impregnated units, at least for the main Cu-mineralised arkose cannot be completely discounted. However, evidence suggests S^{2-} availability was low during initial interaction between the ore fluids as copper was apparently partitioned into silicates (feldspars, chrysocolla) and barite was formed prior to significant sulfide precipitation. This suggests sulfur was initially present as SO_4^{2-} and therefore most probably transported to the trap site(s), possibly in relatively low concentrations, by the ore fluid (i.e., K-rich brine). Sulfide precipitation occurred once *in situ* reduction of ore fluid sulfate generated sufficient S^{2-} to stabilise copper sulfides. The low S^{2-} availability at Ndola West is reflected in the development of a (sulfur-poor) chalcocite plus bornite dominated sulfide assemblage.

Although the total sulfur budget at Ndola West was apparently limited to that provided (as sulfate) by the ore fluid, the limited availability of reduced sulfur was ultimately determined by low hydrocarbon abundances within the Cu-mineralised host rocks. Although Cu-sulfides partially replace barite locally, within the main Cu-mineralised arkose (Fig. 12d and e), preservation of barite is interpreted to reflect the limited availability of organic-derived reductants capable of driving TSR to completion. Further evidence for limited hydrocarbon availability at Ndola West is provided by stable isotopic data for carbonates from within the ore formation (Fig. 2b). Although the carbonate alteration at Ndola West is interpreted to post-date copper mineralisation and is not related to TSR of anhydrite (e.g., Annels, 1974), carbon isotopic values for secondary carbonate ($\delta^{13}C$: +4 to –2 ‰ PDB) do not display the strong negative shift (e.g., $\delta^{13}C < -15$ ‰) indicative of oxidation of light organic-derived carbon (Large et al. (b), 2003).

In addition to elevated levels of copper and barium (reflecting the presence of minor barite), whole-rock geochemical data reveals a marked positive europium anomaly ($Eu/Eu^* = Eu_N / \sqrt{[(Sm_N).(Gd_N)]}$, where the subscript N denotes normalised values: Taylor and McLennan, 1985) at the level of the mineralised arkose. In view of the interpreted redox control on copper mineralisation, it is tempting to interpret the positive europium anomaly as an indication that within the hydrocarbon traps Eu^{3+} introduced in the ore fluid was reduced to the more compatible Eu^{2+}. However modelling by Bodon and Cooke, (1997) indicates that in hydrothermal brines (25 eq. wt % NaCl) at temperatures of 150°C (reasonable lower limit for copper mineralisation in the Zambian Copperbelt) europium is predominantly transported as $EuCl_4^{2-}$ (Eu^{2+}), so reduction of the 'oxidised'ore fluid should make no difference to europium speciation. In hydrothermal fluids close to the haematite–pyrite redox boundary Eu^{3+} is only stable in very acidic fluids ($EuCl^{2+}$, pH<1) or moderately to highly alkaline fluids (EuO_2^-, pH > 8–10) (Bodon and Cooke, 1997). Eu^{2+} is expected to strongly partition into K-feldspar at log f_{O_2} = –45 to –35 (appropriate to K-rich brines in the ZCB, Cooke, 2003). Thus it is perhaps surprising that positive europium anomalies are not developed throughout the Lower Roan (cf. Fig. 2c). In fact, the Cu-mineralised arkose that yields the positive europium anomaly has a relatively low feldspar content, and furthermore neither the most K-feldspar enriched sample (Ndola ore shale) or the most K-feldspar depleted samples (acid altered zone in the hanging wall formation) show any significant europium anomaly. In fact whole-rock europium contents do increase roughly with K-feldspar content. This suggests strong Eu partitioning into another mineral phase only developed within the mineralised arkose, namely barite, is responsible for the positive europium anomaly at this level.

Acknowledgments

I gratefully acknowledge the support of Anglo American, and Peter Mann in particular, for access to the Ndola West core and the provision of useful related data. Katie McGoldrick stained samples for K-feldspar and carbonate stable isotope samples were prepared by Mike Blake. Thin sections were prepared by Simon Stephens and Mike Blake. David Steel and Fernando della Pasqua provided invaluable assistance with the electron microprobe. Discussions with David Selley, Peter McGoldrick, Stuart Bull, David Cooke and Ross Large have contributed substantially to the ideas presented here. As ever, June Pongratz and Mike Blake are thanked for their efforts in formatting this report.

References

Annels, A. E., 1974, Some aspects of the stratiform ore deposits of the Zambian Copperbelt and their genetic significance, in Bartholomé, P., ed.: Gisements stratiformes et provinces cupifères, Société Géologique de Belgique, Liège, p. 235–254.

Bodon, S. B. and Cooke, D. R., 1997, Europium transport in sedimentary brines – Physiochemical controls in the ore-forming environment of McArthur- and Broken Hill-type sediment-hosted Pb-Zn deposits: AMIRA/ARC Project P384A – Sediment-hosted base metal deposits, Report 3, p. 85–90.

Cooke, D. R; Bull, S. W; Large, R. R; McGoldrick, P. J., 2000, The importance of oxidized brines for the formation of Australian Proterozoic stratiform sediment-hosted Pb-Zn (sedex) deposits: Economic Geology, v. 95, p.1-17.

Cooke, D. R., McGoldrick, P., Hitzman, M., Scott, R., and Selley, D., 2003, Geochemical modelling: Implications for mineralising processes in the Zambian Copperbelt, AMIRA P544 Proterozoic Sediment Hosted Copper Deposits, Final Report. This volume.

Darnley, A. G., 1960, Petrology of some Rhodesian Copperbelt orebodies and associated rocks: transactions of the Institution of Mining and Metallurgy, v. 69, p. 137–173.

Eliet, P. P. and Gawthorpe, R. L., 1995, Drainage development and sediment supply within rifts, examples from the Sperchios Basin, central Greece: Journal of the Geological Society of London, v.152, p. 883-893.

Herrmann, W. and Berry, R. F., 2002, MINSQ – a least squares spreadsheet method for calculating mineral proportions from whole rock major element analyses: Geochemistry: Exploration, Environment, Analysis, v. 2, p. 361–368.

Koziy, L., Large, R., Yang J., Bull, S. and Selley, D., 2003, Numerical fluid flow, salinity and heat transfer modelling in an attempt to understand basin scale mineralisation processes in the Zambian Copperbelt: AMIRA P544 Proterozoic Sediment Hosted Copper Deposits, Final Report. This volume.

Large, R. R., Bull, S., Croaker, M., McGoldrick, P., Pollington, N., Scott, R., and Selley, D., 2003(b), Carbon and oxygen isotopic composition of ore-related and sedimentary carbonates in the Roan, Zambian Copperbelt, AMIRA P544 Proterozoic Sediment Hosted Copper Deposits, Final Report. This volume.

Large, R. R., McGoldrick, P., Bull, S., Scott, R. and Selley, D., 2003(a), Lithogeochemistry and halos to ore in the Chambishi Basin: AMIRA P544 Proterozoic Sediment Hosted Copper Deposits, Final Report. This volume.

Machel, H. G., 1989, Relationships between sulfate reduction and the oxidation of organic compounds to carbonate diagenesis, hydrocarbon accumulations, salt domes, and metal sulfide deposits: Carbonates and Evaporites, v. 4, p. 137–151.

McGoldrick, P., Cooke, D. and P544 Team, 2003, Zambian Copperbelt geochemistry, geochemical modelling and stable isotopes: implications for mineralising processes: AMIRA P544 Proterozoic Sediment Hosted Copper Deposits, Final Report. This volume.

McGowan, R. R., Roberts, S., Foster, R. P., Boyce, A. J., Coller, D., 2003, Origin of the copper–cobalt deposits of the Zambian Copperbelt: An epigenetic view from Nchanga: Geology, v. 31, p. 491–500.

Scott, R. J., 2002 (a), Basement - Roan relations at Ndola west: Proterozoic sediment hosted copper deposits, AMIRA/ARC Project P544, May Sponsors Meeting, p. 9.1–9.8.

Scott, R. J., 2002 (b), Style and stratigraphic context of copper mineralisation: Ndola West: Proterozoic sediment hosted copper deposits, AMIRA/ARC Project P544, May Sponsors Meeting, p. 18.1–18.13

Scott, R. J., 2002 (c), Stratigraphy, structure and copper mineralisation, Ndola West, Zambia: AMIRA P544 Proterozoic Sediment Hosted Copper Deposits, Annual Report, p. 10.1–10.33.

Scott, R. Berry, R. Selley, D and Bull, S., 2003 (a), Lufilian metamorphism in the Zambian Copperbelt: Implications for the interpretation of mineral assemblages and alteration paragenesis: AMIRA P544 Proterozoic Sediment Hosted Copper Deposits, Final Report. This volume.

Scott, R., Selley, D. and Cooke, D., 2003 (b), Arenite-hosted copper mineralisation east of the Kafue Anticline: A comparison of tectono-stratigraphic, mineralogical, geochemical and C- and O-isotopic characteristics of small and large deposits: AMIRA P544 Proterozoic Sediment Hosted Copper Deposits, Final Report. This volume.

Selley, D., Bull, S., Croaker, M., Scott, R., Broughton, D. and Pollington, N., 2003 (a), Development of the Lower Roan basin system, western Kafue Anticline: AMIRA P544 Proterozoic Sediment Hosted Copper Deposits, Final Report. This volume.

Selley, D.,, McGoldrick, P., Scott, R. and Bull, S., 2003 (c), Mwambashi B: Keys to arenite-hosted Cu-Co mineralisation: AMIRA P544 Proterozoic Sediment Hosted Copper Deposits, Final Report. This volume.

Selley, D., Scott, R., Large, R., Croaker, M., Bull, S., Pollington, N., 2003 (b), Alteration history of the Roan: AMIRA P544 Proterozoic Sediment Hosted Copper Deposits, Final Report. This volume.

Taylor, S. R. and McLennan, S. M., 1985, The continental crust: its composition and evolution. Blackwell, Oxford.

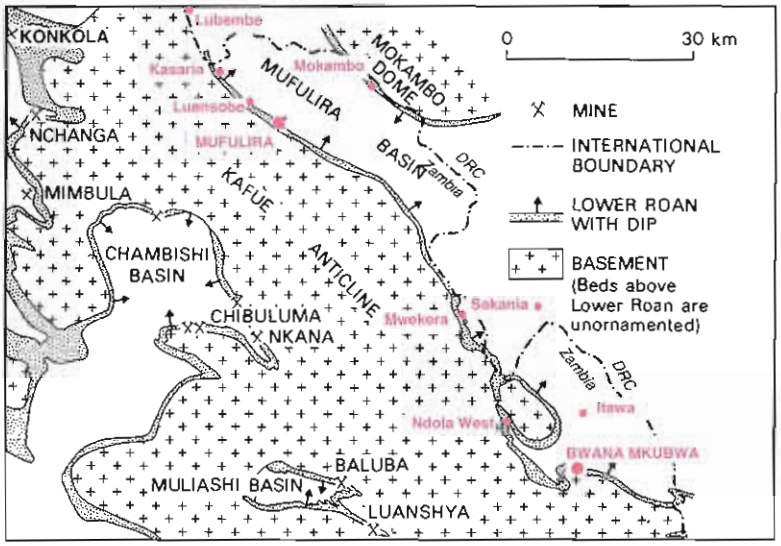

Figure 1. Map of the central portion of the Zambian Copperbelt showing the locations of copper deposits east of the Kafue Anticline (red dots). Ndola West is located approximately 10 km NW of Bwana Mkubwa. After Fleischer et al. (1976).

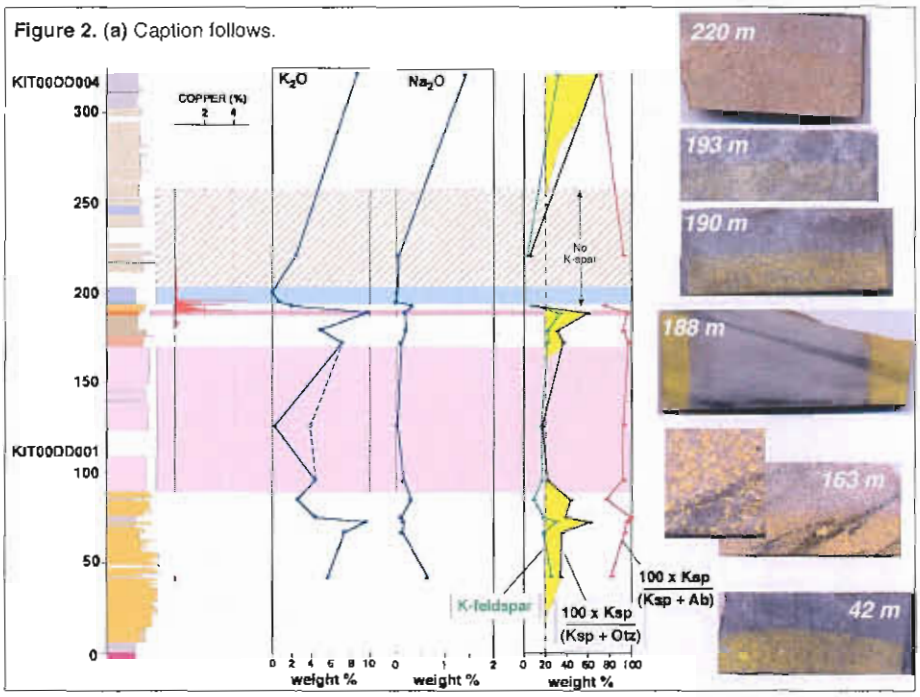

Figure 2. Representative stratigraphic column and selected whole rock geochemical and isotopic data for the eastern limb of the Ndola Syncline. Graphic logs show estimated true thickness of units based on intersections in drill holes KIT00DD001 and DD004, and horizontal dimension of logs is proportional to grain size. Assay data for copper also shown. Coloured bands extending to the right of the graphic logs park the position of the thick pink arkose in the upper hanging wall formation (pink), the Ndola ore shale (brown); sedimentary dolomite and talc schist (pale blue) and a largely K-feldspar-absent zone in the lower part of the hanging wall formation.

(a) Feldspar distribution. Down-hole variation in K_2O and Na_2O highlights zones of potential K-feldspar and albite (or as is more likely the case in the lower part of the hole, scapolite) enrichment respectively. Note that the sample from the central portion of the pink arkose is depleted in K_2O because all detrital feldspar is weathered to kaolinite; its true composition was probably similar to the underlying sample.
The MINSQ program (Herrmann and Berry, 2002) was used to determine approximate proportions of K-feldspar, quartz and albite (assuming no scapolite) from the wholerock analyses. The K-feldspar/quartz ratio (normalised to 100) provides a fairly reliable indicator of K-feldspar metasomatism (yellow shading). The dashed lower limit (at 100 x Ksp / (Ksp + Qtz) = 20%, represents the likely maximum detrital K-feldspar content in unaltered clean arkosic sandstone (e.g. sample from ~163 m, right). K-feldspar / quartz ratios to the right of this line (especially for fine-grained units) indicate addition of secondary K-feldspar. The predicted extent of K-feldspar metasomatism is supported by the abundance and distribution of K-feldspar in samples stained (yellow) for K-feldspar (illustrated at right). The normalised K-feldspar/albite ratio is generally above 90%, but three of the four with significantly lower values occur at levels of sulfide enrichment (see text for further discussion).

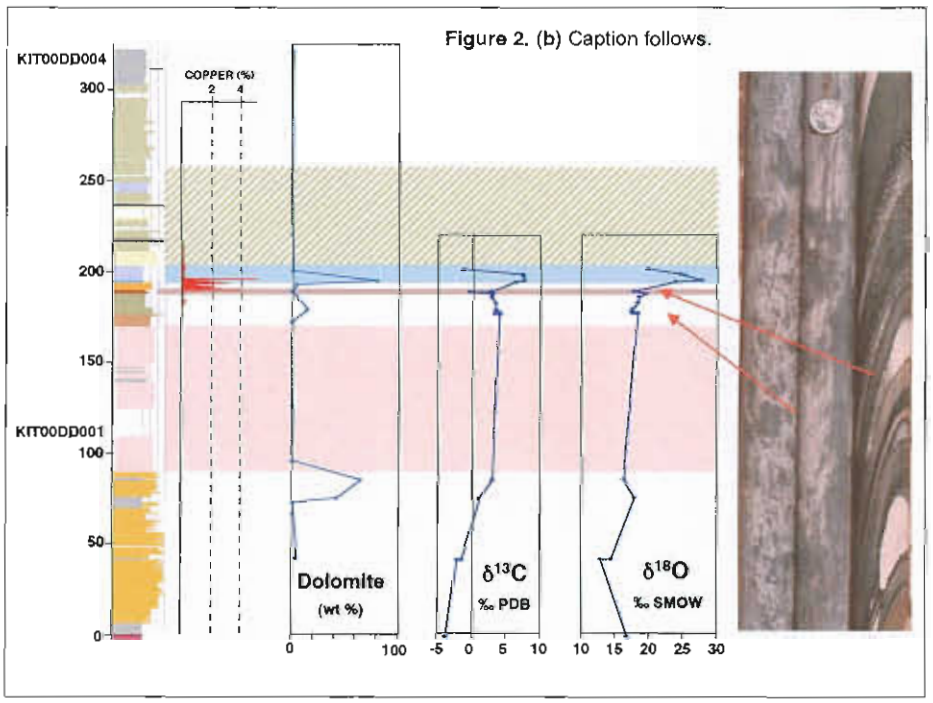

Figure 2. (b) Caption follows.

Figure 2. continued.

(b) Carbonate distribution through the stratigraphic section based on MINSQ estimates of dolomite content from whole rock geochemical data. There is no calcite present in the section. Whole rock geochemical samples from the zone of moderate to intense carbonate alteration in and immediately below the level of the Ndola ore shale, were chose to minimise the affects of carbonate alteration and thus under estimate the intensity of secondary dolomite development in this zone (typical examples of intense, patchy and selective carbonate alteration in core are illustrated at right.
Carbon and oxygen isotopic data from the carbonates clearly delineates zones of sedimentary and secondary carbonate. Note that isotopic data is a composite of information from multiple drill holes, plotted at equivalent stratigraphic position. See Figures 3 and 4 for exact data locations.

Figure 2. (c) Caption follows.

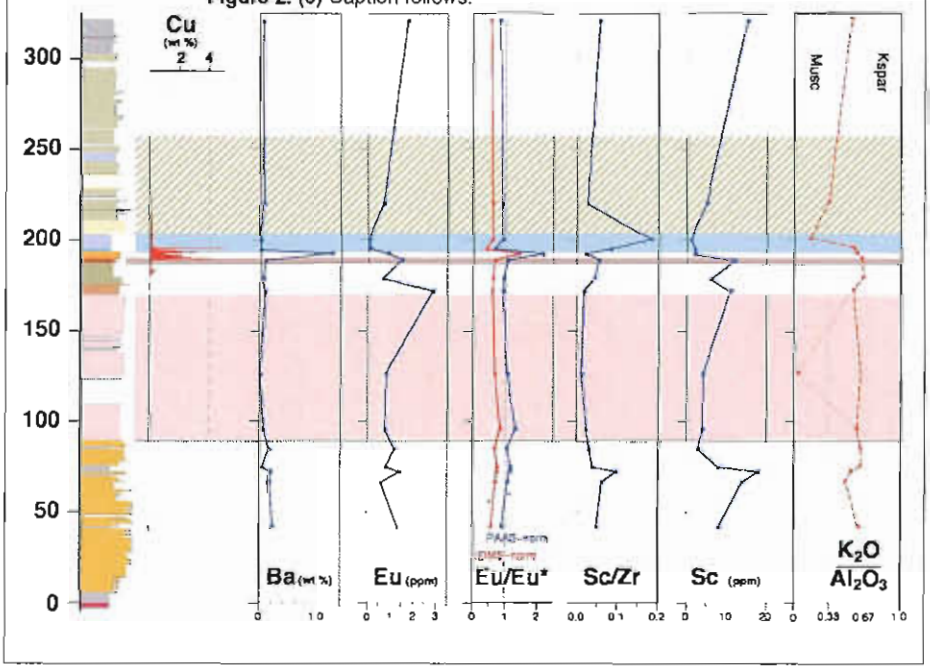

Figure 2 continued
(c) Selected major, minor and trace element data for the Lower Roan section at Ndola West. Barium is significantly enriched at the level of the Cu-mineralised arkose (the only level in the stratigraphy where barite is consistently developed). Lower Ba levels elsewhere in the section probably reflect Ba in feldspars. The europium (Eu) content crudely reflects K-feldspar distribution (e.g. Fig. 2a, approximately reflected by K_2O/Al_2O_3 ratio, right), consistent with the expected partitioning of Eu^{2+} into feldspars. However, only one significant (positive) europium anomaly, at the level of the main Cu mineralised horizon, is evident in the whole-rock data. The magnitude of the europium anomaly is clearly independent of K-feldspar content, and coincident with the only significant Ba enrichment in the section. Accordingly the whole-rock europium anomaly is interpreted to reflect strong partitioning of Eu^{2+} (relative to other LREE) into barite.

Scandium is immobile and principally sourced from original clay. Accordingly variation in Sc contents reflects variations in the argillaceous fraction of the sediments. Variation in K_2O/Al_2O_3 crudely mimics Sc (as well as Eu) indicating the intensity of K-feldspar metasomatism principally reflects original clay content of the sediments. In the absence of provenance changes, the Sc/Zr ratio (both ~immobile elements) also reflects sedimentary fractionation in clastic rocks, with Sc principally sourced from clays and Zr from zircon , enriched in coarser grained and clean sandstones. This ratio highlights smooth variations in the degree of sedimentary reworking (winnowing out of fines) through the footwall succession, with lowest values for the thick pink arkose at the top of the footwall formation. Apparent Sc/Zr anomalies for the dolomite and talc schist are meaningless and arise because of the similarly low concentrations of both Sc and Zr in these units.

GRAPHIC LOGS AND INTERPRETED STRATIGRAPHIC CORRELATIONS: ANGLO-AMERICA NDOLA WEST PROSPECT

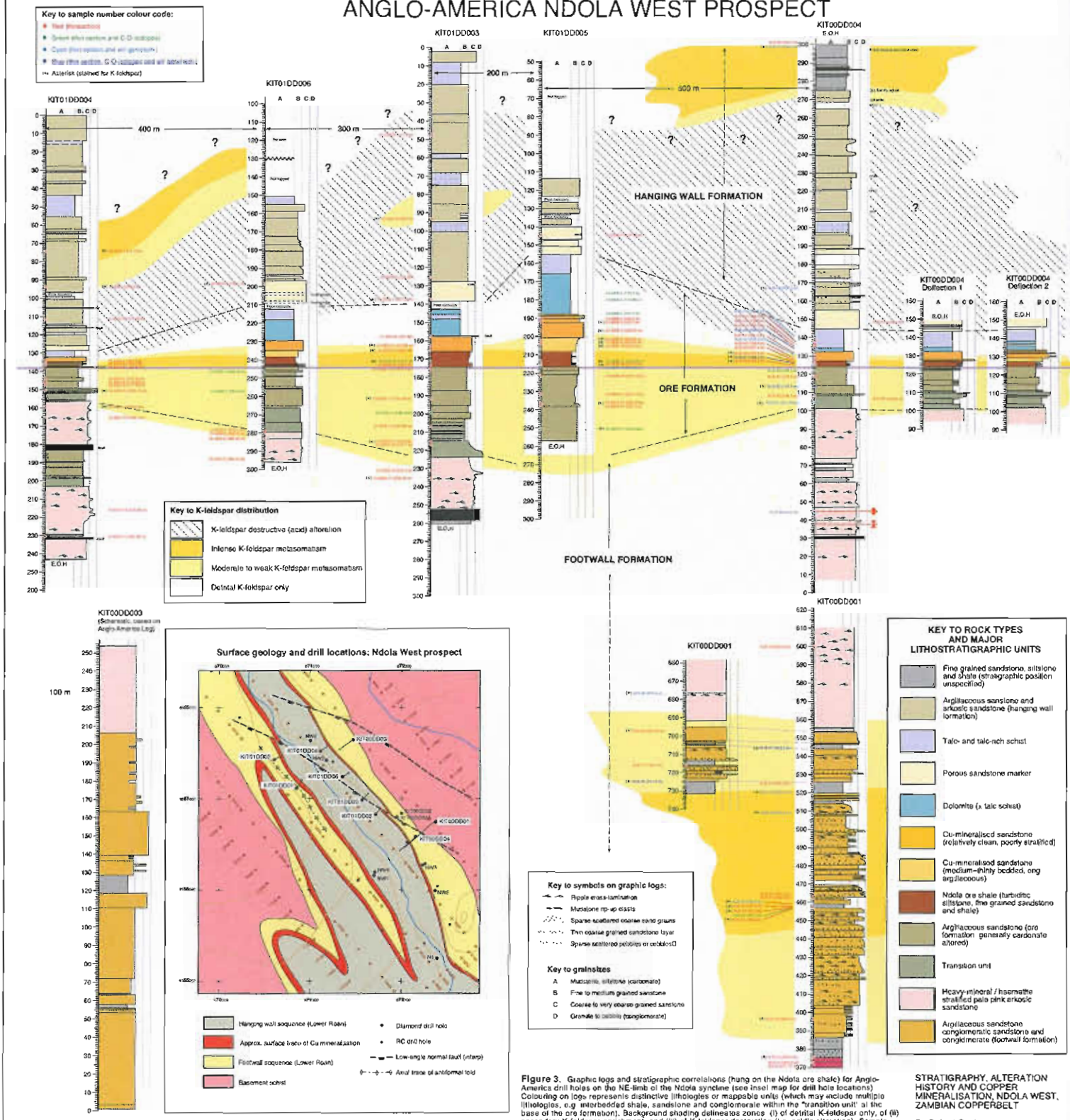

Figure 3. Graphic logs and stratigraphic correlations (hung on the Ndola ore shale) for Anglo-America drill holes on the NE-limb of the Ndola syncline (see inset map for drill hole locations). Colouring on logs represents distinctive lithologies or mappable units (which may include multiple lithologies, e.g. interbedded shale, sandstone and conglomerate within the "transition unit" at the base of the ore formation). Background shading delineates zones: (i) of detrital K-feldspar only, of (ii) secondary K-feldspar enrichment, and (iii) of K-feldspar destruction (i.e. acidic alteration). Sample locations are also shown.

STRATIGRAPHY, ALTERATION HISTORY AND COPPER MINERALISATION, NDOLA WEST, ZAMBIAN COPPERBELT

By Robert Scott

Figure 3

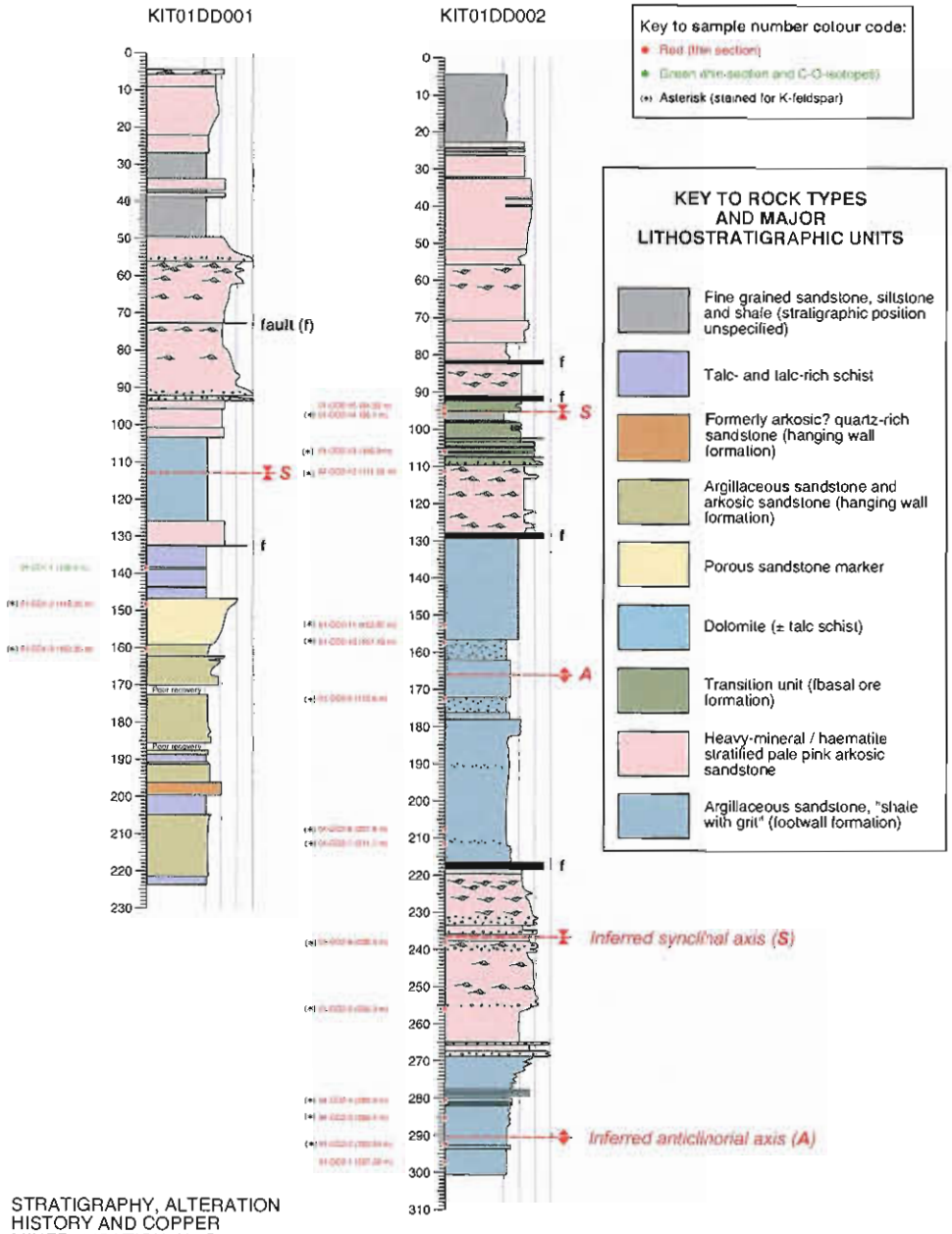

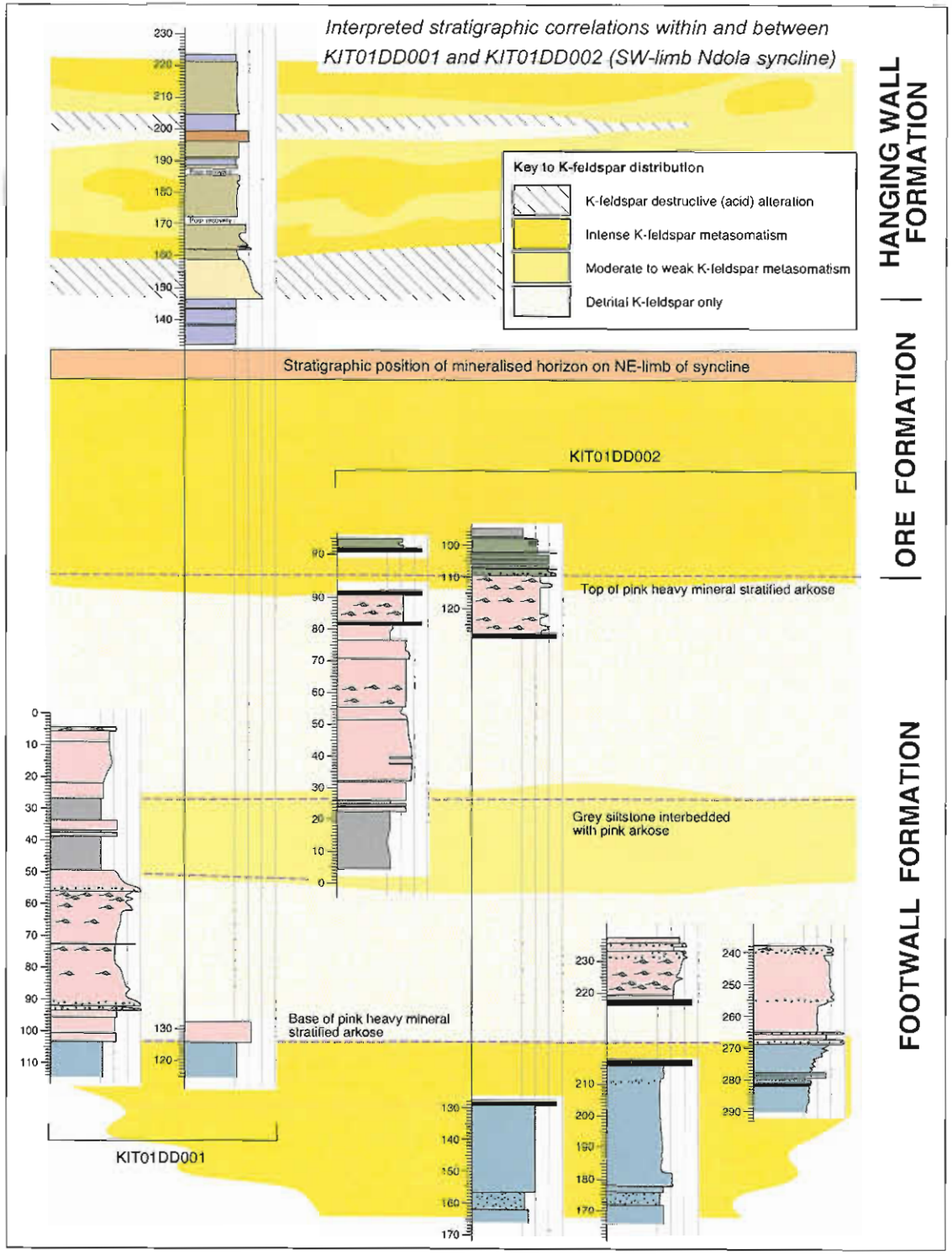

STRATIGRAPHY, ALTERATION HISTORY AND COPPER MINERALISATION, NDOLA WEST, ZAMBIAN COPPERBELT

By Robert Scott

Figure 4. Original graphic logs (above) and stratigraphic correlations (left, including fold and fault repeated units in KIT01DD002) for Anglo-America drill holes on the SW-limb of the Ndola syncline (see Figure 3 for drill hole locations). Colouring on logs represents distinctive lithologies or mappable units (which may include multiple lithologies, e.g. interbedded shale, sandstone and conglomerate within the "transition unit" at the base of the ore formation). Background shading delineates zones (i) of detrital K-feldspar only, of (ii) secondary K-feldspar enrichment, and (iii) of K-feldspar destruction (i.e. acidic alteration). Sample locations are also shown.

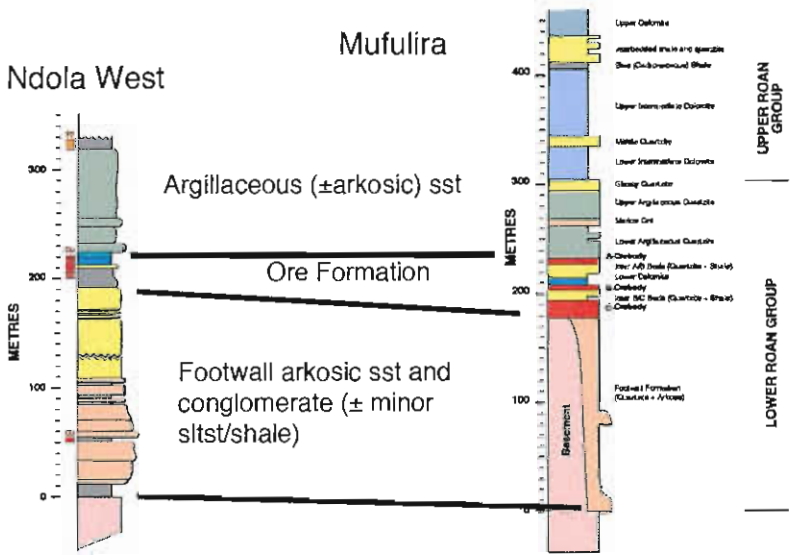

Figure 5. Stratigraphic correlation between Ndola West and Mufulira, on the NE-flank of the Kafue Anticline.

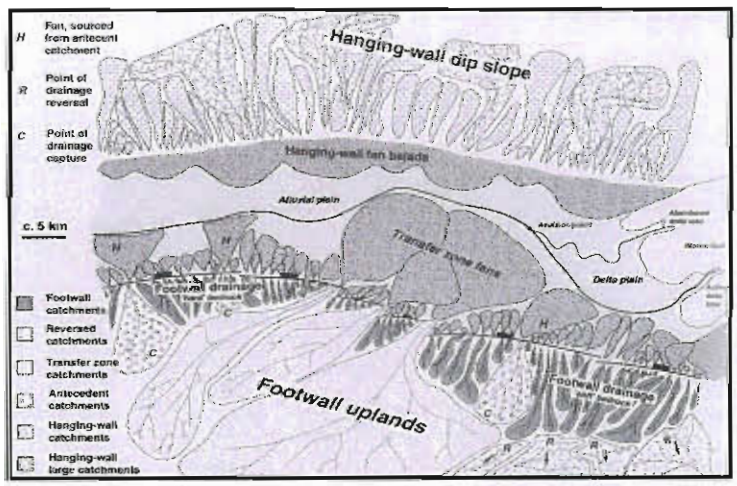

Figure 6. Facies architecture of an asymmetric rift. Note transverse drainage patterns adjacent to range-front faults and on tilted hanging-wall and footwall uplands (dip slopes), and axial drainage (alluvial plain) in the central portion of the rift. Expansion of the axial drainage system due to either (i) widening of the rift, (ii) decrease in sediment supply to transverse fan systems (by, for example, increased fault linkage across transfer zones, the main points of sediment entry into the rift) of (iii) decreased footwall relief, may result in local onlap with earlier formed transverse drainage systems. From Eliet and Gawthorpe, 1995.

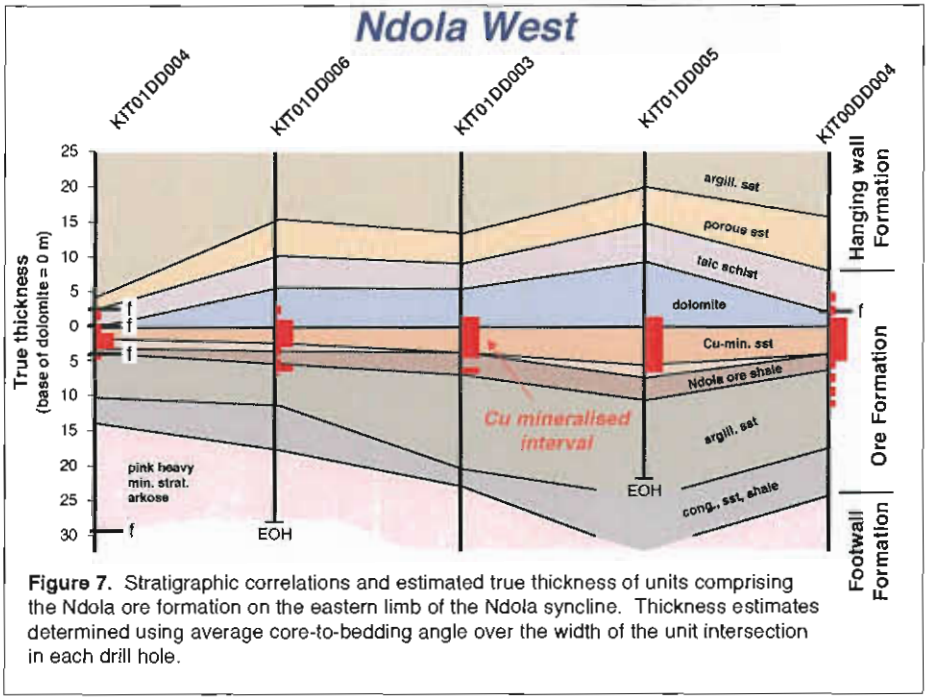

Figure 7. Stratigraphic correlations and estimated true thickness of units comprising the Ndola ore formation on the eastern limb of the Ndola syncline. Thickness estimates determined using average core-to-bedding angle over the width of the unit intersection in each drill hole.

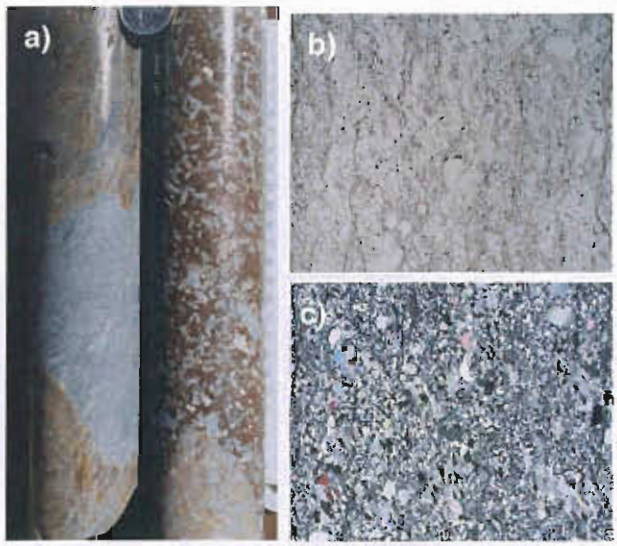

Figure 8. **(a)** Areas of silicification (blue grey) highlight millet-seed textures after gypsum in basal succession of the ore formation (KIT01DD004, 150.15 m) **(b)** PPL and **(c)** XPL photomicrographs of deformed carbonate-altered argillaceous sandstone. Under XPL domains of elongate carbonate crystals (parallel to S_1) are evident and reflect relict strongly deformed carbonate veins (KIT01DD004, 143.4 m).

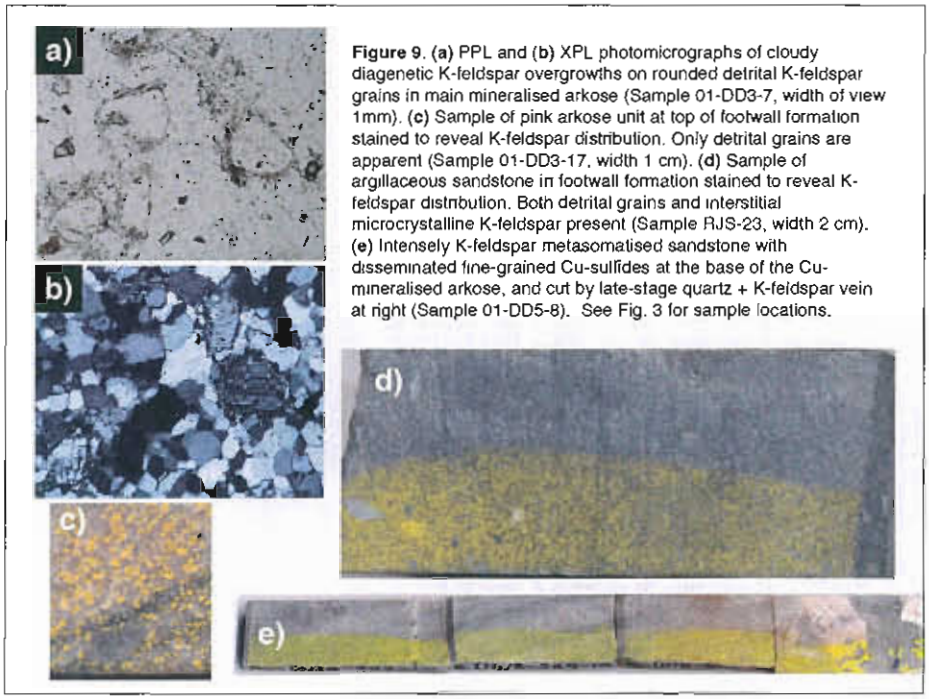

Figure 9. **(a)** PPL and **(b)** XPL photomicrographs of cloudy diagenetic K-feldspar overgrowths on rounded detrital K-feldspar grains in main mineralised arkose (Sample 01-DD3-7, width of view 1mm). **(c)** Sample of pink arkose unit at top of footwall formation stained to reveal K-feldspar distribution. Only detrital grains are apparent (Sample 01-DD3-17, width 1 cm). **(d)** Sample of argillaceous sandstone in footwall formation stained to reveal K-feldspar distribution. Both detrital grains and interstitial microcrystalline K-feldspar present (Sample RJS-23, width 2 cm). **(e)** Intensely K-feldspar metasomatised sandstone with disseminated fine-grained Cu-sulfides at the base of the Cu-mineralised arkose, and cut by late-stage quartz + K-feldspar vein at right (Sample 01-DD5-8). See Fig. 3 for sample locations.

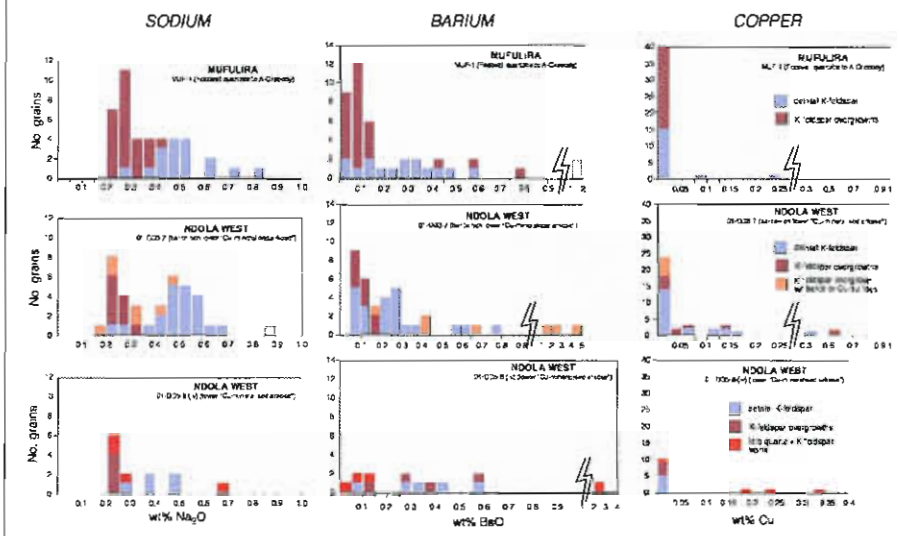

Figure 10. Probe data for detrital and secondary K-feldspar at Mufulira and Ndola West. Main caption follows.

Figure 10. Probe data for detrital and secondary K-feldspar at Mufulira and Ndola West. Samples are a weakly mineralised clean arkosic sandstone from Mufulira (top row), barite-rich, moderate to weakly K-feldspar metasomatised arkose from the central portion of the main Cu-mineralised sandstone at Ndola West (middle row), and strongly K-feldspar metasomatised fine grained sandstone and cross-cutting "late-stage" quartz + K-feldspar vein from the thinly-bedded lower portion of the Cu-mineralised arkose at Ndola West (bottom row). Histograms show the number of probed grains with Na_2O, BaO and Cu contents within the ranges indicated. Note changes in scale on x-axes of some plots.

The probe results indicate diagenetic K-feldspar overgrowths are consistently depleted in Na and generally depleted in Ba relative to detrital K-feldspar. Hydrothermal K-feldspar that is apparently intergrown with barite at Ndola West is variably enriched in Ba (± Cu) relative to both detrital and diagenetic K-feldspar. K-feldspars in "late-stage" fibre veins overprinting disseminated Cu mineralisation at Ndola West have variable Na, Ba and Cu contents but may be significantly enriched in Ba or Cu, relative to detrital K-feldspar (N.B. barite and copper sulfides are both minor phases precipitated in the late veins.

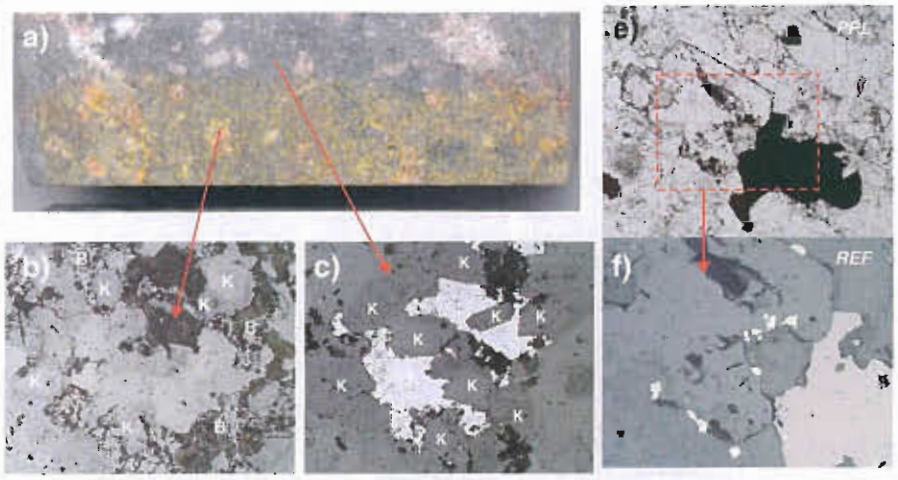

Figure 11. (a) Barite intergrown with K-feldspar (pink and white clots) in Cu-mineralised arkose (KIT01DD03, 165.0 m). **(b)** Photomicrograph showing euhedrally-terminated K-feldspar (K) crystals penetrating barite (B) (REF light, width 1.1 mm). **(c)** Copper sulfides (bright) intergrown with and encasing euhedrally-terminated K-feldspar (K) or overgrowths (REF light, width 1.1 mm). **(d)** Photomicrograph of barite crystal rimmed and partially replaced by Cu-sulfides (KIT01DD05, 196.7 m, PPL, width = 1.1 mm). **(e)** Detail from (d) highlighting paragenetic relations between barite and sulfides (REF light, width = 0.55 mm).

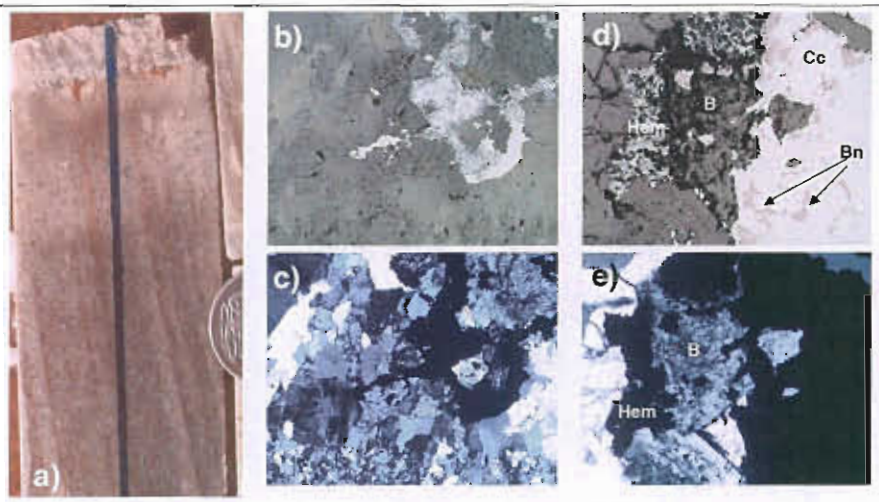

Figure 12. (a) 1 cm wide fibrous quartz + K-feldspar vein cuts intensely K-feldspar metasomatised sandstone with disseminated fine-grained Cu-sulfides at high angle to bedding (KIT01DD005, 203.1 m). Minor Cu-sulfides within the vein were evidently sourced from the adjacent wall rocks. Disseminated sulfides are stripped from the wall rock in the bleached halo adjacent to the vein. **(b)** REF light and **(c)** XPL photomicrographs of copper sulfides (chalcocite + haematite after bornite ± chalcopyrite) intergrown with quartz and K-feldspar in late-stage fibre vein. Wall rock contact (bottom) parallel to long edge of photomicrograph (KIT01DD005, 202 1 m.) **(d)** REF light and **(e)** XPL photomicrographs chalcocite (Cc) and haematite (Hem) after bornite (Bn) that replacing earlier barite (B) in fibre vein illustrated in (a).

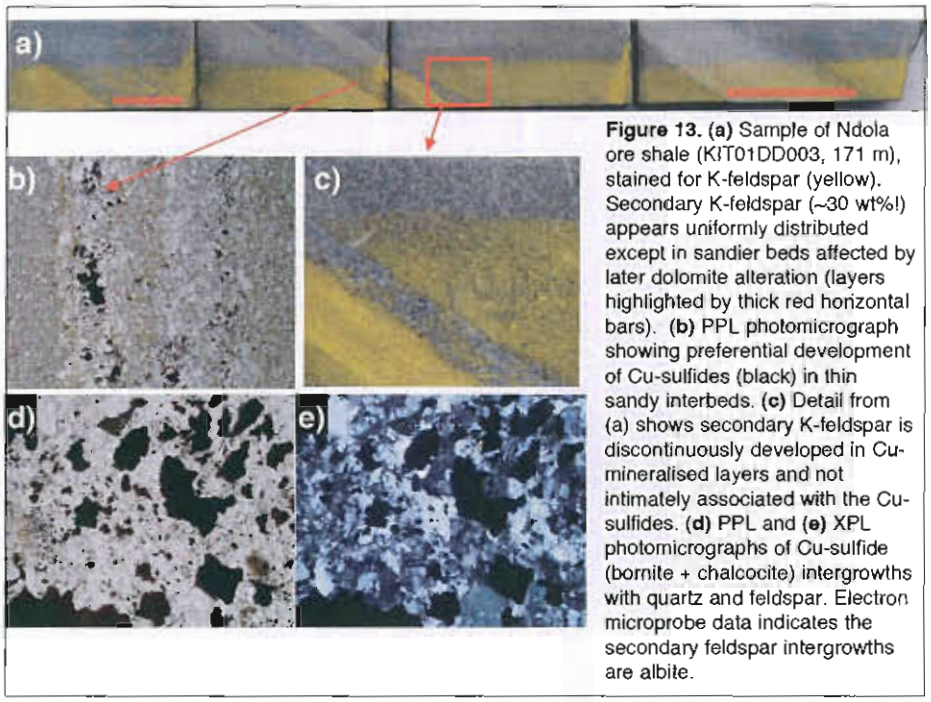

Figure 13. (a) Sample of Ndola ore shale (KIT01DD003, 171 m), stained for K-feldspar (yellow). Secondary K-feldspar (~30 wt%!) appears uniformly distributed except in sandier beds affected by later dolomite alteration (layers highlighted by thick red horizontal bars). **(b)** PPL photomicrograph showing preferential development of Cu-sulfides (black) in thin sandy interbeds. **(c)** Detail from (a) shows secondary K-feldspar is discontinuously developed in Cu-mineralised layers and not intimately associated with the Cu-sulfides. **(d)** PPL and **(e)** XPL photomicrographs of Cu-sulfide (bornite + chalcocite) intergrowths with quartz and feldspar. Electron microprobe data indicates the secondary feldspar intergrowths are albite.

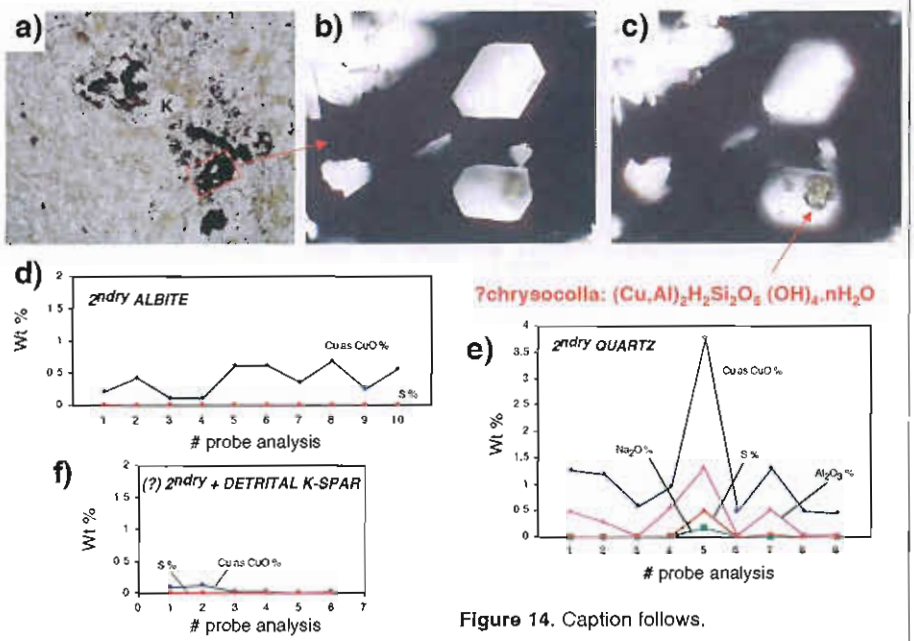

Figure 14. Caption follows.

Figure 14.

(a) PPL photomicrograph of clots of fine-grained Cu-sulfides (black) intergrown with microcrystalline feldspar and quartz. An outsized K-feldspar (K) grain, possibly secondary in origin, occurs between two sulfide clots (Sample KIT01DD003, 171 m, width 1 mm).
(b) PPL photomicrograph shows sulfide grain in (a) encase euhedral crystallites of quartz ± feldspar (width 100 μm).
(c) As for (b) but focus adjusted below the surface of the thin section revealing anhedral translucent inclusion of early-formed (?)chrysocolla.
(d) Probe data for albite intergrown with the copper sulfides indicates elevated Cu but S below detection.
(e) Probe data for microcrystalline quartz and quartz crystallites intergrown with Cu-sulfides indicates elevated Cu, Al but S generally below detection. Analysis #1 is for the euhedral quartz grain containing the green inclusion illustrated in (c).
(f) Cu and S analyses (probe data) for K-feldspar from the same sandstone layer. Analyses #1 and #2 are for the grain labelled "K" in (a). Slightly elevated Cu (S below detection) compared to a definite detrital grain in the same layer (analyses #3–6) support a secondary origin for the grain "K", and likely co-precipitation with the albite + Cu-sulfide + quartz intergrowths.

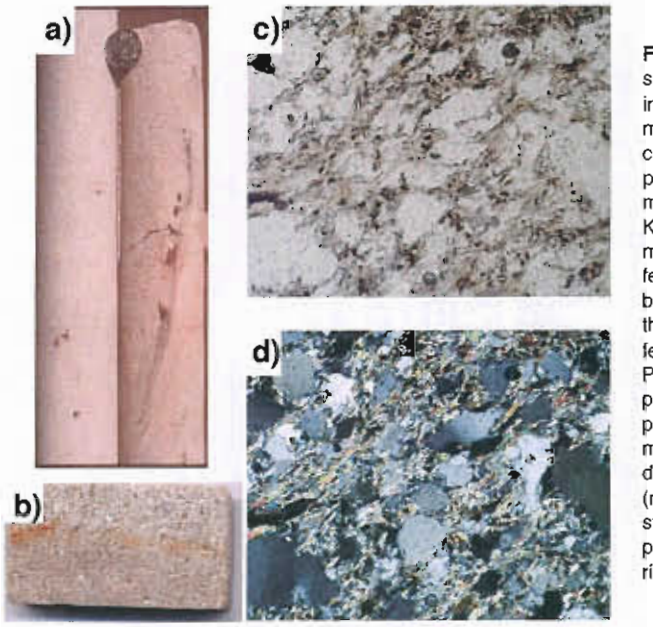

Figure 15. **(a)** Porous sandstone marker unit in KIT01DD005 (~143 m). Note relict pyrite cubes. **(b)** Sample of porous sandstone marker unit in KIT01DD006 (~198.4 m) stained for K-feldspar (below orange brown tide mark left by the chemicals). No K-feldspar is evident. **(c)** PPL and **(d)** XPL photomicrographs of the porous sandstone marker reveal only detrital grains of quartz (no K-feldspar) in a strongly foliated phlogopite + muscovite rich matrix.

Structural development and controls on Cu-Co mineralisation at Nkana-Mindola

Mawson Croaker and David Selley
Centre for Ore Deposit Research, University of Tasmania

Introduction

The origin and timing of Cu mineralisation within the Zambian Copperbelt has been a controversial topic for many decades with syn-genetic, diagenetic and hydrothermal mineralisation models proposed (Garlick, 1961; Sweeney et al, 1986; Annels, 1989). This study deals with one of the largest and more structurally complex Cu–Co deposits, and investigates the origin and timing of mineralisation within the frameworks of basin architecture and deformation history.

Located in the SE corner of the Chambishi Basin, the Nkana-Mindola (NKM) deposit is an economic Cu–Co resource hosted mainly by basal shales-siltstones of the Copperbelt Orebody Member (COM–locally 'Ore Shale') of the Kitwe Formation. All economic mineralisation is currently confined to the NE limb and hinge areas of the NW plunging Nkana Syncline. However low grade Cu mineralisation (0.5% to 1%) is continuous on the SW limb (West Limb Area), totalling an overall mineralised strike distance of approximately 35 km (Slide 4).

Stratigraphy and basin architecture

The Lower Roan sequence at NKM can be divided into the basal coarse-grained Mindola Clastic Formation (MCF) (0–200m thick) and the overlying finer grained Kitwe Formation (KF) (~ 150 m thick) (Slide 5). Previous work by Clemmey (1978) accurately described the gross stratigraphy and sedimentology of the Lower Roan sequence, based on underground exposures at Mindola Shaft and within the Mindola Pit. Clemmey (1978) concentrated his research on the Kitwe Formation, with only minor studies on the basal MCF.

Mindola Clastic Formation

Current research has provided improved constraints on basin development through the analysis of facies architecture recorded at the onset of sedimentation. Significant lateral and vertical thickness changes and facies variations have been identified within the MCF, as have been likewise observed in other parts of the Chambishi Basin (Selley & Bull, 2001; Selley et al., 2002; Bull & Selley, 2003). This complex stratigraphic architecture is evident despite the intense Lufilian deformation, and is indicative of sedimentation within small, tectonically active rift basins. Supporting this interpretation is the preservation of laterally discontinuous sedimentary breccia facies (e.g., 1250L SOB Shaft) contained within more extensive fluvial and deltaic facies. This architecture is typical of embryonic rift settings and records chaotic, coarse grained sediment input across fault scarps.

The compartmentalised character of the MCF basin system is also reflected in macroscopic map patterns. New geological data combined with the extensive archival database reveal abrupt changes in the strike of the basement–MCF contact. Although lack of continuity in datasets prevents detailed facies analysis in these areas, broad changes in stratigraphic architecture have been demonstrated to coincide with these strike changes. An example occurs between 500 m and 1.5 km north of Mindola Shaft, where the regional NW strike of the basement–MCF contact rotates anticlockwise to the WNW (Slide 8). Here there is significant thinning of the MCF, observed

coarser grained facies and reported breccia facies. We interpret changes in the orientation of the basement contact to reflect perturbations in regional fold geometry, inherited from early basin-controlling structures.

Kitwe Formation

The finer-grained siliciclastic-carbonate packages of the KF are distinguishable from the MCF by their laterally persistent bedding geometry. Although broadly layer-cake, four distinct facies variants are recognised within the lower portion of COM (Slide 6). At the northern end of NKM, the COM is typically an interbedded dolomite-argillite sequence, whereas in the southern portion of the NKM and majority of the west limb area, it forms black, carbonaceous-carbonate shale-argillite package. In addition, there are very localised and abrupt facies changes from siltstones-shales to either coarse-grained sandstone facies or massive carbonate rich facies. These local facies variations coincide with a thin or even non-existent MCF, lower Cu grades or barren gaps (Slide 8).

Despite the significant deformation and destruction of primary sedimentary textures within massive carbonate facies, the C–O isotope signature of these units are compatible with published C–O isotopic data from Proterozoic sedimentary carbonate (Slide 7). Moreover, a similar C–O isotopic signature has been obtained from less deformed, but stratigraphically analogous massive carbonate facies at Chambishi SE, where primary microbial textures are preserved (Bull and Selley, 2003).

The distinct change in facies architecture between the Mindola Clastic Formation and Kitwe Formation is interpreted to reflect a significant and abrupt change in basin evolution from small, compartmentalised depocentres, to an opening of the basin system. No sedimentary facies typically associated with active rift margins have been identified within the Kitwe Formation at NKM.

Structural history

Relative to other COM hosted Cu deposits within the Chambishi Basin (e.g., Chambishi and Chambishi SE), the Nkana-Mindola system records an unusually complex deformation history, characterised by particularly high strain within the southern orebody (Slide 10). By contrasting the structural styles of low and high strain domains, this section aims to unravel the affects of the main phase of Lufilian deformation on ore distribution, as well as providing constraints on pre- to early Lufilian deformation.

Low strain domains

The northern portion of NKM, situated on the NE limb of the Nkana Syncline, is a relatively low strain area with some of the best exposures of moderately deformed SW dipping Kitwe Formation occurring in the Mindola Pit. These exposures and underground data from North Shaft and Mindola Shaft reveal significant partitioning of the strain into the shales and siltstones of the COM. The MCF–KF contact at the southern end of the Mindola Pit has two discrete lineations contained within the plane of bedding (Slide 12). An early gently S- to SSW-plunging stretching lineation, defined by scapolite, is oriented slightly oblique to the axis of regional folds, and is interpreted to indicate a pre-folding phase of decoupling at the MCF–KF contact. However, there is no evidence of significant displacement related to this event. The second lineation is defined by steeply SW-plunging quartz-calcite fibres and is interpreted to record a component of flexural slip associated with the main folding event.

On the lower levels of Mindola Shaft, bedding is steeply SW-dipping and significant bedding parallel shear and meso-scale isoclinal folding occur within interbedded dolomite-argillites of the COM (Slide 13). These structures are related to development of the main Nkana Syncline. The increased strain within the COM on the steepened limb of the Nkana Syncline reflects strain partitioning into the shaley COM relative to the underlying coarser grained MCF. None of the small-scale structures are seen in the immediately underlying MCF.

High strain domains

To the south at SOB Shaft, where mining is underway in the hinge zone of the NW plunging Nkana Syncline intense Lufilian deformation is prevalent (Slide 14). This portion of NKM is referred to as the Nkana Synclinorium. Despite the extensive mining over the past decades, severe limitations on access to many areas, lack of preserved diamond cores and poor geological exposures once outside the main ore zones restricts data collection. Only within the Nkana Synclinorium area are there good exposures of the footwall to the COM, and accessible drill core (Slides 15, 16).

Folding and cleavage development

Three discrete deformation phases are recognised within the COM, with the S_2 cleavage commonly been the only cleavage recognised on the mesoscale. Strain partitioning occurs across three rheological-stratigraphic boundaries: the basement–MCF contact, the Lower Conglomerate–KAM contact and the MCF–COM contact. However the larger portion of strain has once again been partitioned within the COM. Although there is evidence of elevated strains extending above the level of the COM, current mining methods rarely exposure significant portions of the Rokana Evaporites or overlying stratigraphy anywhere at NKM. No large scale thrust repetition (in the order of 50 m to 100s m) of the Lower Roan Sequence has been recognised at NKM.

Tight to isoclinal folds with doubly plunging hinge lines, curved axial planes and limb attenuation, characterise the structural style of the COM (Slides 16, 17, 18). Low angle shears, confined largely to the COM, overprint and locally crenulate the S_2 fabric (Slide 18). These relationships indicate that the non-cylindrical fold geometry resulted in part at least from late-stage, shear related modification.

Strain partitioning into the COM has resulted in considerable dissolution and bedding-S_2 parallel shearing. The pre-folding stretching lineation observed in Mindola Pit was either not developed or obliterated within this high strain zone. However late, steep SW- to WSW-plunging lineations and horizontal NW trending lineations are only recognised within the lower portion of the COM.

Veining

Several vein generations were developed within the COM and to a lesser degree in the underlying MCF (Slide 19). The majority of veining is confined to the highest strain areas, such as the hinge zone of the Nkana Syncline. The basal contact of the COM on the eastern flank of the 'C' syncline is commonly characterised by layer-parallel carbonate fibre veins, interpreted to have developed at the onset of shortening. These veins have been intensely deformed due to decoupling along the MCF–COM boundary during the subsequent main progressive fold generation (Slide 19). By far the most common veins occur within S_2 and contain a complex assemblage of qtz-cal-bio-alb-K-feld-anhy-ser.

Metamorphism and metasomatism

Complex and pervasively developed metamorphically-modified alteration assemblages occur largely confined to the MCF–KF contact. These assemblages vary at both meso- and microscopic scales and in relation to the original country rock. Assemblages consist of varying quartz–albite–K-feldspar–biotite (phlogopite)–calcite–anhydrite–chlorite–tremolite–actinolite and accessory minerals of epidote, allanite, apatite, scapolite, tourmaline, sphene, monazite and rutile. The intensity of the alteration appears to be related to changes in the thickness of MCF, distance from MCF–COM contact, position relative to fold hinge and some late moderate angle shears (Slide 16).

C–O isotopes

C–O isotopes results from a suite of mineralised COM lithologies, veins and metamorphic alteration assemblages from the COM and upper MCF show a consistent depleted $\delta^{13}C$ value range of –10 ‰ to –19‰. Small-scale variation of only several per mil $\delta^{18}O$ appears to reflect the relative proportion of carbonaceous matter and degree of metamorphism.

Pervasive alteration of the upper MCF and the lower COM within the high strain zones show very limited variation in C–O isotopes, relative to less altered lithologies (Slide 20). The early generation of carbonate veins have the most depleted $\delta^{13}C$ values (–17 ‰ to –19 ‰). Later syn-S_2 veins have slightly heavier $\delta^{13}C$ values (–11 ‰ –15 ‰) interpreted to reflect processes related to metamorphism within a closed system. Later post S_2 veins have similar $\delta^{13}C$ values (Slide 20).

Mineralisation

Mineralisation at NKM is mainly hosted at the level of the lower COM and to a lesser degree within the immediately underlying MCF. At the broad scale the orebody transgresses the stratigraphy at Mindola. For example the Cu orebody in low strain zones such as the Mindola Pit grossly dips parallel to stratigraphy, however the assay footwall contact can vary up to 5 m above and below COM–MCF contact. Sulfides are disseminated throughout the mineralised zones, however sulfide rich portions are hosted by K-feldspar-albite rich beds. Minor sulfide remobilisation and recrystallisation is seen even in the low strain zones on the scale of centimetres (Slide 21).

Within the high strain zones, such as the hinge zone on and below the 3360 L at SOB Shaft, the overall Cu orebody geometry is now folded and the majority of disseminated sulfides are aligned parallel to S_2. A younger generation of sulfides occur within cal-qtz-feld-bio veins that cross-cut S_2. Significant hinge thickening and remobilisation in the 'C' syncline and 'C' anticline and on the SW limb of the 'C' anticline is evident and results in very complex, meso to macroscale orebody geometries. Vertically limited ore shoots contained within the upper COM and lower Rokana Evaporites Member are the result of remobilisation by post-S_2 shear propagation folds (Slides 22, 23).

Co mineralisation is unevenly distributed within the Cu orebodies at NKM. At the southern end of NKM, high grade Co zones are situated at the base of COM or in the immediately underlying upper portions of the MCF, while towards the north at Mindola Shaft, overall higher grades of Co are within the COM, and commonly towards the upper portion of Cu orebody. High grade cobalt mineralisation is locally partitioned into higher strain domains at Nkana Synclinorium. Co rich, Cu poor intersections are rarely situated outside the actual Cu orebody (Slide 25).

The sulfide paragenesis at NKM is complicated by metamorphism and high strain. To date the gross sulfide paragenesis of Py–Cobalt-rich pyrite–Carrollite–(Chalcopyrite–Bornite)–late Carrollite? would best characterise the entire NKM system. Accessory sulfide minerals identified include molybdenite, sphalerite, pyrrhotite and chalcocite.

Summary and Conclusions

- Significant lateral thickness and facies variation occurs at the onset of sedimentation and relate to an initial stage of active rifting. The positions of compartment-bounding faults are indicated by the coincidence of facies changes within both the MCF and basal COM, and abrupt changes in strike of the MCF–basement contact.
- Facies variation within the basal COM coincide with changes in ore grade. Barren gaps occur in association with arenaceous strata and enigmatic, massive and highly altered carbonate facies. $\delta^{13}C$ signatures of these carbonate units are compatible with those of sedimentary carbonate carbonate facies.
- Changes in facies architecture between the MCF and KF are interpreted to reflect evolution from small, compartmentalised depocentres, to an open basin system.
- Strain increases progressively towards the core of the Nkana Syncline. Highest strains are ubiquitously partitioned into fine-grained facies of the COM, and reflect rheological contrast with underlying basement and/or coarse siliciclastic strata of the MCF. Although evidence exists for an early phase of decoupling at the MCF–COM contact, most small scale structures record deformation related to the regional Lufilian folding event.
- Folding within high strain zones is characteristically non-cylindrical, the result of late stage shear development.

- Alteration is most intense about the MCF–KF contact and comprises a complex metamorphosed assemblage of quartz–albite–K-feldspar–biotite–calcite–anhydrite–chlorite–tremolite–actinolite.
- δ^{13}C signatures of hydrothermal carbonate are characteristically 'light'. Most depleted values were recorded in early formed, layer-parallel calcite veins and are comparable with ore-related hydrothermal carbonate from other deposits in the Copperbelt. Later syn-S_2 veins show slightly heavier δ^{13}C values, the result of metamorphism within a closed system.
- Although there was considerable grain-scale remobilisation of sulfides into the S_2 cleavage and late-stage shears during metamorphism, the broad envelope to mineralisation defines an extensive sheet positioned at the MCF–KF interface. This geometry, albeit slightly transgressive of stratigraphy, is analogous to lesser deformed Ore Shale-hosted deposits (eg. Konkola), and implies mineralisation prior to the regional folding event.

Ongoing work during the second half of the PhD will be focused several issues including (Slide 27):

- A better understanding of the early or pre Lufilian deformation observed in low strain zones;
- Complete, detailed u/g maps of new exposures of high strain zones to further resolve the significance and relationship of deformation to basin architecture, metamorphism and sulfide remobilisation;
- Sulfide paragenesis linked to S-isotopes and possible sulfide chemistry;
- Modelling of C–O isotope data, possibly in conjunction with fluid inclusion work on veins; and
- Significance of Co mineralisation.

References

Annels, A.E., 1989, Ore genesis in the Zambian Copperbelt, with particular reference to the northern sector of the Chambishi Basin, in Boyle, R.W., et al., Sediment-hosted stratiform copper deposits: Geological association of Canada Special Paper 36, p. 427-452.

Bull, S. & Selley, D., 2003. Chambishi basin studies; Chambishi SE Prospect. This volume.

Clemmey, H. 1978. A Proterozoic lacustrine interlude from the Zambian Copperbelt. In Matter, A. and Tucker, M.E. (eds) Modern and ancient lake sediments: proceedings of a symposium. Special Publication of the International Association of Sedimentologists, 2. pp259–278.

Garlick, W.G., 1961. The syngenetic theory. In Mendelsohn, F., ed., The geology of the northern Rhodesian Copperbelt: London, MacDonald, p. 146–165.

Selley, D. & Bull, S., 2001. Stratigraphy and basin geometry at the Chibuluma West copper-cobalt deposit, Zambia. AMIRA P544 Progress Report, Dec 2001. pp. 101–132.

Selley, D., Bull, S., Scott, R., Cooke, D., 2002. Chambishi Basin progress report 2: Basin geometry and its controls on mineralisation at Mwambashi B. AMIRA P544 Progress Report, Dec 2002. pp. 5.1–5.40.

Structural Development and Controls on Cu-Co Mineralisation, Nkana-Mindola

What is the significance of the Lufilian deformation on the distribution-accumulation of Cu and Co sulphides at Nkana-Mindola?

Mawson Croaker

3360L SOB Shaft

Underground Change Room

Deformed Ore Shale, Mindola Shaft.

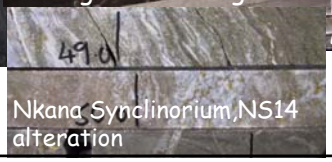
Nkana Synclinorium,NS14 alteration

KEY POINTS

Footwall basin architecture still observed in places despite deformation.

Early lineations unrelated to main fold generation.

No large-scale thrust repetition of stratigraphy.

MCF-Ore Shale contact important rheology boundary.

Large scale fold geometry significantly controlled by basement and MCF.

At Ore Shale level - limb attenuation, flexural slip progressive deformation, late shearing.

Cu Orebody original flat lying, now complexly deformed.

Significant local remobilisation-recrystallisation, Possible continuous use of 'original' fluid conduit pathways.

OUTLINE

Three areas:

Basin architecture.

RELATION TO

Deformation of the Lower Roan.

Briefly discuss mineralisation distribution and remobilisation related to deformation.

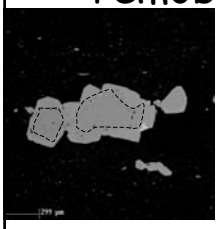

So for the evidence!!

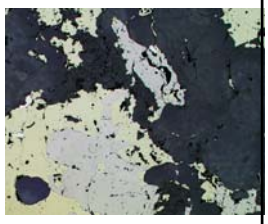

AMIRA/ARC Project P544 *Final Sponsors Meeting* *July 2003*

NKANA-MINDOLA

Significant Cu-Co producer over 60 years from 4 shafts plus open pits.

<u>Structural Overview</u>

Most highly strained Chambishi basin deposit.

Mineralisation occupies hinge and eastern limb of major NW plunging syncline.

Non-cylindrical fold geometry

Interference with WNW trending folds

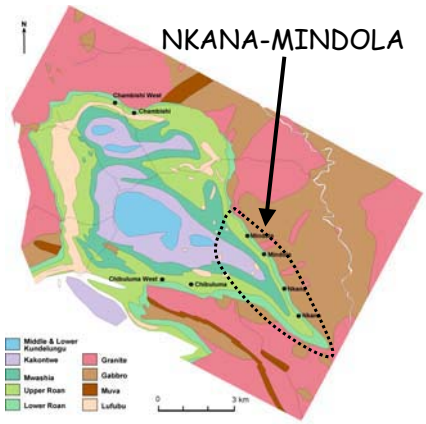

AMIRA/ARC Project P544 *Final Sponsors Meeting* *July 2003*

BASIN ARCHITECTURE – Stratigraphy

- Facies architecture is compatible with that recognised throughout Chambishi Basin
  - two distinct phases of basin growth

- facies variation evident within the Ore Shale
  - barren gaps: ie. link between basin architecture and mineralisation
  - dolomitic barren gaps have d13C isotopic signatures compatible with microbial carbonates from Chambishi SE

- thickness variation in FW

- barren gaps & FW thinning coincide with subtle perturbations in fold geometry

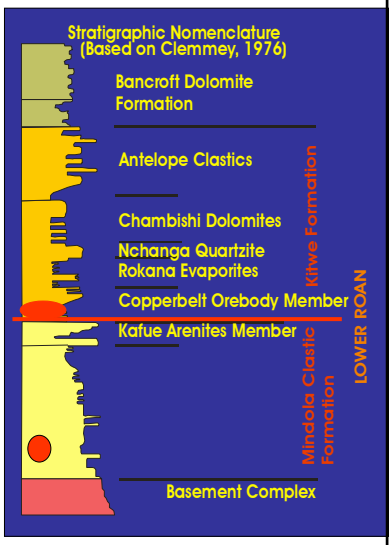

AMIRA/ARC Project P544 *Final Sponsors Meeting* *July 2003*

BASIN ARCHITECTURE – Facies and geometry

- Facies architecture is compatible with that recognised throughout Chambishi Basin
  - two distinct phases of basin growth

- facies variation evident within the Ore Shale
  - barren gaps: ie. link between basin architecture and mineralisation
  - dolomitic barren gaps have d13C isotopic signatures compatible with microbial carbonates from Chambishi SE

- thickness variation in FW

- barren gaps & FW thinning coincide with subtle perturbations in fold geometry

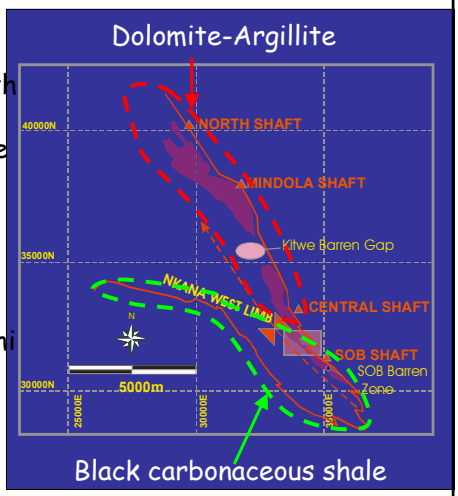

AMIRA/ARC Project P544 *Final Sponsors Meeting* *July 2003*

BASIN ARCHITECTURE – Isotopes

- Facies architecture is compatible with that recognised throughout Chambishi Basin
  - two distinct phases of basin growth
- facies variation evident within the Ore Shale
  - barren gaps: ie. link between basin architecture and mineralisation
  - dolomitic barren gaps have d13C isotopic signatures compatible with microbial carbonates from Chambishi SE.
- thickness variation in FW
- barren gaps & FW thinning coincide with subtle perturbations in fold geometry

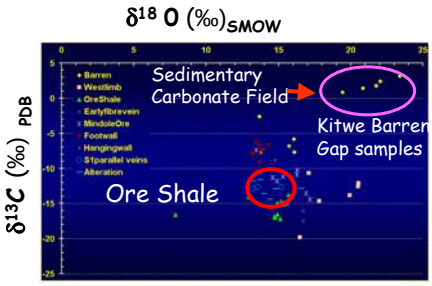

BASIN ARCHITECTURE – Fold geometry.

- Facies architecture is compatible with that recognised throughout Chambishi Basin
  - two distinct phases of basin growth
- facies variation evident within the Ore Shale
  - barren gaps: ie. link between basin architecture and mineralisation
  - dolomitic barren gaps have d13C isotopic signatures compatible with microbial carbonates from Chambishi SE
  - barren gaps & FW thinning coincide with subtle perturbations in fold geometry

thickness variation in MCF

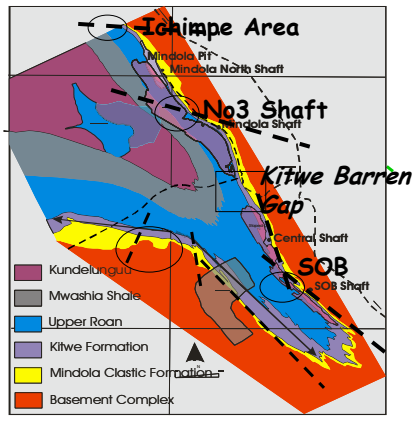

BASIN ARCHITECTURE – In strain zones?

- Facies architecture is compatible with that recognised throughout Chambishi Basin
  - two distinct phases of basin growth
- facies variation evident within the Ore Shale
  - barren gaps: ie. link between basin architecture and mineralisation
  - dolomitic barren gaps have d13C isotopic signatures compatible with microbial carbonates from Chambishi SE
- thickness variation in FW
- barren gaps & FW thinning coincide with subtle perturbations in fold geometry

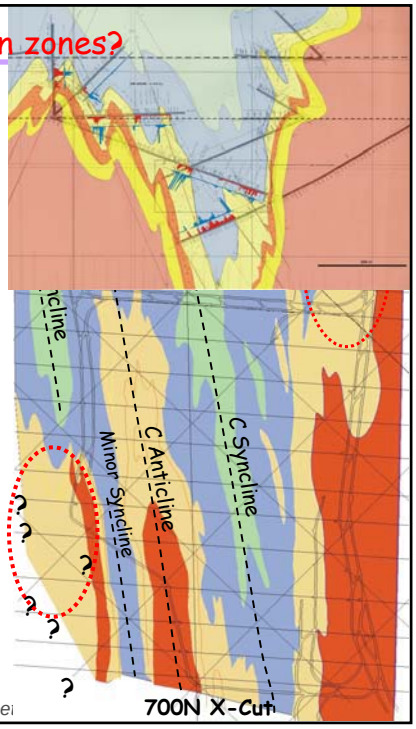

DEFORMATION - NKANA SYNCLINE

Level of strain is variable throughout the system.
laterally: broadly increases towards the hinge of the Nkana Syncline
vertically: higher strains within the Kitwe Formation relative to the Mindola Clastics Formation

1. North Shaft and Mindola Pit ('low strain').
2. Zero Syncline-Anticline – Central Shaft ('moderate strain').
3. 'C' Syncline-Anticline – SOB Shaft ('high strain').

No new data collected from the western limb of Nkana Syncline. Selection of work areas primarily based upon u/g access and quality of drill core.

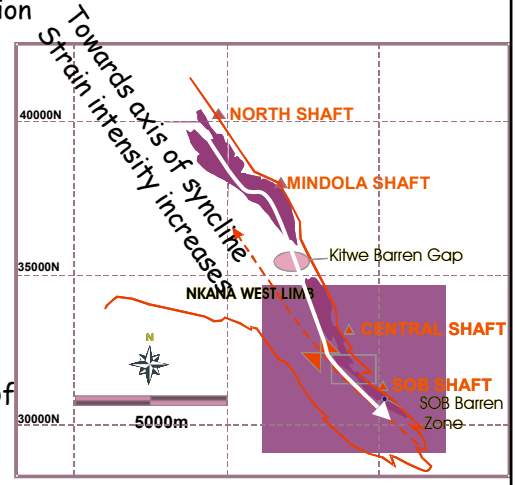

DEFORMATION – Low strain.

Macroscopic Structural Geometry

- near surface portion of orebody located on uniformly & shallowly dipping segment of fold limb
  - 30° SW – WSW dip

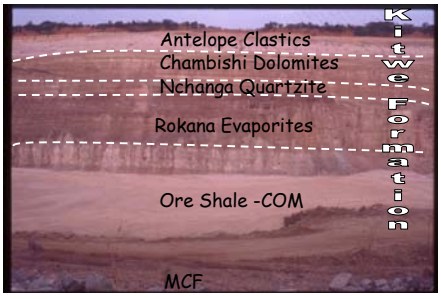

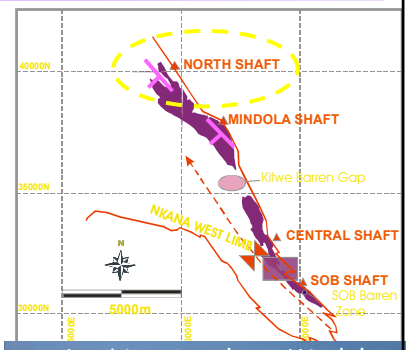

Mesoscopic Structures

- evidence of minor bedding parallel movement within the Ore Shale
  - asymmetric mesoscopic folds
  - axes parallel regional fold trend
- two generations of mineral lineation
  - L1 – attenuated nodules
  - shallow SSW plunge
  - oblique to main fold axis
  - L2 –WSW plunging slickenfibre lineation
- mesoscopic folds and slickenfibre lineation compatible with flexural slip
- L1 stretching lineation unrelated to folding – possible early thrusting

- *both events highlight rheological contrast between FW & Kitwe Fm*

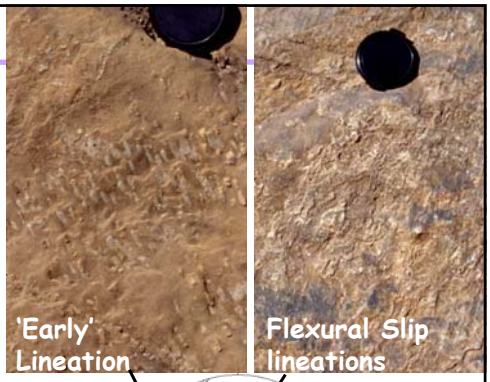

DEFORMATION – Moderate strain, Mindola -1000m.

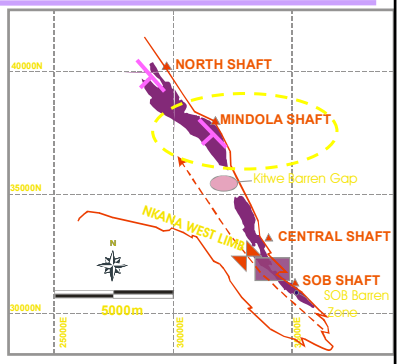

Limb dip increased ~75 degrees

Decoupling at base of Ore Shale intensifies
- Meso-scale isoclinal folding
- shear fabrics
- schistose ore shale

No 'early lineations' recorded.

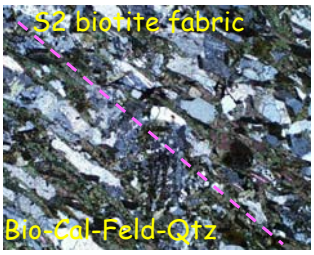

AMIRA/ARC Project P544 *Final Sponsors Meeting* *July 2003*

DEFORMATION – High Strain, SOB Shaft

Overall strain increase throughout MCF & COM

3 discrete phases

BUT strain partitioning occurs across three rheological/ stratigraphic boundaries:
- Basement-MCF
- Lower Conglomerate-KAM
- MCF-Ore Shale

Strain is manifested meso- & macroscopically as:
- upright, high amplitude folds
- shear zones - fold modification
- multiple generation vein arrays.
- significant dissolution and bedding-S2 parallel shearing.

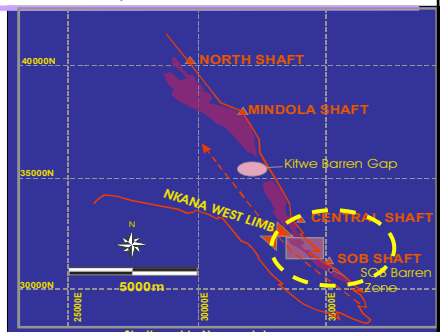

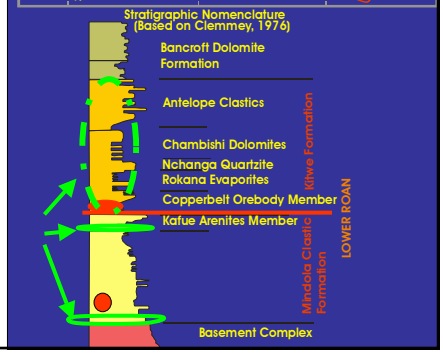

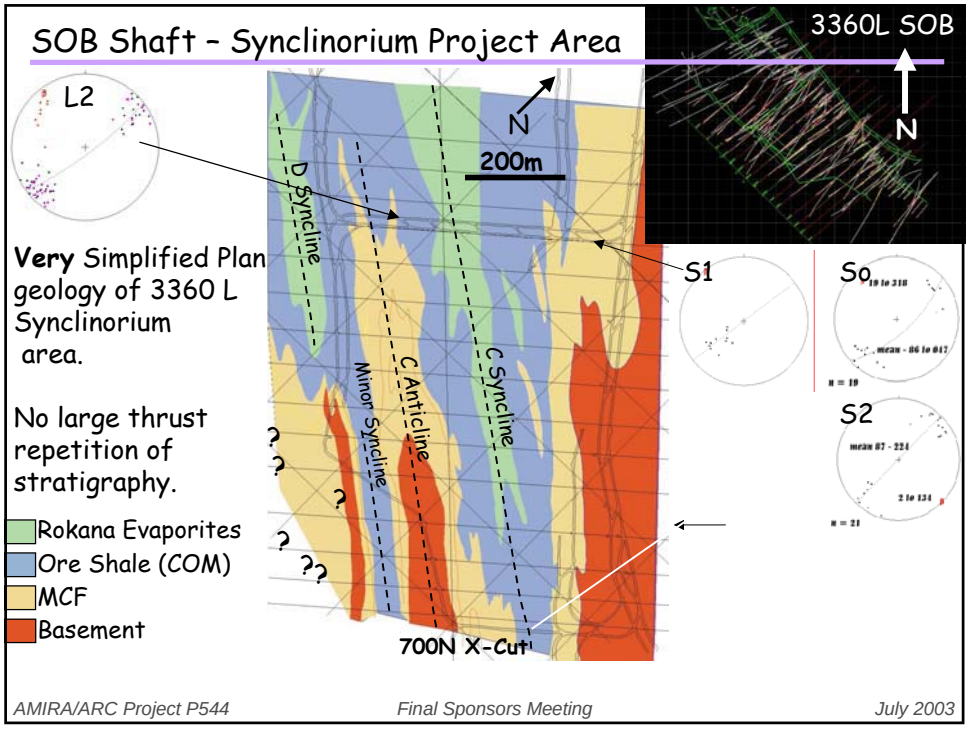
SOB Shaft – Synclinorium Project Area
3360L SOB
N
L2
N
200m
D Syncline
C Anticline
Minor Syncline
C Syncline
S1
So
S2
Very Simplified Plan geology of 3360 L Synclinorium area.
No large thrust repetition of stratigraphy.
Rokana Evaporites
Ore Shale (COM)
MCF
Basement
700N X-Cut
AMIRA/ARC Project P544
Final Sponsors Meeting
July 2003

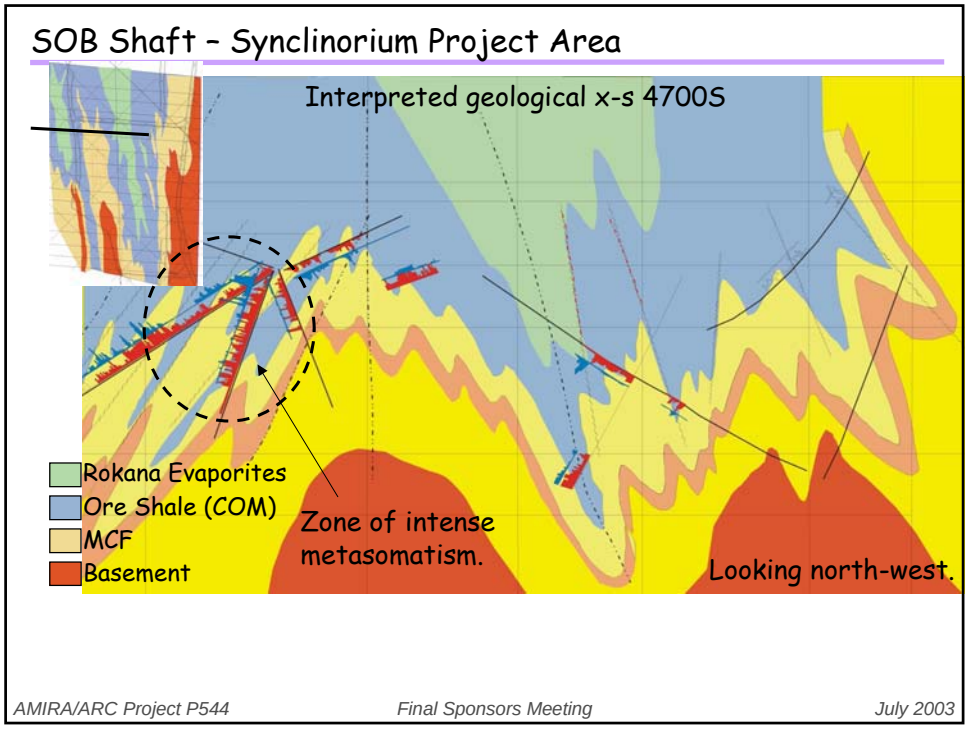
SOB Shaft – Synclinorium Project Area
Interpreted geological x-s 4700S
Rokana Evaporites
Ore Shale (COM)
MCF
Basement
Zone of intense metasomatism.
Looking north-west.
AMIRA/ARC Project P544
Final Sponsors Meeting
July 2003

SOB Shaft – Synclinorium Project Area

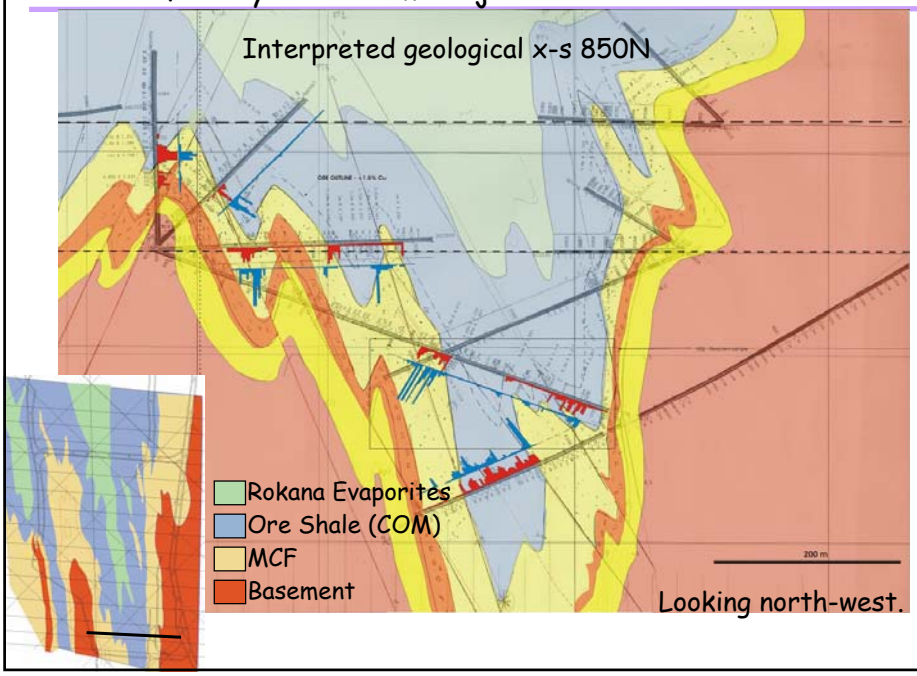

SOB Shaft – Synclinorium Project Area

S0 – easily recognised within MCF, lesser degree in Ore Shale.

S1 – Rarely Observed, eastern end of 4700s cross cut in MCF.

S2 – pervasive, well developed in Ore Shale and KAM.

S3 – Crenulation of S2 in zone of shortening associated with late, low angle shears.

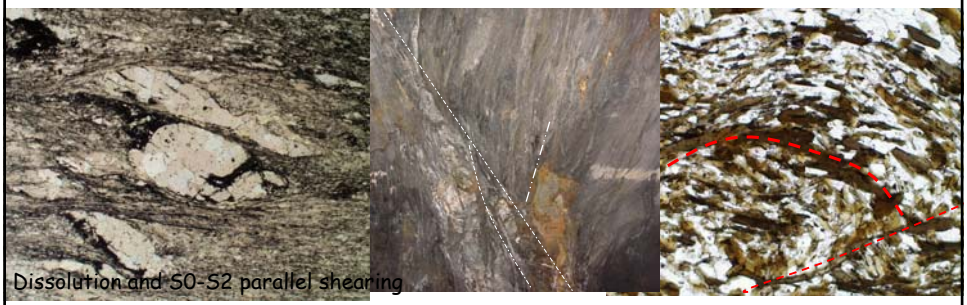

AMIRA/ARC Project P544 *Final Sponsors Meeting* *July 2003*

VEINS - SOB Shaft – Synclinorium Project Area

Early fibre veins (calcite) development at basal portion of Ore Shale (onset of shortening).

S2 parallel veins (qtz-feld-cal-ser) + sulphides.

Post S2 – similar composition to S2 veins + sulphides

Late small tension veins – qtz, unmin.

Veins only locally influence sulphide distribution

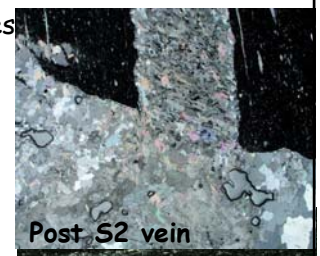

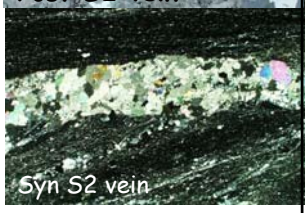

AMIRA/ARC Project P544 *Final Sponsors Meeting* *July 2003*

CARBON AND OXYGEN ISOTOPES

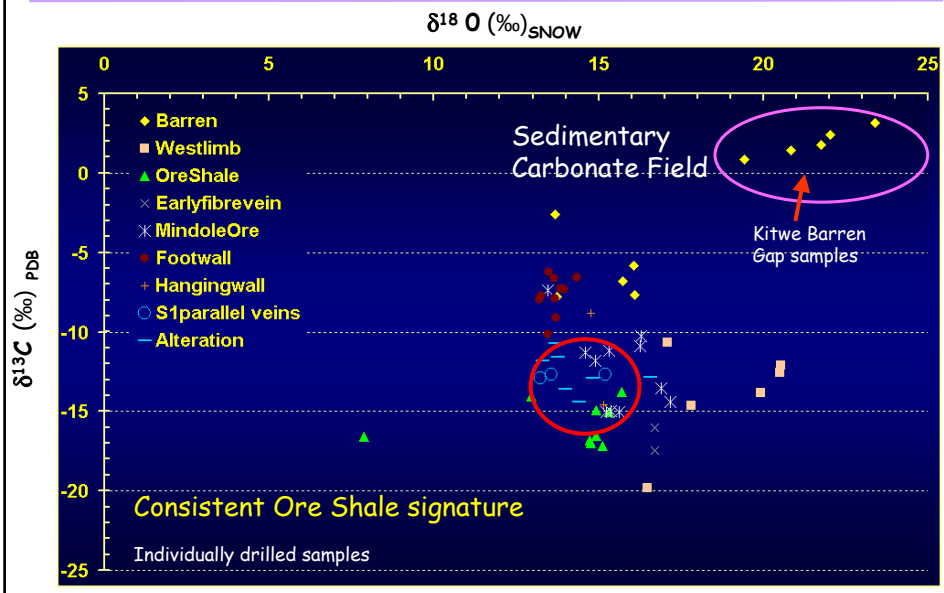

AMIRA/ARC Project P544 *Final Sponsors Meeting* *July 2003*

MINERALISATION – Mindola and North Shaft

Cu-Co Mineralisation primarily hosted in Ore Shale, minor upper 5m of footwall.

Sulphides recrystallised, into S2 cleavage and S0 parallel veins.

K-feld-albite-dolomite phases.

Internal grade variations non-systematic.

Grade contact (+1.6% Cu) up to Maybe up to 3-5m above MCF-Ore Shale Contact.

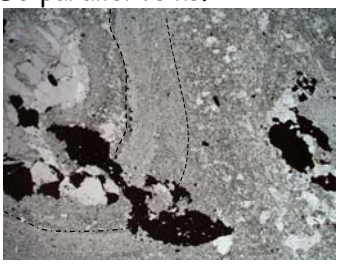

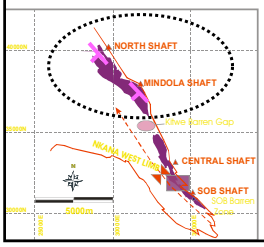

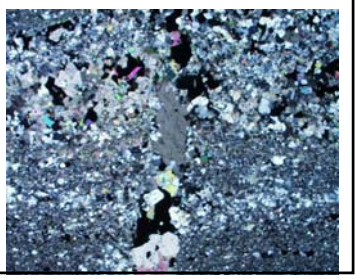

MINERALISATION –SOB Shaft

Cu-Co Mineralisation overall folded geometry.

Higher grade and thicker mineralisation in fold noses.

'Ore Shoot' developed by 1. fault prop. folds in Ore Shale only and 2. local sulphide remobilisation.

High grade cobalt zones within Cu orebody.

Disseminated sulphides in Ore Shale primarily aligned parallel to S2 cleavage or recrystallised post S2.

Sulphide phase mobility relative to metamorphism resulting in complex SOB sulphide paragensis. To date – Py- CoPy – Car – Po – Cpy – Bn - Car

AMIRA/ARC Project P544 *Final Sponsors Meeting* *July 2003*

MINERALISATION –SOB Shaft

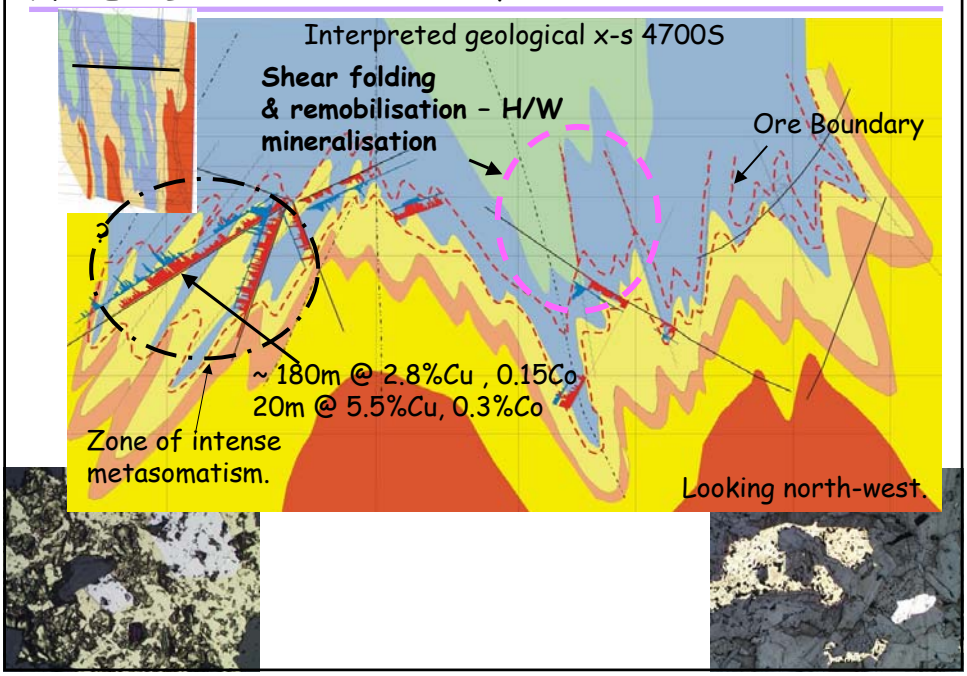

MINERALISATION – SOB Shaft

Disseminated ore in Ore Shale primarily aligned parallel to S2 cleavage.

Sulphide phase mobility relative to metamorphism resulting in complex SOB sulphide paragensis.
To date – Py- CoPy – Car – Po – Cpy – Bn - Car

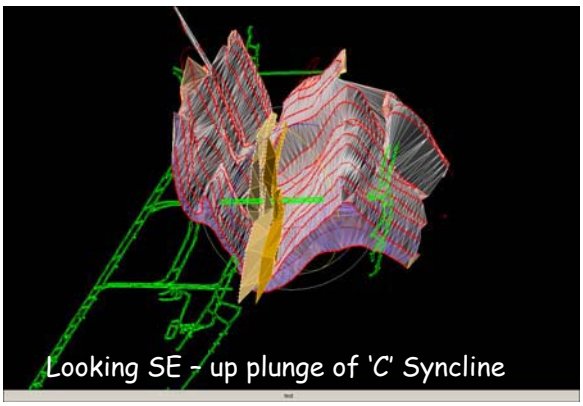

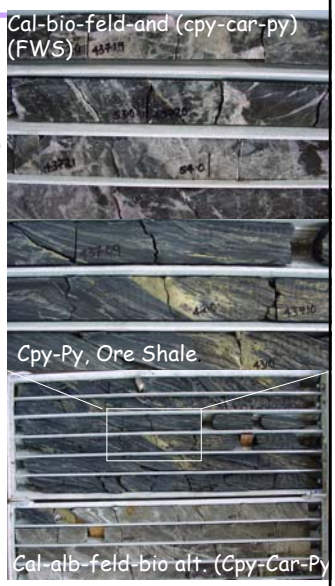

AMIRA/ARC Project P544 *Final Sponsors Meeting* *July 2003*

MINERALISATION –SOB Shaft

Higher grade and thicker mineralisation in fold noses.
'Ore Shoot' developed by 1. fault prop. folds in Ore Shale only
and 2. local sulphide remobilisation.
Significant high grade mineralisation on SW limb of 'C' anticline.

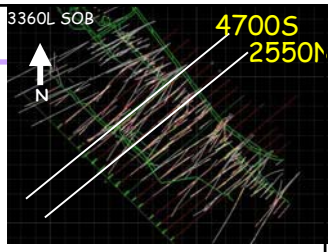

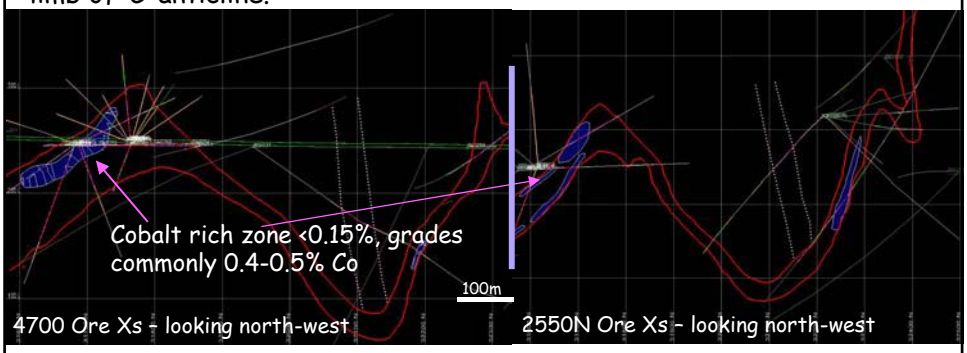

High grade cobalt zones within Cu orebody.

AMIRA/ARC Project P544 *Final Sponsors Meeting* *July 2003*

CONCLUSIONS TO DATE

Evidence of footwall basin architecture still observed in places.

Early lineation unrelated to main fold generation.

MCF-Ore Shale contact important boundary for strain partitioning.

Rheology contrast between MCF-Ore Shale forms polydisharmonic folding

No large scale repetition of stratigraphy.

Broad fold geometry significantly controlled by basement forming original near cylindrical folds. Limb attenuation, non co-axial, flexural slip. Progressive deformation, late shearing.

Orebody geometry folded.

Significant local remobilisation-recrystallisation.

Possible continuous use of 'original' fluid conduit pathways.

AMIRA/ARC Project P544 *Final Sponsors Meeting* *July 2003*

THE FUTURE – Completion……..

Nearing completion of 2nd year of PhD.

Small field season for detailed structural work at new u/g exposures – Further work ascertain metasomatic / metamorphic relationships to Structure, geochemistry and mineralisation. 3360L SOB

Continued sulphide and metamorphic assemblage assessment– petrography, probe, LA-ICPMS?
Linked to sulfur isotopes.

Closer assessment of actually individual sulphide deformation.

Fluid inclusions from veins (SOB) and C-O isotope modelling.

Cobalt Story….? - Where, why and how?

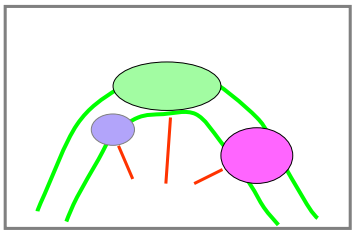

Do the individual sulphide compositions change?

WRITE!*When will my PhD be completed? Late'04.* *hopefully* ***No more money***

AMIRA/ARC Project P544 *Final Sponsors Meeting* *July 2003*

ACKNOWLEDGEMENTS

MOPANI COPPER MINES. Dave Armstrong, Wellington Mukumba, Giddy Mwale, Shaft Geologists and ALL underground workers.

FIRST QUANTUM MINERALS. ZAMBIA – Hugh Carruthers and Mike Stuart.

ZAMANGLO. Peter Mann, Jon Woodhead and staff. 'Spider' for keeping the 'Love Bus' ticking over.

AMIRA SPONSORS, CODES STAFF AND CSM. Dave Selley, Rob Scott and Peter McGoldrick.

University of Tasmania Postgraduate Scholarship.

Maptek for version of Vulcan™

JUNE PONGRATZ.

AMIRA/ARC Project P544 *Final Sponsors Meeting* *July 2003*

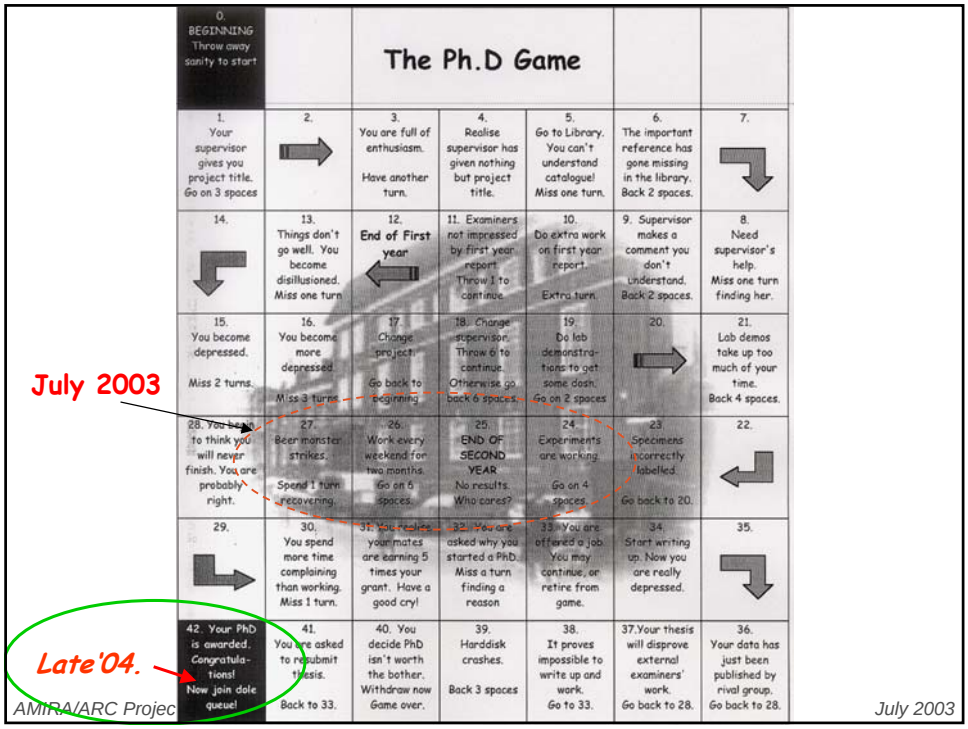
The Ph.D Game
0. BEGINNING Throw away sanity to start
1. Your supervisor gives you project title. Go on 3 spaces
2.
3. You are full of enthusiasm. Have another turn.
4. Realise supervisor has given nothing but project title.
5. Go to Library. You can't understand catalogue! Miss one turn.
6. The important reference has gone missing in the library. Back 2 spaces.
7.
8. Need supervisor's help. Miss one turn finding her.
9. Supervisor makes a comment you don't understand. Back 2 spaces.
10. Do extra work on first year report. Extra turn.
11. Examiners not impressed by first year report. Throw 1 to continue.
12. End of First year
13. Things don't go well. You become disillusioned. Miss one turn
14.
15. You become depressed. Miss 2 turns.
16. You become more depressed. Miss 3 turns
17. Change project. Go back to beginning
18. Change supervisor. Throw 6 to continue. Otherwise go back 6 spaces.
19. Do lab demonstrations to get some dosh. Go on 2 spaces
20.
21. Lab demos take up too much of your time. Back 4 spaces.
22.
23. Specimens incorrectly labelled. Go back to 20.
24. Experiments are working. Go on 4 spaces.
25. END OF SECOND YEAR No results. Who cares?
26. Work every weekend for two months. Go on 6 spaces.
27. Beer monster strikes. Spend 1 turn recovering.
28. You begin to think you will never finish. You are probably right.
29.
30. You spend more time complaining than working. Miss 1 turn.
31. You realise your mates are earning 5 times your grant. Have a good cry!
32. You are asked why you started a PhD. Miss a turn finding a reason
33. You are offered a job. You may continue, or retire from game.
34. Start writing up. Now you are really depressed.
35.
36. Your data has just been published by rival group. Go back to 28.
37. Your thesis will disprove external examiners' work. Go back to 28.
38. It proves impossible to write up and work. Go to 33.
39. Harddisk crashes. Back 3 spaces
40. You decide PhD isn't worth the bother. Withdraw now Game over.
41. You are asked to resubmit thesis. Back to 33.
42. Your PhD is awarded. Congratulations! Now join dole queue!
July 2003
Late'04.
AMIRA/ARC Projec
July 2003

Geochemical and isotopic character of Cu mineralisation in the Tapley Hill Formation, South Australia

Peter McGoldrick and Stuart Bull
Centre for Ore Deposit Research, University of Tasmania

Introduction

Previous workers in South Australia had argued that Cu mineralisation in the the Tapley Hill Formation on the Stuart Shelf, and minor Cu occurrences in the Callana Group in the Adelaide Foldbelt were similar to the Zambian Copperbelt (ZCB) deposits (e.g., Rowlands, 1974). Hence, one of the important aims of P544 was to use the insights gained from our Zambian work to make a more critical comparisons with Cu mineralisation in the Neoproterozoic sequences of South Australia.

This short report re-iterates results from the Emmie Bluff deposit on the Stuart Shelf (McGoldrick - P544 Annual Progress Report 2001), and discusses new geochemical data from drill core from the Boorloo prospect in the northern Willouran Ranges.

Copper mineralisation in the Neoproterozoic of South Australia is, broadly speaking, confined to two stratigraphic levels (Selley 2000). The Callanna Group hosts a number of small structurally controlled epigenetic deposits e.g., Dunn's Mine (Mackay, Selley et al. 2002). Higher in the stratigraphy, stratiform, stratabound and vein-style Cu mineralisation occur in Umberatana Group rocks (mainly in, or near the Tapley Hill Formation (e.g., Emmie Bluff, Myall Creek)).

This report discusses geochemical and isotopic signatures associated with Cu mineralisation in the Tapley Hill Formation at two localities: Emmie Bluff and Boorloo Mine (Slide 1).

Emmie Bluff

Emmie Bluff was discovered by MIM Exploration in the 1980s and is a sub-horizontal stratiform deposit with resource of 24 Mt at 1.3wt% Cu at a depth of about 400 m below the surface. At Emmie Bluff the Tapley Hill Formation is dominated by carbonaceous siltstone and shale, with minor dolomitic sands and gravels. It rests disconformably on deeply weathered and strongly hematised Mesoproterozoic sandstones of the Pandurra Formation, and is overlain by terrestrial hematitic sandstones and basal conglomerate of the Whyalla Formation. (Slide 5)

Copper mineralisation (chalcopyrite, bornite, chalcocite / digenite and pyrite) is mainly confined to carbonaceous and dolomitic siltstones of the Tapley Hill Formation, but Cu sulfides occur sporadically in the basal part of the Whyalla Sandstone. Fine grained sulfides occur as bedding parallel seams and patches, and coarser Cu sulfides are present in veins and in patches in intraclast breccias. Thicker intersections of Tapley Hill Formation rocks contain more visible Cu at their upper and lower contacts (Slide 6).

The Boorloo prospect, in the northern Willouran Ranges, comprises cupriferous carbonate-pyrite veins in a thick Tapley Hill Formation sequence. Host rocks at Boorloo mine comprise a minimum of several hundred metres of carbonaceous and dolomitic siltstone and shale. The lower part of the section contains substantial thicknesses of interbedded coarse clastic (dolomite, siltstone and pyrite fragments) mass flow deposits (Slide 8). Open File reports from Utah's 1970s drilling program indicate typical grades of 1000 to 2000 ppm Cu over one

metre intersections at several levels in drill holes WD004 and WD010 (two samples had more than 1 wt % Cu). However, there are no visible Cu-sulfides in any of the sedimentary rocks in these holes, and visible chalcopyrite is confined to the quartz-carbonate-pyrite veins (Slides 7, 8).

Lithogeochemistry

Emmie Bluff

The main features of the geochemistry of 119 samples from all three units at Emmie Bluff are summarised in McGoldrick 2001 (AMIRA P544 Annual Progress report). The major element chemistry of the Pandurra Formation reflects its mature, leached and ferruginous character, small amounts of illite or muscovite, and virtually no carbonate. In contrast, both the Tapley Hill Formation and the Whyalla Sandstone contain significant carbonate in the form of ferroan dolomite. The K/Al ratios in both these units indicate illite (or muscovite) is the only K-bearing mineral phase. In the Tapley Hill Formation Cu, Co, Zn and Pb are elevated compared to 'typical shales', while Bi, As, Ni, Mo and Tl are not. In thick Tapley Hill Formation intersections, Cu is elevated close to the upper and lower contacts, and displaced from Zn and Pb, which are highest nearer the middle.

Boorloo prospect

The grab samples of shale and siltstone from Boorloo prospect have a chemistry indistinguishable from 'typical shales'. All samples have K/Al ratios suggestive of illite/muscovite, and most contain some dolomite. However, only one of 21 samples has weakly elevated chalcophile metals (e.g., 195 ppm Cu, 126 ppm Co). This sample is unusual in that it contains several percent pyrite. (Slide 9)

Stable isotopes

Previous studies of the Mt Gunson Cu deposit (Knutson et al., 1983) and Cu mineralisation in the Copper Claim and Myall Creek areas (Lambert et al., 1984 a, b) included S isotope data and a limited amount of C/O isotope data. Additional C/O data for the South Australian Neoproterozoic were available from a stratigraphic study by Hill and Walter (2000) and from unpublished work that will form part of Wallace Mackay's PhD thesis. For the study reported here 12 new whole rock C/O isotope analyses were performed on the more carbonate-rich samples from Boorloo prospect lithogeochemistry sample set.

Most of the available C isotope measurements for samples associated with Cu mineralisation are between about –8 and 6‰, $\delta^{13}C$ and the Boorloo samples range from about 0 ‰ to –8 ‰ $\delta^{13}C$ (SLIDE18.11). This is within the secular range defined by Hill and Walter (2000) for much of the South Australian Neoproterozoic. Hence, C in the Boorloo samples can be interpreted as simply having an unmodified seawater isotopic signature. The regional O isotope values show a wide spread, but in the Boorloo samples have a much more limited range. As with C, it is likely that the Boorloo dolomitic shales and siltstones have a seawater O isotope signature.

While, no new S isotope work was undertaken on the Boorloo samples, the published S isotope data for other Cu prospects and deposits display a wide range of $\delta^{34}S$ values from heaviest values of up to 28‰, to lightest values of –18‰ (Lambert et al., 1984 a, b: Knutson et al., 1983). The S isotopes data, together with sulfide textures, were taken to indicate that biogenic sulfate reduction (BSR), operating at low temperatures during early diagenesis, was responsible for producing the sulfide now seen in the deposits (Knutson et al., 1983). The heavier sulfide $\delta^{34}S$ values were thought to be a product of local closed system BSR.

Comparison with the Zambian Copperbelt

The Emmie Bluff stratiform Cu mineralisation shares some similarities in the tenor of some chalcophile elements to Zambian Copperbelt Ore Shale deposits. For instance, Cu, Co, and Ag are anomalous in both). This, together with the siting of Cu mineralisation in reduced facies within dominantly oxidised sequences, suggests oxidised saline brines were

the metal transporting fluid in both Zambia and South Australia. A notable difference at Emmie Bluff is the occurrence of elevated Zn and Pb, either directly associated with the elevated Cu, or displaced toward the middle of thicker Tapley Hill Formation intersections.

Unlike siltstones in the Zambian Copperbelt Ore Shale deposits and, for that matter, the Tapley Hill Formation at Emmie Bluff, siltstone samples from Boorloo show no elevated Cu or related metals. It would appear that the elevated Cu in the exploration assays is reporting from the quartz-carbonate-pyrite veins. This observation suggests the discordant, epigenetic Cu mineralisation in the Boorloo veins was not locally derived from re-mobilisation of low-grade diagenetic- Cu mineralisation in the Tapley Hill Formation.

None of the South Australian deposits show any signs of strong potassic (or sodic) alteration, although silica dissolution and intense hematisation is evident in the footwall rocks at Emmie Bluff. Also, the Ba content of fine grained rocks is in the high tens to low hundreds of ppm range, and typical for 'normal' shales. These observations are is in marked contrast to the broad pervasive alkali alteration and moderate to strong Ba enrichment seen in the mineralised Roan sequences.

Another prominent difference between the South Australian deposits and the ZCB is that none show the isotopically light C and O that is evident in the ZCB deposits (Slide 11).

Finally, our work in P544 suggests that thermo-chemical sulfate reduction is the most important mechanism for producing the reduced S needed to form the ZCB deposits (Cooke et al, 2001, P544 Annual Progress Report; McGoldrick and Cooke, this volume). This process operates best at temperatures above 150°C, and contrasts with the BSR process advocated for the South Australian deposits (BSR operates at temperature below about 120°C, Machel and Krouse, 1995).

References

Hilll, A. C. and M. R. Walter (2000). "Mid-neoproterozoic (~830–750 Ma) isotope stratigraphy of Australia and global correlation." Precambrian Research 100: 181-211.

Knutson, J., T. H. Donnelly, et al. (1983). "Geochemical constraints on the genesis of copper mineralization in the Mount Gunson area, South Australia." Economic Geology 78: 250-274.

Lambert, I. B., T. H. Donnelly, et al. (1984). "Genesis of Late Proterozoic copper mineralisation, Copper Claim, South Australia." Economic Geology 79: 266-273.

Lambert, I. B., J. Knutson, et al. (1984). "Genesis of copper mineralisation, Myall Creek prospect, South Australia." Mineralium Deposits 19: 266-273.

Machel, H. G., H. R. Krouse, et al. (1995). "Products and distinguishing criteria of bacterial and thermochemical sulfate reduction." Applied Geochemistry 10: 373-392.

Mackay, W., D. Selley, et al. (2002). "P544 Sponsors' Field Meeting Locality Guide, The Willouran Range, South Australia." AMIRA/ARC Project P544: 36pp.

Rowlands, N. J. (1974). The gitology of some Adelaidean stratiform copper occurrences. Gismentes Stratiformes et Provinces Cupriferes. J. P. Bartholome. Liege, La Societe Geologique de Belgique: 419-427.

Selley, D. (2000). "Geological framework and copper mineralisation in South Australia." AMIRA P544 Proterozoic Sedimentary Copper Deposits Meeting 2 December 2000: 42pp.

Neoproterozoic Cu mineralisation SA

- Review by David Selley Dec 2001
- Emmie Bluff (Stuart Shelf) PMcG 2001 Annual Report
- Boorloo Mine: this meeting
- Dunn's Mine: Mackay PhD

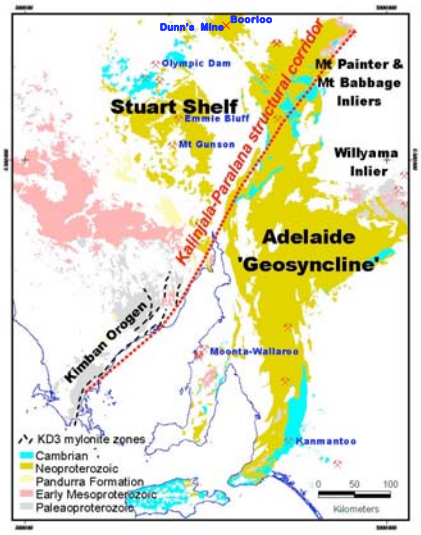

- many of small Cu deposits right through the succession
- broadly speaking (stratiform & stratabound) Cu is at 2 stratigraphic levels:

Callanna Group - Mackay PhD

- small, structurally controlled epigenetic deposits eg., Dunn's Mine

Umberatana Group - Tapley Hill Formation

- e.g., Emmie Bluff, Boorloo Prospect

- This talk compares some of the geochemical features of THF Cu mineralisation at two localities:

  Emmie Bluff on the Stuart Shelf &

  Boorloo Mine in the northern Willouran Ranges

- A description of Callana Group Cu mineralisation at Dunn's Mine will form part of Mackay's PhD

Emmie Bluff

- 24 Mt @ 1.3% Cu as Cu sulfides almost exclusively in carbonaceous, dolomitic siltstones of the Tapley Hill Formation
- On the Stuart Shelf the THF is a condensed sequence
- At EB varies from 0 to more than 40 metres thick

Emmie Bluff

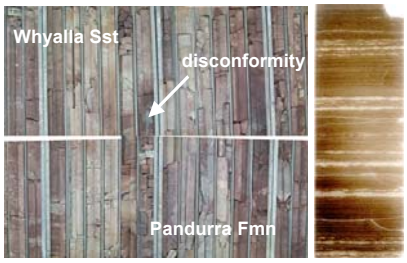

- THF rests unconformably on deeply weathered Mesoproterozoic Pandurra Formation
- Cu sulfides almost exclusively in carbonaceous, dolomitic siltstones of the Tapley Hill Formation
- Little bit Cu in Whyalla Sst at contacts with THF

Emmie Bluff

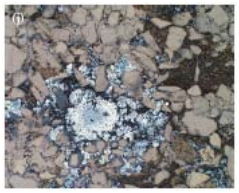

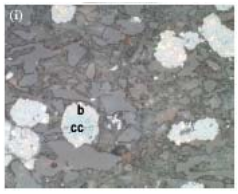

- Both Fe and Cu sulfides (py, cpy, bn, cc, dg)
- Fine grained in seams/beds
- Fine and coarse grained clots, patches and veins in siltstones & intraclasts bxs
- More visible Cu at upper and lower contacts of THF (confirmed by assays)

Boorloo

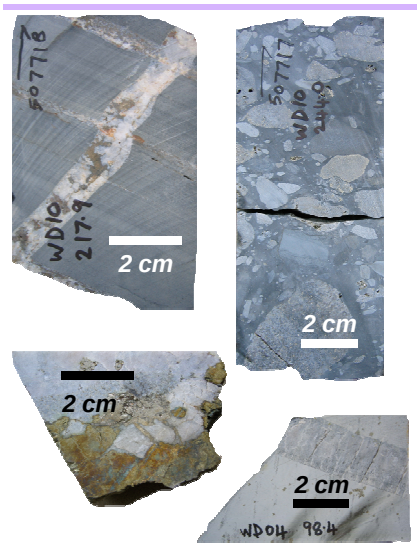

- One of Utah's 'ZCB-style' Cu targets in the Willouran Ranges in the '70s
- Stratabound Cu in lower THF equivalents
- Sporadic metre intersections with 0.x to 1% Cu
- Mainly Fe sulfides as impregnations in clasts and matrix of sedimentary bx units & qz-car veins (cpy assocd with vein py)

AMIRA /ARC P544 Final Meeting July 2003

Boorloo

·Two drill holes provided 21 samples spanning approx. 400 m of THF stratigraphy

·Shale and siltstone dominated upper part of section (WD010)

·Increasing proportion of coarse polymictic debris flow units with interbedded siltstone and shale lower in the section (WD004)

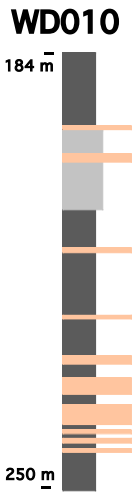

AMIRA /ARC P544 Final Meeting July 2003

Lithogeochemistry I: K_2O v Al_2O_3

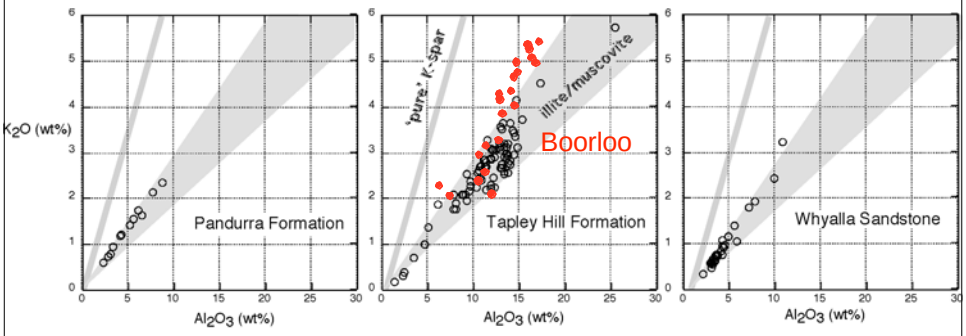

- At EB & Boorloo the sandy units are not arkoses they have not been K-altered

Lithogeochemistry II: Trace Elements

- At Emmie Bluff the THF samples have elevated Cu x 2-10, Co x 5, Zn x 10 & Pb x 25 cf average black shale
- However, Ni, As, Bi, Mo & Tl are not elevated
- In thicker intersections Cu is highest at upper and lower contacts and Zn& Pb are highest in the middle of the THF
- In the Boorloo Mine siltstones none of these elements are elevated
- The Emmie Bluff patterns contrast with the Zambian Ore Shale deposits where Cu is 100 -1000 x, and Co is up to 50 x 'average shale', Bi and Mo are enriched , and Zn and Pb are depleted

C/O isotopes

- Boorloo C/O isotope data are indistinguishable from regional data sets
- Ditto THF Cu deposits (Lambert et al., 1984; Knutson et al; 1983) data

Cf ZCB Ore Shale!

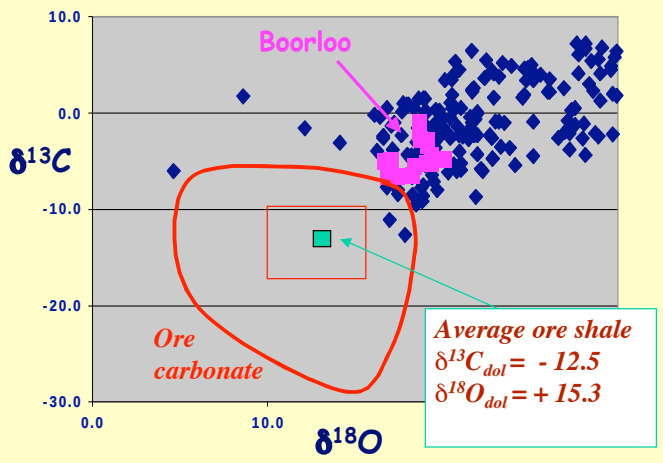

S isotopes

- There is a wide range of published S isotope values for THF associated Cu mineralisation
- Light S (to -15 permil) is common and interpreted as a product of BSR (Knutson et al., 1983; lambert et al., 1984)
- They also explain the heavy S by BSR (?closed system)

Conclusion: biogenic sulfate reduction is an important contributor to sulfide in these deposits

Some support for this from textures e.g., framboidal pyrite

Conclusions

- Tectono-sedimentary setting of THF is not the same as the ZCB Ore Shale
- For THF deposits reducing trap rocks, (relatively) low mineralisation temperatures and similar metal association imply similar (oxidised) metal transporting fluid to ZCB BUT some important differences
- Strong potassic alteration is not evident in THF Cu systems
- Ba is generally low (few 100 ppm)
- No association of very light C with THF mineralisation
- Isotopically light S - impt. biogenic contribution

Alteration, geochemical, and isotopic signatures of stratabound copper mineralisation in the Yeneena Basin, Paterson Orogen, W.A.

Robert Scott
Centre for Ore Deposit Research, University of Tasmania

Summary

This study is based on a review of recent PhD studies of the two major stratabound copper deposits in the Neoproterozoic Yeneena Basin (YB) of central W.A., and a comparison with deposits hosted by similar reduced shale ±carbonate successions in the Zambian Copperbelt (ZCB). This review highlights a number of important differences between stratabound copper deposits in these two areas. In addition to differences in relative timing with respect to basin inversion (i.e. ZCB: pre- to early syn-inversion; YB: syn- to post inversion, syn-greenschist facies metamorphism and cleavage development) several other features suggest the ZCB and YB deposits are the products of fundamentally different mineralising systems. Both the Maroochydore and Nifty deposits in the Yeneena Basin are interpreted to sit relatively high in the stratigraphic section, well into the reduced host-rock package deposited in the "second stage" of (local) basin development. Most of the stratabound Cu deposits in the ZCB (including arenite-hosted deposits) are located at or near the first major (regionally extensive) reduced shale horizon in the sequence. This position marks the approximate boundary between the basal fluvial sandstone-dominated ("first basin stage") and overlying fluvial to shallow marine ("second basin stage") successions.

At least at Nifty, ore-related hydrothermal alteration is strongly localised (structurally- and lithologically-controlled) and essentially restricted to the immediate vicinity of the orebody, unlike the pervasive basin-wide alteration systems responsible for copper mineralisation in the ZCB. Intense ore-related silica–dolomite hydrothermal alteration at Nifty is texturally destructive, and reflects more acidic ore fluid compositions than the pervasive but (generally) non-texturally destructive K-feldspar alteration associated with the Zambian deposits. There is no evidence of K-feldspar metasomatism associated with the Yeneena Basin deposits. ZCB mineralisation is fundamentally controlled by a change in the oxidation state of the oxidised ore fluid following interaction with mobile and in situ hydrocarbon reservoirs. The importance of organic-derived reductants in Zambia is highlighted by strong negative shifts in $\delta^{13}C$ values for ore-stage (and ore-proximal) carbonates, reflecting the incorporation of oxidised isotopically light organic carbon. Ore –stage carbonate alteration and Cu-bearing carbonate veins at Nifty and Maroochydore do not have the very light carbon carbonate signature of the ZCB deposits.

Although both the Maroochydore and Nifty copper deposits in the Yeneena Basin are both interpreted to have formed at similar temperatures (~350°C) during the major deformational (D_2) stage of the <750–680 Ma Miles Orogeny, very different mineralisation models have been proposed for the two systems. Reed's (1996) model for copper mineralisation in the Maroochydore system has more in common with the ZCB systems. Consistent with our present understanding of the ZCB systems, Reed (1996) proposes Cu was transported as a chloride complex in relatively oxidised fluids, via a combination of structurally-enhanced permeability and intergranular flow. Isotopically heterogeneous sulfur sources (diagenetic pyrite and sulfate) were already present at the traps sites and Cu deposition occurred in response to an increase in the H_2S activity and a decrease in fO_2 of the ore fluid. In contrast Anderson (1999)

and Anderson et al. (2001) argued both copper and reduced (isotopically homogeneous) sulfur at Nifty were transported by moderately acidic ore fluids. Copper deposition occurred as a result of cooling and a pH increase of the ore fluid following interaction with the carbonate-rich host rocks. As much of the Broadhurst Formation is carbonate-rich, well-defined (i.e. restricted) structural pathways were implicated in transit of the ore fluid, in order that acidity of the ore fluid was retained until it reached the trap site in the hinge of the Nifty syncline.

Ultimately the differences in the style and chemistry of the Cu-mineralising systems in the Yeneena Basin and Zambian Copperbelt are interpreted to reflect differences in bulk chemistry of the basin fill and the post depositional histories of the respective basins.

Introduction

The two major stratabound shale- and carbonate-hosted deposits in the Neoproterozoic Yeneena Basin (Nifty: 148 Mt @ 1.3% Cu; and Maroochydore: 140 Mt @ 0.5 % Cu, Fig. 1) were discovered using exploration models based on the then current understanding of the Zambian Copperbelt (i.e. syn-genetic and syn-diagenetic genetic models; Haines et al, 1993; Reed, 1996). While syn-genetic exploration models were instrumental in the discovery of these deposits, subsequent PhD studies of both Nifty (Anderson, 1999) and Maroochydore (Reed, 1996) favoured a late-stage syn-deformational, syn-orogenic timing for Cu-mineralisation. This report reviews the settings, style and composition of associated hydrothermal alteration assemblages, and the geochemical and stable isotopic characteristics of stratabound copper deposits of the Yeneena Basin, and compares them to the stratabound copper deposits of the Lower Roan in the Zambian Copperbelt.

Deposit setting

Although broad similarities in the nature of the host rocks exist, the sequence stratigraphic position of stratabound copper deposits in the Yeneena Basin is different to those of the Zambian Copperbelt. Most of the known deposits in the Zambian Copperbelt either sit within the basal siliciclastic package (i.e. Coolbro equivalent) or close to the level of the Ore Shale (first widespread unit deposited under relatively reducing conditions equivalent to basal Broadhurst Formation). In sequence stratigraphic terms the Yeneena basin deposits sit much higher in the section. Both the Maroochydore and Nifty copper deposits are hosted by carbonaceous and dolomitic shales within a 1–2 km thick mixed succession of sandstone, shale and carbonate and minor conglomerate (Broadhurst Formation) (Fig. 2). The amount of sandstone decreases up section, and overall facies are consistent with deposition in an increasingly euxinic low-energy shelf environment (Hickman and Clarke, 1994; Reed, 1996). Reed (1996) estimated the Maroochydore deposit is situated ~1500 m above the basal contact with the underlying Coolbro sandstone. The exact stratigraphic position of the Nifty deposit is unknown but based on the similarity of the host rocks it is probably similar to Maroochydore. Significant primary sulfide mineralisation is restricted to highly silicified carbonaceous and dolomitic shales of the pyrite marker bed and the Nifty Member, within the keel of the Nifty Syncline (Figs 1, 2).

Mineral casts and pseudomorphs after evaporite minerals (gypsum, anhydrite and halite) are sporadically developed throughout the Broadhurst Formation (Reed, 1996; Anderson, 1999). The evaporite casts and pseudomorphs have apparent replacive and displacive habits suggesting a diagenetic origin for the original evaporite minerals. There is no evidence for thick accumulations of evaporites anywhere within the exposed Yeneena Basin succession.

Mineralisation styles

Primary copper mineralisation at the Nifty deposit consists of replacive chalcopyrite and lesser vein-hosted chalcopyrite associated with quartz–dolomite alteration. Chalcopyrite is the only primary copper sulfide developed and occurs as isolated spots and blebs (often replacing or partly replacing pyrite, Fig. 3), in bedding parallel bands, as breccia matrix and within veins and as semi-massive replacement of the host rock and earlier alteration assemblages

(Figs 3, 4). Chalcopyrite also occurs as <100 μm ragged inclusions of replacive origin in syn-mineralisation euhedral pyrite (Anderson, 1999). At Maroochydore chalcopyrite is also the only primary copper sulfide present. Chalcopyrite is variably disseminated through the host succession where it rims and replaces framboidal pyrite. Chalcopyrite is also preferentially developed in syn-deformational (D_2) sites (Fig. 3; discordant and cleavage parallel veins, fold hinges, strain fringes adjacent to more competent minerals and within narrow bedding-parallel shears).

Ore-related hydrothermal alteration

Copper mineralisation at Nifty is associated with intense quartz-dolomite alteration of the carbonaceous and dolomitic shale host rocks, unlike that in any of the Copperbelt deposits. There is a pronounced symmetry of alteration zones with respect to the Nifty shale member, with increasing intensity of silicification towards the high-grade core of the unit (Fig. 5). This pattern suggests ore fluids were strongly channelled into the Nifty Member. Similarly zoned alteration assemblages are not observed at Maroochydore or in the Zambian deposits. The mineralogical zonation (both lateral and vertical) that is observed in the Zambian systems is more likely to reflect variations in chemistry of the trap site rather than flow patterns for the ore fluid.

Yeneena Basin Cu-deposits are not obviously associated with K- or K-feldspar metasomatism although there is some evidence of K-feldspar destruction at Nifty (similar to some ZCB arenite-hosted deposits). The Cu-mineralised Nifty Member shows strong K-depletion, and minor to moderate K-enrichment (~5–6 wt% K_2O) in the immediately overlying units (pyrite marker bed and upper shale). The K_2O distribution is consistent with dissolution of fine-grained K-feldspar from the ore zone by interaction with acidic hydrothermal fluids. Phlogopite is present as an accessory phase and commonly intergrown with sulfides at Maroochydore and K-feldspar–sulfide intergrowths are present but rare. The high Mg content of ferro-magnesian micas in the ZCB is interpreted to ultimately reflect oxidation (Fe to Fe^{3+}) and Mg-enrichments during K-feldspar metasomatism (Scott et al., this volume). However, at Maroochydore and Nifty phlogopite development can be explained by the dolomitic host rocks and potentially high fluorine contents for the micas (Reed, 1996; Anderson, 1999).

The prevalence of K-feldspar metasomatism in the Zambian Copperbelt compared to the Yeneena Basin may ultimately reflect the composition of the constituent sedimentary rocks. The major source of potassium in the ZCB brines is likely to be dissolved salts sourced from the evaporitic successions of the Upper Roan. However, as sandstones throughout the Roan are arkosic (up to 20% K-feldspar in unaltered rocks), and K-feldspar megacrystic granites are a major component of the local basement, wall rock compositions along the fluid flow paths would have helped buffer fluids to high K^+ concentrations. Initial descent and heating of the dense brines in the ZCB, particularly following entry into the basement is likely to have significantly increased the K/Na ratio of the ore fluid through deposition of albite at the expense of wall rock K-feldspar and phyllosilicates (Koziy et al., this volume). In contrast sandstones in the Throssell Group are predominantly quartz-rich (>95% quartz) and there is no evidence for significant accumulations of evaporites (a source for K-rich brines) anywhere within the exposed stratigraphic section.

Yeneena Basin deposits are associated with enrichments in P_2O_5, Sn, and U. Pb and Zn are enriched in the peripheral halo of the copper mineralisation at Nifty and in the hanging wall to disseminated copper mineralisation at Maroochydore. The Cu–Co association at many of the Zambian deposits is not apparent in the Yeneena Basin.

Fluid inclusions and stable isotopic signature

Fluid inclusions

Fluid inclusions from syn-mineralisation veins at Maroochydore and Nifty have similar salinities (8–27 eq. wt % NaCl), homogenisation temperatures

(180°–450°C) and estimated trapping temperatures (median values: 360°–440°C). The compositions and high trapping temperatures of the inclusions are consistent with epigenetic mineralisation at greenschist facies metamorphic conditions (Reed, 1996; Anderson, 1999).

Carbonate C- and O-isotopic signature

Unaltered dolostone and calcareous mudstone from the host sequence at Nifty have $\delta^{13}C$ (0.4 to 4.9‰) and $\delta^{18}O$ (18.8 to 21.4‰), similar to Maroochydore ($\delta^{13}C$: 0.2 to 4.1‰ and $\delta^{18}O$: 19 to 23.3‰, Reed, 1996), but lighter than the majority of unaltered carbonates in the Yeneena Supergroup (Anderson et al., 2001). Syn-mineralisation quartz–dolomite hydrothermal alteration at Nifty has $\delta^{13}C$ in the range –10.3 to 2.4‰ and $\delta^{18}O$ in the range 14.3 to 21.5‰ (Anderson et al., 2001).

$\delta^{13}C$ and $\delta^{18}O$ signatures for carbonate in veins and alteration associated with copper mineralisation at Nifty and Maroochydore show contrasting trends. Maroochydore carbonates are principally shifted towards heavier O, and show a small negative shift in $\delta^{13}C$ relative to unaltered dolostones. The observed fractionation is consistent with carbonate precipitated from a 350°C metamorphic fluid in equilibrium with carbonates in the host sequence. At Nifty both vein and alteration carbonate are shifted to lighter $\delta^{13}C$ and $\delta^{18}O$ values relative to unaltered dolostones. Depletion in ^{13}C (syn-mineralisation carbonate has $\delta^{13}C$ as low as –10.3‰) could simply be explained by decarbonation of the host rocks during the intense silicification associated with mineralisation (Anderson et al., 2001). The strong ^{13}C depletion of secondary carbonate from well mineralised systems the Copperbelt (e.g., $\delta^{13}C$: –15 to –25 ‰) is not observed in the Yeneena deposits, suggesting hydrocarbon involvement, and the oxidation of light organically-derived carbon was of lesser significance in the formation of the Western Australian deposits.

Sulfur isotopic signature

$\delta^{34}S$ sulfur isotopic values for diagenetic framboidal pyrite are $\delta^{34}S$ 16 to –27 ‰ at Nifty (Anderson, 1999) and $\delta^{34}S$ –22 to –31‰ at Maroochydore (Reed, 1996). Pre- to syn-mineralisation euhedral pyrite at Nifty has $\delta^{34}S$ 3.8 to –12‰ (Anderson, 1999) and $\delta^{34}S$ –4.0 to –10‰ at Maroochydore (Reed, 1996). $\delta^{34}S$ sulfur isotopic values for chalcopyrite at Nifty range from 6 to –6 ‰ (Anderson, 1999). At Maroochydore coarse-grained chalcopyrite has $\delta^{34}S$ –13 to –23 ‰ while for fine-grained chalcopyrite the range in $\delta^{34}S$ is –25 to –31 ‰ (Reed, 1996).

The wide range of framboidal pyrite $\delta^{34}S$ values is consistent with bacterial reduction of seawater sulfate in a system closed to SO_4^{2-} (Anderson, 1999; Anderson et al., 2001). The difference between the framboidal pyrite and chalcopyrite $\delta^{34}S$ values at Nifty suggests that sulfur in chalcopyrite was not sourced from existing sulfides or sulfates in the immediate host rocks but was derived from H_2S in the hydrothermal fluid. Furthermore, the relatively narrow range of $\delta^{34}S$ values for both chalcopyrite and euhedral pyrite suggests a homogeneous source for the sulfur (Anderson, 1999; Anderson et al., 2001). In contrast, Reed (1996) argues for a local heterogeneous sulfur source (diagenetic framboidal pyrite and sulfate) for copper mineralisation at Maroochydore. As median $\delta^{34}S$ values for euhedral pyrite and chalcopyrite at Nifty are similar to the median $\delta^{34}S$ value for framboidal pyrite, it is possible homogenisation of footwall sulfur was the source of sulfur for the Nifty deposit. However the $\delta^{34}S$ values are also consistent with either a magmatic source or the inorganic reduction of Proterozoic seawater sulfate, such that the source of the sulfur at Nifty is not well constrained (Anderson et al., 2001)

Mineralisation models

While Reed (1996) and Anderson (1999) both favour a syn-deformational epigenetic origin for copper mineralisation, their models differ in respect to the interpreted source of sulfur, the chemistry of the ore fluids and depositional mechanisms for the copper. At Maroochydore, Reed (1996) argued copper was transported as chloride complex by a combination of structurally-enhanced permeability and intergranular flow during regional deformation. Diagenetic pyrite and sulfate provided a heterogeneous local

sulfur source. Copper deposition was interpreted to be due to increased H_2S activity and decreased fO_2 due to interaction between Cu-bearing fluid and the sulfidic sediments. At Nifty, Anderson (1999) argued the relatively homogeneous $\delta^{34}S$ signature of chalcopyrite suggests sulfur was most likely introduced via H_2S in the ore fluid. Overprinting between alteration assemblages at Nifty suggests the mineralising fluid evolved from a weakly oxidised fluid with low base metal concentrations to a hotter, more saline, moderately acidic reduced fluid with high Cu concentrations. Cooling and a pH increase for the ore fluid due to interaction between acidic ore fluid and carbonate-rich host rocks (driving the fluid to higher pH) are thought to be primary controls on chalcopyrite precipitation.

Comparisons with the Zambian Copperbelt

While some broad similarities exist, in general the style, setting, associated hydrothermal alteration, and C-O-isotopic signature of the Yeneena Basin copper deposits appear to distinguish them from those of the Zambian Copperbelt. Yeneena deposits formed synchronously or after the major phase of cleavage development during compressional deformation of the host rocks. In contrast the Zambian deposits are interpreted to have formed very early (pre-cleavage) in the Lufilian Orogeny. The extent to which copper is remobilised during deformation is often difficult to fully access and remobilisation of copper to structurally-controlled sites can create the impression copper introduction was later than it was. While some features of the Nifty deposit are difficult to reconcile with a late deformational timing, the bulk of the evidence from the Yeneena deposits suggests they formed at higher temperature and at a more advanced stage in the inversion of the basin than the Zambian deposits.

Differences in bulk basin chemistry between the Yeneena Basin (quartz-rich clastic sediments, minor evaporite development) and the Zambian Copperbelt (arkosic clastic sediments, abundant evaporites) are likely to account for the apparent differences in the chemistry of the ore fluids in the two areas. In addition the much shorter time between deposition of the host succession and deformation and greenschist-facies metamorphism in the Yeneena Basin (Scott, this volume), may have inhibited the development of the basin wide fluid circulation systems associated with copper mineralisation in the ZCB (Selley et al.; Koziy et al., this volume). At least in the case of the Nifty deposit, ore fluid access was evidently strongly controlled by syn-deformational structural and lithologic pathways, consistent with expected patterns of fluid flow within less permeable rocks of the deeper crust.

References

Anderson, B., 1999, Structure, alteration and mineralisation of the Nifty Copper Deposit, Western Australia: Unpublished PhD Thesis, University of Tasmania, 225p.

Anderson, B. R., Gemmell, J B. and Berry, R. F., 2001, The geology of the Nifty copper deposit, Throssell Group, Western Australia: implications for ore genesis: Economic Geology, v. 96, p. 1535-1565.

Haines, D. W., Brooke, W. J. L., and Mazzoni, P.P., 1993, Application of conceptual models of sediment-hosted ore deposits in the discovery of the Nifty Copper and adjacent zinc–lead deposits, Yeneena Basin, Western Australia, *in* Kirkham, R.V., Sinclair, W. D., Thorpe, R. I. and Duke, J. M., (Eds.), Mineral deposit modelling: Geological association of Canada, Special Paper 40, p. 75–88.

Hickman, A. H. and Clarke, G. L., 1994, Geology of the Broadhurst 1:100,000 Sheet: Western Australia Geological Survey, 1:100,000 Geological Series Explanatory Notes, 40p.

Hooper, B. G. D., 2002, The Nifty copper deposit, structural and alteration setting: Applied Structural Geology for Mineral Exploration and Mining, Kalgoorlie 2002, Abstract Volume, Australian Institute of Geoscientists, Bulletin 36, p. 87–88.

Koziy, L., Large, R., Yang J., Bull, S. and Selley, D., 2003, Numerical fluid flow, salinity and heat transfer modelling in an attempt to understand basin scale mineralisation processes in the Zambian Copperbelt: AMIRA P544 Proterozoic Sediment Hosted Copper Deposits, Final Report, this volume.

Reed, A., 1996, Structural, stratigraphic, and temporal setting of Neoproterozoic stratabound copper mineralisation at Maroochydore, Paterson Province, Western Australia: Unpublished PhD thesis, University of Western Australia, 289p.

Scott, R., 2003, Architecture and evolution of the Yeneena Basin, Paterson Orogen, W. A.: AMIRA P544 Proterozoic Sediment Hosted Copper Deposits, Final Report, this volume.

Scott, R. Berry, R. Selley, D and Bull, S., 2003, Lufilian metamorphism in the Zambian Copperbelt: Implications for the interpretation of mineral assemblages and alteration paragenesis: AMIRA P544 Proterozoic Sediment Hosted Copper Deposits, Final Report, this volume.

Selley, D., Scott, R., Large, R., Croaker, M., Bull, S., and Pollington, N., 2003 (b), Alteration history of the Roan: AMIRA P544 Proterozoic Sediment Hosted Copper Deposits, Final Report, this volume.

Stratabound Copper deposits of the Yeneena Basin

- Nifty
  - Total resource 148 Mt @ 1.3% Cu
  - includes chalcopyrite resource 110 Mt @ 1.4% Cu, leachable reserve 27.6 Mt @ 1.1% Cu
- Maroochydore
  - 140 Mt @ 0.5% Cu, including 51.3 Mt @ 1.0% Cu, 0.04% Co

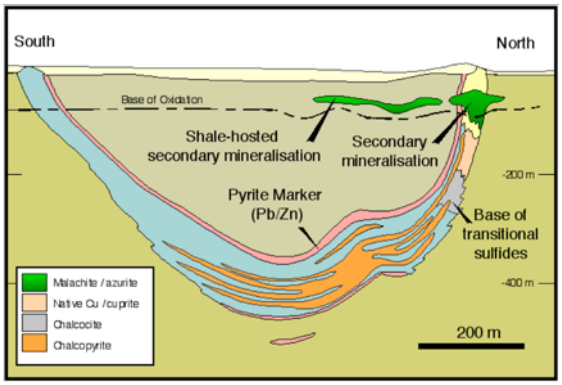

Figure 1. Size and grade of major stratabound copper deposits of the Yeneena Basin, and idealised cross-section of the Nifty ore body showing mineralogical zonation (after Hooper, 2002).

Stratigraphic position of stratabound copper deposits of the Yeneena Basin

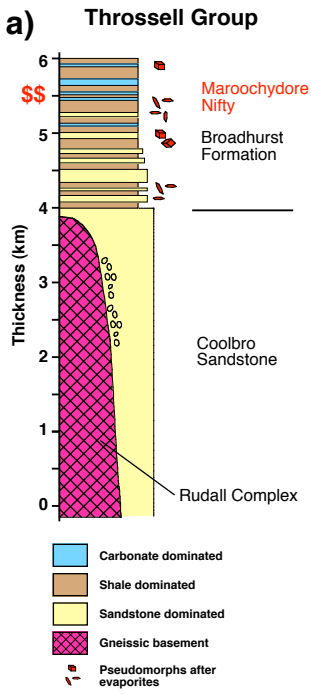

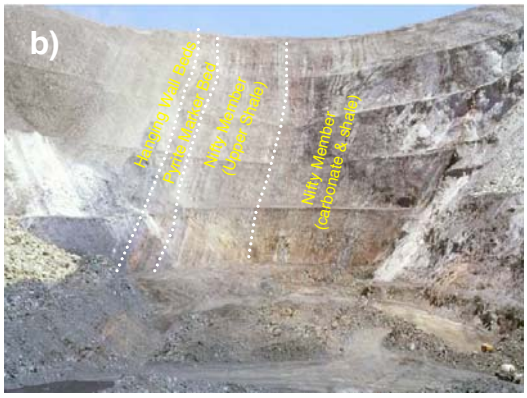

Figure 2. (a) Representative stratigraphic column for the Neoproterozoic Throssell Group in the eastern Yeneena Basin, showing the known (Maroochydore) and inferred (Nifty) positions of the stratabound ore bodies. **(b)** Carbonaceous, dolomitic and sulfidic shales of the Nifty Member host the Nifty deposit.

Mineralisation Styles

Figure 3. Examples of sulfide textures from **(a)** Maroochydore and **(b)** Nifty deposits. Chalcopyrite is the only primary copper sulfide developed, and in these examples it largely rims and replaces diagenetic pyrite. At Nifty, blebby chalcopyrite with replacive textures also occurs in bedding-parallel bands. At both deposits chalcopyrite is developed in syn-deformational sites such as dilatant sites along small-scale faults and in fold hinges, within strain fringes adjacent to more competent minerals and in narrow bedding-parallel shears. In addition, chalcopyrite occurs both deformed (folded) and relatively undeformed (cleavage parallel) veins consistent with syn-deformational emplacement.

Maroochydore
YNC-82, 144 m

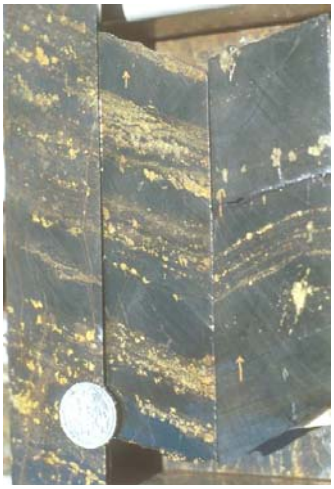

Nifty
THRD 780 W1
386–396 m

Nifty, Drill hole THRD 780 W1

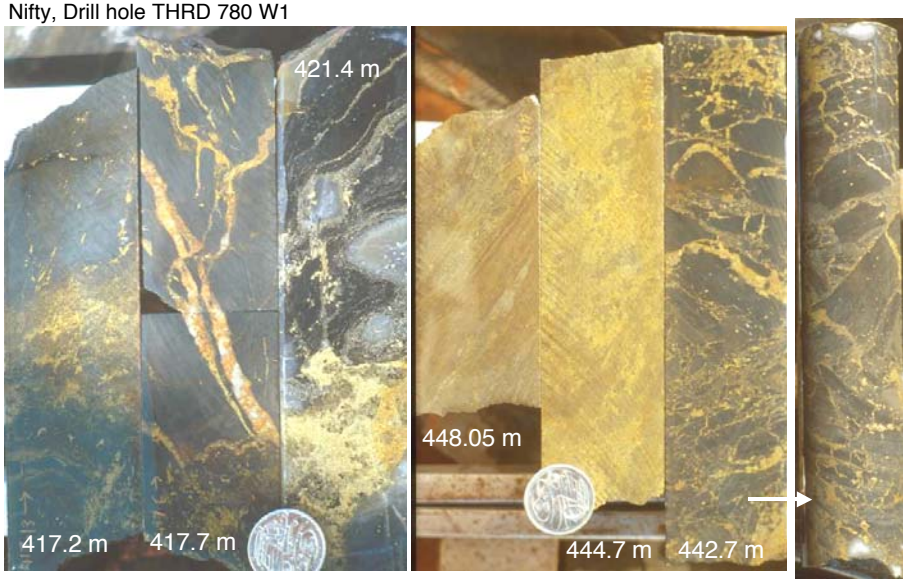

Figure 4. Chalcopyrite at Nifty occurs in a variety of settings ranging from blebby to semi-massive replacement of minerals and beds (417.2 m), syn-deformational veins (417.7 m), semi-massive to massive replacement of altered (intensely silicified) wall rock (421.4, 448.05, 444.7 m) and as a matrix to hydraulic breccias (442.7 m).

Alteration

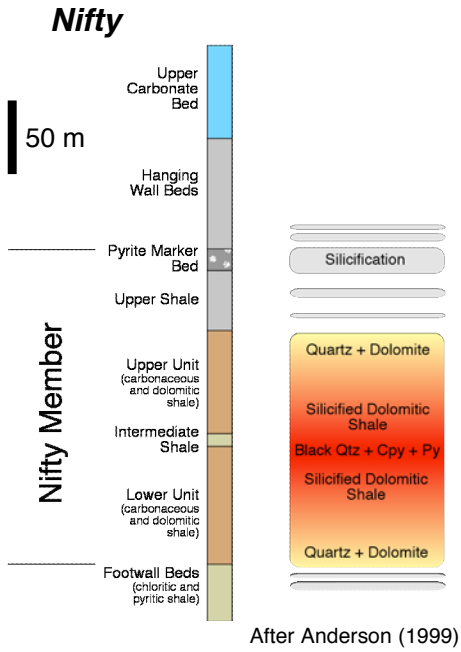

After Anderson (1999)

Nifty

- Intense Qtz-Dolomite Alteration
  - Intensity of silicification increases symmetrically towards ore
  - Stratabound to slightly transgressive
- Nifty Member strong K_2O depletion
- Moderate K_2O enrichment (5–6 wt%) in immediate hanging wall

Maroochydore

- Weak Qtz-Dolomite (±Phlogopite) Alteration
  - Pervasive, no obvious zonation

Figure 5. Alteration mineralogy and zonation associated with the Nifty and Maroochydore deposits.

Yeneena Basin Carbonate C-O Isotopic signature

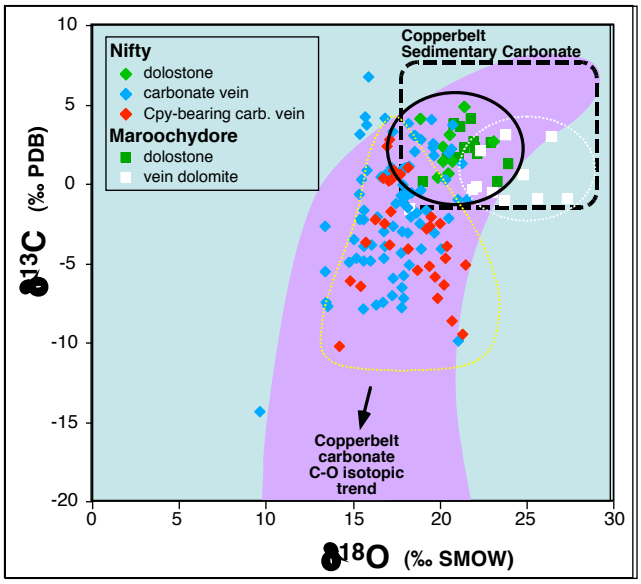

Figure 6. Carbonate C- and O-isotopic signatures for Nifty and Maroochydore, superimposed on the field (purple) for ZCB carbonates. Primary and diagenetic dolostone at the two Yeneena deposits have a similar isotopic signature to sedimentary carbonates from the ZCB, but vein and ore-stage carbonates from the two deposits show different fractionation trends (see text). Neither of the Yeneena Basin deposits have ore-stage carbonate with the highly negative $\delta^{13}C$ values indicating the oxidation of light organic-derived carbon.

Phosphate geochronology and geochemistry of hydrothermal events the Zambian Copperbelt

Galvin Dawson
University of Western Australia, PhD student

This Powerpoint presentation is a progress report for my PhD project which is running in parallel to AMIRA / ARC P544, but is funded separately through University of Western Australia research grants. The samples used for dating have been carefully selected using the improved Zambian geological framework developed during P544.

The study aims to identify and characterise phosphates (xenotime and monazite) found in the unmineralised Roan rocks and associated with Cu mineralisation and use the SHRIMP and other techniques to obtain precise ages. Phosphates paragenetically related to mineralisation may record ages and chemical signatures that relate to the hydrothermal event, and give insights into the timing of Cu mineralisation. Ages obtained for the Roan phosphates will be placed in a broader context of recent regional SHRIMP dating by workers at University of Witwatersrand and the ANU.

At a previous P544 meeting SHRIMP ages were presented that suggested the Zambian Copperbelt (ZCB) phosphates recorded a number of hydrothermal events. The ages obtained could be interpreted statistically in two ways. Either there were four to six separate hydrothermal events at ca. 500, 520, 535 and 560 Ma, and possible events at ca 475 and 615 Ma; or, if the data are pooled, there were only two significant events at ca. 520 and 560 Ma. None of these age determinations were corrected for matrix effects.

It was subsequently discovered that, due to a chemical mismatch between standards and unknowns, the ionisation efficiency varies in different matrices, which means the measured U / Pb and Th / Pb ratios vary giving incorrect ages. It is presently thought that matrix effects for xenotime require changes of up to 30 Ma in the measured age, whereas monazite ages do not change much (5 Ma?).

Applying matrix corrections to the results from the seven SHRIMP sessions to date, yields a single age of about 500 Ma for all the xenotimes analysed so far. Monazites yield two age populations, one at about 535 Ma and one at 500 Ma.

Further work is required to gauge the significance (if any) of these ages with respect to the hydrothermal flow event(s) that produced the Zambian Cu ores. However, some interesting preliminary observations can be made.

SEM imaging of individual phosphate grains shows that the 500 Ma and 530 Ma monazites are morphologically distinct. The older group has 'detrital' cores, and less varied morphology in comparison to the younger group. Furthermore, the older monazites are also geochemically distinct from the younger ones. The former have negative Eu anomalies, lower heavy REE to mid REE ratio and higher Th (and possibly U) contents.

In conclusion, there was clearly at least one significant xenotime- and monazite-forming hydrothermal event in the ZCB rocks at ca. 500 Ma. There was a monazite-only event at 535 Ma. Chemically distinct fluids may have been involved in these two events. More work is needed to confirm the relationship between these events and Cu mineralisation.

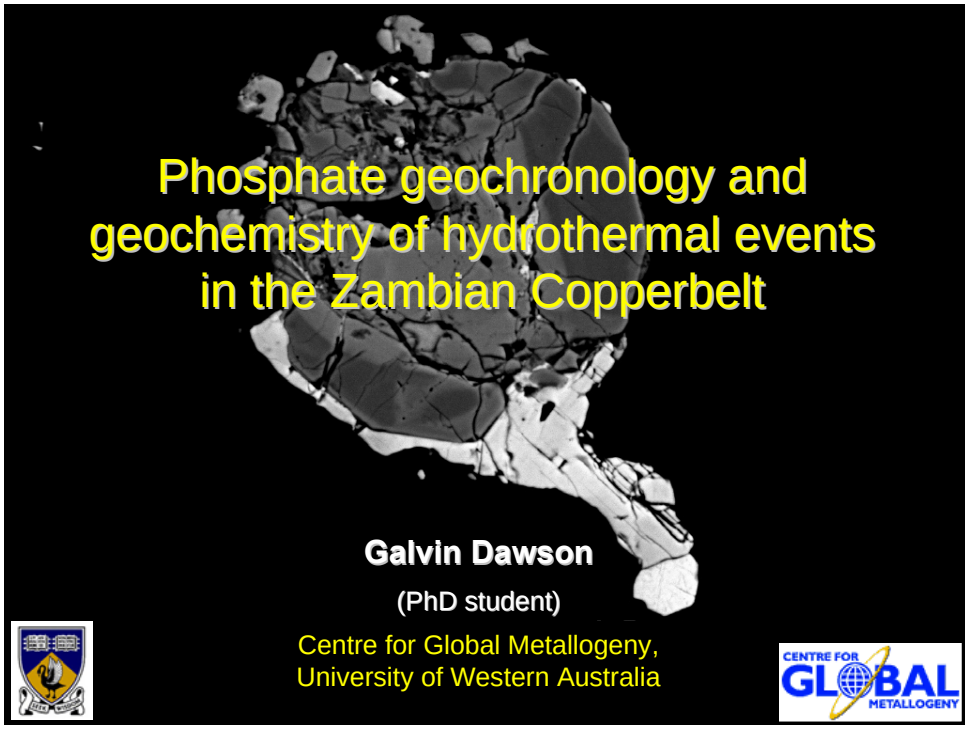

Acknowledgements

- PhD
  - Began in March 2001, UWA
  - External and funded by ARC
  - Running parallel to the AMIRA P544 project
  - Expect to complete PhD mid-late 2004
- Supervisor - Neal McNaughton, UWA
- Ian Fletcher, UWA
- CODES and CSM
  - Dave Selley, Peter McGoldrick
- AMIRA and P544 project sponsors

PhD project aims

- Study area
  - Ndola East (IT-27), Mufulira, Konkola North (KN-18), RCB2 and NS-137
- Identify and characterise phosphates
  - Examine textures and mineral associations
- Phosphate geochronology and geochemistry
- Identify hydrothermal/metamorphic events
- Synthesis and evolution of Zambian Copperbelt

Phosphate Geochronology

- Monazite – (LREE,Th),PO4
- Xenotime – YPO4

- Phosphates form during diagenetic, low-grade metamorphic, hydrothermal, high-grade metamorphic and igneous events
- *In situ* U-Th-Pb dating by SHRIMP (Sensitive High Resolution Ion Microprobe)

Review of Dec 2002 presentation

- Previous geochronology obtained during 4 SHRIMP sessions
  - Xenotime and monazite data combined
- SHRIMP ages were uncorrected for 'matrix effects'
  - individual ages may change
- Phosphate geochemistry was in progress

Either numerous events or…

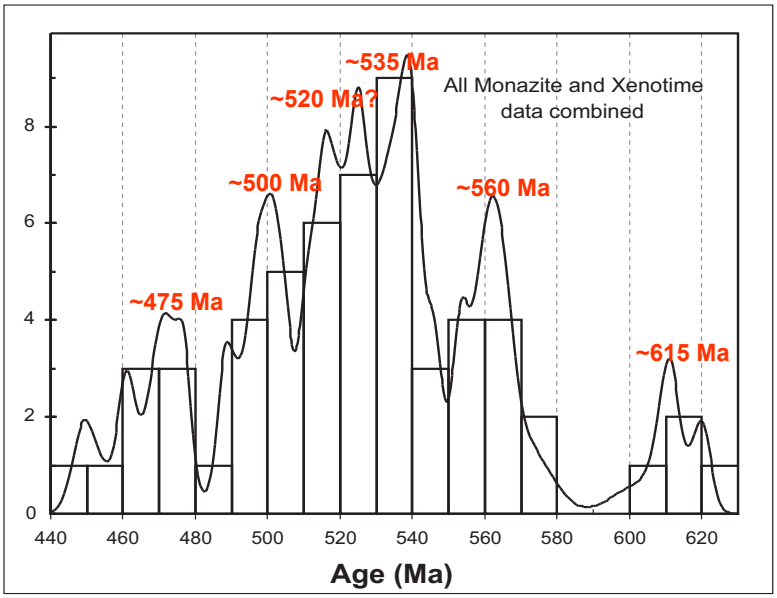

2 main events?

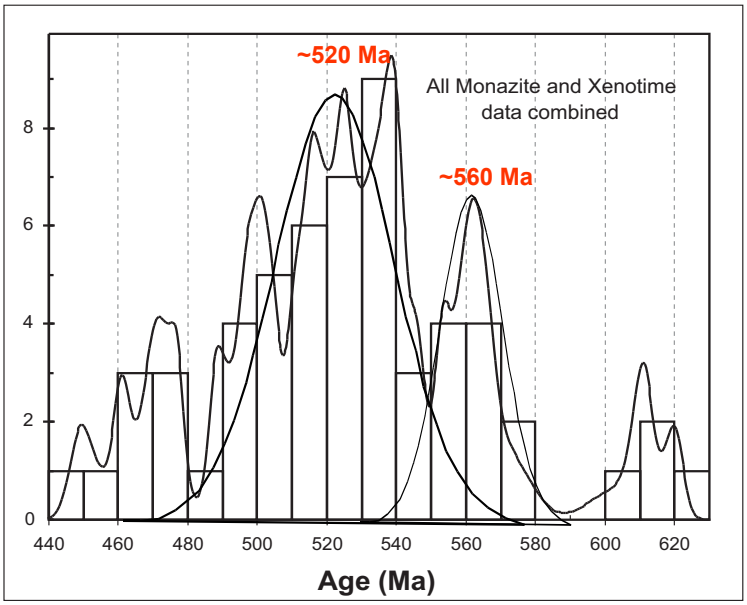

U-Th-Pb geochronology by SHRIMP

A new problem: Matrix Effects

- The chemical mismatch between standard and unknown
- Different matrices mean ionisation efficiency varies
  - Measured U/Pb and Th/Pb ratios vary giving incorrect ages
- This mismatch can be corrected for using U-Th-REE contents and multiple standards of known age
  - 'matrix corrections'
- Need to apply matrix corrections to previously reported data
- Corrections for monazite are less significant than for xenotime (Fletcher pers. comm.)

Geochronology – Matrix Effects

Xenotime

Standards	Uncorrected SHRIMP Age +/-1 σ (Ma)		Corrected SHRIMP Age +/-1 σ (Ma)		Change
Xeno-1 →			**True age = 994**		
C-06	1130	± 11	**1006**	± 33	-11%
C-07	1162	± 2	**987**	± 44	-15%
C-24, 25, 29	1093	± 19	**987**	± 33	-10%
C-113, 114	-	-	**-**	-	-
BS-1 →			**True age = 509**		
C-06	526	± 12	**516**	± 12	-2%
C-07	528	± 7	**504**	± 9	-5%
C-24, 25, 29	492	± 11	**488**	± 11	-1%
C-113, 114	530	± 7	**514**	± 8	-3%

Xenotime – Uncorrected

(3 SHRIMP sessions)

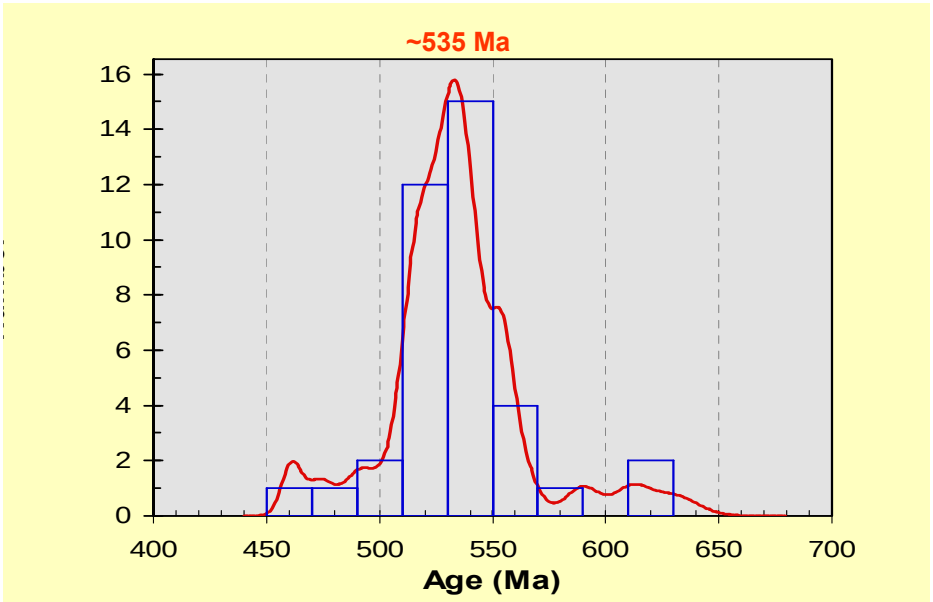

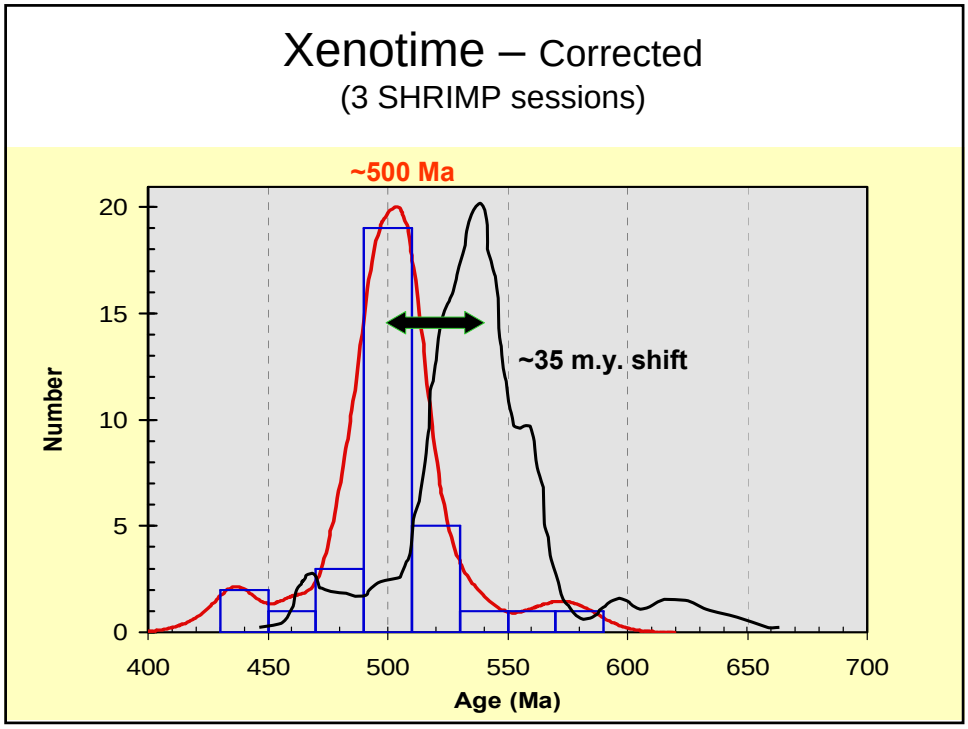
Xenotime – Corrected
(3 SHRIMP sessions)
~500 Ma
~35 m.y. shift
Number
Age (Ma)
0
5
10
15
20
400
450
500
550
600
650
700

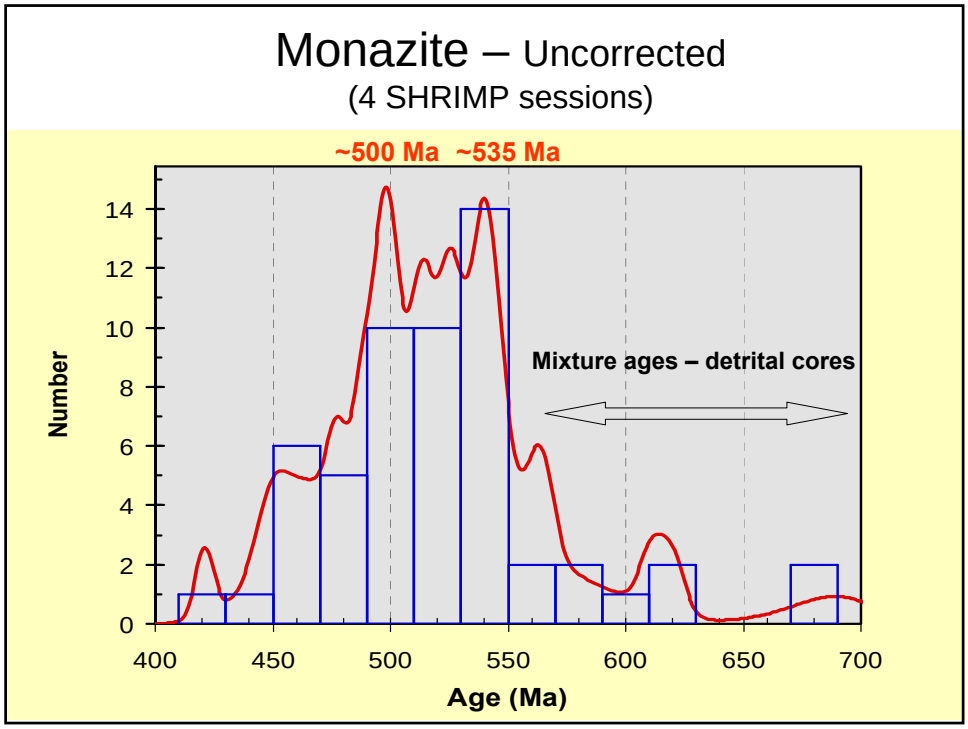
Monazite – Uncorrected
(4 SHRIMP sessions)
~500 Ma ~535 Ma
Mixture ages – detrital cores
Number
Age (Ma)
0
2
4
6
8
10
12
14
400
450
500
550
600
650
700

Two hydrothermal events?

- Xenotime gives only one age ca. 500 Ma
- Monazite gives two ages ca. 535 and 500 Ma
  - Different fluid chemistries?
  - Insufficient Y in 535 Ma fluid?
- Differences between the ca. 535 and 500 Ma monazite populations…
  - Morphology
  - Geochemical signature
  - Spatial relationship to ore

ca. 500 Ma monazites

- variable morphology

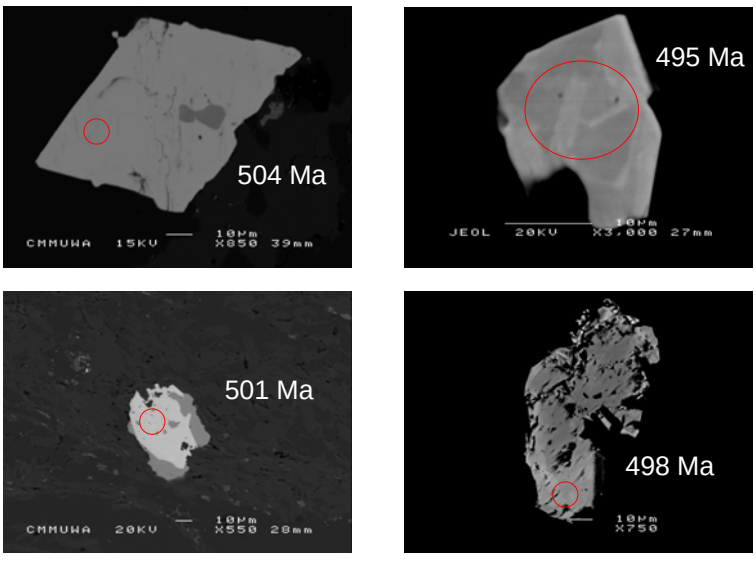

ca. 535 Ma monazites

- High-Th, pitted (detrital?) cores with overgrowths

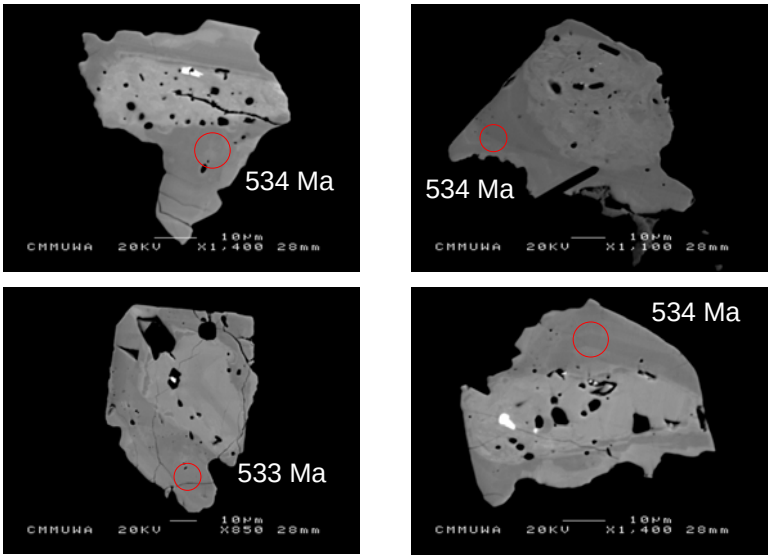

Geochemistry

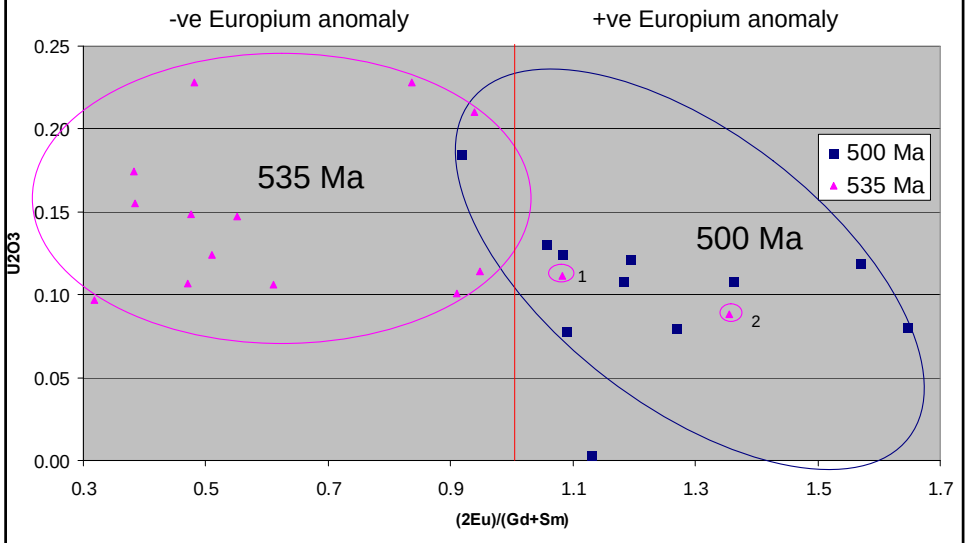

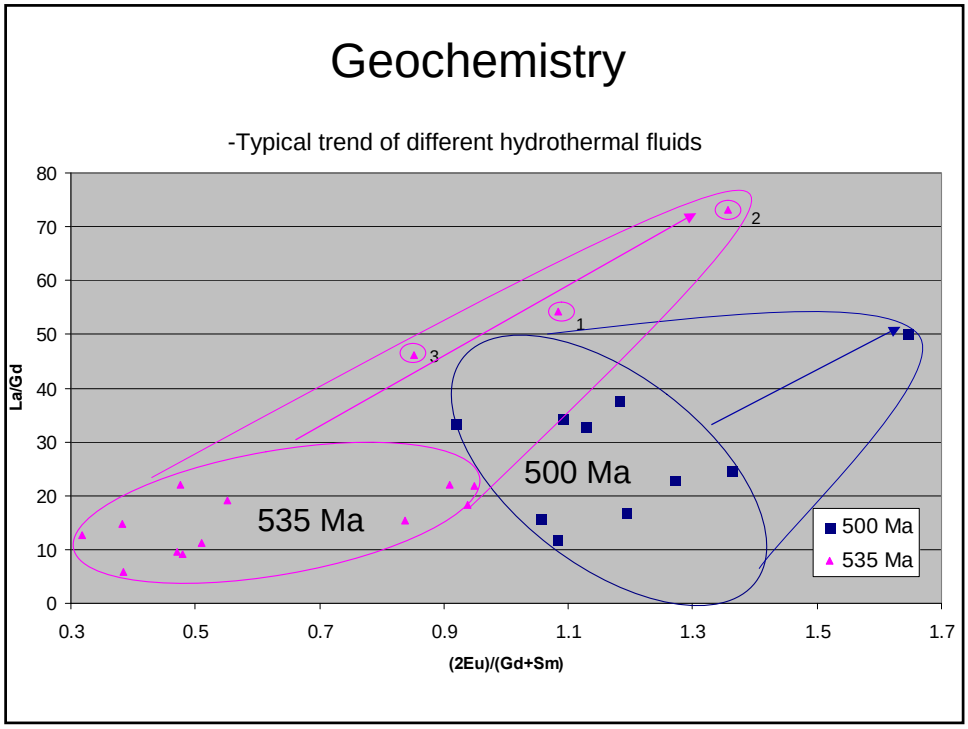
Geochemistry
-Typical trend of different hydrothermal fluids
La/Gd
(2Eu)/(Gd+Sm)
80
70
60
50
40
30
20
10
0
0.3
0.5
0.7
0.9
1.1
1.3
1.5
1.7
1
2
3
500 Ma
535 Ma
500 Ma
535 Ma

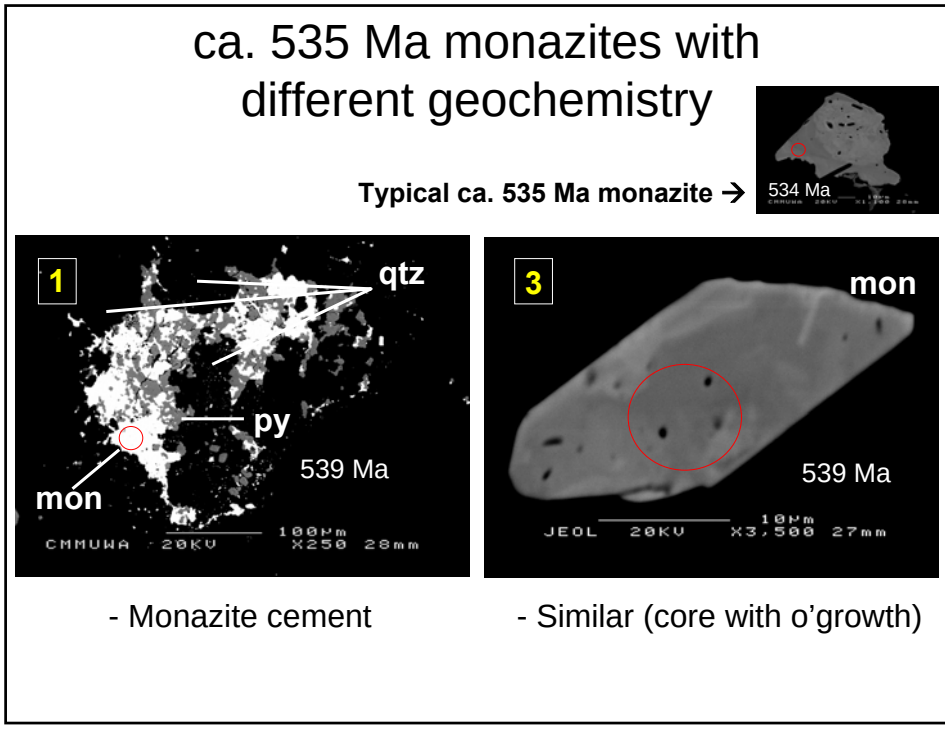
ca. 535 Ma monazites with different geochemistry
Typical ca. 535 Ma monazite →
534 Ma
1
qtz
py
mon
539 Ma
CMMUWA 20KV
3
mon
539 Ma
JEOL 20KV
- Monazite cement
- Similar (core with o'growth)

Textural association of monazite to pyrite

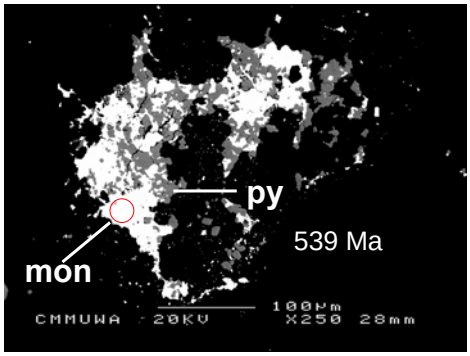

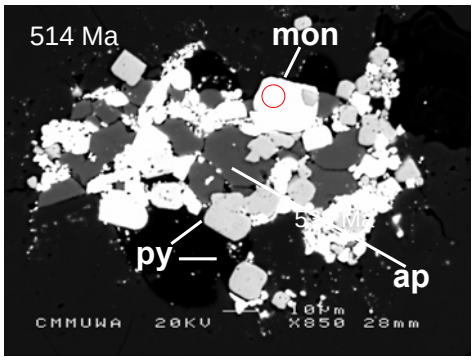

- ca. 535 Ma Monazite and pyrite intergrown

- Monazite post pyrite

Textural association of phosphates to chalcopyrite

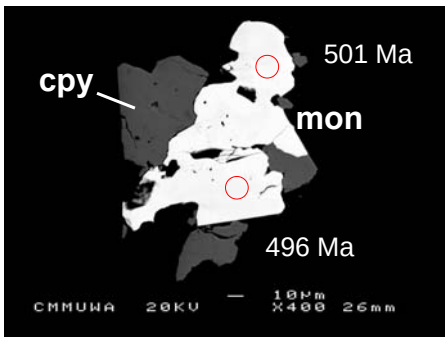

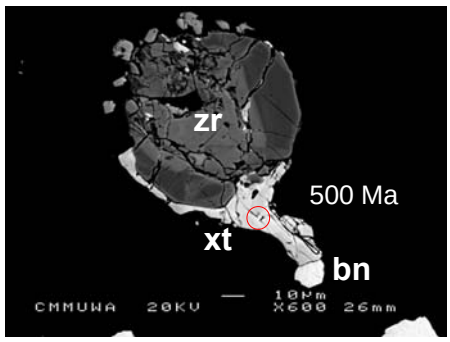

-ca. 500 Ma Monazite post chalcopyrite??

- Timing uncertain

Age of copper mineralisation

- ca. 535 Ma monazites - (IT-27, RCB-2, NS-137, KN-18)
  - 93 % of 535 Ma grains from weakly mineralised zones
- ca. 500 Ma monazites - (NS-137)
  - 10 % of 500 Ma grains from weakly mineralised zones
- Infer copper mineralisation at ca. 535 Ma
- However, database is small!
- Most of the 'mineralised' samples are from Ndola East
  - Weakly mineralised drill-hole!
- Require more 'highly mineralised' samples from high-grade deposits to firm up conclusions

Preliminary conclusions

- Initial hydrothermal/metamorphic event ca. 535 Ma
  - Monazite (-ve Eu anomaly) formed
  - No yttrium in fluid? (no xenotime)
  - Copper mineralisation?
- Second hydrothermal event ca. 500 Ma
  - xenotime and monazite (+ve Eu anomaly) formed
  - Overprinting, but not restricted to ore zones
- Two fluids had different chemistries?
- But… Monazite ages subject to matrix corrections!

Zambian Copperbelt geochemistry, geochemical modelling and stable isotopes: implications for mineralising processes

Peter McGoldrick and David Cooke
Centre for Ore Deposit Research, University of Tasmania

Introduction

This first part of this report focuses on several geochemical and isotopic features of the Zambian Copperbelt (ZCB) deposits not previously discussed in detail in other contributions to the P544 final report. These include Ba solubilities and a discussion of S and C isotopes and organic C patterns. The second part describes chemical modelling of metal solubilities in an oxidised saline brine thought to be a good analogue for the ZCB ore-forming fluid. The results of reacting this fluid with a variety of reducing trap scenarios are then discussed.

The signi cance of barium

All the ZCB deposits examined to date in P544 have anomalous Ba, either directly associated with high-grade ore (e.g., Mwambashi B) or with potassically altered host rocks (e.g., Konkola), or both.

Hence Ba is ore-related, either being introduced with the oxidised Cu fluid, or it is a signature of the reducing trap environment.

The latter suggestion is plausible, as Ba enrichment is seen associated with hydrocarbon reservoir fluids and seeps (Greinert et al., 2002; Fu and Aharon, 1998). The extreme Ba enrichment seen at Mwambashi B may require some build up of Ba in the hydrocarbon reservoir proposed as the trap site for Cu, with this Ba being subsequently incorporated into potassic alteration phases. However, the occurrence of broader areas of Ba enrichments than just the trap sites, and the observation that Ore Shale deposits also show Ba enrichment favours an introduction of Ba with the Cu-transporting fluids.

Such a conclusion places important constraints on the character of the Cu-transporting fluid, because, although the base metals and Co are all soluble in oxidised chloride brines, Ba will be insoluble if the brine contains even small amounts of sulfate (Slide 4). Modern seawater, for instance, contains about 2600 ppm sulfate and only 5–9 ppb Ba. If Ba and Cu are introduced in the same fluid during formation of the Zambian Copperbelt deposits then the ore fluid must have had a substantially different major solute composition to 'normal' seawater. Several types of modern formation waters have low sulfate, but very high total dissolved solids (Hanor 1994; Sullivan, Haszeldine et al. 1994). For instance, deep circulating seawater may loose some sulfate due to retrograde anhydrite precipitation, and in evaporitic basins the ultimate products of seawater evaporation are bittern brines and salts that contain little sulfate. Given the strongly evaporitic character of much of the Upper Roan rocks (Broughton, this volume) both bittern brines and bittern salts are plausible sources of low-sulfate salinity for the ZCB ore fluids.

Organic carbon

Black and dark coloured argillites are common lithologies in the Ore Shale member of the Lower Roan, and dark coloured fine-grained rocks ('black shales') often owe their colour to the presence of organic matter (or its metamorphosed equivalent). Furthermore, Annels (1979) had noted the presence of degraded hydrocarbons in the 'greywackes' at Mufulira. Finally, organic matter, liquid and gaseous hydrocarbons (or H_2S from sour gas) are all potential reductants for the oxidised ZCB metal-transporting fluids (see below).

Hence, an important aim of P544 was to quantify total organic C content of the 'black rocks' of the ZCB deposits. It was hoped these measurements would provide some information concerning original amounts of solid or liquid organic C from in the Lower Roan sequences.

Data for 86 new total organic C (Toc) analyses are depicted on a histogram in Slide 5. There are a range of Toc contents in mineralised and unmineralised rocks, but no simple relationship is observed between grade, mineralogy and Toc content of the rocks. The large majority of samples analysed (mostly from Ore Shale samples) have less Toc than average world shale, and far less than a typical black shale. Generally, Ore Shale samples have more Toc than samples from arenite-hosted deposits, but this is not always the case (e.g., one of the Mufulira samples contains 0.8 wt % Toc).

Hence, the Toc of the Ore Shale is surprisingly low, and one explanation for this is that prior to introduction of the Cu fluid these rocks had more 'normal' Toc, but the mineralising process has destroyed most of this C. The isotopically light C now present in carbonate in these deposits the may be derived from oxidation of larger amounts organic matter once present in the Ore Shale (see below for further discussion).

Sources of reduced sulfur: BSR or TSR?

Carbon isotopes

Isotopically light C in carbonates associated with mineralisation in the ZCB is best explained as ultimately sourced from the oxidation of organic C (see Large et al., this volume). Low temperature, near surface weathering processes will destroy (oxidise) organic matter, but the association of high-grade hypogene Cu ores with isotopically lightest carbonates suggests organic matter oxidation is linked to the ore-forming process.

Microbial metabolic processes will also oxidise reduced C at low temperatures (below about 120°C) and sometimes biogenic sulfate reduction (BSR, see below) can accompany this process.

At higher temperatures (beyond 130°–150°C) the organic matter oxidation is thermally driven and uses sulfate as an electron donor producing sulfide and CO_2 in a process known as thermochemical sulfate reduction (TSR – Machel et al., 1995).

Both BSR and TSR will produce isotopically light CO_2 which can be incorporated in diagenetic (or if ore-related) alteration carbonates. Limited evidence from fluid inclusions (Annels, 1989) suggests temperatures of about 150-200°C for the ZCB ore fluids, too hot for microbial life, hence, TSR is the likely process involved in oxidation of organic matter in the ZCB deposits. Additional support for this interpretation comes from S isotopes in the ZCB deposits (see below).

Sulfur isotopes

As well as investigating the stable isotopes of C from the ZCB, one of the aims of P544 was to re-examine the S isotope systematics of the Lower Roan sequences and the Cu ores. To this end 30 new S isotopic measurements of anhydrite from several stratigraphic levels in the Lower Roan, and two deposit-specific sulfide S isotope studies were undertaken using the laser-ablation S isotope facility at University of Tasmania.

The anhydrite $\delta^{34}S$ values of 19.4‰ ±1.9‰ confirm limited range of sulfate $\delta^{34}S$ values in Roan rocks and ores, and as such the anhydrite values probably represent closely the S isotopic composition of Neoproterozoic seawater sulfate during Lower Roan times.

Published sulfide S isotopes from ZCB deposits display a wide range of values from quite light values (–18‰) to values as heavy as 17‰ (Dechow and Jensen 1965). Light values sometimes observed in the Ore Shale deposits were taken to indicate that open system BSR was an important sulfide-producing process in these deposits. Apparent up section trends to heavier S were interpreted to result from closed system BSR (e.g., Sweeney et al., 1986).

New sulfide S isotope investigations as part of P544 have been undertaken at the Chibuluma W deposit (Selley & Cooke, 2001) and at the Chambishi SE prospect (this report).

Chibuluma W samples show a wide range of relatively heavy S in all sulfides, which Selley & Cooke (2001) argued was likely produced by TSR rather than BSR. Laser ablation measurements on samples collected through two 30 m thick Ore Shale intersections from Chambishi SE (drill holes NN15 and NN45 are depicted on Slide 13. The new data do not reveal any systematic up sequence S isotope variations. In fact, pyrite from a single sample shows $\delta^{34}S$ values ranging from –4 to 11‰ , a range encompassing all other measurements from NN15 and NN45! Pyrrhotite and chalcopyrite have limited within-sample variation, but show a between-sample variation of at least several permil. Hence, the P544 Chambishi SE study fails to reproduce the the pattern of increasingly heavy S up-section described for other Chambishi Basin depsoits by Annels (1989) and at Konkola (Sweeney et al., 1986).

Discussion

These new and old observations for ZCB S isotopes, combined with insights from new ore carbonate C isotopes carried out in P544 provide important constraints on the source of S in the ores, and the processes responsible for generating reduced S to form sulfides.

The heavy sulfide values (at times almost as heavy as the S in Roan sedimentary anhydrite) indicate that S sources are not igneous (i.e., they cannot be derived from direct leaching of sulfides in igneous rocks by circulating hydrothermal fluids, or from magmatic fluids). More likely S is ultimately derived from a large reservoir of heavy S such as Neoproterozoic seawater.

Seawater sourced S will most likely be oxidised and must undergo reduction to sulfide to form Cu ores. As previously mentioned BSR is a viable process for producing reduced S at low temperatures and also metabolising organic matter to produce isotopically light CO_2. For 'open system' BSR the production of isotopically light S is the norm, and certainly open system BSR could not produce the range of heavy and light sulfide S seen in the ZCB deposits. 'Closed sytem' BSR can produce sulfide S isotope signatures ranging from very light to almost as heavy as the sulfate being reduced. However, special geological conditions are required to maintain a closed system long enough to produce large amounts of heavy sulfide. During burial diagenesis of organic matter-rich muds sometimes behave as closed systems, hence, some of the S isotope variability in the Ore Shale deposits might be due to BSR. However, it would be geologically almost impossible to achieve closed system behaviour in the coarser grained Roan rocks, yet arenite-hosted deposits such as Chibuluma show mostly heavy S.

TSR has a pronounced kinetic fractionation effect that will always produce sulfide S that is isotopically lighter than the sulfate being reduced (Machel et al., 1995). The effect is strongly temperature dependent and may be tens of permil at low temperatures, but is small at high temperatures (around 200°C). Hence, TSR could produce a range of light to heavy sulfide within the temperature window previously discussed for the ZCB deposits. Furthermore, 'closed system' behaviour is more likely at the burial depths favourable to TSR, and closed system TSR will ultimately produce sulfide S with an isotopic signature approaching that of the source sulfate.

Hence, TSR is favoured as the mechanism responsible for forming the bulk of the sulfide now present in the ZCB deposits.

How much diagenetic pyrite?

For the most part sulfides in the Ore Shale are ore-related (chalcopyrite±bornite±chalcocite and pyrrhotite±pyrite) assemblages, and much of the unmineralised dark argillite lithologies are sulfide-poor. However, locally pyrite can be an important component of unmineralised Ore Shale (e.g., parts of the Ore Shale at Nkana; the upper third of the Ore Shale at Chambishi SE). Much of this pyrite is fine grained and disseminated through the shale or concentrated in bedding parallel bands, while some

occurs as rims or replacment of nodular evaporites (Annels, 1974) (Slide 15). Microscopically, much of this pyrite consists of coarse to fine grained euhedral and subhedral 'clean' pyrite, however the cores of some grains contain a more porous looking 'spongy' pyrite (Slide 16). While the timing of formation of the ZCB Ore Shale pyrite is not clear, textures like these are typical of early diagenetic Fe sulfides seen in many other sedimentary rocks (e.g., Raiswell and Berner, 1986). It is noteworthy that the isotopically lightest S from Chambishi SE is recorded is from the porous interior of pyrite rimming an evaporite nodule. This observation would be consistent with BSR involvement in early sulfide production.

If early diagenetic Fe-sulfides did form in the Ore Shale, they may be important for several reasons. Firstly, diagenetic sulfides may have been a pre-existing reduced S source for subsequent Cu-fluids. Furthermore, preliminary LA-ICPMS analyses indicate much of the clean pyrite is Co-rich, and the 'spongy' pyrite is elevated in a wide range of chalcophile elements (including Co, Ni and As), hence, if the 'spongy' pyrite was formerly more abundant, it may be a source for some of the metals now seen in the ores. Finally, if pyrite formation began during early diagenesis, its cobaltiferrous character suggests that of the ore metals, Co at least was present in the sedimentary sequence at this time.

At this point in our work it is not possible to quantify the contribution from diagenetic Fe sulfides to the S or metal budgets the ZCB Ore Shale deposits, but from a genetic viewpoint this is an area that warrants further research.

References

Annels, A. E. (1974). Some aspects of the stratiform ore deposits of the Zambian copperbelt and their genetic significance. Gismentes Stratiformes et Provinces Cupriferes. J. P. Bartholome. Liege, La Societe Geologique de Belgique.

Annels, A. E. (1979). "Mulfulira greywackes and their associated sulphides." Transactions/Section B of the Institution ofMining and Metallurgy 88: B15-B24.

Annels, A. E. (1989). Ore genesis in the Zambian Copperbelt, with particular reference to the northern sector of the Chambishi Basin. Sediment-hosted Stratiform Copper Deposits. R. W. Boyle, A. C. Brown, C. W. Jefferson, E. C. Jowett and R. V. Kirkham, Geological Association of Canada. Special Paper 36: 427-452.

Selley, D. and D. Cooke, 2001. Mineral zonation and sulfur isotope systematics of the C hibulima West copper-cobalt deposit, Zambia. AMIRA P544 Annual Progress Report: 133-169.

Dechow, E. and M. L. Jensen (1965). "Sulfur isotopes of some central African sulfide deposits." Economic Geology 60: 894-941.

Fu, B. and P. Aharon (1998). Sources of hydrocarbon-rich fluids advecting on the seafloor in the northern Gulf of Mexico. Transactions - Gulf Coast Association of Geological Societies, vol.48. J. S. Prouty, K. H. Price and V. W. Henderson. New Orleans, Gulf Coast Association of Geological Societies: 73-81.

Greinert, J., S. M. Bollwerk, et al. (2002). "Massive barite deposits and carbonate mineralization in the Derugin Basin, Sea of Okhotsk; precipitation processes at cold seep sites." Earth and Planetary Science Letters 203(1): 165-180.

Hanor, J. S. (1994). The origin of saline fluids in sedimentary basins. Geofluids: Origin and migration of fluids in sedimentary basins. J. Parnell, Geological Society of London. 78: 151-174.

Machel, H. G., H. R. Krouse, et al. (1995). "Products and distinguishing criteria of bacterial and thermochemical sulfate reduction." Applied Geochemistry 10: 373-392.

Raiswell, R. and R. A. Berner (1985). "Pyrite formation in euxenic and semi-euxenic sediments." American Journal of Science 285: 710-724.

Sullivan, M. D., R. S. Haszeldine, et al. (1994). "Late anhydrite cements mark basin inversion: isotopic and formation water evidence, Rotliegend Sandstone, North Sea." Marine and Petroleum Geology 11: 46-54.

Sweeney, M., P. Turner, et al. (1986). "Stable isotope and geochemical studies in the role of early diagenesis in ore formation, Konkola Basin, Zambian copper belt." Economic Geology and the Bulletin of the Society of Economic Geologists 81(8): 1838-1852.

Geochemistry, stable isotopes & chemical modelling: implications for ZCB mineralising processes

Talk Outline

- Ba in ZCB deposits: how much sulfate in ore fluids?
- Toc (total organic carbon) in ZCB deposits
- Isotopically light C in ZCB carbonates
- Sulfur sources (TSR cf BSR)?
- How much diagenetic pyrite?

PMcG

- Metal transport
- Reaction modelling

DRC

Why barium?

Ba is very insoluble in the presence of dissolved sulfate

e.g., Ba content of surface seawater is 5 - 9 ppb!

Either

Ba was carried along with Cu in the ore-forming fluids

Or

Ba-enrichment was pre-ore, but related to processes acting at the trap site e.g., build-up in hydrocarbon waters

If Ba was in the ore fluid then these must have been low sulfate brines

e.g., 1: many evolved basinal brines

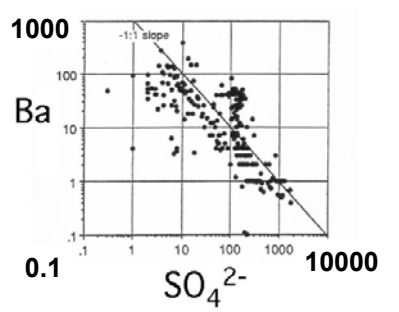

from Hanor 1994

e.g., 2: modern Zechstein formation waters are 12x seawater salinity but <80ppm sulfate

Organic Carbon in ZCB deposits

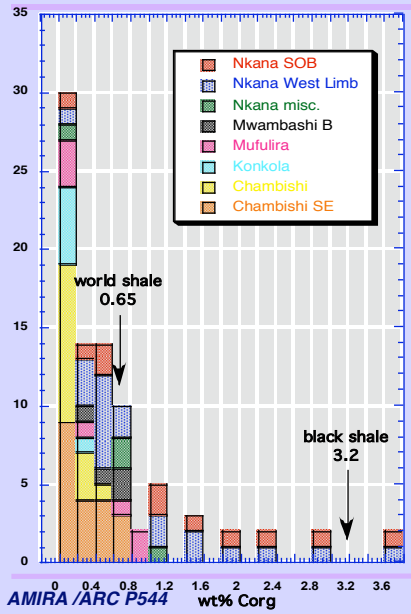

- Range of Corg contents in 'black' rocks from various deposits
- No apparent relationship between grade, mineralogy & Corg content of rocks
- OSh deposits generally have more Corg than arenite-hosted deposits, but not always
- C isotopes imply this was an ore-related process involving PARTIAL TO COMPLETE OXIDATION OF ORIGINAL ORGANIC MATTER

Corg oxidation processes

3 possibilities:

i) Near surface weathering processes

- UNLIKELY; ores are mainly hypogene & association of light C with ore precludes secondary near surface oxidation

Corg oxidation processes

ii) Biologically moderated at low T (<~120°C); this may or may not involve (biogenic) sulfate reduction (BSR)

iii) Thermally driven (at T >130 - 150°: uses sulfate as an electron donor and produces sulfide (TSR)

Corg oxidation processes II

- Both BSR and TSR produce isotopically light CO_2 which may be incorporated into neomorphic carbonate minerals
- Circumstantial evidence favours TSR:
  e.g., thermal conditions during circulation of Cu-fluids & complexity of S isotope signatures in the ores (see below)

Sulfate S isotopes

- More than 30 new anhydrite measurements confirm limited range of sulfate $\delta^{34}S$ values in Roan rocks & ores:

  19.4 permil ±1.9 permil = Neoproterozoic 'seawater' sulfate

Sulfide S isotopes

- Previous P544 work at Chibuluma (Cooke et al., 2001) showed a wide range of (relatively) heavy S in all sulfides
- Data from Chambishi show positive values nearest faulted footwall contact & negative values away from the fault (Hitzman unpub. Data)
- Earlier Copperbelt workers documented a range of S from quite light values (-18 permil) to values as heavy as +17 permil, often with no consistent patterns in different deposits
- lightest values were generally seen in Ore Shale deposits and ascribed to BSR
- Up section trends to heavy sulfide S (Chambishi basin - Annels, 1989; & Konkola - Sweeney et al., 1986) where interpreted as the result of closed system BSR

Sulfide S isotopes (con)

- new laser ablation data for sulfides from the Ore Shale at Chambishi Southeast DO NOT reproduce these patterns of increasingly heavy S up section

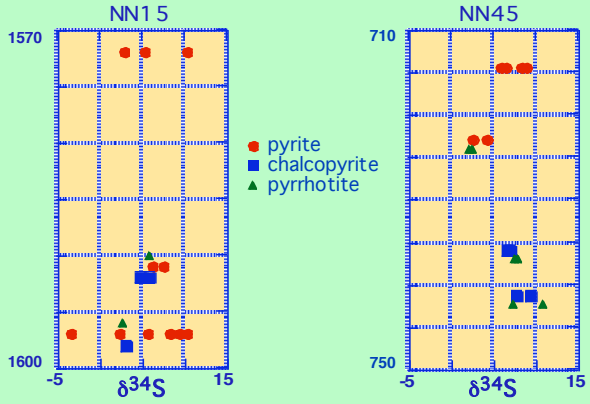

Sulfide S isotopes (con)

- pyrite $\delta^{34}S$ values can span a range of 15 permil in a single sample (encompassing the whole vertical pyrite variation!)
- chalcopyrite and pyrrhotite have limited within sample variation, but a between sample variation of at least several permil

BSR or TSR ?

- 'open system' BSR produces light sulfide from heavy sulfate
- 'closed system' BSR can produce a range of $\delta^{34}S$ signatures from very light to heavy e.g., burial diagenesis of Corg-rich muds
  - but even so light S is the 'norm'

HOWEVER

- The heteregeneity observed in ZCB deposits (now extended to the micro-scale for LA data) would be difficult produce by BSR (particularly in the arenite-hosted deposits)
- TSR isotopic fractionation is temperature dependent (Machel et al., 1995) and does produces sulfide lighter than sulfate

  BUT a 'closed system' is not needed to generate 'heavy' sulfide

HENCE

- TSR is favoured for producing the bulk of the sulfide in ZCB deposits

Diagenetic pyrite?

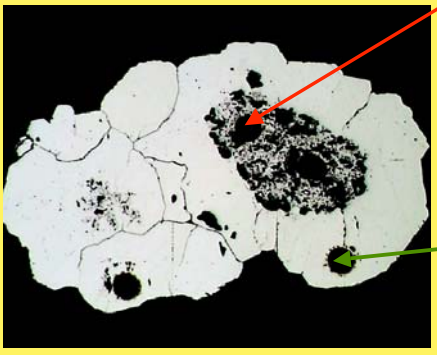

Early diagenetic pyrite
Co: 3507 ppm
Cu: 863 ppm
Pb: 1210 ppm
As: 1743 ppm

Later overgrowth pyrite
Co: 1175 ppm
Cu: 28 ppm
Pb: 29 ppm
As: 7 ppm

Diagenetic pyrite?

Chambishi SE Ore Shale

- Lenticles/nodules of pyrite & finer grained trains of disseminated pyrite are common in the upper third of the Ore Shale at Chambishi SE (Annels, 1974)
- Laser ablation of the cores of some of this coarse pyrite yield the isotopically lightest S seen at Chambishi SE

Diagenetic pyrite? II

Chambishi SE Ore Shale (con)

- Preliminary LA-ICPMS data for these pyrites indicates tha cores are elevated in many trace metals (including Co, Cu, Pb, As and Ni), while the rims are Co-rich, but 'cleaner' wrt other trace metals
- At least some of the fine disseminated pyrite is also the 'clean' Co-rich variety
- The 'porous pyrite' may be early diagenetic pyrite containing biogenic sulfide

When did Co enrichment start?

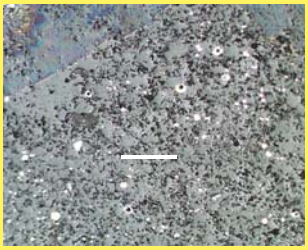

Geochemical modeling: implications for mineralising processes in the Zambian Copperbelt

David R Cooke

Centre for Ore Deposit Research, University of Tasmania

Summary

Numerical simulations of ore forming processes for the Zambian Copperbelt highlight that oxidised metalliferous brines can carry significant amounts of copper, together with Zn, Pb, Ag, Fe and Sb at 150°C. These brines can precipitate zoned Cu-sulfide mineralisation (chalcocite → bornite → chalcopyrite → pyrite) when they interact with solid (e.g., oil shales) or mobile (gas or liquid) hydrocarbon reservoirs. The sequence of sulfide deposition is strongly influenced by the availability of reduced sulfur in the trap site. In cases of mixing with mobile reductants, water-rock interaction may be required to buffer the pH of the resultant fluid, as acidification can inhibit the deposition of bornite and chalcopyrite.

Introduction

This report (Slide 1) uses chemical modelling to test hypotheses concerning fluid compositions and hydrothermal processes that could have operated in the Zambian Copperbelt (ZCB) during ore formation.

Copper solubilities in hydrothermal uids

Copper can occur in two oxidation states in aqueous solutions (Cu^{I}, Cu^{II}), although it is most soluble under hydrothermal conditions in the cuprous form (Cu^{+}). Typically, in saline brines, Cu will be transported as cuprous chloride complexes ($CuCl_{(aq)}$, $CuCl_2^-$, and $CuCl_3^{2-}$). Bisulfide transport of Cu (eg. $Cu(HS)_2^-$) may be important in H_2S-rich fluids and/or high temperature magmatic volatiles, but is unlikely to be relevant for mineralising brines in the ZCB.

Slide 2 illustrates how copper solubilities vary as a function of redox potential (illustrated here as log f_{O2}). Highest copper solubilities (>100 ppm) are predicted to occur under oxidising conditions (left hand side of the diagram). Chalcocite is the stable Cu-sulfide, and hematite is the stable iron-bearing phase. Copper solubilities are lowest under reducing conditions, where pyrite is stable. Note that on this diagram bornite is stable with pyrite under the most reducing conditions portrayed here. However, chalcopyrite will be stabilised in place of bornite by an increase in the pH or a decrease in the total sulfur concentration. Note that ΣCu denotes the total concentration of copper dissolved in solution. It is the sum of the molalities of all individual copper species present in solution, including:

- Cu^+
- $CuCl_{(aq)}$
- $CuCl_2^-$
- $CuCl_3^{2-}$
- $Cu(HS)_2^-$
- $CuSO_{4\ (aq)}$
- $CuOH^+$
- Cu^{2+}
- $CuCl^+$
- $CuCl_{2\ (aq)}$
- $CuCl_3^-$

Slide 2 has been calculated at a temperature of 150ºC, 25 eq. wt % NaCl, ΣS = 0.001 molal and a pH of 4.5. Note that any or all of these variables may not be appropriate for ore formation in the ZCB. Changing any of them will affect the amount of copper that can be dissolved in the hydrothermal fluid for any given log f_{O2} value, but will not change the overall trend from high solubilities under oxidising (SO_4-predominant) conditions, to reducing (H_2S-predominant) condi-

conditions, to reducing (H_2S-predominant) conditions.

Cu-Fe-sulfides have complicated stability relationships, due to strong controls imposed by the redox potential and acidity of the fluid, and by the total dissolved concentrations of sulfur, copper and iron available in the fluid. Complicated Cu-Fe-mineral parageneses can be predicted to form in response to chemical processes such as reduction or neutralisation. For example, the mineral paragenesis predicted by progressive reduction of the copper-bearing fluid plotted on Slide 2 is as follows:

- Hematite + chalcocite ***(A)***
- Siderite + chalcocite
- Siderite + bornite
- Siderite + chalcopyrite
- Pyrite + chalcopyrite
- Pyrite + bornite ***(B)***

Even more complicated parageneses can be hypothesised for acidic fluids (e.g., pH < 3), where chalcocite-pyrite becomes a stable mineral assemblage.

Slide 3 illustrates how copper solubilities vary in relation to Zn, Pb, Ag and Fe as a function of decreasing redox potential (diagram calculated for the same conditions as Slide 2). Note that Zn and Pb are predicted to be more soluble than Cu for all redox conditions portrayed on this diagram. However, during reduction, Cu solubilities decrease markedly under hematite-stable conditions, whereas high Zn and Pb solubilities can persist until pyrite is stabilised as the dominant Fe-mineral. Note how Fe has solubility relationships that contrast markedly with Cu, Pb and Zn. Fe achieves maximum solubility at the siderite-pyrite boundary, and is predicted to be less soluble under hematite-stable conditions and least soluble under pyrite-stable conditions. Although silver is shown to have solubilities greater than copper under reducing conditions, it is important to realise that Ag does not actually achieve such high concentrations in hydrothermal fluids. Substitution of Ag into base metal sulfides via coprecipitation reactions causes a significant decrease in the solubility of Ag in hydrothermal fluids.

Slide 4 illustrates how copper solubilities vary in relation to Ba, Au and Sb as a function of decreasing redox potential (diagram calculated for the same conditions as Slide 2). Sb is predicted to behave in a similar fashion to Cu, albeit with a more extreme change going from oxidising (high solubilities) to reducing conditions (low solubilities). A zone enriched in Sb is predicted to occur in systems where oxidising Cu-bearing fluids are reduced to pyrite-stable conditions. The proviso being that there was sufficient Sb in the starting fluid for saturation to occur. Gold and Cu have an antithetic relationship on Slide 4, suggesting that oxidising Cu-bearing fluids will not carry Au, and that Au solubilities may actually increase on reduction, promoting Au-leaching from the site of Cu deposition. Although the trend is subtle on Slide 4, like Au, Ba is predicted to have lower solubilities under oxidising conditions, and higher solubilities under reducing conditions. The contrast in solubilities is far more pronounced at higher concentrations of aqueous sulfate, and/or higher pH values.

Overall, these modelling results predict that oxidising fluids are effective transporting agents for Cu, and that significant Zn, Pb, Ag, Fe and Sb may be transported together with the copper. If such fluids were responsible for ore formation in the ZCB, then significant Zn-Pb deposits may exist further down the fluid flow path from the Cu deposits, if enough reductant is available to trap Zn and Pb. Au and Ba are unlikely to be significant components of ZCB Cu ores, if the fluid conditions modelled here are relevant to ore formation. More work is required to integrate Co and other elements of interest into these models.

Numerical simulations of ore-forming processes

Brine composition

Slide 5 summarises a hypothetical brine composition used for numerical simulations of ore formation for the ZCB. The following chemical components were used to define the chemical system used in these models:

H^+	H_2O	Cl^-	SO_4^{2-}	HCO_3^-	$SiO_{2\ (aq)}$
Al^{3+}	Ca^{2+}	Mg^{2+}	Fe^{2+}	Na^+	K^+
Mn^{2+}	Zn^{2+}	Cu^+	Pb^{2+}	Ag^+	$AuCl_2^-$
Ba^{2+}	$Sb(OH)_{3\ (aq)}$		Co^{2+}	$O_{2\ (aq)}$	

The hypothetical brine composition has been calculated by making initial assumptions about the initial fluid parameters (temperature = 150°C; salinity = 25 eq. wt % NaCl; Na/K ratios ≈ albite/K-spar stability; pH = 4.5; log $f_{(O2)}$ = 0.01, ∑S = 0.001 molal; ∑C = 1.0 molal). Many of these parameters are very poorly constrained. The temperature and salinity were chosen on the basis of the best 'guesstimate' by the P544 research team, rather than from any detailed fluid inclusion studies. ∑S and ∑C concentrations were estimated from Cooke et al. (2000). If ∑S concentrations are too high in reduced fluids, base metal solubilities will be too low for effective Pb, Zn and Cu transport, Au solubilities will become too high, and sulfosalts will be stabilised in preference to sulfides.

SOLVEQ (Reed, 1982) was used to calculate the concentrations of additional component species (Al, Fe, Mg, Mn, Ba) using a 'forced mineral equilibration' technique. This involved calculating the concentration of the relevant chemical component (e.g., Fe^{2+}) with respect to saturation of the stable mineral phase (e.g., hematite) based on the initial temperature and compositional estimates for the water. The starting fluid is saturated with K-feldspar and dolomite. To maintain charge balance, Na^+ concentrations were adjusted during each forced mineral equilibration step.

The composition of the brine in relation to theoretical metal solubilities is illustrated on Slides 3 and 4. Saturation levels for Zn, Pb, Cu, Ag, Au, Ba, Sb and Co concentrations were calculated by forced mineral equilibration. Metal concentrations were then arbitrarily decreased by up to an order of magnitude in the brine, allowing various depositional mechanisms to be tested for their effectiveness at extracting large quantities of base and precious metals from solution (Slide 5). This method allows us to assess whether a particular mechanism is capable of efficiently extracting base metals from solution.

Cooling

Chemical modelling of ore-forming processes has been undertaken using CHILLER (Reed and Spycher, 1985) and thermodynamic properties from SUPCRT92 (Johnson et al., 1991). Slide 6 shows how ineffective conductive cooling is when considered in isolation as an ore-forming process for oxidising brines. Cooling from 150°C to 50°C caused deposition of quartz, with minor Sb deposition below 60°C. No other metals were predicted to precipitate. It is concluded that conductive cooling is not relevant as an ore-forming process. Furthermore, based on these results, it is predicted that basinal brines undergoing down-T flow within the ZCB will produce domains of silica addition (cementation of pore space), whilst also potentially leaching base metals from the host media.

Mobile hydrocarbons

Slides 7 and 8 summarise the architecture and characteristics of the footwall orebodies of the ZCB (e.g., Chibuluma, Chingola B; diagram from Hitzman, this volume). The location of footwall orebodies is controlled by the sedimentary architecture, with early normal faults and the presence of sedimentary 'seals' important. Slides 9 and 10 summarise the architecture and characteristics of the arenaceous orebodies (e.g., Mufilira, Mwambashi B, Chibuluma, Nchanga footwall orebodies; diagram from Hitzman, this volume). Both groups of deposits are thought to have been controlled by the presence of mobile hydrocarbons (natural gas and petroleum) which served as reductants for oxidised mineralising brines. The reductants were located in physical traps (e.g., Slides 7, 9).

Gas traps

In order to test the effectiveness of gas reservoirs as chemical traps for base metals, a series of simulations of brine-gas interaction are illustrated in Slides 11–16. Slide 11 shows that interaction of the metal bearing brine with methane is not particularly effective at driving ore formation. Chalcocite is predicted to be the only copper mineral to precipitate, together with galena (but not sphalerite). Gangue minerals precipitated include graphite, dolomite, K-feldspar and talc. The onset of talc deposition coincided with

a period of gold-silver-antimony deposition. The pH increased from 4.6 to 5.9 in this simulation, which failed to produce the typical Cu-sulfide mineral zonation typical of the ZCB deposits.

In order to buffer pH, a second brine-methane gas simulation was undertaken in which the host rock was available for chemical reaction (Slide 12). The bulk rock composition used here was an 'arkose' that consisted of quartz (64%), oligoclase (21%) and K-feldspar (15%). The proportion of methane to arkose was 65:35. This simulation produced similar results to the preceding model, with the addition of chlorite as a gangue mineral late in the simulation. Again, a chalcocite-precious metal ore assemblage was predicted to form with no Cu-sulfide mineral zonation.

Because the simulations of brine-methane interaction do not appear to be capable of producing mineralisation typical of the known ZCB mineral deposits, several additional gas-brine simulations have been undertaken (Slides 13–16). These involve H_2S gas, which is potentially the most important chemical constituent of a sour gas reservoir from an ore forming perspective.

Slide 13 illustrates the effect of reacting the metalliferous brine with H_2S gas in isolation from any water-rock interaction processes. This process causes extreme acidification of the brine, with the pH dropping from 4.6 to 2.1. While a variety of copper minerals are predicted to form, the zonation produced by this process comprises chalcocite-bornite-tetrahedrite-covellite, not typical of the ZCB deposits. A large amount of pyrite was predicted to be deposited over a very small reaction interval, together with tetrahedrite, sphalerite and later-forming galena. Although the simulation did not produce aluminosilicate phases, any silicate rock that interacted with the end-product fluid would produce advanced argillic alteration assemblages, which have not been reported from the ZCB.

In order to counteract the strong acidification caused by H_2S dissolution into oxidising brine, several simulations have been undertaken where wallrocks (dolomite or arkose) have been allowed to interact with the fluids and buffer the pH. Slide 14 shows how reaction with a mixture of 50% H_2S gas, 50% dolomite results in initial acidification down to pH 3.2, and then acid neutralisation back towards pH 4.6. The predicted Cu-sulfide zonation is the same as for the H_2S-only simulation, but Cu-minerals ceased deposition when the pH rebounded and a large quantity of sphalerite, galena and acanthite were precipitated as the pH increased back towards 4.6.

In Slide 15, the proportions of dolomite to H_2S gas are 90:10. The presence of an abundant pH buffer allows the pH to remain constant at 4.6–4.7 throughout the simulation. This allowed for the production of more classic ZCB copper sulfide zonation, from chalcocite to bornite to chalcopyrite, with minor late stage boulangerite, tetrahedrite and polybasite in association with sphalerite and galena.

The simulation in Slide 16 used the same arkose used in Slide 12, with the proportions of 65% arkose to 35% H_2S gas. The aluminosilicate minerals proved far less effective than dolomite at buffering acidity, with pH decreasing to 2.5 before rebounding to 3.1. Chalcocite-bornite-tetrahedrite-covellite zonation was predicted, together with the deposition of significant pyrite, sphalerite and galena. By allowing ideal site mixing between pyrite and cattierite, this simulation predicted the deposition of some Co as a solid solution phase within pyrite.

Overall, the results of the gas-brine interaction simulations highlight the following:

- Sour gas reservoirs are more effective traps than methane reservoirs, implying that H_2S gas may be an essential ingredient of a gas trap site
- A pH buffer is required to offset the effects of acidification when H_2S gas dissolves into oxidising brine, which generates sulfuric acid
- Carbonate minerals are predicted to be a more effective pH buffer than feldspars, and dissolution of a carbonate cement in the gas reservoir may provide both the permeability to allow continued brine ingress and the chemical buffer required to prevent acidification
- Provided that acidification is prevented, H_2S gas addition can produce the classic chalcocite-bornite-chalcopyrite mineral zonation from an oxidising brine.

Petroleum reservoirs (organic waters)

It is not possible to chemically simulate the interaction of the mineralising brine with oil, due to a lack of thermodynamic properties for complex liquid hydrocarbon mixtures. Instead, simulations of fluid mixing between the oxidising brine and aqueous organic waters have been undertaken. The organic water comprises acetic acid (1 m) and NaCl (1 m) and has a temperature of 100ºC and pH of 5 (Slide 17). It is intended to be representative of pore waters in contact with liquid hydrocarbons.

Slide 17 illustrates the effects of mixing metalliferous oxidised brine with organic water. The only minerals predicted to be deposited are dolomite, gold and chalcocite. Furthermore, metal speciation is predicted to switch from chloride to acetate complexing when the volume of organic water exceeds the brine, as shown for aqueous Co on Slide 17. This simulation is most likely not relevant to the ZCB.

Because the organic water is devoid of reduced sulfur, several simulations have been undertaken to test whether this process is a chemically viable option for producing zoned ZCB-style ores. Slide 18 shows that with 0.001 m reduced sulfur dissolved in the organic water, a far more complicated sequence of mineral precipitation occurs. Chalcocite deposition is followed by bornite, and then polybasite, tetrahedrite and cobaltiferous pyrite, in conjunction with abundant late stage galena and sphalerite. Dolomite was the only gangue mineral produced. In Slide 19, the concentration of reduced sulfur in the organic water was increased by an order of magnitude to 0.01 m. This caused deposition of a complex sulfide mineral sequence: chalcocite–chalcocite+galena–bornite+galena+sphalerite–chalcocite+galena+sphalerite and then late stage polybasite, boulangerite and cobaltiferous pyrite. This simulation was then repeated using a modified brine where the Pb and Zn contents had been arbitrarily decreased by one order of magnitude prior to the start of the simulation (Slide 20). This simulation produced the most relevant results, with the Cu-sulfide zonation comprising chalcocite –bornite–chalcopyrite–pyrite+chalcopyrite+base metal sulfides–pyrite+bornite+base metal sulfides and sulfosalts–pyrite, with no gangue deposition apart from early dolomite. It is concluded that fluid mixing had potential to produce ZCB-style mineralisation, although it is essential for end-member fluid compositions to be better constrained before this can be tested rigorously.

Water-rock interaction with oil shale (immobile hydrocarbons)

Slides 21 and 22 summarise the architecture and characteristics of the ore shale orebodies of the ZCB (e.g., Konkola, Konkola North, Nkana, Nchanga; diagram from Hitzman, this volume). The ore shale orebodies are apparently controlled by the presence of carbonaceous (reducing) lithologies adjacent to (typically overlying) permeable rock units. Ore formation is thought to have been controlled by the interaction of oxidised mineralising brines with organic carbon-rich ± reduced sulfur rich shales.

Slide 23 lists an oil shale composition used in this simulation of water-rock interaction. The rock has a high content of organic carbon (6.4 wt %) and reduced sulfur (2 wt %). Interaction of the brine with this rock produced the classic ZCB sulfide zonation, from chalcocite to bornite to chalcopyrite + pyrite to pyrite only, demonstrating the chemical effectiveness of this trap mechanism. Alteration minerals produced include K-feldspar, dolomite and graphite (a proxy for pyrobitumen, for which no thermodynamic data are available). The pH remained constant throughout the simulation (Slide 23).

Conclusions

- Oxidising saline brines are inferred to have been the transporting agents for copper and other metals in the ZCB ore-forming fluids
- Interaction with reduced sulfur-bearing trap sites is inferred to have been the critical element for ore deposition
- Mobile hydrocarbons and oil shales had the potential to act as chemical traps for mineralising brines (Slide 24).
- Any mobile hydrocarbon traps most likely needed to contain some reduced sulfur in order to be chemically effective at forcing sulfide deposition. A pH buffer would most likely have also been required in cases where H_2S gas dissolved into the

oxidising brine during the mineralising process

- Interaction of oxidising brine with oil shale is particularly effective at producing zoned Cu-sulfide mineralisation
- Pb and Zn deposition was predicted in most simulations, begging the question "where are the ZCB zinc deposits"?
- Albite was not produced in any simulation and the importance of albite alteration to mineralisation remains to be tested
- Fluid and rock compositions are still poorly constrained, as are the physicochemical conditions of ore formation. Further work is required to provide better constraints on ore-forming conditions, which would then allow for more relevant chemical modelling

References

Cooke, D.R., Bull, S.W., Large, R.R. and McGoldrick, P.J., 2000. The importance of oxidised brines for the formation of Australian Proterozoic stratiform sediment-hosted Pb-Zn deposits. Economic Geology, 95, 1-17.

Johnson, J.W., Oelkers, E.H. and Helgeson, H.C., 1991. SUPCRT92: A software package for calculating the standard molal thermodynamic properties of minerals, gases, aqueous species and reactions from 1 to 5000 bars and 0° to 1000°C. 50 p. Computers & Geoscience.

Reed, M.H., 1982. Calculation of multicomponent chemical equilibria and reaction processes in systems involving minerals, gases and an aqueous phase. Geochim. Cosmochim. Acta, 46: 513-528.

Reed, M.H. and Spycher, N.F., 1985, Boiling, cooling and oxidation in epithermal systems: a numerical approach: *in*: Berger, B.R., and Bethke, P.M., (eds.), Geology and geochemistry of epithermal systems: Reviews in Economic Geology, v. 2, p. 249-272.

Geochemical modelling: implications for mineralising processes in the ZCB

David Cooke, Peter McGoldrick, Murray Hitzman, Robert Scott, David Selley

AMIRA/ARC P544 July 2003

Copper Solubilities

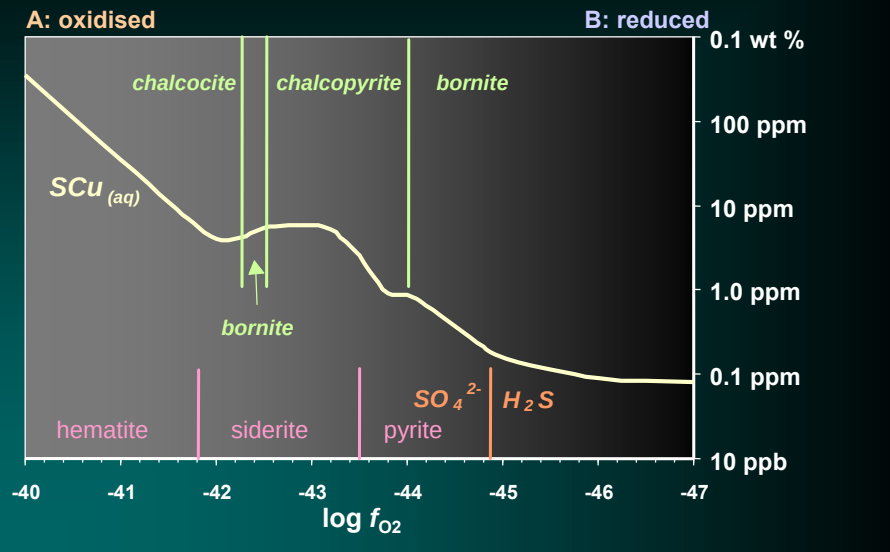

T = 150°C, 25 eq. wt %, pH = 4.5, ΣS = 0.001 m

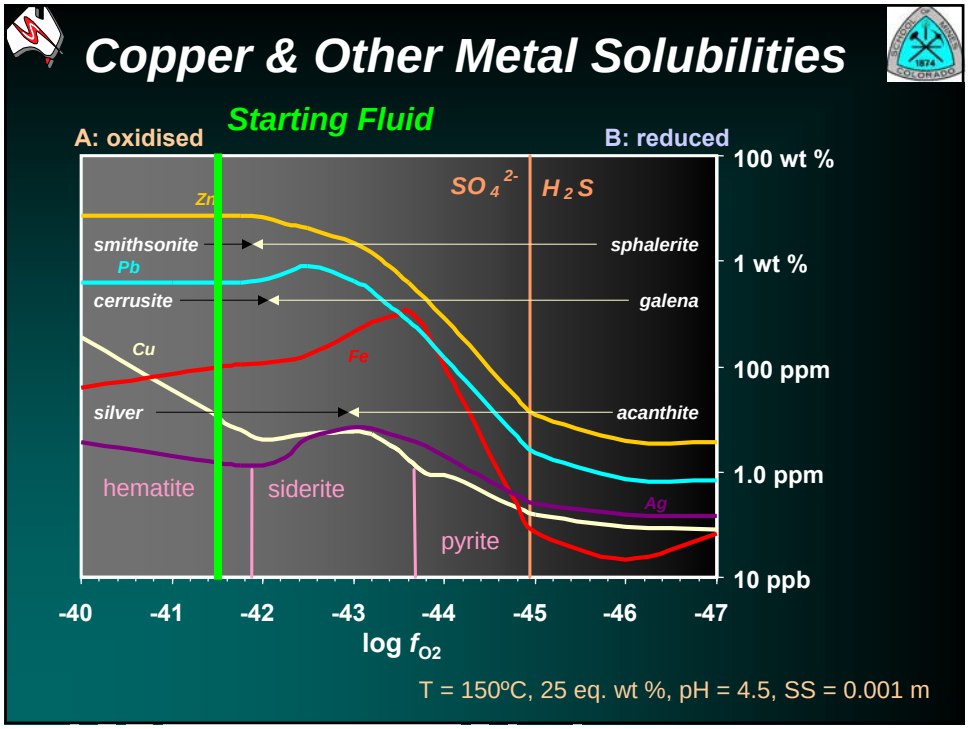
Copper & Other Metal Solubilities
Starting Fluid
A: oxidised
B: reduced
SO_4^{2-}
H_2S
Zn
smithsonite
sphalerite
Pb
cerrusite
galena
Cu
Fe
silver
acanthite
hematite
siderite
pyrite
Ag
100 wt %
1 wt %
100 ppm
1.0 ppm
10 ppb
-40
-41
-42
-43
-44
-45
-46
-47
log f_{O2}
T = 150ºC, 25 eq. wt %, pH = 4.5, SS = 0.001 m

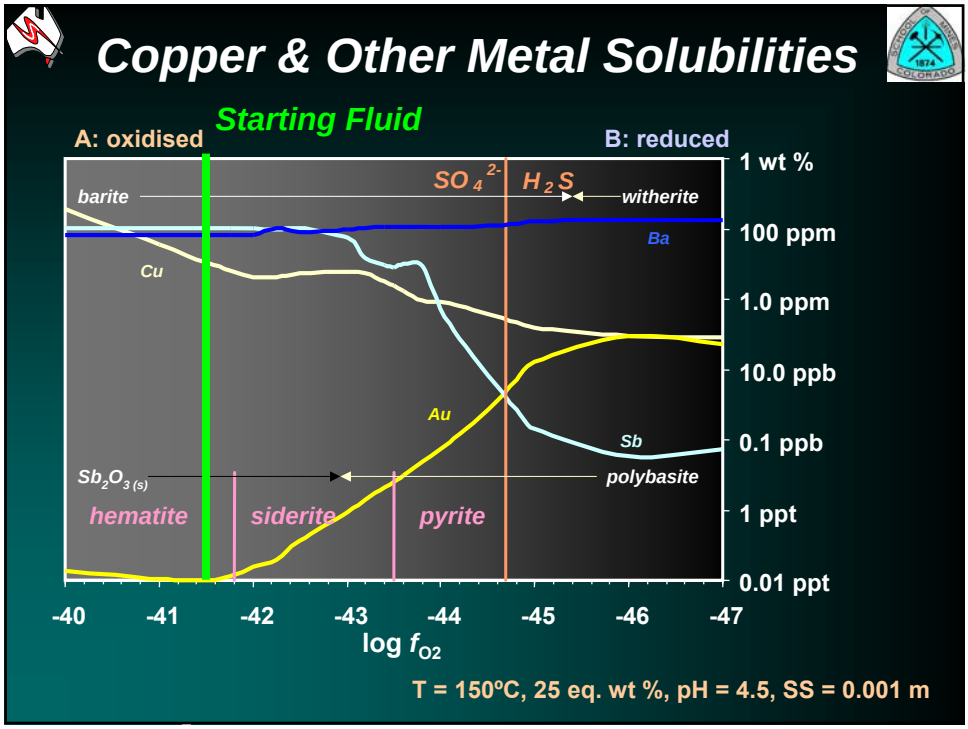
Copper & Other Metal Solubilities
Starting Fluid
A: oxidised
B: reduced
SO_4^{2-}
H_2S
barite
witherite
Ba
Cu
Au
Sb
$Sb_2O_{3\,(s)}$
polybasite
hematite
siderite
pyrite
1 wt %
100 ppm
1.0 ppm
10.0 ppb
0.1 ppb
1 ppt
0.01 ppt
-40
-41
-42
-43
-44
-45
-46
-47
log f_{O2}
T = 150ºC, 25 eq. wt %, pH = 4.5, SS = 0.001 m

Brine Composition

Notes:

- Oxidised (hm-stable) brine - log f_{O2} = -41.5
- Weakly acidic
- Highly saline (~ 25 wt % NaCl eq.)
- Saturated with Kf & dolomite
- Metal-rich, but all metals undersaturated by up to one order of magnitude

Chambishi Basin - NC47 - anhydrite

Component	Concentration
T	150C
pH	4.7
Cl-	149766.3
SO4--	69.6
HCO3-	11226.6
SiO2(aq)	75.6
Al+++	0.0012
Ca++	8885.7
Mg++	940.0
Fe++	34.7
K+	42962.0
Na+	59324.7
Mn++	97.4
Zn++	721.0624 or 72.11
Cu+	67.7
Pb++	388.2634 or 38.83
Ag+	0.20
AuCl2-	1.77E-08
Ba++	6.2
Sb(OH)3	12.318 or 1.23
Co++	32.5

Cooling from 150º to 50ºC

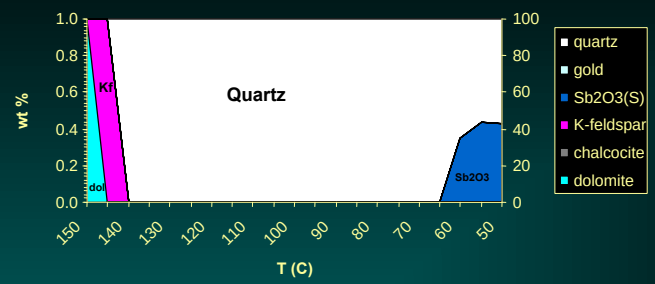

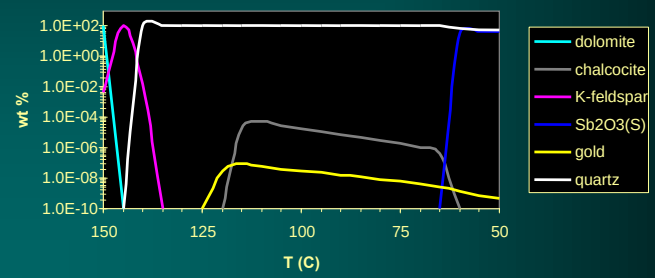

Notes:

- dolomite & K-feldspar saturated at start
- qz is the dominant ppt
- Minor Cu deposition as chalcocite
- Late Sb deposition

pH = 4.66 → *pH = 4.28*

Mineralization - Footwall Orebodies

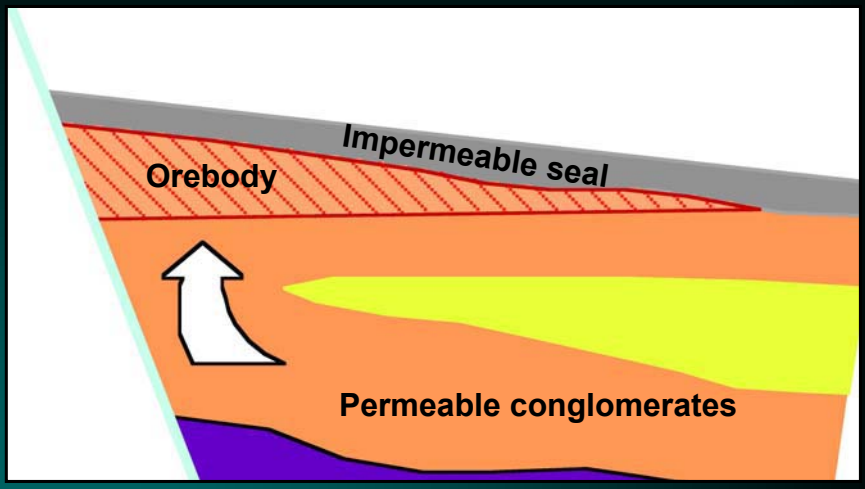

The location of footwall orebodies is controlled by the sedimentary architecture related to early normal faults and the presence of sedimentary "seals."

Footwall Orebodies

Examples:

- Chibuluma
- Chingola B

Ore Deposition:

- Metal-rich, but all metals undersaturated by up to one order of magnitude

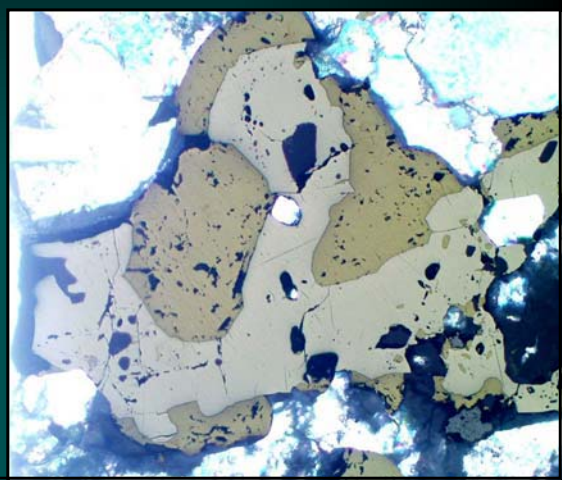

Chibuluma: Cp & py in quartzite - NS137 1300.5 ft

Mineralization - Arenaceous Orebodies

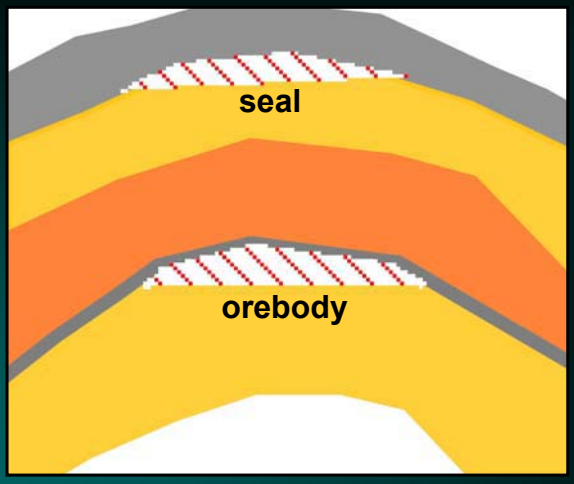

Arenaceous (and probably footwall) orebodies controlled by the former presence of hydrocarbons (natural gas and petroleum) which served as reductants. These reductants were in physical traps.

Arenaceous Orebodies

Examples:

- Mufulira (muscovite alt)
- Mwambashi B (K-spar stable, carbonate-buffered)
- Chibuluma (K-spar stable)
- Nchanga footwall orebodies

Ore Deposition:

- Hydrocarbon traps / sour gas reservoirs (mobile reductants)

Interbedded shales - Mufulira (1240L)

High grade ore - C lens, Mufulira (py overprint)

React brine with CH_4 gas

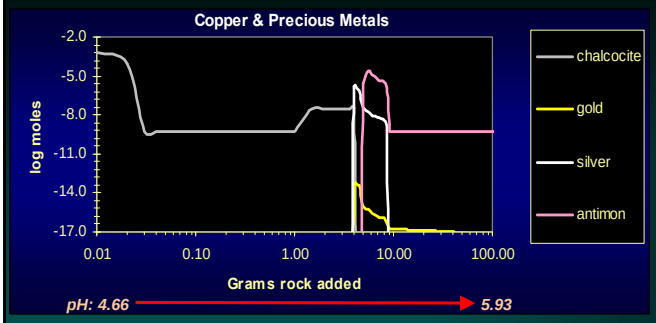

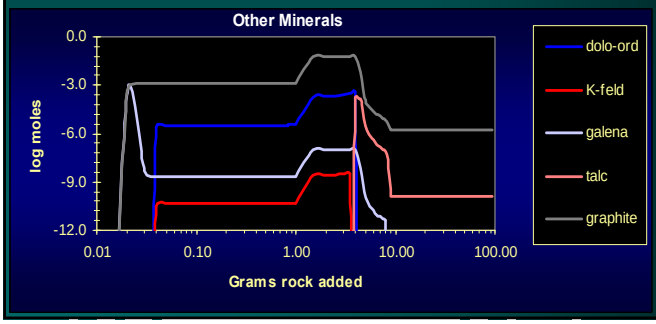

Notes:

- Chalcocite was the only Cu mineral deposited
- pH increase from 4.6 to 5.9
- Deposition of galena, but not sphalerite
- Dolomite deposition followed by talc
- Deposition of gold-silver-antimony

React brine with CH_4 gas & arkose

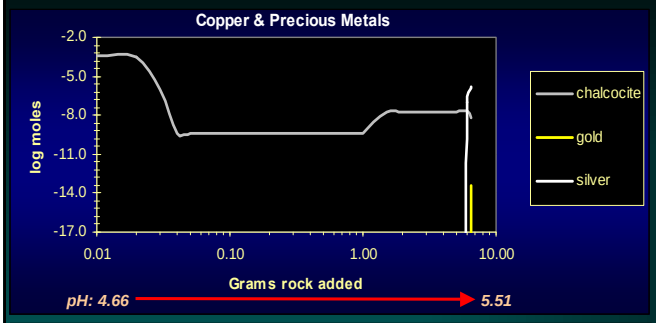

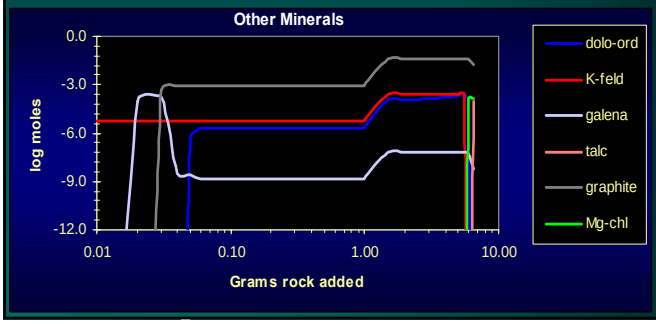

Notes:

- Chalcocite was the only Cu mineral deposited
- pH increase from 4.6 to 5.5
- Deposition of galena, but not sphalerite
- Dolomite deposition followed by chlorite & talc
- Deposition of gold-silver-antimony

React brine with H_2S gas

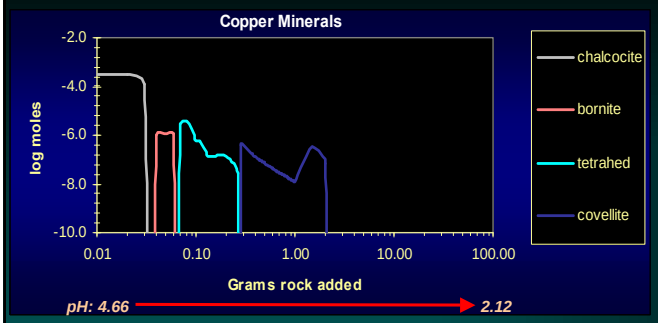

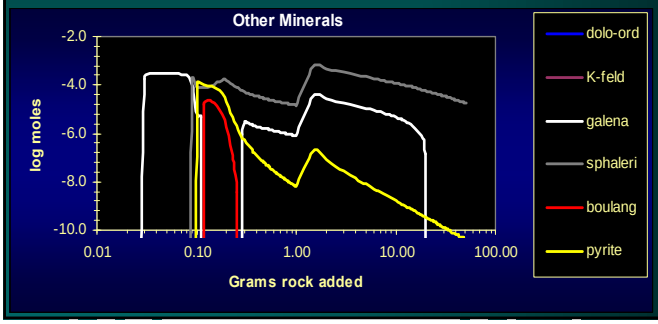

Notes:

- Cc-bn-tet-cov zonation
- Strong acidification from 4.6 to 2.1
- abundant sp & gl precipitation
- Pyrite deposition consumes Fe rapidly
- Simulation terminated with onset of phase separation

React brine with 50% dol, 50% H_2S

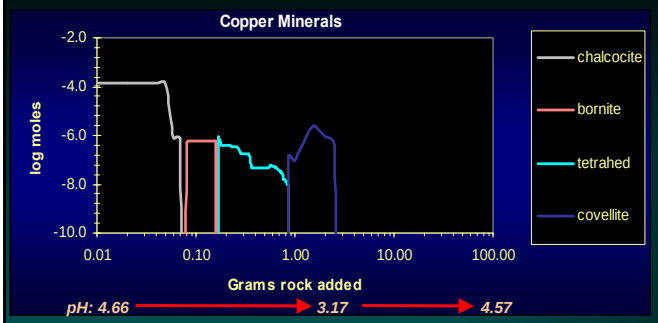

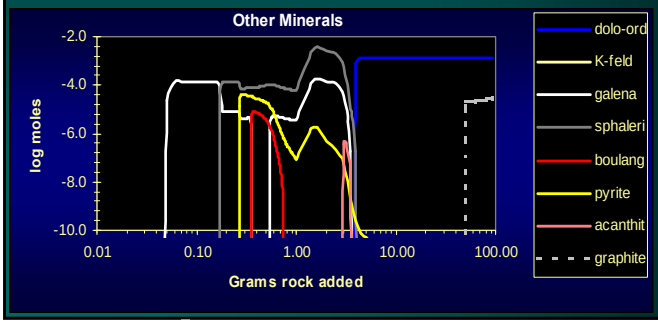

Notes:

- Cc-bn-cov zonation
- Dol dissolution as pH drops to 3.2
- pH then rebounds to 4.6 with onset of dol ppt^{n}
- Ideal site mixing model for Co substitution into py indicates trivial amounts of Co substitution

React brine with 90% dol, 10% H_2S

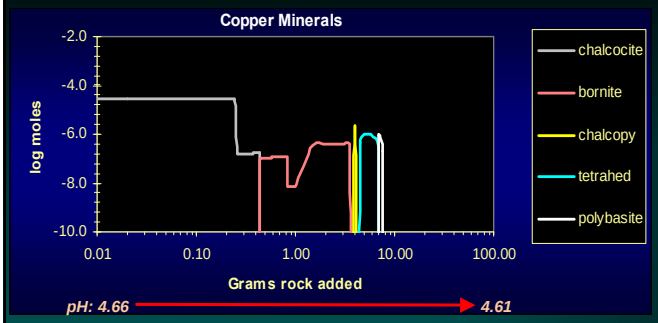

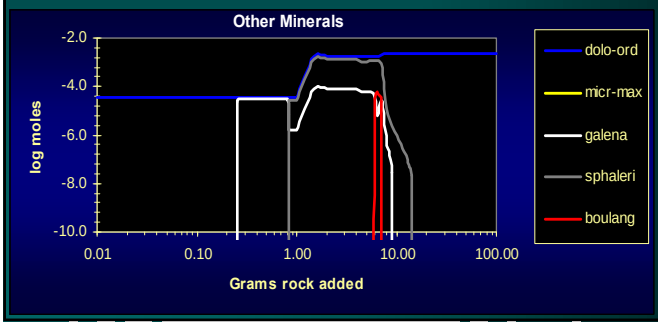

Notes:

- Cc-bn-cp zonation
- Dolomite dissolution and ppt^n buffers pH to 4.6 throughout the simulation
- abundant sp & gl precipitates due to high conc. of Zn & Pb in starting fluid
- No pyrite deposition

React brine with H_2S & arkose

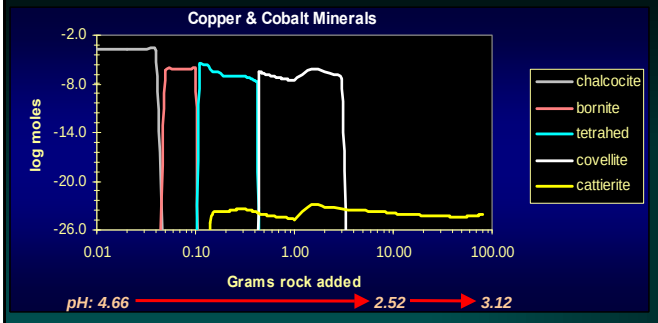

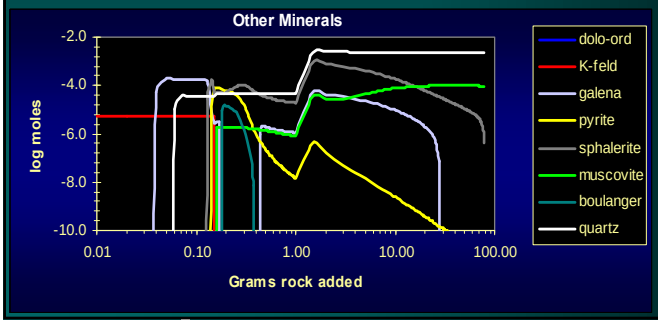

Notes:

- Cc-bn-tet-cov zonation
- Dolomite dissolution and ppt^n buffers pH to 4.6 throughout the simulation
- abundant sp & gl precipitates due to high conc. of Zn & Pb in starting fluid
- No pyrite deposition

Mix with organic water

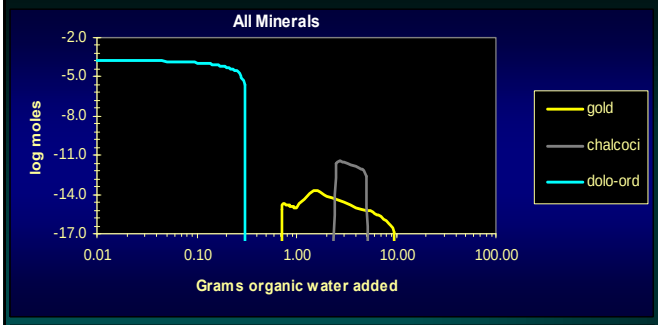

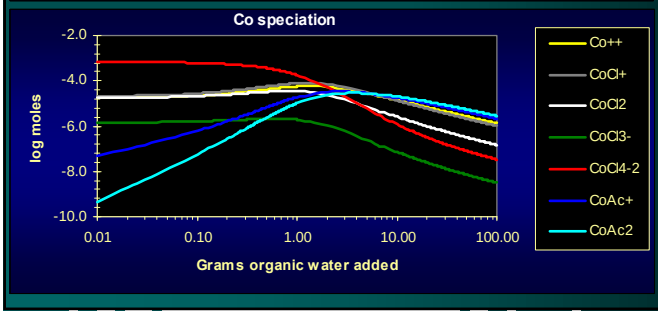

Notes:

- 1 m acetic acid, 1 m NaCl, in 100°C, pH = 5, org. water
- pH increase from 4.6 to 5.0
- Deposition of dolomite, then very minor chalcocite and gold
- Me-acetate complexes form and are predominant when organic water > brine

Mix with organic water & 0.001 m HS^-

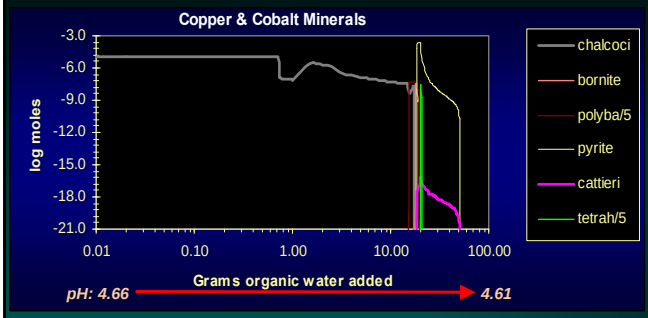

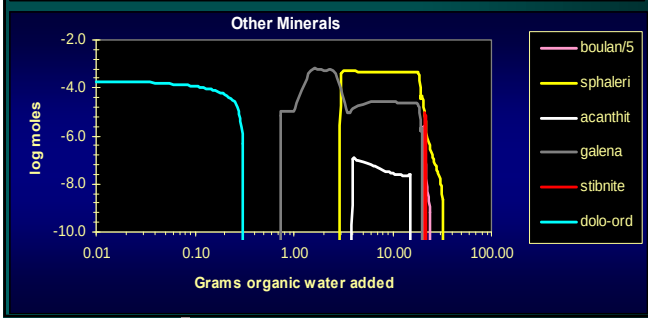

Notes:

- 1 m acetic acid, 0.001 m HS-, 1 m NaCl, in 100°C, pH = 5, org. water
- pH constant
- Deposition of abundant chalcocite, then bn & Cu-Sb sulfosalts
- Late Co-pyrite deposition
- No gangue apart from early dolomite
- sp-gl distal to chalcocite

Mix with organic water & 0.01 m HS^-

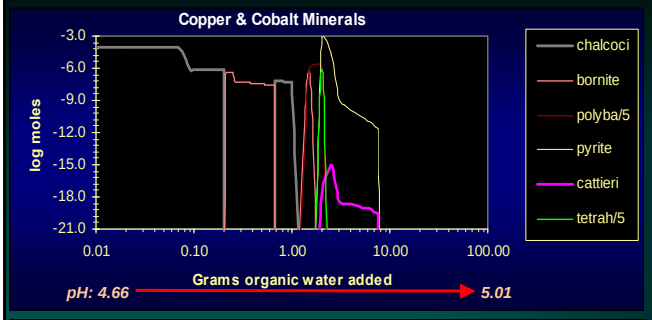

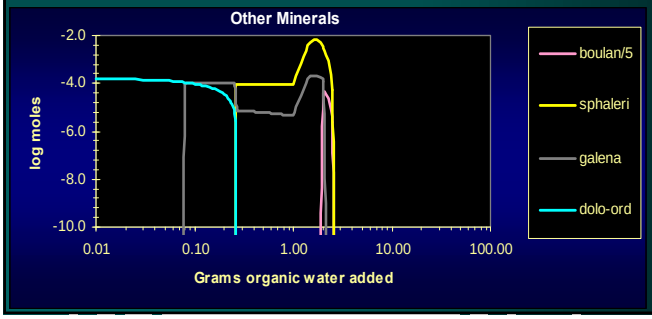

Notes:

- 1 m acetic acid, 0.01 m HS-, 1 m NaCl, in 100°C, pH = 5, org. water
- pH increase from 4.6 to 5
- Deposition of chalcocite - bn - chalcocite & Cu-Sb sulfosalts
- Late Co-pyrite deposition
- No gangue apart from early dolomite
- sp-gl distal to chalcocite

Mix with organic water & 0.01 m HS^-

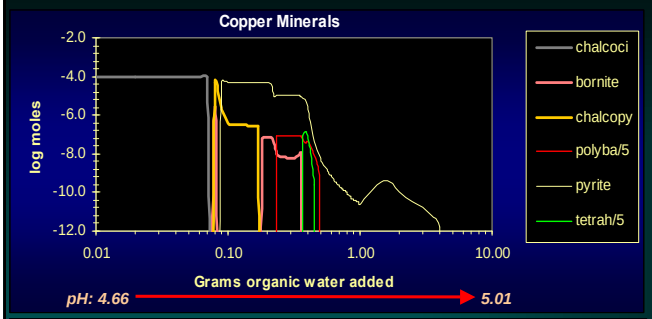

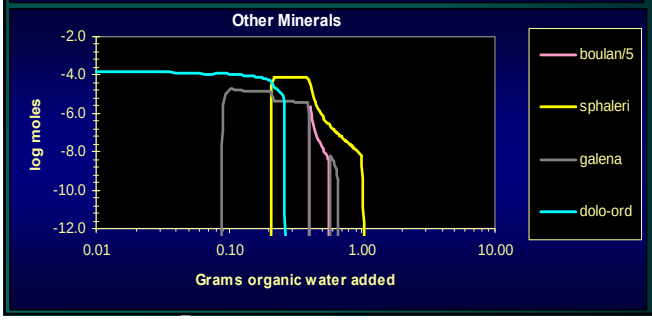

Notes:

- Pb, Zn and Sb conc. decreased by 1 order of magnitude from previous simulation
- pH increase from 4.6 to 5
- Deposition sequence: chalcocite → bn → cp → py+cp+bms → py+bn+bms ± Cu-sulfosalts → py
- No gangue apart from early dolomite

Mineralization - Ore Shale Orebodies

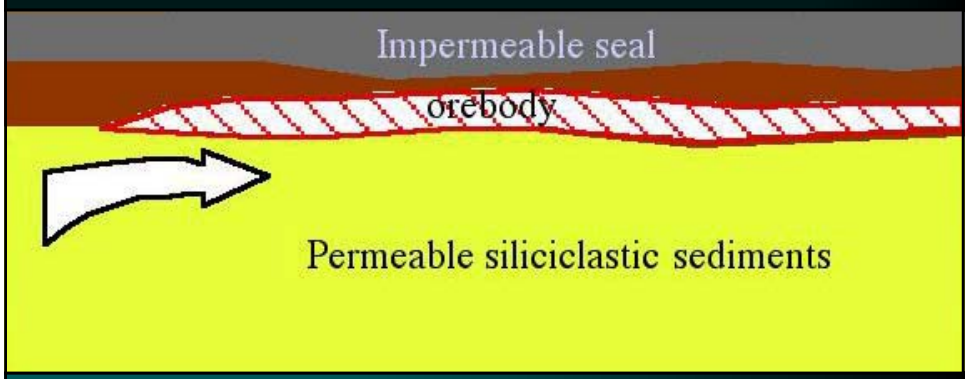

Ore shale orebodies are controlled by the presence of carbonaceous (relatively reducing) lithologies and adjacent (generally stratigraphically below) permeable lithologies.

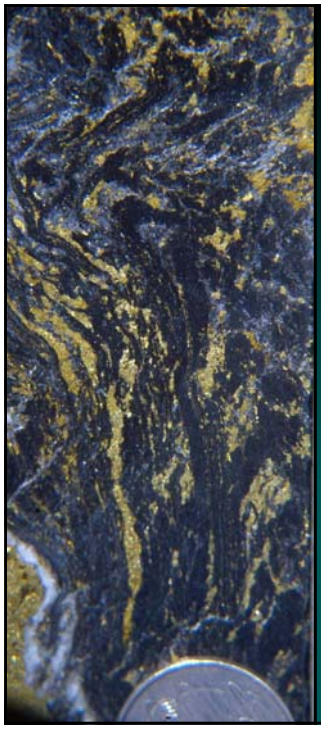

Ore Shale Orebodies

Examples:

- **Konkola / Konkola N**
- **Nkana**
- **Nchanga**

Ore Deposition:

- **Interaction of metalliferous brine with C_{org}-rich ± S-rich shales**

Nkana - NSO4 - 41m

React with Oil Shale

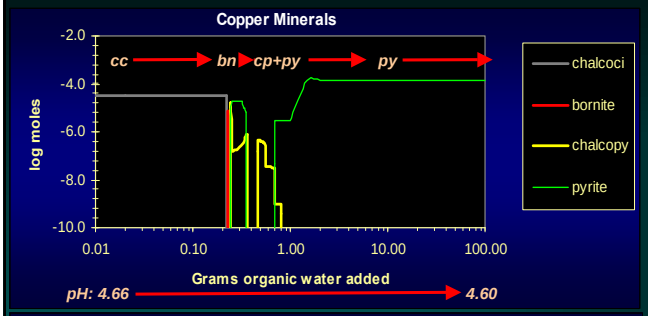

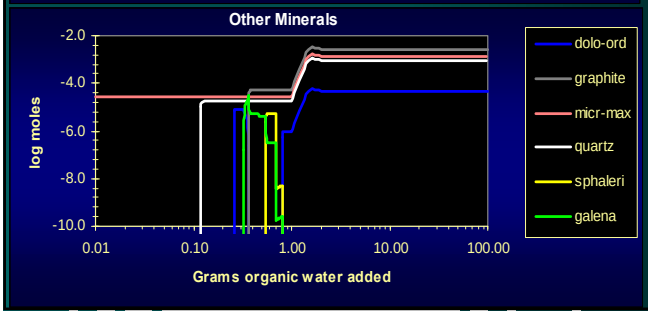

Notes:

- K-spar - dol - qz - graph (pyrobit?) alteration
- pH constant
- sulfide zonation

Rock composition:

- SiO_2 60.2%
- Al_2O_3 14.23%
- Fe_2O_3 2.86%
- MnO 0.019%
- MgO 2.16%
- CaO 3.10%
- Na_2O 0.94%
- K_2O 2.41%
- C_{org} 6.40%
- H_2S 2.00%
- H_2O 5.35%

Conclusions

- Oil shale, mobile hydrocarbons & organic waters are chemically effective traps
- Reduced sulfur is the key - either already present at the trap site, or produced via sulfate reduction
- Where is the Pb & Zn? Should have been very soluble - why didn't they precipitate?

Comparison of Cu mineralised basins: the Zambian Copperbelt, the Polish Kupferschiefer, the Adelaide Fold Belt and the Yeneena Basin

Stuart Bull et al.
Centre for Ore Deposit Research, University of Tasmania

Summary

The giant Cu deposits of the Zambian Copperbelt (ZCB) and the Kupferschiefer of Poland and Germany (PK) have many elements in common. In summary; they occur in relatively thin (<5 km) single cycle basin successions deposited during active rifting and subsequent thermal sag in continental - marginal marine environments; sulfides are focused in and around an organic-rich unit abruptly overlying the basal rift clastics; there is a hangingwall evaporitic and carbonate succession; subsequent sag phase shales and carbonates have low sedimentation rates and restricted thickness.

In contrast, the Adelaide Fold Belt (AFB) has a different basin history involving at least four main basin cycles that have produced a thicker and more complex basin fill, with a dynamic thermal history as a result of high heat-producing basement granites and extensive salt migration. The AFB Cu deposits most often interpreted as PK or ZCB-style are those of the Stuart Shelf. However, we argued that these actually occupy a markedly different tectono-stratigraphic setting in that they occur later in the basin history (higher in the basin fill) and outside the zone of active rifting.

A coherent picture is now emerging of the processes that operated to form the giant ZCB deposits, which highlights the critical role played by evaporates and hydrocarbons. We therefore conclude this comparative study by examining the potential for similar processes to have operated in the PK, AFB and Yeneena Basin.

Introduction

The ZCB has been the focus of the bulk of the multi-disciplinary research carried out in the course of AMIRA / ARC P544 project. As a result, it has become clear that a number of elements of basin geology, for example the facies architecture of early rift-phase clastic sediments, the development of evaporitic facies and hydrocarbon generation, are critical elements in the genesis of world-class stratiform sediment-hosted Cu deposits. The aim of this discussion is to compare and contrast these elements that we now know to be particularly significant in the ZCB; with another basin that is known to host world class examples of similar style mineralisation, the Kupferschiefer of Poland and Germany (PK); and with basins with similar geological elements and / or ages that seem to lack large examples of this deposit type, the Adelaide Fold Belt (AFB) and Yeneena Basin (YB).

The PK was chosen because, as has been noted by previous workers (e.g., Rentzsch, 1974), this mineralised system has many elements in common with the ZCB. This is especially significant since it is essentially unmetamorphosed while the ZCB is biotite grade. Although no detailed studies were carried out in the PK in the current project, there is considerable literature available and a reconnaissance visit was made to the Polish part of the system by some of the authors.

The AFB was selected in the project generation phase of the P544 project as the focus of the major Australian component of the field studies, on the basis that the basin fill was of broadly the same age as that of the

ZCB, and previous studies that proposed Cu mineralisation of similar style was present. Work carried out in the initial phase of the P544 project showed that the latter interpretation is open to question, in that there are considerable differences between the deposits cited as ZCB/Kupferschiefer-style and the actual deposits in Zambia. It also became clear that although the ages and lithostratigraphic elements of the two basins are indeed broadly correlative, the histories of the basin fill are very different. A reconnaissance visit was also made by one of the authors to the Yeneena Basin, a correlative of the AFB in western Australia that also hosts substantial Cu deposits, albeit of an apparently different style to the ZCB examples.

Basin Architecture

The large stratiform Cu deposits of the ZCB occur towards the base of the Neoproterozoic Katanga Supergroup (Slide 3), an intracontinental succession of subaerial to restricted and ultimately open marine sediments. The ore deposits occur in the basal Roan Group, focused in and beneath the carbonaceous siltstones and correlative carbonates of the Ore Shale. This unit represents the abrupt transition from a fluvially dominated clastic footwall succession with abrupt lateral thickness (maximum ~1 km) and facies changes controlled by a closely spaced network of syn-sedimentary faults (Slide 4), to sub-wave base sedimentation controlled by more widely spaced master faults (Selley et al., report 4 this volume; Slide 5). The hangingwall upper Roan succession has an effectively layercake stratigraphy signifying the cessation of active tectonsim (Bull et al., report 3 this volume; Slide 6). It comprises a diverse facies mosaic of coarse- and fine-grained clastics and carbonates, and abundant preservation of primary sulfate evaporite textures attest to deposition in an evaporitic marginal marine environment. The subaerial to restricted marine Roan Group is overlain by fine-grained open marine fine-grained clastics and carbonates of the Mwashia and Kundelungu Groups (Slide 7) interpreted to represent thermal sag phase sedimentation.

The Cu deposits of the Polish Kupferschiefer are also hosted in a relatively thin subaerial to restricted marine succession deposited in an intra-continental rift environment (Slide 8). In this case extension was initiated in the Devonian, and the basal Rotligendes rift phase sediments and bimodal volcanics are around 1 km thick in the area of the deposits (e.g., Jowett, 1986; Slide 9). They are abruptly overlain by the Kupferschiefer (Slide 10), a thin (~1 m) organic-rich shale that, as with the Ore Shale in the ZCB, hosts or immediately overlies the mineralisation. The hanging wall succession comprises cycles of carbonates and evaporates (the Zechstein) that include thick in-situ anhydrite and halite units (Slide 11).

In summary the empirical tectono-stratigraphic characteristics of systems that host known large stratiform sediment-hosted Cu deposits are;

- They occur in relatively thin (<5 km) single cycle basin successions deposited during active rifting and subsequent thermal sag in continental - marginal marine environments.
- The sulfides are focused in and around an organic-rich unit abruptly overlying the basal rift clastics.
- The hangingwall succession includes major evaporite and carbonate units.
- Subsequent sag phase shales and carbonates have low sedimentation rates and restricted thickness.

Although the rocks of the AFB also accumulated in an intra-continental rift setting and are broadly chronostratigraphic equivalents of the ZCB, the basin fill history is substantially different. The stratigraphy comprises a complex multi-phase succession (Slide 13), in which there are at least four major basin phases bounded by regional unconformities (e.g., Preiss, 1987; Selley, 2000). The glacial deposits that mark the base of the Kundelungu in the ZCB (Slide 7) around 2 km above basement are in the third basin cycle, the Umberatana Group, which is underlain by up to 15 km of basin fill. The insulating effect of this thick basin fill, in combination with high heat producing basement granites, has resulted in a dynamic thermal history for the AFB (e.g., Nuemann et al., in press). This has included extensive salt migration (tectonism) in the basin centre where small Cu deposits are spatially associated with salt diapirs (e.g., Selley, 2000).

In terms of the Cu mineralisation, it is the deposits of the Stuart Shelf region (e.g., Mt Gunson; Slide 14) that have most commonly been interpreted as Kupferschiefer and/or ZCB in style (e.g., Maiden, 1989). Although these deposits are clearly of the same broad family, in that they are hosted by reduced fine-grained trap rocks, they occur much higher in the basin stratigraphy than the ore hosts in the ZCB or PK (Slide 14). In addition, there is no significant footwall rift clastic phase on the Stuart Shelf, as it is first onlapped by AFB sediments at Umberatana time (Slide 15). It is therefore difficult to see how the types of mineralizing processes that we advocate to for the ZCB and PK, that are intimately controlled by the architecture of an underlying rift phase aquifer system, could have been responsible for the Cu deposits of the Stuart Shelf.

In fact it is the basal Callana and Burra Groups, below the glacial units (Slide 13) that are the probable direct Roan chrono-stratigraphic correlates. In general terms, the basal Callana Group, which is the direct lower Roan tectono-stratigraphic correlate, has the right ingredients (Slide 16) in that it has basal clastic aquifer successions deposited during active rifting, and both reduced and evaporitic units are present in the overlying stratigraphy. However, because it is at the base of the much thicker basin fill, this succession was largely covered by younger basin phases during sedimentation. In addition, the subsequent Delamarian inversion involved the development of a regional decollement within the evaporitic levels of Callana Group that leaves few windows through the Burra Group into the lower levels of the stratigraphy.

The Yeneena Basin succession is an AFB correlative developed in a structurally complex area at the NW margin of the Centralian Superbasin (Slide 18). In spite of uncertainty with respect to correlation of different stratigraphic elements (Slide 19), it is clear that the Yeneena Basin succession records a similar basin evolution to basal Katangan sequences in the ZCB. In summary (Slide 20); the basal sequences are dominated by clean fluvial sandstones that record initial stages of intracontinental rift development; the upper part of the basal sequence records an abrupt increase in rate of tectonically-controlled subsidence (e.g., Ore Shale-time in the ZCB); subsequent widespread marine transgression led to the rapid development of anoxic depositional environment and transition to 'sag phase' depositional cycle.

Evaporites

In the essentially undeformed and unmetamorphosed PK, the relationship between the evaporites and the Cu mineralisation is clear. On the SE basin margin where the deposits occur, the Zechstein evaporite units are still in situ (Slide 22), indicating that local salt migration and tectonism is not necessary for Cu mineralisation. In fact, where there has been considerable salt migration via diapirism in the basin centre to the N and W (Slide 23) there are no known Cu deposits. We speculate, based on the work of Hanor (1999) in the Gulf Coast that one explanation is the effects of salt migration on the salinity profile in a basin. Where salt is present as a stratiform sheet, salinity and hence metal carrying capacity of the pore fluid, increases linearly with depth. However, where salt has migrated into cross-stratal diapirs pore fluid salinity is much more patchy and generally lower. In current models for the in situ PK the evaporite units act as a regional seal for convective circulation in the footwall clastics (Jowett, 1986). In addition, if access to the salt occurred in fluid upwelling zones subsequent dissolution could also contribute to the salinity of the fluids (e.g., Warren, 1997).

One of the striking features of the ZCB when compared to most Proterozoic successions is the widespread preservation of anhydrite throughout the Roan. Most now occupies diagenetic and/or structural sites, e.g., cements and veins respectively. However, nodular textures clearly indicative of a primary evaporitic origin are frequently preserved from the level of the Ore Shale and into the hanging-wall (Slide 24), and sulfur isotopic studies confirm a seawater origin (McGoldrick, this report). Although halite is not preserved, presumably due to the green-schist facies metamorphism (Scott et al., this volume), the development of widespread stratabound and cross cutting breccias (Slide 24) in the upper Roan is at least part attributed to removal of substantial salt units (Broughton, this volume).

One of the outcomes of P544 research program in the ZCB is the proposal that the dissolution of these hangingwall evaporite units played a critical role in the hydrological regime that led to the generation of the stratiform Cu deposits (Selley et al., this volume; Large et al., this volume). This process could certainly have contributed salinity to the basinal fluids and thereby enhanced their metal carrying capacity. However, it may also have contributed in other less obvious ways. For example, there are no primary evaporates present in the mainly fluvially deposited footwall sandstone aquifers in the Chambishi Basin. However, evaporitic cement components now recrystallised, are present in the form anhydrite and carbonate. These are attributed to the downward migration of dense brines (brine reflux) from the overlying stratigraphy during early diagenesis (Bull et al., this volume). We propose that the preservation of these components till late in basin history may help explain one of the geological contradictions of the ZCB; that while there is considerable evidence for a relatively late (syn onset of inversion?) timing for the mineralisation, the ores are stratiform and the mineralising fluids seem to have used early diagenetic fluid pathways and to be associated with hydrocarbon accumulations (Selley et al., this volume; Hitzman et al., this volume). This is because the persistence of early diagenetic evaporitic cements is one factor that could facilitate generation of ~stratiform zones of secondary porosity later in the basin history and thereby enhance the potential for stratiform Cu mineralisation.

In the AFB, evaporate pseudomorphs are abundant in the basal Callana and Burra Groups, however the salt was extensively remobilised into diapiric breccias through the axis of the basin (Slide 26). This activity is thought to have peaked coincident with Rodinian breakup. Many of the clasts in the diapirs are clearly sourced from the Curdimurka Subgroup, and given the lack of exposure of this lower part of the stratigraphy the distribution of salt diapirs is used to infer its subsurface extent (Slide 17). However many of the clasts are also mafic volcanics and Black Knob Marble from the underlying Arkaroola Subgroup (Slide 27). We therefore contend that the thick stratiform halite units that must have been present to source the diapirs must have been deposited below this level. This becomes important in an exploration context, given the empirical observation that in the basins considered here that are known to host large-scale stratiform Cu mineralisation, it occurs stratigraphically below the thick stratiform evaporite sheets. It suggests that the most prospective parts of the basal AFB stratigraphy would be the lowest levels (Arkaroola Subgroup and correlates) in marginal regions outside the zone of diapirism where stratiform evaporates may have remained in situ (Slide 28) until late in the basin history. One positive factor for this exploration strategy is that it is in these regions, for example in the area of the Northwest Fault – Torrens Hinge Zone (Slide 29), that the Burra Group thins. In addition, geophysical modelling (McKay et al., this report) suggests that upright folds are present in this area that could bring the prospective lower stratigraphic units close to the surface beneath shallow cover.

The other aspect of the geology of the Australian Neoproterozic that is now clear, is that it is not the most subsident part of the system, the AFB, that most resembles the mineralised parts of the Cu-hosting basins. In terms of the palaeogeography of the European Cu system, it is more analogous to the depocentre below the North Sea (pink zone on Europe map; Slide 30), where the basin fill is thicker and the evaporites have been mobilised into diapirs (Slide 28). It is actually the elements of the so called Centralian Superbasin to the NW (Slide 30), where the basin fill is thinner and less complex and stratiform evaporates are preserved in situ, that most closely resembles the PK and ZCB systems and may therefore be more prospective for large stratiform Cu deposits.

In the case of the Yeneena Basin, evaporite minerals (gypsum, anhydrite and halite) of probable diagenetic origin are locally developed throughout Broadhurst Formation (Slide 31). Although these indicate at least sporadic development of evaporitic conditions during sedimentation, there is no evidence that thick evaporitic units were present. However given the generally poor outcrop, and the fact that the system was deposited on the NW margin of the Centralian Superbasin where such units are preserved to the present day, they could well have been present in this system.

Hydrocarbons

Annels (1979) publication on Mufulira (Slide 33) was the first to propose that hydrocarbons were involved in the genesis of a ZCB Cu deposit. The current phase of P544 work has taken this concept further, and we would now contend that hydrocarbon involvement was a critical element in the formation of all of the Chambishi Basin deposits (Selley et al., this volume). Our main lines of evidence are; The geometry and location of the ore bodies within the tectono-stratigraphic architecture of the basin suggests they are after migrated hydrocarbons (footwall) or in situ organic matter (ore shale); The trend to very light C isotopic values of ore-related carbonates (Large et al., this volume) suggest the involvement of thermochemical sulfate reduction which is reliant on the presence of hydrocarbons (McGoldrick et al., this volume).

With regard to the other known mineralised basin considered here, the PK system, the basal Rotleigendes sandstones host producing gas reservoirs in the footwall of the Kupferschiefer, which was itself the source of some of the hydrocarbons. Peryt (1989) recognised that the Cu deposits occupied the same palaeogeographical zones as the gas reservoirs (Slide 35) and suggested that this implied a common origin. In spite of this, we are unaware of any published model for the Kupfershciefer Cu deposits that demonstrates direct correspondence with hydrocarbon traps. In terms of a signature for this hydrocarbon association, as in the ZCB, the lowest C and O isotopic values in carbonate occur in Cu mineralised zones in the organic rich shales (Kupferschiefer; Achim et al., 2001), and this has been attributed to oxidation of organic matter (BSR and TSR). However, in this case the C only shifted by ~ 4‰, and given the maximum temperature attained by Kupferschiefer is ~130°C (Sun & Puttmann, 1997), we interpret this to indicate that thermochemical sulfate reduction was not a major factor in this system.

The hydrocarbon geology of the lower part of the AFB stratigraphy is difficult to evaluate due to the lack of exposure, deformation and metamorphism. However, organic-rich potential source rocks are certainly present in the Curdimurka (and Arkaroola?) Sub-Groups (Slide 37). In terms of an isotopic signature for the former presence of hydrocarbons as is present in the two basins that host large deposits, the situation is complicated by a secular negative isotopic excursion coincident with deposition of the Callana Group (e.g., Hill and Walter, 2000; Slide 38). However, limited data collected in the current project shows no substantial negative C excursion associated with the minor Cu shows in the Curdimurka Subgroup (Slide 39). A similar situation exists for the Yeneena Basin, where although there is certainly a negative C trend associated with the more substantial Cu deposits (Slide 40). They do not show the very light C values characteristic of the ZCB deposits.

Discussion/Conclusions

The characteristics of the basin systems that we know host large-scale stratiform sediment-hosted Cu deposits, the ZCB and the PK are:

- The deposits occur near the base of a relatively thin (<5 km), single cycle basin succession deposited during active rifting and subsequent thermal sag in a continental to marginal to open marine environment.
- The mineralisation is focused in and around an organic rich unit that abruptly overlies the basal rift-phase clastics. In a hydrological sense this represents a redox trap in communication with a footwall aquifer (and basement!).
- The hangingwall succession includes in-situ stratiform evaporite units, and evaporitic components derived from these (e.g., diagenetic cements) were preserved until late in the basin history. We contend that the in situ evaporates act as a seal for convecting brines and contribute to the salinity of the system, and the diagenetic components preserve early permeable fluid pathways.
- Subsequent sag phase shales and carbonates have low sedimentation rates and restricted thickness. This provides a stable thermal regime and time for protracted fluid flow and burial to optimum depths for generation, local migration and trapping/preservation of hydrocarbons. These act as the reductant for oxidised metalliferous brine using similar fluid pathways.

- Although the AFB was chosen as the Australian analogue for the ZCB, it is now apparent that the basin fill is thicker and has a more complex multi-cyclic history.
- A problem with appraising the AFB in terms of its potential to host strictly ZCB style deposits, is that the potential host rocks at the base of the stratigraphy are only exposed in two inliers through the overlying basin fill, and as clasts in diapiric breccias. It may be significant that as far as we are aware, no Cu mineralised black shale clasts have been reported. However, we propose that the most prospective areas of this covered basal sequence would be at the basin margins of outside the zone of salt diapirism. In some of these areas, for example in the Northwest Fault – Torrens Hinge Zone region, the overlying stratigraphic units are thinned and the style of folding is such that the target stratigraphy may be at relatively shallow depths.

A critical question at the close of the P544 research, is whether large stratiform Cu deposits of this type are restricted to the precise tectono-stratigraphic setting in which they occur in the ZCB and PK (and if so why?) or, for example, are organic-rich units higher in the stratigraphy also potential Cu hosts? The answer lies in the correct interpretation of the deposits to the north in the DRC. The origin of these deposits is contentious, at least in part because they are breccia-hosted, but in some models they represent allocthonous pieces of mineralised lower Roan, in which case the answer to the question posed above is yes, and in others the host mine sequence is a separate stratigraphic entity, in which case the answer is no.

References

Annels, A. E. 1979. The genetic relevance of recent studies at Mufulira Mine, Zambia. Ann. Soc. Geol. Belg., v 102, p. 431-449.

Garven, G. and Bull, S. 1999. Fluid flow modelling of the HYC ore system, McArthur Basin, Australia. In Stanley, C.J. (ed.) Proceedings of the Fifth Biennial SGA Meeting and the Tenth Quadrennial IAGOD Symposium, Longdon, UK, August 22-25.

Hanor, J. S. 1999. Geochemistry and origin of metal-rich brines in sedimentary basins. In CODES Special Publication 2. Basins Fluids and Ores, p. 129-146.

Hill, A. C. and Walter, M. R. 2000. Mid-Neoproterozoic (~830-750 ma) isotope stratigraphy of Australia and global correlation. Precambrian Research, v. 100, p. 181-211.

Hitzman, M. W. 2000. Source basins for sediment-hosted stratiform Cu deposits: implications for the structure of the Zambian Copperbelt. J. African Earth Sci. v 30 (4), p. 855-863.

Jowett, E. C. 1986. Genesis of the Kupferschiefer Cu-Ag deposits by convective flow of Rotlegende brines during Triassic rifting. Econ. Geol. v. 81, p. 1823-1836.

Ludwig, H. and Rentzsch, J. 1967. Dans Sanderzproblem. Ein beitrag zur genese des Kupfershiefers. Ber. DGGW, Reihe B, p. 1-12.

Maiden, K. J. 1989. structural traps for stratabound Cu deposits in the Mount Gunson area, South Australia. In Sediment-Hosted Stratiform Cu Deposits: Geological Association of Canada Special Paper 36, p. 543-554.

Neumann N., Sandiford M. & Foden J. in press Regional geochemistry and continental heat flow: Implications for the origin of the South Australian heat flow anomaly.

Peryt, T. M. 1989. Basal Zechstein in southwestern Poland: sedimentation, diagensis, and gas accumulations. . In Sediment-Hosted Stratiform Cu Deposits: Geological Association of Canada Special Paper 36, p. 601-624.

Preiss W. V. (compiler) 1987. The Adelaide Geosyncline-late Proterozoic stratigraphy, sedimentation, palaeontology and tectonics. Geological Survey of South Australia, Bulletin 53, 438 p.

Rentzsch, J. 1974. the Kupferschiefer in comparison with the deposits of the Zambian Copperbelt. Centrenaire de la Societe de Belgique Gisements Stratiformes et Provinces Cupriferes, Liege, p. 395-418.

Rickard, D. T., Willden, M. Y., Marinder, N. E. and Donnelly, T. H. 1979. Econ. Geol. v. 74, p.1255-1285.

Selley, D. 2000. Geological framework and copper mineralisation in South Australia. In AMIRA/ARC project P544, Proterozoic sediment-hosted copper deposits, Report 2.

Warren, J. K. 1997. Evaporites, brines and base metals: fluids, flow and 'the evaporite that was'. Aust. J. Earth Sci. v. 44, p. 149-183.

Wendorff, M. 2001. New exploration criteria for 'megabreccia'-hosted Cu-Co deposits in the Katangan belt, central Africa. In Piestrzynski et al. (eds.), Mineral Deposits at the Beginning of the 21st Century, proceedings of the 6th biennial SGA-SEG meeting, Krakow, Poland. p. 19-22.

Yang, J., Large, R. and Bull, S. 2001. Numerical simulation of transient hydrothermal fluid migration associated with the formation of mineral deposits in the McArthur basin. In Williams, P.J. (ed.) Extended Abstract of 2001 Hydrothermal Odyssey, 228-229. Townsville, Queensland, May 17-19.

1

Comparison of Cu mineralised basins; the Zambian Copperbelt, the Polish Kupferschiefer, the Adelaide Fold Belt & the Yeneena Basin

Stuart Bull et al

AMIRA /ARC ProjectP544 *Final Sponsors Meeting* *July 2003*

2

Introduction

What we are really asking is what factors are common, on varying scales, to the basins that we know host stratiform sediment-hosted Cu-Co mineralisation

How do we recognise systems with similar potential?

This talk will cover

- **Teconostratigraphy**
- **Evaporites**
- **Hydrocarbons**

AMIRA /ARC ProjectP544 *Final Sponsors*

3

Tectono-stratigraphic setting; ZCB

Mineralised Roan stratigraphy accumulated in an intra-continental rift environment

Relatively thin (<2 km) subaerial to restricted marine succession

Post mineralisation transition to thicker (several km), deep marine succession with less obvious structural control - thermal sag?

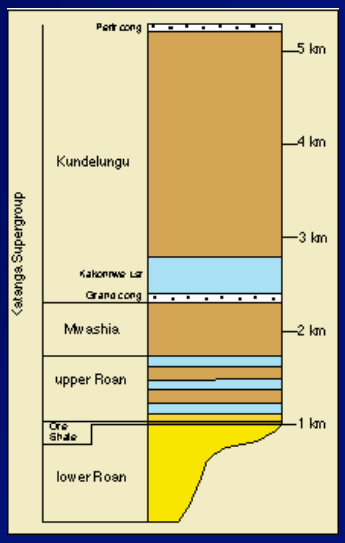

AMIRA /ARC ProjectP544 *Final Sponsors Meeting* *July 2003*

4

Tectono-stratigraphic setting; ZCB

Lower Roan

- arkosic & locally conglomeratic succession
- rapid lateral thickness and facies variation controlled by closely spaced network of normal faults

AMIRA /ARC ProjectP544 *Final Sponsors Meeting* *July 2003*

5

Tectono-stratigraphic setting; ZCB

Ore Shale

- cessation of activity on pre-existing dense normal fault network
- extensive sub-wave base siltstones reflect regional subsidence controlled by widely spaced master faults
- laterally equivalent biohermal carbonates on topographic highs

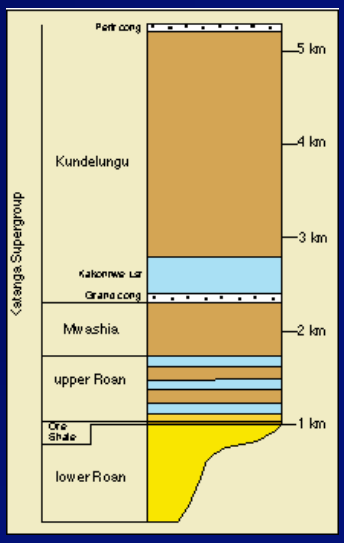

AMIRA /ARC ProjectP544 *Final Sponsors Meeting* *July 2003*

6

Tectono-stratigraphic setting; ZCB

Immediate hangingwall

- layercake stratigraphy
- diverse facies mosaic of coarse- & fine-grained clastics & carbonates deposited in marginal marine environments
- preservation of sulfate evaporites

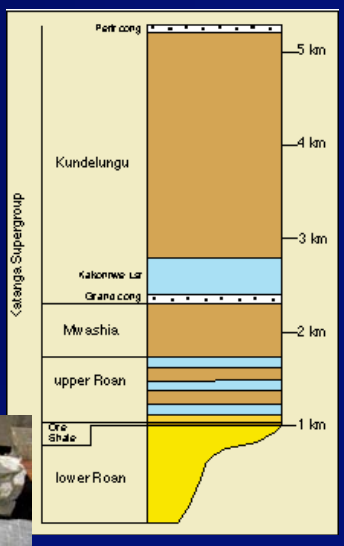

AMIRA /ARC ProjectP544 *July 2003*

7

Tectono-stratigraphic setting; ZCB

Mwashia & Kundelungu

- fine-grained clastics and carbonates
- Open marine - thermal sag phase sedimentation?

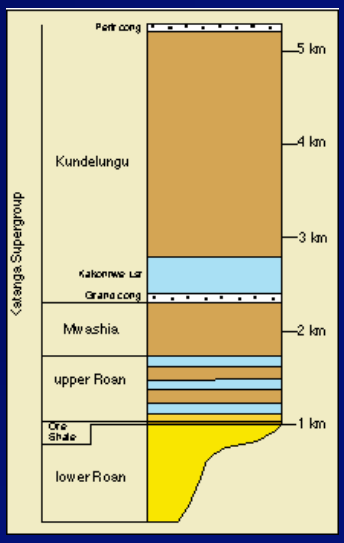

AMIRA /ARC ProjectP544 *Final Sponsors Meeting* *July 2003*

8

Tectono-stratigraphic setting; Kupferschiefer

Relatively thin subaerial to restricted marine succession deposited in an intra-continental rift environment

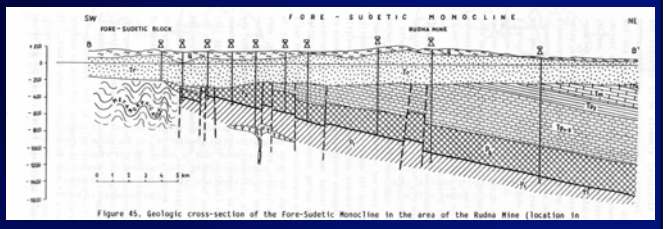

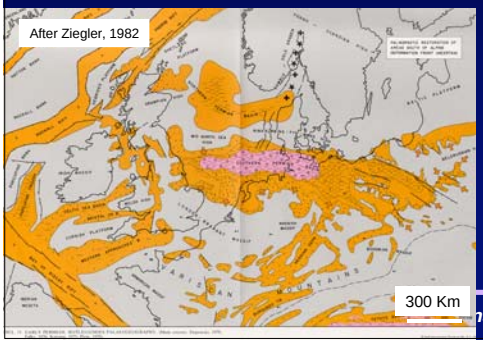

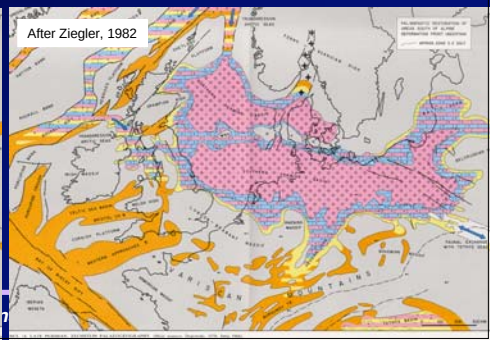

9

Tectono-stratigraphic setting; Kupferschiefer

Rotligendes basal clastic sequence of variable thickness up to ~1 km in the area of the deposits-

In this case includes bimodal volcanics

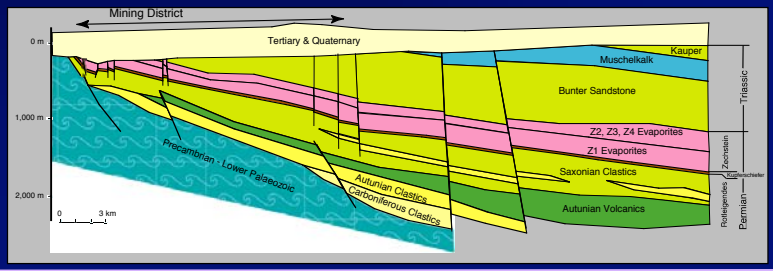

AMIRA /ARC ProjectP544 *Final Sponsors Meeting* *July 2003*

10

Tectono-stratigraphic setting; Kupferschiefer

Abruptly overlain by the Kupferschiefer a thin organic rich shale with carbonate correlates

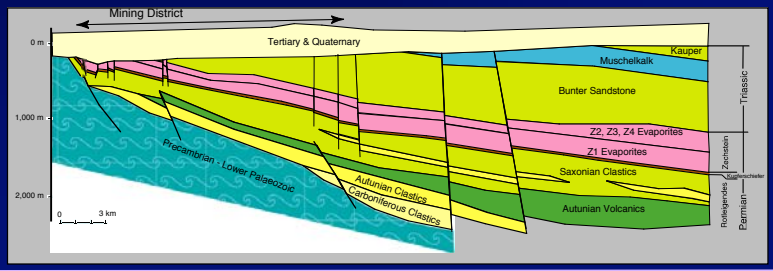

AMIRA /ARC ProjectP544 *Final Sponsors Meeting* *July 2003*

11

Tectono-stratigraphic setting; Kupferschiefer

Overlain by the Zechstein carbonate and evaporitic succession that includes in situ thick massive anhydrite and halite units

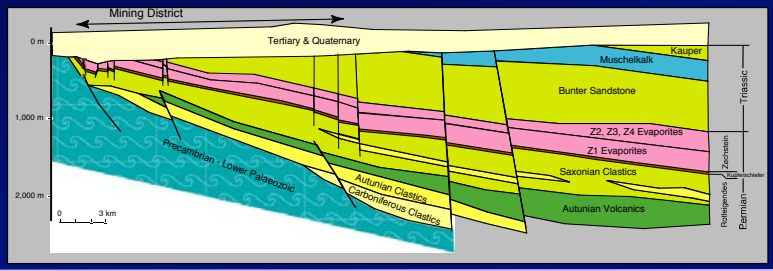

AMIRA /ARC ProjectP544 *Final Sponsors Meeting* *July 2003*

12

Tectono-stratigraphic setting

Summary of empirical characteristics of systems the we know host large scale stratiform sediment-hosted Cu deposits;

- Occur in relatively thin (<5 km) single cycle basin successions deposited during active rifting and subsequent thermal sag in continental - marginal marine environments
- Sulfides focussed in and around an organic-rich unit abruptly overlying the basal rift clastics
- Hangingwall evaporitic and carbonate succession
- Subsequent sag phase shales and carbonates have low sedimentation rates and restricted thickness

Can we really restrict ourselves to this precise tectonostratigraphic setting (and if so why?) or, for example, are organic-rich units higher in the stratigraphy also potential Cu hosts?

AMIRA /ARC ProjectP544 *Final Sponsors Meeting* *July 2003*

13

Tectono-stratigraphic setting; Adelaide Fold Belt

- Intra-continental rift setting - complex (multi-phase) basin succession
- Glacial deposits in third basin cycle (~ Kundelungu) = much thicker basin fill
- Dynamic thermal history - high heat producing basement granites and a thick basin fill that provides insulation
- Thermal regime perturbed by extensive salt migration (tectonism) in the basin centre where Cu deposits spatially associated with salt diapirs

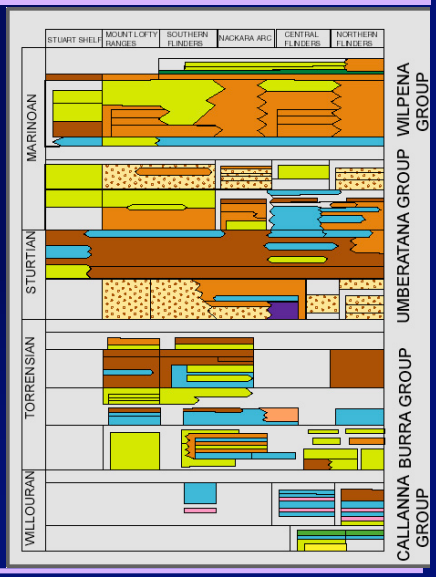

AMIRA /ARC ProjectP544 *Final Sponsors Meeting* *July 2003*

14

Tectono-stratigraphic setting; Adelaide Fold Belt

- Tapley hill Formation Cu deposits on the Stuart Shelf have been interpreted as Kupferschiefer-style

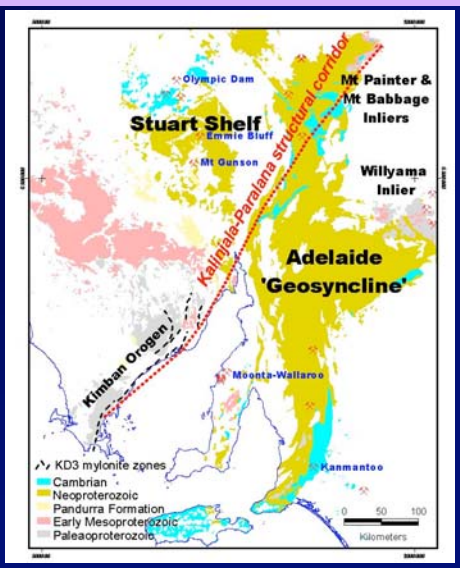

AMIRA /ARC ProjectP544 *Final Sponsors Meeting* *July 2003*

15

Tectono-stratigraphic setting; Adelaide Fold Belt

Reduced trap rocks in the Umberatana Group occur higher in the basin stratigraphy than the ore hosts in the Polish system or the ZCB

On the Stuart Shelf there is no significant footwall rift-phase

Difficult to see how the type of Cu mineralising processes that we are proposing could have operated at Umberatana time

Good time in basin history for stratiform Zn deposits

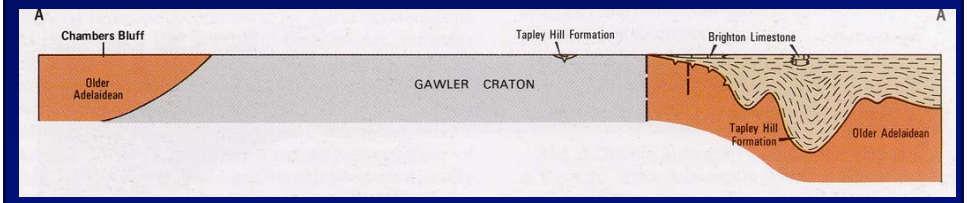

AMIRA /ARC ProjectP544 *Final Sponsors Meeting* *July 2003*

16

Tectono-stratigraphic setting; Adelaide Fold Belt

Basal Callanna and Burra Groups below the glacials are probable chronostratigraphic Roan correlates

Have the right ingredients

- Deposited during active rifting - basal clastic aquifer succession
- Reduced and evaporitic units are present

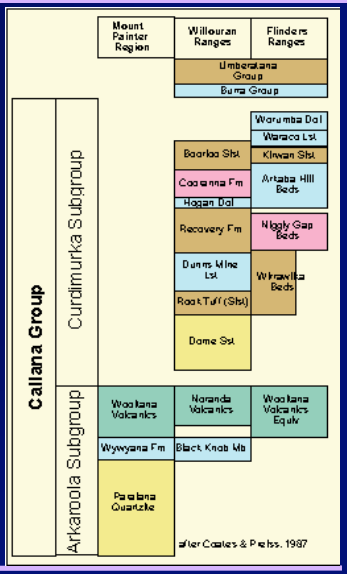

AMIRA /ARC ProjectP544 *Final Sponsors Meeting* *July 2003*

17

Tectono-stratigraphic setting; Adelaide Fold Belt

Problem is because they are at the base of a much thicker basin fill - largely covered by younger basin phases during sedimentation

Delamarian inversion involved a regional decollement within the evaporitic levels of CG - leaves few windows into the lower stratigraphy

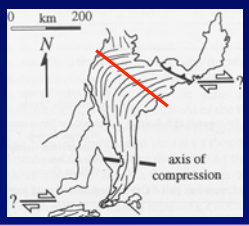

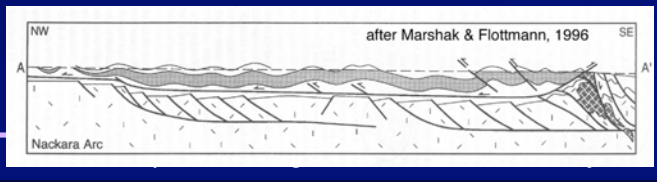

AMIRA /ARC ProjectP544

18

Tectono-stratigraphic setting; Yeneena Basin

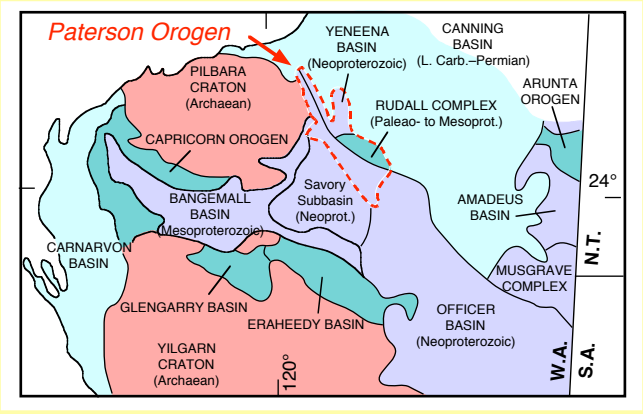

AMIRA /ARC ProjectP544 *Final Sponsors Meeting* *July 2003*

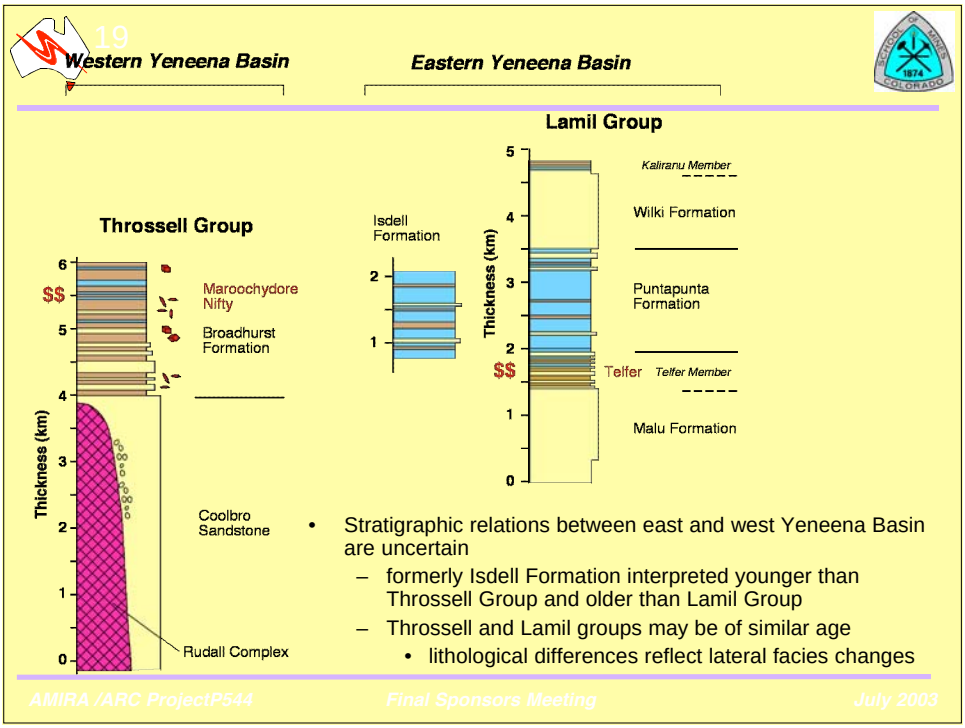
19
Western Yeneena Basin
Eastern Yeneena Basin
Lamil Group
Throssell Group
Isdell Formation
Thickness (km)
Kaliranu Member
Wilki Formation
Puntapunta Formation
Telfer
Telfer Member
Malu Formation
Maroochydore
Nifty
Broadhurst Formation
Coolbro Sandstone
Rudall Complex
• Stratigraphic relations between east and west Yeneena Basin are uncertain
– formerly Isdell Formation interpreted younger than Throssell Group and older than Lamil Group
– Throssell and Lamil groups may be of similar age
• lithological differences reflect lateral facies changes
AMIRA /ARC ProjectP544
Final Sponsors Meeting
July 2003

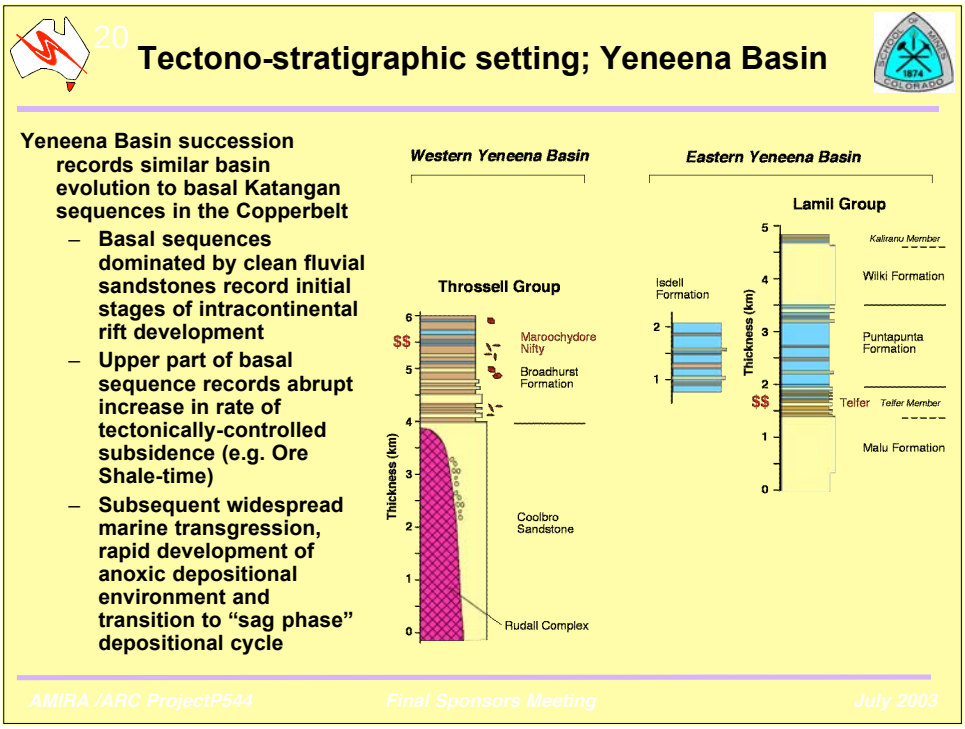
20
Tectono-stratigraphic setting; Yeneena Basin
Yeneena Basin succession records similar basin evolution to basal Katangan sequences in the Copperbelt
– Basal sequences dominated by clean fluvial sandstones record initial stages of intracontinental rift development
– Upper part of basal sequence records abrupt increase in rate of tectonically-controlled subsidence (e.g. Ore Shale-time)
– Subsequent widespread marine transgression, rapid development of anoxic depositional environment and transition to "sag phase" depositional cycle
Western Yeneena Basin
Eastern Yeneena Basin
Lamil Group
Throssell Group
Isdell Formation
Thickness (km)
Kaliranu Member
Wilki Formation
Puntapunta Formation
Telfer
Telfer Member
Malu Formation
Maroochydore
Nifty
Broadhurst Formation
Coolbro Sandstone
Rudall Complex
AMIRA /ARC ProjectP544
Final Sponsors Meeting
July 2003

21

Evaporites

AMIRA /ARC ProjectP544 *Final Sponsors Meeting* *July 2003*

22

Evaporites; Polish Kupferschiefer

Zechstein evaporites still in-situ

Don't need local salt tectonsim to produce Cu deposits

Evaporites act as regional seal and contribute salt and sulfate to the mineralising fluids

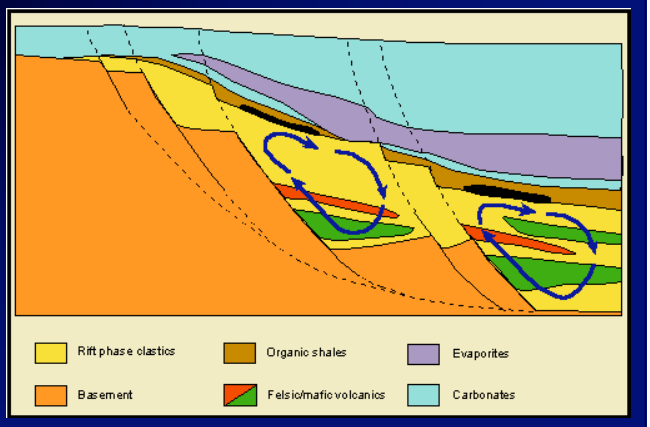

AMIRA /ARC ProjectP544 *Final Sponsors Meeting* *July 2003*

23

Evaporites; Polish Kupferschiefer

Why do the known Cu deposits occur in areas where salt remains effectively in situ?

Hanor, 1999 Gulf Coast work

- margin where evaporites remain in-situ at base of section salinity increases linearly with depth to values of >350g/l
- salinities substantially reduced in basinal areas where salt diapirism has occurred (100-150g/l)

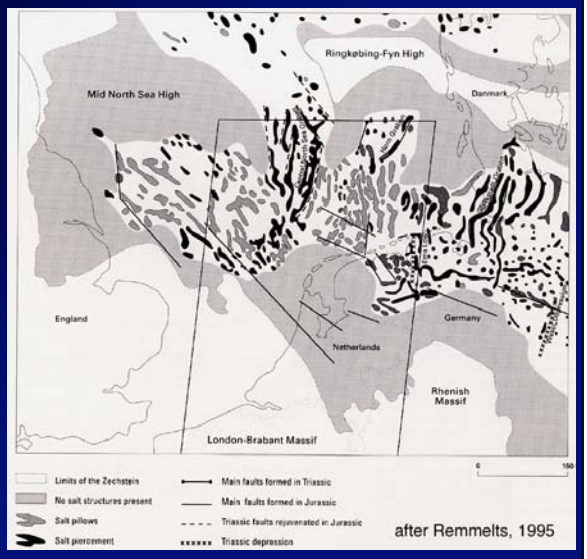

AMIRA /ARC ProjectP544 *Final Sponsors Meeting* *July 2003*

24

Evaporites; Zambian Copper Belt

Evidence of evaporitic processes in the upper ore shale and hangingwall in the form of evaporitic sedimentary facies (eg. Rokana Evaporites)

However main salt units now represented by extensive breccia bodies primarily in the upper Roan

AMIRA /ARC ProjectP544 *Final Sponsors Meeting* *July 2003*

25

Evaporites; Zambian Copper Belt

Significance of sulfate retained to present day?

Unusual situation in Proterozoic basins - other examples include Officer/Amadeus Basin central Australia, Grenville and Bylott Supergroups Arctic Canada

Preservation of evaporites till late in basin history may help explain one of the geological contradictions of the ZCB?

- Considerable evidence for a relatively late (syn onset of inversion?) timing for the mineralisation
- Ores are stratiform and mineralising fluids seem to be using early diagenetic fluid pathways and to be associated with hydrocarbon accumulations

Persistence of early diagenetic evaporitic cements one factor that could facilitate generation of ~stratiform zones of secondary porosity later in the basin history - enhance potential or Cu mineralisation

AMIRA /ARC ProjectP544 *Final Sponsors Meeting* *July 2003*

26

Evaporites; Adelaide Fold Belt

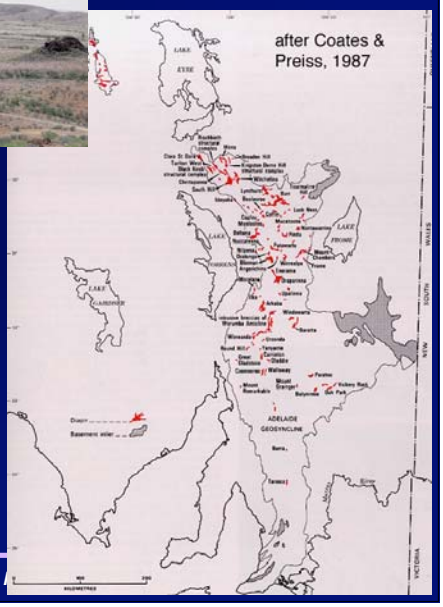

Abundant in the basal Callanna Group

Extensive remobilization (salt tectonics) of evaporitic stratigraphy into diapiric breccias in the basin centre

Peaked coincident with Rodinian breakup

AMIRA /ARC ProjectP544 *Final Sponsors*

27

Evaporites; Adelaide Fold Belt

At what stratigraphic level were the thick mobile evaporites?

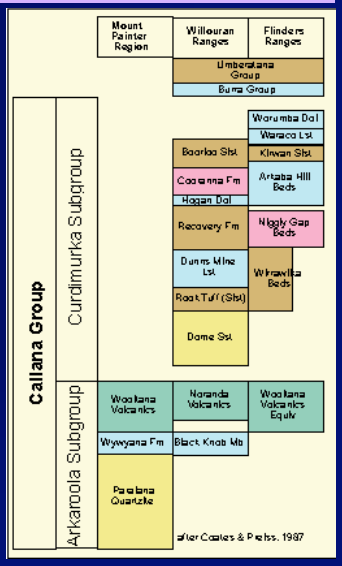

28

Evaporites; Adelaide Fold Belt

Did evaporites remain in situ at the basin margins?

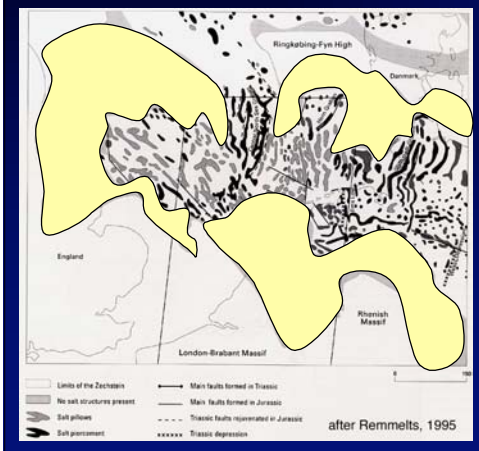

29

Evaporites; Adelaide Fold Belt

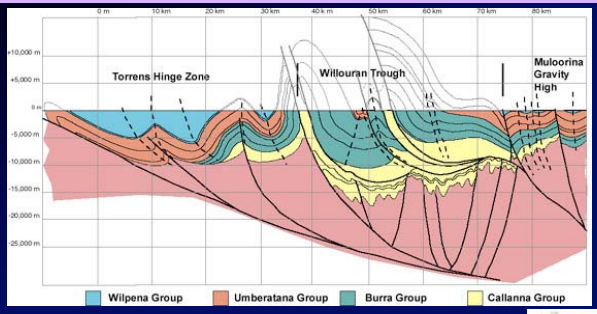

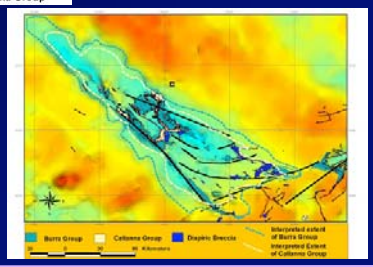

AMIRA /ARC ProjectP544 *Final Sponsors Meeting* *July 2003*

30

Evaporites; Adelaide Fold Belt

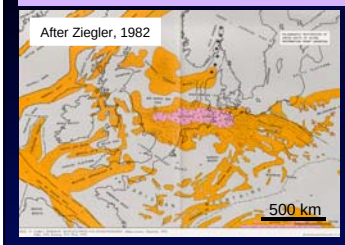

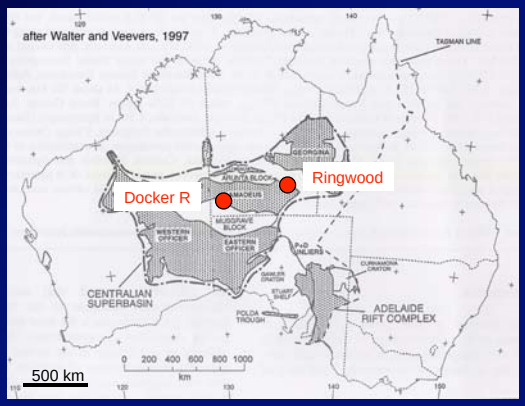

AMIRA /ARC ProjectP544 *Final Sponsors Meeting* *July 2003*

31

Evaporites; Yeneena Basin

- Evaporite minerals (gypsum, anhydrite and halite) of probable diagenetic origin locally developed throughout Broadhurst Formation
- No evidence for thick evaporites anywhere in Yeneena Basin
- If system was deposited on the NW margin of the centralian superbasin they may have been present

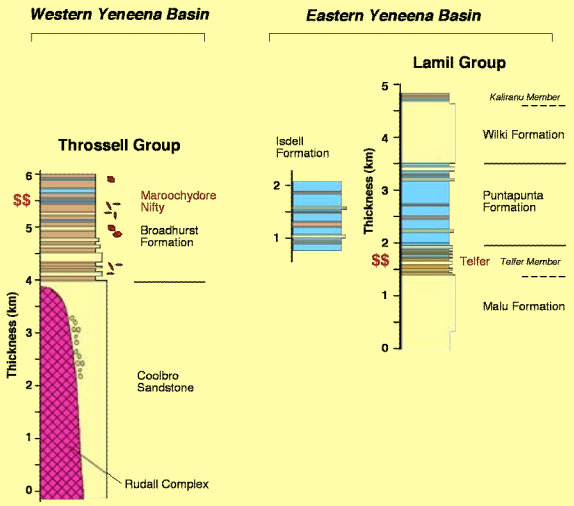

AMIRA /ARC ProjectP544 Final Sponsors Meeting July 2003

32

Hydrocarbons

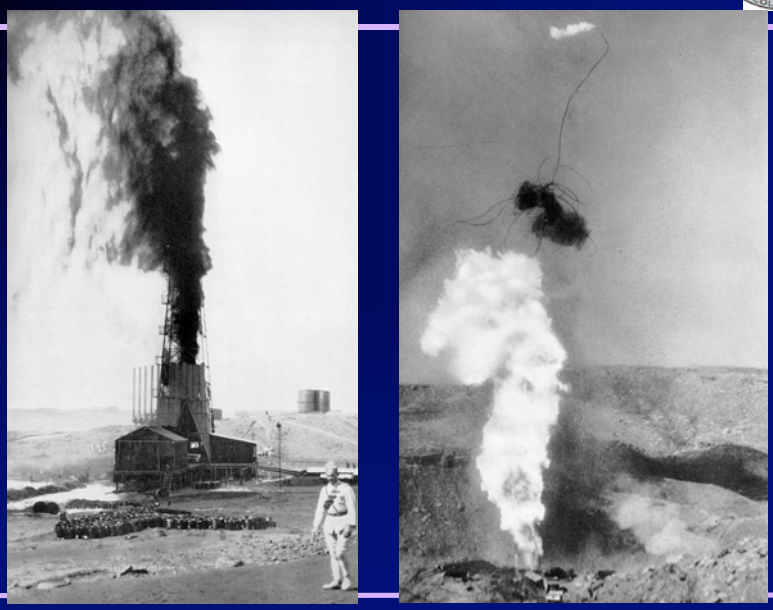

AMIRA /ARC ProjectP544 Final Sponsors Meeting July 2003

33

Hydrocarbons; ZCB

Annels (1978) originally proposed hydrocarbons were involved in the formation of Mufulira

P544 work has taken this further and proposes that hydrocarbons are a critical element in the formation of all Chambishi Basin deposits

Main lines of evidence are

- Geometry and location of the ore bodies within the tectono-stratigraphic architecture of the basin suggests they are after migrated hydrocarbons (footwall) or in situ organic matter (ore shale)
- Light C isotopic values of ore-related carbonates (~TSR)

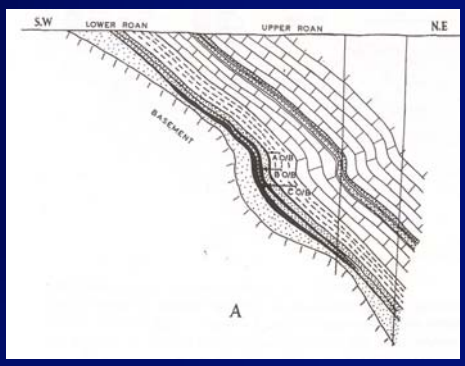

AMIRA /ARC ProjectP544 *Final Sponsors Meeting* *July 2003*

34

Hydrocarbons; Polish Kupferschiefer

The main producing gas reservoir in Europe is the Rotleigendes sandstones in the footwall of the Kupferschiefer that was itself the source of some of the hydrocarbons

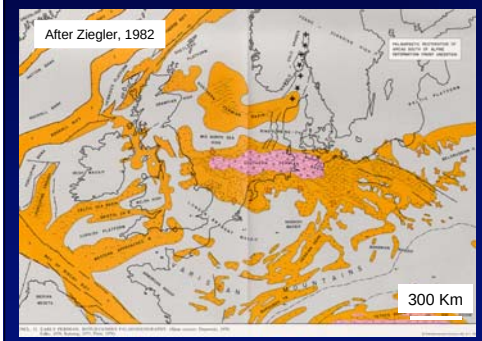

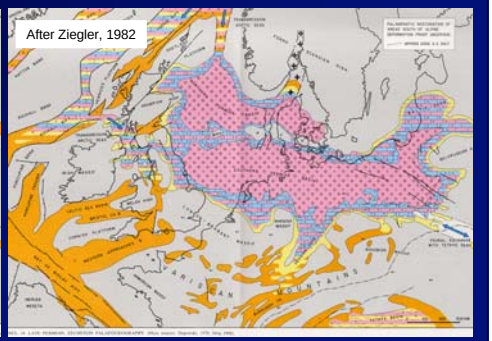

AMIRA /ARC ProjectP544 *Final Sponsors Meeting* *July 2003*

35

Hydrocarbons; Polish Kupferschiefer

Peryt (1989) proposed the Polish examples occupied the same palaeogeographical zones as the Cu sulfide deposits suggesting a common control on location

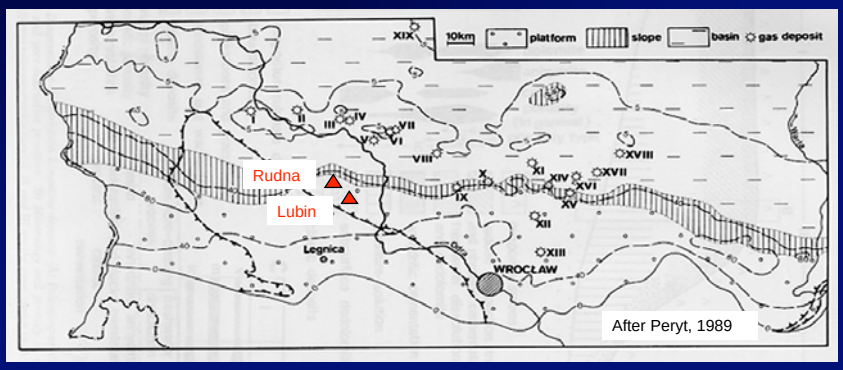

AMIRA /ARC ProjectP544 *Final Sponsors Meeting* *July 2003*

36

Hydrocarbons; Polish Kupferschiefer

Signature of the hydrocarbon association

Lowest C and O in carbonate occur in Cu mineralised zones in the Kupferschiefer (Achim et al., 2001)

- Light C values result from oxidation of organic matter (BSR and TSR)
- C only shifted by ~ 4% (max T attained by Kupferschiefer is ~130°C (Sun & Puttmann, 1997))

AMIRA /ARC ProjectP544 *Final Sponsors Meeting* *July 2003*

37

Hydrocarbons; AFB

Potential source rocks present in Curdimurka (and Arkaroola?) Sub-Groups

Lack of exposure deformation and metamorphism makes petroleum potential difficult to evaluate

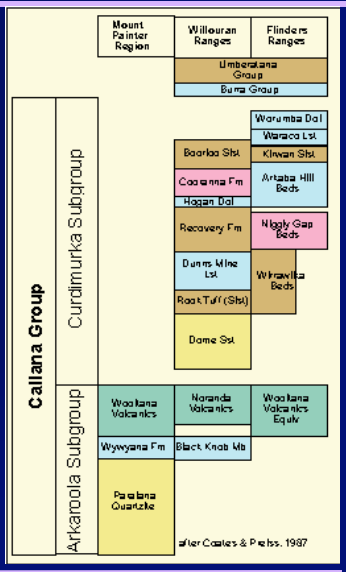

38

Hydrocarbons; AFB

Secular changes in marine C isotopic values have been used to correlate Neopoterozoic basins within Australia and globally

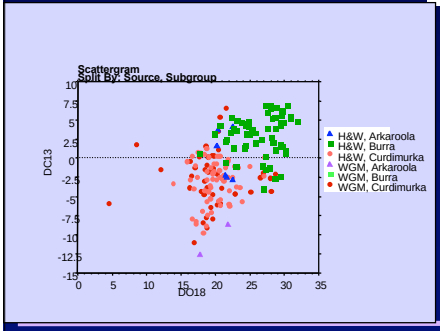

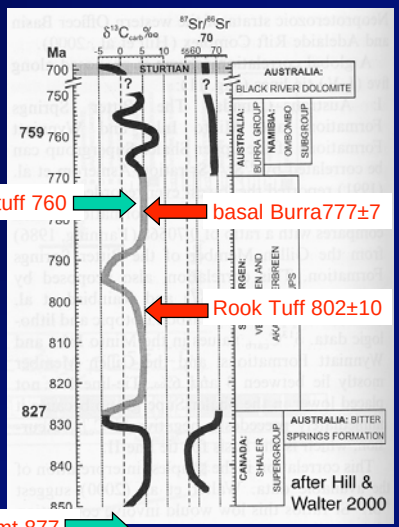

Mwashia tuff 760

basal Burra777±7

Rook Tuff 802±10

NRG bmt 877

39

C & O Isotopes – Callanna & Burra Groups

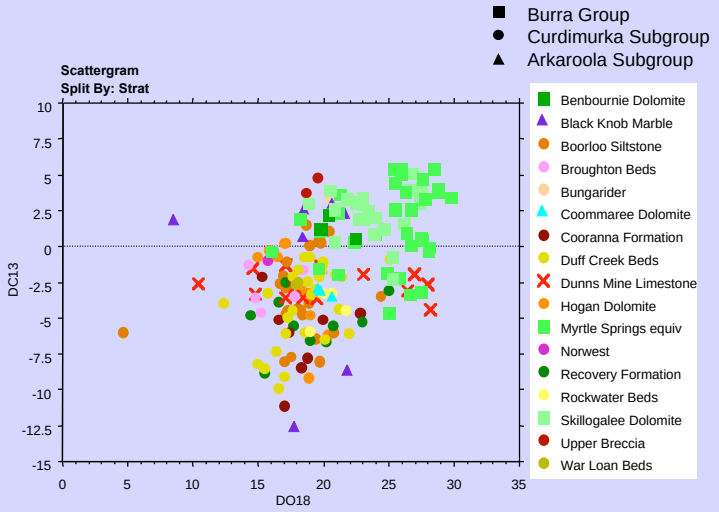

Data from this study and Hills and Walter, 2000

AMIRA /ARC ProjectP544 *Final Sponsors Meeting* *July 2003*

40

Yeneena Basin Carbonate C-O Isotopic signature

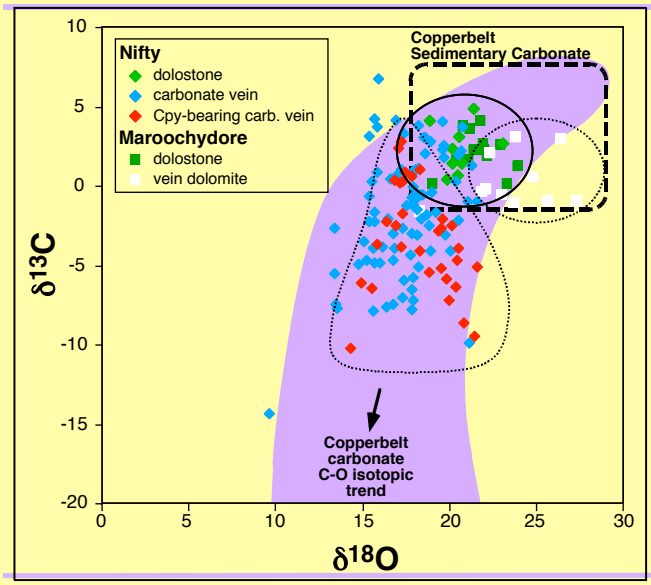

- **Variable C-O isotopic signature of syn-Cu carbonate**
  - **Maroochydore: positive shift in $d^{18}O$ = ppt from 350°C fluid in equilibrium with wall rock carbonate (Reed, 1996)**
  - **Nifty: negative shift in $d^{13}C$ = decarbonation of wall rocks during mineralisation**
- **No strong shift to very light $d^{13}C$ (e.g. -15 – -25 ‰) seen in Zambian Copperbelt**

AMIRA /ARC ProjectP544 *Final Sponsors Meeting* *July 2003*

41

Conclusions

Characteristics of mineralised systems

Occur near the base of relatively thin (<5 km) single cycle basin successions deposited during active rifting and subsequent thermal sag in continental - marginal marine environments

Mineralisation focused in and around an organic rich unit immediately overlying the basal rift clastics

- **redox trap in hydrological communication with footwall aquifer clastics (and basement!)**

Hangingwall in-situ evaporitic succession - preservation of evaporite components till late in the basin history

- **seal and salinity for brines - preserve early permeable pathways**

AMIRA /ARC ProjectP544 *Final Sponsors Meeting* *July 2003*

42

Conclusions

Subsequent sag phase shales and carbonates with low sedimentation rates and restricted thickness

- **stable thermal regime giving time for the system to stew in its own juices**
- **burial to optimum depths for generation, local migration and trapping/preservation of hydrocarbons**
- **act as the reductant for oxidised metalliferous brine using similar fluid pathways**

Can we really restrict ourselves to this precise tectono-stratigraphic setting (and if so why?) or, for example, are organic-rich units higher in the stratigraphy potential Cu hosts?

Answer lies in the Congo

AMIRA /ARC ProjectP544 *Final Sponsors Meeting* *July 2003*

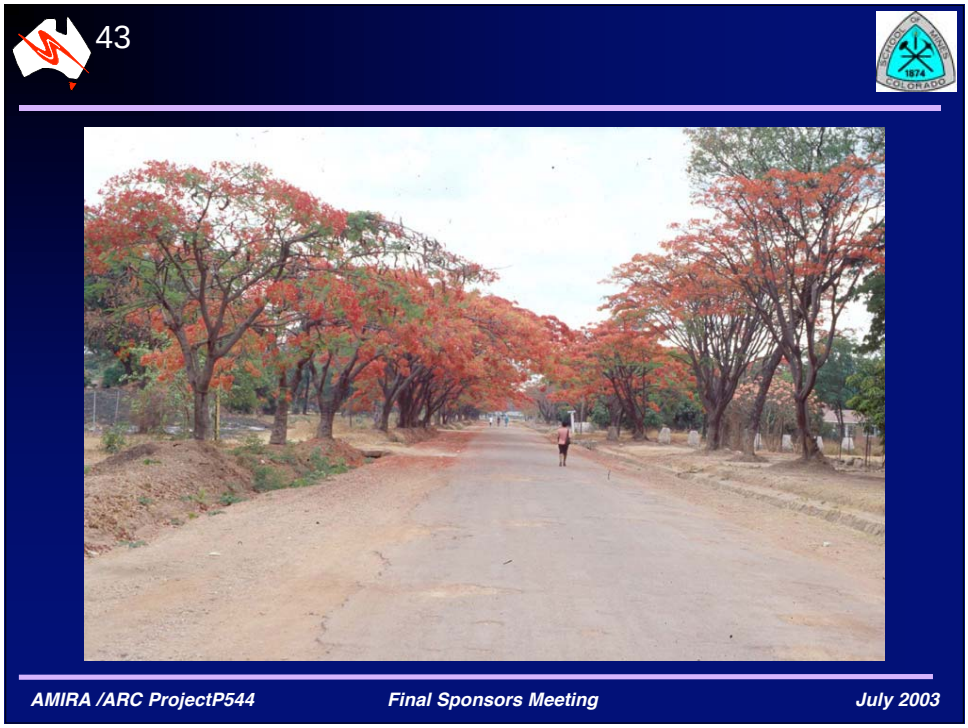
43
AMIRA /ARC ProjectP544
Final Sponsors Meeting
July 2003

Numerical fluid flow, salinity and heat transfer modelling in an attempt to understand basin-scale mineralisation processes in the Zambian Copperbelt

Lyudmyla Koziy, Ross Large, Stuart Bull, Jianwen Yang and Dave Selley
Centre for Ore Deposit Research, University of Tasmania

Summary

As an aid to better understanding fluid flow processes and potential source rocks for the Zambian Copperbelt (ZCB), preliminary numerical fluid flow modelling has been undertaken, coupled to salinity and heat transfer. The computer code used for the modelling is from Yang and Large (2001), and has been previously used to successfully model fluid flow-salinity-heat transfer in the McArthur Basin related to Stratiform Zn–Pb–Ag ore genesis (Large, et al., 2002).

A 43.5 km x 17 km theoretical geological section was constructed, based on our current understanding of the structure, stratigraphy and basin architecture in the ZCB. The geological model section incorporates elements of basement, footwall succession, Ore Shale, hangingwall lower Roan siltstones and carbonates, upper Roan siltstones, carbonates and a layer of salt, Mwashia and overlying Kundelungu shales. Porosity and permeability parameters have been assigned based on our understanding of the sedimentary facies, alteration zones, petrographic evidence and local to regional structures. The most permeable elements assigned in the model are; the Mindola Clastics in the immediate footwall to the Ore Shale; crosscutting breccias in the hangingwall (below salt layer) and fault zones. The least permeable elements assigned are the Ore Shale, hangingwall carbonates and siltstones, the Mwashia shales and the basement.

A one km thick salt layer in the Upper Roan has been assigned a salinity of 30 wt% (the maximum allowable by the computer code). Other sedimentary units have been given lesser initial salinites depending on the interpreted sedimentary environment (evaporitic, marine or lacustrine). A normal geothermal gradient through the basin of 30°C per km has been assumed.

The model has been designed to test fluid flow and temperature gradients associated with the downward flow and convective circulation of saline fluid, from the hanging wall evaporitic salt layer into the Lower Roan stratigraphy and basement. A number of scenarios have been tested by varying the permeability of certain basin elements and fault structures. The results indicate the exciting potential of fluid flow–heat–salinity numerical modelling to test ideas and provide new insights into the ore-forming processes in the ZCB.

Introduction

This preliminary study of fluid flow coupled with heat and salinity transport was undertaken to investigate possible fluid flow pathways in the ZCB, and to determine whether it is feasible to generate large tonnage stratiform sedimentary copper deposits by simple density driven free convection, without appealing to external forces such as gravity drive or tectonic drive. It is not possible, at this stage of our understanding of the ZCB, to construct a balanced cross section of the basin for the time of mineralisation. However, based on our recent work (Broughton, 2003; Bull et al, 2003; Selley et al., 2003), we now know the nature and configuration of the major stratigraphic and structural elements of the

ZCB and this has enabled us to construct a realistic geological model on which to base the numerical flow simulations.

For this modelling exercise we set out to attempt to answer several important questions:

- What is the effect on fluid flow of the interpreted salt layer in the Upper Roan?
- Can fluids circulate deep into the basement, and is the basement a potential source of copper?
- What control do the regional master faults and local basin faults have on temperature distribution and fluid flow?
- What is the effect on fluid flow of changing the permeability of elements of the Roan stratigraphy?
- What is the effect of the hanging wall breccia zones and associated mafic intrusions?

In this preliminary study it was not possible to provide answers to all of these question, however the results provide important insights to many of them.

Numerical modelling methods

We have recently developed a sophisticated finite element computer package using the finite-element Galerkin technique to solve fluid flow, heat transfer and solute transport equations (Yang and Large, 2001). The equations governing density-dependent transport include the Darcy's equation, the continuity equation for the fluid, the solute mass conservation equation, the thermal energy conservation equation, and the constitutive equation related fluid density and viscosity to temperature and salinity. The fluid continuity equation is expressed in terms of *equivalent freshwater head* (Frind, 1982) for the variable density fluid flow system. The details of the computational method, both the principals and the schemes for their implementation into finite element software, are similar to those for pure water hydrothermal system (Yang et al., 1998). In brief, we first update the fluid density and viscosity using the latest salinity and temperature data from the previous time step; then determine the equivalent freshwater head distribution by solving the fluid continuity equation; next we calculate fluid velocity based on the Darcy equation using the updated fluid properties and equivalent freshwater head; and finally we determine the temperature and salinity distribution by solving the thermal energy conservation equation and the solute mass conservation equation respectively. These iteration steps are repeated and not allowed to move on to the next time levels until the preset convergence criteria are satisfied.

A quadrilateral non-orthogonal finite element mesh was designed in such a way as to trace the geometry of hydrostratigraphic units with condensation of grid lines within more permeable units. This made it possible to have a detailed picture of flow, where it is most intensive.

The software being used for the present simulation imposes a restriction onto the size of grid cells; they have to be at least 100 m wide. Because of this restriction, some thin sedimentary units, like the 60 m thick Ore Shale layer, were represented by larger, 100 m wide, finite elements.

Hydrological model of ZCB

A hypothetical geological-hydrological model was developed based on our understanding of basin stratigraphy, structure and basement relationships (Slide 4). The model measures 43.5 km across by 17 km deep and the geological section is a simplified representation of the basin at middle Kundelungu time. Key features include:

(a) a structural framework of first and second order normal faults that control a strongly compartmentalised lower rift clastic succession (Mindola Clastics) and link to a major detachment structure at depth.
(b) An abrupt transition to a thin reduced unit (Ore Shale) that transgresses the normal fault network.
(c) An effectively layercake overlying stratigraphy that includes some clastics (immediately overlying the Ore Shale) but is dominated by carbonates and ultimately shales.
(d) A 1-km-thick halite unit (~salina) in the upper Roan.

The important hydrological units and their assigned permeabilities are listed in Slide 5 and summarised below:

- Basement — given a low permeability due to crystalline and metamorphic nature ($K_H = K_Z = 10^{-16}$ m^2).
- Mindola Clastics — assigned moderate to high permeability due to sandstone and conglomerate lithology ($K_H = 10^{-13}$; $K_Z = 10^{-15}$ m^2), coupled with alteration evidence of extensive fluid flow.
- 'Ore Shale' — assigned a low permeability due to fine grainsize and lack of fractures ($K_H = 10^{-16}$; $K_Z = 10^{-18}$ m^2).
- Hangingwall sandstones and Rokana evaporates; assigned a moderate permeability ($K_H = 10^{-14}$; $K_Z = 10^{-16}$ m^2).
- Upper Roan dolomites; assigned a low permeability due to fine grainsize and early lithification textures ($K_H = 10^{-16}$; $K_Z = 10^{-18}$ m^2).
- Salt layer in Upper Roan at the position of stratiform breccias and albite alteration; assigned a variable permeability from basal layer to top layer:
- Basal layer (where salt is actively dissolved) was given high permeability ($K_H = 10^{-13}$; $K_Z = 10^{-15}$ m^2), middle layer of salt was given a moderate permeability ($K_H = 10^{-14}$; $K_Z = 10^{-16}$ m^2), top layer was given a low permeability ($K_H = 10^{-16}$; $K_Z = 10^{-18}$ m^2)
- Breccias in upper Roan; assigned a very high permeability ($K_H = 10^{-12}$; $K_Z = 10^{-14}$ m^2)
- Lower Mwashia dolomite member; assigned low permeability ($K_H = 10^{-16}$; $K_Z = 10^{-18}$ m^2)
- Upper Mwashia siliciclastic member; assigned moderate permeability ($K_H = 10^{-15}$; $K_Z = 10^{-17}$ m^2)
- Lower and middle Kundelungu forms the uppermost layer of the model; assigned a moderate to high permeability ($K_H = 10^{-14}$; $K_Z = 10^{-16}$ m^2) due to shallow (partly lithified) position in section.
- Faults were assigned a width of 200m and given a high permeability ($K_H = K_Z = 10^{-15}$ 10^{-13}m^2). This was varied in later simulations.

A moderately high geothermal gradient of 30°C/km was used for the modelling, based on the assumption that mineralisation occurred during late diagenesis, and potentially spanned the onset of metamorphism. Thus the initial conditions had T = 445° C at the bottom surface of the model and T = 20°C at the top surface.

The initial salinity profile was chosen based on our interpretation of the basin history (Bull et al., 2003; Selley et al., 2003; Broughton, 2003). The highest salinity was assigned to the salt layer in the Upper Roan (30%NaCl). The next highest salinity was assigned to the clastics in the hanging wall of the ore shale (Roakana Evaporites Member) as they were deposited in a marginal marine sabkha environment (Bull, 2003). The upper Roan dolomites between these two evaporitic successions were assigned a moderate salinity of 10%. As there is evidence for brine reflux associated with the Rokana Evaporites Member, the underlying ore shale, which commonly has sulfate nodules in its upper portion was assigned an initial salinity of 10% in its lower section and 20% in the upper part. To reflect potential additional downward migration of some dense brine, the basement and the footwall clastics were assigned seawater equivalent initial salinities, even though the latter were deposited in largely subaerial environments and would have had meteoric pore waters immediately after deposition.

Previous modelling of salt–brine convection

The first numerical investigation of fluid flow in sedimentary Cu systems is probably that of Jowett (1986) on the Polish Kupferschiefer. This study involved conductive heat flow modelling of a number of geological sections through the area of the mineralisation. The resultant temperatures were then used to calculate the Rayleigh numbers in the area of the Polish mines, to determine whether convective circulation could be expected and to estimate the time required to form the orebodies. Although the effects of salinity were not built into the numerical models in this work, the Zechstein evaporites in the hangingwall of the Kupfershciefer were recognised as the regional seal below which convective fluid flow occurred.

The first fully coupled modelling of fluid, thermal and salinity transfer associated with ore formation in

the form of the McArthur River stratiform Zn deposit in northern Australia has recently been presented by Yang et al. (in press), and is summarised in Large et al (2002). This work showed that because of its effect on the density of the fluids, the distribution of salt within the facies architecture of a basin exerts a strong control on free convective fluid flow patterns. A finite element mesh was used in the study as it enables representation of realistic shaped geological elements, however a limitation of this technique is that the salt unit cannot be modified over the course of a model run. Earlier finite difference modelling by Sarkar et al. (1995) that investigated thermohaline convection in sediments below allochthonous salt sheets in the Gulf Coast had the converse limitation. In these models the salt unit acts as a seal and is progressively eroded with time (e.g. Sarkar 1995). Even though the sediments below the salt layer were given a relatively low vertical permeability (10^{-17} m^2) salt is removed from the base of the sheet at 3–5 m per million years and convective cells develop over a 4 million year period (Slide 6). This implies that if our interpretation of the geology of the ZCB is correct, and ~ 1 km of salt is present in the upper Roan, then this could have supplied salt to basinal fluids, convecting beneath it, for tens of millions of years.

Results and discussion of numerical simulations

Seven separate numerical simulations were run each involving a different case study with different starting parameters, The seven case studies are:

Case 1: Initial conditions as above, with major faults connected through to surface of model, no breccia unit.

Case 2: Major faults are sealed up at the level of Upper Roan Dolomites.

Case 3: As for Case 2 plus permeable breccia unit (k_x=10^{-12} m^2, k_z=10^{-14} m^2) is added in the right-hand side of the section.

Case 4: Permeability of all faults reduced from 10^{-13} m^2 to 10^{-14} m^2 along with the decrease in permeability of the bottom layer of the Upper Roan Salt unit from 10^{-12} m^2 to 10^{-14} m^2.

Case 5: All faults are closed below 9000m (i.e., given same permeability as basement).

Case 6: Isotropic breccia (k_x= k_z=10^{-14} m^2), with all faults closed below 11000 m.

Case 7: Permeability of the faults decreases gradually: k_x= k_z=10^{-14} m^2 above 9000 m, k_x= k_z=10^{-15} m^2 between 9000m and 11000 m, and k_x= k_z=10^{-16} m^2 below 11000 m.

We will not discuss the results of each case study in turn, but have selected particular models to describe, that highlight key features and results, from the modelling.

Model A (Cases 2 & 3)

This model has the starting conditions listed in Slides 4 and 5 and outlined above for Case 3. A breccia unit, with high permeability, was added adjacent to the master fault on the eastern side of the model (Slide 10). The model was run for a period of 1.4 million years, with the following results (Slides 11, 12):

- High salinity brines from the base of the hanging wall salt layer sink down the major faults due to their greater density. (Slide 14)
- The brines sink into the basement, where they are heated and begin to convect. Some brine continues sinking along the faults to depths of 10 to 15 kms, other brines convect up the second order faults, from depths of 5 to 10km, and move into the footwall clastic wedges below the impermeable 'ore shale' (Slide 14)
- The interconnection of the master faults with the deep basement and the Upper Roan salt layer provides an effective mechanism of convective pumping of the heated brine through the basement and then back up and through the Roan sequence. (Slide 13, 14)
- The breccia unit is a focus of major fluid flow, and has a controlling effect on the convection patterns developed in the section (including the basement) below the breccia (Slide 16, 17)

As shown in Slide 12 two major convective flow paths are indicated by the modelling:

Path 1, (black arrows, Slide 12): the master faults control the flow of high salinity brine from the salt layer, through the basement and then back up to the salt layer. Continued dissolution and erosion of the salt layer by the heated brine provides a constant

supply of salinity to the hydrothermal convection cell.

Path 2 (red arrows, Slide 12): the convecting basement brines move up the second order faults and into the footwall clastic wedges of the Lower Roan, where they travel laterally below the impermeable "ore shale". This second path is the one responsible for the copper mineralisation. Copper is leached from the basement by the high salinity heated brines, moves up the second ore faults, and deposits where the Cu-bearing brines come into contact with organic matter in the 'ore shale', or within clastics below the shale.

Graphical analysis of fluid flow in Path 2 through the clastics immediately below the 'ore shale' in the eastern compartment of the model (Slides 17,18; point 2), indicates that after about 1000years the fluids reach a temperature of 210°C, salinity of 10 wt % NaCl and a flow rate of 15 m/yr. Steady state is reached after 1 million years, when the temperature is 260°C, salinity 6 wt% NaCl and flow rates are down to 1 m/yr. These hydrothermal system conditions are compatible with the formation of major copper deposits in and below the shale provided a reductant is present to precipitate the copper sulfide minerals (Slide 23)

Relationship between fluid flow and alteration: The well known temperature and Na/K control on felspar stability suggests that the modelled flow paths may have a relationship to the type of feldspar alteration. Our previous studies (e.g. Large et al., this vol) have shown that K-feldspar alteration characterises the mineralising event, whereas albite alteration is concentrated in the hanging wall breccias and is generally (but not always) unrelated to mineralisation. In Slide 20 it is apparent that albite is generally stable at higher Na^+/K^+ ratio and higher temperature than K-feldspar. Sodic, low temperature, fluids in the salt layer will be in equilibrium with albite. These fluids will cause albite alteration as they sink into the basement and are heated (Slide 20). The basement granites are highly potassic , and this K-felspar will be replaced by albite as the fluids penetrate the basement. This replacement process will cause a gradual decrease in the Na^+/K^+ ratio of the fluids. As the K-enriched fluids rise and cool, they will move into equilibrium with K-felspar, and will cause potassic alteration on their upward trajectory, and as they move laterally through the footwall clastics (Slides 20, 21). Copper deposition will occur in the cooling part of the cycle associated with K-feldspar alteration.

Other Potential ore body sites indicated by the modelling (Slide 26): in addition to the 'ore shale' and footwall clastic wedges, two other sites for potential ore formation are indicated by the modelling:

- Base of the salt layer in the Upper Roan, especially adjacent to the master faults, if a mechanism exists to precipitate sulfides (see next case study)
- Top of the Mwashia or base of Kungelungu where hot metalliferous brines permeate from the top of the faults and cool or react with organic matter. This potential site is revealed by the water/rock ratio simulation in Slide 22, where it is obvious that significant fluid in leaking from the upper terminations of the faults at the Mwashia-Kungelungu contact.

Model B (Case 1)

In this model B the conditions are the same as model A, except for two changes: 1) The master faults are extended through to the top boundary of the model, and 2) the high permeability breccia has been removed from the model.

The results of the model run are shown in Slide 28 (velocity vectors), Slide 30 (temperature contours) and Slide 31 (salinity contours). In summary, cold surface marine fluids flush through the basin via the deep master faults and the aquifers. Saline brines from the salt layer, sink and convect through the lower basin and basement. These two major fluid pathways are shown by the yellow and black arrows in Slide 29. Deep brines, that have circulated through the basement, move up along the secondary faults and are channelled into the clastic footwall wedges to produce Cu ore bodies in and below the 'ore shale' as in Model A. A mixing site is identified as a potential ore body location at the early stages of the simulation (Slide 29), where the cool surface marine fluids convecting through the base of the salt layer, meet with deeper and hotter metalliferous fluids that have cycled through the basement.

Another very significant feature of this model is that the central master fault acts as a discharge fault to the surface. Exhalation of saline brines that have picked up salinity by passing through the salt layer, and leached metals by passing through the basement, could produce SEDEX type Pb–Zn–Cu deposits in the uppermost Kungelungu. The modelling indicates these brines are exhaled at the surface adjacent to the central master fault at temperatures of 150° to 250°C and salinities of 6–12 wt% NaCl.

Model C (Case 7)

Three changes were made to model C, relative to model A: (1) the breccia unit is prescribed to be isotropic, (2) the permeability of the lower salt layer was reduced from $10^{-12}m^2$ to $10^{-14}m^2$, and (3) the permeability of the faults were progressively decreased with depth from $10^{-14}m^2$ to $10^{-16}m^2$, such that the fault permeability was the same as the basement permeability below 11km depth (Slide 33). The changes were made because it was felt that the salt and fault permeabilities used in the previous models were possibly too high, and also to determine whether fluid convection, in the basement, could be stopped by choosing lower fault permeabilities.

The model simulation (Slides 34 & 36) indicates that the low permeabilities selected for the salt layer and faults dampens hydrothermal convection. Fluid flow paths for the early stages of the simulation are shown in Slide 35. The brines take considerably longer to sink into the basement, however with time (after 500,000 years) a broad and deep brine convection system is established, involving both the Roan package and the basement (Slide 37). Hydrothermal fluid temperatures vary from 150° to 350°C across the convection system (Slide 37), and salinity gradually dissipates with time due to the erosion of the salt layer, and mixing with lower salinity basinal fluids (Slide 39). Due to the slower fluid velocities in the convection cells compared with the previous models, development of a large tonnage deposit will involve a much longer period. However the key outcome for this model, is that deep fluid convection involving the basement, is still a viable mechanism to source and leach metals, even when the fault permeabilities have been reduced by one to two orders of magnitude.

Conclusions

- The numerical modelling provides some exciting new insights into the early hydrothermal fluid processes and fluid interaction in the ZCB
- The hanging wall salt layer provides an important source of salinity, and a density contrast to drive brine convection through the basin and underlying basement
- The master faults provide a link between the salt layer and the deep basement, that enables the convection of high salinity brines which have the capacity to leach metals from the basement, and deposit them in and below permeability barriers within the Mindola clastics and "ore shale" package
- Other potential ore body sites are indicated by the modelling; (1)the Upper Roan salt layer and breccias, (2) at the Mwashia–Kungelungu contact adjacent to the terminations of the master faults, and (3) stratiform exhalative deposits in the upper Kungelungu, adjacent to master faults that penetrate the high stratigraphic levels.
- Variations in the permeability of the salt layer and faults leads to changes in the flow paths and time span for effective mineralisation. Reducing the permeability of the master faults dampens the fluid flow, and extends the life of the hydrothermal system. However penetration of brines into the basement remains a key element of the models, even at low fault permeabilities.

References

Broughton, D., 2003, Stratigraphy of the Zambian Copperbelt: AMIRA International P544 Final Meeting Presentation

Bull, S. W., 2003,

Bull, S. W and Selley, D., 2003, Chambishi Basin Studies; Chamishi Southeast Project: AMIRA International P544 Final Meeting Presentation

Frind, E.O., 1982, Simulation of long-term transient density-dependent transport in groundwater: Adv. Water Resources, v. 5, p. 73-88.

Jowett, E. C.,1986, Genesis of Kupfersschiefer Cu-Ag deposits by convective flow of Rotliegend brines during Triassic rifting. Economic Geology, v. 81, p. 1823-1837.

Large, R. R., McGoldrick, P. J., Bull, S. W., Scott, R., and Selley, D.,(2003), Lithogeochemistry and Alteration Halos to Stratiform Copper Mineralisation in the Chambishi Basin, Zambian Copper Belt: AMIRA P5444, Final Report, October, 2003.

Large, R. R., Bull, S., Selley, D., Yang , J., Cooke, D., Garven,

G., and McGoldrick, P. M., 2002, Controls on the formation of giant stratiform sediment-hosted Zn-Pb-Ag deposits, with particular emphasis on the north Australian Proterozoic. In Cooke D. C. and Pongratz J., eds., Giant Ore Deposits; Characteristics, Genesis and Exploration, CODES Special Publication No. 4, University of Tasmania, p. 107-150.

Sarkar, A., Nunn, J. A. and Hanor, J. S. 1995. Free thermohaline convection beneath allochthonous salt sheets - An agent for salt dissolution and fluid flow in Gulf Coast sediments. Journal of Geophysical Research-Solid Earth, v. 100, p. 18085-18092.

Selley, D., Bull, S., Croaker, M., Scott, R., Broughton, D., and Pollington, N., 2003, Development of the Lower Roan basin system, western Kafue Anticline: AMIRA International P544 Final Meeting Presentation

Yang, J., Edwards, R.N., Molson, J.W., and Sudicky, E.A., 1996, Three-dimensional numerical simulation of the hydrothermal system within TAG-like sulfide mounds: Geophysical Research Letters, v. 23, p. 3475-3478.

Yang, J., Latychev, K., and Edwards, R.N., 1998, Numerical computation of hydrothermal fluid circulation in fractured earth structures: Geophysical Jouranal International, v. 135, p. 627-649.

Yang, J., and Large, R.R., 2001, Computational modelling of hydrothermal ore- forming fluid migration in complex earth structures. *in* Xie, H., Wang, Y., and Jiang, Y., eds., Computer Applications in the Minerals Industries: A.A. Balkema Publishers, Lisse, p. 115-120.

Yang, J., Large, R.R., and Bull, S.W., 2001, Numerical simulation of transient hydrothermal fluid migration associated with the formation of mineral deposits in the McArthur Basin. *In* Williams, P.J., eds., A Hydrothermal Odyssey: James Cook University EGRU contribution 59, p. 230.

Yang, J., Bull, S.W., and Large, R.R., in press, Numerical Investigation of salinity in Controlling Ore-forming Fluid Transport in Sedimentary Basins: Example of the HYC Deposit, Northern Australia: submitted to GEOLOGY.

Numerical Fluid Flow, Salinity and Heat Transfer Modelling in an Attempt to Understand Basin-Scale Mineralisation Processes in the Zambian Copperbelt

Lyudmyla Kosiy, Ross Large*, Jianwen Yang, Stuart Bull, Dave Selley & P544 team

AMIRA P544

Aims of Numerical Modelling

- **To test several senarios of fluid flow in the Zambian Basin**
- **In particular to understand the relative importance of certain basin elements on fluid flow:**
  - Salt layer in Upper Roan evaporites
  - Extent and permeability of basin faults
  - Involvement of basement as a source of copper
  - Permeability variations in Roan and overlying sequences
  - Effect of hanging wall breccias

AMIRA P544

Basin Architecture 2D Model

- **A hypothetical model has been developed based on our understanding of the basin stratigraphy, structure and basement relationships**
- **Section measures 50km across X 17km deep**
- **Permeabilities are based on our best estimates from petrography, alteration studies and previous petroleum literature**

AMIRA P544

Basin Architecture 2D Model

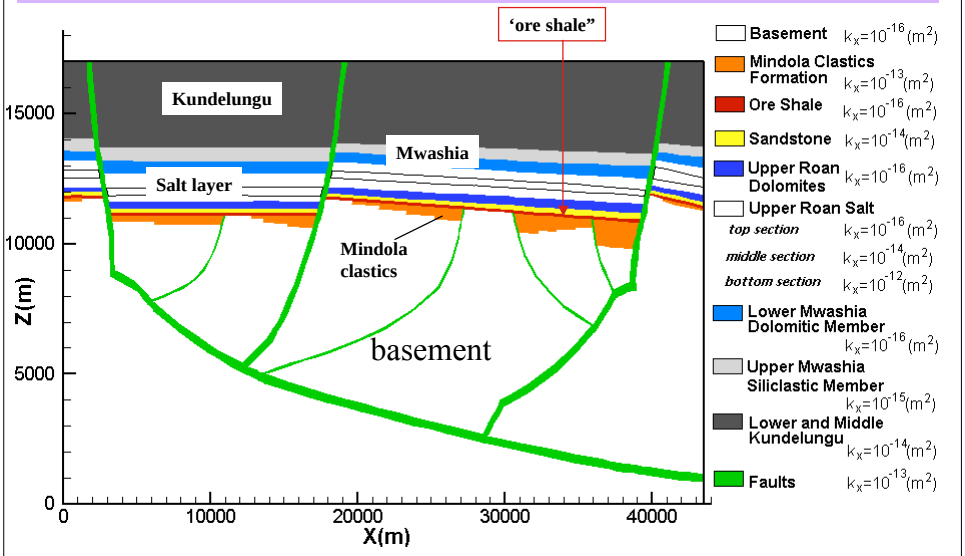

AMIRA P544

Model parameters for flow simulation

rock unit name	colour on the map	permeability in the horizontal direction (m^2)	permeability in the vertical direction (m^2)	thermal conductivity ($Jm^{-1}s^{-1}degree^{-1}$))	initial salinity (‰)
Basement		10^{-16}	10^{-16}	3.0	3.57
Mindola Clastics Formation		10^{-13}	10^{-15}	2.5	3.57
Ore Shale		10^{-16}	10^{-18}	2.5	10.00
Sandstone		10^{-14}	10^{-16}	2.5	20.00
Upper Roan Dolomites		10^{-16}	10^{-18}	2.5	10.00
Upper Roan Salt:					
bottom section		Case1, Case2: 10^{-12} Case3: 10^{-13} Case4, Case5: 10^{-14}	Case1, Case2: 10^{-14} Case3: 10^{-15} Case4, Case5: 10^{-16}	2.5	30.00
middle section		10^{-14}	10^{-16}	2.5	30.00
top section		10^{-16}	10^{-18}	2.5	30.00
Lower Mwashia Dolomitic Member		10^{-16}	10^{-18}	2.5	3.57
Upper Mwashia Siliclastic Member		10^{-15}	10^{-17}	2.5	3.57
Lower and Middle Kundelungu		10^{-14}	10^{-16}	2.0	3.57
Faults		Case1-Case3: 10^{-13} Case4, Case5: 10^{-14}	Case1-Case3: 10^{-13} Case4, Case5: 10^{-14}	2.5	of the surrounding rocks
Breccia (Case3, Case4, Case5)		10^{-12}	10^{-14}	2.5	of the surrounding rocks

AMIRA P544

Testing Salt-Brine Convection

Sub-salt convection after Warren, 1999

Fluids migrating laterally below salt increase in density due to dissolution

Free convection significant even where permeabilities as low as 0.01 md = $1x10^{-17}$ (Sarkar et al., 1995)

- **In this case takes 10 My for steady state convection**
- **3-5 m/My of salt is removed**

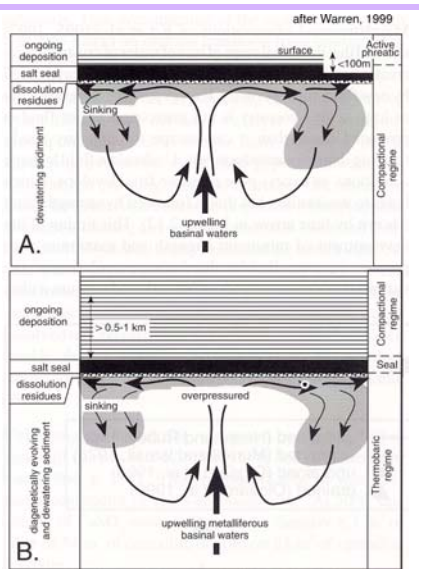

AMIRA P544

Modelling Software

- **Developed by Jianwen Yang at CODES in 2001/02**
- **Used to model hydrothermal brine flow in the McArthur Basin (Yang ,Large and Bull, 2001)**

AMIRA P544

Finite Element Mesh

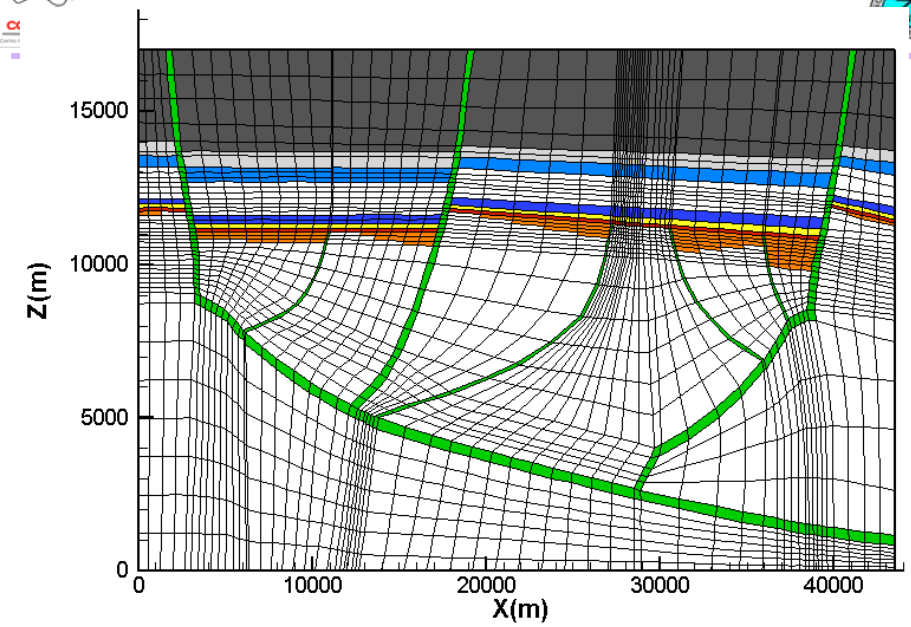

AMIRA P544

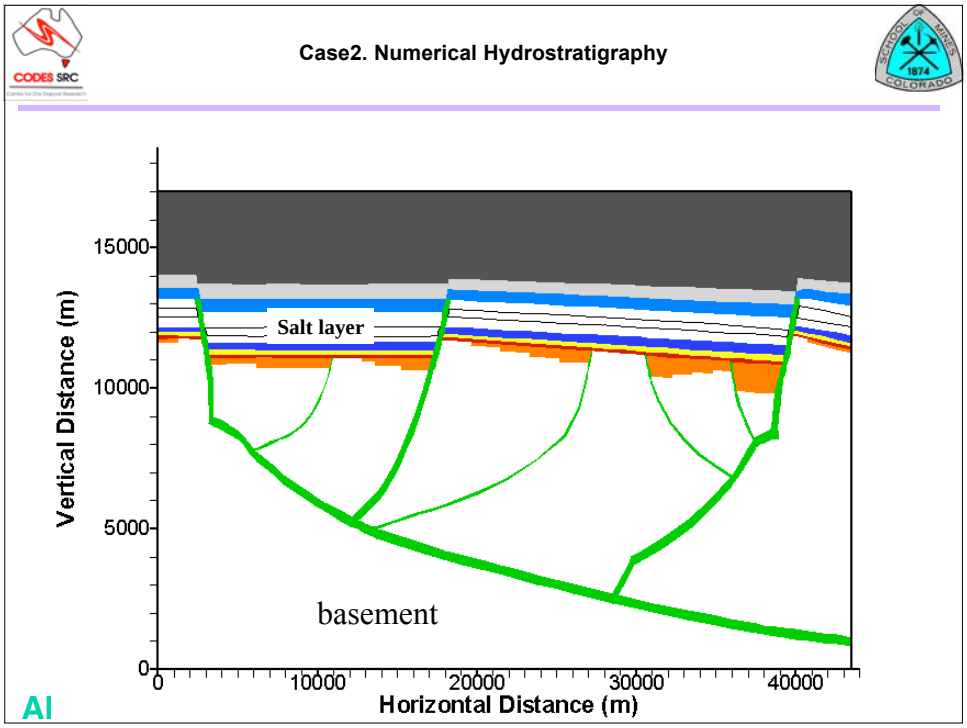
Case2. Numerical Hydrostratigraphy
Salt layer
basement
Vertical Distance (m)
Horizontal Distance (m)
0
5000
10000
15000
0
10000
20000
30000
40000
AI

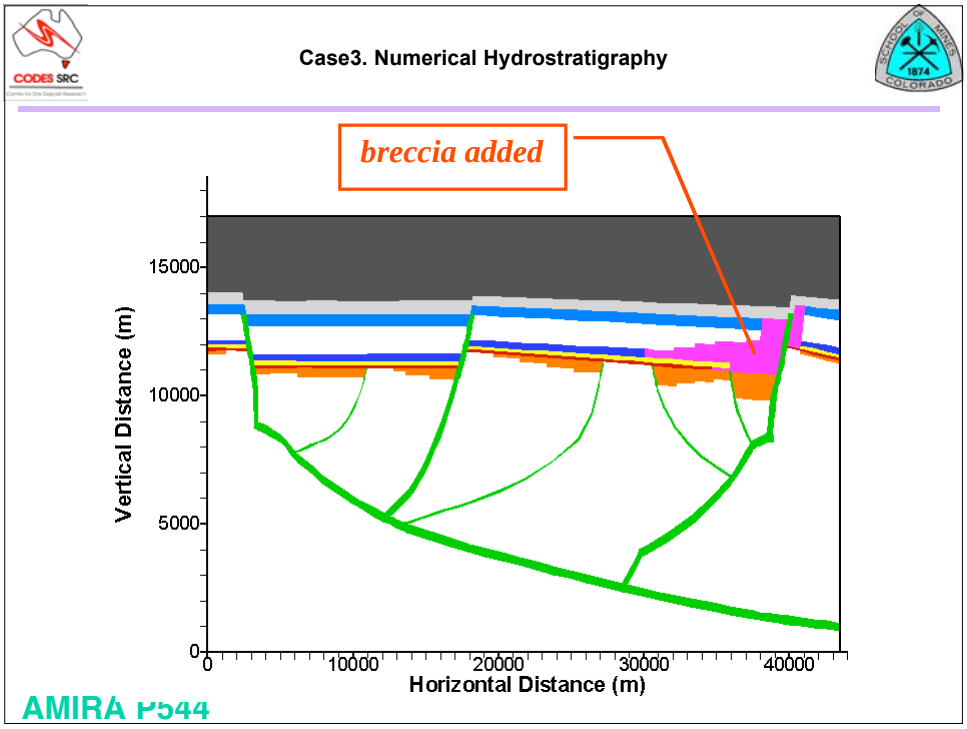
Case3. Numerical Hydrostratigraphy
breccia added
Vertical Distance (m)
Horizontal Distance (m)
0
5000
10000
15000
0
10000
20000
30000
40000
AMIRA P544

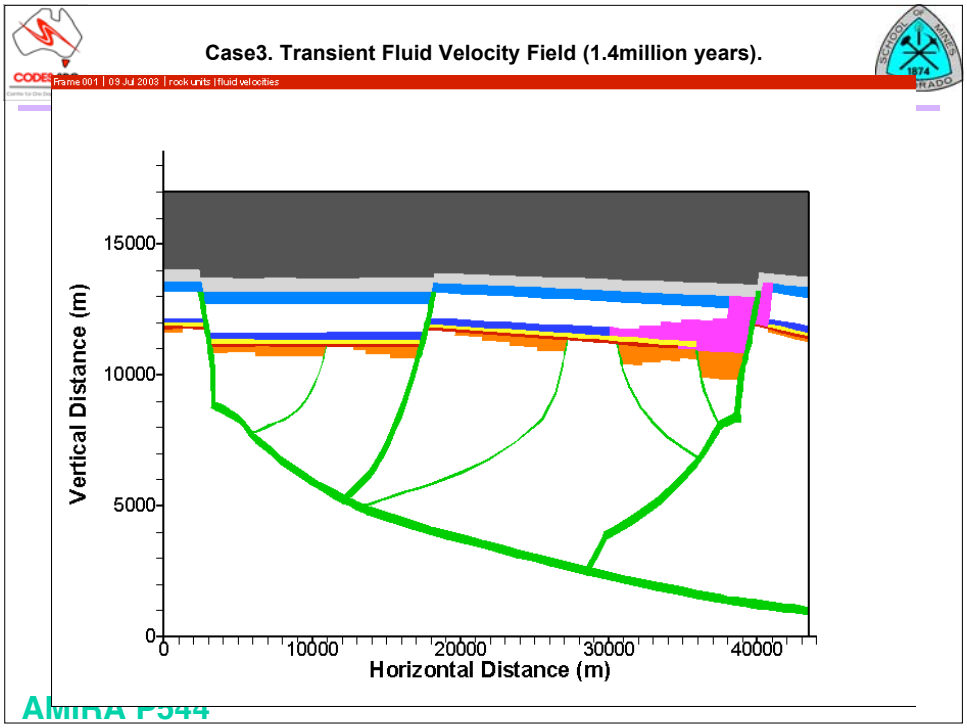
Case3. Transient Fluid Velocity Field (1.4million years).
Frame 001 | 09 Jul 2003 | rock units | fluid velocities
Vertical Distance (m)
15000
10000
5000
0
0
10000
20000
30000
40000
Horizontal Distance (m)
AMIRA P544

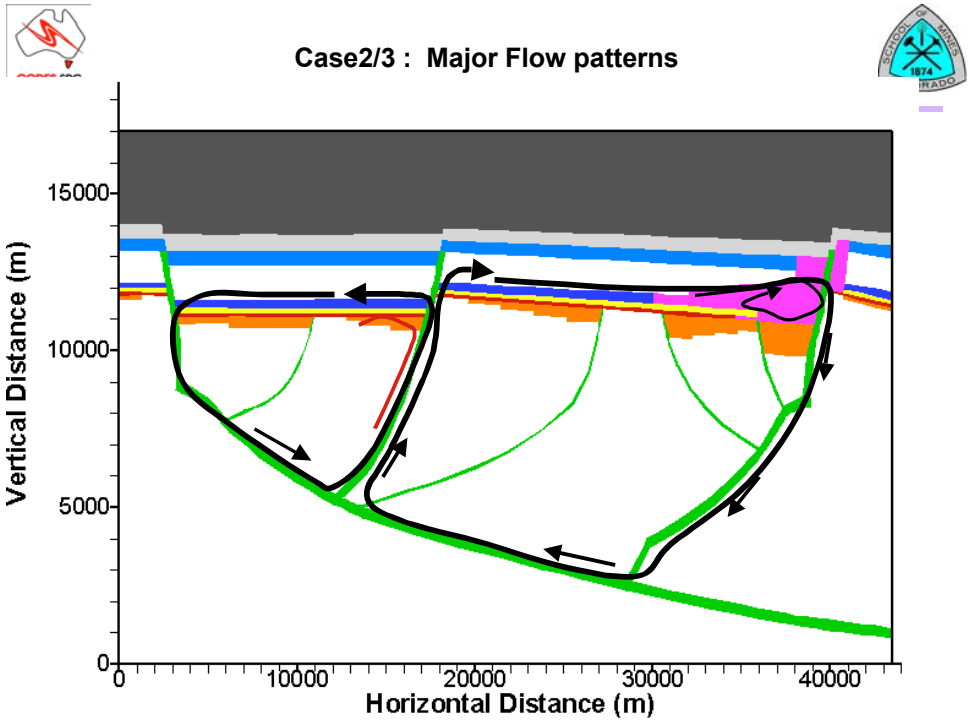
Case2/3 : Major Flow patterns
Vertical Distance (m)
15000
10000
5000
0
0
10000
20000
30000
40000
Horizontal Distance (m)

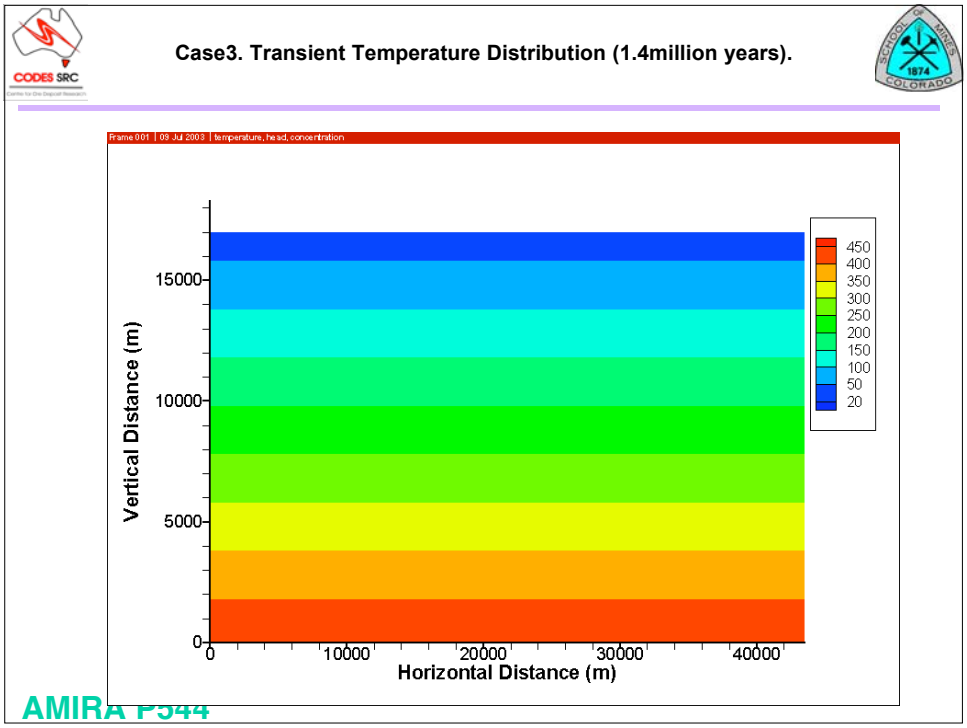
Case3. Transient Temperature Distribution (1.4million years).
Frame 001 | 09 Jul 2003 | temperature, head, concentration
Vertical Distance (m)
15000
10000
5000
0
0
10000
20000
30000
40000
Horizontal Distance (m)
450
400
350
300
250
200
150
100
50
20
AMIRA P544

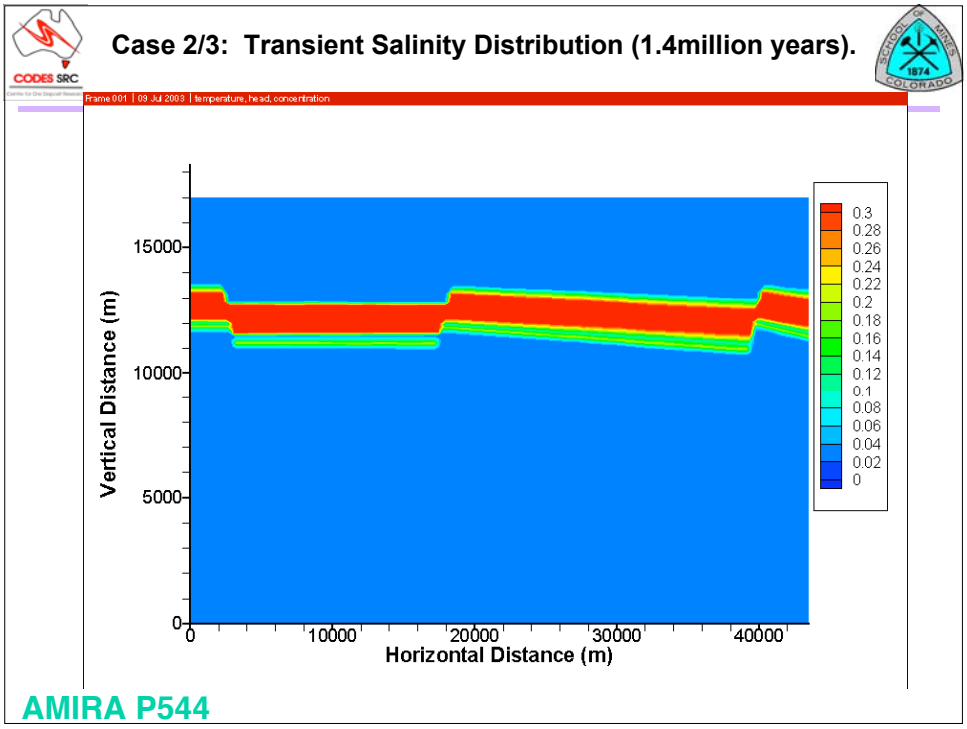
Case 2/3: Transient Salinity Distribution (1.4million years).
Frame 001 | 09 Jul 2003 | temperature, head, concentration
Vertical Distance (m)
15000
10000
5000
0
0
10000
20000
30000
40000
Horizontal Distance (m)
0.3
0.28
0.26
0.24
0.22
0.2
0.18
0.16
0.14
0.12
0.1
0.08
0.06
0.04
0.02
0
AMIRA P544

Interpretation of Case 2/3

- **Brine from salt layer sinks down faults into basement where it heats and begins convecting**
- **The interconnection of master faults and salt layer provides a mechanism of convective pumping of the heated brine through the basement.**
- **This brine has excellent metal leaching capacity**
- **The salt layer is eroded by the convective flow continually providing a powerful heated brine**
- **Secondary faults provide pathways for heated brines to access the Mindola clastics and cause mineralisation in the ore shale and FW clastics**

AMIRA P544

Case3. Detailed Transient Fluid Velocity Field (1.4million years).

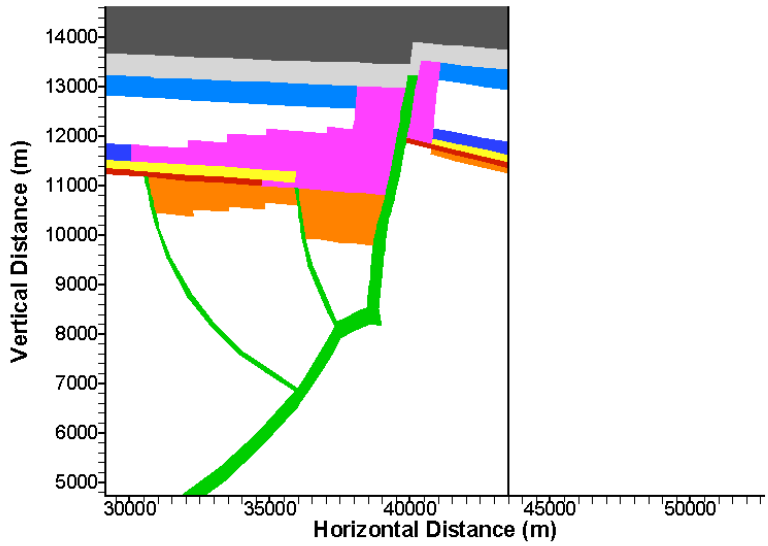

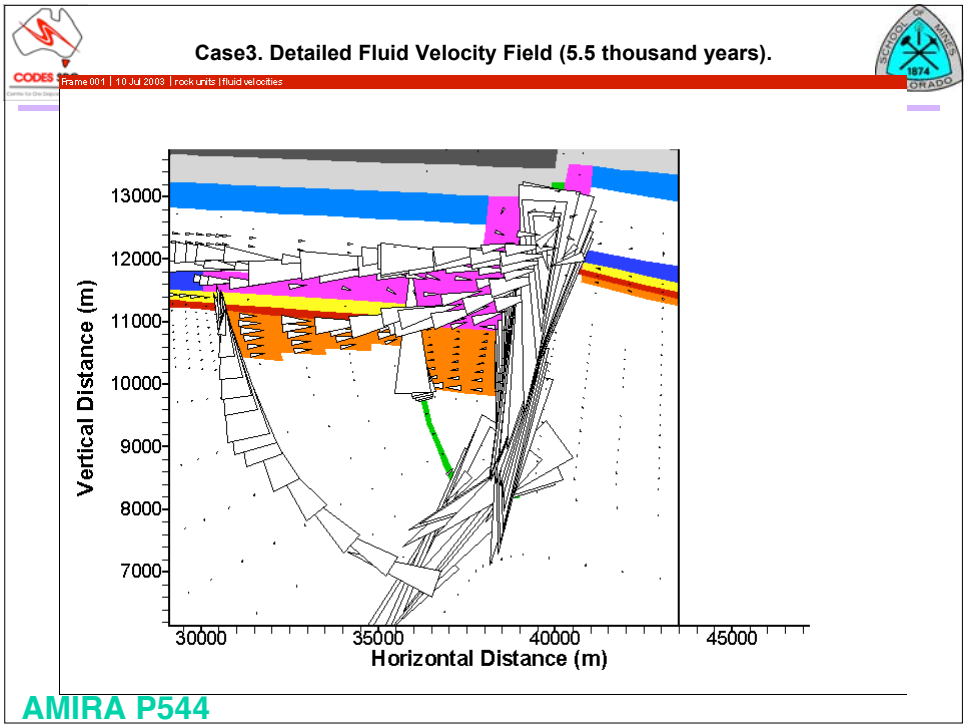
Case3. Detailed Fluid Velocity Field (5.5 thousand years).
Frame 001 | 10 Jul 2003 | rock units | fluid velocities
Vertical Distance (m)
13000
12000
11000
10000
9000
8000
7000
30000
35000
40000
45000
Horizontal Distance (m)
AMIRA P544

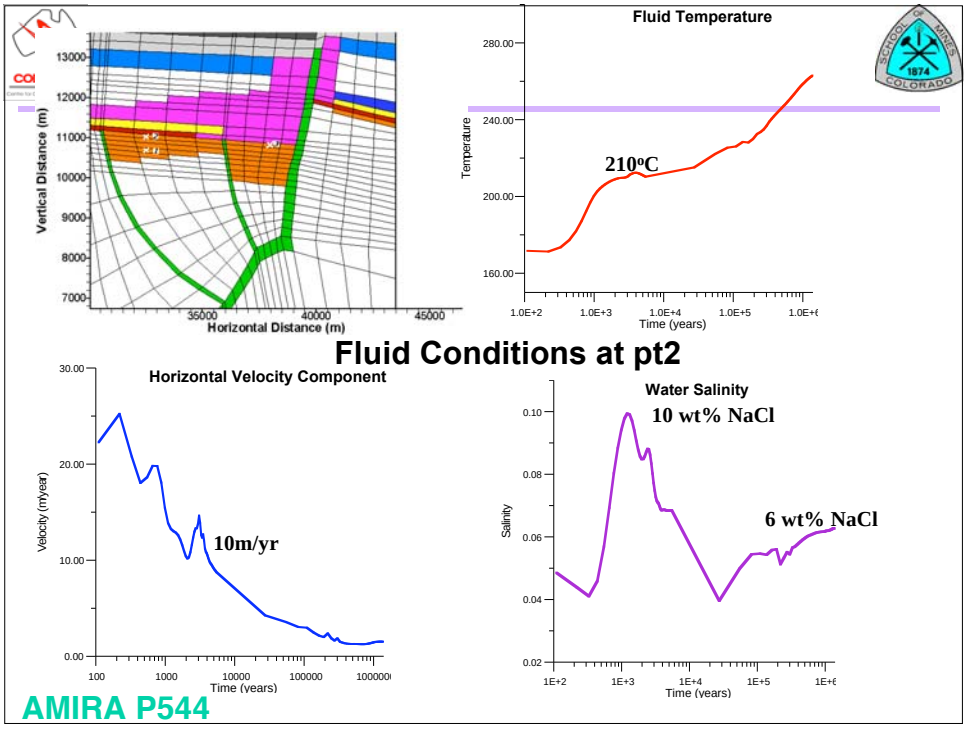
Vertical Distance (m)
Horizontal Distance (m)
Fluid Temperature
Temperature
210°C
Time (years)
Fluid Conditions at pt2
Horizontal Velocity Component
Velocity (m/year)
10m/yr
Time (years)
Water Salinity
10 wt% NaCl
6 wt% NaCl
Salinity
Time (years)
AMIRA P544

Case 2/3: Detailed Transient Salinity Distribution (1.4million years).

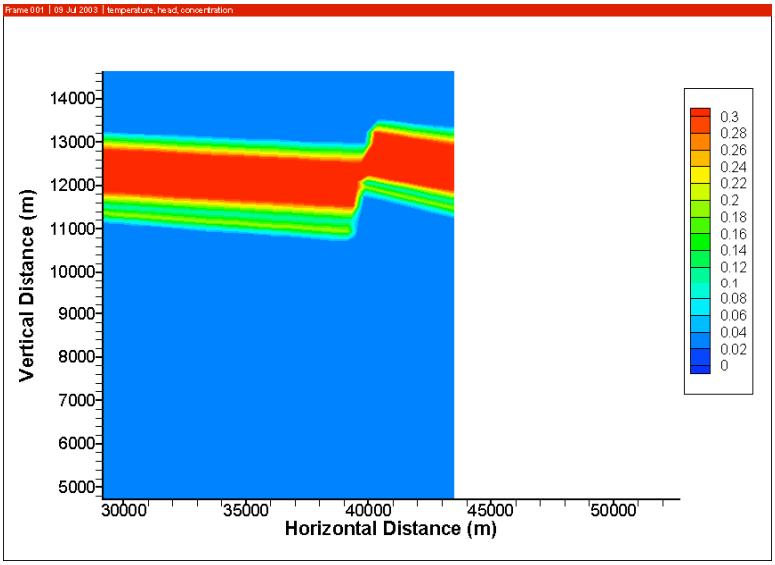

AMIRA P544

Albite - K-feldspar alteration

Convection cycle

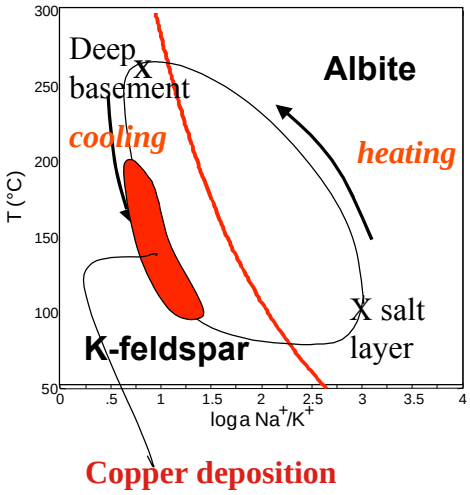

- Albite metasomatism occurs as salty fluid moves down and heats up
- K-felspar metasomatism occurs as fluid moves up from basement and cools
- Cu deposition in favourable horizon in cooling part of cycle associated with K-feldspar alteration

AMIRA P544

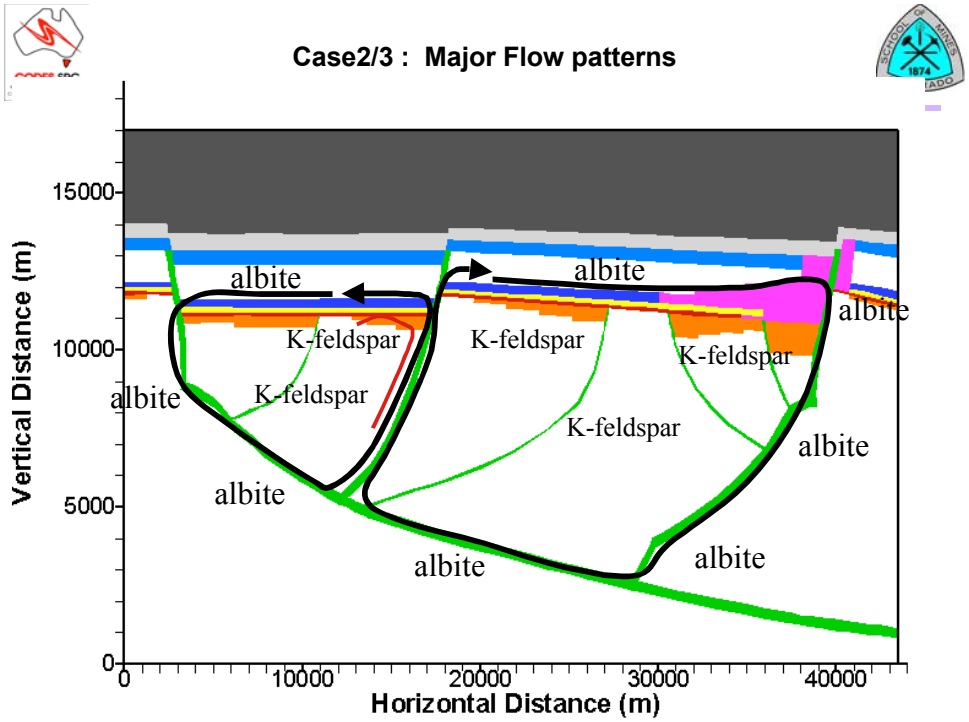
Case2/3 : Major Flow patterns
Vertical Distance (m)
15000
10000
5000
0
0
10000
20000
30000
40000
Horizontal Distance (m)
albite
albite
albite
albite
albite
albite
albite
albite
albite
K-feldspar
K-feldspar
K-feldspar
K-feldspar

Interpretation of Case 2/3

- **Brine from salt layer sinks into lower Roan and basement causing sodium meatsomatism**
- **Brine convects through basement and has potential to leach metals (depending on basement permeability)**
- **Metalliferous brine moves up faults, via convective flow, and into clastics, cooling, and causing K-metasomatism and copper mineralisation (mixing with organic-rich formation waters)**
- **HW breccias have effect of enhancing fluid flow in related FW clastics and basement compartment**

AMIRA P544

Case2/3. Detailed Flow Paths

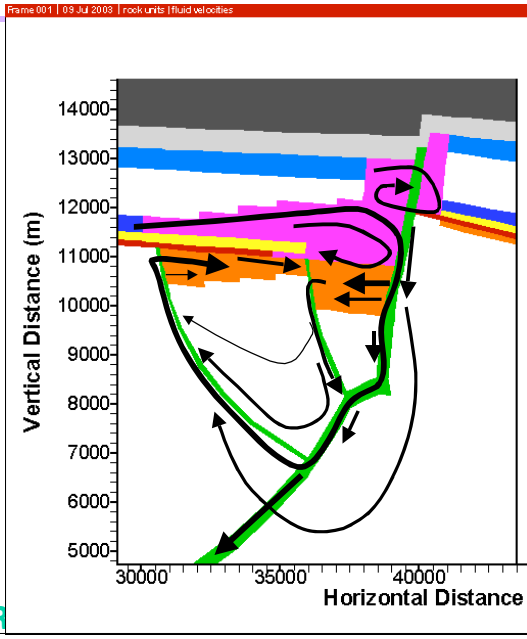

- **Copper ores may form where brines convect through basement (Cu source?), and are focussed up along second-order faults into Mindola clastics**
- **Reaction between Cu-bearing oxidised brine and organic maturation products in "ore shale" and clastics causes sulfide deposition.**

AMIR

Potential other Mineralisation sites

- **Base of salt layer especially adjacent to master faults if precipitating mechanism exists (eg mixing with surface marine re-charge fluids; see next case)**
- **Top of Mwashia where hot brines permeate from top of faults and cool or react with organic layers**

AMIRA P544

Potential ore body sites

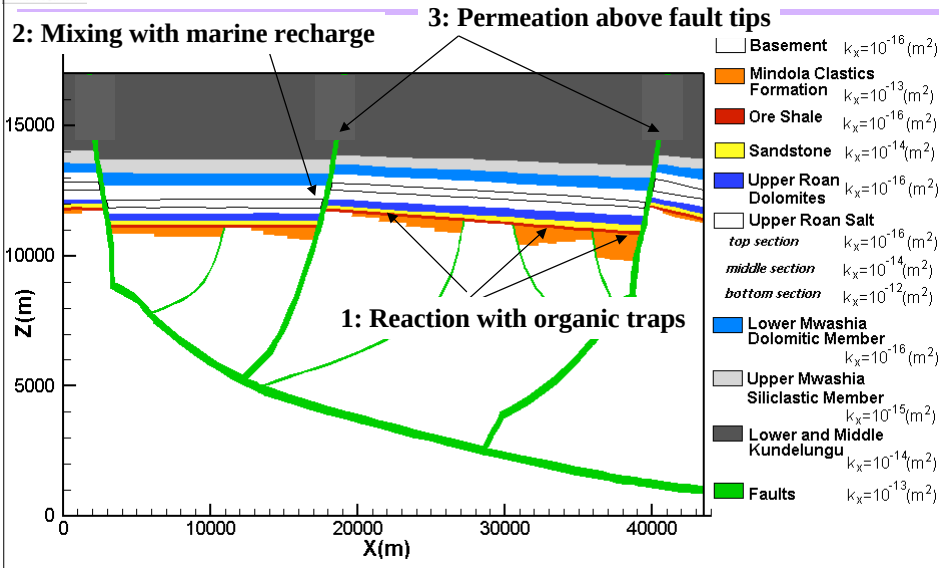

AMIRA P544

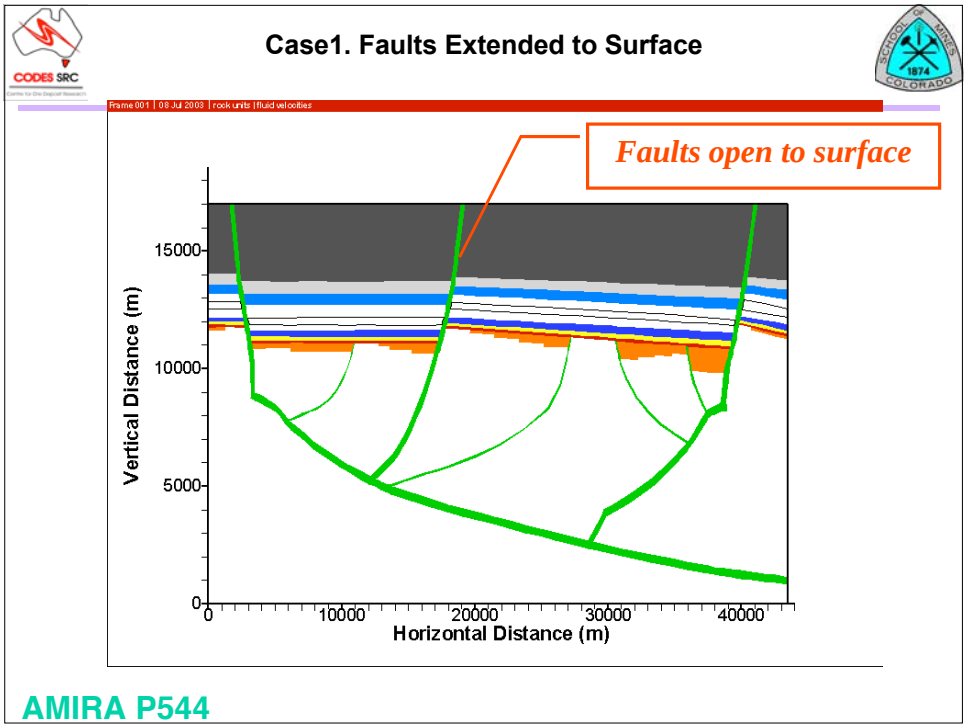
Case1. Faults Extended to Surface
Faults open to surface
Vertical Distance (m)
15000
10000
5000
0
0
10000
20000
30000
40000
Horizontal Distance (m)
AMIRA P544

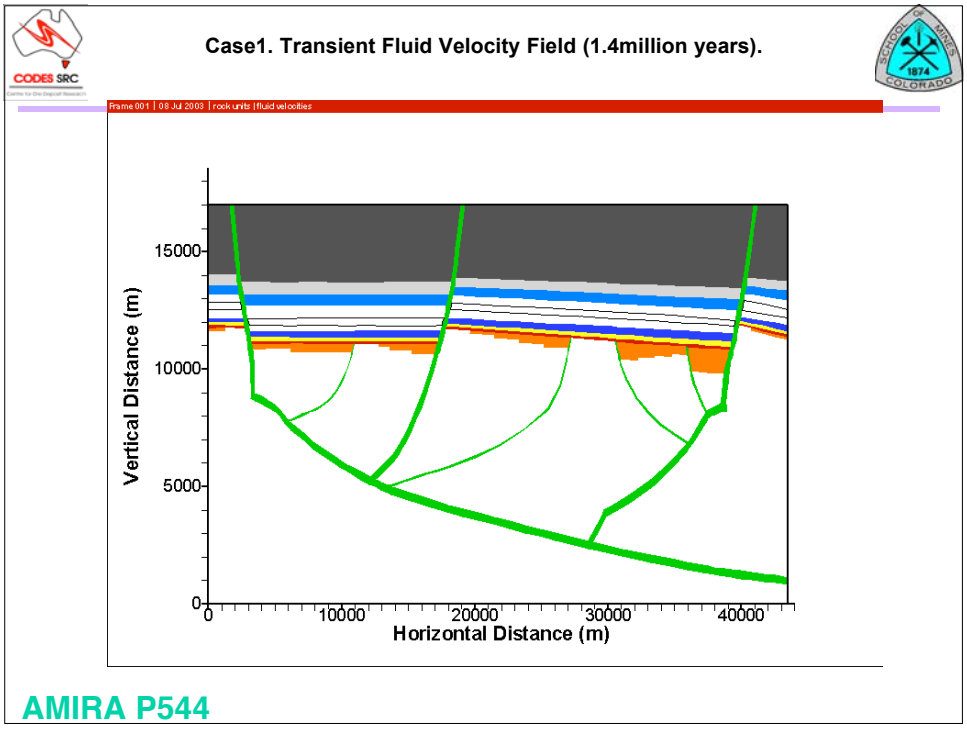
Case1. Transient Fluid Velocity Field (1.4million years).
Vertical Distance (m)
15000
10000
5000
0
0
10000
20000
30000
40000
Horizontal Distance (m)
AMIRA P544

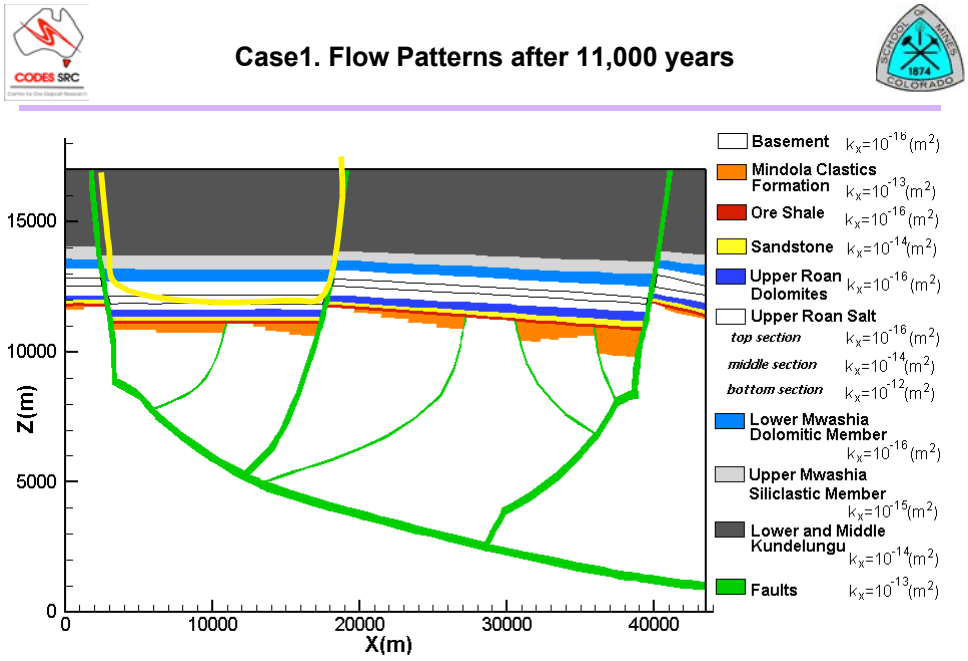
Case1. Flow Patterns after 11,000 years
15000
10000
5000
0
Z(m)
0
10000
20000
30000
40000
X(m)
Basement $k_x=10^{-16}(m^2)$
Mindola Clastics Formation $k_x=10^{-13}(m^2)$
Ore Shale $k_x=10^{-16}(m^2)$
Sandstone $k_x=10^{-14}(m^2)$
Upper Roan Dolomites $k_x=10^{-16}(m^2)$
Upper Roan Salt
top section $k_x=10^{-16}(m^2)$
middle section $k_x=10^{-14}(m^2)$
bottom section $k_x=10^{-12}(m^2)$
Lower Mwashia Dolomitic Member $k_x=10^{-16}(m^2)$
Upper Mwashia Siliclastic Member $k_x=10^{-15}(m^2)$
Lower and Middle Kundelungu $k_x=10^{-14}(m^2)$
Faults $k_x=10^{-13}(m^2)$

AMIRA P544

Case1. Transient Salinity Distribution (1.4million years).

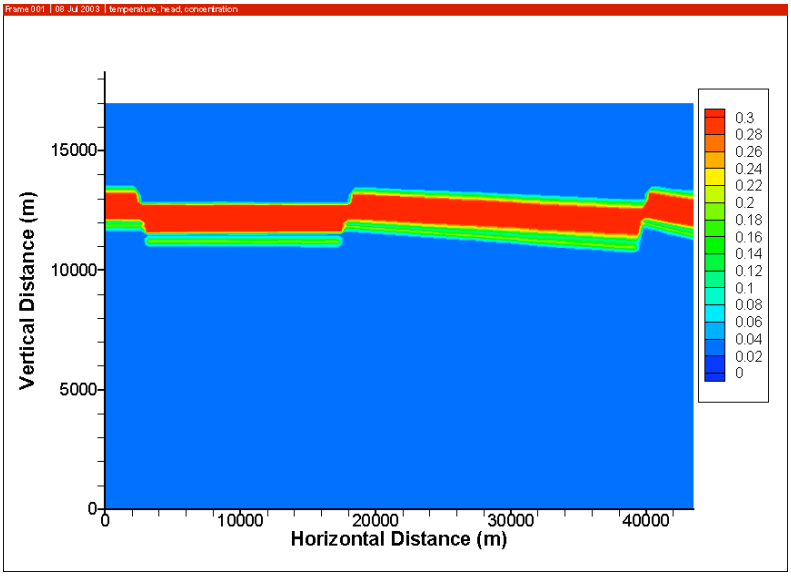

AMIRA P544

Case 1: Interpretation

- **Cold surface marine fluids, flush through the basin via the deep master faults and aquifers**
- **Saline brines from salt layer convect through lower basin and basement**
- **Mixing of deeper Cu-bearing brines with shallower marine fluids could promote copper deposition in the HW breccia zones (eroded salt layer)**
- **Central master fault acts as discharge fault to surface.**
- **Discharge of 150 to 200°C salty fluids toward surface could produce: a)Kipushi type Cu-Pb-Zn pipes or b) SEDEX type Zn-Pb-Ag deposit in Upper Kundelungu**

AMIRA P544

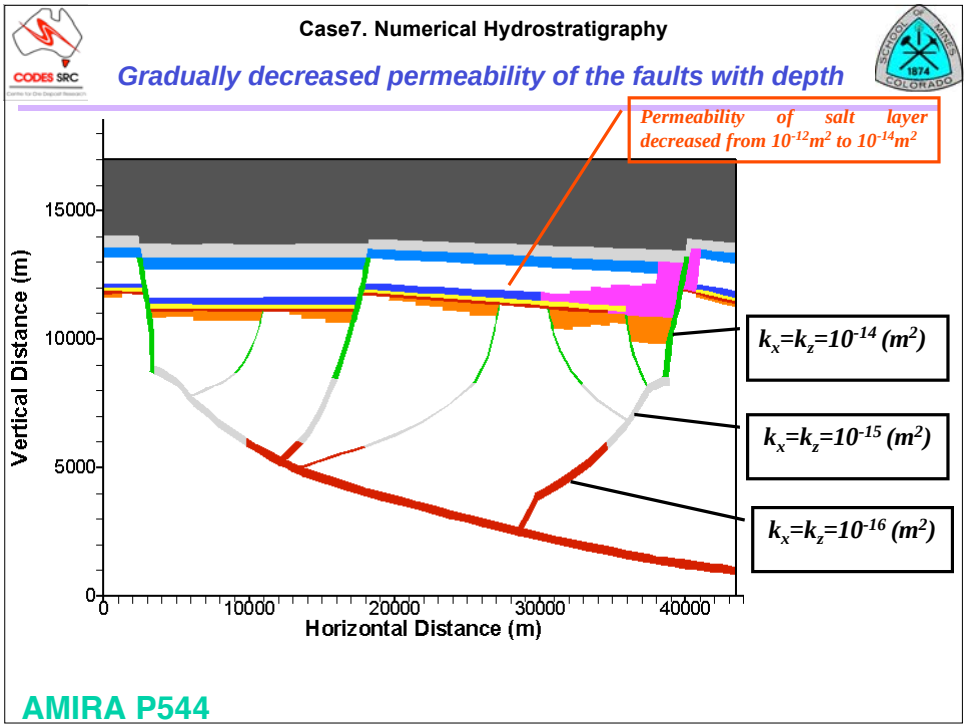
Case7. Numerical Hydrostratigraphy
Gradually decreased permeability of the faults with depth
Permeability of salt layer decreased from 10-12m2 to 10-14m2
kx=kz=10-14 (m2)
kx=kz=10-15 (m2)
kx=kz=10-16 (m2)
Vertical Distance (m)
Horizontal Distance (m)
0
5000
10000
15000
10000
20000
30000
40000
AMIRA P544

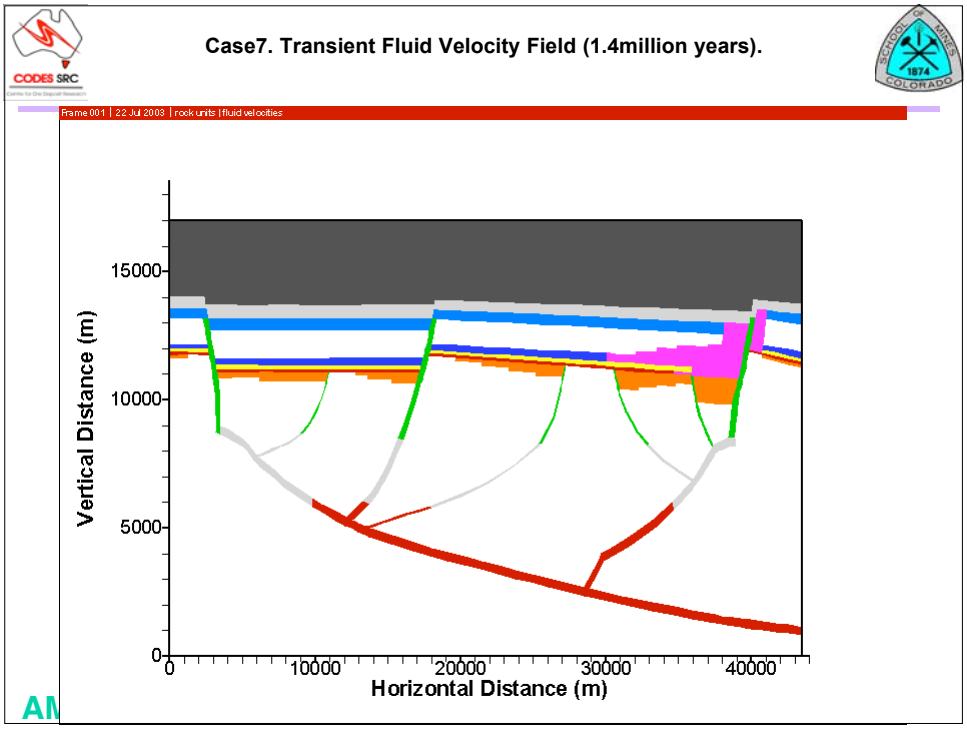
Case7. Transient Fluid Velocity Field (1.4million years).
Frame 001 | 22 Jul 2003 | rock units | fluid velocities
Vertical Distance (m)
Horizontal Distance (m)
0
5000
10000
15000
10000
20000
30000
40000

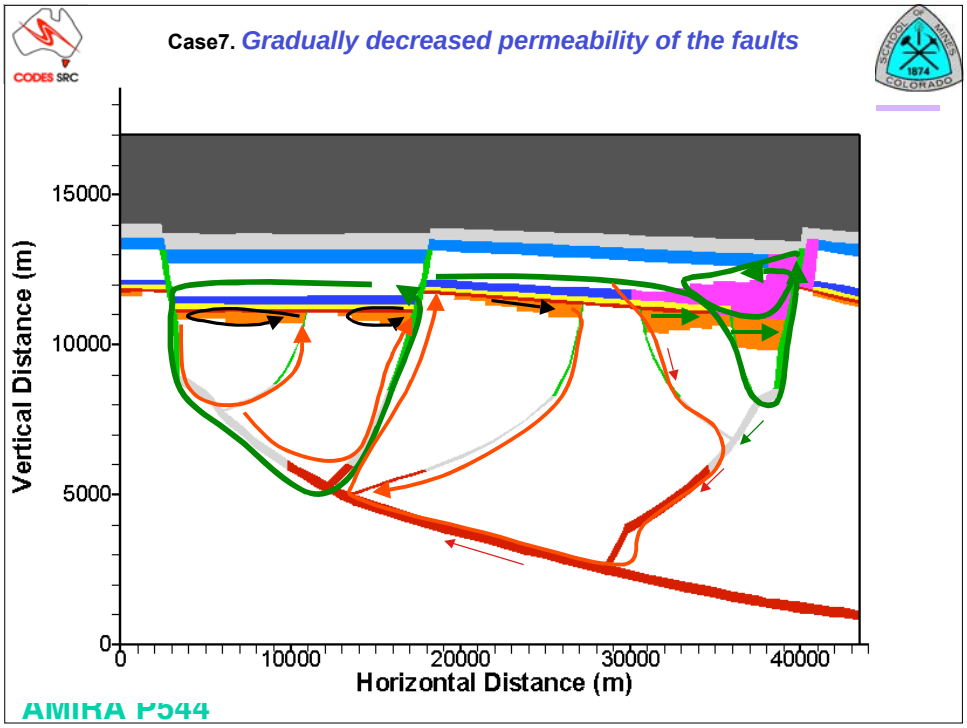
Case7. Gradually decreased permeability of the faults
CODES SRC
Vertical Distance (m)
15000
10000
5000
0
0
10000
20000
30000
40000
Horizontal Distance (m)
AMIRA P544

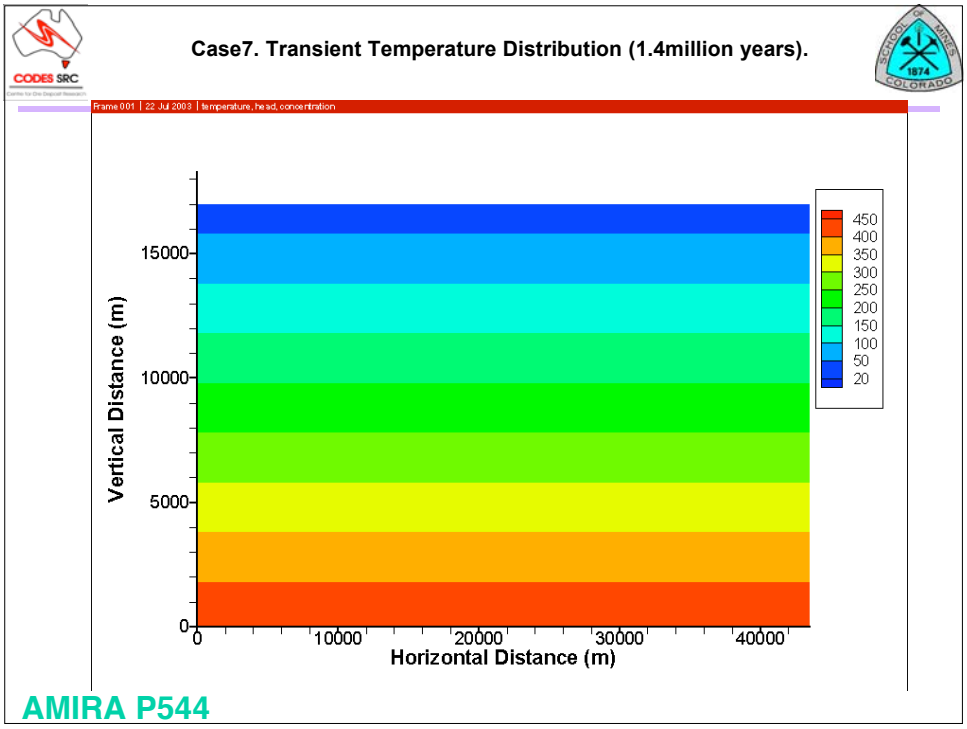
Case7. Transient Temperature Distribution (1.4million years).
CODES SRC
Frame 001 | 22 Jul 2003 | temperature, head, concentration
Vertical Distance (m)
15000
10000
5000
0
0
10000
20000
30000
40000
Horizontal Distance (m)
450
400
350
300
250
200
150
100
50
20
AMIRA P544

Case7: Steady State Temperature Distribution (1.4million years).

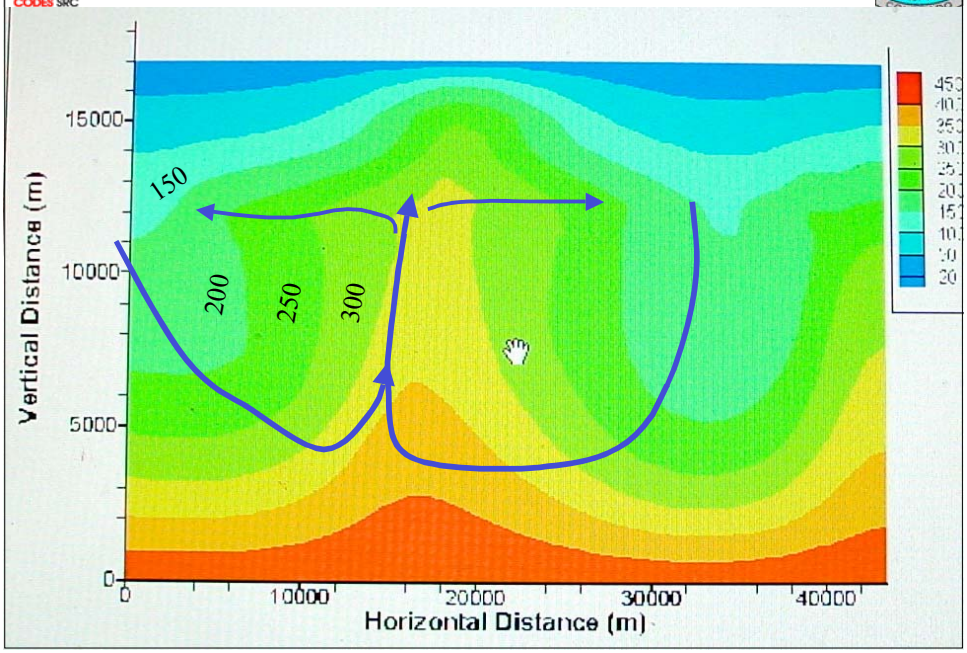

Testing Salt-Brine Convection

Sub-salt convection after Warren, 1999

Fluids migrating laterally below salt increase in density due to dissolution

Free convection significant even where permeabilities as low as 0.01 md = $1x10^{-17}$ (Sarkar et al., 1995)

- **In this case takes 10 My for steady state convection**
- **3-5 m/My of salt is removed**

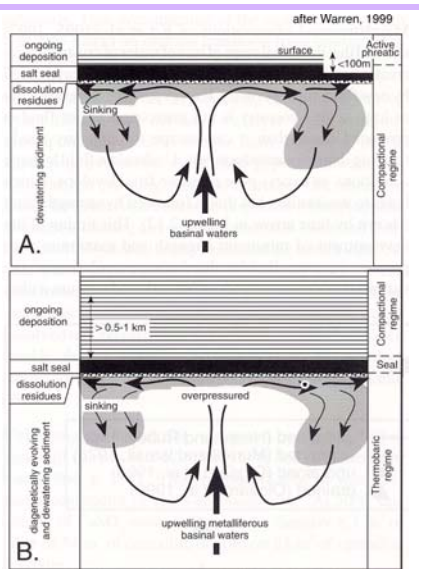

AMIRA P544

Case7. Final Salinity Distribution (1.4million years).

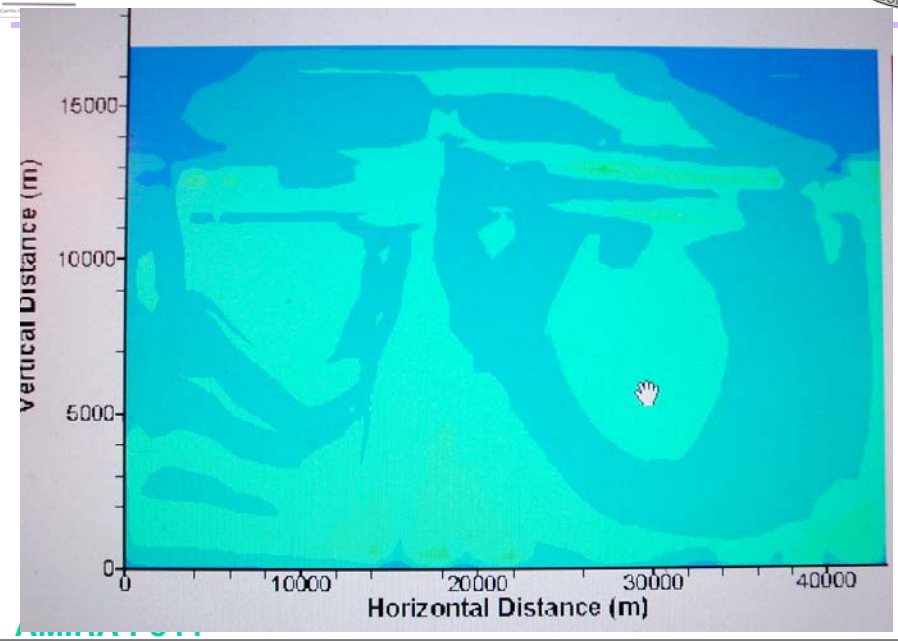

AMIRA P544

Case 7: Interpretation

- **Lower permeabilities in salt layer and faults dampens the hydrothermal system**
- **Less flow through salt layer and thus longer period of concentrated brine circulation**
- **Flow concentrated in FW clastics below "ore shale"**
- **After 0.5 million years a broad and deep brine convection system is established in basement**
- **Good scenario for long-lived, moderate to high temperature hydrothermal system**

AMIRA P544

Fluid Velocity Values (5.5 thousand years)

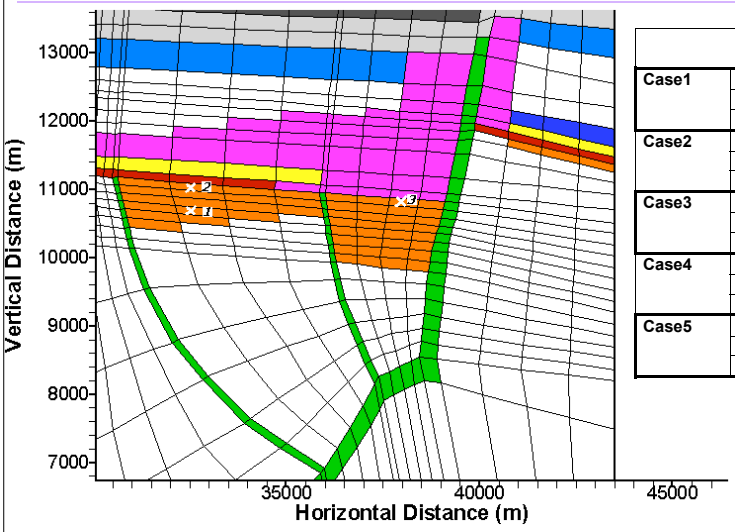

		Fluid Velocity (m/year)
Case1	point 1	5.7
	point 2	8.4
	point 3	14.2
Case2	point 1	5.6
	point 2	9.0
	point 3	11.9
Case3	point 1	5.7
	point 2	8.8
	point 3	1.3
Case4	point 1	0.4
	point 2	6.7
	point 3	3.0
Case5	point 1	1.7
	point 2	4.9
	point 3	1.5

AMIRA P544

Preliminary Conclusions

- **The modelling provides some exciting insites into fluid processes and fluid interaction in the basin**
- **Linked primary and secondary fault-controlled convection cells provide ideal mechanism for generating a metalliferous brine**
- **Brine flow and convection from salt layer into basement, suggests the basement is a likely source for Cu**
- **Other potential orebody deposition sites, in addition to the ore shale and footwall clastics, are suggested by the models**
- **The modelling predicts alteration patterns in the basement that could be used to target new ore body sites**

AMIRA P544

Conclusion: Key Architectural Elements for Sed Cu

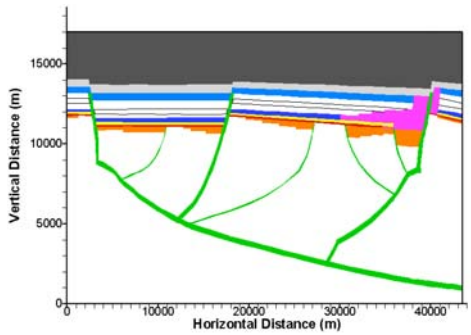

- **Hanging wall evaporites (salt layer)**
- **Clastic wedges sitting on basement**
- **Organic-rich shale which acts as a seal to clastics**
- **Linked fault system which cuts salt layer and penetrates basement**
- **Convective master cells drive the hydrothermal brine**
- **Secondary cells focus metalliferous brine into hydrocarbon-bearing clastic pinch-outs**

AMIRA P544

END

AMIRA P544

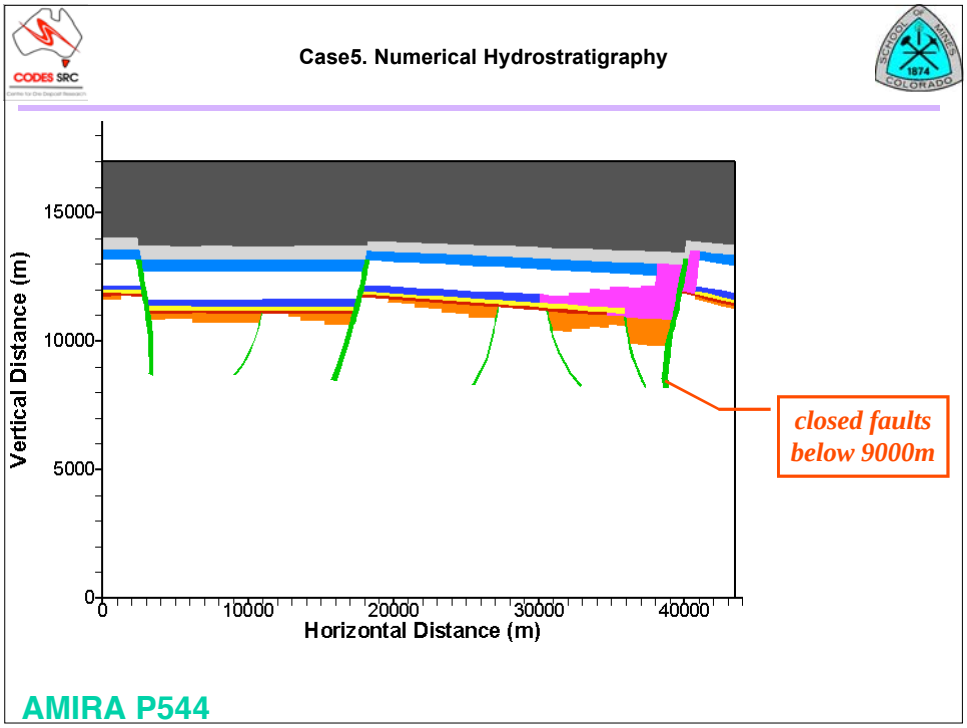
Case5. Numerical Hydrostratigraphy
Vertical Distance (m)
15000
10000
5000
0
0
10000
20000
30000
40000
Horizontal Distance (m)
closed faults below 9000m
AMIRA P544

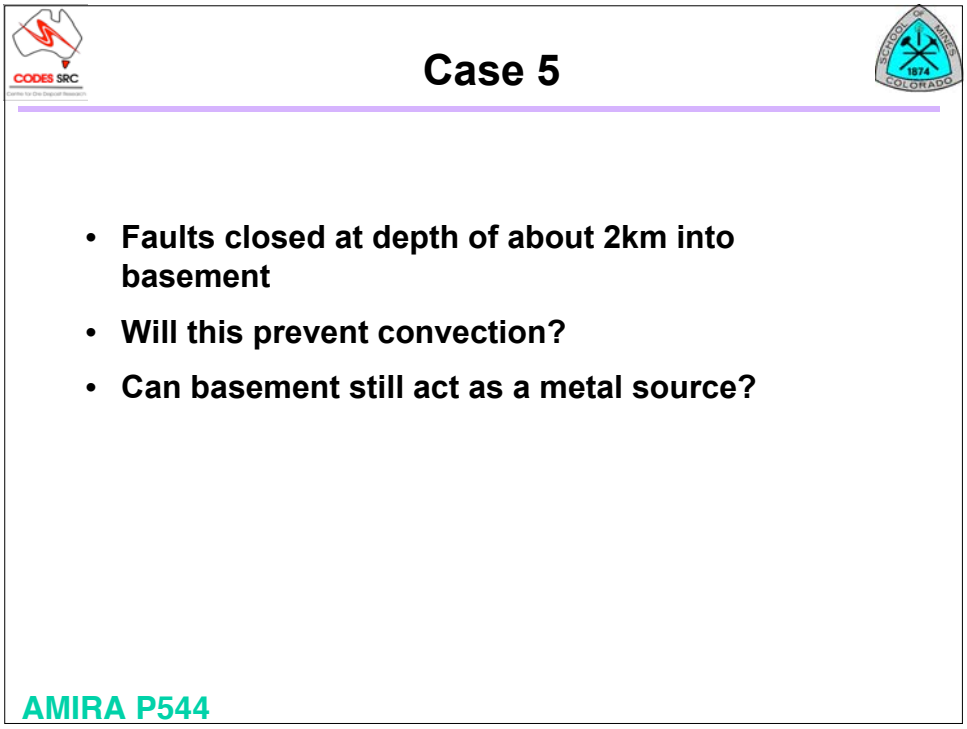
Case 5
• Faults closed at depth of about 2km into basement
• Will this prevent convection?
• Can basement still act as a metal source?
AMIRA P544

Case5. Transient Fluid Velocity Field (11thousand years).

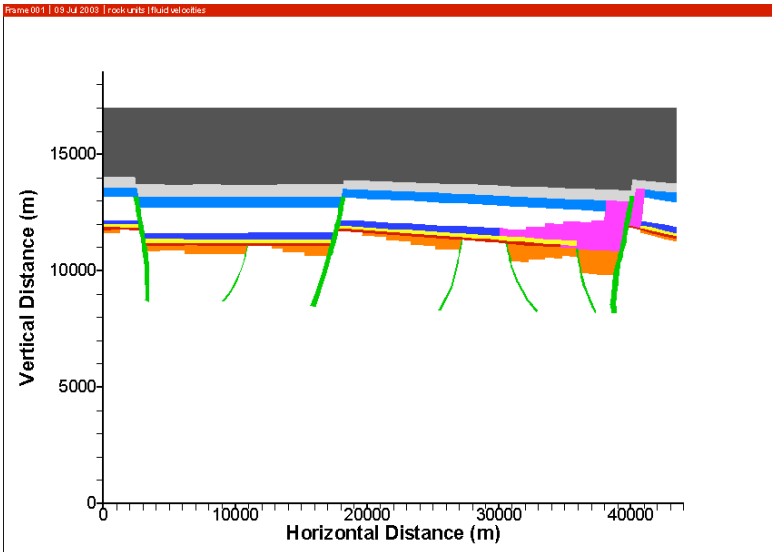

AMIRA P544

Case5. Detailed Transient Fluid Velocity (11thousand years).

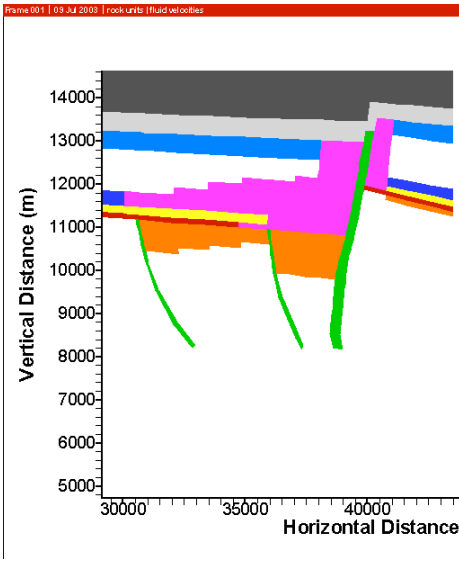

- **Convection confined to breccias and clastics**
- **Little flow in basement**
- **Limited Cu source**
- **Potential Co source in gabbros and breccias**

AMIRA P544

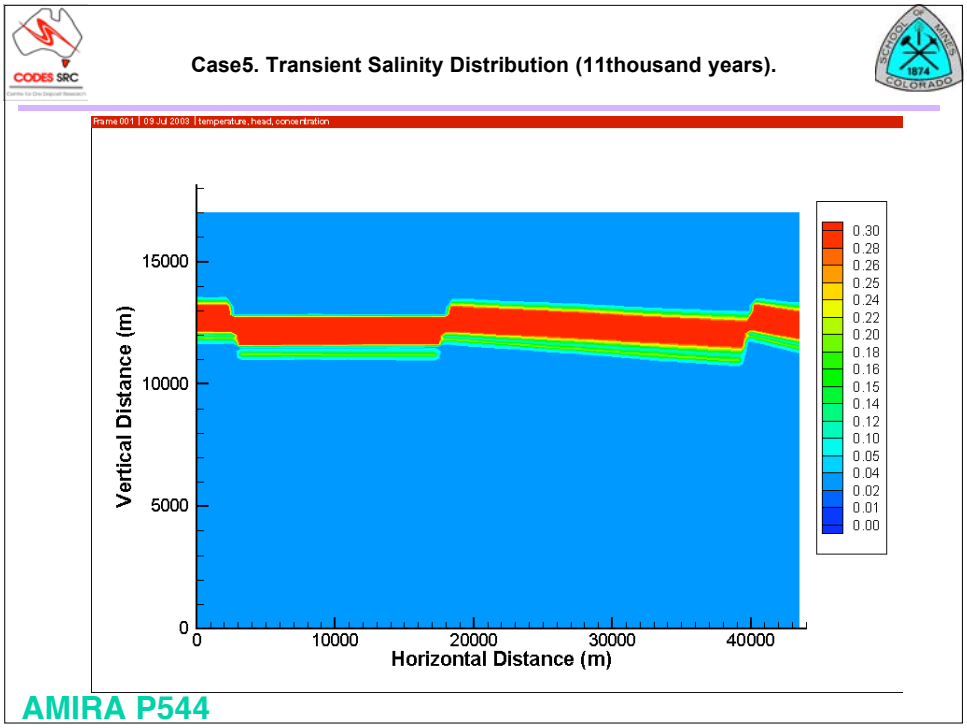
Case5. Transient Salinity Distribution (11thousand years).
Frame 001 | 09 Jul 2003 | temperature, head, concentration
Vertical Distance (m)
15000
10000
5000
0
0
10000
20000
30000
40000
Horizontal Distance (m)
0.30
0.28
0.26
0.25
0.24
0.22
0.20
0.18
0.16
0.15
0.14
0.12
0.10
0.05
0.04
0.02
0.01
0.00
AMIRA P544

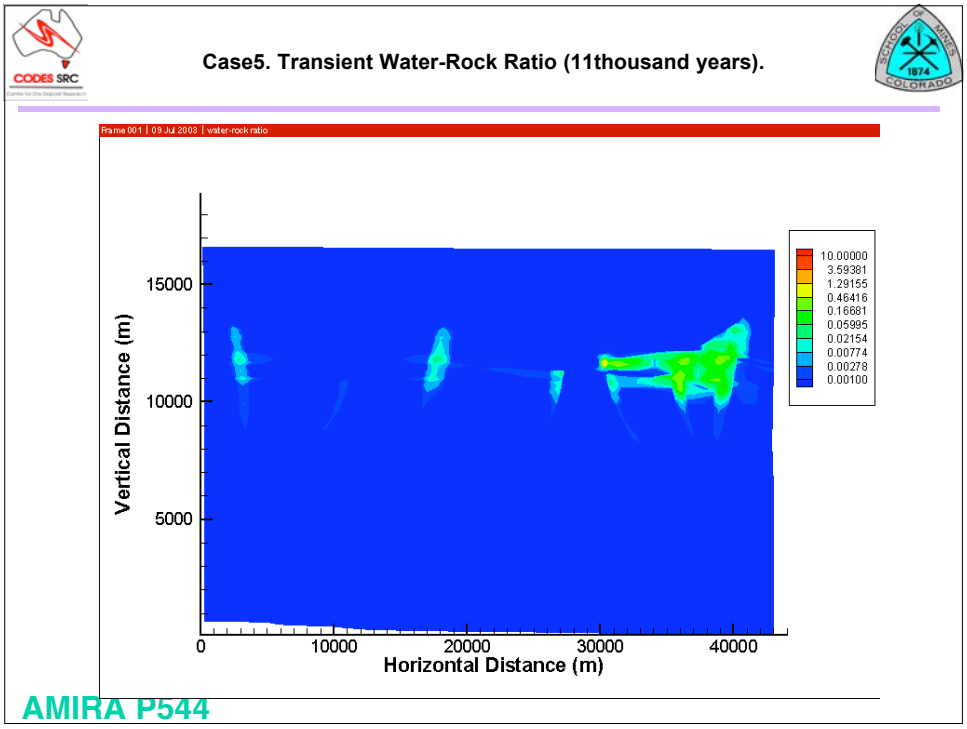
Case5. Transient Water-Rock Ratio (11thousand years).
Frame 001 | 09 Jul 2003 | water-rock ratio
Vertical Distance (m)
15000
10000
5000
0
10000
20000
30000
40000
Horizontal Distance (m)
10.00000
3.59381
1.29155
0.46416
0.16681
0.05995
0.02154
0.00774
0.00278
0.00100
AMIRA P544

Case 5: Interpretation

- **Salt moves down faults into basement**
- **However little circulation of fluids and very little heat flow**
- **No potential to develop widespread potassic alteration**

AMIRA P544

Case 4. Numerical Hydrostratigraphy

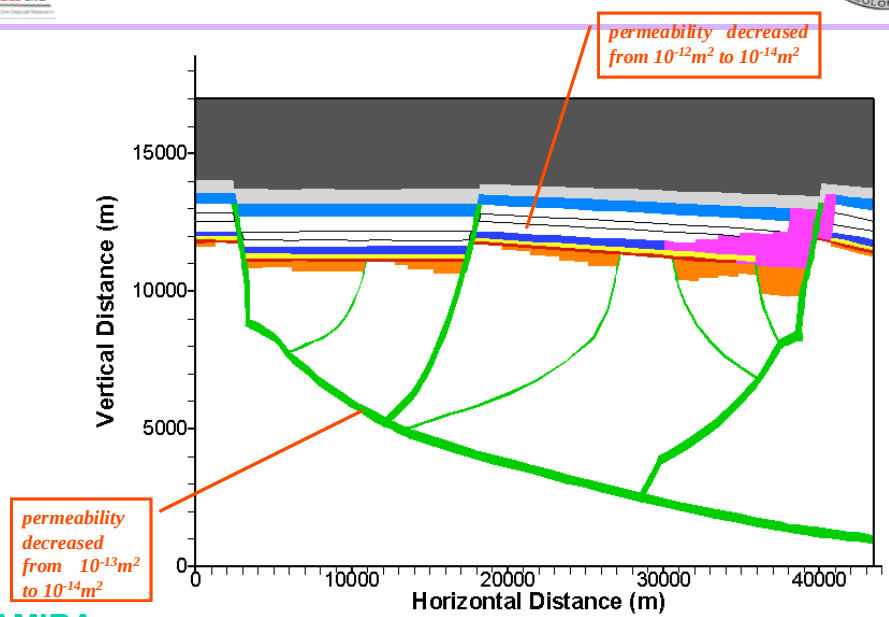

AMIRA P544

Case 4

- **In order to dampen fluid flow through salt layer and basement the permeability of these elements were reduced by one order of magnitude**

AMIRA P544

Case4. Detailed Transient Fluid Velocity (11thousand years).

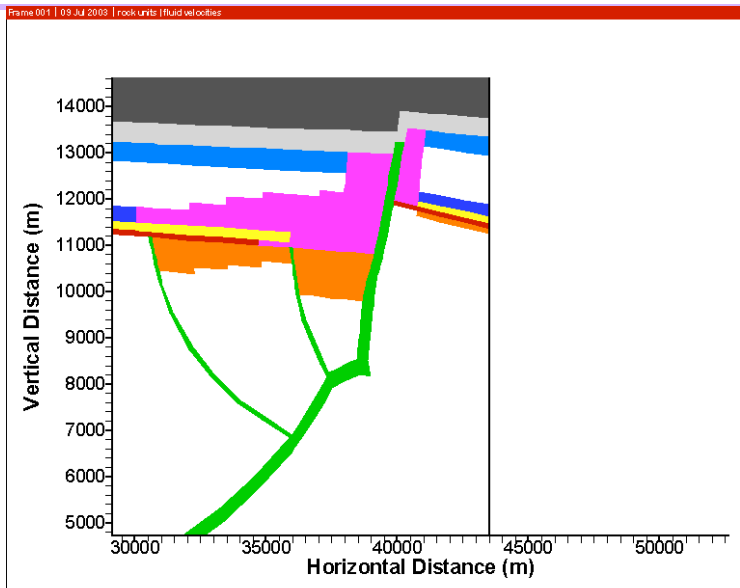

AMIRA P544

Case4. Transient Salinity Distribution (11thousand years).

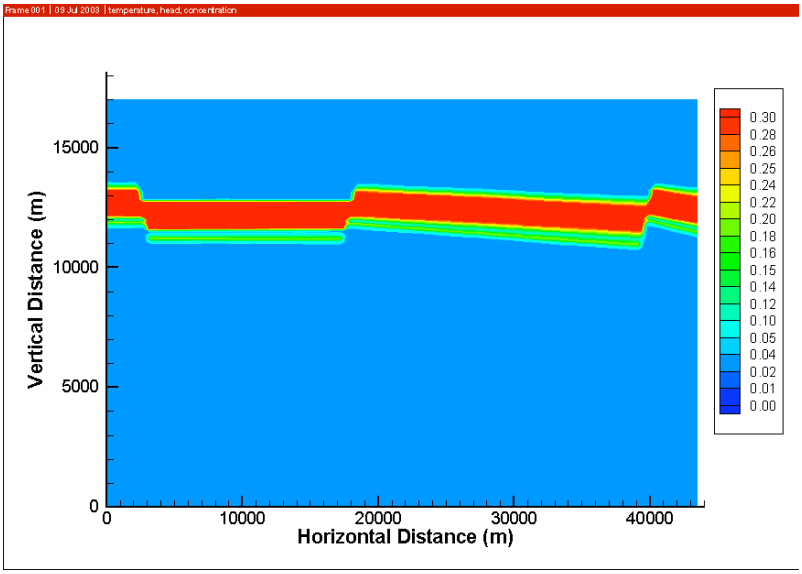

AMIRA P544

Case 4: Interpretation

- **Increased influence of HW breccias**
- **Less flow through salt layer and thus longer period of concentrated brine circulation**
- **Flow concentrated in FW clastics below "ore shale"**
- **Less brine flow into deep basement**
- **Significantly lower temperature of ore fluid compared with cases 1 to 3**

AMIRA P544

Synthesis of P544 data for a genetic and exploration model for the Zambian portion of the African Copperbelt

Murray Hitzman
Colorado School of Mines

The data from P544 allows a new understanding of the Zambian Copperbelt and provides new exploration approaches. This discussion incorporates all the data from P544 together with data gained from field visits in southern Democratic Republic of Congo (DRC). Figures referred to in this contribution are slide numbers of the attached PowerPoint presentation.

Sedimentary architecture/structure

P544 has provided a much more complete understanding of the sedimentary framework from the basement up to the Lower Kundelungu sediments. Work in the Chambishi basin underscores the importance of segmented synsedimentary faults active during early (lowermost) Roan times. Such faults allowed the formation of compartmentalised basins. Lower Roan sediments form an oxidised basal section overlain by a complex, but largely laterally continuous siliciclastic-carbonate sequence with mixed permeability and oxidation state. The ore shale is moderately organic-rich siltstone which in the Zambian Copperbelt represents a regional, probably tectonically controlled, flooding surface. There appears to have been a fundamental re-organisation of faults at the start of ore shale time with fault death, and the generation of a few master faults. These master fault systems provided zones of structural weakness that were reactivated during subsequent Mwashia and Kundelungu sedimentation and into the Lufilian deformation event.

The Upper Roan sequence appears to have been dominated by carbonate and evaporitic sediments, though the evaporites were later dissolved leaving only breccia complexes (largely stratabound, but sometimes crosscutting) and vein anhydrite to mark their presence. The mineralised section in the DRC appears to correlate with the Upper Roan/Lower Mwashia sequence of Congo. Breccias hosting large mineralised blocks in Congo are texturally similar to those in the Upper Roan and Mwashia of Zambia. It is doubtful that Lower Roan equivalent stratigraphy has been observed in most of the DRC Copperbelt opening the possibility of another, previously unrecognised exploration target in this area.

The Mwashia sequence grades upward from a carbonate-rich base to dominantly a siliciclastic sequence, culminating locally in starved, black shale conditions. Chemostratigraphic work suggests that there may be a change in sediment source from a dominantly felsic source in the Roan to a more mafic source during Mwashia times. The Grand Conglomerate is the primary regional marker throughout the African Copperbelt. It appears to consist of both debris flows and glacial diamictites and appears to have been deposited in a tectonically active basin. The Kundelungu between the Grand Conglomerate and the Petite Conglomerate in the Zambian Copperbelt represents a condensed sequence with little evidence of associated tectonic activity.

A major igneous event occurred throughout the African Copperbelt in Mwashia to lower Kundelungu time. It is represented in the Zambian Copperbelt by numerous gabbro sills (age 765–740 Ma) and in the DRC Copperbelt by intrusive and extrusive igneous rocks. Aeromagnetic data in Zambia suggests that the gabbro sills are concentrated along master fault zones.

The Katangan sediments of the African Copperbelt are typical of rift-fill environments. There is no evidence in Zambia or Congo to suggest that the rift responsible for the sediments evolved to oceanic crust. Hence, it appears that this is an intracratonic system, probably analogous to the Permian basins of Europe (Kupferschiefer) (Fig. 16). The relatively thin sedimentary sequence observed in Zambia (<5 km) suggests that the Zambian Copperbelt does not occupy the axial portion of a rift basin (Fig. 17). Rather, it appears that the Zambian district occurs on the shoulders of a basin. While further work is required, it appears that the major basin may occur to the north in the Congo Copperbelt (Fig. 18).

Alteration and lithogeochemistry

Work from P544 has demonstrated that the Katangan sequence from within the Mwashia down into the basement is intensely altered throughout the Zambian Copperbelt. Both potassic and sodic alteration are recognised with potassic alteration generally predating sodic alteration. In many areas, alteration is pervasive, effecting sediments with variable grain size. Preliminary data suggests potassic alteration may occur in the Congo Copperbelt though much more work is required to understand alteration types and timing.

Much of the Lower Roan, and portions of the Upper Roan (as well as the basement locally), throughout the Zambian Copperbelt have undergone potassic metasomatism (Fig. 21). This is seen in increased potassium feldspar and in some cases biotite (formed during later metamorphism). Potassium metasomatism is best developed in stratabound zones, often coarser grained sedimentary layers that presumably had increased permeability relative to adjacent sediments. Though our data is still preliminary, such zones may also contain increased anhydrite. These potassically altered zones contain increased barium (in K-feldspar) and strontium (in anhydrite) relative to non-metasomatised rocks. Potassic alteration was presumably caused by the interaction of a highly saline (>10000 TDS mg/L) brine with the host sediments. Such brine could most easily be produced by evaporite dissolution.

Copper orebodies are largely confined to zones of potassium metasomatism suggesting a genetic link. However, potassic alteration affects much larger areas that those affected by sulfide mineralisation.

Zones of potassic alteration are locally cut by albitic alteration indicating that sodic alteration post-dates potassic alteration. Sodic alteration (also characterised by mariolitic scapolite) is most prominent within stratabound breccia zones within the Upper Roan that may correspond to the position of former evaporates (Fig. 23). Such zones are also the locus of gabbro intrusion. Many of the gabbros are themselves severely sodically altered. Geochemical work on gabbros from outside the Zambian Copperbelt (Barron, 2003) indicates that albitic alteration liberates copper and cobalt from these rocks. It is unclear whether this alteration is associated with copper-cobalt mineralisation and potassic alteration at stratigraphically lower levels. In the Zambian Copperbelt, zones of sodic alteration appear to display copper leaching. However, sodic alteration is associated with significant copper mineralisation higher in the stratigraphic sequence elsewhere in the Lufilian arc (Kansanshi; Broughton et al., 2002), suggesting that such fluids can precipitate copper under the proper conditions. Petrography suggests that albite and scapolite formed largely during Lufilian metamorphism indicating an age of approximately 500 Ma for at least a portion of this alteration event.

Neither potassic nor sodic alteration are direct guides to ore in the Zambian Copperbelt. These styles of alteration are critical, however, in demonstrating that the basin was hydrodynamically active and circulated large volumes of brine necessary to form major ore deposits.

P544 has recognised one probable ore-related alteration type at Mufulira. As noted previously by Annels (1979), the host arenites at Mufulira contain virtually no potassium feldspar though laterally equivalent arenites are feldspathic. This feldspar-destructive alteration forms a halo to the mineralised zone. Our work suggests that this alteration is due to the generation of sulfuric acid from the interaction of mineralizing fluids with sour gas. Thus, delineation of feldspar-absent ('orthoquartzites') or highly aluminous (muscovite- and/or kyanite-rich; see

Barron, 2003) sequences may be good guides to arenite-hosted orebodies.

Lithogeochemistry undertaken as part of P544 has not demonstrated the presence of any robust elemental halos to mineralisation with the exception of copper. Our work suggests that cobalt may form a weak halo around some mineralised zones. However, isotopic studies undertaken during P544 show that several orebodies in Zambia display a broad zone of depletion of carbon isotopic values in carbonate minerals around mineralised zones (Figs 27, 28). Additional work is required to quantify the size of these halos (Fig. 29).

Mineralisation

Mineralisation in the Zambian Copperbelt is fundamentally controlled by a change in oxidation state of the mineralizing fluids (i.e., reduction of fluids). Arenite hosted orebodies are controlled by three-dimensional seals — both stratigraphic pinchouts (Fig. 33) and anticlinal traps (Fig. 34). These physical traps appear to have contained hydrocarbons, either petroleum or natural gas, which served as the reductant. The evidence of the prior presence of hydrocarbons includes pyrobitumen in the greywackes at Mufulira and light carbon and oxygen isotopic values of carbonates spatially associated with sulfides at other deposits suggesting the former presence of natural gas. Many copper mineralised zones also appear to contain less anhydrite than unmineralised potassically altered zones, suggesting that reduction of sulfate was involved in mineralisation.

Ore shale orebodies formed by the interaction of an oxidised mineralised brine flowing through the relatively permeable footwall siliciclastic sediments with the relatively reducing (carbonaceous), and impermeable ore shale (Fig. 35). These orebodies are analogous to those of the Kupferschiefer.

Thus, the data from P544 indicates that reductants are the key to mineralisation in the Zambian Copperbelt. In the arenite-hosted orebodies, mineralisation probably occurred along the hydrocarbon-brine interface within the physical traps (Fig. 50). The level of mineralisation migrated upward through time with hydrocarbon destruction and escape. In the ore shale orebodies mineralisation was focused in portions of the ore shale with higher organic contents and/or increased permeability.

The African Copperbelt has an unusual metals budget compared to other sediment-hosted deposits. It has much higher cobalt and lower silver, zinc, and lead than other districts. Work for P544 has not determined the reasons for this.

The source of copper in the African Copperbelt remains problematic. For most sediment-hosted copper districts the source of metals is relatively well understood — basal red bed sediments, generally with mafic volcanic rocks and detritus. Hitzman (2000) undertook a simple mass balance calculation that indicated that there is an insufficient amount of basal Lower Roan red bed sediments to account for the amount of copper mineralisation. Recognition from P544 that significant thicknesses of sediment up to the level of the Mwashia have been altered and are potential sources of metals has allowed a revision of the original mass balance calculations (Figs 39, 40, 41). Even utilizing these increased thicknesses, there is still apparently more copper leached per tonne of source material than is recognised in either the Kupferschiefer or White Pine. Thus, the implication is that the mineralizing fluids have interacted with copper sources outside of the immediate Zambia Copperbelt area. Two possibilities exist:

- Basement. Fluid modeling done as part of P544 convincingly demonstrates that brines will seek to enter the basement and our petrographic work demonstrates that at least the upper portion of the basement has been severely altered in some areas.
- Lateral fluid flow. Our preliminary understanding of the geology of southern DRC suggests that a thicker basin may occur in this area which may be the real source of the mineralizing fluids.

The age of copper-cobalt mineralisation remains problematic. Based on geological evidence, mineralisation could have been initiated anytime after deposition of the ore shale. Constraints on the age of mineralisation include:

- Mineralisation post the generation of hydrocarbons (e.g., source beds must have reached the oil window.
- Initial mineralisation is post late Upper Roan times if the mineralizing brine source is in the Upper Roan.
- Mineralisation similar in style to that in the Zambian Copperbelt occurs in the Kakontwe and the lower Kundelungu (Lonshi) in the DRC indication mineralisation processes must have been active in Kundelungu or later times.
- Tectonic activity capable of enhancing brine movement occurred during the Mwashia-Grand Conglomerate period (765–740Ma) and during Lufilian deformation (530–490Ma).
- Geochronological work conducted as part of P544 (Re/Os – Broughton and phosphate geochronology – Dawson) consistently gives Lufilian ages (circa 530 Ma) for mineralisation.

Whether mineralisation was continuous or episodic up to the Lufilian deformational event is currently unknown.

Petrographic work indicates that much of the sulfide in the Zambian Copperbelt has recrystallised during Lufilian metamorphism. Isotopic work indicates a very diverse range of sulfide isotopic values indicating that metamorphism did not result in homogenisation of isotopic values. We are still in the process of evaluating the available sulfur isotopic data, and collecting new data, to understand what these isotopic values are telling us. The available data suggests that thermochemical sulfate reduction was probably a key mechanism in mineralisation.

Data from throughout the Zambian Copperbelt indicates a late (Mesozoic to Tertiary) period of extremely deep supergene oxidation (locally over 1 km depth), which has affected many orebodies. The high grade of many orebodies in Zambia may be due, in part, to supergene processes. Supergene oxidation has resulted in the remobilisation of copper and reprecipitation along structures and into more permeable units (caused by groundwater leaching of anhydrite and carbonate cements). P544 data suggests that trace element signatures in chalcocite (Pb, Ag, Bi, Sn) may be useful in discriminating hypogene from supergene sulfides.

Genetic model for the Zambian Copperbelt

The data provided by P544 does allow us to construct a new genetic model for the history of the Zambian Copperbelt. Though geochronology has been a focus of the project, we have been stymied by the apparent resetting of many mineral ages during Lufilian metamorphism. The key dates available are:

- 880 Ma Nchanga granite
- ? Age of Roan sediments
- 765 Volcanic rocks in Mwashia (Congo)
- 765-740 Gabbros in Zambia
- 750 Grand Conglomerate (Sturtian glaciation)
- 670-620 Shinkolobwe U deposit (reliable age?)
- 645 Disseminated Cu mineralisation at Musoshi (Pb-Pb reliable?)
- 600-620 Petite Conglomerate (assuming Marinoan age correlation)
- 560 Hook granite
- 500-535 Xenotime/monazite ages – Zambian Copperbelt
- 510-490 Vein Cu-Mo mineralisation (Nkana, Musoshi, Kansanshi)
- 495 Cooling below 300°C blocking T for Ar in biotite
- 470 Cooling below blocking T for Ar in muscovite

From these dates and the available geological data a model of the geological evolution of the Zambian Copperbelt has been constructed:

- Lower Roan time (Figs 57, 58, 59): An extensional environment leads to the formation of numerous normal fault-related basins filled with complex fluvial-alluvial sediments. In the Zambian Copperbelt this section is relatively thin (<1.5 km), while in southern Congo there may be a much more substantial thickness of similar sediments. A fundamental reorganisation of faults corresponds with the deposition of the ore shale in Zambia and represents a major transgression. The Lower Roan above the ore shale consists of mixed siliciclastic and carbonate sediments, including local evaporites, largely of marine origin.
- Upper Roan time (Figs 60, 61): A restriction of the basin led to evaporite precipitation. The thickest

evaporites were probably deposited in the Congo portion of the basin. The Upper Roan/lower Mwashia of the Zambian Copperbelt correlates with the Mines Group and Dipeta Group in Congo. Initial movement of diagenetic fluids may have resulted in the start of mineralisation in the ore shale. Late in Upper Roan time there may have been a sufficient thickness of sediments, especially in the thicker basin to the north in Congo, to initiate hydrocarbon maturation and migration.

- Mwashia (Fig. 62): The Mwashia is a deepening up sequence going from carbonates to shale. It is possible that the base of the unit represents a regional unconformity though this is difficult to distinguish in the Zambian Copperbelt due to structural dislocation along this surface. A major mafic igneous event occurred throughout the African Copperbelt during Mwashia-Grand Conglomerate time. This event would have helped to mature organic matter in the Roan and would have provided energy to drive fluid flow within the basin. It appears that salt movement was probably initiated during Mwashia time along with the production of brine (Figure 68).
- Grand Conglomerate – Kakontwe – Lower Kundelungu (Fig. 63): The Kundelungu period opens with a period of extension within the basin which may be a continuation of the igneous event in the Mwashia. The global glaciation responsible for the Grand Conglomerate may also have allowed incursion into the basin of brine derived from ocean freezing, however, it would be expected that such a brine would not be as saline as that derived from the dissolution of the Upper Roan evaporites which was probably occurring at this time. The thickness of the sedimentary succession between the Grand Conglomerate and the Petite Conglomerate is generally only several hundreds of metres in the Zambian Copperbelt area, though this interval represents approximately 150 million years. This suggests that this was largely a period of non-deposition. Further stratigraphic work is required in Congo to better understand what is happening in the basin during this period. It is likely that brine-related mineralisation took place during the early portion of this interval, coincident with the tectonic and igneous activity. It is unclear whether mineralisation would have continued throughout this long interval, but it is likely that brines remained within the sequence and could have continued mineralisation.
- Petite Conglomerate – Upper Kundelungu (Fig. 64): The base of this succession is a second worldwide glacial event. This sequence is poorly known in Zambia. In one drill hole, a major thickness (>300 m) of conglomeratic molasse is present suggesting the initiation of Lufilian deformation and the formation of a wedge of foreland clastic sediments.
- Lufilian Deformation (Figs 65, 66): Our present understanding is that this tectonic event prograded from south to north. In the Zambian Copperbelt the event resulted in recrystallisation of the sediments and their included sulfides. Metamorphism and deformation resulted in local mobilisation of sulfides (Nkana – Croaker) but apparently did not in itself generate orebodies as elsewhere in northern Zambia (Kansanshi; Broughton et al., 2002).

Figure 72 schematically displays a time-temperature curve for the Zambian Copperbelt. Based on this analysis it would appear that most mineralisation probably occurred during Mwashia to lower Kundelungu time. However, no reliable geochronological evidence to date gives ages in this time range.

Exploration implications

These data suggest the following key features for discovery of additional Zambian-type orebodies.

- Delineation of early syn-sedimentary faults (aeromag data, thickness variations in the basal Roan clastics, later folds and reverse faults nucleated on such early structures).
- Restriction of exploration to potassically altered zones.
- Definition of 'reduction traps' – physical hydrocarbon reservoirs (anticlinal closures, stratigraphic pinchouts; organic-rich sediments). Any type of reduced zone may be favorable. Zones of anomalously low carbon and oxygen isotopic values in carbonates may help define zones of former reductants.
- Recognition of potassium feldspar free zones in feldspathic arenites indicating acid production by

sour gas destruction associated with mineralisation.
- Recognition of structural zones that may have allowed deep oxidation and lateral migration of copper-rich groundwaters.

The data from P544 suggest the following characteristics should be sought for Copperbelt-type basins.

- Intracratonic basins – those that retain, and do not leak brines. The most favorable sites are on basin shoulders ('horns' of the steer-head rift basin).
- Basins that contain significant (>100s metres) of oxidised, siliciclastic sediments at their base and are composed largely of oxidised fill. However, the basins must also contain relatively restricted zones of reductants (either organic-rich black shales or physically trapped hydrocarbons).
- Evidence of brine production, such as wide-scale potassic and/or albitic alteration, probably derived from evaporite (halite) dissolution. Evidence of evaporites may include, in addition to regional scale alteration, major stratabound and crosscutting breccias and megabreccias.
- Long-lived structural conduits that provide vertical fluid pathways.
- Geologic evidence of a heat engine, such as intrusives and/or volcanic rocks, capable of enhancing fluid flow.
- Widespread trace copper mineralisation at multiple stratigraphic levels.

References

Annels, A.E., 1979, Mufulira greywackes and their associated sulfides: Trans. of the Institute of Mining and Metallurgy, v. 89, p. 15-23.

Barron, J.W., 2003, The stratigraphy, metamorphism, and tectonic history of the Solwezi area, Northwest Province, Zambia: Integrating geological field observations and airborne geophysics in the interpretation of regional geology: Unpub. Ph.D. thesis, Colorado School of Mines, 233p.

Broughton, D.W., Hitzman, M.W., and Stephens, A.J., 2002, Exploration history and geology of the Kansanshi Cu-(Au) deposit, Zambia: Society of Economic Geologists, Special Publication 9. p. 141-153.

Hitzman, M.W., 2000, Source Basins for Sediment-Hosted Stratiform Copper Deposits - Implications for the Structure of the Zambian Copperbelt: Journal of African Earth Sciences, v. 30, p. 855-863.

Synthesis of P544 Data — A Genetic and Exploration Model for the Zambian Portion of the African Copperbelt

Murray W. Hitzman
Colorado School of Mines

AMIRA P544 *Final Sponsors Meeting* July 2003

Outline

- What have we learned from P544 (Zambia)?
  - Sedimentary architecture / Structure
  - Alteration and lithogeochemistry
  - Mineralization
- A Genetic Model for the Zambian Copperbelt
- Brief comparisons with other districts
- Exploration implications for other basins

Comments on comparisons with Congo throughout talk

AMIRA P544 *Final Sponsors Meeting* July 2003

Acknowledgements

- All the corporate sponsors but especially those in Zambia who have helped in so many ways — Anglo American, Avmin, First Quantum, Mopani, and Phelps Dodge.
- Special thanks to Alan Stephens who got me started on this whole venture just after I arrived at CSM.
- Those who first helped me here - ZCCM personnel and especially David Armstrong.
- AMIRA for their support.
- The CODES team that has been a real pleasure to work with and who have taught me so much.
- David Broughton who has done all the heavy lifting.

AMIRA P544 *Final Sponsors Meeting* July 2003

What have we learned from P544 (Zambia)?

Sedimentary Architecture / Structure

Konkola Core Farm

AMIRA P544 *Final Sponsors Meeting* July 2003

Sedimentary Architecture / Structure

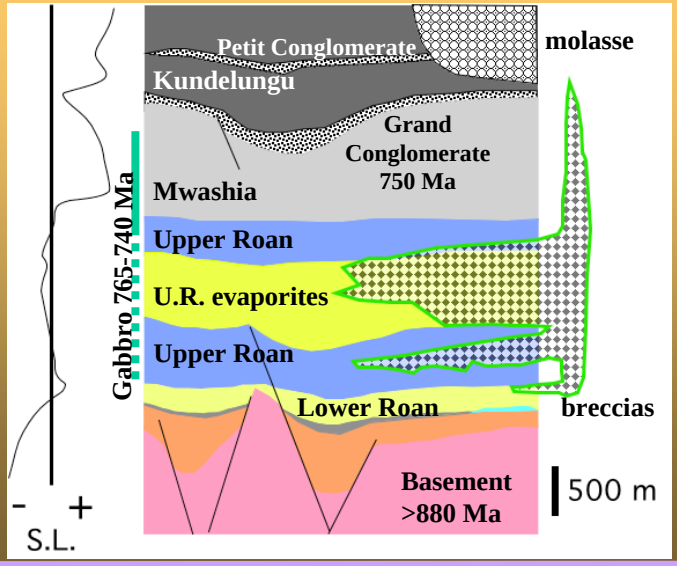

Sedimentary Architecture / Structure

Stratigraphic / structural work has given us a more complete sedimentary framework from the basement to the Lower Kundelungu.

- **Basal Lower Roan siliciclastic rocks:**
  - **Composed of arkosic conglomerates and sandstones derived from granitic and metamorphic basement and deposited in fan-delta environments (*previously known*).**
  - **Sedimentation controlled by short strike length, normal faults (extensional environment) forming compartmentalized basins (*not appreciated previously*).**

Sedimentary Architecture / Structure

- **Lower Roan (ore shale):**
  - **Ore "shale" is moderately organic-rich siltstone representing a regional (probably tectonically controlled) flooding surface.**
  - **Demonstrated facies variation in the ore shale — starved shallow marine to carbonate facies (*previously known*).**
  - **Ore shale horizon overlain by mixed shallow marine sequence.**
  - **Fundamental fault re-organization at start of ore shale time with linkage and generation of master faults (*previously unknown*).**

AMIRA P544 *Final Sponsors Meeting* July 2003

Sedimentary Architecture / Structure

- **Lower Roan (above ore shale):**
  - **Largely layer-cake mixed siliciclastic-carbonate sequence.**
  - **Locally shallow marine with sabhka sequences - evidence of gypsum-facies evaporitic sedimentation.**
  - **"Shale with grit" is regional facies - dewatering textures still enigmatic and will be continuing focus (Broughton).**

AMIRA P544 *Final Sponsors Meeting* July 2003

Sedimentary Architecture

- **Upper Roan:**
  - **Generally layer-cake carbonate-(siliciclastic) sequence.**
  - **Laterally extensive sand layers - tectonic pulses or sea-level variation (?).**
  - **Evidence (breccias and alteration) of major evaporite package within Upper Roan section - may have been in excess of 1 km. Evaporite (with exception of anhydrite) has undergone dissolution. (*previously not appreciated*)**

AMIRA P544 *Final Sponsors Meeting* July 2003

Sedimentary Architecture / Structure

- **Upper Roan breccias:**
  - **The Upper Roan contains abundant breccias making tracing of stratigraphy locally difficult.**
  - **Origins of the breccias are diverse and probably include:**
    - **Sedimentary**
    - **Dissolution / collapse**
    - **Intrusive-related**
    - **Tectonic**
    - **Combinations of events**

AMIRA P544 *Final Sponsors Meeting* July 2003

Sedimentary Architecture / Structure

- **Upper Roan breccias:**
  - **Breccias are very similar to those in Congo (and central Zambia).**
  - **Difference appears to be the scale of the Congo breccias compared to those in Zambia — thicker salt in Congo?**

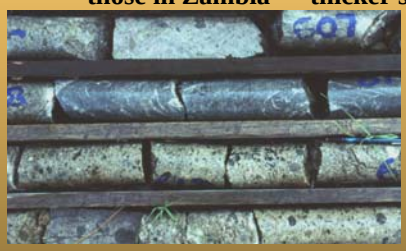

Mufulira, Zambia

Kamoya, Congo

Kalengwa, central Zambia

AMIRA P544 *Final Sponsors Meeting* July 2003

Sedimentary Architecture / Structure

- **Mwashia:**
  - **Grades upward from a carbonate-rich base to dominantly siltstones. It apparently served as a regional "seal" - however, lithogeochemistry suggests it was also regionally altered. (*new data*)**
  - **Chemostratigraphic properties suggest a change in provenance from Roan sediments (i.e. contribution from mafic sources).**
  - **Is Mwashia a separate sedimentary sequence (sedimentologically and in age) from Roan?**

Konkola

Shituru, Congo

AMIRA P544 *Final Sponsors Meeting* July 2003

Sedimentary Architecture / Structure

- **Kundelungu:**
  - **The Grand Conglomerate (750 Ma) serves as a regional marker unit. It appears to consist of both debris flows and glacial diamictites (tectonically active basin conditions?).**
  - **The Kundelungu between the Grand Conglomerate and the Petit Conglomerate in Zambia (now called Nguba in Congo) appears to represent a condensed sequence (starved conditions?) spanning approximately 150 m.y.**

Photomicrograph
Grand Conglomerate

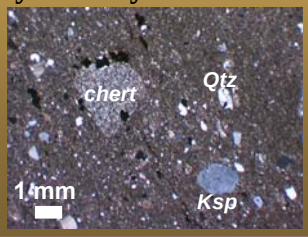

AMIRA P544 *Final Sponsors Meeting* July 2003

Sedimentary Architecture / Structure

- **Gabbros and mafic volcanic rocks:**
  - **Gabbro intrusions in Zambia are concentrated in the Upper Roan section but are recognized from the basement to the Grand Conglomerate. Dating indicates ages of 765-740 Ma. (*new data*)**
  - **Mafic volcanic rocks and gabbro intrusions occur within the Mwashia in Congo.**
  - **Magnetics suggest gabbros may sit on major faults.**

Zambia gabbro

Congo pyroclastics

AMIRA P544 *Final Sponsors Meeting* July 2003

Sedimentary Architecture / Structure

- **Katangan sediments in the Zambian Copperbelt are typical of rift-fill environment. Structures are compatible with extensional (rift) environment.**
- **Zambian Copperbelt does not form a major depocenter - no evidence that Zambian Copperbelt was near center of significant rift basin (thin sequence, absence of volcanic rocks, oceanic crust) or along a continental margin. (*not previously appreciated*)**

AMIRA P544 *Final Sponsors Meeting* July 2003

Sedimentary Architecture / Structure

Good analogue may be intracratonic basins associated with the Kupferschiefer.

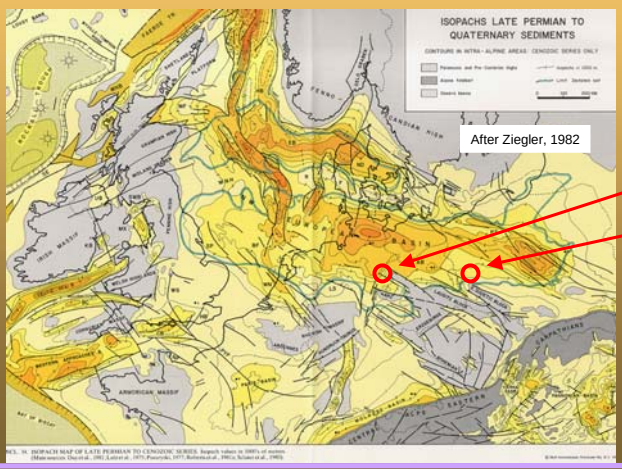

AMIRA P544 *Final Sponsors Meeting* July 2003

Sedimentary Architecture / Structure

Zambia system potentially represents condensed margin of a larger basin system. In rift basin terms this would be on the "steer's horn." (c.f. Stuart Shelf - Adelaide Fold Belt)

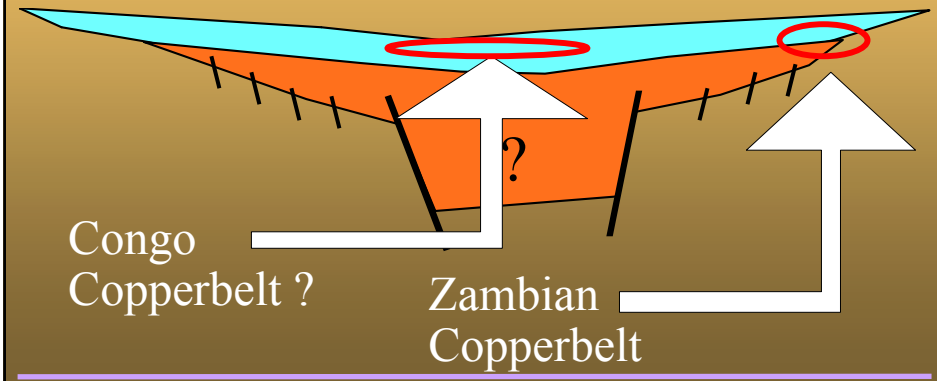

AMIRA P544 *Final Sponsors Meeting* July 2003

Sedimentary Architecture / Structure

Copperbelt area probably comprised of complex downfaulted basin with depocenter just north of Congo-Zambia border. Major basin bounding faults appear to be important ore controls.

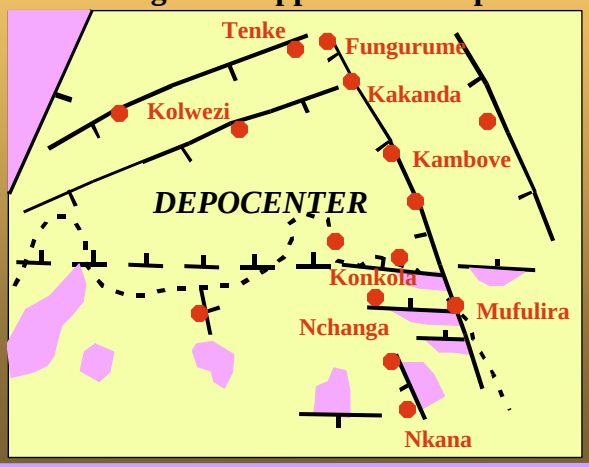

AMIRA P544 *Final Sponsors Meeting* July 2003

What have we learned from P544 (Zambia)?

Alteration and Lithogeochemistry

Lower Roan conglomerate with potassic alteration Chambishi

AMIRA P544 *Final Sponsors Meeting* July 2003

Alteration and Lithogeochemistry

- **Alteration is recognized in the Zambian Katangan sequence from within the Mwashia down into the basement (*new data*). Most intense alteration in Lower Roan.**
- **Both potassic and sodic styles of alteration are observed.**
- **Alteration is commonly pervasive regardless of grain size, even sediments with low apparent permeability may be pervasively altered (*new data*).**

Styles of alteration in the Congo Copperbelt unclear - probable potassic alteration in Mines Group.

AMIRA P544 *Final Sponsors Meeting* July 2003

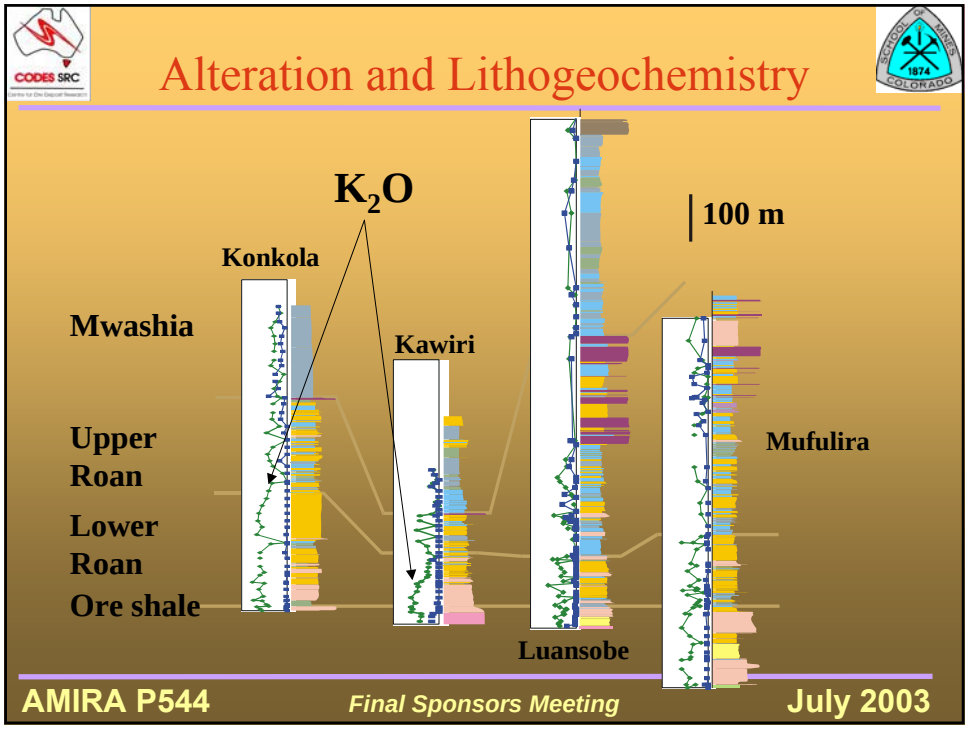
Alteration and Lithogeochemistry
K_2O
100 m
Konkola
Kawiri
Mwashia
Upper Roan
Lower Roan
Ore shale
Luansobe
Mufulira
AMIRA P544
Final Sponsors Meeting
July 2003

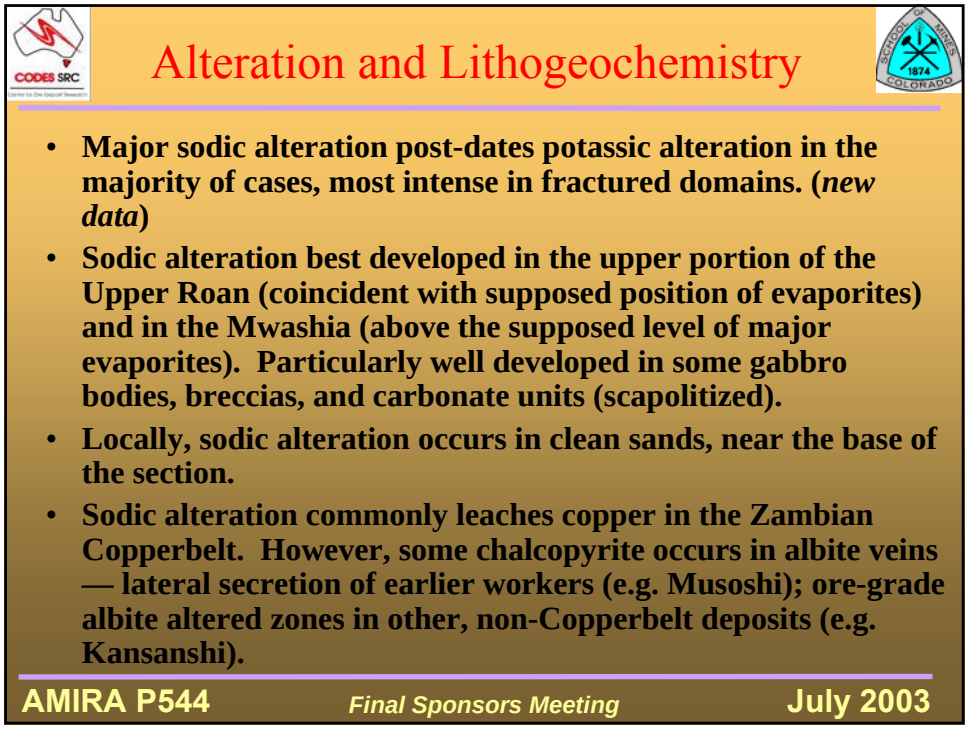
Alteration and Lithogeochemistry
• Major sodic alteration post-dates potassic alteration in the majority of cases, most intense in fractured domains. (*new data*)
• Sodic alteration best developed in the upper portion of the Upper Roan (coincident with supposed position of evaporites) and in the Mwashia (above the supposed level of major evaporites). Particularly well developed in some gabbro bodies, breccias, and carbonate units (scapolitized).
• Locally, sodic alteration occurs in clean sands, near the base of the section.
• Sodic alteration commonly leaches copper in the Zambian Copperbelt. However, some chalcopyrite occurs in albite veins — lateral secretion of earlier workers (e.g. Musoshi); ore-grade albite altered zones in other, non-Copperbelt deposits (e.g. Kansanshi).
AMIRA P544
Final Sponsors Meeting
July 2003

Alteration and Lithogeochemistry

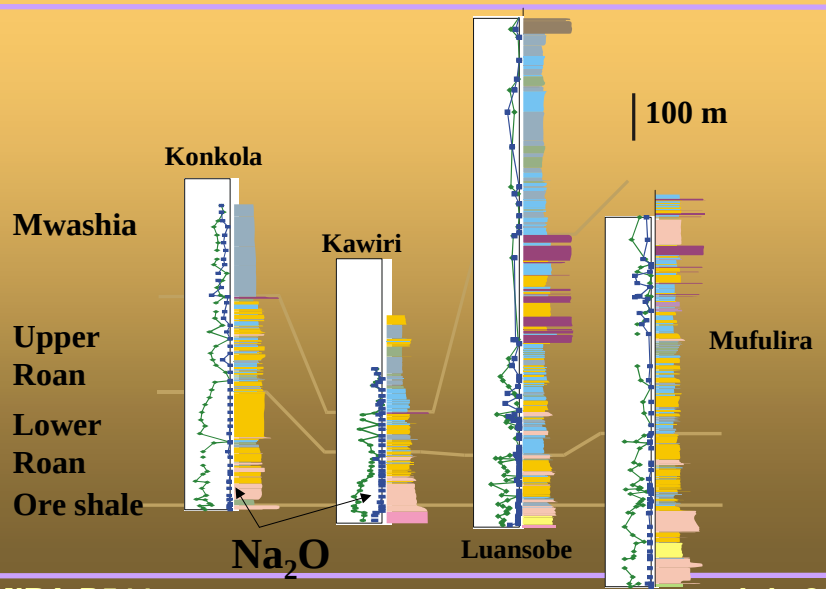

AMIRA P544 *Final Sponsors Meeting* July 2003

Alteration and Lithogeochemistry

- Neither potassic nor sodic alteration are direct guides to ore.
- Both styles of alteration are regional.
- Zambian Copperbelt orebodies occur within zones of potassic alteration but the alteration extends laterally and vertically far beyond ore. (*new data*)

These styles of alteration are critical, however, in showing that the basin was hydrodynamically active and circulated large volumes of brine necessary to form major ore deposits.

AMIRA P544 *Final Sponsors Meeting* July 2003

Alteration and Lithogeochemistry

- One probable ore-related alteration type recognized at Mufulira — K-feldspar destructive (acid) alteration due to generation of sulfuric acid from sour gas.
- Potential guide to ore in other arenite-hosted systems.
- Note that in other areas this alteration may be seen as "orthoquartzites" (some supposed Muva?) or as highly aluminus rocks (kyanite schists in NW Zambia?)

AMIRA P544 *Final Sponsors Meeting* July 2003

Alteration and Lithogeochemistry

- Are there geochemical halos to ore?
- Copper is the only robust elemental halo to mineralization recognized to date. Co may form a larger halo.
- Carbon isotopes also display a broad depletion around mineralized zones - probably due to oxidation of hydrocarbons *(new data)*.

AMIRA P544 *Final Sponsors Meeting* July 2003

Halos to Mineralization - Carbon Isotopes

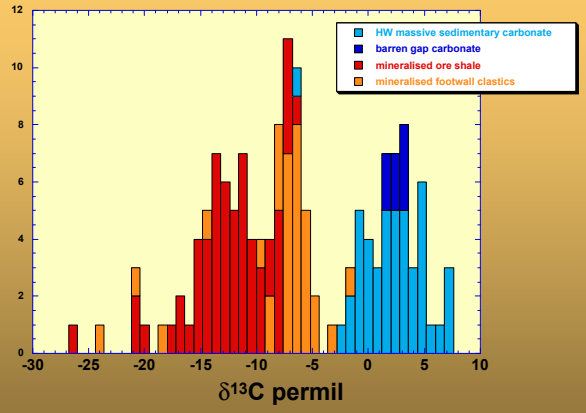

Light carbon isotopes, indicative of oxidation of hydrocarbons, seem to form a broad zone around mineralized areas.

Halos to Mineralization - Carbon Isotopes

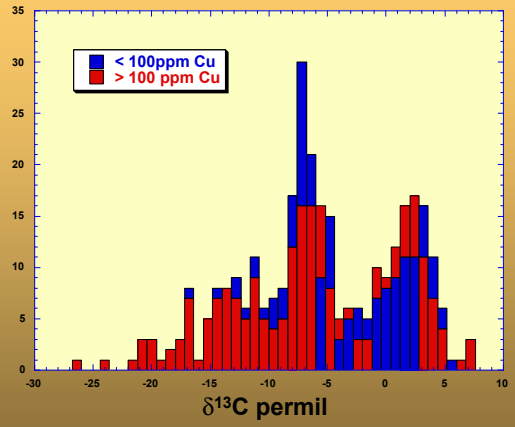

Though the fit is not perfect, most mineralized rocks contain carbonate with relatively depleted carbon isotopic values.

Halos to Mineralization - Carbon Isotopes

Despite recognition that a depleted carbon isotopic signature occurs in the vicinity of orebodies, we do not yet have enough data to quantify the size of these halos.

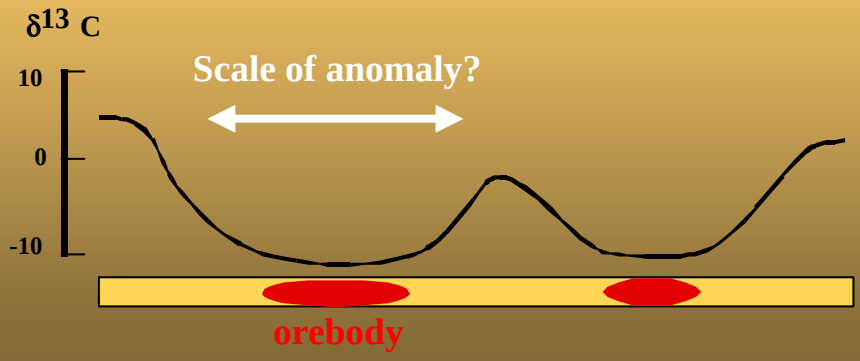

Additional data will be provided by theses - Broughton, Croaker, and Pollington.

AMIRA P544 *Final Sponsors Meeting* July 2003

What have we learned from P544 (Zambia)?

Mineralization

Nkana

AMIRA P544 *Final Sponsors Meeting* July 2003

Mineralization

- **Zambian Copperbelt mineralization is fundamentally controlled by oxidation change. (*suspected before*)**

AMIRA P544 *Final Sponsors Meeting* July 2003

Mineralization

- **Arenite hosted orebodies (e.g. Chibuluma and Mufulira) are controlled by three dimensional seals (stratigraphic pinchouts and/or anticlinal traps). Orebodies controlled by the former presence of hydrocarbons (natural gas and petroleum) which served as reductants.**
- **Ore shale orebodies (e.g. Konkola) are controlled by the presence of carbonaceous (relatively reducing) lithologies.**
- **In both instances, structure is probably critical in guiding fluids.**

AMIRA P544 *Final Sponsors Meeting* July 2003

Mineralization - Arenite Orebodies

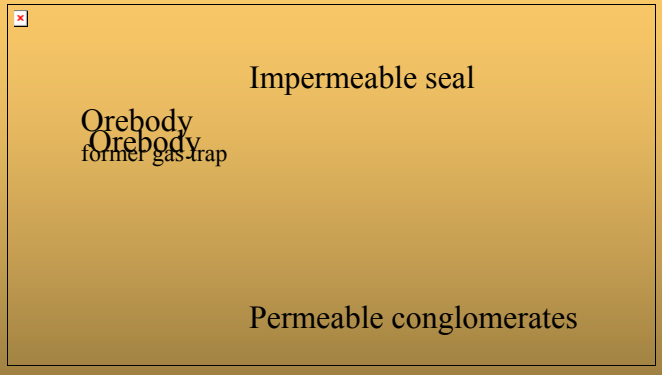

The location of footwall orebodies is controlled by the sedimentary architecture related to early normal faults and the presence of sedimentary "seals."

AMIRA P544 *Final Sponsors Meeting* July 2003

Mineralization - Arenite Orebodies

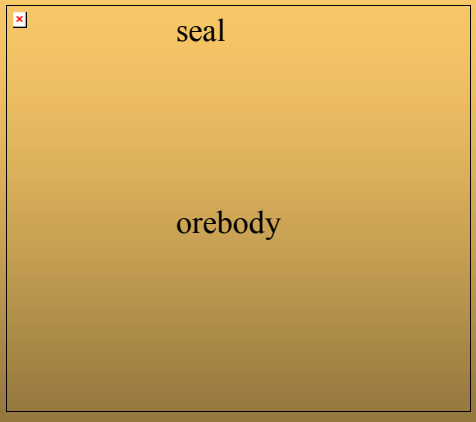

Arenaceous orebodies occur in physical traps (permeable rocks overlain by impermeable rocks). They are controlled by the former presence of hydrocarbons (natural gas and petroleum) which served as reductants.

AMIRA P544 *Final Sponsors Meeting* July 2003

Mineralization - Ore Shale Orebodies

Ore shale orebodies are controlled by the presence of carbonaceous (relatively reducing) lithologies and adjacent (generally stratigraphically below) permeable lithologies.

AMIRA P544 *Final Sponsors Meeting* July 2003

Mineralization — Metals

The Copperbelt is unusual among stratiform, sed-hosted copper districts:

- Locally abundant Co (most of Congo orebodies)
- Very little Ag
- Low to no Zn, Pb

AMIRA P544 *Final Sponsors Meeting* July 2003

Source of Copper

Hitzman (2000) pointed out that the Zambian Copperbelt contained too little "source beds" relative to Kupferschiefer and White Pine districts.

	Dimensions (thickness x width x length) km	Tones of material ($x10^{12}$ tonnes)	Tonnes of known Cu in deposits ($x10^6$)	Average grade leached from source for deposits (ppm)	Tonnes of total Cu in district ($x10^6$)	Average grade leached from source material for districts (ppm)
White Pine	2 x 10 x 40	1.3	7	**5.4**	45	**34**
Kupferschiefer	0.9 x 40 x 160	9.4	52	**5.5**	350	**37**
Zambia	0.25 x 50 x 100	2.1	91	**43**	612	**291**

Source of Copper

Based on data from P544 it appears that sediments below and above the ore shale in Zambia have been altered and are thus possible sources of copper. Redoing the original calculations allows us to investigate whether we now have a sufficient source for metals.

AMIRA P544 *Final Sponsors Meeting* July 2003

Source of Copper

Case 1: 500 m Upper Roan
250 m Lower Roan
100 m basement

	Dimensions (thickness x width x length) km	Tones of material ($x10^{12}$ tonnes)	Tonnes of known Cu in deposits ($x10^6$)	Average grade leached from source for deposits (ppm)	Tonnes of total Cu in district ($x10^6$)	Average grade leached from source material for districts (ppm)
Kupferschiefer	0.9 x 40 x 160	9.4	52	5.5	350	37
Zambia (1)	0.85 x 50 x 100	6.8	91	13.4	612	90

Source of Copper

Case 2: 600 m Upper Roan
300 m Lower Roan
200 m basement

	Dimensions (thickness x width x length) km	Tones of material ($x10^{12}$ tonnes)	Tonnes of known Cu in deposits ($x10^6$)	Average grade leached from source for deposits (ppm)	Tonnes of total Cu in district ($x10^6$)	Average grade leached from source material for districts (ppm)
Kupferschiefer	0.9 x 40 x 160	9.4	52	5.5	350	37
Zambia (2)	1.1 x 50 x 100	8.9	91	10.2	612	69

Source of Copper

Case 3: 600 m Mwashia
600 m Upper Roan
300 m Lower Roan
200 m basement

	Dimensions (thickness x width x length) km	Tones of material ($x10^{12}$ tonnes)	Tonnes of known Cu in deposits ($x10^6$)	Average grade leached from source for deposits (ppm)	Tonnes of total Cu in district ($x10^6$)	Average grade leached from source material for districts (ppm)
Kupferschiefer	0.9 x 40 x 160	9.4	52	**5.5**	350	**37**
Zambia (3)	1.7 x 50 x 100	13.8	91	**6.6**	612	**44**

AMIRA P544 *Final Sponsors Meeting* July 2003

Source of Copper

- Even utilizing extremely generous thicknesses of Lower Roan, and adding alteration of the Upper Roan and portions of the Mwashia and the basement, we still have more copper leached per tonne of source material than either the Kupferschiefer or White Pine (both of which have abundant mafic detritus in the basal clastic rocks).
- Implication is that fluids have interacted with copper sources outside the immediate Zambian Copperbelt area:
  - **Lateral fluid flow (from basin in southern Congo?)**
  - **Basement involvement**

AMIRA P544 *Final Sponsors Meeting* July 2003

Source of Copper

Implication is that fluids have interacted with copper sources outside the immediate Zambian Copperbelt area:

– **Lateral fluid flow -** Where is the adjacent basin? (Congo?) Heat to drive convection?

– **Basement involvement -** Fluid flow models show this is viable. Geologic evidence of deep, widespread alteration of basement?

AMIRA P544 *Final Sponsors Meeting* July 2003

Source of Cobalt

- What is the source of cobalt (which differentiates Copperbelt from other systems)?
- Data suggests timing of cobalt mineralization may be different from main period of copper mineralization. (Documented later in most Congo deposits).
- Cobalt mineralization associated with potassic alteration (Zambia).

AMIRA P544 *Final Sponsors Meeting* July 2003

Source of Cobalt

- What is the source of cobalt (which differentiates Copperbelt from other systems)?

- Least altered gabbros from northern Zambia have up to 60 ppm Co and over 125 ppm Cu - much in pyroxene. During alteration (conversion of pyroxene to hornblende) these metals are expelled and lost to the metamorphic fluid (Barron, 2003).
- Early pyrite and some carbonates also contain elevated cobalt — possible Co sources.

Cobalt liberated during alteration is fixed within copper orebodies lower in section.

AMIRA P544 *Final Sponsors Meeting* July 2003

Metals - Ag, Zn, Pb

- Levels of Ag, Zn, Pb are low in the Copperbelt orebodies compared to other stratiform, sediment-hosted copper districts.
- Metal source beds may have had low Ag, Zn, Pb — geologically unlikely.
- Or, metals may have passed through system (not precipitated) — precipitating higher in the system (Kipushi, Kabwe, etc.?).
- If Ag, Zn, Pb are not precipitating, it suggests the system is reductant (not metal) limited.

AMIRA P544 *Final Sponsors Meeting* July 2003

Reductants - Keys to Mineralization?

May be multiple reductants in the Zambian Copperbelt:

- Arenite orebodies
  - Methane, sour gas (H_2S), petroleum
- Ore Shale orebodies
  - In-situ organic material

AMIRA P544 *Final Sponsors Meeting* July 2003

Reductants - Keys to Mineralization?

- May not be need for large amounts of hydrocarbons (Mufulira exception?).
- We see few "source beds" for hydrocarbons in the Zambian Copperbelt sequence.
- Ore shale could generate some hydrocarbons but such rocks are not abundant in some areas (e.g. eastern side of Kafue anticline).

Hydrocarbons (petroleum and/or gas) do not migrate downward. This suggests possible lateral hydrocarbon migration from downdip adjacent basinal areas with source beds in Lower Roan equivalent strata (lacustrine/marine black shales in basin to north in Congo?).

AMIRA P544 *Final Sponsors Meeting* July 2003

Reductants - Keys to Mineralization?

Hydrocarbons will not mix easily with dense brine (or fresh water). Mixing probably requires:

- Turbulence — fault movement?
- Time — boundary infiltration and movement

AMIRA P544 *Final Sponsors Meeting* July 2003

Reductants - Keys to Mineralization?

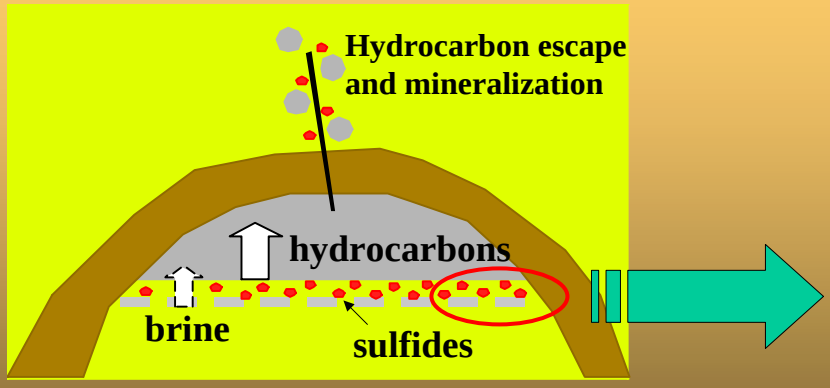

Hydrocarbon-brine boundary moves up with hydrocarbon escape (and destruction). Mineralization on hydrocarbon - brine interface; migrates through time.

AMIRA P544 *Final Sponsors Meeting* July 2003

Reductants - Keys to Mineralization?

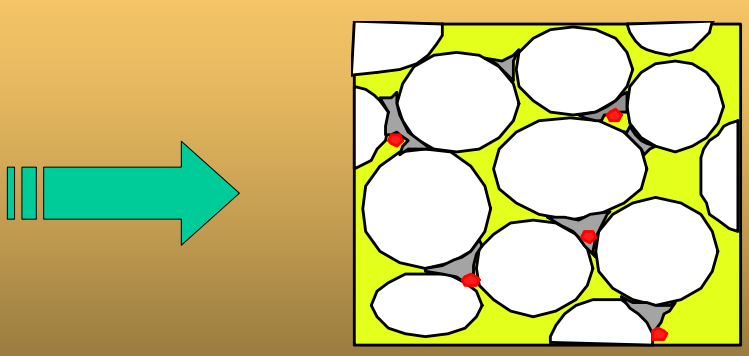

Sulfides precipitate on "dead" oil in pore space below hydrocarbon - brine interface. Does this explain the observed Cu - heavy mineral association?

AMIRA P544 *Final Sponsors Meeting* July 2003

Mineralization - Metamorphism

- Diverse sulfur isotopic signatures of sulfides within and between deposits indicates sulfides have not homogenized during metamorphism.
- Thermochemical sulfate reduction favored mechanism to explain these variations.

"Ore shale" - chalcopyrite - bornite (opaque) cutting and deforming biotite. Movement and recrystallization during deformation. Chambishi

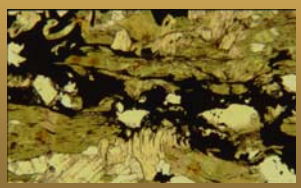

- Sulfide textures indicate most sulfides have recrystallized.

AMIRA P544 *Final Sponsors Meeting* July 2003

Mineralization - Supergene Effects

- Work to date suggests significant, and locally deep (>1 km), supergene alteration, especially along faults.
- Much of the chalcocite is probably supergene.

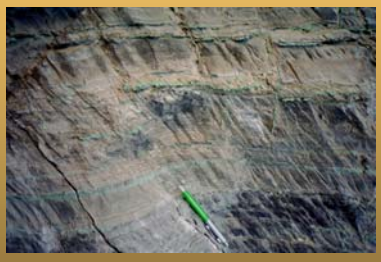

- Trace element signatures (Pb, Ag, Bi, Sn) in chalcocite may serve to differentiate hypogene-supergene chalcocite (*new data*).

AMIRA P544 *Final Sponsors Meeting* July 2003

Genetic Model for the Zambian Copperbelt

AMIRA P544 *Final Sponsors Meeting* July 2003

Key Ages

- 880 Ma — Nchanga Granite (basement)
- Age of Roan sediments?
- 765 — Volcanic rocks in Mwashia
- 765 - 740 — Gabbros
- 750 — Grand Conglomerate (Sturtian glaciation)
- 670 - 620 — Shinkolobwe U deposit (reliable age?)
- 645 — Disseminated mineralization at Musoshi (Pb-Pb— reliable?)
- 600 — Age of Petit Conglomerate
- 560 — Hook Granite
- 500-535 — Xenotime/monazite ages - Copperbelt
- 510 - 490 — Vein Cu-Mo-U mineralization (Kansanshi, Musoshi; Nkana Mo)
- 495 — Cooling below 300°C blocking T for Ar in biotite
- 470 — Cooling below blocking T for Ar in muscovite

AMIRA P544 *Final Sponsors Meeting* July 2003

Structural Architecture

Location of schematic cross section across Copperbelt from north to south.

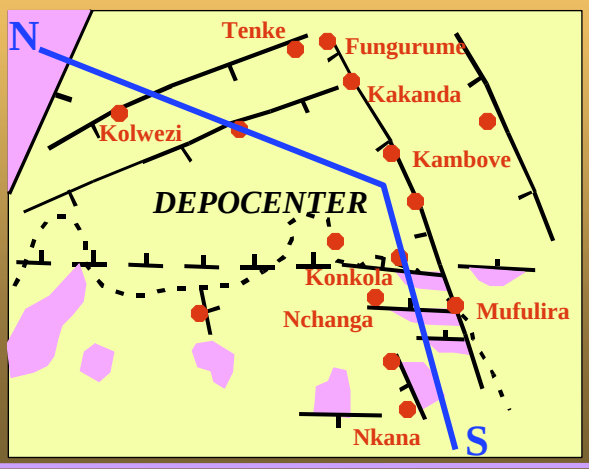

AMIRA P544 *Final Sponsors Meeting* July 2003

Lower Roan Sedimentation

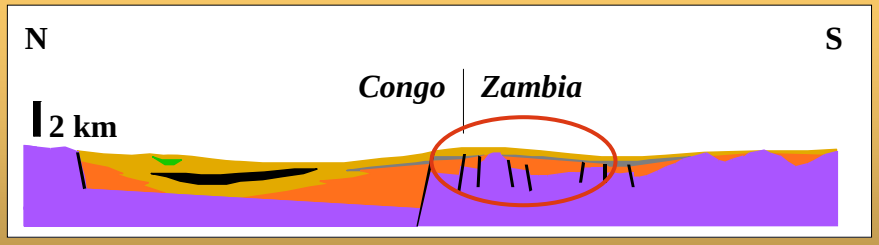

- **Extensional environment (post 880 Ma) leads to complex fluvial/alluvial basal section (lower Roan) dominated by basement-derived arkose.**

AMIRA P544 *Final Sponsors Meeting* July 2003

Lower Roan Sedimentation

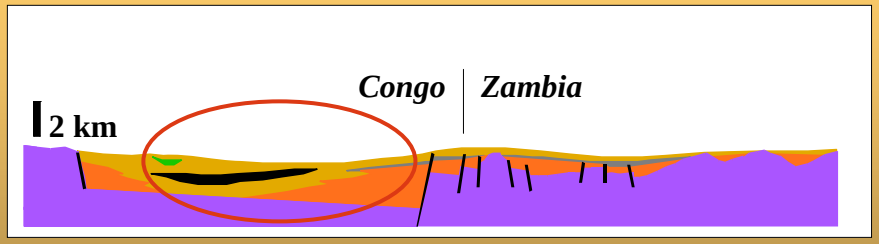

- **Possibility of major basin north of Zambian Copperbelt in southern Congo. Basin could contain >3km red beds (coarse sediments grading up to RAT siltstones) and lacustrine/shallow marine C-rich source rocks.**

AMIRA P544 *Final Sponsors Meeting* July 2003

Lower Roan Sedimentation

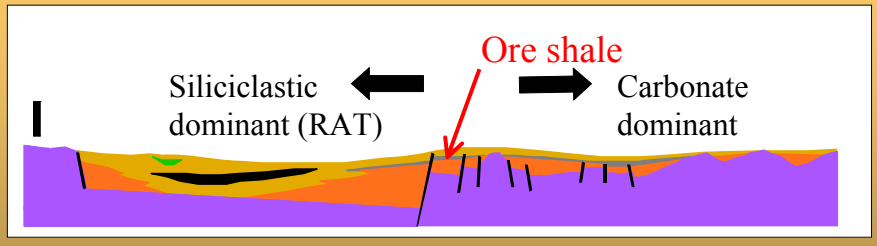

- **In Zambia, relatively thin, coarse-grained basal siliciclastics covered by mixed sequence of siltstones, rare shales ("Ore Shale"), and carbonates.**
- **In Congo, basal sequence poorly observed. Appears to be siliciclastic-dominant (RAT).**

AMIRA P544 *Final Sponsors Meeting* **July 2003**

Lower - Upper Roan Sedimentation Zambian Copperbelt

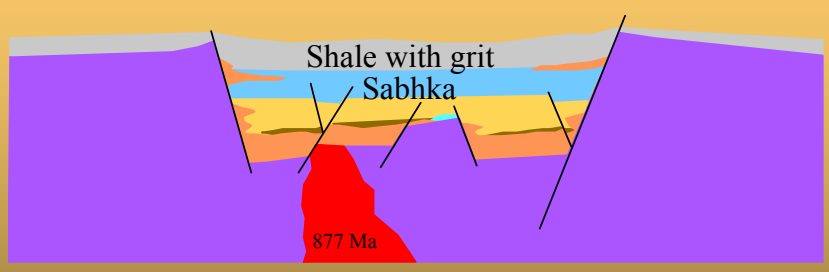

- **Covering of basement topography leads to more mature, layer-cake sedimentary geometry with mixed marine (?) siliciclastic-carbonate facies overlain by sabhka carbonate facies.**
- **Punctuated extensional events provide coarse siliciclastic input.**

AMIRA P544 *Final Sponsors Meeting* **July 2003**

Upper Roan Sedimentation

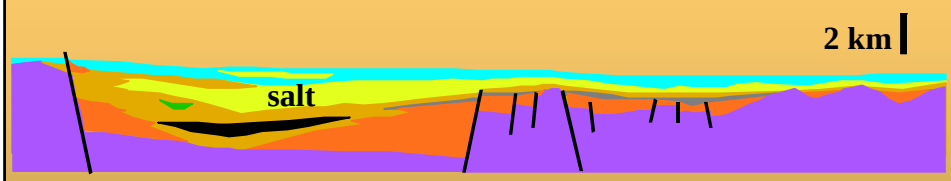

- **Probable restriction of basin leads to evaporite (gypsum + halite) precipitation. Thickest evaporites to north in Congo basin which also has continuing siliciclastic sedimentation (RAT).**
- **Upper Roan (above evaporite) dominated by carbonates - broad, regular sequence (sabkha).**
- **Upper Roan in Zambia correlates with Mines Group and Dipeta in Congo.**

AMIRA P544 *Final Sponsors Meeting* July 2003

Mwashia Sedimentation (~765 Ma)

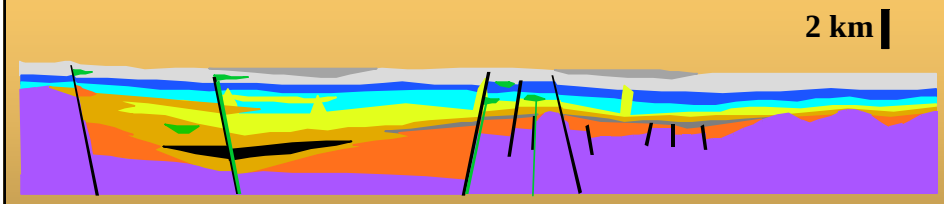

- **Mwashia consists of basal carbonate-rich sediments grading up to siltstones.**
- **Mafic igneous event during Mwashia time - intrusive (gabbro) in Zambia; extrusive and intrusive rocks in Congo.**
- **Evaporite movement probably starts during Mwashia time.**
- **Initiation of copper mineralization (especially ore shale) at this time?**

AMIRA P544 *Final Sponsors Meeting* July 2003

Grand Conglomerate -Nguba

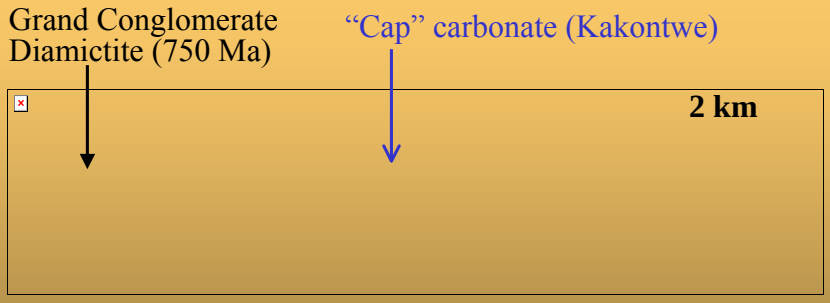

- **Extensional event (765-740 Ma) with continued intrusion of gabbros.**
- **Close to time of Grand Conglomerate - "Snowball Earth."**
- **Extensional event probably caused thermal maturation and migration of hydrocarbons. This event may also have allowed incursion of water (glacial, meteoric?) or glacially-produced brine, evaporite movement and dissolution, and Upper Roan brine formation.**

AMIRA P544 *Final Sponsors Meeting* July 2003

Petite Conglomerate -Kundelungu

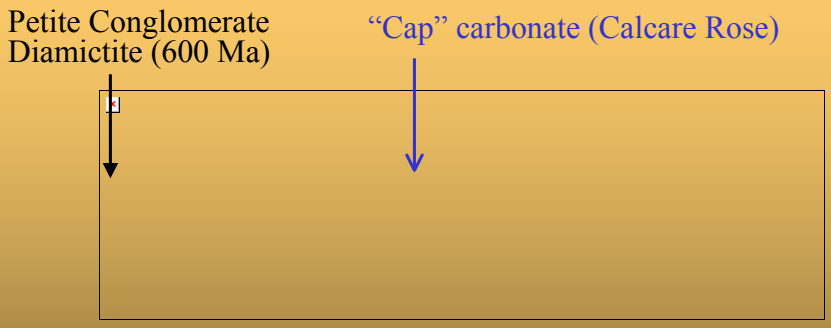

- **Petite conglomerate represents a second major glacial event.**
- **The Kundelungu section above the Petite Conglomerate is dominantly siltstones. The section appears to become coarser grained upsection to the south - onset of uplift?**

AMIRA P544 *Final Sponsors Meeting* July 2003

Lufilian Deformation (~540 - 480 Ma) Zambian Copperbelt

- **Deformation results in upright tight folding in Lower Roan sequence nucleated on early faults.**
- **Structural decoupling near base of Mwashia.**
- **Deformation in upper sequence largely recumbent folds and low-angle (thrust) faults.**
- **Deformation provides energy for movement of remaining brine into basement and overlying rocks.**

AMIRA P544 *Final Sponsors Meeting* July 2003

Lufilian Deformation (~540 - 480 Ma)

- **Progressive deformation from south.**
- **Evaporites provide zones of decoupling. Salt also intrudes upward along structures.**
- **Structural decoupling at Ore Shale, on top of Lower Roan, in salt in Upper Roan, and near base of Mwashia.**

AMIRA P544 *Final Sponsors Meeting* July 2003

Lufilian Salt Tectonics

South **North**

QuickTime™ and a Cinepak decompressor are needed to see this picture.

- Model by Jackson et al. Showing concept of salt breakout for Lufilian Arc.

AMIRA P544 *Final Sponsors Meeting* July 2003

Brine Event (~700 Ma ?)

- **Some breccia formation in Upper Roan section by salt dissolution.**
- **Brine formation and movement downward.**
- **Brine convection and mineralization.**

AMIRA P544 *Final Sponsors Meeting* July 2003

Basin-scale Alteration - Zambia

- **Upper and Lower Roan sections highly altered from brines ("pickled")**
- **General pattern of upper sodic alteration and lower potassic alteration with hematite.**

AMIRA P544 *Final Sponsors Meeting* **July 2003**

Diagenesis - Alteration - Metamorphism

• Diagenesis	• SO_4 + Mg + Na + Ca (dolomitization, albitization)
• Late diagenesis	• Hydrocarbon maturation
• Late diagenesis — syntectonism	• Potassic alteration (deep) K, B, Mg (Cu and Co mineralization); sodic alteration (shallower) with Cu-Co leaching.
• Late diagenesis — synmetamorphism	• Sodic alteration Na, Mg, Ca

AMIRA P544 *Final Sponsors Meeting* **July 2003**

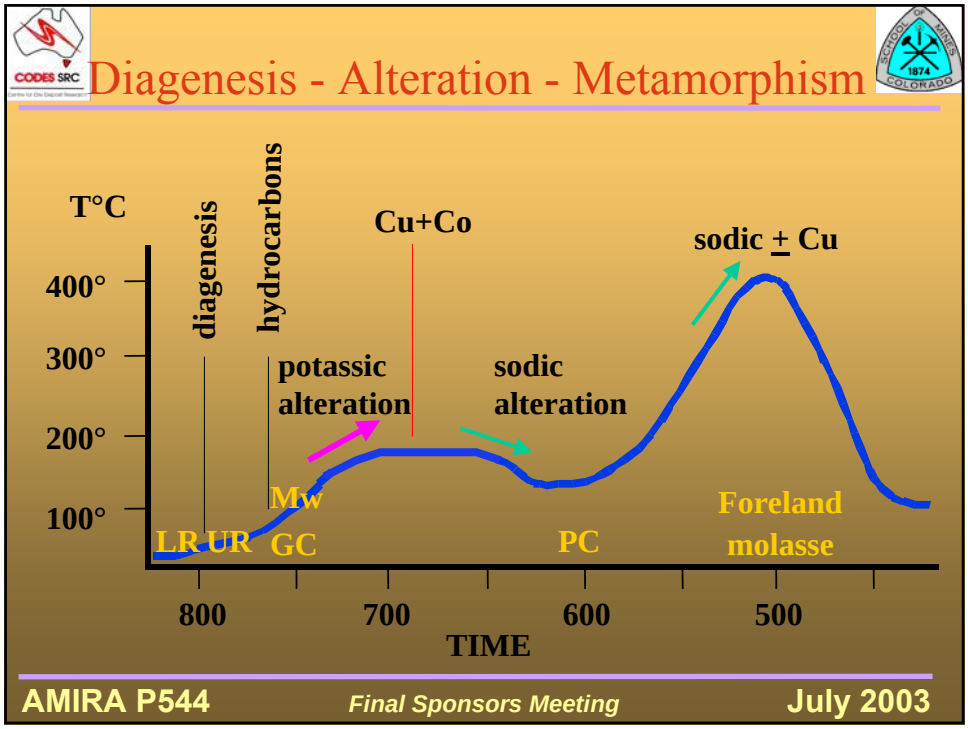
Diagenesis - Alteration - Metamorphism
T°C
400°
300°
200°
100°
diagenesis
hydrocarbons
Cu+Co
sodic ± Cu
potassic alteration
sodic alteration
Mw
LR-UR
GC
PC
Foreland molasse
800
700
600
500
TIME
AMIRA P544
Final Sponsors Meeting
July 2003

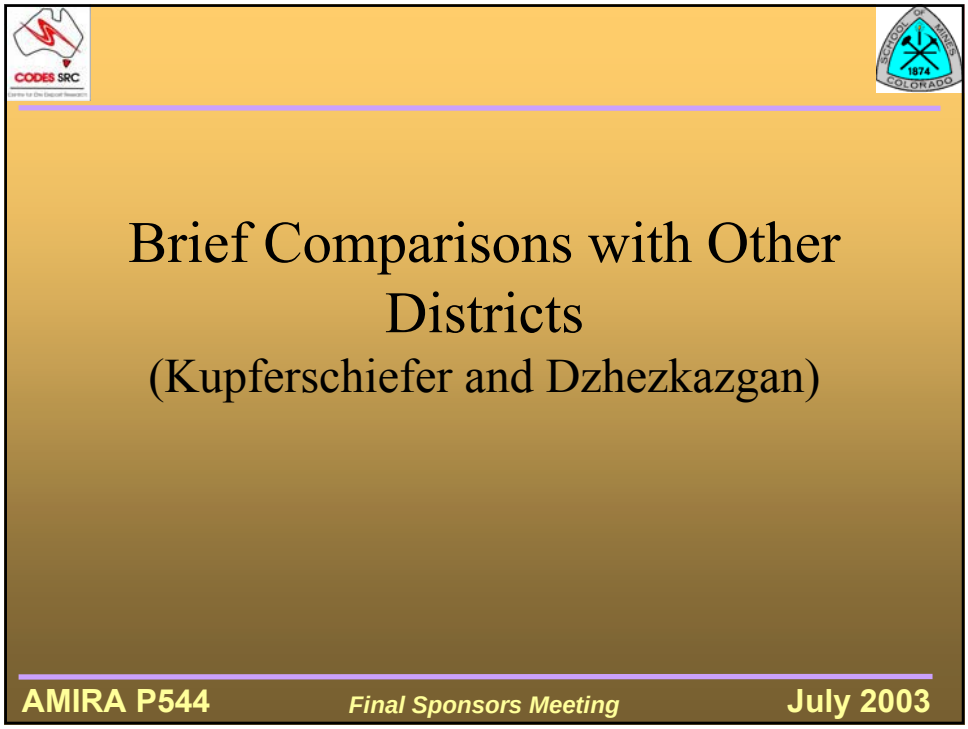
Brief Comparisons with Other Districts
(Kupferschiefer and Dzhezkazgan)
AMIRA P544
Final Sponsors Meeting
July 2003

Comparisons

The Kupferschiefer and Dzhezkazgan districts provide younger analogues to the Zambian Copperbelt.

Comparisons — District Size

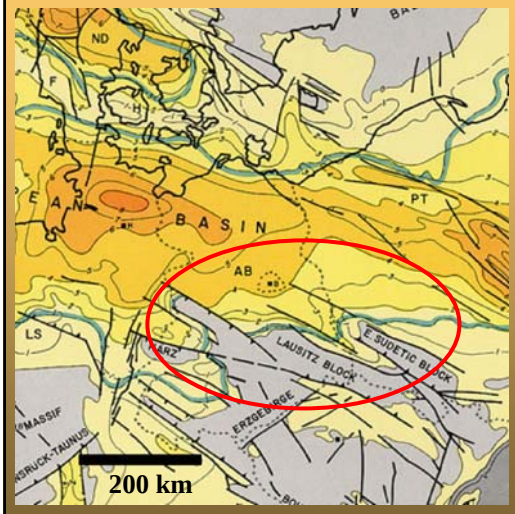

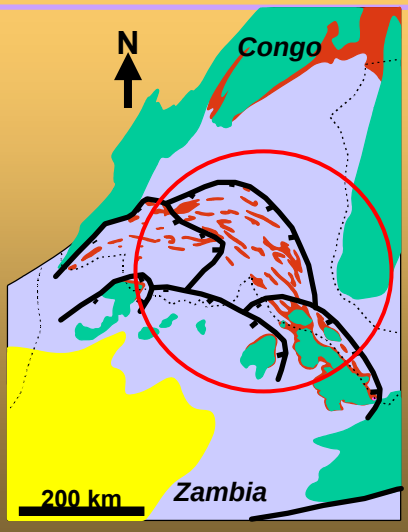

Kupferschiefer African Copperbelt

Comparisons — District Size

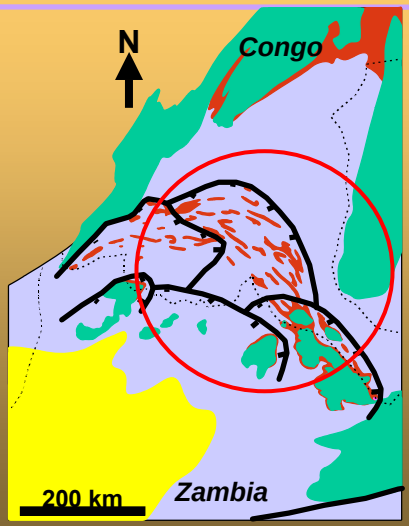

Dzhezkazgan, Kazakhstan | African Copperbelt

AMIRA P544 | Final Sponsors Meeting | July 2003

Kupferschiefer - Analogue for Ore Shale Orebodies

- Kupferschiefer deposits are good analogues to Zambian ore shale deposits.
- Different basin geometries with regards brines - in Zambia brines from above and below carbonaceous shale.
- Note presence of lake facies in Rotliegendes - source rocks for hydrocarbons?

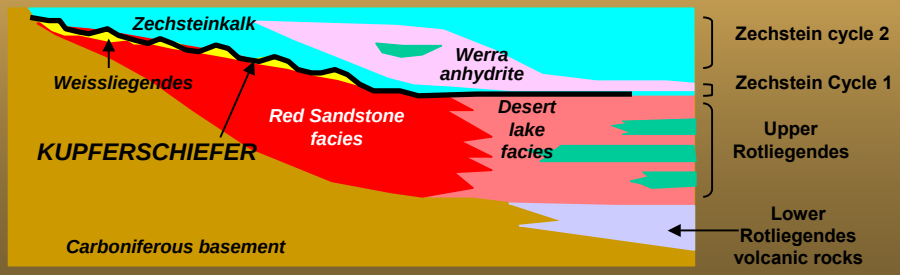

AMIRA P544 | Final Sponsors Meeting | July 2003

Dzhezkazgan - Analogue for Arenaceous Orebodies

- Dzhezkazgan is a structural trap with evidence of hydrocarbons (sour gas) that was then invaded by metalliferous brine - analogue for Mufulira.

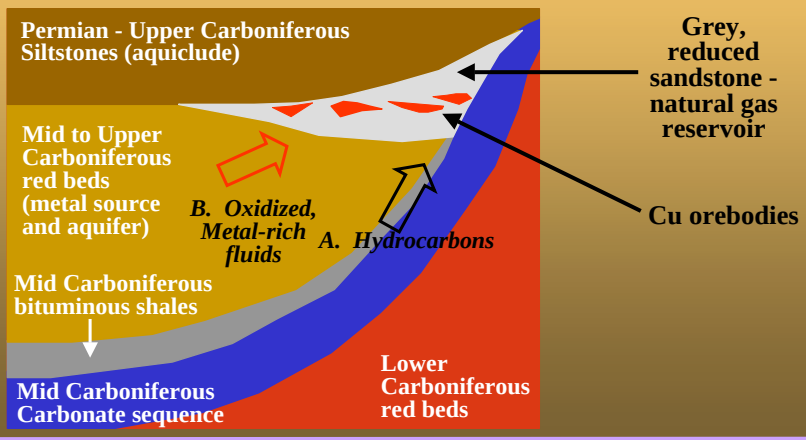

AMIRA P544 *Final Sponsors Meeting* July 2003

Comparisons

A potentially significant difference between Zambia and the other districts may be that Zambia developed a brine pool in the basin that interacted with the host rocks for a long time period (~100 my).

AMIRA P544 *Final Sponsors Meeting* July 2003

Exploration Implications

Implications of the Model

- **Whole basin hydrothermal system. Basin-scale alteration pattern. May not be deposit-specific alteration patterns.**
- **Source of brines is high in sequence.**
- **Convective flow probably concentrated along first-order basin-bounding faults. Understanding structural architecture critical for exploration.**

Implications of the Model (cont.)

- **Delineation of reduced zones within the basin is critical.**
- **Any type of reduced zone may be favorable.**
- **Carbon isotopes on carbonates may help define form zones of reductants.**

AMIRA P544 *Final Sponsors Meeting* July 2003

Implications of the Model (cont.)

- **Multiple deposit types may be present at multiple stratigraphic horizons:**
  - **Zambian Copperbelt type**
  - **Congo Copperbelt type**
  - **Kipushi type**
  - **Kansanshi type**

AMIRA P544 *Final Sponsors Meeting* July 2003

Implications of the Model (cont.)

- Zambian Copperbelt —
  Ore deposits in carbonaceous sedimentary layers and physical gas/oil traps in Lower Roan.

AMIRA P544 *Final Sponsors Meeting* July 2003

Implications of the Model (cont.)

- Congo Copperbelt —
  Ore deposits in now mildly carbonaceous Upper Roan dolosiltstones and dolostones - relict hydrocarbons ???
  (REQUIRES ADDITIONAL RESEARCH)

AMIRA P544 *Final Sponsors Meeting* July 2003

Implications of the Model (cont.)

Breccia pipe hosted deposit (e.g. Kipushi)

- Southern Congo / Central Zambia / Namibia —
  Ore deposits in cross stratal breccia pipes (paleo salt domes) charged with gas/oil cutting Mwashia and Kundelungu sequence. *(REQUIRES ADDITIONAL RESEARCH)*

AMIRA P544 *Final Sponsors Meeting* July 2003

Implications of the Model (cont.)

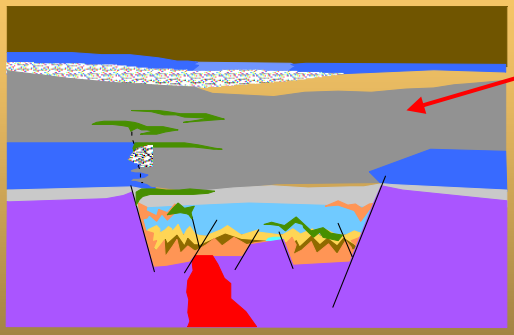

N. Zambia/ S. Congo (e.g. Kansanshi)

- Northern Zambia / Southern Congo —
  Tectonically-induced fluid escape ways into the reduced Mwashia and lower Kundelungu. (e.g. Kansanshi, Shinkolobwe)

AMIRA P544 *Final Sponsors Meeting* July 2003

Exploration for Deposits in Zambia

- Delineation of early, syn-sedimentary faults using aeromagnetics and gravity, thickness variations in the basal Roan clastic rocks, later folds and reverse faults nucleated on early structures.
- Restriction of exploration to potassically altered areas.
- Definition of "reduction traps" — physical hydrocarbon reservoirs (anticlinal closures), stratigraphic pinchouts, and organic-rich sediments. Zones of anomalously low $\delta^{13}C$ may help pinpoint zones.
- Recognition of Ksp destructive zones in arenites indicating acid production by sour gas destruction associated with mineralization.
- Recognition of structural zones that may have allowed deep oxidation and lateral migration of copper-rich groundwaters (supergene deposits).

AMIRA P544 *Final Sponsors Meeting* July 2003

Exploration for other Copperbelt-type Basins

- Intracratonic basins — those that retain, and do not leak, brines.
- Basins that contain significant (>100's meters) thicknesses of oxidized, siliciclastic sediments at their base and are composed largely of oxidized fill. Mafic volcanic detritus is favorable.
- Basins that contain(ed) restricted zones of reductants — either organic-rich black shales or physically trapped hydrocarbons.
- Evidence of brine production — widespread potassic and/or sodic alteration derived from evaporite dissolution. Evidence for evaporites (in addition to regional alteration) includes major stratabound and cross-cutting breccias and megabreccias.

AMIRA P544 *Final Sponsors Meeting* July 2003

Exploration for other Copperbelt-type Basins (cont.)

- Evaporites survive to late in basin history and/or brines present in basins for long time periods (millions of years).
- Geologic evidence of a heat engine, such as intrusive and/or volcanic rocks, to move evaporite-generated brine.
- Long-lived structural conduits that provide fluid pathways.
- Widespread trace copper mineralization.
- Alteration must have had a significant affect on petrophysical properties - are fluid pathways mappable from geophysical datasets?

AMIRA P544 *Final Sponsors Meeting* July 2003

Good Hunting!

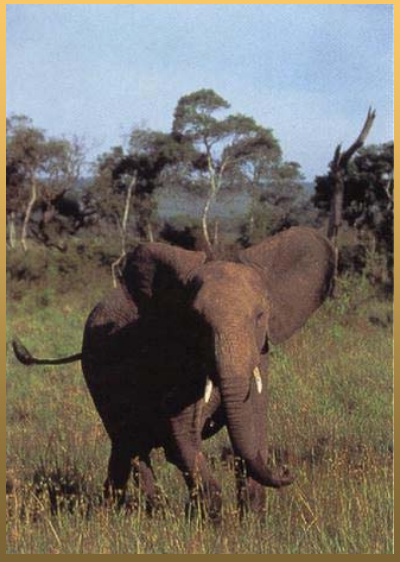

There are still elephants to find …

AMIRA P544 *Final Sponsors Meeting* July 2003